UNIVERSIDAD MICHOACANA DE SAN NICOLÁS DE HIDALGO

INSTITUTO DE INVESTIGACIONES QUÍMICO BIOLÓGICAS

Título de la Tesis:

PARTICIPACIÓN DE LA SUBUNIDAD Gpb1 DE PROTEÍNAS G HETEROTRIMÉRICAS EN LA VIRULENCIA DE *Mucor circinelloides*

Que para obtener el grado de Doctor en Ciencias en Biología Experimental

Presenta:

Maestro en Ciencias Marco Iván Valle Maldonado

Asesor: Doctor en Ciencias en Biología Experimental Víctor Meza Carmen

Comité Evaluador: D.C. Carlos Cortés Penagos

D.C. J. Félix Gutiérrez Corona (Universidad de Guanajuato)

D.C. Martha Isela Ramírez Díaz

D.C. Homero Reyes de la Cruz

Morelia, Mich., Agosto 2020

AGRADECIMIENTOS

A mis padres Olimpia Maldonado Monje y Aureliano Valle Rangel, por haberme criado y haberme dado las herramientas durante mi formación académica, que ahora formalmente concluye. A Eréndira, Gabriel y Uriel por ser mis hermanos y compañeros de juegos y bromas durante toda la vida.

A la Universidad Michoacana de San Nicolás de Hidalgo, y al Instituto de Investigaciones Químico Biológicas por brindarme la oportunidad de cursar un posgrado que incluyó dos etapas: maestría y doctorado

Al D.C. Víctor Meza Carmen por asesorar permanentemente mi trabajo durante todos mis estudios de posgrado y contribuir significativamente en la formación de mi pensamiento crítico. Especialmente estoy agradecido por haberme brindado las oportunidades de colaborar con grupos externos a la UMSNH.

Al Laboratorio Estatal de Salud Pública de Michoacán por facilitar el desarrollo satisfactorio de los ensayos durante mis estudios de posgrado y permitir mi desarrollo profesional.

Al D.C. Irvin E. Jácome Galarza, por su constante enseñanza en la aplicación y entendimiento de técnicas de Biología Molecular, y por permitirme llegar a su coordinación primero como estudiante y luego como Químico Analista.

A mi comité evaluador, que incluye a los D.C. Martha Isela Ramírez Díaz, Homero Reyes de la Cruz, Carlos Cortés Penagos, y J. Féliz Gutiérrez Corona de la Universidad de Guanajuato por sus contribuciones intelectuales para la realización de este trabajo.

A mis compañeros del Laboratorio de Diferenciación Celular a los M.C. José Alberto Patiño Medina, Nancy Yadira Reyes Mares, David Vargas Tejeda, Sharel Pamela Díaz Pérez, Viridiana Alejandre Castañeda, Ma. Dolores Vázquez Rivera y Guadalupe Maldonado Herrera por ser mis amigos en el laboratorio y por contribuir a que la productividad del laboratorio fuera mayor durante el periodo de mis estudios.

A mis compañeros del Laboratorio De Biología Molecular del Laboratorio Estatal de Salud Pública, los Q.F.B. Alejandro Soria Cruz, Iván Alejandro Sánchez Novoa, Alexis Villaseñor Fraga, Christian Josué Serrato Morales, María Elena Silva Martínez, José Edgar Vidales Becerril, Itzi Yanet Ortega Valencia, Jorge Trejo Mejía, por su valiosa amistad y compañerismo especialmente en estos tiempos de pandemia.

A la M.S.P. Gloria Alicia Figueroa Aguilar por las facilidades prestadas para la conclusión de este proyecto de investigación.

Al Dr. Soo Chan Lee y al M.C. Sandeep Vellanki por haberme recibido y su importante ayuda en la estancia de investigación que realicé en la Universidad de Texas en San Antonio, Estados Unidos de América. Durante el periodo Septiembre-Noviembre de 2019. Thank you!

A los D.C. Diego Delgado Álvarez y Olga Callejas Negrete por su valiosa ayuda en la estancia de investigación realizada en el Laboratorio Nacional de Microscopía Avanzada, CICESE en Ensenada, Baja California. Durante Diciembre de 2018.

A Marycarmen, por tu amistad y compañerismo durante este último año y medio.

A CONACyT por haberme otorgado becas para mis estudios de posgrado.

ÍNDICE

INDICE DE FIGURAS

INDICE DE TABLAS

Página

Tablas Suplementarias del artículo Valle-Maldonado et al., 2020

ABREVIATURAS Y SÍMBOLOS

AC: Adenilato ciclasa

ADP: Adenosín difosfato

AMPc: Adenosín monofosfato cíclico

DNA: Ácido desoxribonucleico

GAP: Proteína activadora de GTPasa (GTPase-activating protein).

GDP: Guanosín difosfato

GTP: Guanosín trisfosfato

GPCR: Receptor acoplado a proteínas G (G Protein Coupled Receptor)

kDa: kilo Daltons

PGH: Proteínas G Heterotriméricas

PKA: Proteína cinasa A

RGS: Regulador de señalización de proteínas G (Regulator of G-protein signaling)

RNA: Ácido Ribonucleico

RT-qPCR: Reacción en cadena de la polimerasa con transcriptasa inversa en tiempo real

PREFIJOS

M: Mega ($1x10^{6}$)

k: kilo ($1x10^{3}$)

μ: micro ($1x10^{-6}$)

n: nano ($1x10^{-9}$)

RESUMEN

Las proteínas G heterotriméricas son elementos cruciales en la regulación de un repertorio muy amplio de funciones biológicas en eucariotes. En hongos, estas proteínas controlan la diferenciación celular, la reproducción, la respuesta a nutrientes, la patogénesis, entre otros procesos. *Mucor circinelloides* es un patógeno oportunista fúngico en humanos. En nuestro grupo de trabajo reportamos previamente que este organismo tiene el repertorio más grande de proteínas G heterotriméricas en el reino Fungi. Específicamente, este mucoral expresa tres genes que codifican para subunidades beta (Gpb1, Gpb2, Gpb3) de proteínas G heterotriméricas. Adicionalmente, reportamos que el gen que codifica para la subunidad Gpb1 presentó niveles de transcrito incrementados durante el crecimiento micelial comparado con esporas o el crecimiento levaduriforme. La interrupción del gen que codifica para la subunidad Gpb1, demostró su relevancia para un desarrollo adecuado durante la transición levadura-micelio, y para el desarrollo de micelio durante el crecimiento en bajas concentraciones de oxígeno. Los ensayos de infección en ratones por esporas mutantes de interrupción del gen gpb1 (Δ*gpb1*) mostraron un fenotipo con reducción significativa en la virulencia, la invasibidad de tejido y en la respuesta inflamatoria del huesped en comparación con la cepa silvestre. Este hallazgo podría ser atribuido a un crecimiento filamentoso reducido en los tejidos animales. En este contexto, la interrupción del gen de la subunidad regulatoria (PkaR1) de la proteína cinasa A (PKA) también fue evaluada y mostró fenotipos similares a Δ*gpb1*. Los fenotipos de Δ*gpb1* fueron suprimidos genéticamente por la sobreexpresión de *pkaR1,* lo que indica que la ruta de la PKA está bajo control de Gpb1 en *M. circinelloides* durante estos procesos. Adicionalmente, durante el crecimiento en bajas condiciones de oxígeno, los niveles de cAMP fueron muchos más altos en la cepa Δ*gpb1* comparados con la cepa Silvestre, pero similares con los de la cepa Δ*pkaR1.* Estos resultados revelaron que *M. circinelloides* posee una ruta de transducción de señales a través de la cual Gpb1 y PkaR1 controlan el crecimiento micelial en respuesta a bajos niveles de oxígeno.

Los resultados de este trabajo son importantes para entender la función de la subunidad Gpb1 de proteínas G heterotriméricas en la fisiología de este mucoral.

Palabras clave: cAMP, dimorfismo, *Mucor circinelloides*,Virulencia fúngica, Proteínas G heterotriméricas, Proteína cinasa A.

Abstract

Heterotrimeric G proteins are keystone elements that critically regulate a wide repertoire of biological functions in eukaryotes. In fungi, these proteins control cellular differentiation, reproduction, response to nutrients, pathogenesis, among others. *Mucor circinelloides* is a fungal opportunistic in humans. In our group we have previously reported that this organism harbors the largest repertoire of heterotrimeric G proteins in the Fungi kingdom. Specifically, this Mucoral expresses three heterotrimeric G-protein beta subunits (Gpb1, Gpb2, Gpb3). The Gpb1-encoding gene is upregulated during mycelial growth compared with that in the spore or yeast stage. *gpb1* deletion mutation analysis revealed its relevance for an adequate development during the dimorphic transition and for hyphal growth under low oxygen concentrations. Infection assays in mice indicated a phenotype with considerably reduced virulence and tissue invasiveness in the deletion mutants (Δ*gpb1*) and decreased host inflammatory response in comparison with the wild-type strain. This finding could be attributed to the reduced filamentous growth in animal tissues compared with that of the wild-type strain. Mutation in a regulatory subunit of cAMP-dependent protein kinase A (PKA) subunit (PkaR1) resulted in similar phenotypes to Δ*gpb1*. The defects exhibited by the Δ*gpb1* strain were genetically suppressed by *pkaR1* overexpression, indicating that the PKA pathway is controlled by Gpb1 in *M. circinelloides* during these processes. Moreover, during growth under low oxygen levels, cAMP levels were much higher in the Δ*gpb1* than in the wild-type strain, but similar to those in the Δ*pkaR1* strain. These findings reveal that *M. circinelloides* possesses a signal transduction pathway through which the Gpb1 heterotrimeric G subunit and PkaR1 control mycelial growth in response to low oxygen levels.

The results of this study are important to understand the function of the Gpb1 subunit at the pathophysiology of this Mucoral.

Key words: *Mucor circinelloides*, Fungal virulence, Heterotrimeric G proteins, hyphae, Protein kinase A.

I. INTRODUCCIÓN

1.1 Generalidades de los hongos

Los hongos son organismos eucariontes heterótrofos que son componentes indispensables de los ecosistemas, ya que contribuyen de manera importante a la conservación del ciclo del carbono (Bennet et al., 2002). Debido a su habilidad de producir una amplia variedad de enzimas extracelulares, son capaces de degradar todo tipo de materia orgánica, descomponiendo componentes del suelo, y por lo tanto regulando el balance de carbono y de nutrientes (Žifčáková et al., 2016). Frecuentemente, algunos hongos, denominados endófitos, colonizan el sistema radicular de una planta, mejorando la absorción de agua y de nutrientes de dicha planta. Mientras que ésta provee a los hongos de carbohidratos formados a partir de la fotosíntesis. De hecho, esta simbiosis ha sido hallada en todas las plantas estudiadas en ecosistemas naturales (Singh et al., 2011).

Estructuralmente los hongos, además de la membrana celular, y a diferencia de las células de mamíferos, presentan pared celular. Dicha estructura tiene diversas funciones, entre las cuales están: mantener rigidez y la forma celular, el intercambio de iones, la protección de la radiación UV a través de la presencia de pigmentos, y en el caso de patógenos, regular la interacción con sistemas de defensa del hospedero (Martins et al., 2019). La pared celular está compuesta de polisacáridos y proteínas estructurales, de los cuales los principales polisacáridos son glucana, quitina y quitosana (Abo Elsoud y El Kady, 2019). La membrana celular fúngica contiene ergosterol a fin de brindar permeabilidad y la fuidez, cabe mencionar que este compuesto no se encuentra en los demás eucariotes (Rodrigues, 2018). Generalmente, los hongos pueden encontrarse en un estado haploide, el cual se caracteriza en que cada célula tiene una sola copia de material genético, en un estado diploide el cual tiene dos copias del material genético, o existiendo también casos de polipliodía (Todd et al., 2017).

El tamaño del genoma de los hongos oscila entre 8.97 y 177.57 millones de pares de bases de DNA (Mohanta y Bae, 2015). A manera de comparación el genoma

del ser humano cuenta con 3000 millones de pares de bases (Walbot y Petrov, 2001), mientras que el de la bacteria *Escherichia coli* tiene 4.6 millones de pares de bases (Blattner et al., 1997).

A pesar de que los hongos son muy diversos en su naturaleza, en cuanto a fisiología celular y genética, estos comparten componentes similares con las células animales o vegetales. Por ejemplo, la multicelularidad, las estructuras citoesqueléticas, el ciclo celular, el ritmo circadiano, la señalización intracelular, la reproducción sexual, el desarrollo y la diferenciación celular (Galagan et al., 2005).

1.1.1 Criterios de clasificación

Como consecuencia de la relación que guardan con otros organismos, los hongos se clasifican como saprofitos (cuando obtienen sus nutrientes de organismos muertos), simbiontes (al vivir en cooperativismo con otros organismos) o parásitos (viviendo de otros organismos generando un daño) (Baron, 1996). Es importante mencionar que los organismos fúngicos pueden combinar dichas interacciones en respuesta a ciertas variaciones ambientales (Redman et al., 2001).

La espora es una estructura de dispersión en hongos, y es consecuencia de eventos de reproducción sexual o asexual. Las estructuras anatómicas de donde provienen estas esporas representó un criterio de clasificación de los hongos. Más concretamente, si derivan de un saco llamado asco se les llamó ascomicetos, si provienen de un basidio se les llamó basidiomicetos, o zigomicetos para una estructura denominada zigoesporangio (Sharma, 2005).

Actualmente, la clasificaciones filogenéticas más aceptadas (Hibbett et al., 2007; Spatafora et al., 2016, Bass et al., 2018) de los hongos se obtuvieron mediante el uso de técnicas de biología molecular, que incluyen la comparación de las secuencias de un conjunto de genes altamente conservados entre las especies. Tal es el caso de los RNA ribosomales 28S, 18S y 5.8S, α-tubulina y β-tubulina; los cuales se encuntran codificados en el núcleo. Los hongos forman un grupo

monofilético que en conjunto engloban al Reino Fungi. Dentro del subreino *Dikarya,* se encuentran los Phyla *Ascomycota* y *Basidiomycota*. De igual manera pertenecen al Reino Fungi los Phyla *Chytridiomycota, Blastocladiomycota, Cryptomycota, Zoopagomycota* y *Mucoromycota.*

1.1.2 Phylum *Mucoromycota*

Anteriormente, los hongos zigomicetos fueron clasificados debido a características morfológicas en un único *Phylum* monofilético llamado *Zygomycota,* dichos hongos fueron considerados como un linaje primitivo del reino *Fungi* (Tanabe et al., 2005). Esto por la carencia de estructuras fructíferas complejas y la mayoría de los representantes tienen hifas cenocíticas (sin septos) durante todo o parte de su ciclo de vida. Sin embargo, los resultados obtenidos por análisis filogenéticos no mostraron que el *Phylum* fuera monofilético, en su lugar se propuso la existencia de dos Phyla *Zoopagomycota* y *Mucoromycota* (Spatafora et al., 2016).

El *Phylum Zoopagomycota* contiene a las subdivisiones Entomophtoromycotina, Kickxellomycotina y Zoopagomycotina, y constituye el linaje más primitivo de los anteriormente llamados zigomicetos y contiene especies que son primariamente parásitos y patógenos de animales pequeños, y de otros hongos (Davis et al., 2019). Taxonómicamente el *Phylum Mucoromycota* alberga a las subdivisiones Glomeromycotina, Mortierellomycotina, y Mucoromycotina (Spatafora et al., 2016); y principalmente consiste en hongos endófitos de raíces, descomponedores de material vegetal e importantemente algunos géneros pueden ser patógenos oportunistas en humanos, como es el caso de los géneros *Rhizopus*, *Lichteimia , Mucor, Cunninghamella*, *Rhizomucor, Apophysomyces* y *Saksenaea* (Ertugrul y Ariakn-Akdagli, 2014).

A su vez, la subdivisión Mucoromycotina contiene a los órdenes *Endogonales, Umbelopsidales* y *Mucorales* (White et al., 2006). Del orden *Mucorales* se encuentran géneros como *Mucor, Phycomyces, Rhizopus y Rhizomucor.* Por pertenecer a un linaje basal, los hongos mucorales han sido utilizados como modelo de estudio para estudiar la evolución fúngica (Ma et al., 2009, Corrochano

et al., 2016). Existen mucorales dimórficos como es el caso de *Rhizopus oryzae* (Karmakar et al., 2012) y *Mucor circinelloides* o monomórficos filamentosos como es el caso de *Phycomyces blakesleeanus* (Cerdá-Olmedo, 2001). Los mucorales tienen importancia industrial, tal es el caso de *Rhizopus oryzae* y *R. microsporus* empleados en la fermentación de muchos alimentos de la comida asiática como el tempeh, el cual se obtiene a partir de la soya (Nout y Rombouts, 1990; Hartanti et al., 2015). *R. oryzae* también es productor de ácidos orgánicos, etanol (Thongchul et al., 2010, Meussen et al., 2012) y enzimas hidrolíticas (Takahashi et al., 1978, De Souza et al., 2019). No obstante varios mucorales son patógenos para humanos y causan la infección conocida como mucormicosis (Battaglia et al., 2011).

1.1.3 Mucormicosis

Existen aproximadamente 1.5 millones de especies diferentes de hongos en la tierra, pero solamente se conocen unas 300 que pueden causar enfermedades en humanos (Garcia-Solache y Casadevall, 2011; Hawksworth, 2001). Esto debido a que las especies fúngicas patógenas de humanos deben satisfacer cuatro condiciones básicas: tolerancia a crecer e temperaturas altas, habilidad para invadir al huésped humano, capacidad de lisar y absorber el tejido humano y resistencia del sistema inmune humano (Köhler et al., 2015).

La mucormicosis es una infección fúngica emergente causada por los mucorales pertenecientes a los géneros: *Rhizopus*, *Lichteimia* (anteriormente conocido como *Absidia), Mucor, Cunninghamella*, *Rhizomucor, Apophysomyces* y *Saksenaea* (Ertugrul y Ariakn-Akdagli, 2014). Siendo los géneros más comunes causantes de esta infección son *Rhizopus* (73%) y *Mucor* (13%) (Almyroudis et al.,2006).

La inmunosupresión es un factor de predisposición para la mucormicosis, con la infección generalmente limitada a pacientes con afecciones hematológicas, transplantes de células madre hematopoyéticas, transplantes de órganos sólidos y diabetes (Hammond et al., 2011; Rammaert et al., 2012). La mucormicosis es la

tercer micosis más frecuente en orden de importancia después de la candidiasis y aspegillosis en pacientes con transplantes de células madre hematológicas y alogénicas. Basados en la localización anatómica, la mucormicosis puede clasificarse en una de las seis formas: (a) rinocerebral, (b) pulmonar, (c) cutánea, (d) gastrointestinal, (e) diseminada y (f) otras presentaciones poco comunes. Dichas condiciones además de la rapidez del diagnóstico pueden determinar el pronóstico final de la enfermedad (Petrikkos et al., 2012). La forma rinocerebral es la más frecuente y suele asociarse a pacientes diabéticos descompensados o con enfermedades hematológicas (Zaballos et al., 2003). Se ha reportado recientemente un aumento alarmante en la incidencia mundial de la mucormicosis (Prakash y Chakrabarti, 2019).

Esta infección, cuando es invasiva está asociada a altos niveles de mortalidad. En este sentido, se ha reportado que la tasa de mortalidad de la mucormicosis en pacientes que recibieron transplante de órganos sólidos oscila entre un 49% y un 71% (Aslani et al., 2007; Almyroudis et al., 2006). En años recientes se han logrado avances sustanciales en el tratamiento de la infección fúngica mucormicosis. Diversos reportes indican la importancia de la excisión quirúrgica de tejido necrótico o infectado, siempre y cuando sea factible. Basado en su seguridad y eficacia, las formulaciones lípidicas de amforeticina B son el tratamiento estándar para atender la mucormicosis (Spellberg e Ibrahim, 2010). Además, se ha demostrado que el uso de un quelante de hierro denominado deferasirox mejora el pronóstico en modelos animales que padecieron mucormicosis (Spellberg et al., 2012).

1.2 Mucor circinelloides

1.2.1 Generalidades

M. circinelloides es un mucoral dimórfico (Lübbehüsen et al., 2003). Es un modelo de estudio en la regulación de la diferenciación celular ylas respuestas celulares a la luz (Murcia-Flores et al., 2007). Adicionalmente, ha sido estudiado dado que es

un patógeno emergente en pacientes inmunodeprimidos (Bastidas et al., 2012), se le ha asociado también a la contaminación de frutos como el noni (Nishijima et al., 2011) y alimentos fermentados como el yogurt (Snyder et al., 2016); además recientemente se le considera como una fuente de ácidos grasos para la obtención de fuentes de energía renovables como el biodiesel (Zininga et al., 2019). Su metabolismo fermentativo ha sido investigado a la par de la obtención de etanol, además de que se ha evaluado el rendimiento de esta producción modificando condiciones de crecimiento (Wikandari et al., 2012). En este sentido, a fin de explicar la asociación entre los metabolismos fermentativo y oxidativo, en nuestro grupo de trabajo, realizamos la caracterización del gen *adh1* el cual codifica para un alcohol deshidrogenasa. Nuestros hallazgos indicaron que el producto de dicho gen regula el efecto Crabtree y puede actuar ya sea como una enzima fermentativa u oxidativa, dependiendo de las condiciones nutricionales (Rangel-Porras et al., 2019).

Uno de los eventos diferenciativo más estudiados en *M. circinelloides* es el dimorfismo (Lübbehüsen et al., 2003, Valle-Maldonado et al., 2015b). No obstante *M. circinelloides* presenta otros eventos diferenciativos, como la síntesis de carotenos, inducida por la presencia de luz (Murcia-Flores et al., 2007, Zhang et al., 2016), generando crecimiento radial que presenta tonalidad amarillenta a diferencia de colonias crecidas en ausencia de luz que son albinas. Adicionalmente el desarrollo de estructuras reproductivas y la esporulación también son regulados positivamente por la presencia de luz.

M. circinelloides ha sido empleado como huésped heterólogo para la producción de enzimas relevantes de carácter industrial. Se ha evaluado, el efecto del dimorfismo en el proceso de producción y actividad enzimática de glucosa oxidasa. Se reportó una mayor producción de esta enzima durante la morfología levaduriforme (Bredenkamp et al., 2010). A su vez, se han generado cepas que acumulan licopeno de manera exacerbada, lo cual podría ser una alternativa para la producción industrial de licopeno (Zhang et al., 2017).

El genoma de este organismo ha sido secuenciado (Corrochano et al., 2016) y está disponible en la red (http://genome.jgi-psf.org/Mucci2/Mucci2.home.html). El material genómico de este organismo está distribuido en 9 cromosomas tratándose de 11,719 genes en 36.6 millones pares de bases (Mb) (http://www.ncbi.nlm.nih.gov/genome/2804). Durante la última década, el desarrollo de herramientas moleculares, ha permitido la manipulación del genoma de este hongo (Gutiérrez, et al., 2011; Vellanki et al., 2018). En nuestro grupo de trabajo hemos validado al gen *tfc-1*, como un gen normalizador para ensayos de RT-qPCR durante el dimorfismo de este mucoral (Valle-Maldonado et al., 2015a). Este gen codifica para una subunidad del factor de transcripción TFIIIC, el cual a su vez forma parte de ensamblaje del complejo de preiniciación de la RNA polimerasa III.

1.2.2 Transiciones morfológicas en *M. circinelloides*

La estructura de dispersión y resiliencia a las condiciones adversas en el género *Mucor* es la espora. Existiendo tres tipos de ellas: 1) zigosporas productos de la recombinación genética en la reproducción sexual, y dos tipos de esporas generadas asexualmente: 2) las esporangiosporas que pueden servir como mecanismo de dispersión y se generan a partir de una estructura diferenciada llamada esporangio y 3) las artrosporas aseguran la supervivencia bajo condiciones de crecimiento adversas y se producen al diferenciarse crecimientos maduros de micelio que se diferencian hacia cadenas de artrosporas (Orlowski, 1991). La reproducción sexual sucede cuando hay fusión de hifas de origen homotálico o heterotálico y conduce finalmente a la formación de zigosporas.

La zigospora es una morfología resiliente que permanece en reposo durante periodos prolongados de tiempo, semanas o meses. El detectarse señales ambientales favorables se produce la germinación y se genera una estructura alargada conocida como esporangioforo, el cual presenta un cuerpo esférico en la punta conocida como esporangio del cual se almacenan y se desprenden las esporangiosporas. Las esporangiosporas tienen forma elipsoidal y aunque son derivadas exclusivamente del hábitat miceliar del género *Mucor,* éstras son

capaces de desarrollar la morfología levaduriforme o miceliar dependiendo de la disponibilidad de oxígeno y la fuente de carbono (Lübbehüsen et al., 2003). Si las esporangiosporas se encuentra en anaerobiosis se favorece el crecimiento isotrópico (levadura), mientras que en condiciones aeróbicas el crecimiento de *M. circinelloides* es polarizado (filamentos). Además del ambiente gaseoso, el crecimiento levaduriforme en el caso de *M. rouxii* requiere que una fuente de carbono fermentable (Bartnicki-Garcia, 1968).

Los crecimientos polarizados e isotrópico de *M. circinelloides* no son terminales y puede haber transiciones de levadura a micelio o de micelio a levadura, esto al modificar las condiciones de crecimiento (McIntyre et al., 2002). Las hifas multinucleadas del género *Mucor* son cenocíticas, al no presentar septos (divisiones). Adicionalmente, las levaduras son esféricas y multinucleadas (Ocampo et al., 2012).

La artrospora es la estructura menos estudiada y entendida del género *Mucor*, sin embargo su funcionalidad ha sido propuesta como un mecanismo de supervivencia ya que se forma al fin del crecimiento exponencial o bajo condiciones nutricionales desfavorables (Orlowski, 1991; Lübbehüsen et al., 2003).

1.2.3 Genes involucrados en la regulación de la diferenciación morfológica y virulencia en *M. circinelloides*

La calcineurina es una fosfatasa específica de serina-treonina, la cual es activada por el complejo Ca^{2+}-calmodulina. Esta enzima está compuesta por dos subnidades: la subunidad catalítica A, la cual tiene la actividad de fosfatasa y la subunidad regulatoria B, la cual une al calcio y a la subunidad A; la unión del calcio activa el complejo enzimático, permitiendo la disociación de ambas subunidades. En *M. circinelloides* fueron identificados tres genes que codifican para subunidades catalíticas (CnaA-CnaC) y un solo gen homólogo de la subunidad regulatoria (CnbR) (Lee et al., 2013). Es de resaltar que la via de la calcineurina controla la morfogenésis y la virulencia en este mucoral. La

interrupción del gen *cnbR* que codifica para la subunidad regulatoria de la calcinerurina condujo a un crecimiento monofórmico levaduriforme a pesar de la presencia de condiciones aeróbicas tanto en medio sólido como en líquido; esta mutante es avirulenta en contra de *Galleria mellonella* a diferencia de la cepa silvestre (Lee et al., 2013). Adicionalmente, cuando se interrumpió el gen *cnaA,* el cual codifica para una de las subunidades catalíticas de la calcineurina en este hongo, el fenotipo mostró un tamaño de la esporangiospora y virulencia significativamente mayores en relación con la cepa silvestre (Lee et al., 2013). De manera similar en nuestro grupo de trabajo hemos reportado que los productos de los genes *gpa11* y *gpa12*, los cuales codifican para subunidades alfa de proteínas G heterotriméricas regulan el tamaño de la esporangiospora en este mucoral (Patiño-Medina et al., 2019). En este mismo trabajo se reportó que los resultados de medición de mRNA sugieren una relación genética y funcional entre los genes *gpa11* y *gpa12* con la ruta de la calcineurina *en M. circinelloides* (Patiño-Medina et al., 2019a). Recientemente se ha reportado la caracterización funcional de un gen llamado *bycA* el cual codifica para una permeasa de aminoácidos. Este gen fue asociado con la calcineurina, esto debido ya que la cepa doble mutante Δ*cnbR*Δ*bycA es* capaz de crecer filamentosamente en medio sólido suprimiendo el fenotipo de la cepa Δ*cnbR* la cual solo puede generar crecimiento levadurifome (Vellanki et al., 2020).

En nuestro grupo de trabajo, hemos reportado que la interrupción del gen *adh1* (cepa M5)*,* el cual codifica para una alcohol deshidrogenasa, durante condiciones anaeróbicas genera células hinchadas siendo incapaz de generar levaduras, a diferencia de la cepa silvestre (Rangel-Porras et al., 2019). Adicionalmente, en un trabajo posterior reportamos que la cepa M5 exhibió mayor virulencia que la cepa silvestre R7B en contra del modelo murino (Díaz-Pérez et al., 2020). El sobrenadante libre de células de la cepa M5 contenía concentraciones más altas de acetaldehído, lo que en parte explica el efecto tóxico exarcerbado en comparación con la cepa silvestre (Díaz-Pérez et al., 2020). Además, hemos validado la acumulación del transcrito mediante RT-qPCR de este gen como un

marcador de crecimiento levaduriforme en este hongo (Valle-Maldonado et al., 2015a).

Adicionalmente, en nuestro laboratorio hemos caracterizado funcionalmente a los cuatro genes (*arf1*-*arf*4) que codifican para proteínas G monoméricas de la familia Arf (ADP-ribosylation-factor) en este hongo (Patiño-Medina et al., 2018). Los productos de dichos genes participan en la regulación del transporte vesicular. La interrupción del gen *arf2* provoca una reducción siginificativa (80%) en la formación de levaduras comparado con la cepa silvestre (Patiño-Medina et al., 2018). Por otro lado, la interrupción del gen *arf1* condujo a una reducción en la cantidad y longitud de hifas durante el crecimiento aeróbico en relación a la cepa silvestre (Patiño-Medina et al., 2018). Además, la totalidad de las cuatro mutantes sencillas de los genes *arf1-4* mostraron mayor virulencia en contra de los modelos de ratón y nematodo en comparación con la cepa silvestre (Patiño-Medina et al., 2018).

Es importante mencionar que además de los genes *arf1-4*, el genoma de *M. circinelloides,* contiene al menos dos genes que codifican para proteínas Arl (Arf-like), *arl1*-*arl2* (Patiño-Medina et al., 2019b). La incapacidad de generar una mutante Δ*arl1* homocarionte sugiere que es esencial para el crecimiento de este mucoral. Además, la cepa Δ*arl1*$^{(+)(-)}$ mostró una reducción en la cantidad y longitud de hifas durante el crecimiento aeróbico en relación a la cepa silvestre (Patiño-Medina et al., 2019b). Adicionalmente, se demostró que ambos genes *arl1* y *arl2* participan en el tráfico vesicular al localizar adecuadamente a los endosomas en la hifa. La mutante heterocarionte Δ*arl1*$^{(+)(-)}$ secretó al medio de cultivo componentes de naturaleza proteica que presentan un efecto tóxico en contra del modelo de nematado en comparación con la cepa silvestre (Patiño-Medina et al., 2019b). Cabe mencionar que también en nuestro grupo de trabajo recientemente comprobamos que los productos de los genes *arl1* y *arl2* están involucrados positivamente en la formación de mitocondrias en este mucoral, controlando el metabolismo oxidativo (Patiño-Medina et al., 2020).

Además de lo anterior, se ha asociado a la ruta cAMP-PKA en la regulación del dimorfismo de *M. circinelloides*. La PKA consiste en dos subunidades regulatorias (PKAR) que se unen e inhiben la actividad de dos subunidades catalíticas (PKAC). La unión del AMPc a las cadenas PKAR resulta en la liberación de las subunidades PKAC y se desencadena la cascada de fosforilación de sustratos proteicos específicos en residuos de serina y treonina que resulta en cambios en la morfogénesis y en el dimorfismo. El gen que codifica para la subunidad regulatoria PkaR1 fue sobreexpresado y dicha cepa mutante presentó un fenotipo de hiperramificación en crecimiento en medio sólido (Wolff et al., 2002). Posteriormente, se reportó que la interrupción del gen *pkaR1* condujo a la disminución de la longitud de la hifa durante la transición morfológica levadura-micelio (Ocampo et al., 2009). Cabe mencionar que el gen que codifica para la isoforma *pkaR4*, es esencial, ya que su interrupción generó células heterocariontes, y esta mutante muestra un defecto en la emisión del tubo germinativo (Ocampo et al., 2012). Adicionalmente, la participación de PKA en el crecimiento polarizado en *Mucor* ha sido evidenciada usando análogos de AMPc como N^6-monobutiril-AMPc, N^6-benzoil-AMPc (Sorol et al., 2000). Estos análogos estructurales imitan la actividad del AMPc y el fenotipo resultante es crecimiento levaduriforme en condiciones aérobicas. La regulación en el dimorfismo conferida por el AMPc es muy relevante , ya que la remoción de los análogos del AMPc provocó una inmediata transición morfológica de crecimiento isotrópico a filamentoso (Wolff et al., 2002; Ocampo et al., 2009).

Es importante mecionar que se ha reportado que los niveles de AMPc y la actividad de PKA están incrementados en el crecimiento levaduriforme durante el dimorfismo en *M. circinelloides* en comparación con el crecimiento filamentoso (Lee et al., 2013, Vellanki et al., 2020).

1.3 Proteínas G en la transducción de señales

La supervivencia requiere que los organismos seamos capaces de responder efectivamente a los estímulos ambientales. La adaptabilidad es una capacidad

clásica y característica de los seres vivos, y consiste en la habilidad de un organismo o de una parte del mismo para identificar un cambio negativo o positivo en el medio ambiente y poder reaccionar a éste.

La regulación genético-molecular de la percepción y respuesta a estimulos en los seres vivos implica un proceso complejo llamado transducción de señales. El cual consiste en la transferencia de información desde un ambiente externo hacia el interior de la célula. Este sistema está compuesto por un elemento sensor o "receptor" para detectar la señal, un componente "amplificador", que aumenta la intensidad de la señal intracelularmente regulando los niveles de segundos mensajeros y un elemento "transductor" que realiza la labor de convertir la señal detectada por el receptor a una forma que pueda ser entendida y convertida a respuesta por el amplificador. Existen ciertas señales que por su naturaleza química pueden ingresar a la célula (aquellas moléculas lipofílicas, como las vitaminas A y D y la hormona tiroidea) y pueden atravesar la membrana celular hacia el interior de la célula donde pueden tener un efecto biológico afectando la expresión a nivel transcripcional o traduccional (Brivanlou y Darnell, 2002). La diversidad de los estímulos externos es muy amplia, e incluye señales acústicas, cambios de temperatura, nutrientes, luz, hormonas, entre otros factores (Krauss, 2003).

1.3.1 Receptores involucrados en transducción de señales

El primer componente partipante en un sistema transducción de señales en eucariotas son los receptores. Dichos elementos que reconocen señales de diversos tipos, entre los cuales destacan:

-Receptores intracelulares. Se hallan localizados intracelularmente y cuando se presenta la unión de ligando migran hacia el núcleo, donde el complejo ligando-receptor directamente regula la transcripción génica. Dado que la localización de esta clase de receptores es intracelular y actúan directamente en el núcleo como factores de transcripción, comúnmente se les ha llamado receptores nucleares. Dentro de los receptores de esta clase se encuentran la gran familia de receptores

de esteroides, como el estrógeno y la progesterona, y otras sustancias solubles en lípidos como el ácido retinoico y hormona tiroidea (Sever y Glass, 2013). Adicionalmente, los receptores de esta clase presentan un motivo de unión a ligando, además de un dominio de unión a DNA y de un dominio activador transcripcional (Huang et al., 2010). En hongos se ha descrito en el ascomiceto *S. cerevisiae*, la enzima PDR1 reconoce al antifúngico cicloheximida lo que provoca la activación de una vía que confiere resistencia a este fármaco. Dicho mecanismo implica la regulación de la expresión de genes que codifican para transportadores de fármacos, como es el caso de PDR5 el cual es un transportador pleiotrofico dependiente de ATP (Naar y Thakur, 2009; Balzi et al., 1994; Gao et al., 2004.).

-Receptores que presentan actividad enzimática intrínseca. Dentro de este tipo de receptores se encuentran aquellos que tienen actividad catalítica de tirosin-cinasa (por ejemplo el receptor de la insulina, receptores del factor de crecimiento derivado de plaquetas, factor de crecimiento de fibrobastos , o del factor de crecimiento epidermal). También incluyen a los receptores con actividad enzimática de serin-treonina cinasas (por ejemplo los receptores de activina y factor de crecimiento transformante-β). Otro tipo de receptores incluirían a las tirosin-fosfatasas (por ejemplo la proteína CD45 de células T y macrófagos) (Koretzky et al., 1990), y finalmente los receptores con acitividad de guanilato ciclasas (por ejemplo los receptores de péptido natriurético). Un ejemplo de receptores con actividad enzimática intrínseca en hongos incluye a la rodopsina-guanilato ciclasa en el hongo acuático *Blastocladiella emersonii* la cual como respuesta a la luz modula la formación de GMPc (Scheib et al., 2015).

-Receptores acoplados a proteínas G. Este tipo de receptores se denominan GPCRs (por sus siglas en inglés, G-Protein Coupled Receptors). Se tratan de receptores de siete pasos transmembranales que se encuentran conformados por tres asas intracelulares y tres asas extracelulares, contando con un extremo amino extracelular y con un extremo carboxilo intracelular. Se trata de un grupo muy numeroso de receptores, que en humanos representa el grupo más amplio de

receptores membranales. El genoma humano codifica al menos 791 GPCRs. Y representan el 30-40 % de los blancos moleculares de todos los fármacos modernos (Wacker et al., 2017).

Dentro de este tipo de receptores se encuentran: los receptores olfatorios, los receptores adrenérgicos y algunos receptores de hormonas: angiotensina, glucagón, bradiquinina y vasopresina (Huang y Tesmer, 2011). Estos receptores se encuentran presentes en todos los eucariontes, desde hongos hasta mamíferos. Un ejemplo de este tipo de receptores en ascomicetos es el receptor para detectar feromonas denominado PRE-2 en *Neurospora crassa* (Cabrera et al., 2015). Es importante mencionar que los receptores acoplados a proteínas G, transmiten la detección de la señal a las proteínas G heterotriméricas.

1.3.2 Proteínas G

Dentro de los componentes transductores de señales se encuentran las proteínas G, reciben su nombre porque unen e hidrolizan nucleótidos de guanina (McCudden et al., 2005). Se trata de componentes muy importantes en la transducción de señales, una muestra de la importancia del aporte al conocimiento de estas proteínas es que los investigadores Alfred Gilman y Martin Rodbell ganaron el premio Nobel de Medicina en 1994 por su descubrimiento. Las proteínas G incluyen dos familias generales: monoméricas y heterotriméricas ambas involucradas en diversas funciones celulares.

Dentro de las proteínas G monoméricas existen las familias Ras*,* Rho, Ran, Rab y Arf (Takai et al., 2001). Ha sido demostrada la participación de la familia Ras en procesos de oncogénesis (Repasky et al., 2004), la familia Rho ha sido involucrada en la regulación de la organización de actina, del ciclo celular y de la expresión celular (Etienne-Manneville y Hall, 2002). Por su parte, lafamilia Ran participa en el transporte nucleocitoplásmico de RNA y proteínas (Weis, 2003). A su vez, la familia Rab cumple la funcion de regular el transporte vesicular y el

tráfico de proteínas entre diferentes organelos de las rutas endocíticas y exocíticas (Zerial y McBride, 2001). Finalmente, la familia Arf está involucrada en la regulación del tráfico vesicular (Nielsen et al., 2008, Patiño-Medina et al., 2018).

La otra gran familia de las proteínas G está compuesta por las proteínas G heterotriméricas.

1.3.2.1 Proteínas G heterotriméricas en hongos

Las proteínas G heterotriméricas (PGH) sirven a modo de intermediario entre el receptor localizado en la membrana plasmática y los efectores intracelulares, se tratan del componente transductor de señales. Estructuralmente están compuestas de tres proteínas distintas: una subunidad Gα, una subunidad Gβ y una subunidad Gγ (McCudden et al., 2005).

La subunidad Gα une el nucleótido GDP o GTP, determinando el estado de inactivación o activación del complejo, respectivamente. La subunidad Gα muestra homología con las subunidades G pequeñas, debido a que ambas tienen actividad de GTPasa y comparten los dominios, llamadas caja G (G1-G5) que cumplen dichas funciones (Sprang 1997). Sin embargo las diferencias con las proteínas G monoméricas consisteen que la subunidad Gα es más grande, por lo regular entre (35-45 kDa) en comparación con las subunidades G pequeñas (20-25 kDa). Además, por lo general las subunidades Gα presentan un motivo caracaterístico susceptible a miristoilación (MGXXXS) en el extremo amino terminal de la proteína (Buss et al., 1987), y otro motivo susceptible a ADP-ribosilación por la tóxina del cólera (RSRVK) en la caja G2 (Van Dop et al., 1984), Además, las subunidades Gα presentan otro motivo susceptible a ADP-ribosilación por la tóxina pertussis (CAAX) en el extremo carboxilo terminal (West et al., 1985). Finalmente, las proteínas G monoméricas carecen de los residuos necesarios para la interacción con la subunidad Gβ que estan presentes en las subunidades Gα (Takai et al., 2001).

Los análisis evolutivos de las subunidades Gα fúngicas indicaron que estas subunidades tienen una distribución en cuatro grupos (I-IV), esta clasificación fue derivada de la funcionalidad de las subunidades Gα de mamífero (Bölker, 1998).

El grupo I fue relacionado con las subunidades $G\alpha_i$ las cuales inhiben la actividad de la adelinato ciclasa. Por su parte, el grupo III fue asociado con las subunidades Gαs que estimulan la actividad de la adelinato ciclasa. Mientras que los grupos II y IV no han sido relacionados a subunidades de mamíferos (Bölker, 1998; Li et al., 2007).

Las subunidades Gβ presentan característicamente siete motivos dipéptido WD y un residuo W^{105} indispensable para la interacción con la subunidad Gα (Whiteway et al., 1994). La cristalización de subunidades Gβ ha descrito su estructura terciaria como un propulsor de siete laminas β circularizado con una hélice α en el extremo amino terminal (Wall et al., 1995). Por su parte las subunidades Gγ, presentan característicamente el motivo CaaX, siendo “a” un residuo alifático, en el extremo carboxilo terminal susceptible a farnesilación o geranilación necesario para la interacción con las membranas (Mulligan y Farber 2011). Las subunidades Gγ presentan los residuos L^{16} y N^{20} necesarios para la interacción con la subunidad Gβ. Referentemente, a su estructura terciaria, ésta ha sido descrita como dos hélices α unidas por un asa (Wall et al., 1995). En cuanto a las subunidades Gβ y Gγ, éstas forman un dímero muy estable que en condiciones fisiológicas no se disocia (Schwindinger y Robishaw, 2001).

1.3.2.2 Proteínas G heterotriméricas en *M. circinelloides*

Con anterioridad, se realizó la identificación de cuatro subunidades Gα en el *M. circinelloides* (Meza-Carmen et al., 2006). Posteriormente en nuestro grupo de trabajo reportamos que *Mucor circinelloides* presenta el repertorio más grande de proteínas G heterotriméricas en el Reino *Fungi,* con doce subunidades Gα, tres subunidades Gβ y tres subunidades Gγ (Valle-Maldonado et al., 2015b). En ese mismo manuscrito, al analizar filogenéticamente las secuencias Gβ y Gγ fúngicas propusimos una clasificación para estas subunidades por primera vez y también la

existencia de un posible evento de coevolución debido a la distribución en cuatro grupos (I-IV) para ambos tipos de subunidades, dependiendo de los Phyla fúngicos. En los grupos I están ascomicetos filamentosos, en los grupos II están basidiomicetos, en los grupos III se encuentran los mucorales, y en el grupo IV están ascomicetos levaduriformes y dimórificos (Valle-Maldonado et al., 2015b).

El mecanismo canónico de estucturación del heterotrímero de PGH implica dos posibles conformaciones:

-Heterotrímero asociado inactivo. Esta es la conformación cuaternaria que tiene el heterotrímero cuando la subunidad Gα está asociada a las subunidades Gβ y Gγ, las cuales están adyacentes entre sí. La subunidad Gα tiene unido GDP en esta conformación. Importantemente, el heterotrímero está anclado en la membrana plasmática mediante las subunidades Gα, y Gγ. Éstas subunidades puede ser susceptibles para presentar modificaciones postraduccionales (miristoilación para Gα y farnesilación o geranil-geranilación para Gγ) que favorecen la interacción con la membrana celular. La subunidad Gα además tiene contacto con el receptor, funcionalmente este heterotrímero se encuentra inactivo (Tesmer, 2010).

-Heterotrimero disociado activado. Al percibirse una señal extracelular por medio del receptor, se promueve el intercambio del GDP por GTP en la subunidad Gα. Lo anterior implica un cambio conformacional de la subunidad Gα, que altera la interacción con el dímero Gβγ, lo que a su vez produce una disociación del trímero. A continuación, las unidades de señalización, correspondientes a la subunidad Gα-GTP y el dímero Gβγ, se encuentran separadas, a esta conformación se le conoce como activa. A su vez, cada una de éstas unidades de señalización son capaces de interactuar con distintos efectores generando específicamente diversas respuestas fisiológicas (Tesmer, 2010).

Los complejos de señalizacion de las proteínas G heterotriméricas activados transmiten la señal a proteínas efectoras que tienen actividad enzimática, entre los cuales están las fosfodiesterasas específicas de GMPc (Artemeyev et al., 1992), la

adelinato ciclasa (Levitzki y Bar-Sinai, 1991), las fosfolipasas (Smrcka et al., 2012) o canales iónicos como: canales de K^+, Ca^{2+} o Cl^- (Zhang, 2011, Zhang et al., 2011).

La activación de estas proteínas efectoras puede conducir a cambios en la concentración intracelular de compuestos químicos conocidos como segundos mensajeros, como el GMPc, AMPc, diacilglicerol o inositol trifosfato, Ca^{2+}, entre otras, los cuales funcionalmente desencadenan reacciones fisiológicas específicas (Neer, 1994).

1.3.2.3 Regulación de la actividad de las proteínas G

El grado de actividad de las proteínas G es regulado por las tasas de intercambio de GDP por GTP en la subunidad Gα y a su vez por la velocidad de hidrólisis del GTP a GDP. El primer proceso es catalizado por enzimas llamadas factores de intercambio de nucleótidos de guanina (GEF, por sus siglas en inglés, Guanine Exchange Factors). Así mismo, se ha propuesto que los mismos receptores GPCRs pueden tener actividad GEF (Kahn, 2014), esto cuando ocurre la unión del ligando y la activación correspondiente del receptor.

Sin embargo, se ha reportado la existencia de proteinas tipo GEF que no son receptores GPCR. Tal es el caso de RIC8 en el ascomiceto *Neurospora crassa*. Mutantes carentes de este gen, muestran una disminución drástica de los niveles de proteína de las subunidades GNA1-3 (Gα) y GNB-1 (Gβ) y de la adenilato ciclasa CR-1 en comparación con la cepa silvestre. De igual manera, en la mutante carente de RIC8 se reportaron afectaciones fenotípicas asociadas con bajos niveles de AMPc como fueron una disminución en el crecimiento vegetativo, desarrollo sexual y asexual (Wright et al., 2011).

La hidrólisis del GTP unido a las subunidades Gα de las proteínas G se regula por una familia de proteínas denominadas proteínas activadoras de GTPasa (GAP, por sus siglas en inglés, GTPase-Activating Protein). Un ejemplo de lo anterior en un modelo fúngico es el caso de la enzima Sst2 de *S. cerevisiae* la cual se une a la forma activa (Gα-GTP) de Gpa1p, la cual es una subunidad Gα, dicha unión

regula negativamente la señalización al favorecer la inactivación de la subunidad Gα (Gα-GDP) (Dohlman et al., 1996). Con lo anterior, se demuestra la importancia funcional de las proteínas GEFs y GAPs las cuales son reguladoras de la señalización por proteínas G y se denominan por sus siglas en inglés RGSs .

1.3.2.4 Mecanismos no canónicos de asociación de las proteínas G heterotriméricas en hongos

Se ha reportado recientemente que las proteínas G heterotriméricas pueden realizar funciones no canónicas, debido a la interacción con nuevos efectores, activación independientemente de receptores y la localización celular diferente a la membrana plasmática.

La detección de glucosa en la levadura *Saccharomyces cerevisiae* es un mecanismo no canónico de actividad de las PGH, Esto porque se ha demostrado la participación del receptor Gpr1 y la subunidad Gα, Gpa2p, mientras que no ha sido comprobada la participación de las subunidades Ste4p (Gβ) ni Ste18p (Gγ) presentes en este organismo. La evidencia disponible hasta el momento mostró que la subunidad Gpa2p (Gα) en estas condiciones funciona sin la participación de las subunidades Gβ ni Gγ. Además, se ha demostrado que las subunidades Gpa2p y Ste4p no interactúan entre sí lo cual refuerza la teoría de que no forman un parte de un heterotrímero (Versele et al., 2001).

En este mismo organismo se ha comprobado de igual manera, que las subunidades Gα, Gβ y Gγ (Gpa2p, Ste4p y Ste18p, respectivamente) pudieran estar en una configuración activada a niveles normalmente vistos solo en presencia de ligando, de manera espontánea en ausencia de receptor, esto sucede cuando el gen que codifica para el componente Sst2, un elemento RGS (Siekhaus y Dubrin, 2005) es mutado. Se ha identificado la existencia de proteínas activadoras de señalización de proteínas G, independientes de receptor AGS (por sus siglas en inglés: receptor-independent activators of G-protein signaling). Estas proteínas son capaces de interactuar y activar a la subunidad Gα o al dímero Gβγ de manera específica (Blumer et al., 2005). Un ejemplo de lo anterior la proteína

AGS1, en mamíferos, incrementa el intercambio de GTP en la subunidades $G\alpha_i$ y $G\alpha_o$ actuando como un GEF, en la ausencia del receptor (Cismowski et al., 1999, Blumer y Lanier, 2014).

1.4 Función de subunidades Gβ fúngicas

La primera identificación de una subunidad Gβ (Ste4p) fúngica se reportó *S. cerevisiae* (Whiteway y col., 1989).

A partir de ese momento ha habido mucho interés en el estudio de estas subunidades Gβ fúngicas debido a que son subunidades homólogas a las de mamífero. Las subunidades Gβ fúngicas tienen porcentajes altos de identidad respecto a las de mamífero, un ejemplo es CPG-1 en *Cryphonectria parasitica* que tiene una identidad mayor al 65% en comparación a GNB1 de humano (Kasahara y Nuss, 1997).

Además, se ha demostrado el papel relevante de las subnidades Gβ fúngicas en la regulación de la morfología, reproducción y virulencia.

Hasta la fecha han sido caracterizadas funcionalmente 19 subunidades Gβ fúngicas (Tabla S3), todas ellas pertenecientes al subreino Dikarya, que incluye a los Phyla *Ascomycota* y *Basidiomycota*.

En el ascomiceto fitopátogeno *Fusarium verticilloides,* el producto del gen *gbb1,* el cual codifica para una subunidad Gβ*,* regula positivamente la síntesis de la micotóxina fumonisina B y la dirección del crecimiento polarizado en este hongo (Sagaram y Shim, 2007). En contraste, en *Monascus ruber*, la subunidad Gβ Mgb1 es un regulador negativo de la producción de la micotóxina citrinina (Li et al., 2014).

De manera similar en otro fitopatógeno filamentoso *C. parasitica,* la interrupción de *cpgb-1,* cuyo producto es una subunidad Gβ, condujo a una reducción significativa

de la pigmentación, reproducción asexual y de la capacidad virulenta en contra del tejido de *Castanea sativa* (Kasahara y Nuss, 1997).

La verticilosis es una infección fúngica frecuente en el tomate. Se reportó que la interrupción del gen que codifica para la subunidaf Gβ, *vgb*, en *Verticillium dahliae,* condujo a un fenotipo que mostró una reducción de la virulencia en contra de esta planta (Tzima et al., 2012).

El género *Magnaporthe* incluye hongos patógenos de arroz que producen la enfermedad denominada piriculariosis. Dicha infección produce las mayores pérdidas económicas ocasionadas por fitopatógenos. En *Magnaporthe grisea,* se comprobó que MGB1, una subunidad Gβ es un regulador positivo de la virulencia en conta de plantas de arroz (Nishimura et al., 2003).

Un aspecto importante que regulan positivamente las subunidades Gβ es la reproducción: KlSte4p en *Kluyveromyces lactis* (Navarro-Olmos et al., 2010), GPB1 en *Cryptococcus neoformans* (Wang et al., 2000), STE4 en *Candida albicans* (Dignard et al., 2008).

En nuestro grupo de trabajo, medimos los niveles de transcrito de los tres genes que codifican para subunidades Gβ (*gpb1*, *gpb2* y *gpb3*) durante el dimorfismo de *M. circinelloides* . Encontrando que el gen gpb1 presenta los mayores niveles de mRNA durante el crecimiento filamentoso (Valle-Maldonado et al., 2015b).

2. ANTECEDENTES

Las subunidades Gβ fúngicas son parte del heterotrímero que componen a las proteínas G heterotriméricas y son elementos importantes en la transducción de señales al regular el crecimiento, la reproducción y de la capacidad virulenta en estos organismos (Tzima et al., 2012). *Mucor circinelloides* es un patógeno oportunista en humanos y presenta el repertorio más grande de proteínas G heterotriméricas en el Reino *Fungi* (Valle-Maldonado et al., 2015b). Es un hongo dimórfico, que presenta mayor virulencia en su crecimiento filamentoso (Lee et al., 2013). Los niveles de transcrito del gen *gpb1*, el cual codifica para una subunidad Gβ son significativamente mayores en dicha morfología, respecto a los otros dos genes que codifican a subunidades Gβ, *gpb2* y *gpb3* presentes en este mucoral.

Los participantes moleculares en el crecimiento filamentoso y la regulación de la virulencia en *M. circinelloides* se conocen parcialmente.

3. JUSTIFICACIÓN

En hongos se ha descrito la participación de subunidades Gβ de proteínas G heterotriméricas en la regulación de la virulencia.

M. circinelloides es un hongo dimófirco el cual ha sido reportado como patógeno oportunista de humanos, siendo relevante en los años recientes debido al incremento en su incidencia. En este organismo, el gen que codifica para la subunidad Gpb1 de proteínas G heterotriméricas presenta el mayor nivel de transcrito en micelio, el cual es la morfología virulenta, respecto a los demás genes que codifican para proteínas G heterotriméricas. La evaluación funcional de la subunidad Gpb1 permitirá demostrar su participación en la virulencia de este organismo.

4. HIPÓTESIS

La subunidad Gpb1 de proteínas G heterotriméricas regula la ruta PKA y controla positivamente la virulencia del hongo *M. circinelloides* a través del desarrollo micelial.

5. OBJETIVOS

5.1 Objetivo General

Dilucidar la función de la subunidad Gpb1 de proteínas G heterotriméricas en la ruta PKA y en la virulencia de *M. circinelloides* asociada al desarrollo micelial.

5.2 Objetivos Particulares

A) Determinar la participación de la subunidad Gpb1 en el dimorfismo *de M. circinelloides*.

B) Evaluar la regulación de la virulencia de *M. circinelloides* por parte de la subunidad Gpb1.

C) Analizar la participación del producto del gen *gpb1* en la regulación del crecimiento micelial a través de la vía PKA.

6. METODOLOGÍA EXPERIMENTAL GENERAL

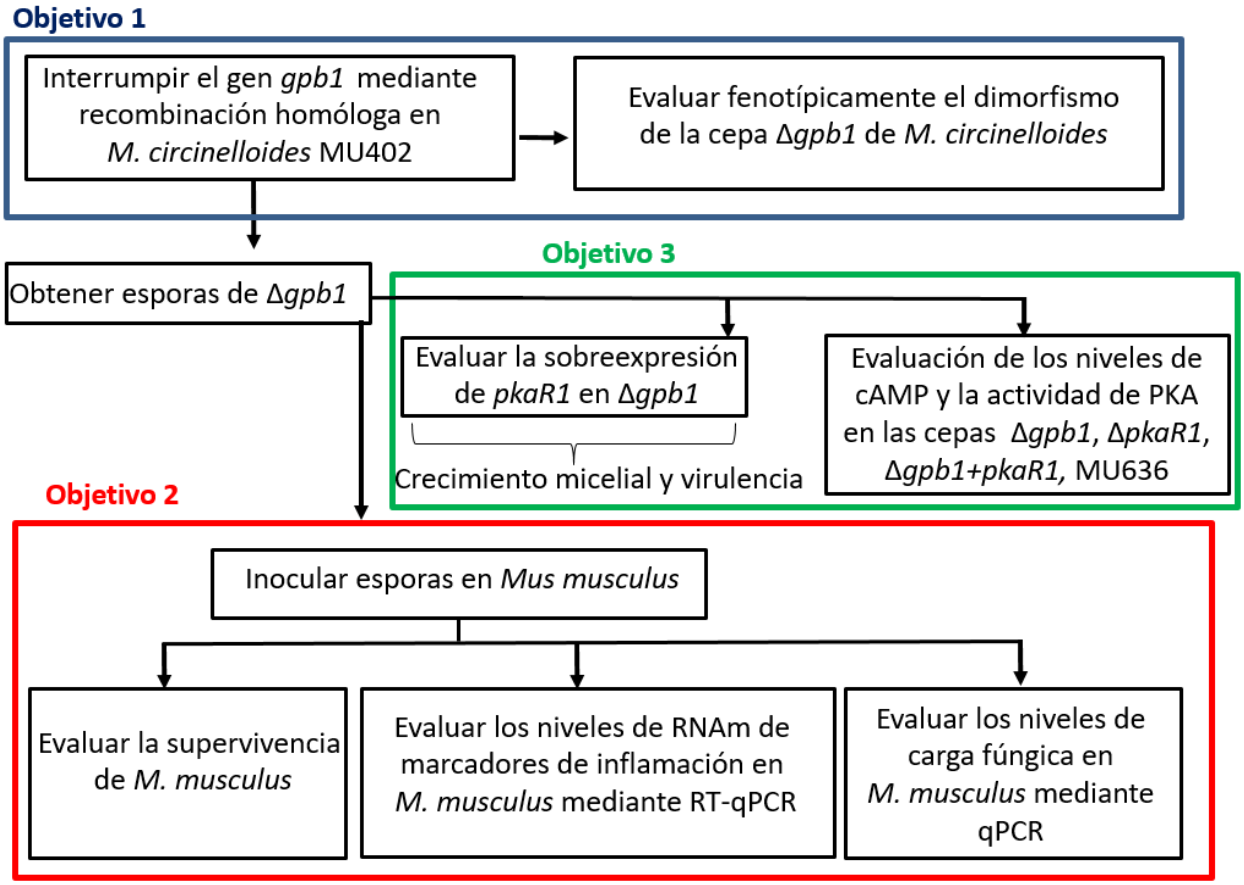

7. MATERIALES Y MÉTODOS

8. RESULTADOS

Las dos secciones (**7 MATERIALES Y MÉTODOS**, y **8 RESULTADOS**) de la presente tesis, se presentan siguiente en el manuscrito:

Valle-Maldonado, M.I., Patiño-Medina, J.A., Pérez-Arques, C., Reyes-Mares, N.Y., Jácome-Galarza, I.E., Ortíz-Alvarado, R., Vellanki, S., Ramírez-Díaz, M.I., Lee, S.C., Garre, V., Meza-Carmen V. 2020. The heterotrimeric G-protein beta subunit Gpb1 controls hyphal growth under low oxygen conditions through the protein kinase A pathway and is essential for virulence in the fungus *Mucor circinelloides*. *Cell Microbiol* 19: e13236

Received: 12 December 2019 | Revised: 24 May 2020 | Accepted: 9 June 2020
DOI: 10.1111/cmi.13236

RESEARCH ARTICLE

WILEY

The heterotrimeric G-protein beta subunit Gpb1 controls hyphal growth under low oxygen conditions through the protein kinase A pathway and is essential for virulence in the fungus *Mucor circinelloides*

Marco Iván Valle-Maldonado[1] | José Alberto Patiño-Medina[1] | Carlos Pérez-Arques[2] | Nancy Yadira Reyes-Mares[1] | Irvin Eduardo Jácome-Galarza[3] | Rafael Ortíz-Alvarado[4] | Sandeep Vellanki[5] | Martha Isela Ramírez-Díaz[1] | Soo Chan Lee[5] | Victoriano Garre[2] | Víctor Meza-Carmen[1]

[1]Instituto de Investigaciones Químico Biológicas, Universidad Michoacana de San Nicolás de Hidalgo, Ciudad Universitaria, Morelia, Mexico

[2]Departamento de Genética y Microbiología, Facultad de Biología, Universidad de Murcia, Murcia, Spain

[3]Laboratorio Estatal de Salud Pública del Estado de Michoacán, Morelia, Mexico

[4]Facultad de Quimico Farmacobiología, Universidad Michoacana de San Nicolás de Hidalgo, Morelia, Mexico

[5]South Texas Center for Emerging Infectious Diseases (STCEID), Department of Biology, The University of Texas at San Antonio, San Antonio, Texas

Correspondence
Víctor Meza-Carmen, Laboratorio de Diferenciación Celular, Instituto de Investigaciones Químico Biológicas, Universidad Michoacana de San Nicolás de Hidalgo, Ciudad Universitaria, 58030 Morelia, Michoacán, Mexico.
Email: victor_meza2004@yahoo.com.mx

Funding information
Consejo Nacional de Ciencia y Tecnología, Grant/Award Number: CB- 2011-01-167071; Coordinación de la Investigación Científica, Grant/Award Number: 2.36

Abstract

Mucor circinelloides, a dimorphic opportunistic pathogen, expresses three heterotrimeric G-protein beta subunits (Gpb1, Gpb2 and Gpb3). The Gpb1-encoding gene is up-regulated during mycelial growth compared with that in the spore or yeast stage. *gpb1* deletion mutation analysis revealed its relevance for an adequate development during the dimorphic transition and for hyphal growth under low oxygen concentrations. Infection assays in mice indicated a phenotype with considerably reduced virulence and tissue invasiveness in the deletion mutants (Δ*gpb1*) and decreased host inflammatory response. This finding could be attributed to the reduced filamentous growth in animal tissues compared with that of the wild-type strain. Mutation in a regulatory subunit of cAMP-dependent protein kinase A (PKA) subunit (PkaR1) resulted in similar phenotypes to Δ*gpb1*. The defects exhibited by the Δ*gpb1* strain were genetically suppressed by *pkaR1* overexpression, indicating that the PKA pathway is controlled by Gpb1 in *M. circinelloides*. Moreover, during growth under low oxygen levels, cAMP levels were much higher in the Δ*gpb1* than in the wild-type strain, but similar to those in the Δ*pkaR1* strain. These findings reveal that *M. circinelloides* possesses a signal transduction pathway through which the Gpb1 heterotrimeric G subunit and PkaR1 control mycelial growth in response to low oxygen levels.

KEYWORDS
cAMP, dimorphism, G proteins, hyphae, *Mucoral*, mucormycosis

1 | INTRODUCTION

Mucor circinelloides is a versatile fungus that displays several morphologies, including hyphae and yeast growth. The presence of a carbon source and availability of oxygen are the main factors that lead the spores to germinate as hyphae or yeast. Hyphae development requires oxygen independently of the carbon source; meanwhile the yeast growth requires an anaerobic atmosphere and fermentable

carbon source (De la Cruz et al., 2007; Lübbehüsen, Nielsen, & McIntyre, 2003; Orlowski, 1991). The ability to grow as either yeast or mycelia has allowed dimorphic species of *Mucor* to adapt to diverse biological environments, using fermentative or oxidative metabolism (Morin-Sardin, Nodet, Coton, & Jany, 2017; Orlowski, 1991).

Importantly, this fungus has been used as a model organism to elucidate the molecular mechanisms of the rare but lethal disease called mucormycosis (Baldin & Ibrahim, 2017; López-Fernández et al., 2018; López-Muñoz et al., 2018; Patiño-Medina et al., 2018). Certain strains of *M. circinelloides* also have the potential for use in biotechnological processes such as biodiesel production and the biocontrol of animal-parasitic nematodes (Khan et al., 2019; Morin-Sardin et al., 2017; Rodrigues Reis et al., 2019). Additionally, *M. circinelloides* is a model Mucorales fungus with robust tools for genetic manipulation (Nagy et al., 2017; Nicolás et al., 2018; Trieu et al., 2017; Vellanki et al., 2018). This fungus has been studied as a model system for the understanding of cellular processes including dimorphism (Lübbehüsen et al., 2003; Valle-Maldonado et al., 2015), the light perception that stimulates carotenogenesis and spore production (Corrochano & Garre, 2010) and RNA silencing (Nicolás & Garre, 2016).

In several fungi, such as *Candida albicans* and *Aspergillus fumigatus*, hyphal growth is critical for mycelial development and an adequate invasion of their biological niche (Brand, 2012). Hyphal growth involves an apical extension of new cells that are organised in the hyphal tip, which is responsible for sensing environmental conditions (Brand & Gow, 2009).

Several reports indicate that mycelial growth in *M. circinelloides* is involved in its virulence. A mutation in the *cnbR* gene, which encodes a regulatory subunit of calcineurin, leads to monomorphic yeast morphology even in the presence of oxygen. The Δ*cnbR* mutant is less virulent than the wild type (WT) strain (Lee, Li, Calo, & Heitman, 2013). Interestingly, the mutation in *adh1*, which encodes an alcohol dehydrogenase, led to mycelial monomorphic growth (Rangel-Porras et al., 2019), with an exacerbated virulent phenotype that was explained by higher levels of secreted acetaldehyde (Díaz-Pérez et al., 2020). These results suggest that mycelial growth in *M. circinelloides* is critical for the development of a fully virulent phenotype.

The heterotrimeric G-protein signalling pathway is omnipresent among eukaryotic organisms, and it is responsible for regulating specific responses to a myriad of signals involved in growth, differentiation, virulence, etc. (Li, Wright, Krystofova, Park, & Borkovich, 2007). Heterotrimeric G-proteins are signal transducers, which are canonically attached to the G-protein coupled receptor. They are composed of a GTPase Gα subunit coupled to a dimer (Gβγ) (Li et al., 2007). These proteins are involved in the regulation of fungal hyphae growth (Lin, Alspaugh, Liu, & Harris, 2015). In *Saccharomyces cerevisiae* grown under limited nitrogen with normal glucose conditions, the glucose receptor Gpr1 increases cAMP through Gpa2 (a Gα subunit) by activating adenylyl cyclase, which regulates the pseudohyphal differentiation event (Pan, Harashima, & Heitman, 2000). Moreover, hyphal growth is involved in the pathogenesis of some fungi; for example, the heterotrimeric Gβ subunit (Gpb1) is needed in *Fusarium oxysporum* for hyphal growth and to cause infection in the plant host (Delgado-Jarana, Martínez-Rocha, Roldán-Rodriguez, Roncero, & Di Pietro, 2005). Several effectors downstream of the heterotrimeric subunits transduce the signalling, ion channels, phosphodiesterases and adenylyl cyclases, among others, to produce the hyphal physiological response (Li et al., 2007).

The addition of cAMP to cultures of diverse dimorphic species of *Mucor* stimulates yeast growth, even in aerobic conditions (Kubo & Mihara, 2007; Orlowski, 1991). Accordingly, it has been reported that in *M. circinelloides*, intracellular cAMP accumulation is higher in yeast compared to hyphal growth (Vellanki et al., 2020). In eukaryotes, it has been reported that cAMP activates the protein kinase A (PKA) pathway by binding to the regulatory subunit (PkaR) that leads to its dissociation from the catalytic subunit (PkaC), which activates several transcription factors that control the final morphological fate of the cell (Choi, Jung, & Kronstad, 2015). The fungal PKA pathway is involved in several functions, including asexual sporulation, nutrient sensing, growth and virulence (Demuyser, Van Genechten, Mizuno, Colombo, & Van Dijck, 2018; Fuller & Rhodes, 2012; Kozubowski, Lee, & Heitman, 2009; Liu et al., 2018).

In *M. circinelloides*, the mRNA levels from *pkaR1*, which encode the regulatory subunit of protein kinase A, are higher during mycelial growth compared with spore or yeast cells (Ocampo et al., 2009; Valle-Maldonado et al., 2015). *pkaR1* mRNA levels are also elevated after shifting from anaerobic yeast growth to aerobic filamentous growth (Ocampo et al., 2009). Additionally, PkaR1-encoding gene overexpression stimulates hyperbranching in *M. circinelloides* (Wolff, Appel, Petersen, Poulsen, & Arnau, 2002). Mutation in *pkaR1* causes reduction of the hyphal length compared with that of the WT during the yeast-to-hyphae transition (Ocampo et al., 2009).

We previously described in *M. circinelloides* the most extensive repertoire of heterotrimeric G proteins in the fungal kingdom: 12 Gα, three Gβ, and three Gγ subunits (Valle-Maldonado, Jácome-Galarza, Díaz-Pérez, et al., 2015). Accordingly, it has been proposed a whole-genome duplication in Mucoromycotina fungi that could explain the increased number of genes that encode signal transduction proteins (Corrochano et al., 2016). Phylogenetic analysis revealed the existence of four phylogenetic groups (I-IV) for fungal Gβ subunits. The three Gβ subunits (Gpb1, Gpb2 and Gpb3) encoded in the genome of *M. circinelloides* belong to group III, which is composed of subunits from Mucorales exclusively (Valle-Maldonado, Jácome-Galarza, Díaz-Pérez, et al., 2015). It is noteworthy that group III is the only fungal Gβ group with no members that have been functionally characterised to date. Among all Gβ subunits, the expression of *gpb1* is highly elevated during mycelial growth compared to spore or yeast growth, suggesting the importance of Gpb1 during hyphal growth in *M. circinelloides* (Valle-Maldonado, Jácome-Galarza, Díaz-Pérez, et al., 2015). Based on this information, we speculate that Gpb1 positively controls mycelial growth.

In this work, we provide evidence that the Gpb1 gene is a positive regulator of dimorphic transitions, virulence and filamentous growth under low oxygen levels by controlling cAMP levels through the PKA pathway in *M. circinelloides*. This is, to our knowledge, the first report

of the functional characterisation of a Gβ subunit from a non-Dikarya fungus.

2 | RESULTS

2.1 | Gpb1 is expressed preferentially during mycelial growth

Our group previously quantified the mRNA levels of the 18 heterotrimeric G-protein-encoding genes in spores, yeast or mycelia in the R7B strain of *M. circinelloides* through reverse transcription quantitative polymerase chain reaction (RT-qPCR) using the ΔCt method. Some genes had morphology-dependent expression patterns, such as *gpa11* and *gpa12*, which are highly expressed in the spore morphology (Valle-Maldonado, Jácome-Galarza, Díaz-Pérez, et al., 2015). By re-analysing the raw data (Valle-Maldonado, Jácome-Galarza, Díaz-Pérez, et al., 2015) with a ΔΔCt approach, we found that among all 18 heterotrimeric G subunit-encoding genes, the *gpb1* gene was expressed highly (approximately 7-fold) in mycelia compared to spore or yeast growth (Figure S1). We consistently made similar observations here in MU402, a strain derived from R7B that was used as a recipient strain in transformation experiments, which showed higher mRNA levels of Gpb1 among the three Gβ subunit-encoding genes during mycelial growth compared with spores or yeast stages (Figure 1). This suggests that Gpb1 may have an important role in hyphal development or filamentation in *M. circinelloides*.

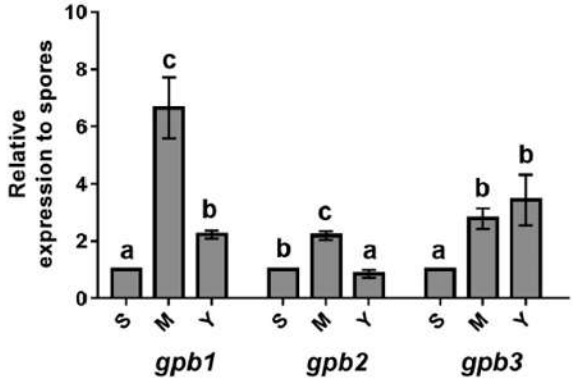

FIGURE 1 Transcript levels of heterotrimeric Gβ-encoding genes in spores, mycelia and yeast from the MU402 strain of *M. circinelloides*. Total RNA was isolated from spores (S), mycelia (M) or yeast (Y) from *M. circinelloides* strain MU402. These vegetative growths were obtained after spores were incubated for 6 hr in YPG medium, aerobically or anaerobically. A delta–delta Ct analysis (ΔΔCt) was carried out for three Gβ (*gpb1-3*) encoding genes. Bars represent relative gene transcripts for each gene during vegetative growth (mycelium or yeast) compared to the spore stage. The data are represented as the average from three independent biological replicates, ± correspond to standard error (*SE*). Significance testing was performed using ANOVA with Fisher's exact test for each gene independently. For each G beta subunit-encoding gene, the different letters above the bars denote statistically significance; values with identical letter were not considered significantly different ($p < .05$)

2.2 | Gpb1 is involved in the dimorphic transition development of *M. circinelloides*

The high expression of the *gpb1* gene during mycelial growth (Figure 1), suggest that Gpb1 could have a function during aerobic growth. Therefore, to study the roles of the *gpb1* gene in development, we generated deletion mutants (Figure S2). The homologous recombination event in the *gpb1* locus was verified by PCR, Southern blot and RT-qPCR (Figure S2). Three independent clone Δ*gpb1* mutants (*leuA*$^-$, *pyrG*$^+$) were selected for further characterisation; the phenotypes displayed by these mutants were similar across all of the experiments. We employed the MU636 (*leuA*$^-$, *pyrG*$^+$) strain as a wild-type (WT) control, with exception of the virulence rate similar phenotypes were also observed with the MU402 strain.

Spore germination analyses in liquid or on solid media revealed no significant differences in aerobic germination rate, morphology, biomass or radial growth between the Δ*gpb1* and WT strains (Figure S4).

Despite both Δ*gpb1* and WT strains exhibit the yeast phenotype in anaerobic conditions (Figure 2a), Δ*gpb1* mutants developed into yeast slightly faster, and produced 14% more biomass than the WT strain (Figure 2b, c). The quantification of *adh1* transcript in yeast cells from 6 hr, revealed a moderate (32.86%), yet significant increase in mRNA levels in Δ*gpb1* compared with the WT strain (Figure 2d). *adh1* encodes an alcohol dehydrogenase I that its transcript accumulates mainly in yeast compared with mycelium or spores cells (Valle-Maldonado, Jácome-Galarza, Díaz-Pérez, et al., 2015).

Based on these results, we hypothesised that Gpb1 participates partially as a regulator of yeast development under anaerobic condition in this fungus.

In order to describe the morphological phenotype of this Δ*gpb1* strain in more detail, we characterised the dimorphic transitions. Indeed, the yeast-to-hyphae transition in Δ*gpb1* resulted in a shorter hyphae compared with that of the WT strain at 2 and 4 hr (Figure 3a, b). Moreover, Δ*gpb1* grown in YPG medium showed a significant delay (approximately 50%) in the development of hyphae at 1 and 2 hr after the transition compared to the WT strain (Figure 3c)), although, in YNB medium, this delay in the hyphal growth was not present (Figure S5a). Previously, we had described *pkaR1*, which encodes a protein kinase regulatory subunit, as molecular marker whose transcripts accumulate more mycelial growth in *M. circinelloides* (Valle-Maldonado, Jácome-Galarza, Díaz-Pérez, et al., 2015). The mRNA quantification in the yeast-to-hyphae transition of *adh1* and *pkaR1* showed that the Δ*gpb1* strain had a modest but significant increase of expression of *adh1* and significantly decreased transcript levels of *pkaR1* compared to the WT strain (Figure 3d, e).

Additionally, in the hyphae-to-yeast transition, Δ*gpb1* showed more yeast cells than the WT strain (Figure 4a, b, Figure S5b). The mRNA quantification in the hyphae-to-yeast transition of *adh1* and *pkaR1*, showed similar results as the yeast-to hyphae transition

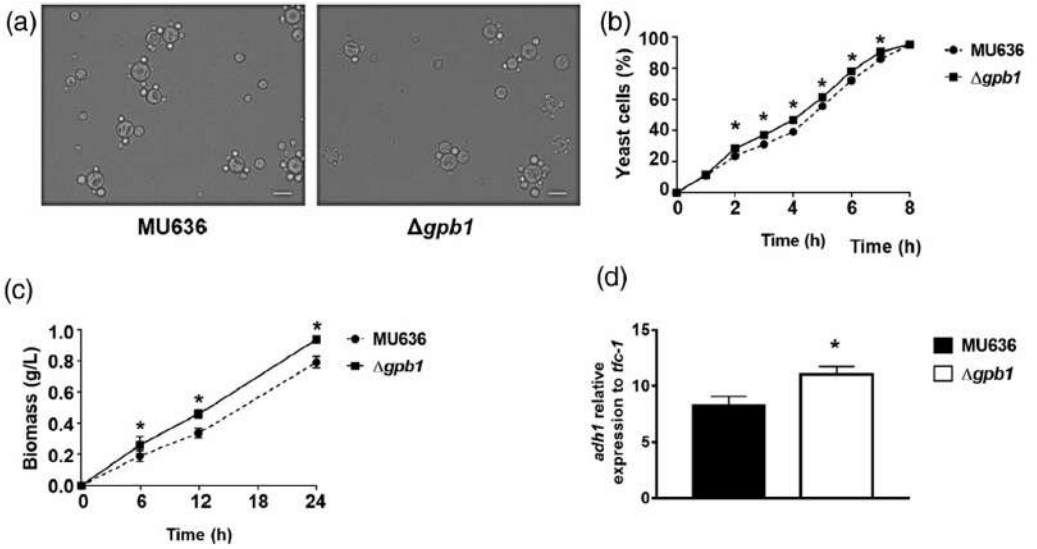

FIGURE 2 Effect of *gpb1* mutation on anaerobic growth of *M. circinelloides*. (a) Cellular morphology. Microphotographs taken by light microscopy (40×) reveal the morphology of yeast cells of the Δ*gpb1* and MU636 strains grown anaerobically for 10 hr in liquid YPG. Scale bar = 20 μm. (b) Cellular germination in YPG medium. The Δ*gpb1* and MU636 strains were grown anaerobically in liquid rich YPG medium and yeast cells were counted hourly. (c) Biomass production. Biomass accumulation in the indicated strains in aerobic cultures in rich YPG medium. (d) Transcript levels of *adh1*. Relative mRNA levels of the *adh1* (were determined for Δ*gpb1* and MU636 yeasts that had been incubated anaerobically for 6 hr in YPG. The data are represented as the average from three independent biological replicates, ± correspond to standard error (*SE*). Significance testing was performed using ANOVA with Fisher's exact test. For each condition, asterisks denote statistical significance, ($p < .05$)

(Figure 4c, d). Together, the data suggest that Gpb1 might be required for maintenance of filamentous growth during dimorphic transitions.

2.3 | Gpb1 and PkaR1 are likely in the same signalling pathway controlling the dimorphic transitions of *M. circinelloides*

The phenotype of the Δ*gpb1* mutant that produced shorter hyphae during the yeast-to-hyphae transition is similar to that of the Δ*pkaR1* (Ocampo et al., 2009). In fact, both strains showed similar morphologies during yeast-to-hyphae and hyphae-to-yeast transitions (Figure 5a), suggesting that Gpb1 and PkaR1 could be involved in the same signalling pathway.

To examine if PkaR1 is downstream of Gpb1 in *M. circinelloides*, we expressed the WT allele of *pkaR1* in Δ*gpb1* by targeted integration of *pkaR1* under the strong promoter pZRT in the *carRP* locus. The phenotype shown by the Δ*gpb1* strain overexpressing *pkaR1* was similar to the WT strain during morphological transitions (yeast-to-hyphae or hyphae-to-yeast) (Figure 5a), suggesting that the overexpression of *pkaR1* suppresses the phenotype of the Δ*gpb1* strain.

To examine that the morphological observations in Figure 5a are congruent with the expression of molecular markers, the mRNA levels of *pkaR1* and *adh1* were quantified after the yeast-to-hyphae transition (Figure 5b, c). We found that Δ*gpb1* cells, after the shift to hyphal growth, contain lower transcript of *pkaR1* and higher *adh1* mRNA levels compared with the WT (Figure 5b, c). Interestingly, the *pkaR1* mRNA levels in the Δ*gpb1* + *pkaR1* strain were similar to those mRNA levels from the WT strain during this transition (Figure 5b).

The mRNA levels of *adh1* accumulated more in Δ*pkaR1* compared with those of the WT strain after the yeast-to-hyphal transition (Figure 5c). Interestingly, the complementation with *gpb1* or the overexpression with *pkaR1* in the Δ*gpb1* strain restored the mRNA levels of *adh1*, compared with the those of WT after the yeast-to-hyphae transition (Figure 5c).

After the hyphae-to-yeast transition, the *pkaR1* and *adh1* mRNA levels were lower and higher, respectively, in the Δ*gpb1* strain compared with those of the WT (Figure 5d, e). Interestingly, Δ*pkaR1* contained *adh1* mRNA levels similar to those of Δ*gpb1* (Figure 5e), and *pkaR1* overexpression in the Δ*gpb1* strain restored the mRNA levels of *adh1* in this transition to levels similar to those of the WT strain (Figure 5d, e).

Moreover, the direct observation of the cellular morphologies (Figure 5a) revealed a delay of formation of hyphae during the yeast-to-hyphae transition for both mutants Δ*gpb1* and Δ*pkaR1* (29.3–31.0%) compared with wild type, Δ*gpb1* + *gpb1* or the Δ*gpb1* + *pkaR1* strains that showed 74.33–76.77% of hyphal cells in transition (Table S2). In the case of the hyphae-to-yeast transition, we found that the Δ*gpb1* and Δ*pkaR1* were more prone to develop yeast cells (86.3–90.0%) compared with the wild type, Δ*gpb1* + *gpb1* or the Δ*gpb1* + *pkaR1* strains that showed 42.67–45.67% (Table S2). These morphological

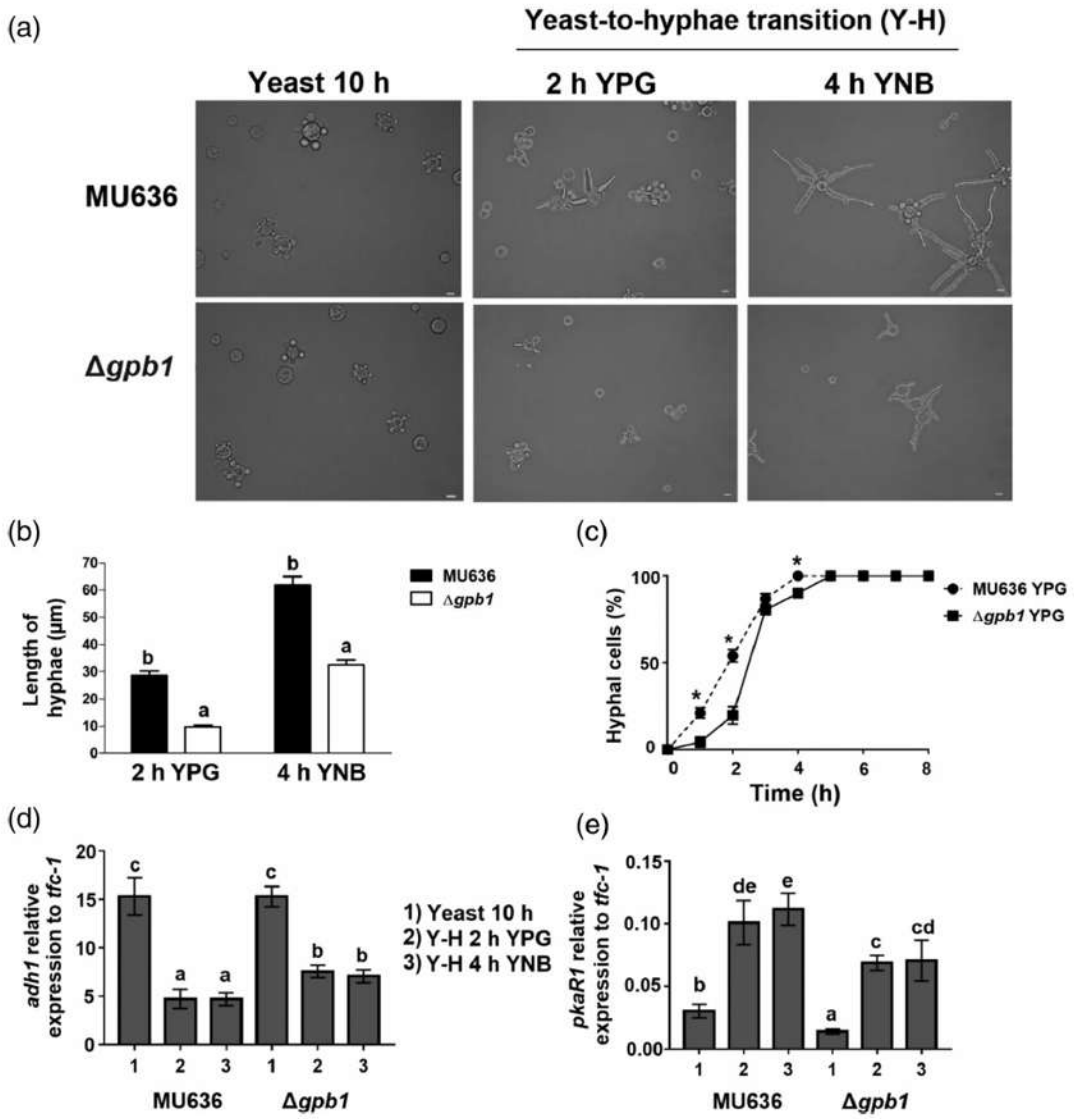

FIGURE 3 Effect of *gpb1* mutation on yeast-to-hyphae transition in *M. circinelloides*. (a) Cellular morphology. Δ*gpb1* and MU636 spores were incubated anaerobically in medium for 10 hr, then the resulting yeast cells were washed and transferred to fresh YPG or YNB media supplemented with leucine and uridine and grown aerobically to promote the yeast-to-hyphae transition. Microphotographs taken by light microscopy (40×) reveal morphology in liquid YPG and YNB at 2 and 4 hr of aerobic growth for the Δ*gpb1* and MU636 strains. Scale bar = 20 µm. (b) Length of hyphae. Length of hyphae from Δ*gpb1* and MU636 after the yeast-to-hyphae transition was determined for YPG and YNB media supplemented with leucine and uridine at 2 and 4 hr under aerobic conditions. (c) Hyphae cell determination. The percentage of hyphae cells was determined in YPG medium hourly for Δ*gpb1* and MU636 after the yeast-to-hyphae transition was induced. Hyphae cell was considered independently of the number or length of the hyphae per mother cell. Relative mRNA levels of the *adh1* (d) and *pkaR1* (e) genes were determined for Δ*gpb1* and MU636 yeasts that had been incubated anaerobically for 10 hr in YPG (1) and cells under the yeast-to-hyphae transition, in YPG (2) or YNB (3) at 2 and 4 hr of aerobic growth. ΔCt analysis was performed to compare mRNA and gene expression levels between samples. The data are represented as the average from three independent biological replicates, ± correspond to standard error (*SE*). Significance testing was performed using ANOVA with Fisher's exact test. For each condition, the different letters or the presence of asterisks above the bars or on the lanes denote statistical significance. Values with identical letter were not considered significantly different ($p < .05$)

phenotypes correlate with the mRNA levels of *pkaR1* and *adh1* during dimorphic transitions; these genes are the molecular markers of filamentous and yeast growth respectively (Figure 5b–e).

All these data indicate that PkaR1 is downstream of the Gpb1 subunit in the signalling pathway, and the deletion of either *gpb1* or *pkaR1* led to phenotypes that are less prone to maintain or

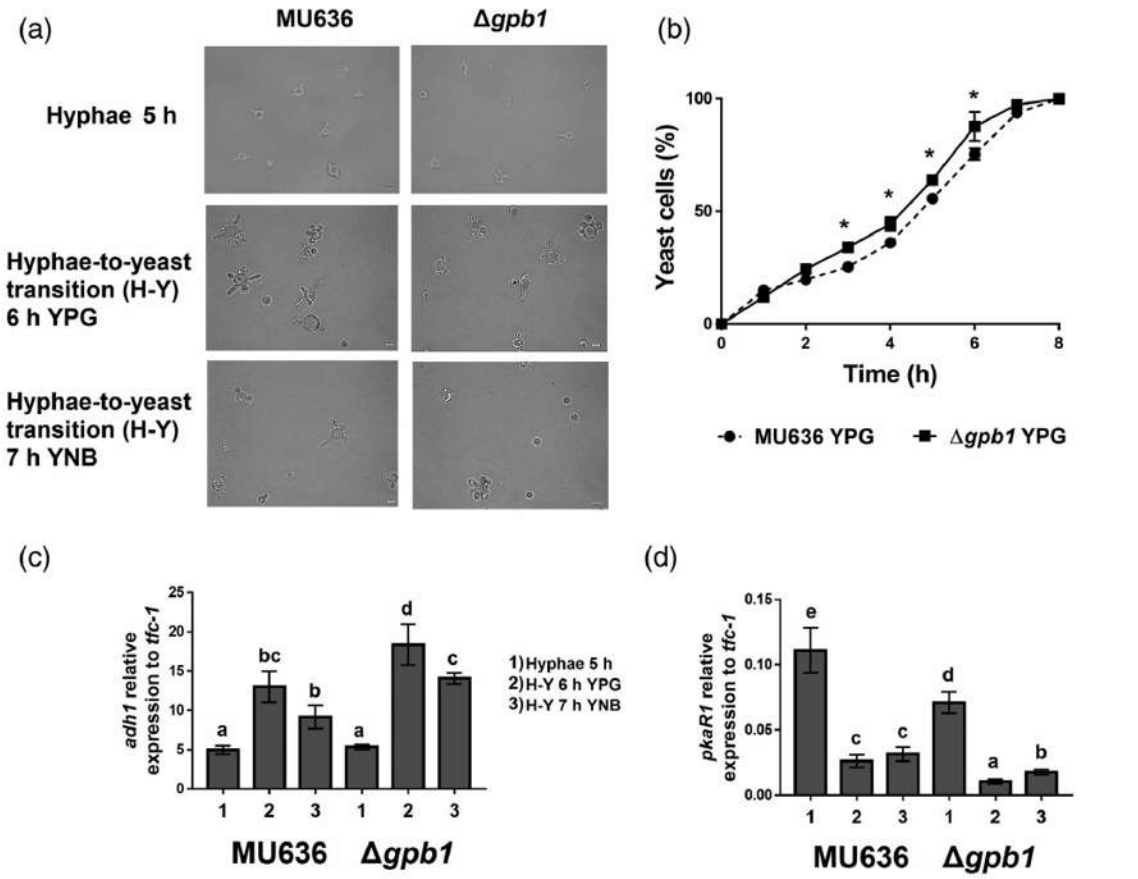

FIGURE 4 Effect of *gpb1* mutation on hyphae-to-yeast transition in *M. circinelloides*. (a) Cellular morphology. Δ*gpb1* and MU636 spores were incubated aerobically in YPG medium for 5 hr, then the resulting hyphae cells were washed and transferred to fresh YPG or YNB media and grown anaerobically to promote the hyphae-to-yeast transition. Microphotographs taken by light microscopy (40×) revealed morphology in liquid YPG and YNB at 6 and 7 hr of anaerobic growth, respectively, for Δ*gpb1* and MU636 strains. Scale bar = 20 μm. (b) Yeast cell determination. The percentage of yeast cells was determined hourly for Δ*gpb1* and MU636 after the hyphae-to-yeast transition was induced. Relative mRNA levels of the *adh1* (c) and *pkaR1* (d) genes were determined for Δ*gpb1* and MU636 germlings that had been incubated for 5 hr aerobically in YPG (1) and cells under the hyphae-to-yeast transition, in YPG (2) and YNB (3) at 6 and 7 hr of anaerobic growth. ΔCt analysis was performed to compare mRNA and gene expression levels between samples. The data are represented as the average from three independent biological replicates, ± correspond to standard error (*SE*). Significance testing was performed using ANOVA with Fisher's exact test. For each condition, the different letters or the presence of asterisks above the bars or on the lanes denote statistical significance; values with identical letter were not considered significantly different ($p < .05$)

generate hyphae development after dimorphic transitions compared with the WT.

2.4 | The *gpb1* gene is required for virulence of *M. circinelloides*

Since the Δ*gpb1* strain is less prone to produce hyphae compared with the WT after dimorphic transitions (Figures 3 and 4), and the filamentous morphology is associated with a more virulent phenotype compared with the yeast morphology (Lee et al., 2013), we hypothesised that the Δ*gpb1* strain would be less virulent compared with the WT. To test this hypothesis, we used diabetic murine host system that has been previously employed to test virulence (Patiño-Medina et al., 2018; Patiño-Medina et al., 2019).

In the diabetic mouse host model, both Δ*gpb1* and Δ*pkaR1* strains exhibited a significantly attenuated virulence compared with the WT strain; showing Δ*pkaR1* a more virulent phenotype than the Δ*gpb1* strain (Figure 6a). We measured the fungal load in mouse tissue using *tfc-1* to indirectly determine the degree of invasion of the fungus, as previously reported (Patiño-Medina, Vargas-Tejeda, et al., 2019). The livers infected with Δ*gpb1* spores showed lower levels of the *tfc-1* fungal gene marker during qPCR compared with the levels from tissues infected with the WT (Figure 6b). Similarly, the Δ*pkaR1*-

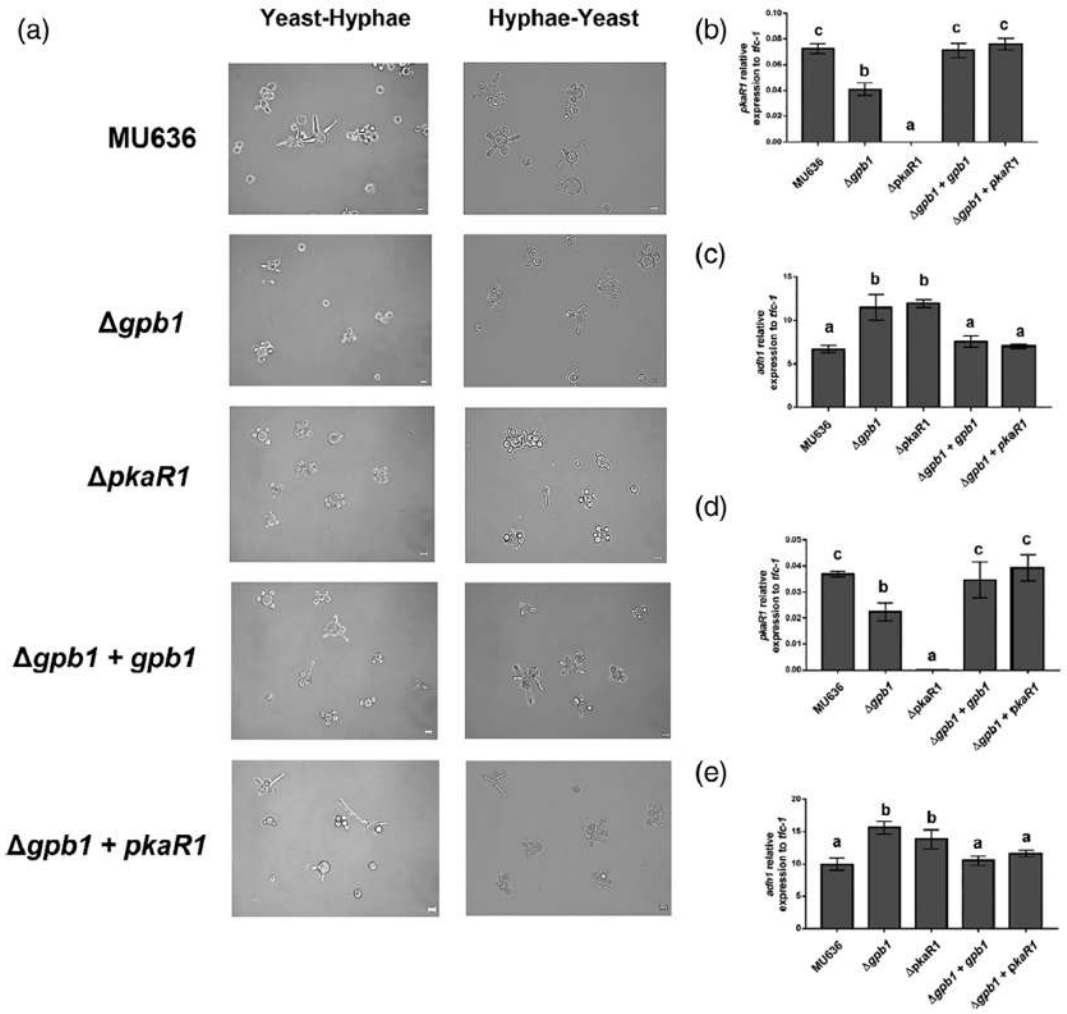

FIGURE 5 Genetic suppression of *gpb1* deletion in the dimorphic transitions by *pkaR1* overexpression in *M. circinelloides*. (a) Morphological yeast-to-hyphae or hyphae-to-yeast transitions were evaluated for the MU636, Δ*gpb1*, Δ*pkaR1*, Δ*gpb* + *gpb1* and Δ*gpb1* + *pkaR1* strains in *M. circinelloides* in YPG medium, following the methodology described previously. Microphotographs taken by light microscopy (40×) reveal the morphology of the mentioned strains. Scale bar = 20 μm. Total RNA was isolated from cells harvested at 2 hr during the yeast-to-hyphae transition (b, c) or at 6 hr during the hyphae-to-yeast (d, e) transition. The transcript levels of the *pkaR1* (b, d) and *adh1* (c, e) genes were determined by reverse transcription quantitative polymerase chain reaction (RT-qPCR); these genes are validated molecular markers associated with, respectively, mycelia and yeast morphologies in *M. circinelloides*. The ΔCt expression analysis employed the *tfc-1* gene as a normaliser. The data are represented as the average from three independent biological replicates, ± correspond to standard error (*SE*). Significance testing was performed using ANOVA with Fisher's exact test. For each condition, the different letters above the bars denote statistical significance; values with identical letter were not considered significantly different ($p < .05$)

inoculated groups showed higher levels of *tfc-1* compared with the Δ*gpb1* groups, but lower levels compared with those injected with the WT strain (Figure 6b). Furthermore, the restored Δ*gpb1* + *gpb1* or the overexpressing Δ*gpb1* + *pkaR1* strains resulted in similar liver fungal loads compared with those of the WT strain (Figure 6b). Lower levels of mRNA of the cellular stress marker *BIP* and the inflammation markers *IL-6*, *IL-1β* and *TNF-α* were found in the liver tissue that was infected with Δ*gpb1* spores compared with those of the WT strain, the restored Δ*gpb1* + *gpb1* and the overexpressing Δ*gpb1* + *pkaR1* strains (Figures 6c–f). These data indicate that Gpb1 and PkaR1 are required for tissue invasion, as well as cellular damage and inflammatory response in the hosts.

In order to determine whether the less virulent character of the Δ*gpb1* strain could be a result of a higher sensitivity to phagocytosis by macrophage, we grew the spores in the presence of the oxidant stressor hydrogen peroxide (H_2O_2). We found that the spores from

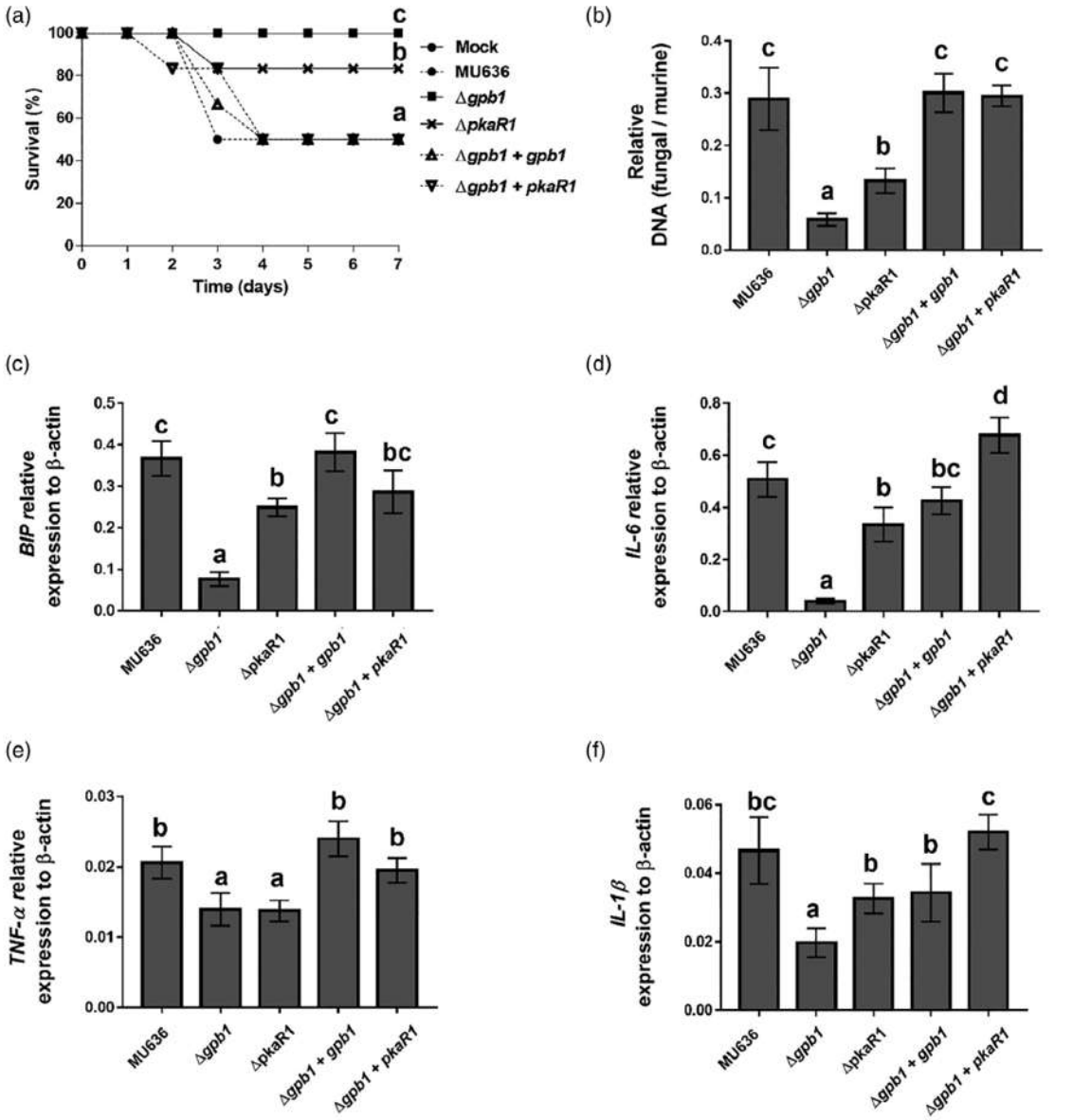

FIGURE 6 Genetic suppression of *gpb1* deletion by *pkaR1* overexpression in virulence regulation in *M. circinelloides*. (a) Spores (2×10^7) from the MU636, Δ*gpb1*, Δ*pkaR1*, Δ*gpb1* + *gpb1* and Δ*gpb1* + *pkaR1* strains were intraperitoneally injected into streptozotocin-induced diabetic mice and survival was monitored daily for a week. (b) Fungal burden in the mice was determined by quantitative polymerase chain reaction (qPCR) using the *tfc-1* gene from *M. circinelloides* and β-actin from *Mus musculus* 15 days post-infection. A ΔCt analysis was performed to compare the relative abundance of the fungal DNA compared with that of the murine DNA. The mRNA levels of inflammation markers *BIP* (c), *IL-6* (d), *TNF-α* (e), and *IL-1β* (f) were determined by reverse transcription quantitative polymerase chain reaction (RT-qPCR) from mouse livers infected with the corresponding spores 15 days post-infection. The data are represented as the average from three independent biological replicates, ± correspond to standard error (*SE*). Significance testing was performed using ANOVA with Fisher's exact test. The different letters above the bars or on the lanes denote statistical significance; values with identical letter were not considered significantly different ($p < .05$)

the Δ*gpb1* and Δ*pkaR1* strains showed lower colony survival compared with the WT, Δ*gpb1* + *gpb1* and the Δ*gpb1* + *pkaR1* strains (Figure 7a). After 6 hr of co-cultures with macrophages, we observed that the WT, Δ*gpb1* + *gpb1* and Δ*gpb1* + *pkaR1* strains displayed apparently an increase in the hyphal growth compared to the Δ*gpb1* and Δ*pkaR1* strains (Figure 7b).

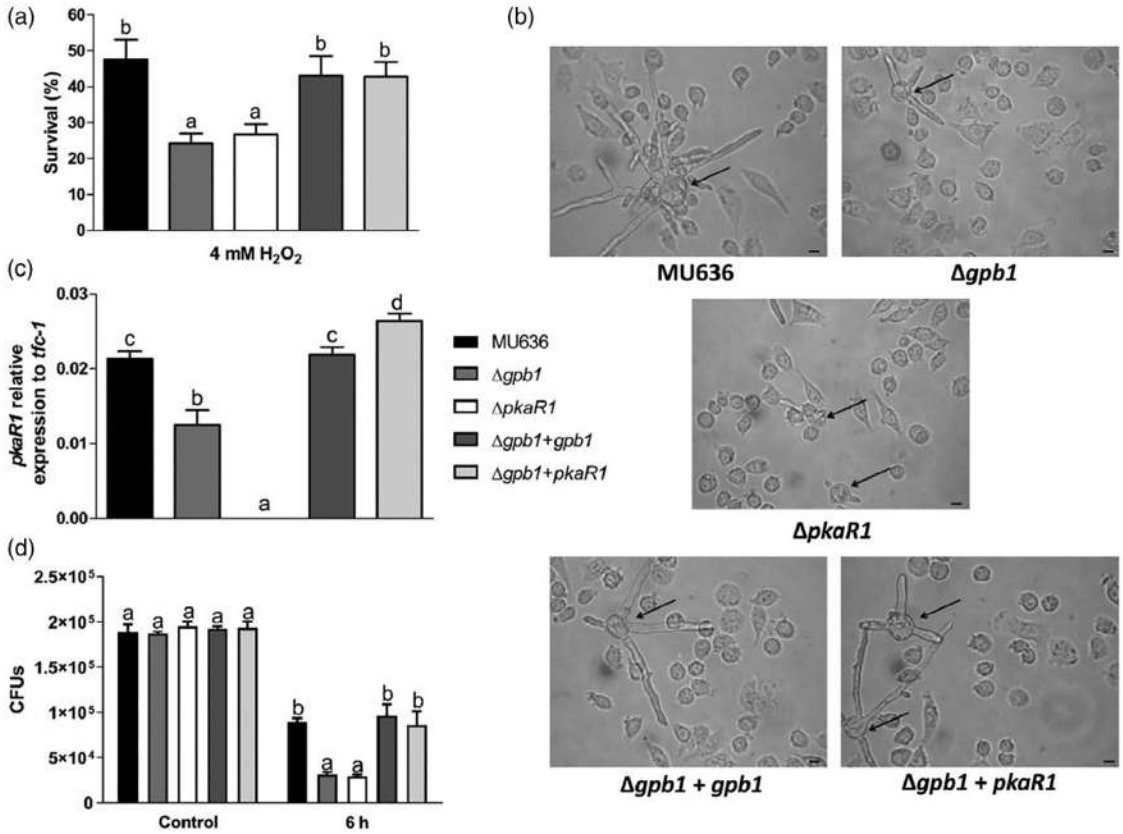

FIGURE 7 Effect of *gpb1* or *pkaR1* deletion on survival of spores after confrontation with macrophages. Spores from the MU636, Δ*gpb1*, Δ*pkaR1*, Δ*gpb1* + *gpb1* and Δ*gpb1* + *pkaR1* strains were incubated with or without 4 mM H_2O_2 at 28°C. (a) Survival was calculated after 24 hr of growth by dividing the number of colonies in treated samples by the number of colonies in untreated samples. (b) Macrophages were seeded at 8×10^5 cells/well in DMEM basal medium and cocultured with 2×10^5 spores from *M. circinelloides* for 6 hr. Germination of spores interacting with macrophages was observed under direct observation by light microscopy (40×). Scale bar = 20 μm. Arrows indicate hyphae germination. (c) *pkaR1* mRNA levels were quantified by reverse transcription quantitative polymerase chain reaction (RT-qPCR) at 6 hr after initiation of spore and macrophage interactions. ΔCt analysis was performed to compare mRNA and gene expression levels between samples. (d) Quantitation of CFUs from spores after 6 hr of incubation with mouse macrophages. The CFUs from the control correspond to the spores in DMEM basal medium without macrophage confrontation. Figures show the average and *SD* of three independent experiments, ± correspond to standard error (*SE*). Significance testing was performed using ANOVA with Fisher's exact test. The different letters above the bars indicate statistical significance; values with identical letter were not considered significantly different ($p < .05$)

In order to quantify the hyphal growth, we used and indirect approach based on the quantitation of the mRNA levels of *pkaR1*, which is a validated molecular marker of hyphal development in *M. circinelloides* (Díaz-Pérez et al., 2020; Patiño-Medina, Vargas-Tejeda, et al., 2019; Valle-Maldonado, Jácome-Galarza, Gutiérrez-Corona, et al., 2015). The results showed that the WT, Δ*gpb1* + *gpb1* and Δ*gpb1* + *pkaR1* strains contain higher levels of mRNA of *pkaR1*, compared with the Δ*gpb1* and Δ*pkaR1* strains (Figure 7c), correlating with lower hyphal development in either the Δ*gpb1* or Δ*pkaR1* strains. Additionally, we quantified the CFUs produced from spores that survived the digestion by the macrophage after 6 hr of interaction. Spores from the WT, Δ*gpb1* + *gpb1* and Δ*gpb1* + *pkaR1* strains produced significantly more CFUs (290.3–310.3%) after the macrophage interaction than the Δ*gpb1* and Δ*pkaR1* strains (Figure 7d). These results indicate that the spores from the Δ*gpb1* and Δ*pkaR1* strains mutant strains are more susceptible to be digested by the macrophages than the spores from the WT, Δ*gpb1* + *gpb1* and Δ*gpb1* + *pkaR1* strains. All these results suggest that Gpb1 and PkaR1 are positive regulators of virulence in *M. circinelloides* in diabetic mice.

2.5 | The G beta subunit *gpb1* controls hyphal growth under lower oxygen in *M. circinelloides*

We observed that the Δ*gpb1* strain is more prone to generate or maintain the yeast morphology compared with the WT during both

dimorphic transitions (Figures 3 and 4). Growth under restricted oxygen levels has been reported to regulate morphogenesis in other dimorphic fungal pathogens such as *C. albicans* (Setiadi, Doedt, Cottier, Noffz, & Ernst, 2006). Moreover, oxygen levels in the peritoneal cavity and intestinal tissues are around 5.3–7.6% (Carreau et al., 2011; Ortiz-Prado et al., 2019; Renvall & Niinikoski, 1980), considering that the spore inoculation of *M. circinelloides* spores was performed in this murine anatomical area, it is possible that similar oxygen levels could be present during the infection. Based on this information, we hypothesised that the Δ*gpb1* strain would generate more yeast cells under lower oxygen conditions compared with the WT. In order to determine the effect of low oxygen levels, we induced hyphal morphology under constant shaking at 160 r.p.m., which leads to 14.4 ± 1.2% dissolved oxygen, contrary to shaking at 50 r.p.m. which leads to 7.3 ± 0.56% dissolved oxygen. As shown in Figure S4, the Δ*gpb1* strain showed similar a hyphae germination rate as the WT at 160 r.p.m. However, at 50 r.p.m., the WT generated 80% hyphae and 20% yeast cells after 8 hr (Figure 8a), but the Δ*gpb1* strain showed 90% yeast cells and 10% hyphae. The Δ*pkaR1* strain showed 88% yeast cells and 12% hyphae, whereas the Δ*gpb1* + *gpb1* or the Δ*gpb1* + *pkaR1* showed similar percentages of morphologies as the WT strain (Figure 8a). The morphologies found during the growth at low oxygen levels (7.3 ± 0.56%) indicate that deletion of *gpb1* or *pkaR1* increased the development of yeast cells compared with the WT (Figure 8b)).

The Δ*gpb1* strain grown in low oxygen had lower mRNA levels of *pkaR1* and higher *adh1* mRNA levels, compared with the WT and other strains shown in Figure 8c, d. Remarkably, the overexpression of *pkaR1* in the Δ*gpb1* strain restored the hyphae/yeast proportion to that of the WT (Figure 8a) and the mRNA levels of *adh1*. On the other hand, the mRNA levels of *pkaR1* in the Δ*gpb1* + *gpb1* strain were similar to the Δ*gpb1* + *pkaR1* strain and the WT (Figure 8c, d). The quantification of transcript levels of *pkaR1* and *adh1* in the livers of mice infected with the different strains indicates that liver tissue infected with Δ*gpb1* or Δ*pkaR1* contained higher mRNA levels of *adh1*, as well as lower levels of mRNA of *pkaR1* for Δ*gpb1* (similar to those levels found *in vitro* for these mutant strains), compared with those tissues infected with the WT or the Δ*gpb1* + *gpb1* strains (Figure 8e, f).

These results indicate that Gpb1 and PkaR1 are positive regulators of filamentous growth of *M. circinelloides* in low oxygen conditions *in vitro*. They also likely regulate *in vivo* morphology in tissues like the peritoneal cavity where the oxygen levels are around 5.3 to 6.7% (Renvall & Niinikoski, 1980) or in the intestinal tissues with 7.6% dissolved oxygen (Carreau et al., 2011; Ortiz-Prado et al., 2019).

It is interesting to note that the mutation of *gpb1* did not lead to a full defect either during dimorphic transitions (Figures 4 and 5) or low oxygen condition growths (Figure 8a). This could be explained in part due *M. circinelloides* harbours three *gpb* genes (*gpb1*-*gpb3*) and based on the previous (Valle-Maldonado, Jácome-Galarza, Díaz-Pérez, et al., 2015) and this new transcription pattern analysis during dimorphism in the wild-type R7B and MU402 strains might suggest that *gpb2* could have a principal role during hyphal growth, and *gpb3* might be important for hyphal and yeast development in this fungus (Figure 1). In order to know if a compensatory role could exist for *gpb2* and *gpb3* in Δ*gpb1*, their mRNA levels were quantified in the Δ*gpb1* strain. The mutation of *gpb1* led to the mRNA increase of *gpb2* during hyphal (52.78%) or low oxygen level cultures (32.01%) respect to the wild-type strain. Meanwhile, mRNA levels from *gpb3* were also increased in the Δ*gpb1* strain, but in lesser extend compared with *gpb2* (Figure S6). These results suggest that Gpb2 and/or Gpb3 could partially compensate the absence of Gpb1 in *M. circinelloides* during these growth conditions, although more experiments are needed to confirm this suggestion.

Additionally, we searched for transcription factors consensus motifs in the promoter regions (1 kb upstream of ATG start codon) of the *gpb1*, *gpb2* and *gpb3* genes in *M. circinelloides* in order to determine a putative transcription factor that could be involved in the hyphal growth of *M. circinelloides*. We found that only for the promoter region of the *gpb1* and not the other two *gpb* genes (*gpb2* and *gpb3*), a putative consensus motif (CATTCTT) for the transcription factor TEC1p at 50 bp upstream of the ATG codon (Figure S7a) (Heise et al., 2010; Hwang, Chambon, & Davidson, 1993). In this extent, it has been demonstrated in *C. albicans* that TEC1 transcription factor is expressed mainly in the hyphal morphology (Schweizer, Rupp, Taylor, Röllinghoff, & Schröppel, 2000). Moreover, its disruption showed that this gene is a positive regulator of hyphal development and virulence in this fungus (Schweizer et al., 2000).

In order to determine whether any TEC1p homologue was present in *M. circinelloides*, we used the TEC1p of *S. cerevisiae* as a bait to query the genome of this organism (https://genome.jgi.doe.gov/Mucci2/Mucci2.home.html). At least two TEC1p homologues (Tec1 and Tec2, with ID numbers: 84676 and 106,595 respectively) were found (Figure S7b). These sequences contain the characteristic structural motifs and the TEA/ATSS domain in Tec1 (Heise et al., 2010). In addition, Tec1 and Tec2 share 54.6 and 53.12% at sequence identity within the TEA/ATSS domain when compared with TEC1p of *S. cerevisiae* (Figure S7b). These analyses suggest that the hyphal transcription factor Tec1 or/and Tec2 in *M. circinelloides* could participate in the regulation of expression of *gpb1* during hyphal growth.

2.6 | The G beta subunit *gpb1* negatively controls the cAMP levels in *M. circinelloides* experiencing low oxygen levels

The PKA signalling pathway is regulated by cAMP, a secondary messenger, whose production is modulated by heterotrimeric G-proteins (Sassone-Corsi, 2012). The yeast morphology of dimorphic *Mucor* species is stimulated by the addition of cAMP (Orlowski, 1991). Our data indicated that the Δ*gpb1* strain was more prone to generate and maintain yeast morphology during dimorphic transitions or upon growth under low oxygen levels. These results suggest that Δ*gpb1* could contain higher intracellular cAMP levels compared with the WT. To demonstrate this hypothesis, the intracellular cAMP levels were measured

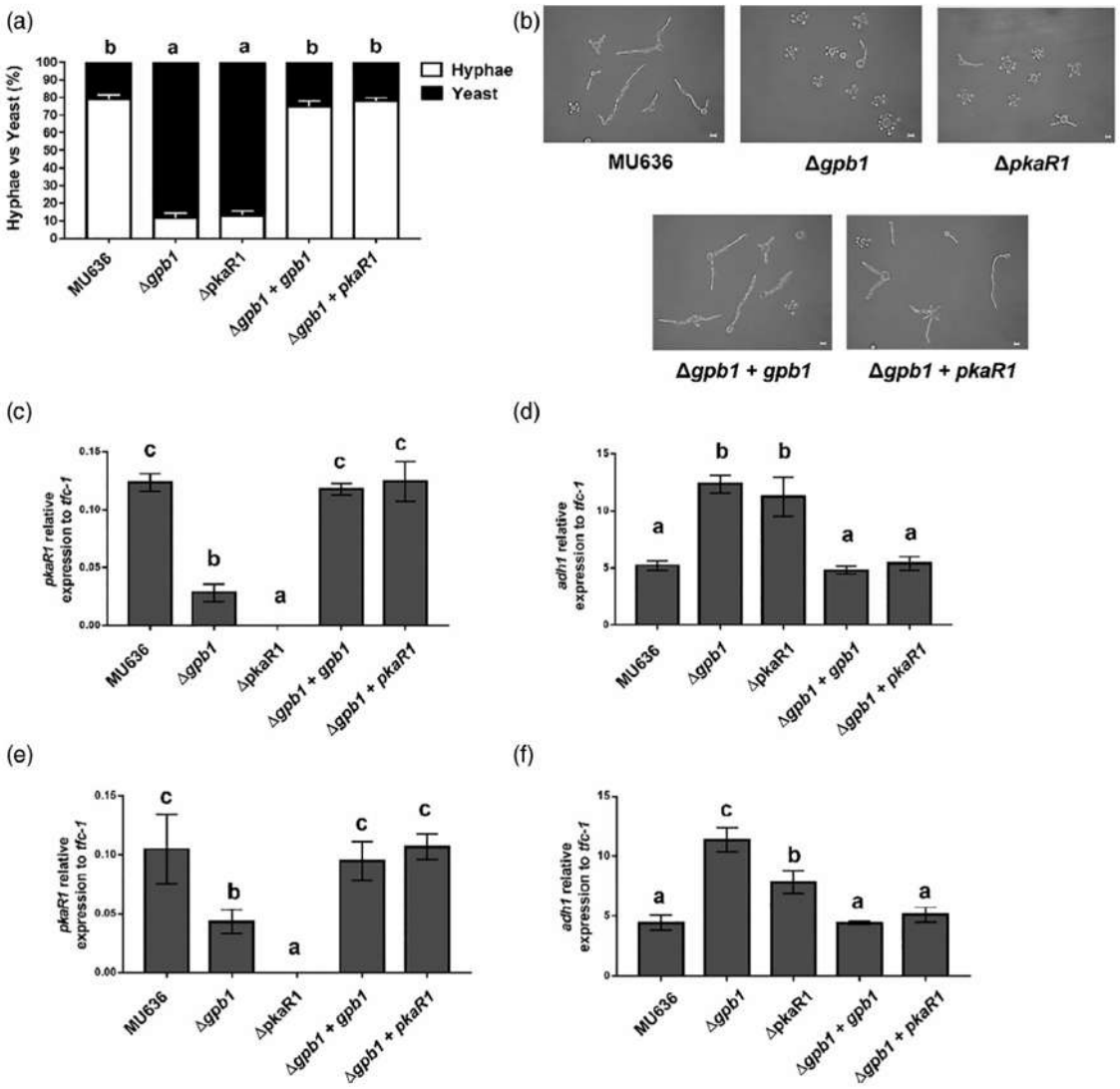

FIGURE 8 Effect of oxygen concentration on the morphology of Δ*gpb1* from *M. circinelloides*. Spores from the MU636, Δ*gpb1*, Δ*pkaR1*, Δ*gpb1* + *gpb1* and Δ*gpb1* + *pkaR1* strains of *M. circinelloides* were inoculated onto YPG media and incubated with constant shaking (50 r.p.m.). (a) Hyphae and yeast abundances were counted at 8 hr. (b) Microphotographs taken by light microscopy (40×) reveal representative cellular morphology. Scale bar = 20 μm. Total RNA was isolated from cells at 8 hr of incubation and the transcript levels of the *pkaR1* (c) or the *adh1* (d) genes were determined by RT-qPCR; these genes are validated molecular markers associated with, respectively, mycelia and yeast morphologies in *M. circinelloides*. Diabetic-induced BALB/c mice were intraperitoneally inoculated with 20×10^6 spores from the MU636, Δ*gpb1*, Δ*pkaR1*, Δ*gpb1* + *gpb1* or Δ*gpb1* + *pkaR1* strains. At day seven, the mice were euthanised. Total RNA was isolated from their livers and mRNA levels of *pkaR1* (e) or the *adh1* (f) genes were determined by RT-qPCR. The ΔCt expression analysis employed the *tfc-1* gene as a normaliser. Bars represent the mean of three independent assays, and error bars correspond to the standard error (*SE*). Significance testing was performed using ANOVA with Fisher's exact test. The different letters above the bars denote statistical significance; values with identical letter were not considered significantly different ($p < .05$)

during low oxygen growth conditions. Our results show that Δ*gpb1* and Δ*pkaR1* contain significantly higher cAMP levels compared to the Δ*gpb1*-restored, Δ*gpb1*-overexpressing *pkaR1* and WT strains (Figure 9a). Since high PKA activity has been associated with yeast development in this fungus (Lee et al., 2013), we evaluated strains grown in low oxygen levels for PKA activity. Our results showed that Δ*gpb1* and Δ*pkaR1* display significantly higher PKA activity compared with the other strains (Figure 9b). These results demonstrate that Gpb1 positively regulates hyphal growth by controlling the PKA pathway.

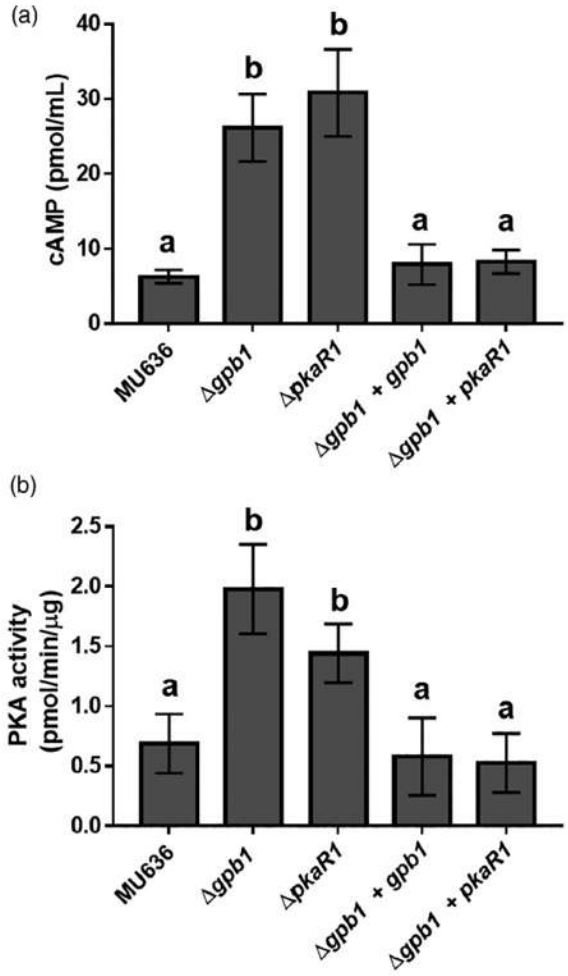

FIGURE 9 *Gpb1 is* involved in the regulation of cAMP levels and PKA activity in *M. circinelloides*. Spores from the MU636, Δ*gpb1*, Δ*pkaR1*, Δ*gpb1* + *gpb1* and Δ*gpb1* + *pkaR1* strains from *M. circinelloides* were inoculated into YPG media and incubated with constant shaking (50 r.p.m.) for 8 hr, and intracellular cAMP levels (a) and PKA activity (b) were detected. The data are represented as the average from three independent biological replicates, ± correspond to standard error (*SE*). Significance testing was performed using ANOVA with Fisher's exact test. The different letters above the bars indicate statistical significance; values with identical letter were not considered significantly different ($p < .05$)

3 | DISCUSSION

This work provides evidence that the key regulator Gpb1 is highly expressed during mycelial growth and is necessary for hyphal development during dimorphic transitions in low oxygen levels, contributing to *M. circinelloides* virulence.

Heterotrimeric G-proteins are keystones in the regulation of fungal morphogenesis (Li et al., 2007). In *M. circinelloides*, twelve Gα, three Gβ and three Gγ subunits have been described, giving it the most extensive repertoire of these subunits in the fungal kingdom currently reported (Valle-Maldonado, Jácome-Galarza, Díaz-Pérez, et al., 2015). To our knowledge, 19 fungal Gβ subunits have been functionally characterised to date (Table S3). All of these subunits belong to phylogenetic groups I (filamentous ascomycetes), II (basidiomycetes) or IV (dimorphic or yeast ascomycetes) (Table S3); group III is composed of subunits from Mucorales including the three Gβ subunits from *M. circinelloides*. Notably, none of the subunits in group III had been functionally characterised.

gpb1 mRNA levels are highly elevated during mycelial growth (Valle-Maldonado, Jácome-Galarza, Díaz-Pérez, et al., 2015) compared with the rest of the Gβ subunits (Figure 1), suggesting a role of this gene in the regulation of mycelial morphology. Mycelial growth in *M. circinelloides* has been reported to cause virulence (Díaz-Pérez et al., 2020; Lee et al., 2013). Several factors stimulate mycelial growth in *M. circinelloides*: presence of oxygen, non-fermentable carbon sources and inorganic nitrogen sources (McIntyre, Breum, Arnau, & Nielsen, 2002; Orlowski, 1991). Host components may promote the virulence of this fungus, as blood serum also stimulates hyphal germination of the spores (Patiño-Medina, Vargas-Tejeda, et al., 2019).

This work demonstrates that the prevalent morphology of *M. circinelloides* under low oxygen levels (approximately 7%) is hyphal (Figure 8). Although the deletion of *gpb1* did not alter mycelial morphology development during growth at relatively high oxygen concentrations (pproximately 14%), during dimorphic transitions or oxygen limitation in the Δ*gpb1* strain clearly increased yeast development compared with the WT strain. The defect could be critical for infection and virulence as mycelial development is required and low oxygen levels are prevalent during fungal infection of the tissues (Grahl, Shepardson, Chung, & Cramer, 2012). Virulence assays using diabetic mice confirmed that the *gpb1* gene is required for virulence, where the Δ*gpb1* strain was not able to invade mouse tissue like the WT or the Δ*gpb1* + *gpb1* restored strains (Figure 6). This could be explained in part because of the more sensitivity to H_2O_2 and the higher proportion of yeast cells formed as a result of Gpb1 loss in a low-oxygen tissue environment. These yeast cells could be more effectively killed by macrophages (Figure 7) as has been described (Lee et al., 2013). These results are in accord with the mycelial morphology prevalence in host tissues infected with *M. circinelloides* (Dizbay et al., 2009; Khan, Ahmad, Brazda, & Chandy, 2009).

The data presented here are consistent with other relevant human pathogenic fungi that have been shown to become filamentous in hypoxic or anoxic *in vitro* conditions, such as the dimorphic pathogen *C. albicans* (Setiadi et al., 2006), the monomorphic filamentous fungi *A. fumigatus* (Hall & Denning, 1994) and *F. oxysporum* (Gunner & Alexander, 1964). Similarly, it was reported in the entomopathogenic fungus *Isaria fumosorosea* that the relative abundance of hyphae or yeast in an *in vitro* culture is regulated by oxygen availability (Jackson, 2012). In concordance, the filamentous growth of the pathogenic fungi *C. albicans* is critical for its virulence (Da Silva Dantas et al., 2016), and this morphology is positively regulated by low oxygen

levels (Setiadi et al., 2006). Moreover, transcriptome analysis in this organism when grown under oxygen limitation has shown that hypha-specific genes were up-regulated compared with growth under higher oxygen conditions (Setiadi et al., 2006).

Given that Δ*gpb1* showed shorter hyphae during yeast-to-hyphae transitions (Figure 3), and that a similar phenotype had been already reported for the Δ*pkaR1* strain (Ocampo et al., 2009), we attempted to elucidate a possible functional relationship between these two genes. The Δ*pkaR1* strain showed similar phenotypes compared with Δ*gpb1*, as it was more prone to develop yeast under low oxygen conditions (Figure 8). It also showed attenuated virulence and fungal invasion (Figure 6) compared with the WT strain. For fungal heterotrimeric G-proteins, it has been reported that genes that participate in the same signalling pathway usually displayed similar altered phenotypes when they were disrupted individually (Landry & Hoffman, 2001; Landry, Pettit, Apolinario, & Hoffman, 2000; Whiteway et al., 1989; Yang, Poole, & Borkovich, 2002).

Co-participation of *gpb1* and *pkaR1* in regulating hyphal growth under low oxygen levels and virulence was supported by restoring WT phenotypes following *pkaR1* overexpression in the Δ*gpb1* strain (Figures 8 and 9). The functional relationship between Gpb1 and PkaR1 might rely on the Gpb1-mediated regulation of adenylyl cyclase activity, which in turn increases cAMP levels to activate PKA (Choi et al., 2015). The increased cAMP levels and PKA activities found

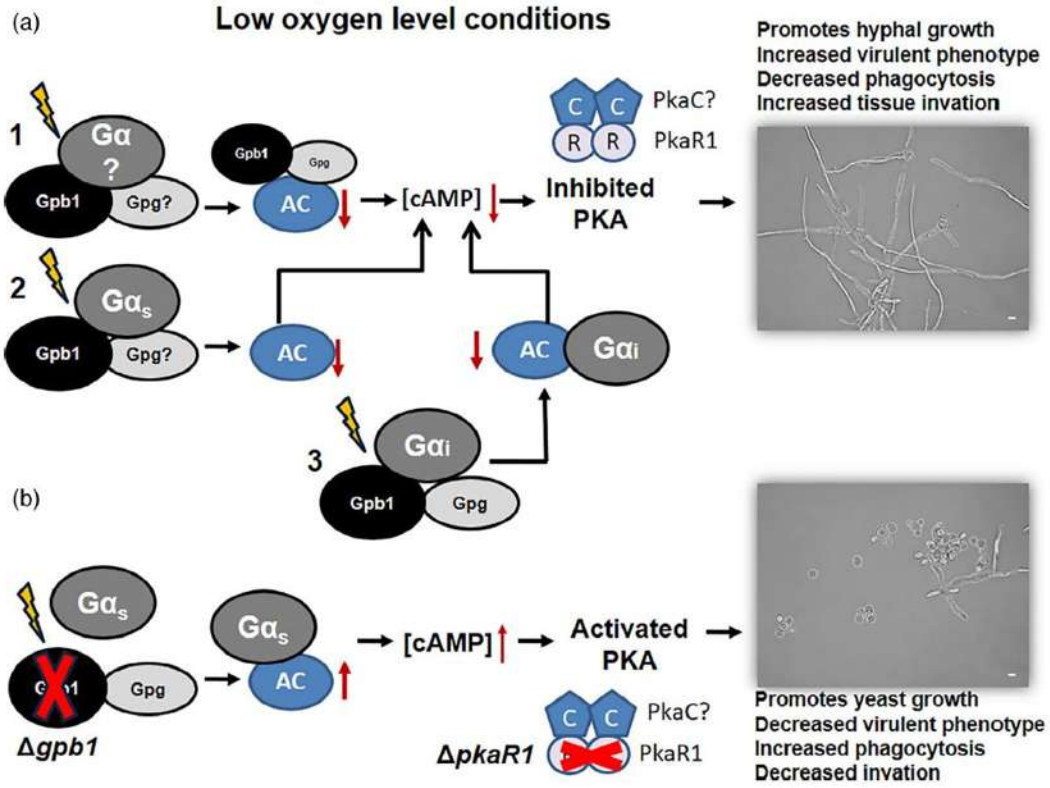

FIGURE 10 Possible models to explain the regulatory role of Gpb1 in *M. circinelloides* grown under low oxygen growth conditions. The low oxygen levels during the growth of spores generate unknown signal(s) that maintain hyphal growth in the WT strain. (a) Gpb1 is a putative regulator of adenylyl cyclase (AC) activity in *M. circinelloides* under low oxygen conditions. (1) Gpb1 is part of an activated Gβγ heterodimer that intrinsically exerts a direct inhibitory modulation on adenylyl cyclase (Tang & Gilman, 1991). (2) Gpb1 is part of a Gβγ dimer that antagonistically binds to the Gα stimulatory (Gαs) subunit, inhibiting indirectly the AC activity (Mehrabi et al., 2009). (3) Gpb1 is part of a Gβγ dimer that binds to Gα inhibitory (Gαi), the unknown signal release the dimer Gβγ and the Gαi that inhibits the AC activity (Chen, Choi, & Nuss, 1996). All of these scenarios decrease cAMP levels through the inhibition of AC. Lower levels of cAMP do not stimulate the dissociation of the regulatory subunits (PkaR) from the catalytic subunits (PkaC), which finally promotes hyphal morphology with an increased virulent phenotype. (b) In contrast, the lack of Gpb1 or PkaR1 through the disruption of either *gpb1* or *pkaR1* affects cAMP levels and PKA activity. The deletion of *gpb1* would not result in the promotion of formation of the inhibitory Gβγ dimer leading to unrepressed AC or an adequate Gαs Gαi signalling that modulates the AC. Accordingly, it has been described that the incorrect formation of the heterotrimer (in this case by the lack of Gpb1) would lead to impairment of signalling (Landry et al., 2000; Landry & Hoffman, 2001). All these scenarios in the Δ*gpb1* strain would activate AC, increasing cAMP levels and promoting the activation of the PKA pathway. Moreover, the lack of *pkaR1* releases the catalytic subunits (PkaC), activating the PKA pathway. Lack of Gpb1 or PkaR1 results in increased yeast growth under low oxygen levels and a reduced virulence phenotype

in both Δ*gpb1* and Δ*pkaR1* mutants (Figure 9) might be responsible for the increased yeast development during growth under low oxygen conditions (Figure 8), considering that the addition of a cAMP analogue favoured yeast growth in other *Mucor* species (Pereyra, Mizyrycki, & Moreno, 2000; Pereyra, Zaremberg, & Moreno, 1992).

The levels of intracellular cAMP are a result of the combined effect of adenylyl cyclase-modulated synthesis of cAMP and phosphodiesterase-dependent degradation of cAMP. In such a context, it has been demonstrated that physical interaction of Rlα, a mammalian regulatory subunit of the PKA, and RegA, a phosphodiesterase leads to an increase by several folds of the catalytic activity of the latter. Thus, it was concluded that Rlα, a *pkaR1* homologue, is a positive activator of the phosphodiesterase activity of RegA (Moorthy, Gao, & Anand, 2011). Although we do not have a clear cut explanation in *M. circinelloides*, it might be possible that the deletion of *pkaR1* in low oxygen conditions, leads to the decrease of phosphodiesterase catalytic activity of a RegA homologue(s) in *M. circinelloides* contributing the higher cAMP detected in this strain.

Both cAMP levels and hyphal growth have been reported to be positively regulated by Gβ subunits in other fungi, including *F. oxysporum* (Jain, Akiyama, Kan, Ohguchi, & Takata, 2003), *Neurospora crassa* (Yang et al., 2002) and *Mycosphaerella graminicola* (Mehrabi, Barek, Van der Lee, Waalwijk de Wit, & Kema, 2009). However, in *M. circinelloides*, it is likely that Gpb1 negatively regulates the activity of adenylyl cyclase and promotes hyphal growth under low oxygen conditions. Different scenarios could explain the Gpb1-dependent regulation of the PKA pathway in *M. circinelloides* when grown under low oxygen (Figure 10). We are currently trying to determine the other subunits (Gα and Gγ) of the heterotrimeric protein that are interacting with Gpb1 to control the PKA pathway to promote hyphal development under low oxygen, and in consequence regulate the virulence process. Notably, to our understanding, this is the first report of the functional characterisation of a Gβ subunit in an early diverging fungus.

4 | CONCLUSIONS

Gpb1 is functionally associated with PkaR1 and up-regulates virulence and its deletion generates reduced hyphal growth during dimorphic transitions, as well as reduced hyphal growth under low oxygen levels by controlling the cAMP–PKA pathway. Thus, *gpb1* deletion mutants are more prone to develop yeast cells, which are correlated with a non-virulent, less invasive phenotype that results in decreased cellular damage and inflammation in mouse tissue. This study demonstrates the participation of Gpb1 and PkaR1 in the regulation of the yeast–hyphae fate of *M. circinelloides* that could contribute to controlling the infection event.

5 | EXPERIMENTAL PROCEDURES

5.1 | Fungal strain and growth media

The *M. circinelloides* f. *lusitanicus* MU402 strain (*leuA*$^-$, *pyrG*$^-$) (Nicolás, De Haro, Torres-Martínez, & Ruiz-Vázquez, 2007), a uracil and leucine auxotroph derived from the R7B strain, was used as a recipient strain to knock out the *gpb1* gene. The MU636 strain (*leuA*$^-$, *pyrG*$^+$) derived from *M. circinelloides* MU402 was also employed in this work (Navarro-Mendoza et al., 2019). A Δ*pkaR1* strain was provided by Dr. Silvia Rossi from Universidad de Buenos Aires, Argentina (Ocampo et al., 2009) (Table 1). Spores were obtained from cultures of *M. circinelloides* grown on plates with yeast–peptone–glucose (YPG) medium containing 3 g yeast extract, 10 g gelatine peptone, 20 g glucose, supplemented as needed with uracil (200 mg/L) and 15 g of bacteriological agar in 1 L at pH 4.5. Spore harvesting, counting and preservation were carried out as previously reported (Valle-Maldonado, Jácome-Galarza, Gutiérrez-Corona, et al., 2015). Minimal medium casaminoacids (MMC) selective culture medium was used, containing 10 g/L casaminoacids, 20 g/L glucose, 0.5 g/L yeast nitrogen without amino acids (Nicolás et al., 2007), supplemented with uracil (200 mg/L) as needed and 15 g/L of agar when solid media were made.

5.2 | Spore germination and growth quantification in aerobic, self-anaerobic and low oxygen conditions

Aerobic growth was obtained in a 250-ml flask with 25 ml of YPG, inoculated with 5×10^5 spores of *M. circinelloides* per millilitre. Liquid cultures were maintained at 28°C for 24 hr with constant shaking at 160 r.p.m. Anaerobic growth was obtained in 125-ml flasks with 125 ml of YPG medium inoculated with 5×10^5 spores of

TABLE 1 *Mucor circinelloides* strains used in this study

Strain	Genotype	Parental strain	Source
R7B	*leuA*$^-$	*M. circinelloides* f. *lusitanicus* CBS 277.49	Roncero, 1984
MU402	*leuA*$^-$, *pyrG*$^-$	R7B	Nicolás et al., 2007
MU636	*leuA*$^-$, *pyrG*$^+$	MU402	Navarro-Mendoza et al., 2019
Δ*gpb1*	*gpb1*$^-$, *leuA*$^-$, *pyrG*$^+$	MU402	This work
Δ*pkaR1*	*pkaR1*$^-$, *leuA*$^-$, *pyrG*$^+$	MU402	Ocampo et al., 2009
Δ*gpb1* + *gpb1*	*leuA*$^+$, *pyrG*$^+$, *carRP*$^-$	Δ*gpb1*	This work
Δ*gpb1* + *pkaR1*	*leuA*$^+$, *pyrG*$^+$, *carRP*$^-$	Δ*gpb1*	This work

M. circinelloides per mL, as described previously (Salcedo-Hernandez & Ruiz-Herrera, 1993).

It has been described that oxygen levels in the culture media are modulated by changing the revolutions per minute (r.p.m.) during shaking (Somerville & Proctor, 2013). Moreover, we have already described the use of this methodology to generate low oxygen levels in the liquid cultures (Patiño-Medina et al., 2020). Low oxygen levels in the YPG media were achieved by constant shaking at 50 r.p.m. on an orbital incubator, leading to 7.3 ± 0.56% dissolved oxygen, similar oxygen levels are present in the peritoneal cavity (5.3–6.7%) (Renvall & Niinikoski, 1980) or in the intestinal tissues (7.6%) (Carreau, El Hafny-Rahbi, Matejuk, Grillon, & Kieda, 2011; Ortiz-Prado, Dunn, Vasconez, Castillo, & Viscor, 2019), these anatomical areas in where the spores were inoculated in the mice. Meanwhile, 160 r.p.m. led to approximately 14.4 ± 1.2% dissolved oxygen. Oxygen levels were determined using an oximeter (HI9146; Hanna Instruments Ltd., Leighton Buzzard, UK). Germination percentage was calculated for all conditions, as hyphal cells or budding yeasts counted in 100 cells total.

To determine dry weight, mycelia and yeast cells were collected from liquid cultures by filtration, washed twice with distilled H_2O and dried in pre-weighed filter papers (Whatman No. 5). Filters were dried for 96 hr at 80°C and, after cooling, the dry weight of the cells was determined.

5.3 | Dimorphic transitions: Yeast-to-hyphae and hyphae-to-yeast

Yeast and hyphal cells were obtained from *M. circinelloides* anaerobic and aerobic cultures, respectively, and were utilised for morphogenetic transition experiments, as previously described (De la Cruz et al., 2007).

Briefly, transitions were obtained as follows: for hyphae-to-yeast, spores were initially grown aerobically for 5 hr, after that, filtrated cells were inoculated into fresh culture medium and were grown anaerobically for 3 hr as described previously (De la Cruz et al., 2007). For yeast-to-hyphae transition, spores were initially grown anaerobically for 10 hr to enforce yeast growth followed by collection filter through and inoculation into new culture medium, which were grown aerobically for 3 hr. All growth conditions employed YPG medium at constant temperature (28°C).

5.4 | Spore production and radial growth

To produce spores, YPG media supplemented with uracil were inoculated with each strain (50 spores). The plates were incubated for 6 days at 28°C in the presence of light and then spores were harvested and counted using a hematocytometer chamber.

The radial growth of *M. circinelloides* was monitored by inoculating 50 spores on the centre of YPG plates supplemented with uracil and the colony diameter was measured daily over 6 days.

5.5 | Total RNA and genomic DNA isolation

Biological samples from *M. circinelloides*, mouse tissues and macrophages were used to isolate total RNA and genomic DNA using an RNAeasy mini kit and a QIAamp DNA Mini Kit respectively (Qiagen, Venlo, Netherlands).

Biomass of *M. circinelloides* was collected at indicated times after aerobic or anaerobic growth and filtered through filter paper (Whatman No 6, Sigma-Aldrich, St. Louis, MO) and washed with sterile distilled water. Secondly, approximately 30 mg of mycelia samples were transferred into a tube of MagNA Lyser Green Beads (Roche Life Science, Penzberg, Germany) pre-cooled on ice. Seven hundred microlitres of the denaturing RLT buffer from RNeasy Mini Kit (Qiagen, Venlo, Netherlands) were added immediately before homogenization. The cell disruption was performed in the MagNA Lyser Instrument (Roche Life Science, Penzberg, Germany), as described previously (Valle-Maldonado, Jácome-Galarza, Gutiérrez-Corona, et al., 2015). For DNA extraction, the samples were treated with RNAse A (Roche Life Science, Penzberg, Germany). Purity of the extracted DNA and RNA from samples was confirmed using agarose gels and spectrophotometer.

5.6 | Quantitative reverse transcription polymerase chain reaction (qRT-PCR)

Primers and hydrolysis probes for *gpb1* to *gpb3*, *tfc-1*, *adh1*, *pkaR1* are described previously (Valle-Maldonado, Jácome-Galarza, Díaz-Pérez, et al., 2015; Valle-Maldonado, Jácome-Galarza, Gutiérrez-Corona, et al., 2015). The *tfc-1* gene a previously validated control gene that encodes for a subunit of the transcription factor TFIIIC, was used for qRT-PCR normalisation (Valle-Maldonado, Jácome-Galarza, Gutiérrez-Corona, et al., 2015). We also analysed the expression of *IL-1β*, *IL-6*, *TNF-α*, *BIP* and *β-act* (internal control) from *Mus musculus* (Díaz-Pérez et al., 2020; Patiño-Medina et al., 2019). The reactions of qRT-PCR were performed as described previously (Valle-Maldonado, Jácome-Galarza, Díaz-Pérez, et al., 2015). *gpb1-gpb3* mRNA levels from MU402 strain were quantified using a ΔΔCt (Figure 1) analysis, as well as the *gpa*, *gpb* and *gpg* genes mRNA levels using the previous raw data from R7B strain (Figure S1) already reported (Valle-Maldonado, Jácome-Galarza, Díaz-Pérez, et al., 2015).

5.7 | Targeted deletion of *gpb1* from *M. circinelloides*

The *gpb1* 5′ and 3′ upstream regions were coupled with the *pyrG* selection gene using an overlap-PCR approach. In this process, three PCR fragments containing overlapping sequences between *gpb1* and *pyrG* were PCR-amplified using the following oligonucleotides (Table S1): gpb1-pUFwd and gpb1-pURev-pyrG, which amplified 1-kb from the 5′ upstream region of the start translation codon of *gpb1*;

and oligonucleotides gpb1-pDRev and gpb1-pDFwd-pyrG, which amplified 1-kb from the 3′ downstream region of the stop translation codon of *gpb1*. In oligonucleotide gpb1-pURev-pyrG, an added nucleotide sequence at the 3′ end hybridised to the 5′ ends of *pyrG*; and in oligonucleotide gpb1-pDFwd-pyrG, an added nucleotide sequence at its 5′ end hybridised to the 3′ end of *pyrG*. The gene *pyrG* was PCR-amplified using the oligonucleotides PyrG-Sac-Fwd and PyrG-Sac-Rev, with pMAT1700 as a template. Three individual PCR reactions were performed to obtain three DNA fragments. The *gpb1* 5′ region, *pyrG* (2 kb), and the *gpb1* 3′ region, which were all purified by agarose gels. Overlapping PCR was performed using 100 L of each template; 10 μM each of the oligonucleotides gpb1-pUFwd and gpb1-pDRev and 1 μl of Herculase II Fusion Enzyme (Agilent Technologies), at a molar ratio of 1:2:1, were used to generate the replacement fragment for *gpb1*.

Protoplasts obtained from germlings of the MU402 strain were transformed with the replacement DNA fragments (3 μg/transformation) according to a previously described protocol (Gutiérrez, López-García, & Garre, 2011). Transformants were obtained under selective conditions on MMC agar plates lacking uracil for single deletion mutants or YNB agar plates lacking uracil and leucine for the double mutants. Monosporic cultures were obtained after five cycles of sporulation in either selective medium or rich medium, at which point, 100% of the spores could grow on the selective medium, indicating the transformation of all nuclei.

5.8 | Molecular identification of *gpb1* mutant strains from *M. circinelloides*

5.8.1 | PCR and southern blot confirmation of *gpb1* gene deletion

Transformants with homologous recombination of the *gpb1* locus with the *pyrG* marker were selected PCR using the oligonucleotides gpb1-C-Fwd (forward) and pyrG-R2 (reverse) (Table S1) that hybridise in the selectable marker sequence to determine a homologous integration event; a positive recombination event was determined by PCR amplification of 1.12-kb band. A lack of amplification band indicated the WT genotype (Figure S2).

Additionally, a total of 1 μg of genomic DNA from MU402 and the transformants were digested with *Hin*cII. DNA was separated by electrophoresis and transferred to nylon membranes (HybondTM-N+, Amersham Biosciences, UK) following the recommended protocol. Southern blot hybridization was performed under stringent conditions. DNA probes were labelled with [α-^{32}P] dCTP using Ready-To-Go Labelling Beads (GE Healthcare Life Science), and they were prepared as follows: it was added 1 μl of Gene Ruler DNA Ladder Mix, 50 ng of DNA probe (1 kb) that was directly amplified from genomic DNA from *M. circinelloides* using the primer pairs that amplified the 5′ upstream region UTR of the start translation codon from *gpb1*, 2 μl of hexanucleotide mixture and double distilled water to complete a total volume of 6 μl.

5.9 | Construction of Δ*gpb1* complemented with the *gpb1* and *pkaR1* overexpressed strains

The complemented Δ*gpb1* + *gpb1* and Δ*gpb1* + *pkaR1* strains (*pyrG*$^+$, *leuA*$^+$, *carRP*$^-$) were obtained by integrative transformation with the *gpb1* or *pkaR1* WT allele at the *carRP* gene locus of the Δ*gpb1* (*pyrG*$^+$, *leuA*$^-$, *carRP*$^+$) strains (Figure S3). The *carRP* gene encodes a lycopene cyclase that catalyses the transformation of lycopene to beta-carotene. Beta-carotene is a yellow–orange pigment responsible for the yellowish colouration of this fungus. As a result of silencing the *carRP* gene, the complemented strains had albino colonies instead of the yellowish colonies of the MU402 or Δ*gpb1* strains. The transformation fragments included about 1.1 kb upstream of the start of the *carRP* gene open reading frame (ORF) and approximately 1.1 kb downstream of the stop codon. The vector plasmid employed was pMAT1476 (Rodríguez-Frómeta, Gutiérrez, Torres-Martínez, & Garre, 2013). These two fragments border the *leuA* (4.4 kb) and *gpb1* (2.5 kb) or *pkaR1* (2.5 kb) genes. The *gpb1* gene is under the regulation of its native promoter and terminator sequences in Δ*gpb1* + *gpb1* strain and is under the regulation of promoter pZRT in MU402 + *gpb1*; the *pkaR1* gene is under the regulation of promoter pZRT, used previously (Rodríguez-Frómeta et al., 2013), in both strains. The size of these transformation fragments is around 6.6 kb for the *pyrG* fragments and 9 kb for the *leuA* fragments (Figure S3). For selection, spores from individual colonies from the MMC or YNB minimal media were transferred after 5 days onto new minimal medium agar plates at 28°C and used for subsequent sporulation cycles until homokaryotic albino colonies were observed.

5.10 | Promoter analysis of G beta subunit-encoding genes from *M. circinelloides*

A typical fungal length promoter covers around 600–1000 bp (Haverty, Hansen, & Weng, 2004; Liu & Ringnér, 2007; Patil, Li, & Walter, 2004). Consequently, we searched for transcription factors in the promoter regions (1 kb upstream of ATG start codon), of the *gpb1*, *gpb2* and *gpb3* in *M. circinelloides*. We employed the Search Transcription Factor tool using the TF database of *S. cerevisiae* (http://www.yeastract.com/formfindregulators.php).

5.11 | Ethics statement

The mouse virulence model protocol was carried out following the recommendations of the Mexican Federal Regulations for the Use and Care of Laboratory Animals (approval no. NOM-062-ZOO-1999; Especificaciones técnicas para la producción, cuidado y uso de los animales de laboratorio/Technical specifications for production, use and care of laboratory animals) (SAGARPA, 2001). The Internal Biosecurity and Bioethics Committee of Instituto de Investigaciones Químico Biológicas de la Universidad Michoacana de San Nicolás de Hidalgo first reviewed the experimental protocols and then approved them (trade number 06-13/2016).

5.12 | Mouse-killing assays

Spore virulence of this fungus was assessed in mice as described previously (Rodríguez-Andrade et al., 2016), with minor modifications. Briefly, male BALB/c mice (12–16 weeks old, weighing approximately 20 g) were treated with streptozotocin (200 mg/kg; Sigma) to induce a diabetic state (≥ 250 mg/dl glucose). Each group of mice (n = 6 mice each) was inoculated with 2×10^7 spores from each mutant strains along with the WT by intraperitoneal injection.

5.13 | Macrophages spore killing assay

Mouse RAW 267.4 monocytes/macrophages (TIB-71) were purchased from American Type Culture Collection (Manassas, VA). Cells were maintained in Dulbecco's modified Eagle's medium (DMEM; Sigma-Aldrich St. Louis, MO) supplemented with 10% fetal bovine serum (Sigma-Aldrich, St. Louis, MO), 100 U/ml penicillin, and 100 μg/ml streptomycin (basal medium) at 37°C in an atmosphere containing 5% CO_2 for 24 hr before treatment.

Macrophages were seeded at 8×10^5 cells/well in DMEM basal medium without antibiotics and incubated at 37°C in six-well plates. After incubation ovemight, the basal medium in each well was replaced with fresh medium, and the macrophages were then co-cultured with 2×10^5 spores from *Mucor circinelloides* in DMEM medium for 6 hr. Immediately after, the macrophage and spore pellets were recovered by centrifugation at 2000 × *g* for 5 min and resuspended in 0.1 ml of sterile distillate water and separated into two tubes with 0.05 ml each. One of the tubes was frozen and used until nucleic acid extraction was done. Meanwhile, the other tube was diluted (1:50) and used to plate 200 of the initial spores in order to evaluate CFU on YPG solid medium. For the CFU assay, the control was the spores in DMEM basal medium without macrophage interaction. The CFU were quantified 24 hr after incubation in the presence of light at 28°C.

5.14 | Image analysis

An Olympus CKX41 microscope equipped with a 40× objective lens and a DMC-T25 camera (Panasonic, Kadoma, Japan) was used to capture images of spores or spore germination. Hyphal lengths and spore sizes were determined using QCapture Pro 7 and Leica Application Suite software.

5.15 | Quantification of intracellular cAMP levels and protein kinase A activity

Spores from the MU636, Δ*gpb1*, Δ*pkaR1*, Δ*gpb1* + *gpb1* or Δ*gpb1* + *pkaR1* strains were inoculated into YPG media and incubated with constant shaking (50 r.p.m.) for 8 hr. Biological samples obtained under these conditions were used in either cAMP or PKA measurements.

Cells intended for cAMP measurements were separated from media and frozen in liquid nitrogen. Upon nitrogen evaporation, 60 mg of cells were weighed and resuspended in 1 ml of 0.1 M HCl, and 250 μl of glass beads (0.1 mm) (BioSpec Products, Inc., Bartlesville, OK) were added. Samples were homogenised by three pulses at full speed for 30 s with 1 min incubation on ice intermittently in a bead beater (Model 607; BioSpec Products, Inc.). The supernatants were measured for cAMP using the Direct cAMP ELISA kit (Enzo Life Science, San Diego, CA). Protocols were followed according to the manufacturer's instructions. The optical density was measured at 405 nm on a microplate reader (Bio-Rad Benchmark; Bio-Rad Laboratories, Hercules, CA).

5.15.1 | PKA activity

We obtained crude protein extract (0.5 μg) from each sample, and PKA-specific kinase activity was quantified by using the PKA Colorimetric Activity Kit (Invitrogen, Carlsbad, CA) as described previously (Lee et al., 2013).

5.16 | Statistical analysis

All the data were evaluated by analysis of variance (ANOVA, statistically significant differences ($\alpha \leq .05$) shown in letters. Fisher's exact test was used for analysis.

ACKNOWLEDGMENTS

We would like to thank to SEP-CONACYT for the grant (CB-2011-01-167071) for partially funding this project and CIC/ UMSNH for the grant 2.36, grants. MIV-M, JA P-M and NY R-M were postgraduate students with a CONACyT scholarship. S C-L was supported in part by a Young Investigator Pilot Award in the Max and Minnie Tomerlin Voelcker Foundation.

CONFLICT OF INTEREST

The authors declare that they have no conflict of interest.

AUTHOR CONTRIBUTIONS

Marco I. Valle-Maldonado, J. Alberto Patiño-Medina, Carlos Pérez-Arqués, Nancy Y. Reyes-Mares, Rafael Ortiz-Alvarado, Sandeep Vellanki, Martha I. Ramirez-Diaz—data acquisition, analysis and data interpretation; Martha I. Ramirez-Diaz, Soo C. Lee, Victoriano Garre—reagents, analysis; Martha I. Ramirez-Diaz, Soo C. Lee and Victoriano Garre—critical analysis, data interpretation and critical revision of the article for intellectual content; Victor Meza-Carmen—conception and design of the work, data analysis and interpretation and drafting of the article with important contribution from Soo C. Lee and Victoriano Garre.

ORCID

Víctor Meza-Carmen https://orcid.org/0000-0003-2838-7211

REFERENCES

Baldin, C., & Ibrahim, A. S. (2017). Molecular mechanisms of mucormycosis-the bitter and the sweet. *PLoS Pathogens*, *13*(8), e1006408. https://doi.org/10.1371/journal.ppat.1006408

Brand, A. (2012). Hyphal growth in human fungal pathogens and its role in virulence. *International Journal of Microbiology*, *2012*, 517529. https://doi.org/10.1155/2012/517529

Brand, A., & Gow, N. A. (2009). Mechanisms of hypha orientation of fungi. *Current Opinion in Microbiology*, *12*(4), 350–357. https://doi.org/10.1016/j.mib.2009.05.007

Carreau, A., El Hafny-Rahbi, B., Matejuk, A., Grillon, C., & Kieda, C. (2011). Why is the partial oxygen pressure of human tissues a crucial parameter? Small molecules and hypoxia. *Journal of Cellular and Molecular Medicine*, *15*(6), 1239–1253. https://doi.org/10.1111/j.1582-4934.2011.01258.x

Chen, B., Gao, S., Choi, G. H., & Nuss, D. L. (1996). Extensive alteration of fungal gene transcript accumulation and elevation of G-protein-regulated cAMP levels by a virulence-attenuating hypovirus. *Proceedings of the National Academy of Sciences of the USA*, *93*(15), 7996–8000. https://doi.org/10.1073/pnas.93.15.7996

Choi, J., Jung, W. H., & Kronstad, J. W. (2015). The cAMP/protein kinase A signaling pathway in pathogenic basidiomycete fungi: Connections with iron homeostasis. *Journal of Microbiology (Seoul, Korea)*, *53*(9), 579–587. https://doi.org/10.1007/s12275-015-5247-5

Corrochano, L. M., & Garre, V. (2010). Photobiology in the Zygomycota: Multiple photoreceptor genes for complex responses to light. *Fungal Genetics and Biology: FG & B*, *47*(11), 893–899. https://doi.org/10.1016/j.fgb.2010.04.007

Corrochano, L. M., Kuo, A., Marcet-Houben, M., Polaino, S., Salamov, A., Villalobos-Escobedo, J. M., … Grigoriev, I. V. (2016). Expansion of signal transduction pathways in fungi by extensive genome duplication. *Current Biology*, *26*(12), 1577–1584. https://doi.org/10.1016/j.cub.2016.04.038

Da Silva Dantas, A., Lee, K. K., Raziunaite, I., Schaefer, K., Wagener, J., Yadav, B., & Gow, N. A. (2016). Cell biology of *Candida albicans*-host interactions. *Current Opinion in Microbiology*, *34*, 111–118. https://doi.org/10.1016/j.mib.2016.08.006

De la Cruz, J. O., García-Soto, J., Uriostegui, C., Carranza, L., Novoa, G., Reyna, G., & Martínez-Cadena, G. (2007). Differential expression of Rho1GTPase and Rho3GTPase during isotropic and polarized growth of *Mucor circinelloides*. *Canadian Journal of Microbiology*, *53*(2), 168–176. https://doi.org/10.1139/w06-128

Delgado-Jarana, J., Martínez-Rocha, A. L., Roldán-Rodríguez, R., Roncero, M. I., & Di Pietro, A. (2005). *Fusarium oxysporum* G-protein beta subunit Fgb1 regulates hyphal growth, development, and virulence through multiple signalling pathways. *Fungal Genetics and Biology: FG & B*, *42*(1), 61–72. https://doi.org/10.1016/j.fgb.2004.10.001

Demuyser, L., Van Genechten, W., Mizuno, H., Colombo, S., & Van Dijck, P. (2018). Introducing fluorescence resonance energy transfer-based biosensors for the analysis of cAMP-PKA signalling in the fungal pathogen *Candida glabrata*. *Cellular Microbiology*, *20*(10), e12863. https://doi.org/10.1111/cmi.12863

Díaz-Pérez, S. P., Patiño-Medina, J. A., Valle-Maldonado, M. I., Lopez-Torres, A., Jácome-Galarza, I. E., Anaya-Martínez, V., … Meza-Carmen, V. (2020). Alteration of fermentative metabolism enhances *Mucor circinelloides* virulence. *Infection and Immunity*, *88*(2), e00434–e00419. https://doi.org/10.1128/IAI.00434-19

Dignard, D., André, D., & Whiteway, M. (2008). Heterotrimeric G-protein subunit function in *Candida albicans*: Both the alpha and beta subunits of the pheromone response G protein are required for mating. *Eukaryotic Cell*, *7*(9), 1591–1599. https://doi.org/10.1128/EC.00077-08

Dizbay, M., Adisen, E., Kustimur, S., Sari, N., Cengiz, B., Yalcin, B., … Sugita, T. (2009). Fungemia and cutaneous zygomycosis due to *Mucor circinelloides* in an intensive care unit patient: Case report and review of literature. *Japan Journal of Infectious Diseases*, *62*(2), 146–148.

Fuller, K. K., & Rhodes, J. C. (2012). Protein kinase A and fungal virulence: A sinister side to a conserved nutrient sensing pathway. *Virulence*, *3*(2), 109–121. https://doi.org/10.4161/viru.19396

Ganem, S., Lu, S. W., Lee, B. N., Chou, D. Y., Hadar, R., Turgeon, B. G., & Horwitz, B. A. (2004). G-protein beta subunit of *Cochliobolus heterostrophus* involved in virulence, asexual and sexual reproductive ability, and morphogenesis. *Eukaryotic Cell*, *3*(6), 1653–1663. https://doi.org/10.1128/EC.3.6.1653-1663.2004

Grahl, N., Shepardson, K. M., Chung, D., & Cramer, R. A. (2012). Hypoxia and fungal pathogenesis: To air or not to air? *Eukaryotic Cell*, *11*(5), 560–570. https://doi.org/10.1128/EC.00031-12

Gummer, J. P., Trengove, R. D., Oliver, R. P., & Solomon, P. S. (2012). A comparative analysis of the heterotrimeric G-protein Gα, Gβ and Gγ subunits in the wheat pathogen *Stagonospora nodorum*. *BMC Microbiology*, *12*, 131. https://doi.org/10.1186/1471-2180-12-131

Gunner, H. B., & Alexander, M. (1964). Anaerobic growth of *Fusarium oxysporum*. *Journal of Bacteriology*, *87*, 1309–1316.

Guo, L., Yang, L., Liang, C., Wang, J., Liu, L., & Huang, J. (2016). The G-protein subunits FGA2 and FGB1 play distinct roles in development and pathogenicity in the banana fungal pathon *Fusarium oxysporum* f. sp. cubense. *Physiological and Molecular Plant Pathology*, *93*, 29–38. https://doi.org/10.1016/j.pmpp.2015.12.003

Gutiérrez, A., López-García, S., & Garre, V. (2011). High reliability transformation of the basal fungus *Mucor circinelloides* by electroporation. *Journal of Microbiological Methods*, *84*, 442–446. https://doi.org/10.1016/j.mimet.2011.01.002

Hall, L. A., & Denning, D. W. (1994). Oxygen requirements of *Aspergillus* species. *Journal of Medical Microbiology*, *41*(5), 311–315. https://doi.org/10.1099/00222615-41-5-311

Haverty, P. M., Hansen, U., & Weng, Z. (2004). Computational inference of transcriptional regulatory networks from expression profiling and transcription factor binding site identification. *Nucleic Acids Research*, *32*(1), 179–188. https://doi.org/10.1093/nar/gkh183

Heise, B., Van Der Felden, J., Kern, S., Malcher, M., Brückner, S., & Mösch, H. U. (2010). The TEA transcription factor Tec1 confers promoter-specific gene regulation by Ste12-dependent and -independent mechanisms. *Eukaryotic Cell*, *9*(4), 514–531. https://doi.org/10.1128/EC.00251-09

Hwang, J. J., Chambon, P., & Davidson, I. (1993). Characterization of the transcription activation function and the DNA binding domain of transcriptional enhancer factor-1. *The EMBO Journal*, *12*(6), 2337–2348.

Jackson, M. A. (2012). Dissolved oxygen levels affect dimorphic growth by the entomopathogenic fungus *Isaria fumosorosea*. *Biocontrol Science and Technology*, *22*(1), 67–79. https://doi.org/10.1080/09583157.2011.642339

Jain, S., Akiyama, K., Kan, T., Ohguchi, T., & Takata, R. (2003). The G protein beta subunit FGB1 regulates development and pathogenicity in *Fusarium oxysporum*. *Current Genetics*, *43*(2), 79–86. https://doi.org/10.1007/s00294-003-0372-9

Kaneko, I., Iyama-Kadono, M., Togashi-Nishigata, K., Yamaguchi, I., Teraoka, T., & Arie, T. (2013). Heterotrimeric G protein β subunit GPB1 and MAP kinase MPK1 regulate hyphal growth and female fertility in *Fusarium sacchari*. *Mycoscience*, *54*(2), 148–157. https://doi.org/10.1016/j.myc.2012.09.008

Kasahara, S., & Nuss, D. L. (1997). Targeted disruption of a fungal G-protein beta subunit gene results in increased vegetative growth but reduced virulence. *Molecular Plant-Microbe Interactions*, *10*(8), 984–993. https://doi.org/10.1094/MPMI.1997.10.8.984

Khan, M. A. K., Yang, J., Hussain, S. A., Zhang, H., Garre, V., & Song, Y. (2019). Genetic modification of *Mucor circinelloides* to construct stearidonic acid producing cell factory. *International Journal of Molecular Sciences*, *20*(7), e1683. https://doi.org/10.3390/ijms20071683

Khan, Z. U., Ahmad, S., Brazda, A., & Chandy, R. (2009). *Mucor circinelloides* as a cause of invasive maxillofacial zygomycosis: An emerging dimorphic pathogen with reduced susceptibility to posaconazole. *Journal of Clinical Microbiology*, *47*(4), 1244–1248. https://doi.org/10.1128/JCM.02030-08

Kozubowski, L., Lee, S. C., & Heitman, J. (2009). Signalling pathways in the pathogenesis of *Cryptococcus*. *Cellular Microbiology*, *11*(3), 370–380. https://doi.org/10.1111/j.1462-5822.2008.01273.x

Kubo, H., & Mihara, H. (2007). cAMP promotes hyphal branching in *Mucor globosus*. *Mycoscience*, *48*(3), 187–188. https://doi.org/10.1007/S10267-007-0348-6

Landry, S., & Hoffman, C. S. (2001). The git5 Gbeta and git11 Ggamma form an atypical Gbetagamma dimer acting in the fission yeast glucose/cAMP pathway. *Genetics*, *157*(3), 1159–1168.

Landry, S., Pettit, M. T., Apolinario, E., & Hoffman, C. S. (2000). The fission yeast git5 gene encodes a Gbeta subunit required for glucose-triggered adenylate cyclase activation. *Genetics*, *154*(4), 1463–1471.

Lee, S. C., Li, A., Calo, S., & Heitman, J. (2013). Calcineurin plays key roles in the dimorphic transition and virulence of the human pathogenic zygomycete *Mucor circinelloides*. *PLoS Pathogens*, *9*(9), e1003625. https://doi.org/10.1371/journal.ppat.1003625

Li, L., He, L., Lai, Y., Shao, Y., & Chen, F. (2014). Cloning and functional analysis of the Gβ gene Mgb1 and the Gγ gene Mgg1 in *Monascus ruber*. *Journal of Microbiology (Seoul, Korea)*, *52*(1), 35–43. https://doi.org/10.1007/s12275-014-3072-x

Li, L., Wright, S. J., Krystofova, S., Park, G., & Borkovich, K. A. (2007). Heterotrimeric G protein signaling in filamentous fungi. *Annual Review of Microbiology*, *61*, 423–452. https://doi.org/10.1146/annurev.micro.61.080706.093432

Lin, X., Alspaugh, J. A., Liu, H., & Harris, S. (2015). Fungal morphogenesis. *Cold Spring Harbor Perspectives in Medicine*, *5*(2), a019679. https://doi.org/10.1101/cshperspect.a019679

Liu, Y., & Ringnér, M. (2007). Revealing signaling pathway deregulation by using gene expression signatures and regulatory motif analysis. *Genome Biology*, *8*(5), R77. https://doi.org/10.1186/gb-2007-8-5-r77

Liu, Y., Yang, K., Qin, Q., Lin, G., Hu, T., Xu, Z., & Wang, S. (2016). G protein α subunit GpaB is required for asexual development, aflatoxin biosynthesis and pathogenicity by regulating cAMP signaling in *Aspergillus flavus*. *Toxins (Basel)*, *10*(3), e117. https://doi.org/10.3390/toxins10030117

López-Fernández, L., Sanchis, M., Navarro-Rodríguez, P., Nicolás, F. E., Silva-Franco, F., Guarro, J., … Capilla, J. (2018). Understanding *Mucor circinelloides* pathogenesis by comparative genomics and phenotypical studies. *Virulence*, *9*(1), 707–720. https://doi.org/10.1080/21505594.2018.1435249

López-Muñoz, A., Nicolás, F. E., García-Moreno, D., Pérez-Oliva, A. B., Navarro-Mendoza, M. I., Hernández-Oñate, M. A., … Mulero, V. (2018). An adult zebrafish model reveals that Mucormycosis induces apoptosis of infected macrophages. *Scientific Reports*, *8*(1), 12802. https://doi.org/10.1038/s41598-018-30754-6

Lübbehüsen, T. L., Nielsen, J., & McIntyre, M. (2003). Characterization of the *Mucor circinelloides* life cycle by on-line image analysis. *Journal of Applied Microbiology*, *95*(5), 1152–1160. https://doi.org/10.1046/j.1365-2672.2003.02098.x

McIntyre, M., Breum, J., Arnau, J., & Nielsen, J. (2002). Growth physiology and dimorphism of *Mucor circinelloides* (syn. racemosus) during submerged batch cultivation. *Applied Microbiology and Biotechnology*, *58*(4), 495–502. https://doi.org/10.1007/s00253-001-0916-1

Mehrabi, R., M'Barek, S. B., Van der Lee, T., Waalwijk de Wit, P., & Kema, G. (2009). Gα and Gβ proteins regulate the cyclic AMP pathway that is required for development and pathogenicity of the phytopathogen *Mycosphaerella graminicola*. *Eukaryotic Cell*, *8*(7), 1001–1013.

Moorthy, B. S., Gao, Y., & Anand, G. S. (2011). Phosphodiesterases catalyze hydrolysis of cAMP-bound to regulatory subunit of protein kinase a and mediate signal termination. *Molecular & Cellular Proteomics*, *10*(2), M110.002295. https://doi.org/10.1074/mcp.M110.002295

Morin-Sardin, S., Nodet, P., Coton, E., & Jany, J. L. (2017). Mucor: A Janus-faced fungal genus with human health impact and industrial applications. *Fungal Biology Reviews*, *31*(1), 12–32. https://doi.org/10.1016/j.fbr.2016.11.002

Muller, P., Leibbrandt, A., Teunissen, H., Cubasch, S., Aichinger, C., & Kahmann, R. (2004). The Gbeta-subunit-encoding gene bpp1 controls cyclic-AMP signaling in *Ustilago maydis*. *Eukaryotic Cell*, *3*(3), 806–814. https://doi.org/10.1128/EC.3.3.806-814.2004

Nagy, G., Szebenyi, C., Csernetics, Á., Vaz, A. G., Tóth, E. J., Vágvölgyi, C., & Papp, T. (2017). Development of a plasmid free CRISPR-Cas9 system for the genetic modification of *Mucor circinelloides*. *Scientific Reports*, *7*(1), 16800. https://doi.org/10.1038/s41598-017-17118-2

Navarro-Mendoza, M. I., Pérez-Arqués, C., Pachal, S., Nicolás, F. E., Mondo, S. J., Ganguly, P., … Garre, V. (2019). Early diverging fungus *Mucor circinelloides* lacks centromeric histone CENP-A and displays a mosaic of point and regional centromeres. *Current Biology*, *29*(22), 3791–3802. https://doi.org/10.1016/j.cub.2019.09.024

Navarro-Olmos, R., Kawasaki, L., Domínguez-Ramírez, L., Ongay-Larios, L., Pérez-Molina, R., & Coria, R. (2010). The β subunit of the heterotrimeric G protein triggers the Kluyveromyces lactis pheromone response pathway in the absence of the γ Subunit. *Molecular Biology of the Cell*, *21*(3), 489–498. https://doi.org/10.1091/mbc.E09-06-0472

Nicolás, F. E., De Haro, J. P., Torres-Martínez, S., & Ruiz-Vázquez, R. M. (2007). Mutants defective in a *Mucor circinelloides* dicer-like gene are not compromised in siRNA silencing but display developmental defects. *Fungal Genetics and Biology: FG & B*, *44*(6), 504–516. https://doi.org/10.1016/j.fgb.2006.09.003

Nicolás, F. E., & Garre, V. (2016). RNA interference in fungi: Retention and loss. *Microbiology Spectrum*, *4*(6). https://doi.org/10.1128/microbiolspec.FUNK-0008-2016

Nicolás, F. E., Navarro-Mendoza, M. I., Pérez-Arques, C., López-García, S., Navarro, E., Torres-Martínez, S., & Garre, V. (2018). Molecular tools for carotenogenesis analysis in the mucoral Mucor circinelloides. *Methods in Molecular Biology (Clifton, N.J.)*, *1852*, 221–237. https://doi.org/10.1007/978-1-4939-8742-9_13

Nishimura, M., Park, G., & Xu, J. R. (2003). The G-beta subunit MGB1 is involved in regulating multiple steps of infection-related morphogenesis in *Magnaporthe grisea*. *Molecular Microbiology*, *50*(1), 231–243. https://doi.org/10.1046/j.1365-2958.2003.03676.x

Ocampo, J., Fernandez-Nuñez, L., Silva, F., Pereyra, E., Moreno, S., Garre, V., & Rossi, S. (2009). A subunit of protein kinase A regulates growth and differentiation in the fungus *Mucor circinelloides*. *Eukaryotic Cell*, *8*(7), 933–944. https://doi.org/10.1128/EC.00026-09

Orlowski, M. (1991). *Mucor* dimorphism. *Microbiological Reviews*, *55*(2), 234–258.

Ortiz-Prado, E., Dunn, J. F., Vasconez, J., Castillo, D., & Viscor, G. (2019). Partial pressure of oxygen in the human body: A general review. *American Journal of Blood Research*, *9*(1), 1–14.

Pan, X., Harashima, T., & Heitman, J. (2000). Signal transduction cascades regulating pseudohyphal differentiation of *Saccharomyces cerevisiae*. *Current Opinion in Microbiology*, *3*(6), 567–572. https://doi.org/10.1016/S1369-5274(00)00142-9

Patil, C. K., Li, H., & Walter, P. (2004). Gcn4p and novel upstream activating sequences regulate targets of the unfolded protein response. *PLoS Biology*, *2*(8), e246. https://doi.org/10.1371/journal.pbio.0020246

Patiño-Medina, J. A., Maldonado-Herrera, G., Pérez-Arques, C., Alejandre-Castañeda, V., Reyes-Mares, N. Y., Valle-Maldonado, M. I., … Meza-Carmen, V. (2018). Control of morphology and virulence by ADP-ribosylation factors (Arf) in *Mucor circinelloides*. *Current Genetics*, *64*(4), 853–869. https://doi.org/10.1007/s00294-017-0798-0

Patiño-Medina, J. A., Valle-Maldonado, M. I., Maldonado-Herrera, G., Pérez-Arques, C., Jácome-Galarza, I. E., Díaz-Pérez, C., … Meza-

Carmen, V. (2019). Role of Arf-like proteins (Arl1 and Arl2) of *Mucor circinelloides* in virulence and antifungal susceptibility. *Fungal Genetics and Biology: FG & B*, *129*, 40–51. https://doi.org/10.1016/j.fgb.2019.04.011

Patiño-Medina, J. A., Valle-Maldonado, M. I., Vargas-Tejeda, D., Chávez-Jacobo, V. M., Corrales-Escobosa, A. R., Ramírez-Emiliano, J., … Meza-Carmen, V. (2020). Arf-like proteins (Arl1 and Arl2) are involved in mitochondrial homeostasis in *Mucor circinelloides*. *Fungal Biology*, *124*(7), 619–628. https://doi.org/10.1016/j.funbio.2020.02.016

Patiño-Medina, J. A., Vargas-Tejeda, D., Valle-Maldonado, M. I., Alejandre-Castañeda, V., Jácome-Galarza, I. E., Villegas-Moreno, J., … Meza-Carmen, V. (2019). Sporulation on blood serum increases the virulence of *Mucor circinelloides*. *Microbial Pathogenesis*, *137*, 103737. https://doi.org/10.1016/j.micpath.2019.103737

Pereyra, E., Mizyrycki, C., & Moreno, S. (2000). Threshold level of protein kinase A activity and polarized growth in *Mucor rouxii*. *Microbiology (Reading, England)*, *146*(8), 1949–1958. https://doi.org/10.1099/00221287-146-8-1949

Pereyra, E., Zaremberg, V., & Moreno, S. (1992). Effect of dibutyryl-cAMP on growth and morphology of germinating *Mucor rouxii* sporangiospores. *Experimental Mycology*, *16*(2), 93–101. https://doi.org/10.1016/0147-5975(92)90015-J

Rangel-Porras, R. A., Díaz-Pérez, S. P., Mendoza-Hernández, J. M., Romo-Rodríguez, P., Alejandre-Castañeda, V., Valle-Maldonado, M. I., … Gutiérrez-Corona, J. F. (2019). Alcohol dehydrogenase 1 participates in the Crabtree effect and connects fermentative and oxidative metabolism in the Zygomycete *Mucor circinelloides*. *Journal of Microbiology (Seoul, Korea)*, *57*(7), 606–617. https://doi.org/10.1007/s12275-019-8680-z

Renvall, S., & Niinikoski, J. (1980). Kinetics of oxygen in peritoneal cavity. Effects of chemical peritonitis and intraperitoneally administered colloids in rats. *The Journal of Surgical Research*, *28*(2), 132–139. https://doi.org/10.1016/10.1016/0022-4804(80)90156-0

Rodrigues Reis, C. E., Bento, H. B. S., Carvalho, A. K. F., Rajendran, A., Hu, B., & De Castro, H. F. (2019). Critical applications of *Mucor circinelloides* within a biorefinery context. *Critical Reviews in Biotechnology*, *39*(4), 555–570. https://doi.org/10.1080/07388551.2019.1592104

Rodríguez-Andrade, E., Hernández-Ramírez, K. C., Díaz-Peréz, S. P., Díaz-Magaña, A., Chávez-Moctezuma, M. P., Meza-Carmen, V., … Ramírez-Díaz, M. I. (2016). Genes from pUM505 plasmid contribute to *Pseudomonas aeruginosa* virulence. *Antonie Van Leeuwenhoek*, *109*(3), 389–396. https://doi.org/10.1007/s10482-015-0642-9

Rodríguez-Frómeta, R. A., Gutiérrez, A., Torres-Martínez, S., & Garre, V. (2013). Malic enzyme activity is not the only bottleneck for lipid accumulation in the oleaginous fungus *Mucor circinelloides*. *Applied Microbiology and Biotechnology*, *97*(7), 3063–3072. https://doi.org/10.1007/s00253-012-4432-2

Roncero, M. I. G. (1984). Enrichment method for the isolation of auxotrophic mutants of *Mucor* using the polyene antibiotic *N*-glycosylpolyfungin. *Carlsberg Research Communication*, *49*, 685–690. https://doi.org/10.1007/BF02907499

Rosén, S., Yu, J. H., & Adams, T. H. (1999). The *Aspergillus nidulans* sfaD gene encodes a G protein beta subunit that is required for normal growth and repression of sporulation. *The EMBO Journal*, *18*(20), 5592–5600. https://doi.org/10.1093/emboj/18.20.5592

Sagaram, U. S., & Shim, W. B. (2007). *Fusarium verticillioides* GBB1, a gene encoding heterotrimeric G protein beta subunit, is associated with fumonisin B biosynthesis and hyphal development but not with fungal virulence. *Molecular Plant Pathology*, *8*(4), 375–384. https://doi.org/10.1111/j.1364-3703.2007.00398.x

Salcedo-Hernandez, R., & Ruiz-Herrera, J. (1993). Isolation and characterization of a mycelial cytochrome aa3-deficient mutant and the role of mitochondria in dimorphism of *Mucor rouxii*. *Experimental Mycology*, *17*(2), 142–154. https://doi.org/10.1006/emyc.1993.1013

Sassone-Corsi, P. (2012). The cyclic AMP pathway. *Cold Spring Harbor Perspectives in Biology*, *4*(12), a011148. https://doi.org/10.1101/cshperspect.a011148

Schweizer, A., Rupp, S., Taylor, B. N., Röllinghoff, M., & Schröppel, K. (2000). The TEA/ATTS transcription factor CaTec1p regulates hyphal development and virulence in *Candida albicans*. *Molecular Microbiology*, *38*(3), 435–445. https://doi.org/10.1046/j.1365-2958.2000.02132.x

Secretaría de Agricultura, Ganadería, Desarrollo Rural, Pesca y Alimentación (SAGARPA) NORMA Oficial Mexicana NOM-062-ZOO-1999. (2001). Especificaciones técnicas para la producción, cuidado y uso de los animales de laboratorio. *Diario Oficial de la Federación*, *2*, 107–167 (In Spanish).

Setiadi, E. R., Doedt, T., Cottier, F., Noffz, C., & Ernst, J. F. (2006). Transcriptional response of *Candida albicans* to hypoxia: Linkage of oxygen sensing and Efg1p-regulatory networks. *Journal of Molecular Biology*, *361*(3), 399–411. https://doi.org/10.1016/j.jmb.2006.06.040

Somerville, G. A., & Proctor, R. A. (2013). Cultivation conditions and the diffusion of oxygen into culture media: The rationale for the flask-to-medium ratio in microbiology. *BMC Microbiology*, *13*, 9. https://doi.org/10.1186/1471-2180-13-9

Tang, W. J., & Gilman, A. G. (1991). Type-specific regulation of adenylyl cyclase by G protein beta gamma subunits. *Science*, *254*(5037), 1500–1503. https://doi.org/10.1126/science.1962211

Trieu, T. A., Navarro-Mendoza, M. I., Pérez-Arques, C., Sanchis, M., Capilla, J., Navarro-Rodríguez, P., … Nicolás, F. E. (2017). RNAi-based functional genomics identifies new virulence determinants in Mucormycosis. *PLoS Pathogens*, *13*(1), e1006150. https://doi.org/10.1371/journal.ppat.1006150

Tzima, A. K., Paplomatas, E. J., Tsitsigiannis, D. I., & Kang, S. (2012). The G-protein β subunit controls virulence and multiple growth- and development related traits in *Verticillium dahliae*. *Fungal Genetics and Biology: FG & B*, *49*(4), 271–283. https://doi.org/10.1016/j.fgb.2012.02.005

Valle-Maldonado, M. I., Jácome-Galarza, I. E., Díaz-Pérez, A. L., Martínez-Cadena, G., Campos-García, J., Ramírez-Díaz, M. I., … Meza-Carmen, V. (2015). Phylogenetic analysis of fungal heterotrimeric G protein-encoding genes and their expression during dimorphism in *Mucor circinelloides*. *Fungal Biology*, *119*(12), 1179–1193. https://doi.org/10.1016/j.funbio.2015.08.009

Valle-Maldonado, M. I., Jácome-Galarza, I. E., Gutiérrez-Corona, F., Ramírez-Díaz, M. I., Campos-García, J., & Meza-Carmen, V. (2015). Selection of reference genes for quantitative real time RT-PCR during dimorphism in the zygomycete *Mucor circinelloides*. *Molecular Biology Reports*, *42*(3), 705–711. https://doi.org/10.1007/s11033-014-3818-x

Vellanki, S., Billmyre, R. B., Lorenzen, A., Campbell, M., Turner, B., Huh, E. Y., … Lee, S. C. (2020). A novel resistance pathway for calcineurin inhibitors in the human-pathogenic Mucorales *Mucor circinelloides*. *mBio*, *11*(1), e02949–e02919. https://doi.org/10.1128/mBio.02949-19

Vellanki, S., Navarro-Mendoza, M. I., Garcia, A., Murcia, L., Perez-Arques, C., Garre, V., … Lee, S. C. (2018). *Mucor circinelloides*: Growth, maintenance, and genetic manipulation. *Current Protocols in Microbiology*, *49*(1), e53. https://doi.org/10.1002/cpmc.53

Wang, P., Perfect, J. R., & Heitman, J. (2000). The G-protein beta subunit GPB1 is required for mating and haploid fruiting in *Cryptococcus neoformans*. *Molecular and Cellular Biology*, *2*(1), 352–362. https://doi.org/10.1128/mcb.20.1.352-362.2000

Welton, R. M., & Hoffman, C. S. (2000). Glucose monitoring in fission yeast via the *gpa2* Gα, the *git5* Gβ and the *git3* putative glucose receptor. *Genetics*, *156*(2), 513–521.

Whiteway, M., Hougan, L., Dignard, D., Thomas, D. Y., Bell, L., Saari, G. C., … MacKay, V. L. (1989). The STE4 and STE18 genes of yeast encode potential beta and gamma subunits of the mating

factor receptor G protein. *Cell*, *56*(3), 467–477 10.1016/0092-8674(89)90249-3.

Wolff, A. M., Appel, K. F., Petersen, J. B., Poulsen, U., & Arnau, J. (2002). Identification and analysis of genes involved in the control of dimorphism in *Mucor circinelloides* (syn. *racemosus*). *FEMS Yeast Research*, *2*(2), 203–213. https://doi.org/10.1111/j.1567-1364.2002.tb00085.x

Yang, Q., Poole, S. I., & Borkovich, K. A. (2002). A G-protein beta subunit required for sexual and vegetative development and maintenance of normal G alpha protein levels in *Neurospora crassa*. *Eukaryotic Cell*, *1*(3), 378–390. https://doi.org/10.1128/ec.1.3.378-390.2002

Yu, H. Y., Seo, J. A., Kim, J. E., Han, K. H., Shim, W. B., Yun, S. H., & Lee, Y. W. (2008). Functional analyses of heterotrimeric G protein G alpha and G beta subunits in *Gibberella zeae*. *Microbiology*, *154*(2), 392–401. https://doi.org/10.1099/mic.0.2007/012260-0

SUPPORTING INFORMATION

Additional supporting information may be found online in the Supporting Information section at the end of this article.

How to cite this article: Valle-Maldonado MI, Patiño-Medina JA, Pérez-Arques C, et al. The heterotrimeric G-protein beta subunit Gpb1 controls hyphal growth under low oxygen conditions through the protein kinase A pathway and is essential for virulence in the fungus *Mucor circinelloides*. *Cellular Microbiology*. 2020;e13236. https://doi.org/10.1111/cmi.13236

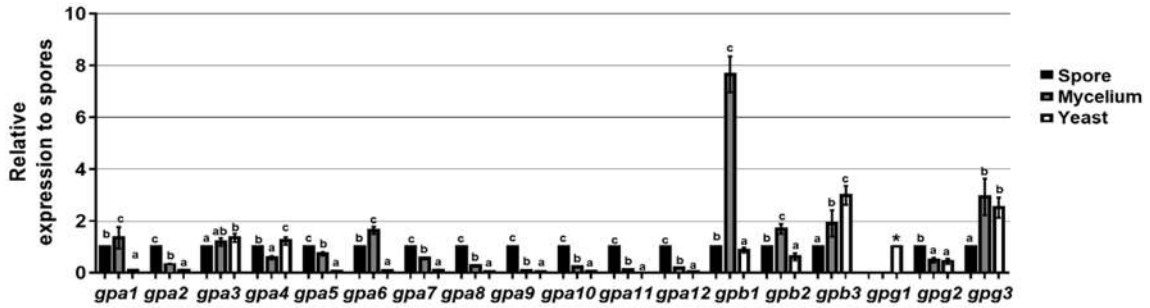

Figure S1. Transcript levels of heterotrimeric G-protein-encoding genes in spores, mycelium and yeast in the R7B strain from *M. circinelloides*. Raw Ct-data from RT-qPCR were retrieved from Valle-Maldonado et al., 2015b. Jácome-Galarza, Díaz-Pérez, et al., 2015 and a novel ΔΔCt was carried out for 12 Gα (*gpa1-12*), 3 Gβ (*gpb1-3*) and 3 Gγ (*gpg1-3*) encoding genes. Spores were incubated for 6 h in liquid YPG rich media, in aerobic or self-anaerobic conditions that led to mycelium or yeast, respectively. Bars represent relative gene transcript for each gene during vegetative growth (mycelium or yeast) compared to the spore stage. Asterisk stands for the *gpg1* gene that was only detected in the yeast morphology. The data is represented as the average from three independent biological replicates, ± correspond to standard error (SE). Significance testing was performed using ANOVA with Fisher´s exact test. For each gene the different letters above the bars denote statistical significance, values with identical letter were not considered significantly different ($p<0.05$).

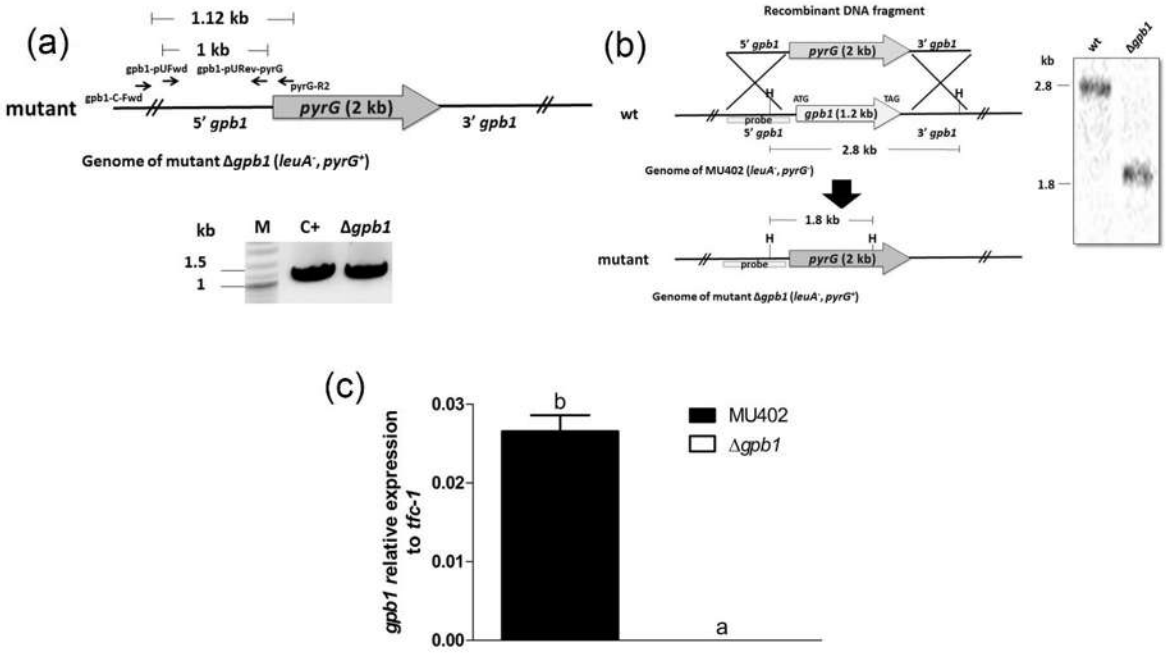

Figure S2. Deletion of *gpb1* in *M. circinelloides*. The 5′ and 3′ regions (1.1 kb for each) upstream and downstream from the start and stop codons, respectively, of *gpb1* were designed to flank the *pyrG* selection marker for gene deletion. The recombinant fragment was used to transform protoplasts of the strain MU402 (*pyrG*$^{-}$, *leuA*$^{-}$) is shown. (a) Molecular confirmation by PCR of the Δ*gpb1* strain, the lane C+ showed the amplicon (1.0 kb) that cover the 5´region that flanks the recombinant *gpb1* fragment; the lane Δ*gpb1* showed the amplicon (1.12 kb) that confirms the integration of the transformation fragment in the *gpb1* locus. (b) Molecular confirmation by Southern blotting was performed using specific probes for *gpb1* gene. DNA samples from transformed and parental (MU402) strains were digested with the indicated restriction enzyme (H, *Hinc*II) and the corresponding

bands to each genotype were observed (WT: 2.8 kb and Δ*gpb1*: 1.8 kb). (c) mRNA levels of *gpb1* was quantified by RT-qPCR using total RNA isolated from spores of each strain, a ΔCt analysis was performed. The data is represented as the average from three biological replicates of independent cultures, ± correspond to standard error (SE). Significance testing was performed using ANOVA with Fisher´s exact test. The different letters above the bars denote statistical significance, values with identical letter were not considered significantly different ($p<0.05$).

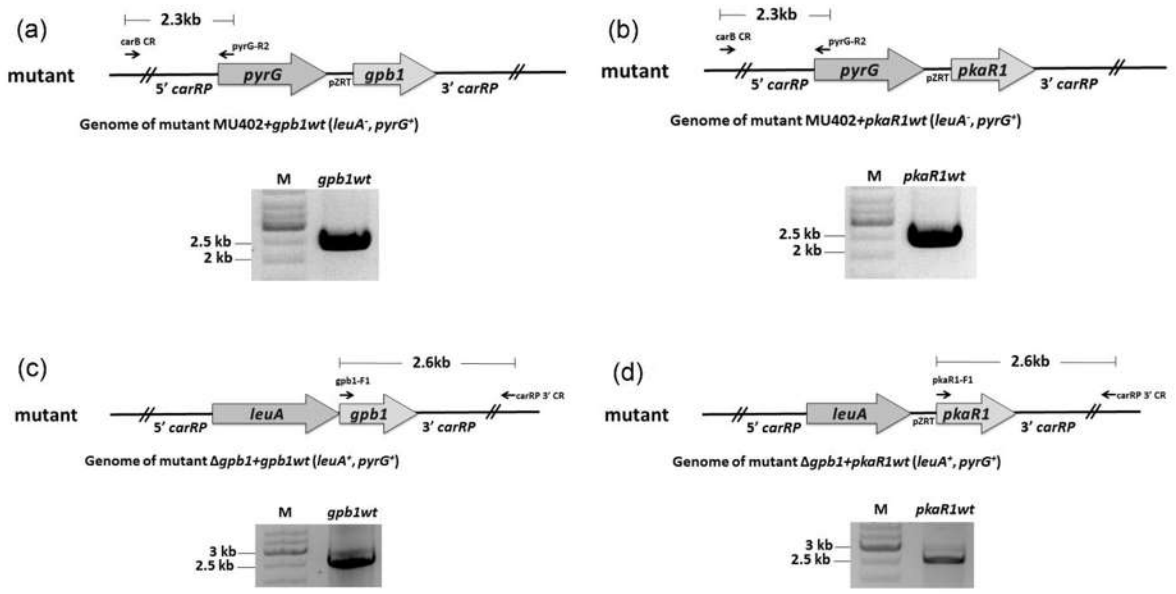

Figure S3. Generation of the complemented Δ*gpb1*+g*pb1* and over expressed Δ*gpb1*+*pkaR1* strains in *M. circinelloides*. The overexpressed mutants MU402+*gpb1* and MU402+*pkaR1* are derivated of the MU402 strain that was transformed by the *gpb1* (a) or *pkaR1* (b) wild-type allele at the *carRP* locus. Similarly, the complemented Δ*gpb1*+g*pb1* (c) and over expressed Δ*gpb1*+*pkaR1* (d) strains (*pyrG*$^{+}$, *leuA*$^{+}$, *carRP*$^{-}$) were obtained by integrative transformation with the *gpb1* or *pkaR1* wild-type allele at the *carRP* gene locus of the Δ*gpb1* strain (*pyrG*$^{+}$, *leuA*$^{-}$, *carRP*$^{+}$). We used a transformation fragment that contained about 1.1 kb upstream of the start of the *carRP* gene ORF and approximately 1.1 kb downstream the stop codon. These two fragments flank the *leuA* (4.4 kb) and *gpb1* (2.5 kb) or pkaR1 (2.5 kb). The molecular confirmation of the integration of the transformation fragment was done by PCR, the presence of an amplicon of 2.3 kb revealed the integration of *gpb1* or *pkaR1* in MU402 (a and b); meanwhile the

integration of *gpb1* or *pkaR1* in Δ*gpb1* was confirmed by the presence of an amplicon of 2.5 kb (c and d). *gpb1* gene is under the regulation of its native promoter and terminator sequences in Δ*gpb1* and it is under the regulation of promoter pZRT in MU402; *pkaR1* gene is under the regulation of promoter pZRT in both strains. The size of those transformation fragments is around 6.6 kb for the *pyrG* fragments and 9 kb for the *leuA* fragments. The complemented strains resulted in albino colonies instead of the MU402 or Δ*gpb1* yellowish colonies.

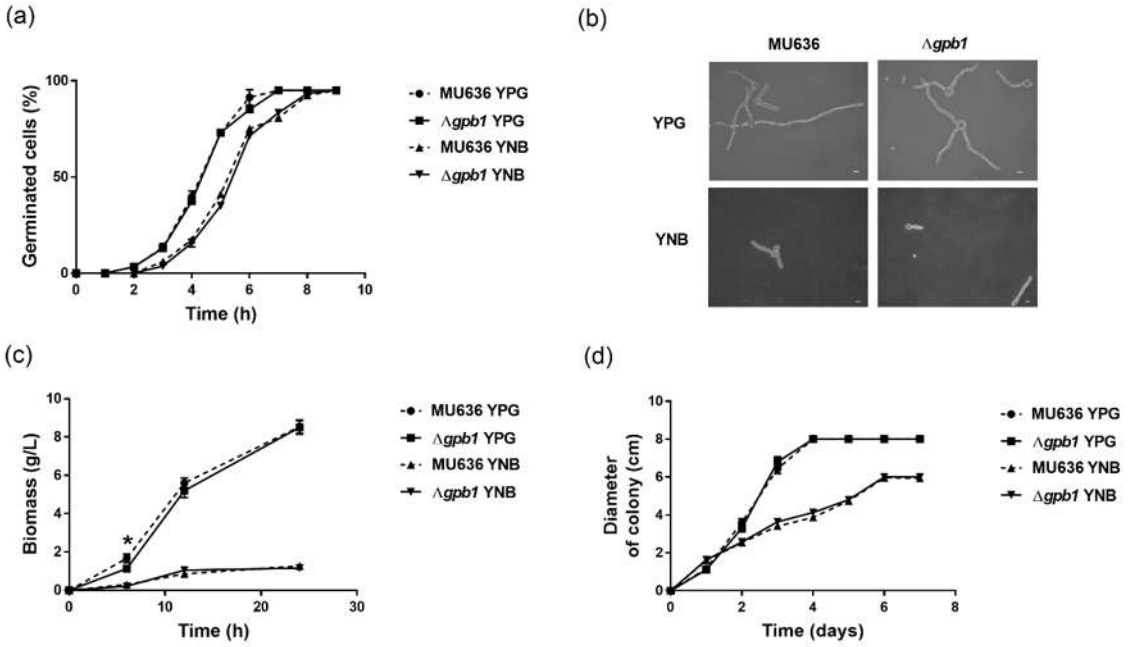

Figure S4. Effect of *gpb1* mutation on aerobic growth of *M. circinelloides*. (a) Aerobic germination. Δ*gpb1* and MU636 strains were grown aerobically in liquid rich or minimal media (YPG or YNB, respectively) and germinules were counted hourly. (b) Cellular morphology. Microphotographs taken by light microscopy (40 ×) reveal morphology of germinules in liquid YPG and YNB, at 6 or 8 h, of aerobic growth for Δ*gpb1* and MU636 strains. Scale bar =20 µm. (c) Biomass production. Biomass was filtered, dried and weight wa determined from Δ*gpb1* and MU636 aerobic cultures in rich and minimal media at 6, 12 and 24 hours of growth. (d) Radial growth. Radial growth was determined daily for Δ*gpb1* and MU636 strains on solid YPG or YNB media. Three independent experiments were conducted. Statistically significant differences are indicated by asterisks (ANOVA and Fisher's tests; $p \leq 0.05$).

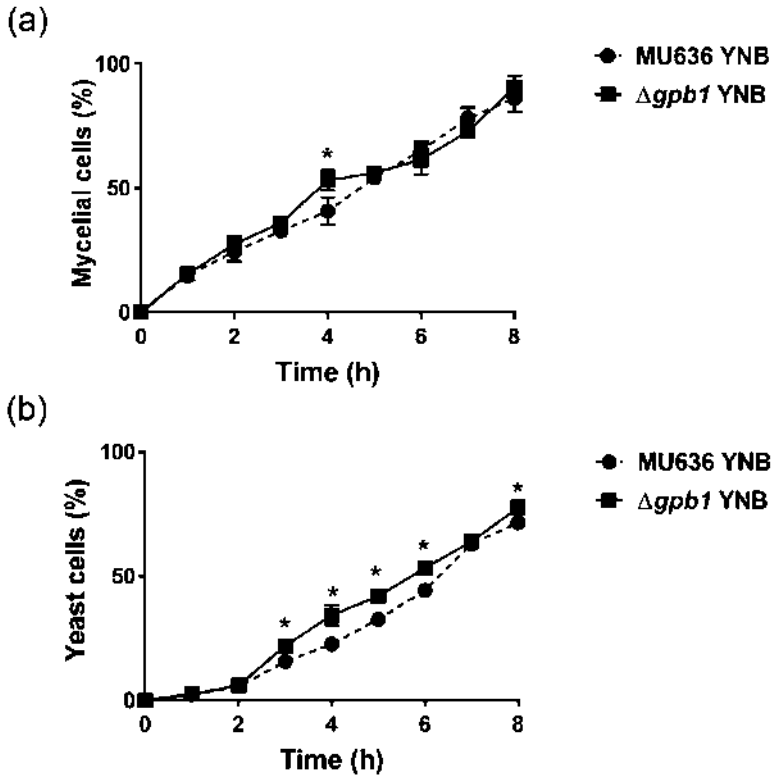

Figure S5. Effect of *gpb1* mutation on filamentous and yeast cells count in yeast-hyphae or hyphae-yeast transitions in YNB medium in *M. circinelloides*. Δ*gpb1* and MU636 spores were incubated anaerobically in YPG medium for 10 h, then the resulting yeast cells were washed and transferred to fresh YNB medium supplemented with leucine and uridine and grown aerobically to promote the yeast-hyphae transition. (a) Filamentous cells determination. The

percentage of hyphae cells was determined hourly for Δ*gpb1* and MU636 after the yeast-to-hyphae transition was induced. Δ*gpb1* and MU636 spores were incubated aerobically in YPG medium for 5 h, then the resulting germlings were washed and transferred to fresh YNB media and grown anaerobically to promote the hyphae-yeast transition. (b) Yeast cells determination. The percentage of yeast cells was determined hourly for Δ*gpb1* and MU636 after the yeast-mycelium transition was induced. The data is represented as the average from three independent biological replicates, ± correspond to standard error (SE). Significance testing was performed using ANOVA with Fisher's exact test. For each condition the asterisks above the bars denote statistically significance, ($p \leq 0.05$).

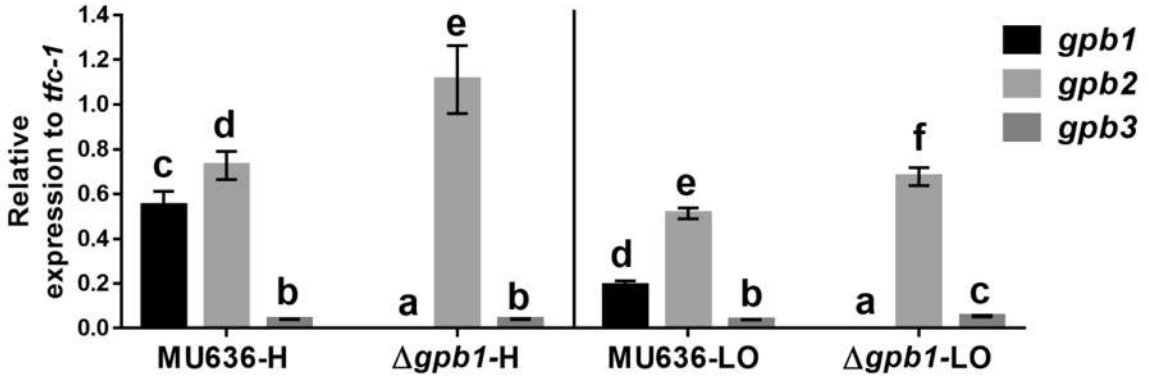

Figure S6. Transcript levels of heterotrimeric Gβ-encoding genes in aerobic and low oxygen cultures from the Δ*gpb1* and MU636 strain of *M. circinelloides*. Total RNA was isolated from vegetative growths obtained after spores from Δ*gpb1* or MU636 strains were incubated for six hours in YPG medium aerobically (H) or after eight hours in low oxygen conditions (LO) as reported previously. mRNA levels of the three Gβ (*gpb1-3*) encoding genes were determined by RT-qPCR A delta Ct analysis (ΔCt) was carried out, using the validated *tfc-1* gene as normalizer. The data is represented as the average from three independent biological replicates, ± correspond to standard error (SE). Significance testing was performed using ANOVA with Fisher´s exact test. For each gene the different letters above the bars denote statistically significance, values with identical letter were not considered significantly different ($p<0.05$).

(a)

CATTCTTAATTTTGAGCCTTTTTTTTCGACAC**TATA**CATTTCCATCATC**ATG**

(b)

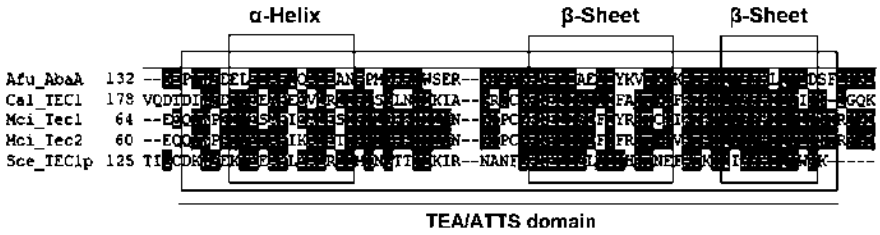

Figure S7. Tec1p homologues in *M. circinelloides*. (a) An analysis in the promoter region of the *gpb1* gene was carried out, a putative consensus sequence (CATTCTT) for the TEC1p transcription factor, the TATA box and the start codon are depicted in bold and underlined letters. (b) Two putative homologues of Tec1p in *Mucor circinelloides* (Mci_Tec1 and Mci_Tec2; ID numbers, 84676 and 106595, respectively) were aligned using ClustalW with AbaA (XP_750232.1) from *Aspergillus fumigatus* (Afu), TEC1 (AOW28471.1) from *C. albicans* (Cal) and TEC1p (NP_009639.3) from *Saccharomyces cerevisiae* (Sce), GenBank accession numbers are shown in parenthesis. The TEA/ATTS DNA-binding domain, and the structural motifs which consist of an α-helix and two β-sheets are shown with boxes (Hwang, Chambon, & Davidson, 1993).

Table S1. Oligonucleotides used for PCR assays

Name	Sequence 5'-3´	Tm(°C)/GC%
gpb1-pUFwd	gtactCTCGAGCTGAAACTTTAACCGTGAGACCTTT	72.84/44.44
gpb1-pURev-pyrG	**caagtaccaatgctgaggca**AGCAAATGATTCCCTTCAACTCAAAC	76.36/43.48
gpb1-pDFwd-pyrG	**cgatagcatggccagtgtac**CTTGATTTCGATACACTGGCCC	78.09/52.38
PyrG-Sac-FWR	GCACCGgagctcTGCCTCAGCATTGGTACTTG	76.66/59.38
PyrG-Sac-REV	GTGTGGgagctcGTACACTGGCCATGCTATCG	76.33/59.38
gpb1-pDRev	ctggcGAATTCTCAGTAGCTCCCTCTTTTTCCAC	73.51/50
gpb1-C-Fwd	TGGCACATATTAGGTCAAAATGTTGCTATCGATCC	70.73/40
pyrG-R2	ATCCCACCAGAAGGAGTACATGG	66.5/52.1
carB CR	GAGTTATGAACGCGGAATACTTCAGG	66.31/46.15
gpb1-F1	**caaaataactaaatctcgag**CATCATGCCAAATACAAACAACG	71.7/34.88
pkaR1-F1	**caaaataactaaatctcgag**ATGATCACTGACGAACATCCG	71.93/39.02
carRP 3' CR	TTGTGTCTTGGGTTTTCTTC	59.2/40

Lowercase letters represent restriction sites.

The lowercase and bold letters show the region that hybridizes to the *pyrG*, *leuA* or *pZRT* sequences.

Table S2. Effect of Gpb1 in hyphal and yeast cells proportions during dimorphic transitions of *M. circinelloides*

	Yeast-to-Hyphae Transition		**Hyphae-to-Yeast Transition**	
	Cellular count (%)		Cellular count (%)	
Strain	**Yeast**	**Hyphae**	**Yeast**	**Hyphae**
MU636	25.67 ± 2.52	74.33 ± 2.52	45.67 ± 5.51	54.33 ± 5.51
Δgpb1	70.67 ± 2.08	29.33 ± 2.08	86.33 ± 4.04	13.67 ± 4.04
ΔpkaR1	69 ± 2.08	31 ± 2.08	90 ± 3.61	10 ± 3.61
Δgpb1 +gpb1	24.33 ± 3.51	75.67 ± 3.51	45.67 ± 6.43	54.33 ± 6.43
Δgpb1 +pkaR1	23.33 ± 3.79	76.67 ± 3.79	42.67 ± 4.51	57.33 ± 4.51

Dimorphic transitions were done by independent triplicates assays; ± stand for the standard deviation. Yeast (%) or hyphae (%) represent the cellular morphologies observed after the transitions.

Table S2. Functions of fungal Gβ subunits

Subunit Group	Organism	Phylum	Function	Reference
CGB1 Group I	*Cochliobolus heterostrophus*	Ascomycota	Positive regulator of female fertility, conidiation and virulent capacity against maize	Ganem et al., 2004.
CPGB-1 Group I	*Cryphonectria parasitica*	Ascomycota	Negative regulator of vegetative growth. Positive regulator of virulent capacity agains chesnut stems.	Kasahara & Nuss 1997.
Fgb1 Group I	*Fusarium oxysporum*	Ascomycota	Positive regulator of hyphal growth and virulent capacity against tomato plants. Positive regulator of cAMP levels.	Jain, Akiyama, Kan, Ohguchi, & Takata, 2003 Guo et al., 2016
Fgb1 Group I	*Fusarium sacchari*	Ascomycota	Negative regulator of filamentous growth. Positive regulator of reproduction	Kaneko et al., 2013.
Gba1 Group I	*Stagonospora nodorum*	Ascomycota	Indispensable for infecting the wheat plant, and for asexual sporulation.	Gummer, Trengove, Oliver, & Solomon, 2012.
GBB1 Group I	*Fusarium verticillioides*	Ascomycota	Positive regulator of the production of the mycotoxin fumonisin and the hyphal polarity.	Sagaram, & Shim 2007.
GNB-1 Group I	*Neurospora crassa*	Ascomycota	Positive regulator of reproduction. Positive regulator of cAMP levels.	Yang, Poole, & Borkovich, 2002.
GzGPB1 Group I	*Gibberella zeae*	Ascomycota	Negative regulator of the production of mycotoxins deoxynivalenol and zearalenone.	Yu et al., 2008.

Continues on next page

Subunit Group	Organism	Phylum	Function	Reference
MGB1 Grupo I	*Magnaporthe grisea*	Ascomycota	Positive regulator of conidiation and virulent capacity against rice plants.	Nishimura, Park, & Xu, 2003.
Mgb1 Group I	*Monascus ruber*	Ascomycota	Positive regulator of vegetative growth and asexual sporulation. Negative regulator of the production of the mycotoxin citrinin.	Li, He, Lai, Shao, & Chen, 2014.
MgGPB1 Group I	*Mycosphaerella graminicola*	Ascomycota	Positive regulator of filamentation and pathogenicity. Positive regulator of cAMP levels.	Mehrabi et al., 2009.
SfaD Grupo I	*Aspergillus nidulans*	Ascomycota	Positive regulator of vegetative growth. Negative regulator of sporulation.	Rosén, Yu, & Adams, 1999.
Vgb Group I	*Verticillium dahliae*	Ascomycota	Positive regulator of the virulent capacity against tomate plants. Negative regulator of sporulation.	Tzima, Paplomatas, Tsitsigiannis, & Kang, 2012.
Bpp1 Group II	*Ustilago maydis*	Basidiomycota	Positive regulator of reproduction and repressor of yeast growth.	Muller et al., 2004.
GPB1 Group II	*Cryptococcus neoformans*	Basidiomycota	Positive regulator of mating and haploid fruiting.	Wang, Perfect & Heitman, 2000.
Git5 Group IV	*Schizosaccharomyces pombe*	Ascomycota	Response to glucose.	Welton & Hoffman 2000.
KlSte4p Group IV	*Kluyveromyces lactis*	Ascomycota	Positive regulator of reproduction.	Navarro-Olmos et al., 2010.

Continues on next page

Table S2. Functions of fungal Gβ subunits (Continuation)

Subunit Group	Organism	Phylum	Function	Reference
STE4 Group IV	*Candida albicans*	Ascomycota	Positive regulator of reproduction.	Dignard, André, & Whiteway, 2008.
STE4 Group IV	*Saccharomyces cerevisiae*	Ascomycota	Indispensable for the reproduction of haploid cells.	Whiteway et al. 1989.

9. DISCUSIÓN

Los resultados de este trabajo indican que el gen *gpb1* presenta altos niveles de transcrito durante el crecimiento micelial. La cepa mutante Δ*gpb1* presentó una disminución de la virulencia posiblemente correlacionado con el decremento del crecimiento filamentoso durante las transiciones morfológicas y en bajas concentraciones de oxígeno. Se identificó la relación funcional Gpb1 y PkaR1 en la regulación positiva del crecimiento filamentoso y de la virulencia en este mucoral.

Las proteínas G heterotriméricas (PGH) son reguladores clave en la morfogénesis fúngica (Li, et al., 2007). Previamente en nuestro grupo de trabajo identificamos los genes que codifican para PGH en el mucoral dimórfico *M. circinelloides.* Interesantemente el repertorio consistió en 12 subunidades Gα, 3 Gβ y 3 Gγ, siendo el más numeroso reportado en un organismo en el Reino Fungi (Valle-Maldonado et al., 2015). Adicionalmente, en el misma investigación se realizó una clasificación filogenética para las subunidades Gβ y Gγ. Para ambos tipos de subunidades la distribución fue de la siguiente manera: grupo filogénetico I (ascomicetos filamentosos), grupo filogénetico II (basidiomicetos), grupo filogénetico III (mucorales) y grupo filogénetico IV (ascomicetos levaduriformes y dimórficos) (Valle-Maldonado et al., 2015).

Hasta la fecha, se han caracterizado funcionalmente 19 subunidades Gβ fúngicas (Tabla). Todas estas subunidades pertecen a los grupos filogéneticos I, II o IV. Notablemente ninguna de las subunidades del grupo filogénetico III, el cual contiene subunidades Gβ de mucorales, había sido caracterizado hasta la fecha.

Los niveles de transcrito del gen *gpb1* se encuentran elevados durante el crecimiento micelial (Valle-Maldonado et al., 2015) en comparación con los otros genes que codifican para subunidades Gβ (Figura 1), sugiriendo una posible participación de este gen en la regulación del crecimiento micelial. Se ha demostrado que existe una asociación entre niveles altos de transcrito de genes que codifican para subunidades Gα durante un estadío en particular y la función

biológica de dichos genes en *M, circinelloides*. Por ejemplo, los genes *gpa11* y *gpa12* que codifican para subunidades Gα, presentan altos niveles de transcrito durante el estadío de espora respecto a los demás genes que codifican para subunidades Gα (Valle-Maldonado et al., 2015b), interesantemente la doble mutante que tiene ambos genes interrumpidos mostró un aumento significativo en el tamaño y velocidad de germinación de la espora (Patiño-Medina et al., 2019a).

El crecimiento micelial en *M. circinelloides* ha sido asociado a una mayor virulencia en este hongo (Díaz-Pérez et al., 2020; Lee et al., 2013). Se ha reportado que varios factores estimulan el crecimiento micelial en *M. circinelloides*: la presencia de oxígeno, y la disponibilidad de fuentes de carbono fermentables y de nitrógeno inorgánico (McIntyre et al., 2002; Orlowski, 1991). De igual manera, es probable que algunas señales provenientes del hospedero pudieran promover la virulencia en este hongo, se ha demostrado que suero proveniente de sangre estimula la germinación micelial de esporas (Patiño-Medina et al., 2019).

Los resultados de este trabajo demuestran que la morfología prevalente en bajas condiciones de oxígeno (~7%) es micelial (Figura 8). La interrupción del gen *gpb1* no alteró el crecimiento micelial durante crecimiento en crecimiento aeróbico en condiciones alta concentración de oxígeno (~14%). Sin embargo, durante las transiciones dimórficas o durante crecimiento en limitación de oxígeno, la cepa Δ*gpb1* mostró un aumento significativo en la formación de levaduras en comparación con la cepa silvestre. Este defecto podría ser relevante para la regulación de la infección y virulencia, ya que el desarrollo de micelio es necesario para la infección fúngica de tejidos, los cuales presentan niveles de oxígeno bajos (Grahl et al., 2012).

Los ensayos de virulencia usando ratones diabéticos, confirmaron que el gen *gpb1* es necesario para la regulación de la virulencia; la cepa Δ*gpb1* no fue capaz de invadir el tejido de ratón al nivel de la cepa silvestre o la cepa complementada Δ*gpb1* + *gpb1* (Figura 6). Lo anterior podría ser explicado en parte por la mayor sensibilidad a H_2O_2 y la mayor proporción de levaduras formadas como resultado de la pérdida de Gpb1 en un ambiente tisular de baja concentración de oxígeno.

Estas levaduras pueden ser fagocitadas con mayor facilidad por los macrófagos (Figura 7), como ha sido descrito (Lee at al., 2013). Estos resultados son concordantes con la prevalencia de morfología micelial en la infección del tejido del hospedero por parte de *M. circinelloides* (Dizbay et al., 2009; Khan et al., 2009).

Los resultados obtenidos en este trabajo son consistentes con otros patógenos fúngicos relevantes de humanos que han mostrado su capacidad de desarrollar crecimiento filamentoso en condiciones hipóxicas o anóxicas *in vitro* como es el caso del dimórfico patógeno *Candida albicans* (Setiadi et al., 2006), y los ascomicetos filamentosos monomorficos *Aspergillus fumigatus* (Hall y Denning, 1994) y *Fusarium oxysporum* (Gunner y Alexander, 1964). Similarmente, ha sido reportado que en el hongo entomopatógeno *Isaria fumosorosea* la proporción relativa de crecimiento micelial o levadurifome está regulada por la disponibilidad de oxígeno (Jackson, 2012).

De manera similar el crecimiento filamentoso del ascomiceto patógeno *Candida albicans* es un factor crítico para regular su virulencia (Da Silva Dantas, et al., 2016), y esta morfología está positivamente regulada por la presencia de bajos niveles de oxígeno (Setiadi et al., 2006). Adicionalmente, un análisis transcriptómico en este ascomiceto mostró que durante un crecimiento bajos condiciones limitantes de oxígeno, los genes específicos del crecimiento filamentoso acumularon una mayor cantidad de transcrito en relación al crecimiento bajo condiciones más altas de oxígeno (Setiadi et al., 2006).

Dado que la mutante Δ*gpb1* mostró hifas más cortas durante la transición de levadura a micelio (Figura 3), el cual es un fenotipo similar al descrito previamente para la cepa Δ*pkaR1* (Ocampo et al., 2009). Fue de nuestro interés dilucidar la posible relación funcional entre estos dos genes. La cepa Δ*pkaR1* mostró fenotipos similares comparados con Δ*gpb1*. Δ*pkaR1* fue significativamente más propensa a desarrollar levaduras en bajas condiciones de oxígeno (Figura 8). De igual manera, mostró una disminución en la virulencia y en la invasión fúngica del tejido murino (Figura 6) comparado con la cepa silvestre. En el caso de las

proteínas G heterotriméricas fúngicas, se ha reportado que genes que participan en la misma ruta de señalización muestran usualmente fenotipos con las mismas alteraciones cuando fueron interrumpidos individualmente (Landry y Hoffman, 2001; Landry et al., 2000; Whiteway et al., 1989; Yang, et al., 2002).

La co-participación de *gpb1* y *pkaR1* en la regulación de crecimiento micelial en bajas condiciones de oxígeno se sugiere fuertemente al restaurar los fenotipos de la cepa silvestre al sobreexpresar a *pkaR1* en la cepa Δ*gpb1* (Figuras 5 y 8). La relación funcional entre Gpb1 y PkaR1 pudiera derivar en la regulación de actividad de la actividad de adenilato ciclasa (AC) la cual incrementa la niveles de cAMP que activan a la PKA (Choi et al., 2015). Los niveles aumentados de cAMP y actividad de PKA encontrados en ambas mutantes Δ*gpb1* y Δ*pkaR1* (Figura 9), pudieran ser responsables del aumento del desarrollo levaduriforme durante bajas condiciones de oxígeno (Figura 8), esto debido a que la adición de un análogo de cAMP favoreció el crecimiento levaduriforme en otras especies del género *Mucor* (Pereyra et al., 2000; Pereyra et al., 1992).

Los niveles de cAMP intracelulares son el resultado del efecto combinado de la síntesis de cAMP a través de la actividad de AC y la degradadación dependiente de fosfodiesterasa. En dicho contexto, en mamíferos se ha demostrado que la interacción física de RIα, una subunidad regulatoria de PKA, y RegA, una fosfodiesterasa aumenta la actividad catalítica de esta última. Por lo tanto, se concluyó que RIα es un activador positivo de la actividad de fosfodiesterasa de RegA (Moorthy et al., 2011). A pesar de que no tenemos una explicación definitiva en *M. circinelloides*, es posible que la interrupción de *pkaR1* en bajas condiciones de oxígeno, condujo a la disminución de la actividad catalítica de al menos un homologo a RegA en este mucoral y finalmente contribuyendo al cAMP aumentado detectado en esta cepa (Figura 9).

En otros hongos se ha reportado que tanto los niveles de cAMP como el crecimiento filamentoso son regulados positivamente por subunidades Gβ, incluyendo a *F. oxysporum* (Jain et al., 2003), *N. crassa* (Yang et al., 2002) y *Mycosphaerella graminícola* (Mehrabi et al., 2009). Sin embargo, en *M.*

circinelloides, es posible que Gpb1 regule negativamente la actividad de AC y promueva el crecimiento filamentoso en bajas condiciones de oxígeno.

Existen escenarios distintos que pudieran explicar la regulación de la ruta PKA mediada por Gpb1 en *M. circinelloides* durante el crecimiento en bajas condiciones de oxígeno (Figura 10).

A) Una de las posibilidades implicaría que la subunidad Gpb1 fuese un regulador de la actividad de la adelinato ciclasa. Esta posible actividad puede ser explicada concretamente en alguna de las siguientes formas.

1) Gpb1 forma parte de un heterodímero Gβγ activo que intrínsecamente ejerce una modulación inhibitoria de la adenilato ciclasa en *M. circinelloides* durante bajas condiciones de oxígeno. Este tipo de actividad ha sido descrita para el dímero Gβγ (Tang & Gilman, 1991).

2) Gpb1 forma parte de un heterodímero Gβγ que antagonisticamente se una a una subunidad Gα estimulatoria (Gαs) de la AC por lo tanto inhibiendo indirectamente la actividad de AC (Mehrabi et al., 2009).

3) Gpb1 forma parte de un heterodímero Gβγ el cual se une a una subunidad Gα inhibitoria (Gαi) de la AC, la señal desconocida liberan al dímero Gβγ y a la subunidad Gαi que inhibe la actividad de la AC (Chen et al., 1996).

Los posibles escenarios anteriores implican la disminución de los niveles de cAMP como consecuencia de la inhibición de la AC. Los niveles bajos de cAMP no estimulan la disociación de las subunidades regulatorias (PkaR) de las subunidades catalíticas (PkaC), lo que finalmente promueve el crecimiento polarizado con un fenotipo con virulencia aumentado.

B) En contraste, la carencia de Gpb1 o PkaR1 a través de la interrupción de ya sea *gpb1* o *pkaR1* afecta los niveles de cAMP y la actividad de PKA. La interrupción de *gpb1* impediría la formación del dímero inhibitorio Gβγ, lo que ocasionaría la no represión de la actividad AC. O bien también se

pudiera impedir una correcta señalización de subunidades Gαs o Gαi que modularían la actividad de AC. De manera semejante, se ha reportado que la formación incorrecta del heterotrimero (en este caso la carencia de Gpb1) conduciría a una transducción de señales defectuosa (Landry et al., 2000; Landry y Hoffman, 2001). Todos estos escenarios en la cepa Δ*gpb1* activarían a la AC, aumentando los niveles de cAMP y promoviendo la activación de la ruta PKA. Además, la carencia de *pkaR1* libera a las subunidades catalíticas (PkaC), activando la ruta PKA. La interrupción de Gpb1 o PkaR1 resulta en un crecimiento levaduriforme aumentado en bajas condiciones de oxígeno y un fenotipo con virulencia reducida.

Notablemente, para nuestro entendimiento, este es el primer reporte de la caracterización funcional de una subunidad Gβ en un hongo mucoral.

.

10. CONCLUSIÓNES

- El producto del gen *gpb1* está funcionalmente asociado con PkaR1, y es un regulador positivo de la virulencia, y su interrupción generó un crecimiento filamentoso reducido durante las transiciones dimórficas.
- Nuestros resultados indican que Gpb1 regula positivamente el crecimiento filamentoso durante bajas condiciones de oxígeno al modular la ruta cAMP-PKA.
- El hecho que la mutante Δ*gpb1* sea proclive a generar levaduras, puede explicar el fenotipo avirulento y con menor capacidad invasiva, daño celular e inflamación en el modelo murino.

11. PERSPECTIVAS

Identificar a la(s) subunidad(es) Gα y Gγ que regulan junto con Gpb1 y PkaR1 el crecimiento filmentoso en bajas condiciones de oxígeno.

12. ADDENDA

En este apartado se muestran las publicaciones resultados de la colaboración con nuestro grupo de trabajo durante mis estudios de doctorado (artículos completos).
.

Además, están mostradas las publicaciones derivadas de otros proyectos de investigación realizados durante mi maestría (sólo portadas). Esto es relevante ya que la pregunta de investigación de este trabajo se deriva de dichas publicaciones.

Artículos publicados con arbitraje internacional

1. Valle-Maldonado, M.I., Jácome-Galarza, I.E., Gutiérrez-Corona, F., Ramírez-Díaz, M.I., Campos-García, J., Meza-Carmen, V. 2015a. Selection of reference genes for quantitative real time RT-PCR during dimorphism in the zygomycete *Mucor circinelloides*. *Mol Biol Rep* 42(3): 705-711

2. Valle-Maldonado, M.I., Jácome-Galarza, I.E., Díaz-Pérez, A.L., Martínez-Cadena, G., Campos-García, J., Ramírez-Díaz, M.I., Reyes-De la Cruz, H., Riveros-Rosas, H., Díaz-Pérez, C., Meza-Carmen, V. 2015b. *Fungal Biol* 119(12):1179-1193.

3. Hernández-Ramírez, K.C., Chávez-Jacobo, V.M., **Valle-Maldonado, M.I.**, Patiño-Medina. J.A., Díaz-Pérez, S.P., Jácome-Galarza, I.E., Ortiz-Alvarado, R., Meza-Carmen, V., Ramírez-Díaz, M.I. 2017. Plasmid pUM505 encodes a Toxin-Antitoxin system conferring plasmid stability and increased *Pseudomonas aeruginosa* virulence. *Microb Pathog* 112: 259-268.

4. Patiño-Medina, J.A., Maldonado-Herrera, G., Pérez-Arques, C., Alejandre-Castañeda, V., Reyes-Mares, N.Y., **Valle-Maldonado, M.I.**, Campos-García J, Ortiz-Alvarado, R., Jácome-Galarza, I.E., Ramírez-Díaz, M.I., Garre, V., Meza-Carmen, V. 2018. Control of morphology and virulence by ADP-ribosylation factors (Arf) in *Mucor circinelloides*. *Curr Genet* 64(4):853-869.

5. Patiño-Medina, J.A., **Valle-Maldonado, M.I.**, Maldonado-Herrera, G., Pérez-Arques, C., Jácome-Galarza, I.E., Díaz-Pérez, C., Díaz-Pérez, A.L., Araiza-Cervantes, C.A., Villagomez-Castro, J.C., Campos-García, J., Ramírez-Díaz, MI, Garre V, Meza-Carmen V. 2019. Role of Arf-like proteins (Arl1 and Arl2) of *Mucor circinelloides* in virulence and antifungal susceptibility. *Fungal Genet Biol* 129:40-51.

6. Rangel-Porras, R.A., Díaz-Pérez, S.P., Mendoza-Hernández, J.M., Romo-Rodríguez, P., Alejandre-Castañeda, V., **Valle-Maldonado, M.I.**, Torres-Guzmán, J.C., González-Hernández, G.A., Campos-Garcia, J., Arnau, J., Meza-Carmen, V., Gutiérrez-Corona, J.F. 2019. Alcohol dehydrogenase 1 participates in the Crabtree effect and connects fermentative and oxidative metabolism in the Zygomycete *Mucor circinelloides*. *J Microbiol* 57(7):606-617.

7. Patiño-Medina, J.A., Vargas-Tejeda, D., **Valle-Maldonado, M.I.**, Alejandre-Castañeda, V., Jácome-Galarza, I.E., Villegas-Moreno, J., Nuñez-Anita, R.E., Ramírez-Díaz, M.I., Ortiz-Alvarado, R., Meza-Carmen, V. 2019. Sporulation on blood serum increases the virulence of *Mucor circinelloides*. Microb Pathog 137:103737. doi: 10.1016/j.micpath.2019.103737.

8. Patiño-Medina, J.A., Reyes-Mares, N.Y., **Valle-Maldonado, M.I.**, Jácome-Galarza, I.E., Pérez-Arques, C., Nuñez-Anita, R.E., Campos-García, J., Anaya-Martínez, V., Ortiz-Alvarado, R., Ramírez-Díaz, M.I., Lee, S.C., Garre, V., Meza-Carmen, V. 2019. Heterotrimeric G-alpha subunits Gpa11 and Gpa12 define a transduction pathway that control spore size and virulence in *Mucor circinelloides*. *PLoS One* 14(12):e0226682.

9. Díaz-Pérez, S.P., Patiño-Medina, J.A., **Valle-Maldonado, M.I.**, López-Torres, A., Jácome-Galarza, I.E., Anaya-Martínez, V., Gómez-Ruiz, V., Campos-García, J., Nuñez-Anita, R.E., Ortiz-Alvarado, R., Ramírez-Díaz, M.I., Gutiérrez-Corona, J.F., Meza-Carmen, V. 2020. Alteration of

Fermentative Metabolism Enhances *Mucor circinelloides* Virulence. *Infect Immun* 88(2)i: e00434-19.

10. Patiño-Medina, J.A., **Valle-Maldonado, M.I.**, Vargas-Tejeda, D., Chávez-Jacobo, V.M., Corrales-Escobosa, A.R., Ramírez-Emiliano, J., Ruiz-Herrera, L.F., Ramírez-Díaz, M.I., Garre, V., Meza-Carmen, V. 2020. Arf-like proteins (Arl1 and Arl2) are involved in mitochondrial homeostasis in *Mucor circinelloides*. *Fungal Biol* 124(7):619-628.

11. Hernández-Ramírez, K.C., Valerio-Arellano, B., **Valle-Maldonado, M.I**., Ruíz-Herrera, L.F., Meza-Carmen, V., Ramírez-Díaz, M.I. 2020. Virulence Conferred by PumA Toxin from the Plasmid-Encoded PumAB Toxin-Antitoxin System is Regulated by Quorum System. *Curr Microbiol*. doi: 10.1007/s00284-020-02083-3.

Artículos de divulgación:

12. Meza-Carmen, V., **Valle-Maldonado, M.I**., 2014. SENTIR O NO SENTIR. ESE ES EL DILEMA. Saber Más Número 14. ISSN: 2007-7041.

13. **Valle-Maldonado, M.I**., Meza-Carmen, V .2019. Hongos: los inquilinos de nuestro cuerpo. Saber Más Número 19. ISSN: 2007-7041.

Mol Biol Rep
DOI 10.1007/s11033-014-3818-x

Selection of reference genes for quantitative real time RT-PCR during dimorphism in the zygomycete *Mucor circinelloides*

Marco I. Valle-Maldonado · Irvin E. Jácome-Galarza · Félix Gutiérrez-Corona · Martha I. Ramírez-Díaz · Jesús Campos-García · Víctor Meza-Carmen

Received: 18 February 2014 / Accepted: 7 November 2014

Abstract *Mucor circinelloides* is a dimorphic fungal model for studying several biological processes including cell differentiation (yeast-mold transitions) as well as biodiesel and carotene production. The recent release of the first draft sequence of the *M. circinelloides* genome, combined with the availability of analytical methods to determine patterns of gene expression, such as quantitative Reverse transcription-Polymerase chain reaction (qRT-PCR), and the development of molecular genetic tools for the manipulation of the fungus, may help identify *M. circinelloides* gene products and analyze their relevance in different biological processes. However, no information is available on *M. circinelloides* genes of stable expression that could serve as internal references in qRT-PCR analyses. One approach to solve this problem consists in the use of housekeeping genes as internal references. However, validation of the usability of these reference genes is a fundamental step prior to initiating qRT-PCR assays. This work evaluates expression of several constitutive genes by qRT-PCR throughout the morphological differentiation stages of *M. circinelloides*; our results indicate that *tfc-1* and *ef-1* are the most stable genes for qRT-PCR assays during differentiation studies and they are proposed as reference genes to carry out gene expression studies in this fungus.

Keywords Dimorphism · *Mucor circinelloides* · Quantitative real time RT-PCR · Reference genes

Introduction

Mucor circinelloides is a fungus belonging to the class of zygomycetes, which exhibits a wide range of morphological stages in accordance with culturing conditions. For example, in cultures carried out in the presence of a fermentable carbon source and oxygen, the spores of *M. circinelloides* germinate and grow in the form of hyphae and eventually lead to mycelium, but in the absence or under low levels of oxygen, the spores develop into yeast cells [1–3]. This zygomycete is also capable of developing yeast-like cells from starting hyphae and vice versa under appropriate culturing conditions, a phenomenon that has been termed morphological transition [2]. By other hand, it had been described that *M. circinelloides* shows physiological photo-response [4], is also considered an opportunistic pathogen in immunosuppressed patients [5], and had been proposed as an alternative for production of biodiesel as a renewable energy source [6]. On the other hand, the development of molecular tools to analyze the biological role of certain genes in *M. circinelloides*, such as protoplast

Marco I. Valle-Maldonado, Irvin E. Jácome-Galarza have contributed equally to this work.

Electronic supplementary material The online version of this article (doi:10.1007/s11033-014-3818-x) contains supplementary material, which is available to authorized users.

M. I. Valle-Maldonado · M. I. Ramírez-Díaz · J. Campos-García · V. Meza-Carmen (✉)
Laboratorio de Biotecnología Microbiana, Instituto de Investigaciones Químico Biológicas, Universidad Michoacana de San Nícolás de Hidalgo, 58030 Morelia, Michoacán, Mexico
e-mail: victor_meza2004@yahoo.com.mx

I. E. Jácome-Galarza
Laboratorio Estatal de Salud Pública del Estado de Michoacán, 58279 Morelia, Michoacán, Mexico

F. Gutiérrez-Corona
División de Ciencias Naturales y Exactas, Departamento de Biología, Universidad de Guanajuato, 36050 Guanajuato, Guanajuato, Mexico

Published online: 13 November 2014

FUNGAL BIOLOGY 119 (2015) 1179–1193

British Mycological Society promoting fungal science

journal homepage: www.elsevier.com/locate/funbio

Phylogenetic analysis of fungal heterotrimeric G protein-encoding genes and their expression during dimorphism in *Mucor circinelloides*

Marco Iván VALLE-MALDONADO[a], Irvin Eduardo JÁCOME-GALARZA[b], Alma Laura DÍAZ-PÉREZ[a], Guadalupe MARTÍNEZ-CADENA[c], Jesús CAMPOS-GARCÍA[a], Martha Isela RAMÍREZ-DÍAZ[a], Homero REYES-DE LA CRUZ[a], Héctor RIVEROS-ROSAS[d], César DÍAZ-PÉREZ[e], Víctor MEZA-CARMEN[a,*]

[a]Instituto de Investigaciones Químico Biológicas, Universidad Michoacana de San Nicolás de Hidalgo, Ciudad Universitaria, 58038, Morelia, Mich., Mexico
[b]Laboratorio Estatal de Salud Pública del Estado de Michoacán, 58279, Morelia, Mich., Mexico
[c]División de Ciencias Naturales y Exactas, Universidad de Guanajuato, 36000, Guanajuato, Gto., Mexico
[d]Departamento de Bioquímica, Facultad de Medicina, Universidad Nacional Autónoma de México, 04510, Mexico D.F., Mexico
[e]Departamento de Ingeniería Agroindustrial, División de Ciencias de la Salud e Ingenierías, Campus Celaya-Salvatierra, Universidad de Guanajuato, 38000, Salvatierra, Gto., Mexico

ARTICLE INFO

Article history:
Received 27 February 2015
Received in revised form
8 August 2015
Accepted 10 August 2015
Available online 29 August 2015
Corresponding Editor:
Teun Boekhout

Keywords:
Expression profile
Gene expression
G protein phylogeny
Signal transduction
Zygomycetes

ABSTRACT

In fungi, heterotrimeric G proteins are key regulators of biological processes such as mating, virulence, morphology, among others. *Mucor circinelloides* is a model organism for many biological processes, and its genome contains the largest known repertoire of genes that encode putative heterotrimeric G protein subunits in the fungal kingdom: twelve Gα (McGpa1–12), three Gβ (McGpb1–3), and three Gγ (McGpg1–3). Phylogenetic analysis of fungal Gα showed that they are divided into four distinct groups as reported previously. Fungal Gβ and Gγ are also divided into four phylogenetic groups, and to our understanding this is the first report of a phylogenetic classification for fungal Gβ and Gγ subunits.

Almost all genes that encode putative heterotrimeric G subunits in M. circinelloides are differentially expressed during dimorphic growth, except for McGpg1 (Gγ) that showed very low mRNA levels at all developmental stages. Moreover, several of the subunits are expressed in a similar pattern and at the same level, suggesting that they constitute discrete complexes. For example, McGpb3 (Gβ), and McGpg2 (Gγ), are co-expressed during mycelium growth, and McGpa1, McGpb2, and McGpg2, are co-expressed during yeast development. These findings provide the conceptual framework to study the biological role of these genes during *M. circinelloides* morphogenesis.

* *Corresponding author*. Laboratorio de Biotecnología Microbiana, Instituto de Investigaciones Químico Biológicas, Universidad Michoacana de San Nicolás de Hidalgo, Ciudad Universitaria, 58030, Morelia, Mich., Mexico. Tel./fax: +52 443326 5788x120.
E-mail address: victor_meza2004@yahoo.com.mx (V. Meza-Carmen).
http://dx.doi.org/10.1016/j.funbio.2015.08.009
1878-6146/

Microbial Pathogenesis 112 (2017) 259–268

Contents lists available at ScienceDirect

Microbial Pathogenesis

journal homepage: www.elsevier.com/locate/micpath

Plasmid pUM505 encodes a Toxin–Antitoxin system conferring plasmid stability and increased *Pseudomonas aeruginosa* virulence

K.C. Hernández-Ramírez [a], V.M. Chávez-Jacobo [a], M.I. Valle-Maldonado [a], J.A. Patiño-Medina [a], S.P. Díaz-Pérez [a], I.E. Jácome-Galarza [b], R. Ortiz-Alvarado [c], V. Meza-Carmen [a], M.I. Ramírez-Díaz [a, *]

[a] Instituto de Investigaciones Químico-Biológicas, Universidad Michoacana, Morelia, Michoacán, Mexico
[b] Laboratorio Estatal de Salud Pública, Secretaría de Salud Michoacán, Morelia, Mexico
[c] Facultad de Químico-Farmacobiología, Universidad Michoacana, Morelia, Mexico

ARTICLE INFO

Article history:
Received 6 June 2017
Received in revised form
20 September 2017
Accepted 28 September 2017
Available online 29 September 2017

Keywords:
Pseudomonas
Plasmid
Virulence
Toxin-antitoxin system
Plasmid stability

ABSTRACT

Pseudomonas aeruginosa plasmid pUM505 possesses a pathogenicity island that contains the *pumAB* genes that encode products with sequence similarity to Toxin–Antitoxin (TA) modules. RT-PCR assays on the overlapping regions of the *pumAB* genes generated a bicistronic messenger RNA, suggesting that they form an operon. When the *pumAB* genes were cloned into the pJET vector, recombinant plasmid pJET-*pumAB* was maintained under nonselective conditions in *Escherichia coli* cells after six daily subcultures, whereas pJET without *pumAB* genes was lost. These data indicate that *pumAB* genes confer post-segregational plasmid stability. In addition, overexpression of the PumA protein in the *E. coli* BL21 strain resulted in a significant growth inhibition, while BL21 co-expressing the PumA and PumB proteins did not show growth inhibition. These results indicate that *pumAB* genes encode a TA system where the PumB protein counters the toxic effects of the PumA toxin. Furthermore, *P. aeruginosa* PAO1 transformants with the *pumA* gene increased *Caenorhabditis elegans* and mouse mortality rate and improved mouse organ invasion, effects neutralized by the PumB protein. Moreover, purified recombinant His-PumA protein decreased the viability of *C. elegans*, indicating that the PumA protein could acts as a toxin. These results indicate that PumA has the potential to promoter the PAO1 virulence against *C. elegans* and mice when is expressed in absence of PumB. This is the first description, to our knowledge, of a plasmid-encoded TA system that confers plasmid stability and encoded a toxin with the possible ability to increase the *P. aeruginosa* virulence.

1. Introduction

Pseudomonas aeruginosa is a versatile Gram-negative bacterium that is ubiquitously distributed in different terrestrial, aquatic, animal, human, and plant environments [38]. *P. aeruginosa* is one of the most important opportunistic pathogens in humans. Patients with chronic diseases or with compromised immune systems, such as immunodeficiency or burns, are at greater risk of infection [32]. In addition, *P. aeruginosa* uses a shared subset of virulence factors to elicit disease in both plants and animals [33]. The conjugative plasmid pUM505 is an IncI type of 123 kilobases (kb) in size, originally isolated from a *P. aeruginosa* clinical strain, which confers resistance to chromate ions and inorganic mercury [10]. Sequence analysis revealed that pUM505 carries several adaptive genes, including *umuD*, which functions as a transcriptional regulator of SOS genes [14], as well as several genes related to virulence [35]. It has been suggested that pUM505 could provide *Pseudomonas* strains with a wide variety of adaptive traits that can comprise selective factors for the distribution and prevalence of this plasmid in diverse environments [34]. The predicted products of Open Reading Frames (ORF) 123 and 124 from pUM505 exhibit sequence similarity to Toxin–Antitoxin (TA) systems [34]. TA systems are small genetic modules found in bacterial mobile genetic elements, as well as in bacterial chromosomes, which currently are group into the six types of TA systems [23,28]. The toxins of all characterized

* Corresponding author. Instituto de Investigaciones Químico-Biológicas, Universidad Michoacana, Edificio B-3, Ciudad Universitaria, 58030 Morelia, Mich., Mexico.
E-mail address: marthaisela_ramirez@hotmail.com (M.I. Ramírez-Díaz).

https://doi.org/10.1016/j.micpath.2017.09.060
0882-4010/

template, and the fragment was subsequently cloned into the pJET1.2/blunt vector. In order to amplify the *pumA* and *pumB* genes independently, primers OD_2 and OR_1 and the OD_3 and OR_2 were used, respectively (Table S1) (Fig. 1a). The amplified fragments were also purified and cloned into the pJET1.2/blunt vector. Recombinant plasmids were transferred by electroporation to *E. coli* JM101 and transformants were selected on LB agar plates with Ampicillin.

For subcloning *pumAB* genes or *pum* individual genes into the pUCP20 vector, recombinant plasmids from pJET derivatives were digested with restriction enzymes *Bam*HI and *Xba*I, and DNA fragments were ligated onto the corresponding sites of pUCP20. Recombinant plasmids were transferred by electroporation to *P. aeruginosa* PAO1 or *E. coli* JM101 and the transformants were selected by culturing on LB agar with Carbenicillin or Ampicillin, respectively.

2.5. Plasmid stability tests

For stability tests, *E. coli* JM101 (pJET-*pumAB*) cultures were grown in NB without Ampicillin selection at 37 °C with shaking for 24 h. Serially diluted samples were then plated on nutrient agar with or without Ampicillin. Plates were incubated for 24 h at 37 °C and Colony-Forming Units (CFU) were measured for each condition. The initial cultures were then diluted 1:50 in fresh medium without antibiotic, incubated for 24 h, and the CFU were measured; the described procedure was repeated daily for up to 6 days. As a negative control of plasmid stability, the same procedure was followed using cultures of *E. coli* JM101 (pJET-*orf131*). To confirm the presence or absence of plasmids pJET-*pumAB* or pJET-*orf131*, CFU were obtained from nutrient agar plates with and without Ampicillin, and agarose gel electrophoresis of plasmid DNA isolated by a mini-prep procedure was performed.

2.6. Overexpression and purification of Toxin–Antitoxin proteins

The *pumA* gene coding region, as well as the DNA region from the *pumA* start codon to the *pumB* stop codon (for co-expression of both PumA and PumB proteins), were amplified by PCR using isolated pUM505 plasmid as the template; the primers employed were Dir123pTrc and Rev123pTrc or ODpTrc2A123-4 and ORpTrc2A123-4, respectively (Table S1). The amplified fragments were cloned into the pJET1.2/blunt vector, and the recombinant plasmids were transferred by electroporation to *E. coli* JM101 and transformants were selected on LB agar plates with Ampicillin. The *pumA* gene coding region was obtained after digesting the plasmid with the restriction enzymes *Pst*I and *Hind*III, and the *pumAB* region was obtained by enzyme digestion with *BamH*I and *Hind*III; both fragments were purified and subcloned into their corresponding restriction enzyme sites of the pTrcHisC or pTrcHis2A vectors, respectively. Recombinant plasmid pTrcHis-*pumA* encodes the tagged His-PumA recombinant protein of ~16 kDa that possesses a 6X-His tag at the N-terminal end. Recombinant plasmid pTrcHis-*pumAB* encodes the PumA protein of a theoretical 11.1 kDa in size and the tagged PumB-His recombinant protein of ~17 kDa that possesses a 6X-His tag at the C-terminal end. Fragment directionality was verified by sequencing with the pTrcHis Forward primer (Thermo Fisher Scientific, Waltham, MA, USA). The recombinant plasmids were transferred by electroporation to *E. coli* BL21-CodonPlus® (DE3)-RP, followed by selection of transformants on LB agar plates with Ampicillin. Overnight cultures of *E. coli* BL21 (pTrcHis-*pumA*) or *E. coli* BL21 (pTrcHis-*pumAB*) were diluted 1:50 into 250 ml of fresh NB medium and cultured with shaking at 37 °C until $OD_{600} = 0.5$. Overexpression of His-PumA and PumA/PumB-His (in co-expression) proteins was induced with 1 mM IsoPropyl-β-D-ThioGalactopyranoside (IPTG) and the cultures were incubated for an additional 6 h. Cells were harvested by centrifugation at 7500 rpm for 30 min at 4 °C; the pellets were suspended in loading buffer [25 mM Tris (Tris [hydroxymethyl] amino methane)-HCl pH 6.8, 1% SDS (Sodium Dodecyl Sulfate), 0.35 mM β-mercaptoethanol, 12.5% glycerol, and 0.005% bromophenol blue] and heated for 5 min at 95 °C. Overproduction of the His-PumA and PumB-His recombinant proteins were verified by SDS-PAGE using a Tris-glycine buffer.

His-PumA and PumB-His proteins purification was performed as described by Ref. [42]. Cells were disrupted by sonic oscillation for clarification and debris was removed by centrifugation. The supernatant was loaded onto a Nickel-NTA resin (Qiagen) packed into a column. The His-PumA and PumB-His proteins were recovered by elution with 200 mM Imidazole as described by Ref. [4]. Purification was monitored by recombinant protein detection by SDS-PAGE followed by staining with Coomassie blue.

For Western blot assays, a duplicate of the previously mentioned polyacrylamide gel was transferred onto a nitrocellulose membrane (Hybond ECL). The membrane was incubated 1 h at 37 °C with HisProbe-HRP (Thermo, Rockford, IL, USA) diluted at a 1:1000 ratio, and the bound probe was visualized with the Super Signal West Pico reagent (Thermo Fisher Scientific, Waltham, MA, USA).

2.7. Bacterial growth assays

Liquid cultures of *P. aeruginosa* PAO1 or *E. coli* JM101 containing the pUC-*pumA* recombinant plasmid were utilized to evaluate the effects of PumA protein expression. Overnight cultures were diluted 1:50 in 250 ml of fresh NB medium and growth was monitored at intervals by measuring OD_{600}. Serially diluted samples were then plated on nutrient agar with Ampicillin and incubated for 24 h at 37 °C and the CFU were measured.

In addition, the effects of His-PumA protein overexpression or the PumA and PumB-His proteins co-expression in *E. coli* BL21 were assayed by measuring their growth in liquid medium in the presence or absence of the IPTG inducer. Overnight cultures of *E. coli* BL21 (pTrcHis-*pumA*) or *E. coli* BL21 (pTrcHis-*pumAB*) were diluted 1:50 in 250 ml of fresh NB medium, and growth was monitored at intervals by measuring OD_{600}. At this point, PumA protein overexpression and PumAB proteins co-expression were induced by adding 1 mM of IPTG, and bacterial growth was monitored at intervals by measuring OD_{600}.

2.8. RT-qPCR assays

For *pumA* gene expression measurement from the BL21 (pTrcHis-*pumA*) strain, cultures were incubated for 6 h after their induction with 1 mM of IPTG, and cells were harvested by centrifugation. Total RNA was isolated and quantified as described in the RNA isolation method mentioned previously. Oligonucleotide primers and hydrolysis probes for RT-qPCR of the *pumA* gene and the *16S* rRNA reference genes (listed in Table S1) were designed employing Biosearch Technologies software (www.biosearchtech.com/support/applications/realtimedesign-software) and were purchased from Biosearch Technologies (Novato, CA, USA). Amplification of the *pumA* gene and the *16S* rRNA genes was performed using the 5′ exonuclease probe RT-qPCR method. RT-qPCR was performed with total RNA samples (500 ng) and the SuperScript III Platinum One-Step RT-qPCR Reagent kit (Thermo Fisher Scientific, Waltham, MA, USA) on the LightCycler 480 II System (Roche Molecular Diagnostics, Pleasanton, CA, USA). Amplification signal curves were analyzed at absorption wavelengths of 530 nm. Appropriate positive and non-template controls were included in each test run. Relative expression of the *pumA* gene was normalized with expression values obtained from *16S* rRNA genes from

P. aeruginosa (accession number AE004091; region: 722096–723631) or *E. coli* (accession number AJ605115). Estimation of relative gene expression was performed via the classical calibration dilution curve and slope calculation. A five-fold dilution series (500–0.05 ng total RNA) was prepared and utilized as sample in the RT-qPCR. Efficiency (E) was obtained from standard curves utilizing the formula $E = (10^{-1/\text{slope}} - 1) \times 100$. Relative expression levels were determined with the efficiency correction method, which takes into account amplification efficiencies between target and reference genes [31].

2.9. Virulence assays

2.9.1. Caenorhabditis elegans killing assays

C. elegans Bristol N2 [6] worms were synchronized by hypochlorite isolation of eggs from gravid adults, followed by hatching of eggs in S-basal medium [39]. L1 larvae were transferred onto NGM (Nematode Growth Medium) [39] in plates seeded with the *E. coli* OP50 strain previously grown on the plates as a food source and incubated at 20 °C for 4–5 days until they reached the young adult phase. Worms were rinsed off the plates and washed in S-basal medium. Cultures of *P. aeruginosa* strains were grown overnight in M9 broth at 37 °C, centrifuged, and the pellets were suspended in fresh M9 broth and grown to an $OD_{600} = 0.4$. For each experiment, 20 worms were dispensed into each well of a 24-well Costar plate (Corning, Inc., Corning, NY, USA). The worms were incubated with 1×10^5 ($\pm 1 \times 10^4$) CFU of the bacterial strain contained in a total volume of 1 ml, and the plates were incubated for 36 h at 20 °C and scored for live worms at 6, 12, 24, and 36 h. *P. aeruginosa* PAO1 (pUCP20) and M9 medium were used as a positive and negative control, respectively. A worm was considered dead when it no longer responded (moved) to a touch stimulus. Worms that died as a result of becoming adhered to the wall of the plate were excluded from the analysis. For all assays, bacterial concentrations were confirmed by dilution, plating, and counting. Two independent assays with two replicates were conducted for each worm group. By supernatant effects assays the cultures of *P. aeruginosa* strains were grown overnight in M9 broth at 37 °C and centrifuged to obtain the supernatant. The worms were incubated with 100 μl of the bacterial strain supernatant in a total volume of 1 ml and the plates were incubated for 36 h at 20 °C and scored for live worms at 6, 12, 24, and 36 h. Two independent assays with two replicates per experiment were conducted for each worm group.

PumA protein toxicity on *C. elegans* was determined by His-PumA purified protein incubation. A total of 20 worms were dispensed into each well of 24-well plates (Corning) and incubated with 10, 25, 50, or 100 μg ml^{-1} of His-PumA protein in a volume of 100 μl, and the plates were incubated for 48 h at 20 °C and scored for live worms at 6, 12, 24, 36, and 48 h. *C. elegans* was incubated in M9 medium, and M9 containing protein elution buffer with or without 0.2 M of Imidazole were used as negative controls. Additionally, His-PumA protein toxicity to *C. elegans* was analyzed after their denaturation by heating at 95 °C for 2 h or by hydrolysis utilizing 100 μg ml^{-1} of Pronase E (Sigma-Aldrich). Finally, the PumA toxicity effect neutralized by PumB protein was determined by *C. elegans* incubation in presence of His-PumA and PumB-His purified proteins in a ratio 1:1 and 1:2. Two independent experiments with two replicates were performed for each worm group.

2.9.2. Mouse virulence experiments

The protocol for mouse manipulation assays followed the recommendations for animal manipulation issued by SAGARPA (Secretaría de Agricultura, Ganadería, Desarrollo Rural, Pesca y Alimentación, México), 2001.

To assess the virulence and colonization ability of *Pseudomonas* strains, groups of 10, 8–10-week-old male BALB/c mice weighing 18–22 g were used. The virulence assays were conducted as described by Ref. [35] and inoculated (100 μl) with as single dose administered by tail-vein injection with 3×10^6 ($\pm 3 \times 10^5$) CFU. Mouse survival was monitored each day. Two independent assays were conducted for each group.

To assess the colonization ability of *P. aeruginosa* PAO1 bearing *pumAB* genes, the mice were anesthetized with sodium pentobarbital (24 mg/kg) and inoculated via tail-vein administration with 5×10^6 ($\pm 5 \times 10^5$) CFU contained in a volume of 100 μl as described by Ref. [35]. At 48 h post-inoculation, the mice were euthanized and samples were taken for analysis. Heart, lungs, and kidneys were removed by dissection, weighed, and homogenized in 10 mM $MgSO_4$ utilizing a mortar and pestle. Organ homogenates were serially diluted in 10 mM $MgSO_4$ and plated on LB agar for CFU determination. Three independent assays were conducted for each mouse group. For all assays, bacterial inoculum concentrations were confirmed by dilution, plating, and CFU determination.

2.10. Statistical analysis

Data analysis was carried out with GraphPad Prism 5 software. ANalysis Of VAriance (ANOVA) employing the Tukey test was performed for all *Pseudomonas* assays. In addition, a Student t-test was carried out for the analysis of the expression assays. $P < 0.05$ was considered statistically significant.

3. Results and discussion

3.1. The pumAB genes of plasmid pUM505

Owing to their similarity with previously characterized proteins, ORF 123 and 124 from the pathogenicity island of pUM505 were reported to encode a probable TA system [34]. These ORF were renamed as *pumA* and *pumB* genes for the pUM505 Toxin–Antitoxin system. PumA is a predicted protein of 99 aa (GenBank accession number AEQ93530) that was previously reported to exhibit 55% sequence identity with the RelE protein (toxic component) of the TA system from *Klebsiella pneumoniae* (ZP_06016753) [34]. A recent BLAST analysis showed that the *pumA* gene encodes a protein that is 73% identical to an uncharacterized addiction module killer protein from *Pseudomonas putida* (NCBI Reference Sequence WP_011005862). Additionally, an amino acid sequence alignment with proteins of the RelE toxin superfamily with known biological function was conducted. The alignment revealed that the PumA protein possesses only 22% identity to MjRelE from *Methanococcus jannaschii*, 18% to YoeB from *E. coli*, and 14% to PhRelE from *Pyrococcus horikoshii* (Fig. S1, Supplementary Material). The low identity of PumA with RelE-like proteins is not surprising, in that it has been reported that amino acid sequences of RelE-like proteins are quite divergent, even those originating from the same or closely related bacterial species [16]. In general, RelE-like sequences present 24–47% similarity among themselves and 15–28% identity with the canonical RelE protein from *E. coli* K-12 [15]. Although highly divergent at the primary sequence level, the PumA protein contains a secondary structure predicted by the MINNOU program that is characteristic of toxins of the RelE superfamily, constituted by five-stranded β-sheet flanked on one side by α-helices α1 and α2 and, on the other side, by α-helix α3 [15] (Fig. S1, Supplementary Material). It has been reported that, despite very low conservation at the amino acid sequence level, RelE-like proteins share secondary and tertiary structures with similar folding [16]. Additionally, PumA contains conserved-type residues (Val4, Val41, Val44, Ile53, Val61, and Val81) and highly-conserved residues (Asp40, Arg52, His54, and Arg60) that are

found in the MjRelE and YoeB proteins (Fig. S1, Supplementary Material). The mutation of Arg62 in MjRelE, which corresponds to Arg65 of PhRelE, renders a toxin inactive [15]; the Arg62 residue located in MjRelE corresponds to Arg60 in the PumA sequence. This analysis suggested that PumA could belong to the RelE toxin family.

The *pumB* gene encodes a putative transcriptional regulator of 96 aa (GenBank accession number AEQ93531) with 92% identity to the antitoxin HTH protein (Helix-Turn-Helix xenobiotic-resistant family-like proteins) from *Pseudomonas alcaligenes* (AAD40346) [34]. The PumB protein contains a predicted HTH DNA-binding domain (Fig. S2, Supplementary Material) that is characteristic of the Xre family of antitoxins, and this domain has often been found in characterized antitoxins [44]. In type II TA systems, the antitoxin is generally a DNA-binding protein that binds to the operator of the operon to repress its own transcription. In the majority of cases, the HTH motif is located at the N-terminal domain of the antitoxins [11]. Examples of the existence of the HTH motif in solved structures of antitoxins include PezA [21], as well as HigA [37]. However, the HTH motif of PumB was located at the C-terminal region of the protein (Fig. S2, Supplementary Material). A similar position of the HTH motif was found in the functional antitoxin MqsA of *E. coli* [8]. This analysis suggests that the PumB protein could function as an HTH-type antitoxin protein.

As mentioned previously, the *pumA* gene encodes a putative RelE-type toxin, while the *pumB* gene encodes a putative HTH-type antitoxin, and it is suggested that these genes encode a hybrid TA system. In general, it has been assumed that each toxin family is associated with a specific antitoxin family; for instance, RelE proteins are frequently associated with RelB antitoxins [17]. However, many hybrid systems exist in which a TA locus contains a toxin of one class and an antitoxin of another class [3]. Together, these results suggest that *pumAB* genes from plasmid pUM505 encode a putative TA hybrid system.

3.2. *pumAB genes form an operon*

The *pumA* and *pumB* genes exhibited a genetic arrangement where *pumA*, which encodes a putative toxin, was located upstream of *pumB*, which encodes an antitoxin (Fig. 1a). In the majority of TA systems, antitoxin genes are located upstream of their cognate toxin genes, suggesting that antitoxins appear to possess an advantage over their cognate toxins with regard to their production [44]. However, there are exceptional cases in which toxin genes are located upstream of their cognate antitoxin genes, suggesting that these differences in gene order might exert a subtle effect on the toxin-to-antitoxin ratio in the cell, which in turn regulates toxin function [44]. Additionally, sequence analysis revealed that *pumA* and *pumB* genes contain a putative σ^{70} promoter that showed at the non-typical −35 to −10 box in the 5′ region of *pumA* (Fig. 1a); no promoter region was identified for *pumB*, suggesting that these two genes constitute an operon that could be expressed from the *pumA* promoter. In type II TA systems, toxin and antitoxin genes are commonly co-transcribed, forming operons [13], suggesting an evolutionary advantage of the close vicinity of coding regions. Additionally, *pumAB* genes have overlapped coding regions; the stop codon of *pumA* and the initiation codon of *pumB* share four nucleotides (Fig. 1a). Overlapping of coding sequences is a conserved feature of paired TA systems [23].

To investigate the existence of a possible transcriptional linkage of the *pumAB* genes, RT-PCR analyses were performed. Primers were designed to amplify complementary DNA (cDNA) synthesized from a transcript spanning the overlapping *pumAB* region (Fig. 1a). When total RNA from exponential-phase cultures of the *P. aeruginosa* PAO1 (pUM505) strain was probed, a sole ~440-bp DNA fragment, covering the overlapping region, was detected (Fig. 1b, lane 2). No corresponding fragment was detected in the negative control (Fig. 1b, lane 1). A less intense DNA band was observed with RNA obtained from stationary-phase cultures (Fig. 1b, lane 3), which is in agreement with previous reports of TA systems displaying higher expression levels in the exponential growth phase [26]. These data demonstrate that the *pumAB* genes are co-transcribed into a bicistronic mRNA, and strongly suggest that they form an operon.

3.3. *The pumAB genes confer plasmid stability*

Since the function of plasmid-encoded TA systems is related to plasmid stabilization, we investigated whether *pumAB* genes are able to promote plasmid maintenance. Because pUM505 additionally to possess the putative TA system contains several genes probably related with the partition, segregation, maintenance, and stabilization of plasmids, as well as *parA*, *parB*, *xerD*, *xerC*, and *ssb*, respectively, [34], in order to test this, *pumAB* genes were first cloned into the Ampicillin (Ap)-resistance pJET vector and the recombinant plasmid pJET-*pumAB* obtained was transferred to the *E. coli* JM101 strain. Plasmid segregation was tested by measuring CFU in *E. coli* JM101 (pJET-*pumAB*) and JM101 (pJET-*orf131*) strains after 24-h consecutive subcultures in non-selective NB medium; samples were withdrawn each day, diluted, and plated on nutrient agar with or without Ap, as described under Methods. CFU of pJET-*orf131*-containing cells decreased in each subculture on the Ap plates from day 3 (corresponding to 216 generations) and, after day 6 (corresponding to 432 generations), these were undetectable (Fig. 2). In contrast, CFU counts in transformants bearing the pJET-*pumAB* plasmid remained without significant changes throughout the assay. Agarose gel electrophoresis of mini-prep plasmid DNA isolations from the subcultures confirmed the absence of plasmid bands from pJET-*orf131* clones, as well as the presence of recombinant plasmid in clones from pJET-*pumAB* transformants (Fig. S3, Supplementary Material). These data indicate that the presence of *pumAB* increases the stability of the pJET plasmid and suggest that they do so by means of a post-segregation killing mechanism

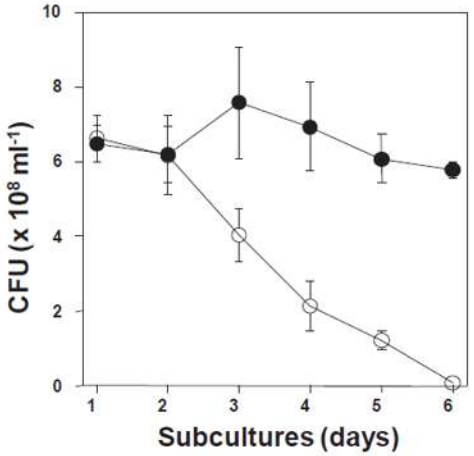

Fig. 2. Plasmid stability conferred by *pumAB* genes from pUM505. Cultures were grown in Nutrient Broth at 37 °C with shaking, and consecutive 24-h subcultures were performed without antibiotic selection. Serial dilutions from each subculture were plated on Nutrient agar medium with Ampicillin, and CFU were counted as described under Methods. Symbols: (○), *E. coli* JM101 (pJET-*orf131*) as a negative control; (●), *E. coli* JM101 (pJET-*pumAB*). Data shown are the means of three independent assays in duplicate with Standard Error (SE) bars shown.

involving a TA system, probably composed of the PumA toxin and its PumB cognate antitoxin.

3.4. Overexpression of the pumA gene inhibits E. coli growth

To investigate whether a functional toxin is encoded by *pumA* of pUM505, this gene, including its putative promoter, was subcloned into the pUCP20 shuttle vector; recombinant plasmid pUC-*pumA* was transferred to the *P. aeruginosa* PAO1 strain, and growth kinetics in liquid cultures was measured. The presence of the pUC-*pumA* plasmid did not cause growth inhibition in PAO1 cells (Fig. S4a, Supplemental Material). This effect was not expected because the *pumA* gene was identified in a plasmid from a *Pseudomonas* strain and, as was shown, is expressed in this strain together the *pumB* gene as an operon (Fig. 1b). However, an explanation to this result may be attributed to the fact that the *pumA* gene is not expressed in PAO1 under its own promoter into the pUC20 vector. However, another possibility could be that the product encoded by the *pumA* gene was less toxic to PAO1 than to *E. coli*, bearing in mind that the function of *pumAB* genes in plasmid stability was determined in *E. coli*. To discern between these possibilities, *pumA* gene expression was determined by RT-qPCR assays from cultures of *P. aeruginosa* PAO1 containing the recombinant pUC-*pumA* plasmid. The results showed that the *pumA* gene was expressed in the *P. aeruginosa* PAO1 strain (Fig. S4c, Supplemental Material). The latter suggested that this gene is functional in this strain. To determine whether the product of the *pumA* gene affects the growth of *E. coli* cells, recombinant plasmid pUC-*pumA* was transferred to *E. coli* JM101 and growth kinetics in liquid cultures were analyzed. The results demonstrated no differences in the growth of *E. coli* cells through the presence of the pUC-*pumA* plasmid (Fig. S4b, Supplemental Material). Additionally, the results of expression by RT-qPCR analysis showed that the *pumA* gene was expressed in this strain (Fig. S4c, Supplemental Material). These results noted that when PumA is expressed in physiological levels, it does not affect cell growth, suggesting that a high expression level is required. In *Mycobacterium tuberculosis*, a correlation between the expression levels of the VapC toxin from TA systems and its ability to confer a toxic phenotype has been reported [2]. To determine whether the overexpression of PumA affects bacterial growth, the *pumA* gene was subcloned into the pTrcHisC expression vector under the control of an IPTG-inducible promoter, and recombinant plasmid pTrcHis-*pumA* was transferred to the *E. coli* BL21 strain. Growth kinetics with or without IPTG induction was then measured in BL21 derivatives. BL21 cells containing the vector alone, with IPTG, exhibited no harmful effects on growth. In contrast, IPTG-induced BL21 transformants containing recombinant plasmid pTrcHis-*pumA* displayed clear growth inhibition as compared with non-induced transformants (Fig. 3a), and these results were consistent with a decrease in the CFU count (Fig. S5, Supplemental Material). Additionally, *pumA* gene expression levels with or without IPTG induction were determined, and the results showed an increase of about 70 times of the *pumA* transcript with respect to the non-induced condition (Fig. 3b), indicating that overexpression of PumA affects *E. coli* growth. Several reports demonstrated that overexpression of the toxins of TA systems produced cell growth inhibition; for example, in *E. coli* K-12 (MG1655), RelE, MazF, YeeV, and YkfI toxins inhibited bacterial growth when they were ectopically overexpressed [7,30]. Additionally, has been reported that some toxins caused cell growth inhibition when they were heterologously and ectopically overexpressed in *E. coli* BL21, as well as the VapC-3 and Tox28 toxins from *Acidithiobacillus ferrooxidans*, YoeB from *Streptococcus suis*, and YoeB from *Staphylococcus equorum* [9,26,46]. Therefore, our results indicated that, like others toxins from TA systems, a high expression level of the *pumA* gene is required to affect bacterial growth, suggesting that PumA functions as a toxin in *E. coli*. Since many genes can be toxic to cells when they are overexpressed, it was important to determine whether cell growth inhibition by PumA is neutralized by expressing its cognate antitoxin. We compared the growth of *E. coli* BL21, in which the *pumA* was expressed either individually or together with its cognate *pumB*, under the control of the same inducible promoter, to determine whether *pumB* allowed cell growth in the presence of the inducer. The *pumAB* gene pair was cloned into the pTrcHis2A vector and transferred to *E. coli* BL21, as described in Methods. When co-expression of PumA and PumB-His proteins was induced by IPTG, BL21 cells did not exhibit growth inhibition in comparison with the strain with individual His-PumA overexpression (Fig. 3a). These results were consistent with the CFU count (Fig. S5, Supplemental Material), suggesting that PumB protein could neutralize the growth inhibitory effect of PumA. Overexpression of recombinant His-PumA and PumB-His proteins was verified by SDS-PAGE and by Western blot analysis (Fig. S6, Supplementary Material). In type II TA systems, the major role of the antitoxin is to neutralize the toxic function of its cognate toxin mediated by the toxin-binding domain [44]. The majority of the TA systems from *E. coli* and *Mycobaterium smegmatis* tested experimentally showed that the toxin inhibited bacterial growth, indicating an effect that is neutralized by its cognate antitoxin [36]. These results indicate that PumA acts as a toxic protein in *E. coli* and that its effects are neutralized by the presence of PumB protein, which supports the notion that these proteins form a functional TA system in *Pseudomonas*.

3.5. Expression of the pumA gene has the potential to increases P. aeruginosa virulence

It has been reported that some strains of *P. aeruginosa*, such as the highly virulent PA14 strain, can kill the *C. elegans* nematode, utilizing virulence factors that are also required for pathogenesis in mammalian or plant hosts [40]. In addition, chromosomally encoded TA systems may be related to the virulence of bacterial pathogens [13,41]. To determine whether the *pumAB* TA system from pUM505 participates in *P. aeruginosa* virulence, assays to test their ability to kill *C. elegans* were conducted. Since the pUM505 contains several genes that are related with the virulence of *P. aeruginosa* [35], *pumAB* genes were cloned, either paired or individually, in the pUCP20 vector, and recombinant plasmids pUC-*pumAB*, pUC-*pumA* and pUC-*pumB* were transferred to *P. aeruginosa* PAO1. The results revealed that transformants containing the *pumAB* genes displayed similar viability levels as compared to the vector-only PAO1control strain (~60% of worms killed in 36 h) (Fig. 4a), suggested that in the conditions carried out the PumAB TA system is not involved in the virulence of *P. aeruginosa*. However, interestingly transformants with the *pumA* gene in the same conditions assayed increased PAO1 ability to kill worms at ~95% at 36-h post-incubation as compared to the control strain, whereas transformants with plasmid constructions containing *pumB* displayed similar viability levels as compared to the control strain (~60% of worms killed in 36 h) (Fig. 4a). In order to rule out the possibility that the virulence effects observed may be due to differences in the growth rate of the transformants analyzed, growth assays were performed and the results exhibited no harmful effects on growth among the transformants (Fig. S7, Supplementary Material). These data indicate that the *pumA* gene product improves the ability of PAO1 to kill *C. elegans*, this effect is neutralized by the *pumB* gene product. Additionally, the effect of the supernatant from *Pseudomonas* strains on the *C. elegans* viability was assayed and the results showed that the supernatant from *P. aeruginosa* contained the *pumA* gene was able to kill the ~75% of worms in 36 h of incubation;

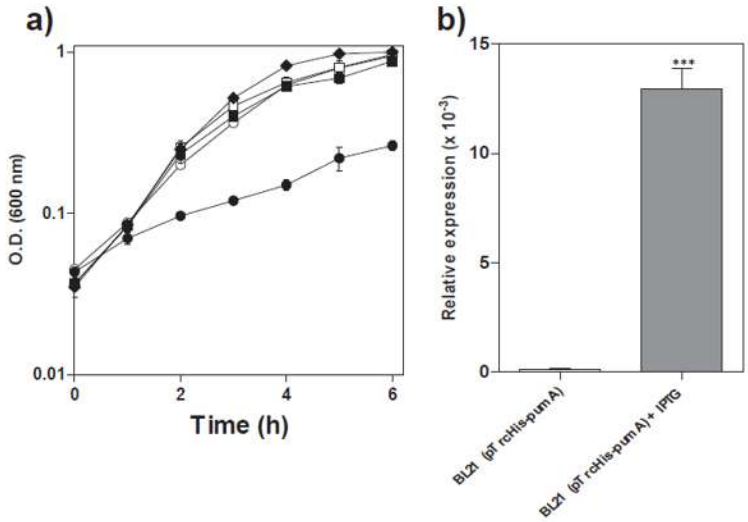

Fig. 3. Overexpression of *pumA* inhibits bacterial growth and the PumB protein neutralized this effect. (**a**) Cultures were grown at 37 °C with shaking in Nutrient Broth, and growth was monitored at intervals as Optical Density (OD) at 600 nm (OD_{600}) with a spectrophotometer. Symbols: (◆), *E. coli* BL21 (pTrcHisC) with 1 mM IPTG; (●) or (○), *E. coli* BL21 (pTrcHis-*pumA*) with or without 1 mM IPTG, respectively; (■) and (□), *E. coli* BL21 (pTrcHis-*pumAB*) with or without 1 mM IPTG, respectively. The data shown are means from the duplicates of three independent assays with Standard Error (SE) bars shown. (**b**) Expression levels of *pumA* from cultures of *E. coli* BL21 (pTrcHis-*pumA*) strain with or without 1 mM IPTG determined by RT-qPCR as described under Methods. Values represent the means of two independent determinations in duplicate with Standard Error (SE) bars shown, normalized with respect to transcription of the *16S* gene from *E. coli*. Statistical analysis was conducted with Student *t*-test to compare the expression, and significant differences ($p < 0.0001$) are indicated by asterisks (***).

whereas *P. aeruginosa* strains contains the *pumB* or *pumAB* genes showed similar killer (~25%) than the *P. aeruginosa* control strain (Fig. S8, Supplementary Material), suggested that the toxin could be secreted to the media growth by the bacteria or release from bacterial lysis to generate toxic effects on the bacterial host. In Rickettsia containing *vap*BC TA systems has been suggested that the toxic effect of on its host could be related to the release of toxin in host cell cytoplasm from a TA complex that is secreted or released following rickettsial death [5]. In addition, comparative genomic studies have shown that the presence of TA systems is significantly associated with the pathogenicity of bacteria [13]. *M. tuberculosis* contains at least 30 functional TA systems, whereas its non-pathogenic counterpart, *M. smegmatis*, has three functional TA systems [36]. Furthermore, TA modules have been shown to be involved in the virulence of *Salmonella* and *Leptospira interrogans* [13,22]. These results suggest that a toxin from a plasmid-encoded TA system might contribute to increasing the virulence of its host.

Additionally, to determine whether the PumA protein is able to kill *C. elegans,* worms were incubated with increasing concentrations of purified His-PumA protein. The results showed that 10 μg ml^{-1} of His-PumA protein was able to kill ~55% of worms in 36 h, and that this effect increased at ~70% with 100 μg ml^{-1} of recombinant protein (Fig. 4b). These harmful effects were not observed when the worms were incubated only with the buffers used for protein elution in these assays (Fig. S9, Supplementary Material). Similar results were previously reported to the VapC toxin from the VapBC TA system of *Rickettsia* spp, this protein was toxic to mammalian cells when injected into the cytoplasm as a free toxin [5]. Additionally, we determined the toxic effect of PumA on *C. elegans* after its denaturalization. The results demonstrated that worm death levels comprised up to ~35 or ~45% when PumA was denaturized by heat or by protease E treatment, respectively, as compared to non-denaturized protein at the same concentration that was able to kill the ~70% of worms (Fig. 4c). The denaturized protein decreased in lethality toward *C. elegans*, suggesting that the toxic effect was not provided by the components of the reaction mix, since a similar worm death was observed between treatments and also suggest that correct structure of the protein is required for its function. Finally, the neutralization of the toxicity of PumA on *C. elegans* by the PumB protein was analyzed, and the results showed that when the worms were incubated simultaneously with PumA and PumB proteins in a 1:2 (toxin:antitoxin) radio, the toxic effect of PumA decrease 50%; whereas, in a 1:1 radio no changes in the toxicity was observed (Fig. 4d), supporting the role of neutralization of PumB and suggested a molar relationship between PumA and PumB proteins. The ratio of the toxin:antitoxin of TA systems had been described is important to determine the stoichiometry of the TA protein complex as well as to regulate the transcription of the TA systems, this phenomenon was termed as conditional cooperativity that reflects that excess toxin often perturbed operator binding by TA complexes [19]. An example of this cooperativity are the CcdAB system from F plasmid of *E. coli*, where both modules form a (CcdA)2–(CcdB)2 complex which binds DNA to regulate the repression state of the *ccd* operon, and the addition of CcdB extra to protein-DNA complex lead an operon derepression [1]. Together, these results indicated that the PumA protein affects the worm viability and suggest that this protein in absence of PumB possess the potential to function as a toxin. It had been described that under non-stress conditions, the toxicity of RelE toxin from RelEB system of *E. coli* is neutralized by the RelB antitoxin by forming a tight non-toxic RelBE complex; but under environmental stress conditions, the antitoxin is degraded by cellular proteinases and RelE is activated [12]. In *Streptomyces cattleya* DSM 46488 it was described that the *relBE2sca* operon transcription was induced under osmotic stress, along with the ClpP proteinase genes, and subsequent *in vivo* analysis showed that the antitoxin was degraded by ClpP [25]. This reports suggests that in some bacterial growth conditions is possible that the decrease in the antitoxins levels allow that the toxin perform its toxic effects.

To test if pUM505 *pumA* gene may also has the ability to increase

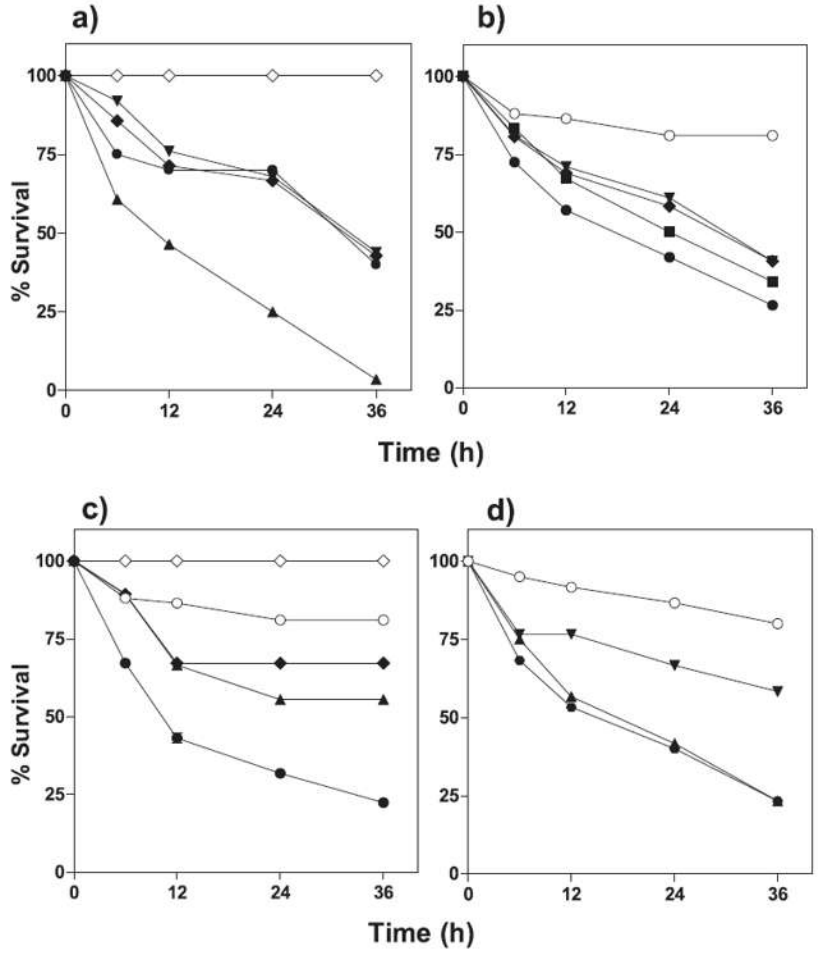

Fig. 4. The product of *pumA* gene kills *Caenorhabditis elegans*. (**a**) Effects of *P. aeruginosa* transformants with *pumAB* genes on *C. elegans* viability. Groups of 20 worms were incubated with 1×10^5 ($\pm 1 \times 10^4$) Colony-Forming Units (CFU) of the indicated strains, as described under Methods. Mixtures were incubated at 20 °C and scored for live worms at the indicated times. Symbols: (◊), M9 medium; (●), *P. aeruginosa* PAO1 pUCP20; (◆), *P. aeruginosa* PAO1 (pUC-*pumAB*); (▲), *P. aeruginosa* PAO1 (pUC-*pumA*), and (▼), *P. aeruginosa* PAO1 (pUC-*pumB*). (**b**) Effects of the PumA protein on *C. elegans* viability. Groups of 20 worms were incubated with purified His-PumA as described under Methods. Mixtures were incubated at 20 °C and scored for live worms at the indicated times. Symbols: (○), M9 medium with 0.2 M Imidazole; (▼), (◆), (■), and (●), M9 medium with 10, 25, 50, or 100 μg ml^{-1} of His-PumA, respectively. (**c**) Effects of previously denaturized His-PumA on *C. elegans* viability. Symbols: (◊), M9 medium; (○), M9 medium with 0.2 M Imidazole; (●), M9 medium with 100 μg ml^{-1} of His-PumA; (▲), and (◆), M9 medium with 100 μg ml^{-1} of His-PumA denaturized by Pronase E or by heat, respectively. (**d**) Neutralization of the PumA protein effects on *C. elegans* viability by PumB. Groups of 20 worms were incubated with purified His-PumA with or without PumB as described under Methods. Mixtures were incubated at 20 °C and scored for live worms at the indicated times. Symbols: (○), M9 medium with 0.2 M Imidazole; (●), M9 medium with 5 μg ml^{-1} of His-PumA, (▲) and (▼), M9 medium with 5 μg ml^{-1} of His-PumA with 1:1 or 1:2 (His- PumA:PumB-His) ratio, respectively. The data shown are means from the duplicates of two independent assays.

the virulence in an animal model, a total of 3×10^6 ($\pm 3 \times 10^5$) CFU of PAO1-derivative strains were individually inoculated by intravenous (i.v.) administration, and mouse survival was monitored each day. It was found that mice infected with *P. aeruginosa* PAO1 (pUC-*pumA*) led to 20% lethality at day 3 post-inoculation, and reached 60% lethality at day 12 compared with mice inoculated with *P. aeruginosa* (pUCP20) or with *P. aeruginosa* (pUC-*pumB*), which both maintained 100% survival until day 12 post-inoculation (Fig. 5a). This result indicates that the toxin encode by the *pumA* gene increase the pathogenicity of *P. aeruginosa* in a mammalian host. Additionally, the effect of the *pumA* on mouse colonization was determined with the previously mentioned PAO1-derivative strains, as described under Methods. The presence of the *pumA* gene significantly increased PAO1 CFU in mouse heart (two-fold), lung (six-fold), and kidney (six-fold) as compared with those inoculated with transformants with the plasmid containing the *pumB* gene, which yielded CFU counts similar to those of the empty-vector strain (Fig. 5b). To determine whether the expression of the PumB antitoxin could neutralize the virulence effects supplied by the presence of the *pumA* gene, mice were inoculated with *P. aeruginosa* transformants containing *pumAB* genes. The results showed that the CFU count was similar to that of the empty-vector strain or to that of the plasmid containing the *pumB* gene (Fig. 5b). These data indicate that PumA expressed alone possess the ability to increases PAO1 invasiveness into mouse organs, an event neutralized by the *pumB* product. Several chromosomal TA systems have been shown to cause increased virulence in their bacterial hosts against animals, including TA systems from *E. coli* [27],

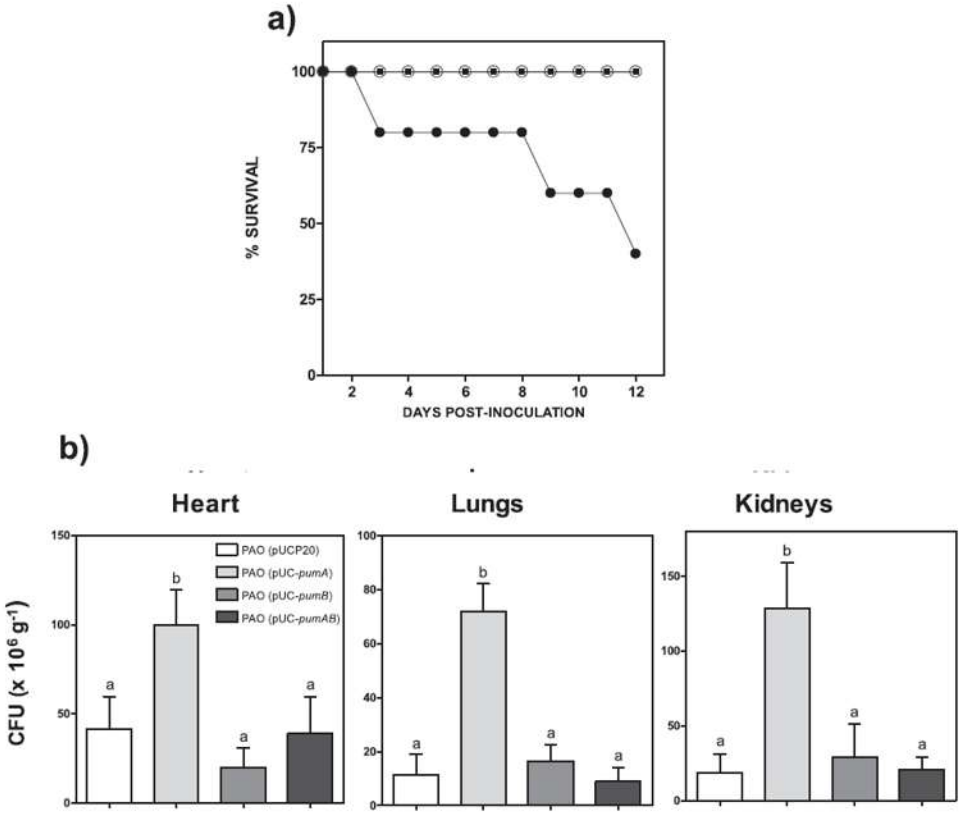

Fig. 5. Mouse virulence by *Pseudomonas aeruginosa* strains. (**a**) Bacterial virulence in mice was determined performing inoculations with a total of 3×10^6 ($\pm 3 \times 10^5$) Colony-Forming Units (CFU) by intravenous (i.v.) administration. Mouse survival was monitored daily for 12 days. Symbols, mice inoculated with: (○), *P. aeruginosa* PAO1 (pUCP20); (■) *P. aeruginosa* PAO1 (pUC-*pumB*), and (●), *P. aeruginosa* PAO1 (pUC-*pumA*). Plots show the mean data pulled from two independent experiments expressed as percentages of mice surviving post-infection in each experimental group. (**b**) Mouse invasivity by *P. aeruginosa* strains. Groups of 10, 8–10-week-old male BALB/c mice were infected with 5×10^6 ($\pm 5 \times 10^5$) CFU of the indicated strains, as described under Methods. At 48 h post-inoculation, heart, lungs, and kidneys were removed by dissection and their homogenates were serially diluted and plated on Luria Broth agar for determination of CFU counts. Control corresponds to the PAO1 pUCP20 strain. Values are the means of three independent experiments conducted for each mouse group. One-way ANalysis Of VAriance (ANOVA) with Tukey post-hoc test was used to compare the strains, and significant differences ($p < 0.05$) are indicated with the letters a and b.

Salmonella typhimurium [13], *M. tuberculosis* [36], *L. interrogans* [22] however, this relationship has not been reported for elements of plasmid-encoded TA systems. These results further confirmed that *pumAB* genes encode a TA system, comprising the PumA toxin and its cognate PumB antitoxin, being the toxin the element with capacity to generate toxic effects. To our knowledge, this is the first toxin from a plasmid-encoded TA system from *P. aeruginosa* that has demonstrated participation in virulence. The increase of PAO1 virulence and the invasion by PumA toward the organisms employed in this work (invertebrates and mammals) suggest that the virulence mechanism involved may be conserved in these evolutionarily divergent hosts. The mechanism by which the PumA toxin exerts its toxic actions is currently under study.

In conclusion, pUM505 contains *pumAB* that encodes a TA system conferring plasmid stability and encodes a toxin with potential to increasing *P. aeruginosa* virulence in animal models.

Funding source

This work was supported by grants from Coordinación de la Investigación Científica (UMSNH; 2.6, 2.35) and Consejo Nacional de Ciencia y Tecnología (CONACYT; 181747, 167071). KCH-R, VMC-J, MIV-M, JA P-M and SPD-P were supported by postgraduate fellowships from CONACYT.

Conflicts of interest

The authors declare no conflict of interest.

Acknowledgments

We thank M.P. Chávez-Moctezuma and R.I. Reyes-Gallegos for their valuable technical support in mouse tissue invasion assays.

Appendix A. Supplementary data

Supplementary data related to this article can be found at https://doi.org/10.1016/j.micpath.2017.09.060.

References

[1] H. Afif, N. Allali, M. Couturier, L. Van Melderen, The ratio between CcdA and

CcdB modulates the transcriptional repression of the *ccd* poison-antidote system, Mol. Microbiol. 41 (2001) 73–82.
[2] B.A. Ahidjo, D. Kuhnert, J.L. McKenzie, E.E. Machowski, B.G. Gordhan, V. Arcus, G.L. Abrahams, V. Mizrahi, VapC toxins from *Mycobacterium tuberculosis* are ribonucleases that differentially inhibit growth and are neutralized by cognate VapB antitoxins, PLoS One 6 (2011) e21738.
[3] V. Anantharaman, L. Aravind, New connections in the prokaryotic toxin-antitoxin network: relationship with the eukaryotic nonsense-mediated RNA decay system, Genome Biol. 4 (2003) R81.
[4] J. Aranda, M.E. Garrido, P. Cortés, M. Llagostera, J. Barbé, Analysis of the protective capacity of three *Streptococcus suis* proteins induced under divalent-cation-limited conditions, Infect. Immun. 76 (2008) 1590–1598.
[5] G. Audoly, R. Vincentelli, S. Edouard, K. Georgiades, O. Mediannikov, G. Gimenez, C. Socolovschi, J.L. Mège, C. Cambillau, D. Raoult, Effect of rickettsial toxin VapC on its eukaryotic host, PLoS One 6 (2011) e26528.
[6] S. Brenner, The genetics of *Caenorhabditis elegans*, Genetics 77 (1974) 71–94.
[7] B.L. Brown, D.M. Lord, S. Grigoriu, W. Peti, R. Page, The *Escherichia coli* toxin MqsR destabilizes the transcriptional repression complex formed between the antitoxin MqsA and the *mqsRA* operon promoter, J. Biol. Chem. 288 (2013) 1286–1294.
[8] J.M. Brown, K.J. Shaw, A novel family of *Escherichia coli* toxin-antitoxin gene pairs, J. Bacteriol. 185 (2003) 6600–6608.
[9] P. Bustamante, M. Tello, O. Orellana, Toxin-antitoxin systems in the mobile genome of *Acidithiobacillus ferrooxidans*, PLoS One 9 (2014) e112226.
[10] C. Cervantes, H. Ohtake, L. Chu, T.K. Misra, S. Silver, Cloning, nucleotide sequence and expression of the chromate resistance determinant of *Pseudomonas aeruginosa* plasmid pUM505, J. Bacteriol. 172 (1990) 287–291.
[11] W.T. Chan, D. Balsa, M. Espinosa, One cannot rule them all: are bacterial toxins-antitoxins druggable? FEMS Microbiol. Rev. 39 (2015) 522–540.
[12] S.K. Christensen, M. Mikkelsen, K. Pedersen, K. Gerdes, RelE, a global inhibitor of translation, is activated during nutritional stress, Proc. Natl. Acad. Sci. U. S. A. 98 (2001) 14328–14333.
[13] M.A. De la Cruz, W. Zhao, C. Farenc, G. Giménez, D. Raoult, C. Cambillau, J.P. Gorvel, S. Méresse, A toxin-antitoxin module of *Salmonella* promotes virulence in mice, PLoS Pathog. 9 (12) (2013) e1003827.
[14] A. Díaz-Magaña, N. Alva-Murillo, M.P. Chávez-Moctezuma, J.E. López-Meza, M.I. Ramírez-Díaz, C. Cervantes, A plasmid-encoded UmuD homologue regulates expression of *Pseudomonas aeruginosa* SOS genes, Microbiology 161 (2015) 1516–1523.
[15] D. Francuski, W. Saenger, Crystal structure of the antitoxin-toxin protein complex RelB-RelE from *Methanococcus jannaschii*, J. Mol. Biol. 393 (2009) 898–908.
[16] N. Goeders, P.L. Drèze, L. Van Melderen, Relaxed cleavage specificity within the RelE toxin family, J. Bacteriol. 195 (2013) 2541–2549.
[17] R. Grady, F. Hayes, Axe-Txe, a broad-spectrum proteic toxin antitoxin system specified by a multidrug-resistant, clinical isolate of *Enterococcus faecium*, Mol. Microbiol. 47 (2003) 1419–1432.
[18] M.R. Green, J. Sambrook, Molecular Cloning: a Laboratory Manual, fourth ed., Cold Spring Harbor Laboratory, Cold Spring Harbor, NY, USA, 2012.
[19] F. Hayes, B. Kędzierska, Regulating toxin-antitoxin expression: controlled detonation of intracellular molecular timebombs, Toxins (Basel) 6 (2014) 337–358.
[20] F. Hayes, L. Van Melderen, Toxins-antitoxins: diversity, evolution and function, Crit. Rev. Biochem. Mol. Biol. 46 (2011) 386–408.
[21] S.K. Khoo, B. Loll, W.T. Chan, R.L. Shoeman, L. Ngoo, C.C. Yeo, et al., Molecular and structural characterization of the PezAT chromosomal toxin-antitoxin system of the human pathogen *Streptococcus pneumoniae*, J. Biol. Chem. 282 (2007) 19606–19618.
[22] K.K. Komi, Y.M. Ge, X.Y. Xin, D.M. Ojcius, D. Sun, W.L. Hu, X. Zhao, X. Lin, J. Yan, ChpK and MazF of the toxin-antitoxin modules are involved in the virulence of *Leptospira interrogans* during infection, Microbes Infect. 17 (2015) 34–47.
[23] R. Leplae, D. Geeraerts, R. Hallez, J. Guglielmini, P. Drèze, L. Van Melderen, Diversity of bacterial type II toxin-antitoxin systems: a comprehensive search and functional analysis of novel families, Nucleic Acids Res. 39 (2011) 5513–5525.
[24] L.L. Li, J.E. Malone, B.H. Iglewski, Regulation of the *Pseudomonas aeruginosa* quorum-sensing regulator VqsR, J. Bacteriol. 189 (2007) 4367–4374.
[25] P. Li, C. Tai, Z. Deng, J. Gan, M.R. Oggioni, H.Y. Ou, Identification and characterization of chromosomal relBE toxin-antitoxin locus in *Streptomyces cattleya* DSM46488, Sci. Rep. (2016), https://doi.org/10.1038/srep32047.
[26] N. Nolle, C.F. Schuster, R. Bertram, Two paralogous *yef*M-*yoe*B loci from *Staphylococcus equorum* encode functional toxin-antitoxin systems, Microbiology 159 (2013) 1575–1585.
[27] J.P. Norton, M.A. Mulvey, Toxin-antitoxin systems are important for niche-specific colonization and stress resistance of uropathogenic *Escherichia coli*, PLoS Pathog. 8 (2012) e1002954.
[28] R. Page, W. Peti, Toxin-antitoxin systems in bacterial growth arrest and persistence, Nat. Chem. Biol. 12 (2016) 208–214.
[29] S.J. Park, W.S. Son, B.J. Lee, Structural overview of toxin-antitoxin systems in infectious bacteria: a target for developing antimicrobial agents, Biochim. Biophys. Acta 1834 (2013) 1155–1167.
[30] K. Pedersen, S.K. Christensen, K. Gerdes, Rapid induction and reversal of a bacteriostatic condition by controlled expression of toxins and antitoxins, Mol. Microbiol. 45 (2002) 501–510.
[31] M.W. Pfaffl, A new mathematical model for relative quantification in real-time RT-PCR, Nucleic Acids Res. 29 (2001) 2000–2007.
[32] J. Quick, N. Cumley, C.M. Wearn, M. Niebel, C. Constantinidou, C.M. Thomas, M.J. Pallen, N.S. Moiemen, A. Bamford, B. Oppenheim, N.J. Loman, Seeking the source of *Pseudomonas aeruginosa* infections in a recently opened hospital: an observational study using whole-genome sequencing, BMJ Open 4 (11) (2014) e006278.
[33] L.G. Rahme, F.M. Ausubel, H. Cao, E. Drenkard, B.C. Goumnerov, G.W. Lau, S. Mahajan-Miklos, J. Plotnikova, M.W. Tan, J. Tsongalis, C.L. Walendziewicz, R.G. Tompkins, Plants and animals share functionally common bacterial virulence factors, Proc. Natl. Acad. Sci. U. S. A. 97 (2000) 8815–8821.
[34] M.I. Ramírez-Díaz, A. Díaz-Magaña, V. Meza-Carmen, L. Johnstone, C. Cervantes, C. Rensing, Nucleotide sequence of *Pseudomonas aeruginosa* conjugative plasmid pUM505 containing virulence and heavy-metal resistance genes, Plasmid 66 (2011) 7–18.
[35] E. Rodríguez-Andrade, K.C. Hernández-Ramírez, S.P. Díaz-Peréz, A. Díaz-Magaña, M.P. Chávez-Moctezuma, V. Meza-Carmen, R. Ortíz-Alvarado, C. Cervantes, M.I. Ramírez-Díaz, Genes from pUM505 plasmid contribute to *Pseudomonas aeruginosa* virulence, Ant. Van Leeuwenhoek 109 (2016) 389–396.
[36] A. Sala, P. Bordes, P. Genevaux, Multiple toxin-antitoxin systems in *Mycobacterium tuberculosis*, Toxins 6 (2014) 1002–1020.
[37] M.A. Schureck, T. Maehigashi, S.J. Miles, J. Marquez, S.E. Cho, R. Erdman, et al., Structure of the *Proteus vulgaris* HigB-(HigA)2-HigB toxin-antitoxin complex, J. Biol. Chem. 289 (2014) 1060–1070.
[38] A.M. Sousa, M.O. Pereira, *Pseudomonas aeruginosa* diversification during infection development in cystic fibrosis lungs- a review, Pathogens 18 (2014) 680–703.
[39] T. Stiernagle, Maintenance of *C. elegans*, Worm book 11 (2006) 1–11.
[40] M.W. Tan, S. Mahajan-Miklos, F.M. Ausubel, Killing of *Caenorhabditis elegans* by *Pseudomonas aeruginosa* used to model mammalian bacterial pathogenesis, Proc. Natl. Acad. Sci. U. S. A. 96 (1999) 715–720.
[41] S.J. Unterholzner, B. Poppenberger, W. Rozhon, Toxin-antitoxin systems: biology, identification, and application, Mob. Genet. Elem. 1 (2013) 3 e26219.
[42] S. Watanabe, Y. Takada, Amino acid residues involved in cold adaptation of isocitrate lyase from a psychrophilic bacterium, Colwellia Maris. Microbiol. 150 (2004) 3393–3403.
[43] S.E. West, H.P. Schweizer, C. Dall, A.K. Sample, L.J. Runyen-Janecky, Construction of improved *Escherichia-Pseudomonas* shuttle vectors derived from pUC18/19 and sequence of the region required for their replication in *Pseudomonas aeruginosa*, Gene 148 (1994) 81–86.
[44] Y. Yamaguchi, J.H. Park, M. Inouye, Toxin-antitoxin systems in bacteria and archaea, Annu. Rev. Genet. 45 (2011) 61–79.
[45] C. Yanisch-Perron, J. Vieira, J. Messing, Improved M13 phage cloning vectors and host strains: nucleotide sequences of the M13mp18 and pUC19 vectors, Gene 33 (1985) 103–119.
[46] C. Zheng, J. Xu, S. Ren, J. Li, M. Xia, H. Chen, W. Bei, Identification and characterization of the chromosomal yefM-yoeB toxin-antitoxin system of *Streptococcus suis*, Sci. Rep. 14 (2015) 13125.
[47] K.S. Makanrova, Y.I. Wolf, E.V. Koonin, Comprehensive comparative-genomic analysis of type 2 toxin-antitoxin systems and related mobile stress response systems in prokaryotes, Biol. Direct. 3 (2009) 4–19.

Current Genetics
https://doi.org/10.1007/s00294-017-0798-0

ORIGINAL ARTICLE

Control of morphology and virulence by ADP-ribosylation factors (Arf) in *Mucor circinelloides*

J. Alberto Patiño-Medina[1] · Guadalupe Maldonado-Herrera[1] · Carlos Pérez-Arques[2] · Viridiana Alejandre-Castañeda[1] · Nancy Y. Reyes-Mares[1] · Marco I. Valle-Maldonado[1] · Jesus Campos-García[1] · Rafael Ortiz-Alvarado[3] · Irvin E. Jácome-Galarza[4] · Martha I. Ramírez-Díaz[1] · Victoriano Garre[2] · Victor Meza-Carmen[1]

Received: 13 October 2017 / Revised: 5 December 2017 / Accepted: 13 December 2017

Abstract

Mucor circinelloides is a dimorphic fungus used to study cell differentiation that has emerged as a model to characterize mucormycosis. In this work, we identified four ADP-ribosylation factor (Arf)-encoding genes (*arf1–arf4*) and study their role in the morphogenesis and virulence. Arfs are key regulators of the vesicular trafficking process and are associated with both growth and virulence in fungi. Arf1 and Arf2 share 96% identity and Arf3 and Arf4 share 89% identity, which suggests that the genes arose through gene-duplication events in *M. circinelloides*. Transcription analysis revealed that certain *arf* genes are affected by dimorphism of *M. circinelloides*, such as the *arf2* transcript, which was accumulated during yeast development. Therefore, we created knockout mutants of four *arf* genes to evaluate their function in dimorphism and virulence. We found that both *arf1* and *arf2* are required for sporulation, but these genes also perform distinct functions; *arf2* participates in yeast development, whereas *arf1* is involved in aerobic growth. Conversely, *arf3* and *arf4* play only minor roles during aerobic growth. Moreover, we observed that all single *arf*-mutant strains are more virulent than the wild-type strain in mouse and nematode models, with the *arf3* mutant being most virulent. Lastly, *arf1*/*arf2* and *arf3*/*arf4* double mutations produced heterokaryon strains that did not reach the homokaryotic state, indicating that these genes participate in essential and redundant functions. Overall, this work reveals that Arfs proteins regulate important cellular processes in *M. circinelloides* such as morphogenesis and virulence, laying the foundation to characterize the molecular networks underlying this regulation.

Keywords ADP-ribosylation factor · Arf protein · Fungal virulence · *Mucor* · Secretion · Vesicle trafficking

Introduction

Mucormycosis is a fungal infection produced by Mucorales, including *Mucor circinelloides*, which is the second species isolated from patients after *Rhizopus oryzae* (Roden et al. 2005). The high mortality rates, unusual antifungal drug resistance and its emerging character have encouraged the researches to identify the molecular mechanisms involved in the ability to infect humans (Trieu et al. 2017). Arf proteins are key regulators of the vesicular trafficking process and are associated with both growth (Lee et al. 2008a) and virulence in fungi (Labbaoui et al. 2017). Therefore, this work takes advantage of the possibility of genetically manipulating *M. circinelloides* to analyze the involvement of Arf proteins in virulence and dimorphism.

Mucor circinelloides exhibits several interesting developmental processes in response to environmental signals, such as dimorphism, which depends on the culture growth

Communicated by M. Kupiec.

Electronic supplementary material The online version of this article (https://doi.org/10.1007/s00294-017-0798-0) contains supplementary material, which is available to authorized users.

✉ Victor Meza-Carmen
victor_meza2004@yahoo.com.mx

[1] Laboratorio de Diferenciación Celular, Instituto de Investigaciones Químico Biológicas, Universidad Michoacana de San Nicolás de Hidalgo, Ciudad Universitaria, 58030 Morelia, Michoacan, Mexico

[2] Departamento de Genética y Microbiología, Facultad de Biologia, Universidad de Murcia, 30100 Murcia, Spain

[3] Facultad de Químico Farmacobiología, Universidad Michoacana de San Nicolás de Hidalgo, Morelia, Michoacan, Mexico

[4] Laboratorio Estatal de Salud Pública del Estado de Michoacán, 58279 Morelia, Michoacan, Mexico

Published online: 20 December 2017

conditions. Thus, sporangiospore can develop either as mycelia or yeast cells in function of mostly the atmosphere and carbon-source conditions (Lübbehüsen et al. 2003). *M. circinelloides* also accumulates carotenoids in response to light presence and are the precursors of trisporic acid which is involved in sexual reproduction in Mucorales (Avalos and Limón 2015). Moreover, the ability of *M. circinelloides* to infect humans may be associated with morphological changes as it occurs in other fungi (Wang and Lin 2012). In eukaryotes, adequate growth and development depend on sensing and transmission of environmental signals and, in several such signalling pathways, G proteins function as critical regulators (Bahn et al. 2007). Intriguingly, several G proteins in *M. circinelloides* are involved in the process leading to fungal dimorphism. For example, Rho1 and Rho3 are differentially expressed during polarised growth (De La Cruz et al. 2007), and several genes encoding heterotrimeric G proteins exhibit differential expression pattern during dimorphism (Valle-Maldonado et al. 2015a); however, the biological functions of these genes have not been studied. Furthermore, elements of the protein kinase A pathway have been reported to regulate the morphology of *M. circinelloides* (Ocampo et al. 2009, 2012), and a correlation between morphology and virulence in *M. circinelloides* was revealed by a mutation in *cnbR*, the gene that encodes the regulatory subunit of calcineurin; the mutation led to monomorphic yeast growth and reduced virulence (Lee et al. 2013).

ADP-ribosylation factors (Arfs) are small G proteins of the Ras superfamily that were initially described biochemically as allosteric modulators of cholera-toxin activity (Kahn and Gilman 1984; Moss and Vaughan 1998). Subsequent studies indicated that Arf proteins are involved in vesicle trafficking in the secretion pathway in *Saccharomyces cerevisiae* and localised in the Golgi apparatus in mammalian cells (Stearns et al. 1990a). The Arf family is composed of Arf, Arl (Arf-like), and Sar (secretion-associated and Ras-related)proteins, which are all involved in vesicle biogenesis (Kahn et al. 2006).

Vesicle trafficking is one of the most critical processes in protein targeting; vesicles transport molecules between organelles inside cells, or transport molecules inside and outside cells, which involves exocytic and endocytic processes. Arf proteins not only control the localisation and function of cargo molecules in vesicles (Mizuno-Yamasaki et al. 2012), but also participate in the biogenesis of organelles such as peroxisomes (Agrawal and Subramani 2013) and regulation of mitochondrial morphology and function (Ackema et al. 2014).

In fungi, the specialised vesicular body Spitzenkörper, which contributes to the apical growth of the fungal mycelium, relies on vesicle flux (Dijksterhuis and Molenaar 2013). Thus, Arf proteins could be particularly relevant to Spitzenkörper generation and, accordingly, certain small G proteins have been found to be involved in the polarisation of fungal filamentous growth (Park and Bi 2007). The small GTPase Sec4, a Rab-related protein, was detected in tip-located vesicles in *Aspergillus niger* (Punt et al. 2001), and the Rab protein YPT-1 from *Neurospora crassa* was reported to play a critical role in the functioning of the machinery that maintains vesicular flux (Sánchez-León et al. 2015).

In *S. cerevisiae*, three ARF-encoding genes have been reported (Hsu and Lee 2013; Stearns et al. 1990a) and, in mammals, Arf proteins are divided into three classes, I–III (Jackson and Bouvet 2014); fungal Arfs are phylogenetically grouped into classes I and III of mammalian Arfs (Yorimitsu et al. 2014). Yeast ARF1 and ARF2, which are class I proteins, participate in the exocytic pathway and are essential, because the *ARF1/ARF2* double-mutant is not viable (Stearns et al. 1990a). Conversely, yeast ARF3, which belongs to class III, is involved in cytoskeletal organisation (Lambert et al. 2007) and appears to function in endocytosis (Smaczynska-de et al. 2008). In *Aspergillus nidulans*, ArfB—the *S. cerevisiae* ARF3 homologue—is involved in polarised growth and endocytosis (Lee et al. 2008a). Recently, the dimorphic human pathogen *Candida albicans* was shown to harbour five ARF homologues: three ARF genes(1–3) and two ARL genes(1 and 3); intriguingly, reduction in *ARF2* expression caused alterations in polarised growth and virulence, whereas the *ARL1* product was also required for invasive filamentous growth (Labbaoui et al. 2017).

In this study, our main goal was to identify the *arf* genes of *M. circinelloides* and characterise their function during dimorphism and virulence by generating and examining gene-knockout mutants. We report that some of the *arf* gene mutants showed altered morphology and virulence via regulation of protein secretion. Our findings identify potentially pivotal roles of *arf* genes in *M. circinelloides*.

Materials and methods

Fungal strain and growth media

Mucor circinelloides R7B (*leuA*$^-$), derived from the (−) mating-type *M. circinelloides f. lusitanicus*CBS 277.49 (Roncero 1984), was used for *arf* gene expression analysis. The recipient strain used for knocking out *arf* genes was MU402 (*leuA*$^-$, *pyrG*$^-$) (Nicolás et al. 2007), a uracil and leucine auxotroph derived from R7B. Spores were obtained from *M. circinelloides* cultures grown on plates with yeast–peptone–glucose (YPG) medium (pH 4.5); 1 L medium contained 3 g yeast extract, 10 g peptone, 20 g glucose, and 15 g bacteriological agar, and was supplemented with 200 mg/L uracil as required. Spores were harvested, counted, and preserved as previously reported (Valle-Maldonado et al.

2015a). The selection culture medium used was yeast nitrogen base (YNB) (Sigma, USA) or MMC (minimal medium casamino acids), which contained 10 g/L casamino acids, 20 g/L glucose, and 0.5 g/L yeast nitrogen without amino acids; both media were supplemented with uracil (200 mg/L) as required; 15 g/L agar was added when solid media were prepared.

Aerobic and self-anaerobic spore germination and growth quantification

Aerobic growth was performed in 250-mL flasks containing 25 mL YPG medium inoculated with 5×10^5 spores/mL of *M. circinelloides*; the liquid cultures were maintained at 28 °C for up to 24 h with constant shaking. Self-anaerobic spore germination was performed using 125-mL flasks containing 125 mL YPG medium inoculated with 5×10^5 spores /mL of *M.circinelloides*, as previously described (Salcedo-Hernandez and Ruiz-Herrera 1993). Germination percentage under aerobic or anaerobic conditions was calculated from the number of germinules or budding yeasts in 100 cells.

To determine dry weights, mycelia or yeast cells were collected from liquid cultures through filtration, washed twice with distilled H_2O, and dried on pre-weighed filter papers (Whatman No 5, Maidstone, Kent, UK). Filters were dried for 96 h at 80 °C and, after cooling the dry weights of the cells were measured.

Sporulation assay and radial growth

Sporulation was quantified by inoculating 50 spores from *M. circinelloides* on plates containing uracil-supplemented YPG medium. The plates were incubated for 5 days in the presence of light and the spores were harvested and counted in a haemocytometer chamber.

The radial growth of *M. circinelloides* was monitored by inoculating 50 spores at the centre of YPG plates supplemented with uracil, followed by measurement of the increase in colony diameter daily for 5 days.

Image analysis

An Olympus CKX41 microscope equipped with a 40× objective lens and a DMC-T25 camera (Panasonic, Kadoma, Japan) was used to capture images of spores or spore germination. Lengths were determined using QCapture Pro 7™ and Leica application suite software.

Identification of Arf-encoding genes in *M. circinelloides*

Genes that were homologous to *S. cerevisiae* genes encoding ARFs (*ARF1, ARF2*, and *ARF3*) were identified in the genome database (2.0) of *M. circinelloides* (http://genome.jgi-psf.org/Mucci2/Mucci2.home.html). The criteria for identifying Arf proteins from *M. circinelloides* included evaluation of identity percentages and the detection of conserved domains. Alignments were performed in Clustal W (Thompson et al. 1994). The ID numbers of the Arf homologues from *M. circinelloides* that were used in protein alignments, dendrograms, and identity scores were as follows: Arf1, 157293; Arf2, 156501; Arf3, 155350; and Arf4, 32250. The accession numbers for Arfs from other species were as follows: *A. nidulans*: ArfA, AN1126 and ArfB, AN5020; *C. albicans*: ARF1, CR_08700C_A, ARF2, C3_04950W_A, and ARF3, CAA99291; *Fusarium oxysporum f. sp. lycopersici*: Arf1, KNA94255.1 and Arf2, KNA94254.1; *N. crassa*: Arf1, EAA29781.1 and Arf6, EAA28162.1; *S. cerevisiae*: ARF1, CAA98769, ARF2, CAA65622, and ARF3, CAA99291; *Schizosaccharomyces pombe*: ARF1, AAC37347.1 and ARF6, CAB51340.1; *Ustilago hordei*: Arf6, CCF50382.1; *Homo sapiens*: ARF1, NP_001019398, ARF3, NP_001650, and ARF6, CAG46762.

Genomic DNA isolation

Mucor circinelloides DNA was isolated as described previously (Van Heeswijck and Roncero 1984). Mycelium samples grown for 12 h were filtered through Whatman filter paper and then preserved at −20 °C until processing. Frozen samples were mechanically lysed by powdering in liquid nitrogen using a mortar and pestle. DNA was extracted as follows: 0.4 mL extraction buffer (10 mM Tris–HCl, pH 8, 0.4 M NaCl, 2 mM EDTA) was added to approximately 100 mg powder (mycelium sample), and then 80 µL sodium dodecyl sulphate (SDS) (10%) was added, followed by 8 µL proteinase K (20 mg/mL); after incubation for 1 h at 60 °C, 320 µL 5 M NaCl was added, and the samplewas centrifuged for 30 min at 12,000 × *g*. The supernatant was collected, mixed with 0.6 volumes of isopropanol, and incubated at −20 °C for 10 min. After centrifugation for 20 min at 12,000 × *g*, the pellet was washed (twice) with an equal volume of 70% ethanol and centrifuged again at 12,000 × *g*. The excess ethanol was removed and the DNA sample was dried at 37 °C. Finally, the pellet was resuspended in 50 µL sterile water. RNA was cleaved by the addition of 3 µL RNase A (Thermo Fisher Scientific, Waltham, MA, USA) and incubation at 37 °C for 10 min, following which the DNA samples were stored at −70 °C.

Total RNA isolation

Mucor circinelloides biological samples were collected at various time points after aerobic or anaerobic growth, filtered through a filter paper (Whatman No. 5), and washed

with distilled water. RNA was isolated following procedures described previously (Valle-Maldonado et al. 2015b).

Oligonucleotide design and quantitative reverse transcription-polymerase chain reaction (qRT-PCR)

Mucor circinelloidesarf gene-specific primers and hydrolysis probes featuring minimal secondary structures were designed using Biosearch Technologies software (http://www.biosearchtech.com) (Novato, CA, USA) to ensure the specificity of all detections during qRT-PCR assays (Table S1). The qRT-PCR assays, amplification-efficiency estimation, relative expression-level calculation, and data analysis were performed as described previously (Valle-Maldonado et al. 2015b).

Targeted *arf* gene disruption in *M. circinelloides*

Δarf1 and *Δarf2*

The *arf1* recombinant fragment was generated by PCR amplification from the genomic DNA of the R7B strain: a 1.1-kb fragment corresponding to the 5′ upstream region from the translation start codon of *arf1* was amplified using the oligonucleotides *arf1*-5′FWR and *arf1*-5′REV (Table S2); *arf1*-5′REV included a *Sac*I restriction site at its 3′ end. Moreover, a 1.1-kb fragment corresponding to the 3′ downstream region from the translation stop codon of *arf1* was PCR-amplified using the oligonucleotides *arf1*-3′FWR and *arf1*-3′REV; whereas *arf1*-3′FWR contained a *Sac*I restriction site at its 5′ end, *arf1*-3′REV contained an *Xba*I restriction site at its 3′ end. The gene *pyrG* was also PCR amplified using the genomic DNA from R7B strain as the template; a 2-kb amplicon was obtained using the oligonucleotides *pyrG*-FWR and *pyrG*-REV, both of which contained *Sac*I restriction sites at their 5′ ends.

The 5′ and 3′ open reading frame (ORF) flanking regions of *arf1* and *pyrG* were independently cloned into pJET1.2/blunt vector (Thermo Fisher Scientific), and the resulting plasmids were named pArf1-5′ (for the 5′ region), pArf1-3′ (for the 3′ region), and pPyrG (for *pyrG*). The presence of the *Sac*I sites allowed *pyrG* to be subcloned into the plasmid pArf1-3′ previously digested with *Sac*I; the resulting plasmid containing the fusion of the *arf1* 3′ region and *pyrG* was named pArf1-3′-PyrG. Finally, the 5′-region fragment of *arf1* was obtained after digestion with *Sac*I and *Xba*I and then purified and subcloned into the pArf1-3′-PyrG vector previously digested with *Sac*I and *Xba*I; the vector and the fragment were ligated and the resulting plasmid was named pArf1-3′-PyrG-5′.

The *arf2* recombinant fragment coupled with the *pyrG* selection gene was generated by fusion-PCR, where three PCR fragments containing overlapping sequences were amplified using these oligonucleotides (Table S2): oligonucleotides (1) *arf2*-UFwd and (3) *arf2*-Urev-*pyrG*, which amplified 1 kb from the 5′ upstream region of the start translation codon of *arf2*, and oligonucleotides (2) *arf2*-Drev and (4) *arf2*-DFwd-*pyrG*, which amplified 1 kb from the 3′ downstream region of the stop translation codon of *arf2*. In oligonucleotide *arf2*-Urev-*pyrG*(3), an added nucleotide sequence at the 3′ end hybridised to the 5′ end of *pyrG*, and in oligonucleotide (4) *arf2*-DFwd-*pyrG*, an added nucleotide sequence at its 5′ end hybridised to the 3′ end of *pyrG*. *pyrG* was PCR-amplified using the oligonucleotides *pyrG*-FWR and *pyrG*-REV, with pMAT1700 (Trieu et al. 2017) as the template.

Three individual PCRs were performed to obtain the *arf2* 5′ region, *pyrG* (2 kb), and the *arf2* 3′ region, which were all purified. Fusion PCR was performed using 100 ng/μL of each template; 10 μM each of the oligonucleotides (1) *arf2*-UFwd and (2) *arf2*-Drev and 1 μL of the enzyme Herculase II fusion enzyme (Agilent Technologies), at the ratio of 1:2:1, were used.

To generate the *Δarf1*/*Δarf2* double-mutant, the plasmid pArf1-3′-PyrG-5′ previously obtained for *arf1* mutation was used. The gene *leuA*, which is required for leucine synthesis (Van Heeswijck and Roncero 1984), was obtained after PCR with oligonucleotides *leuA*-FWR and *leuA*-REV (Table S2), followed by annealing into the plasmid pLeu4 (Arnau and Strøman 1993); *Sac*I restriction sites were added to both oligonucleotides at their 5′ ends. Both *leuA* (3.7 kb) and the pArf1-3′-PyrG-5′ vector were digested with *Sac*I, and both products were ligated using the enzyme T4 DNA ligase; the resulting plasmid was named pArf1-5′-LeuA-3′.

Δarf3 and *Δarf4*

The entire ORFs of *arf3 and arf4*, including a 1-kb region upstream from the ATG codon (5′ region) and a 1-kb region downstream from the stop translation codon (3′ region), were PCR amplified using two pairs of oligonucleotides, FW-*arf3* and RV-*arf3* for *arf3*, and *Sac*I-FW-*arf4* and *Xba*I-RV-*arf4* for *arf4* (Table S2), and the genomic DNA from *M. circinelloides* MU402 was used as the template. The 2.9- and 2.7-kb fragments generated for *arf3* and *arf4*, respectively, were cloned into pUC18 (Thermo Fisher Scientific, Waltham, MA, USA) generating the vectors pMAT1573 (*arf3*) and pMAT1574 (*arf4*). Subsequently, pMAT1573 and pMAT1574 were used as templates to amplify entire vectors, except for the *arf3 and arf4* ORFs, using Herculase (Agilent Technologies, Santa Clara, CA, USA) and the following pairs of oligonucleotides (Table S2): *Bgl*II-FWD-*arf3* and *Bgl*II-REV-*arf3* for pMAT1573, and *Bam*HI-FWD-*arf4* and *Bam*HI-REV-*arf4* for pMAT1574. In both PCR-amplification events, two amplicons of similar size were obtained

(4.7 kb), which were then digested with *Bgl*II and stored at −20 °C.

The selection marker *pyrG* was excised using *Bam*HI digestion from the vector pEMP1 (Benito et al. 1995), and was subsequently purified and ligated into the *Bgl*II site in the vectors pMAT1573 and pMAT1574 (containing the 5′ and 3′ regions for each gene) to generate the final vectors pMAT1576 for the *arf3* recombinant fragment and pMAT1577 for the *arf4* recombinant fragment.

The 5′-*pyrG*-3′ recombinant fragments from the vectors pMAT1576 and pMAT1577 were obtained after double-digestion with *Sph*I/*Sac*I and *Sac*I/*Xho*I for *arf3* and *arf4* recombinant fragments, respectively.

To obtain the *Δarf3*/*Δarf4* double-mutant strain, the plasmid pMAT1573, in which *arf3* was previously cloned, was used as the template, and the entire plasmid (except for the *arf3* ORF) was PCR amplified using the oligonucleotides *Pst*I-FW-*arf3* and *Pst*I-REV-*arf3*; this amplicon contained the 5′ and 3′ ORF flanking regions (1 kb each) from *arf3* at its ends. Next, the amplicon was digested with *Pst*I and, concurrently, the plasmid pLeu4, containing the cloned *leuA*, was also digested with *Pst*I. The DNA fragment corresponding to *leuA* (4.2 kb) was cloned into the plasmid pMAT1573 that was previously digested with *Pst*I; this yielded the plasmid pMAT1579, in which the recombinant fragments of *arf3* flanked *leuA*. This final recombinant fragment was used to transform the *Δarf4* strain to generate the double-mutant strain. To mutate the *arf* genes, all the recombinant fragments were PCR amplified and the corresponding amplicons were used to transform *M. circinelloides* protoplasts.

Protoplasts obtained from *M. circinelloides* MU402 strain were transformed with the recombinant DNA fragments (3 µg/transformation) according to a previously described protocol (Gutiérrez et al. 2011). Transformants were obtained under selection conditions on MMC agar plates lacking uracil. Monosporic cultures were obtained after five cycles of sporulation in either selection medium or rich medium, at which point 100% of the spores could grow on the selection medium, indicating transformation of all nuclei.

Molecular identification of arf-mutant strains from *M. circinelloides*

PCR confirmation

arf1 deletion: In the case of the mutant genotype, a 1.6-kb amplicon was generated by PCR when the following oligonucleotide pair was used: *arf1*-5′CR, which hybridises outside the 5′ end of the recombination fragment used to delete *arf1*, and *pyrG*10, which hybridises inside the selection-marker sequence. No amplicon was obtained from the wild-type strain. As the PCR control for positive amplification, we used the oligonucleotides *arf1*-3′FWR and *arf1*-3′REV (Table S2), which hybridise in the flanking 3′non-coding region of *arf1*; positive amplification was expected to generate a 1.1-kb amplicon for both wild-type and mutant genotypes (Fig. S1). *arf2* deletion: The PCR-based approach used for confirming *arf1* deletion was also used for confirming homologous recombination of mutated *arf2* in the genome. The use of the oligonucleotides *arf2*-5′CR and *pyrG*R2 (Table S2) generated a 1.3-kb amplicon in the case of the mutant, whereas no amplification suggested a wild-type genotype. As the PCR control, we used oligonucleotides (4) *arf2*-DFwd-*pyrG* and (2) *arf2*-Drev, which hybridise with the flanking 3′ noncoding region of *arf2*; positive amplification was expected to generate a 1.1-kb amplicon for wild-type and mutant genotypes (Fig. S1). *arf3* deletion:*arf3* deletion was confirmed by PCR with oligonucleotides FW-*arf3* and RV-*arf3* (Table S2), which hybridise in the flanking region outside the recombination fragment; the generation of 5.5- and 2.9-kb amplified bands indicated the *arf3*-deletion genotype and wild-type genotype, respectively (Fig. S1). *arf4* deletion: To confirm *arf4* deletion, PCR was performed using the oligonucleotides FW-INT-*arf4* and RV-INT-*arf4* (Table S2), which hybridise in the flanking region outside the recombination fragment; amplified bands of 5.4- and 2.7-kb indicated the *arf4*-deletion genotype and wild-type genotype, respectively (Fig. S1).*arf1*/*arf2* deletion:A confirmed *arf2*-deleted mutant strain was used, and the second mutagenesis event in *arf1* was confirmed by performing PCR with the oligonucleotides *arf1*-5′FWR and *arf1*-3′REV; a 3.1-kb amplicon was indicative of the *Δarf2* genotype, whereas a 5.9-kb PCR band indicated the *arf1*-mutant genotype (Fig. S2).*arf3*/*arf4* deletion: a confirmed *arf4*-deleted mutant strain was used, and the second mutagenesis event in *arf3* was confirmed by performing PCR with the oligonucleotides FW-*arf3* and RV-*arf3*; 2.9- and 6.4-kb amplicons indicated the Δ*arf3*-mutant and Δ*arf4*-mutant genotypes, respectively (Fig. S2).

Southern-blot

Genomic DNA (1 µg) from different strains of *M. circinelloides* was digested with restriction enzymes adequate for each *arf* mutant strain, and the DNA was electrophoresed and transferred to nylon membranes (Hybond^{TM}-N+, Amersham Biosciences, Little Chalfont, UK) according to a recommended protocol (Sambrook and Russell 2001). Southern-blot hybridisation was performed under stringent conditions. DNA probes were labelled with [α-^{32}P]dCTP using Ready-To-Go Labeling Beads (GE Healthcare Life Science, Chicago, IL, USA). For Southern-blotting experiments, DNA probes were directly amplified from genomic DNA using the following primer pairs to identify the mentioned strains: *Δarf1* strain, *arf1*-3′FWR and *arf1*-3′REV;

Δarf2 strain, *arf2*-DFwd-*pyrG* and *arf2*-Drev; *Δarf3* strain, SN3-FW and SN3-RV; and *Δarf4* strain, SN4-FW and SN4-RV (Table S2).

qRT-PCR confirmation

Total RNA isolated from each *arf*-mutant strain was used as the template and qRT-PCR was performed to determine all *arf* transcript levels, as described previously (Valle-Maldonado et al. 2015b). The mRNA quantitation from the *arf*-mutant strains is shown in Figs. S2 and S3.

Complementation of *Δarf2* strain of *M. circinelloides*

The *arf2* wild-type ORF was PCR-amplified using the genomic DNA of *M. circinelloides* R7B as the template and the oligonucleotides *arf2*-FWR-*Xho*I and *arf2*-REV-*Not*I, which introduced restriction sites for *Xho*I and *Not*I at the 5′ and3′ ends, respectively.

The gene encoding constitutively active Arf2-GTP was obtained using fusion-PCR with wild-type *arf2* ORF as the template and the oligonucleotides *arf2*-FWR-*Xho*I and Mutarf2-2, which generated a 290-bp amplicon; in a second PCR amplification with Mutarf2-1 and *arf2*-REV-*Not*I, a 590-bp PCR band was obtained. A third PCR was performed using both amplicons as templates and the oligonucleotides *arf2*-FWR-*Xho*I and *arf2*-REV-*Not*I; this generated a 792-bp amplicon. The expected mutation of the codon encoding Q71L in the *arf2* ORF was confirmed by DNA sequencing.

Wild-type and constitutively active *arf2* genes were cloned in pEUKA4 vector(Wolff and Arnau 2002) under the control of *gpd1* promoter from *M. circinelloides* in the *Xho*I and *Not*I sites; the resulting plasmids were confirmed based on restriction patterns and DNA sequencing. Both recombinant plasmids were used to transform the *Δarf2* strain and selection was performed in YNB (Difco, Franklin Lakes, NJ, USA) medium.

Mouse- and *Caenorhabditis elegans*-killing assays

The protocol used for studies with the mouse virulence model followed the recommendations of the Mexican Federal Regulations for the Use and Care of Animals (NOM-062-ZOO-1999) (Especificaciones técnicas para la producción, cuidado y uso de los animales de laboratorio/Technical specifications for production, use and care of laboratory animals) (SAGARPA, 2001).

To assess the virulence of *M. circinelloides* strains, we used methods described previously (Rodríguez-Andrade et al. 2016) with modifications. Briefly, groups of six male BALB/c mice (12–16 weeks old, weighing ~ 20 g) were treated with streptozotocin (200 mg/kg) (Sigma, USA) to induce a diabetic state, and then inoculated with 2×10^7 spores from different strains of *M. circinelloides*; the spores were suspended in saline solution and injected intraperitoneally into mice, the survival of which was then monitored daily. Three independent assays were conducted for each group.

C. elegans Bristol N2 (Brenner 1974) worms were synchronised by hypochlorite isolation of eggs from gravid adults, after which the eggs were hatched in S-basal medium (Stiernagle 2006). L1 larvae were transferred onto NGM (nematode growth medium) (Stiernagle 2006) plates seeded with *Escherichia coli* OP50 strain, which was previously grown on the plates as a food source, and incubated at 20 °C for 4–5 days until the larvae reached the young-adult phase. Worms were rinsed from the plates and washed in S-basal medium. *M. circinelloides* strains were grown at 28 °C for 24 h in YPG medium supplemented with uracil and, after centrifugation, cell-free media were recovered via filtration through Millipore 0.2-µm filters for use in further experiments. For each experiment, 10–20 worms were dispensed into each well of 24-well plates (Costar; Corning, Inc., Corning, NY, USA), followed by incubation with 1 mL cell-free media; the plates were incubated at 18 °C for 48 h, and live worms were scored at 6, 12, 24, and 48 h. For statistical purposes, two replicates per experiment were used. YPG medium was used as a negative control. A worm was considered dead when it no longer responded (moved) to a touch stimulus. Any worm that died because of sticking to the plate wall was excluded from the analysis. Three independent assays were conducted for each worm group. In certain experiments, the cell-free media (1 mL) obtained from the different *M. circinelloides* strains were incubated with 25 µL pronase (equivalent to 5 U; Sigma, USA) for 2 h at 37 °C before use in the *C.elegans*-killing assays.

Protein in cell-free media on *arf* mutant strains was quantified using the Bradford method (BioRad, Hercules, CA, USA).

Statistical analysis

All data were evaluated using analysis of variance (ANOVA). Fisher's test was used for analysis; significant differences ($p \leq 0.05$) are indicated using letters or asterisks.

Results

Identification of Arf-encoding genes in *M. circinelloides*

We searched the *M. circinelloides* genome *in silico* for Arf homologues using ARF1–ARF3 from *S. cerevisiae* and identified four homologues (Arf1–Arf4) (Fig. 1), all of which contain the canonical motif and domains characteristic of

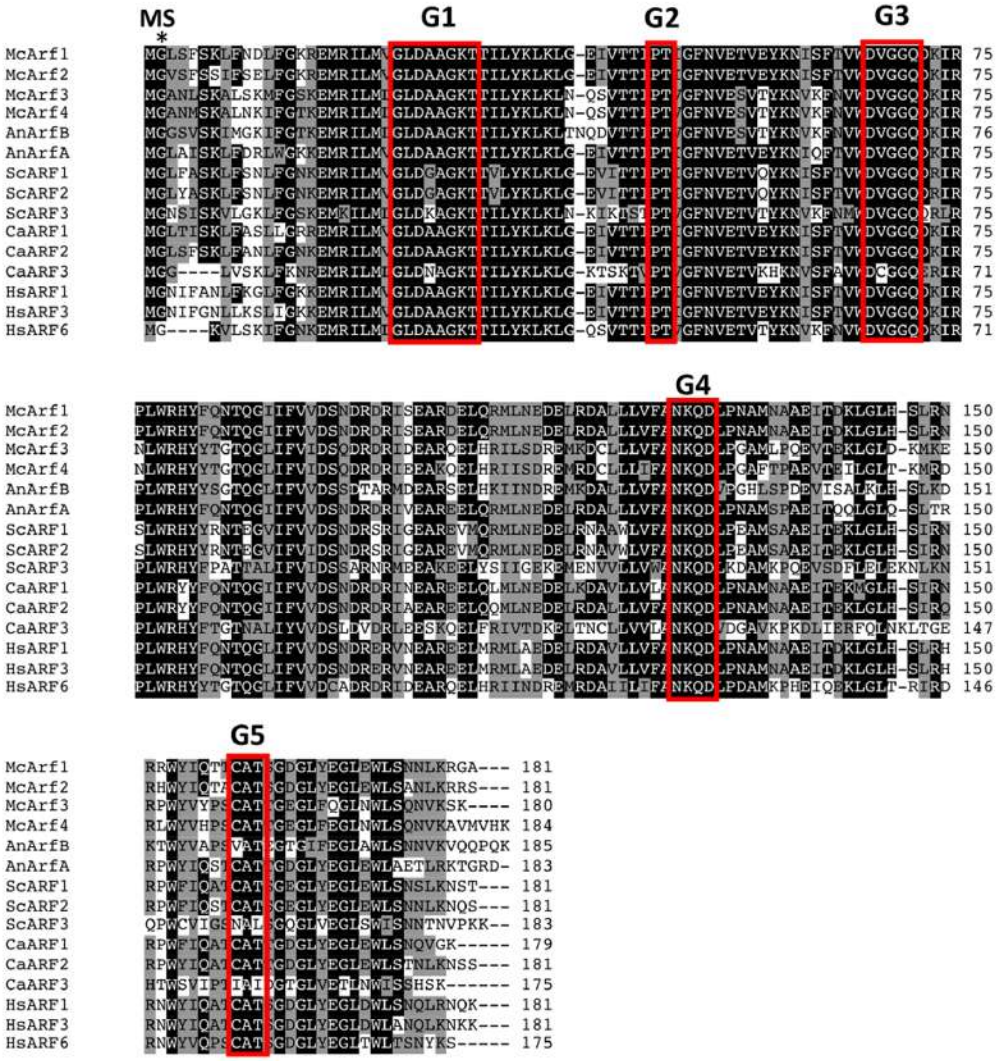

Fig. 1 Amino acid sequences alignment of putative Arf proteins from *M. circinelloides*. Four putative Arf proteins (Arf1–Arf4) from *M. circinelloides* (Mc) were aligned with Arf proteins described in *A. nidulans* (An), *S. cerevisiae* (Sc), *C. albicans* (Ca), and *H. sapiens* (Hs). Guanine nucleotide-binding domains formed by G1–G5 motifs are shown in boxes. The consensus sequences for G1 (GxxxxGKS/T), G2 (PT), G3 (DxxGQ/H/T), G4 (T/NKxD), and G5 (C/SAK/L/T) and the myristoylation site (MS) were obtained from Wennerberg et al. (2005). Shaded areas in black correspond to identical amino acids in the protein sequences

Arf proteins (Colicelli 2004), including glycine at position 2, the amino acidic residue that could be myristoylated (Fig. 1). The G1–G5 motifs required for the guanine nucleotide-binding site are present in all four putative Arfs (Fig. 1). All Arf ORFs contain one or more introns and, intriguingly, *arf1* and *arf2* contain the same number of exons/introns in approximately the same position (Fig. S4). The four Arf proteins from *M. circinelloides* share approximately 65–96% identity with each other in their amino acid sequences (Table S3), and 61–81% identify with ARF1 from *S. cerevisiae* (Table S4). Arf1 and Arf2 from *M. circinelloides* share 96% identity in their amino acid sequence (Table S3), which suggests that these proteins could be functionally redundant. Moreover, these proteins show nearly 80% identity with ARF1 and ARF2 from *S. cerevisiae* (Table S4), and are grouped with ARF1 and ARF3 from *H. sapiens* (Fig. S5), which indicates that the Arf1 and Arf2 from *M. circinelloides* are class I Arfs (Labbaoui et al. 2017); certain Arfs from class I are involved in the exocytic pathway. Arf3 and Arf4 from *M. circinelloides* share nearly 88% identity (Table S3), which

suggests that these proteins could also be functionally redundant. In addition, these proteins share up to 75% identity with ArfB from *A. nidulans*. Interestingly, Arf3 and Arf4 are highly similar (up to 80% identity) to ARF6 from *H. sapiens* (Tables S3 and S4) and are grouped as class III Arfs together with ArfB from *A. nidulans* and ARF3 from *S. cerevisiae* (Fig. S5) (Labbaoui et al. 2017); certain class III Arfs have been reported to function in the endocytic pathway.

Arf mRNA levels during dimorphism in *M. circinelloides*

Next, we measured the mRNA levels of *arf1–arf4* during *M. circinelloides* dimorphism. We performed qRT-PCR using total RNA isolated from spores or vegetative cells (mycelia or yeast) after 6-h growth to detect each transcript level during the dimorphism of *M. circinelloides*. The amplification efficiency for the *arf* hydrolysis probes was > 90% (Table S5), which is an adequately high value for accurate mRNA quantification (Valle-Maldonado et al. 2015b).

qRT-PCR assays yielded the following results (Fig. 2). The *arf1* mRNA showed increased accumulation during vegetative growth, and the mRNA levels were approximately 3- and fourfold higher in mycelia and yeast cells than in spores, respectively. Intriguingly, *arf2* was also differentially expressed, and its mRNA mainly accumulated during yeast development and exhibited up to sixfold increase compared to the level in the spore stage. In the case of *arf3*, the mRNA levels were generally lower under all conditions tested, but accumulated mainly during the mycelial growth stage, accumulating to ~ threefold higher levels than that in the spore or yeast stage. In contrast, *arf4* mRNA was detected during dimorphism, but its expression pattern was not altered during any of the morphological stages examined. Collectively, these data indicate that the *arf* genes in *M. circinelloides* are actively transcribed during dimorphism, and that the mRNA levels of *arf1, arf2*, and *arf3* are influenced by this event, with the effect being most pronounced for *arf2*, the mRNA of which accumulated mainly during yeast development.

Deletion of *arf* genes in *M. circinelloides*

Recombinant *arf* fragments containing ~ 1-kb regions corresponding to the 5′ upstream and 3′ downstream sequences from the start and stop translation codons, respectively, of each *arf* gene were used to flank the selection marker *pyrG* (Fig. 3). These recombinant fragments were purified and used to transform protoplasts of the strain MU402 (*leuA*$^-$, *pyrG*$^-$). Transformants grown in selection medium (MMC) were recovered and, subsequently, successive vegetative-cycle growth in selection medium was performed to obtain homokaryon *arf* mutants. After five cycles, all the selected transformants showed 100% *ura*$^+$ spores, which suggested the homokaryon phenotype.

The homologous-recombination event in each *arf* locus was confirmed by Southern blotting. A specific hybridisation band was observed in each *arf*-mutant strain, which indicated a single integration event in the specific *arf* locus (Fig. 3). Furthermore, qRT-PCR results showed null expression for the specific *arf* gene deleted in each *arf*-mutant strain (Fig. S3).

To create *Δarf1*/*Δarf2* and *Δarf3*/*Δarf4* double-mutant strains, the previously generated (and confirmed) *Δarf2* and *Δarf4* single-mutant strains were used as the recipient strains for *arf1* and *arf3* deletion, respectively. The mutagenesis

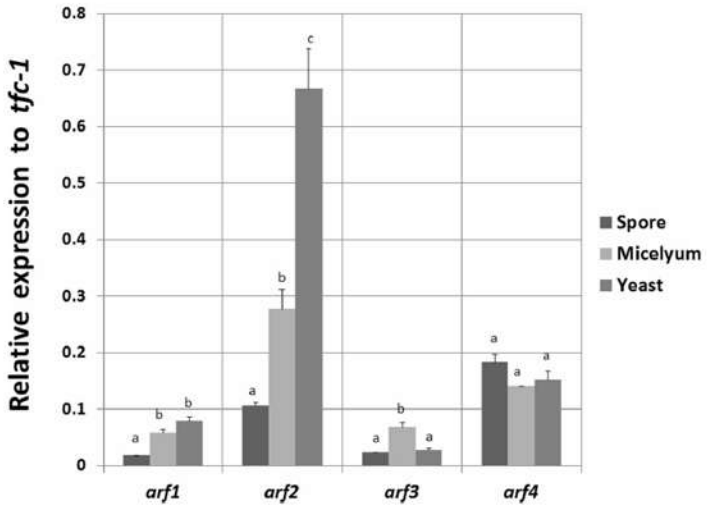

Fig. 2 mRNA quantitation of *arf* genes from *M. circinelloides*. Transcript levels of *arf1–arf4* were measured during sporulation and vegetative growth after 6 h of incubation using qRT-PCR. Transcript levels were quantified relative to *tfc-1* expression. Three independent experiments were conducted and the average is shown; bars correspond to standard error (SE). Statistically significant differences are indicated by different letters (ANOVA and Fisher's tests; $p \leq 0.05$)

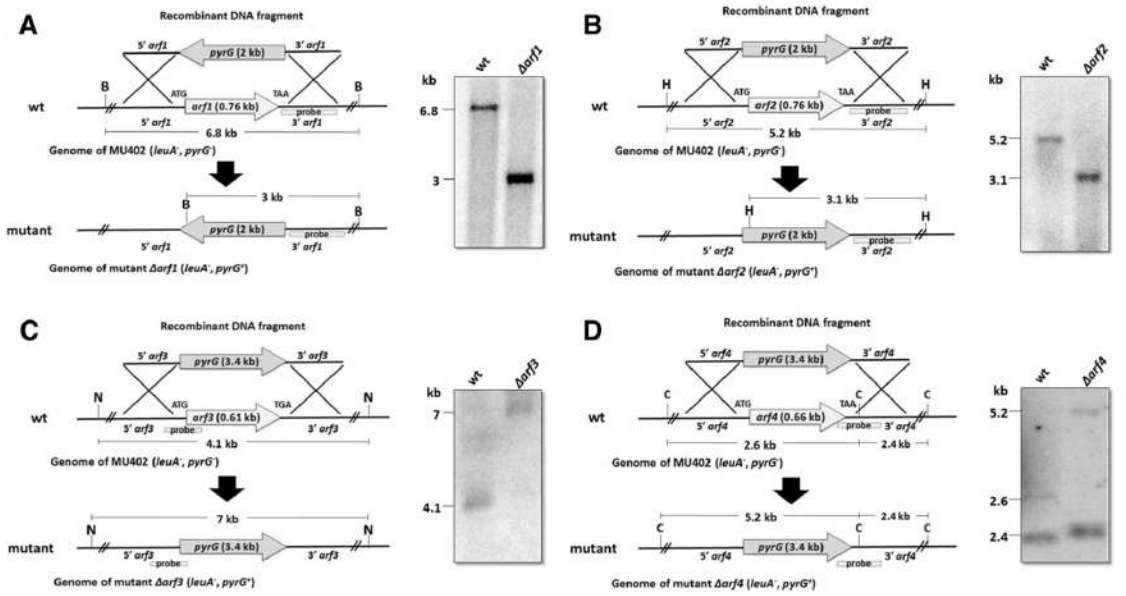

Fig. 3 Deletion of *arf* genes in *M. circinelloides*. **a** *arf1*; **b***arf2*; **c** *arf3*; and **d** *arf4*. The 5′ and 3′ regions upstream and downstream from the start and stop codons, respectively, were used to flank the *pyrG* selection marker. The diagrams show the recombinant fragments that were used to transform protoplasts of the strain MU402 (*pyrG*⁻, *leuA*⁻). Molecular confirmation by Southern blotting performed using specific probes for each *arf* gene showed specific recombination in the corresponding *arf* locus. Genomic DNA samples from transformed and parental (MU402) strains were digested with the indicated restriction enzymes (B, *Bgl*II; H, *Hin*dIII; N, *Nsi*I; *C*, *Cla*I)

strategy was similar to that described for obtaining the single *arf* mutants, but *leuA* was used as the selection-marker gene for transformation (Fig. S2). Ten putative *Δarf3*/*Δarf4* or *Δarf1*/*Δarf2* double-mutant strains were screened using PCR for the double mutation, which revealed that successful deletion of the second *arf* gene in each putative double-mutant strain led to a heterokaryon genotype in the second mutated *arf* (Fig. S2). Expression analysis confirmed the heterokaryon phenotype for each double-mutation event (Fig. S2). The inability to obtain homokaryon mutants suggests essential and redundant roles for the *arf1*/*arf2* and *arf3*/*arf4* pairs of genes in *M. circinelloides* growth.

Biological role of *arf* genes during aerobic growth in *M. circinelloides*

To determine the role of *arf* genes during aerobic growth, each *arf*-mutant strain was analysed by direct observation under a light microscope after aerobic germination (Fig. 4a).

The *arf* mutations did not alter aerobic germination rate in terms of the time required for the first hyphae to emerge, independent of the length or number of hyphae per mother cell (Fig. 5a). Although the germination rates were almost identical for all *arf*-mutant strains, the *Δarf1* strain showed notable differences during aerobic germination (Fig. 4a). For example, in this strain, an average of 7–8 hyphae appeared per mother cell compared to ~ 3–4 hyphae per mother cell in the other strains (including wild-type) (Fig. 5b). Moreover, in the *Δarf1* strain, the mother cell was bigger (26.7 µm in diameter) than that in the wild-type strain (20.6 µm) (Fig. 5c), whereas the hyphae were shorter (average 52 µm) than those in the other strains (average 88 µm) (Fig. 5D). These defects during aerobic germination of the *Δarf1* strain could contribute to the diminished growth in liquid and solid culture media exhibited by this mutant strain (Fig. S6). Furthermore, complementation of the *Δarf1* strain was not possible with either wild-type *arf1* or the gene encoding the constitutively active Arf1-GTP (three independent transformation experiments were performed in each case), which suggests a potential defect in the cell wall and/or plasma membrane. The *Δarf2* strain did not exhibit the phenotypes of the enlarged mother cell, multiple hyphae, and shortened hyphae that were observed in the *Δarf1* strain during aerobic germination (Fig. 5). However, the double-mutant $\Delta arf1^{(+)(-)}/\Delta arf2$ strain showed longer hyphae similar to the *Δarf4* strain (average 112 µm) when compared to the MU402 wild-type strain (Fig. 5d). The

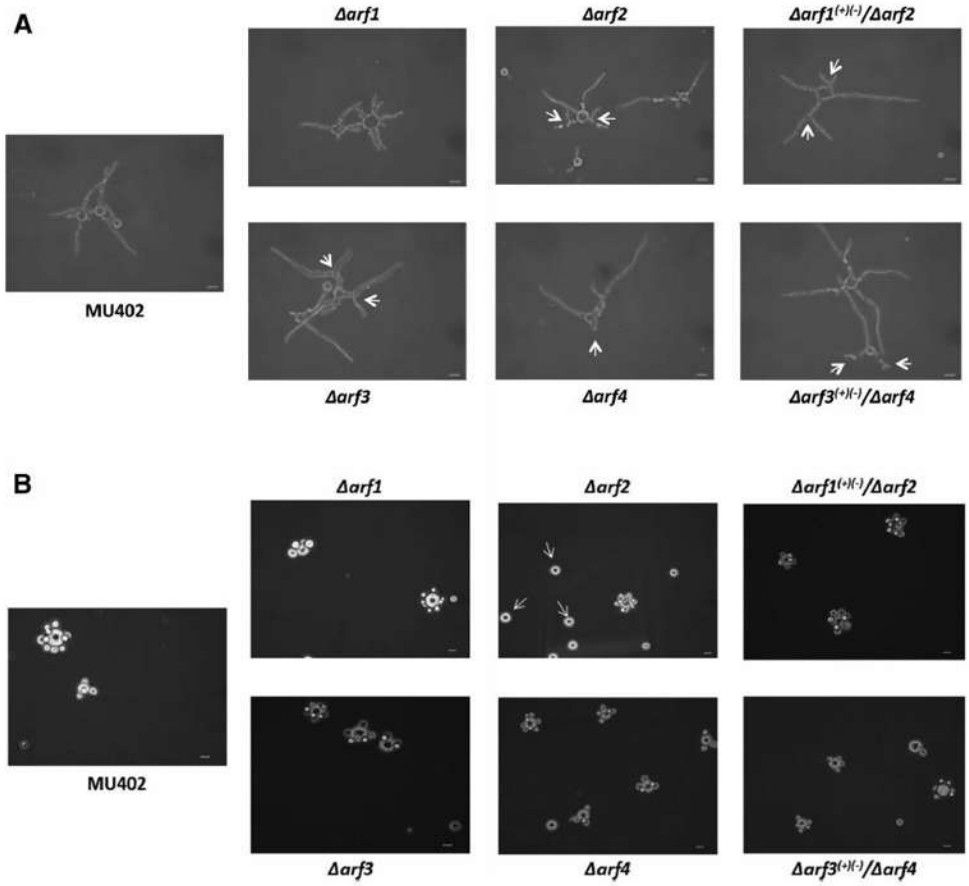

Fig. 4 Effect of *arf* mutation on aerobic germination of M. circinelloides. Morphology of spore germination examined using light microscopy (40 ×). Growth in YPG medium under conditions of **a** aerobic germination (after 4 h of growth; the arrows indicate dichotomies) and **b** anaerobic germination (after 5 h of growth; swollen spores are indicated by arrows). Scale bar = 20 µm

Δarf2 and the double-mutant *Δarf1*$^{(+)(-)}$*/Δarf2* strains also showed a reduction in radial growth on solid media similar to the *Δarf1* strain (Fig. S6).

The *Δarf3*,*Δarf4*, and the double-mutant *Δarf3*$^{(+)(-)}$*/Δarf4* strains did not show drastic changes during aerobic growth, although approximately 30% of the hyphae in these mutants showed dichotomy in their tips (Fig. 4).

Biological role of *arf* genes during anaerobic growth in *M. circinelloides*

Analysis of mRNA levels suggested that Arf2 could be functionally relevant during yeast growth. Anaerobic germination was performed to test this hypothesis. Morphological examination under a light microscope revealed that all *arf*-mutant strains could develop the yeast morphology (Fig. 4b), except for *Δarf2*, which showed a marked reduction (80%) in yeast development; most of the spores in the *Δarf2* strain reached the swollen stage, but yeast cells were not produced at the same rate as in the wild-type strain (Fig. 6a). Notably, genetic complementation of the *Δarf2* strain with either wild-type *arf2* or the gene encoding constitutively active Arf2-GTP restored the capacity of forming yeast cells to the same level as the wild-type strain (Fig. 6b, c). Moreover, the *Δarf2* strain showed reduction in *adh1* (a marker linked to fermentative metabolism under anaerobic growth in *M. circinelloides*) mRNA levels when it was incubated for 24 h under anaerobic conditions, contrary to what was observed with the wild-type strain and the complemented strains (Fig. 6d; Rangel-Porras et al. 2005; Valle-Maldonado et al. 2015b). Finally, during anaerobic growth, *Δarf3, Δarf4*, and the double-mutant

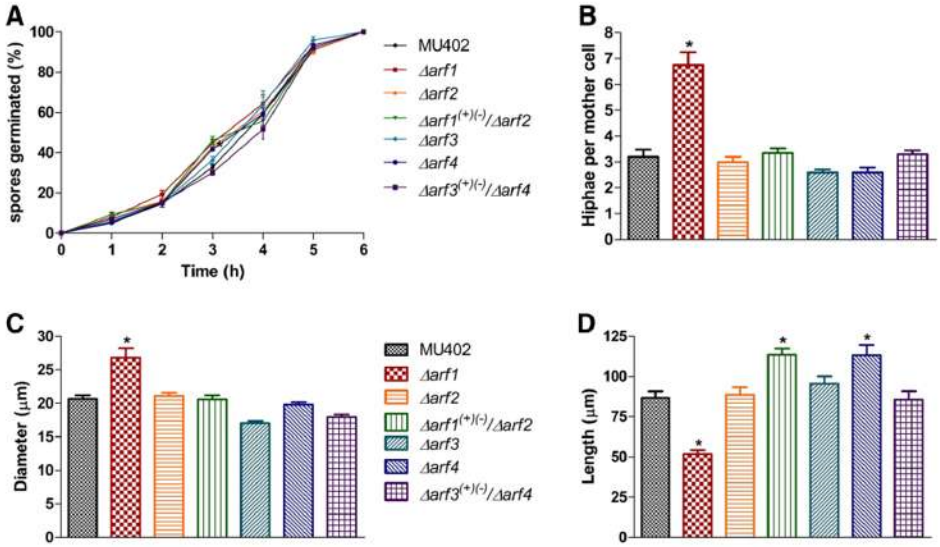

Fig. 5 Biological role of *arf* genes from *M. circinelloides* in aerobic germination. **a** Spores from *arf*-mutant and wild-type MU402 strains were cultured under aerobic germination conditions in YPG medium, and spore germination was registered at the indicated times. **b** Number of primary hyphae per mother cell. **c** Diameter of the mother cell. **d** Hyphal length registered at the indicated times. The experiments were conducted thrice independently. Statistically significant differences are indicated by asterisks (ANOVA and Fisher's tests; $p \leq 0.05$)

Δarf3$^{(+)(-)}$*/Δarf4* strains did not display visible changes under light-microscopy compared to the wild-type strain (Fig. 4b); however, these mutant strains exhibited slightly higher germination rates (Fig. 6a).

Role of Arf proteins in sporangiospore production in *M. circinelloides*

Arf proteins control the first steps in vesicle biogenesis, which ultimately results in the transportation of materials required for the formation of new cellular structures such as the cell wall and cellular membranes. This provided the rationale for measuring the size of the sporangiospores produced by the *arf* mutants (Fig. 7a), which revealed that the mutant *Δarf1* strains produced larger spores and the rest of the mutants produced smaller spores than the wild-type strain as mentioned below: *Δarf1*, 11.7. µm; *Δarf2*, 9.45 µm; *Δarf1*$^{(+)(-)}$*/Δarf2*, 9 µm; *Δarf3*, 8.23 µm; *Δarf4*, 7.86 µm; *Δarf3*$^{(+)(-)}$*/Δarf4*, 7.52 µm, and wild-type, 10.77 µm (Fig. 7b).

Moreover, quantification of spore production revealed that *arf1, arf2*, and *arf1*/*arf2* mutations reduced sporangiospore production by 90% compared to that of the wild-type strain, and that *arf3, arf4*, and *arf3*/*arf4* mutations decreased sporangiospore production, although only by 30–40%, compared to the MU402 wild-type strain (Fig. 7c).

Deletion of *arf1* and *arf3* in *M. circinelloides* increases virulence

The virulence of *arf* mutants was analysed in a mouse model of diabetes, because diabetes is a risk factor for mucormycosis (Binder et al. 2014). Spores from each single-knockout mutant strain were intraperitoneally injected into mice, the survivals of which were quantified. Notably, all the mutants were more virulent than the wild-type strain, with *Δarf3* being most virulent and leading to the death of all mice by day 3 post-inoculation (Fig. 8a); by comparison, the *Δarf1* strain caused nearly 70% death within 3 days after inoculation, and the *Δarf2* and *Δarf4* strains were even less virulent, leading to the death of 30 and 40% mice by the end of the experiment, respectively.

Molecules involved in fungal virulence are secreted, most of which must be enclosed in vesicles to reach the cell exterior. Since certain Arf-family members have been reported to function in the secretion pathway, we investigated how molecules secreted by *M. circinelloidesarf*-mutant strains affect virulence in a nematode (*C. elegans*) model. Worms were seeded in the presence of cell-free media collected from wild-type and *arf*-mutant strains grown for 24 h under aerobic conditions, and the survival of the worms over time was measured. The mycelial cell-free medium from the *Δarf3* strain exhibited the highest

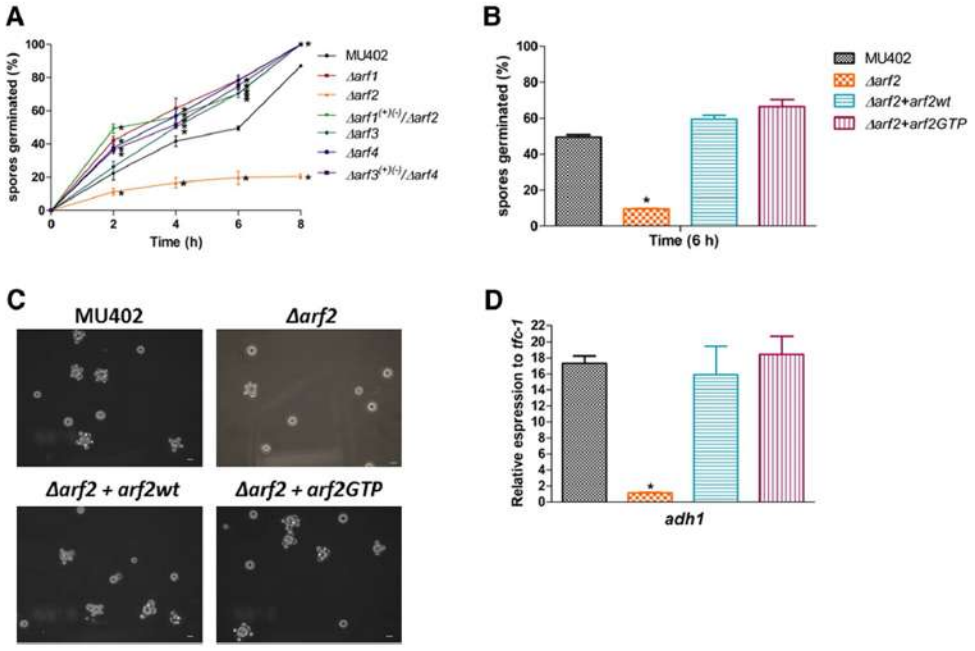

Fig. 6 Arf2 controls yeast development in *M. circinelloides*.**a** Anaerobic germination of spores from *arf*-mutant and wild-type strains in YPG medium at the indicated times. **b** Anaerobic spore germination after 6 h of growth in the *Δarf2* strain complemented with wild-type *arf2* or the gene encoding constitutively active Arf2 (Arf2-GTP). **c** Light microscopy examination of the morphology of the restored *Δarf2* strains under anaerobic growth. **d** Quantification of *adh1* mRNA levels after 24 h of growth under anaerobic growth conditions in the complemented *Δarf2* strains. Scale bar = 20 µm. Three independent experiments were conducted. Statistically significant differences are indicated by asterisks (ANOVA and Fisher's tests; $p \leq 0.05$)

virulence against nematodes, causing the death of 70% of the nematodes by 48 h after inoculation; by comparison, the *Δarf1* cell-free medium caused the death of nearly 50% of the nematodes, and the mycelial cell-free media from the *Δarf2* and *Δarf4* strains were even less virulent (65% survival) (Fig. 8b). Interestingly, when the mycelial cell-free media were treated with a protease, the survival rates increased to nearly the rate measured with the cell-free medium from the MU402 wild-type strain or with sterile YPG medium (Fig. 8c), which indicates that certain proteins secreted during mycelial growth act as virulence factors. Protein quantitation of the cell-free media of *arf* mutant strains did not always correlate with protein over-secretion in the culture media and the virulence phenotype. Our results showed that *Δarf1*, *Δarf2*, and *Δarf4* mutant strains significantly over-secreted 13, 20, and 13% proteins to the culture media, respectively, compared to the wild-type strain MU402 (Fig. S7). However, no significant differences of the protein content in the culture media of the $\Delta arf1^{(+)(-)}/\Delta arf2$, *Δarf3*, and $\Delta arf3^{(+)(-)}/\Delta arf4$ mutants were observed compared to that of the wild-type strain (Fig. S7).

Discussion

Vesicle trafficking is a key process via which molecules are delivered to their target organelles within a cell and transported into or out of eukaryotic cells. Arf proteins represent one of the main regulators involved in vesicle biogenesis (Kahn et al. 2006).

Arf-family members are present in all eukaryotic cells, and more than one member is present in every organism studied thus far (Jackson and Bouvet 2014). Here, four Arf members were identified in the dimorphic opportunistic human pathogen *M. circinelloides*. Sequence-similarity analysis suggests that the pairs Arf1-Arf2 and Arf3-Arf4 are the result of the duplication of two ancestral genes (Corrochano et al. 2016). The mRNAs of *arf1–arf3* accumulated differentially during dimorphism of *M. circinelloides*, but *arf4* mRNA levels were not influenced by the growth conditions

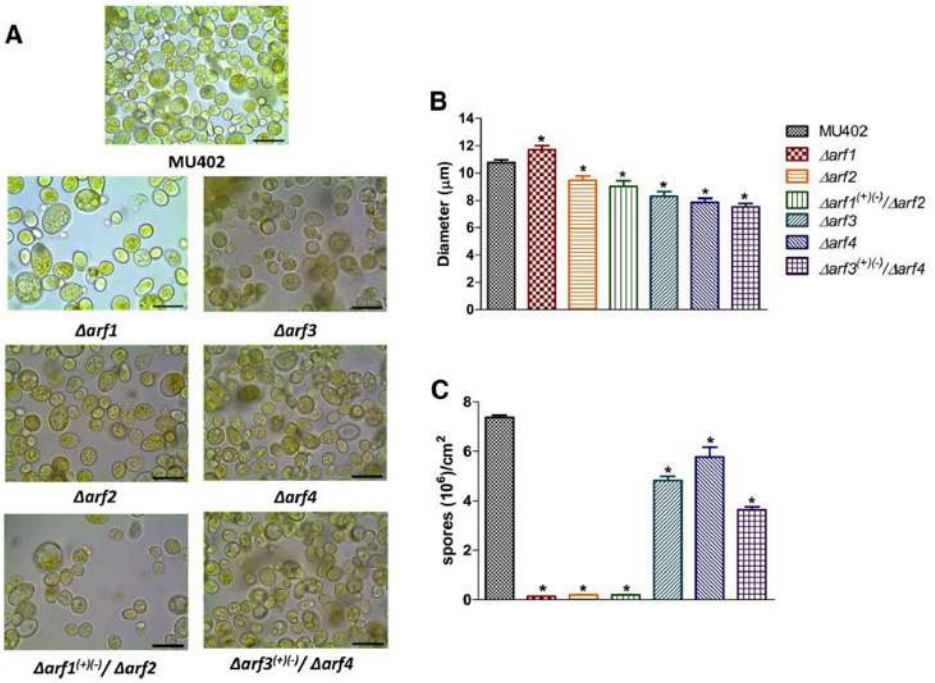

Fig. 7 Spore generation in *arf*-mutant strains of *M. circinelloides*. **a** Spores from different strains of *M. circinelloides* were examined using light microscopy (100 ×); scale bar = 20 μm. **b** Spore size determined through direct measurement from 100 cells, and **c** spore production on YPG solid medium after 5 days of incubation. The experiments were conducted thrice independently. Statistically significant differences are indicated by asterisks (ANOVA and Fisher's tests; $p \leq 0.05$)

tested. Moreover, *arf3* mRNA accumulated in the mycelium stage, whereas *arf2* mRNA accumulated mainly during yeast development.

Arf1 and Arf2 share 95.5% identity, and our observation of the heterokaryon genotype of the *arf1*/*arf2* double-mutant strain suggests that the presence of both Arf1 and Arf2 is essential for *M. circinelloides* growth. Similarly, ARF1 and ARF2 from *S. cerevisiae* share 96% identity and certain common functions, and although the *ARF1* mutation leads to comparatively more severe phenotypes such as lower growth rate and cold sensitivity compared to the *ARF2* mutant strain, the *ARF1*/*ARF2* double-mutant strain was not viable (Stearns et al. 1990a).

Interestingly, the *arf1* mutation led to more severe defects during aerobic growth compared to the dysfunction of the other *arf* genes in *M. circinelloides*. In addition, the absence of ARF1 homologues led to abnormal mitochondrial morphologies and dysfunction in *S. cerevisiae*, *C. elegans*, and mammalian cells (Ackema et al. 2014). The *arf1* mutant strain from *M. circinelloides* probably has similar defects in mitochondrial function that could explain its decreased growth rate. Currently, studies are underway to identify mitochondrial dysfunction and/or biogenesis in this mutant strain.

Conversely, the *arf2* gene of *M. circinelloides* was highly expressed during the yeast stage, and the *arf2*-knockout mutant showed a lower anaerobic germination rate than the other *arf* mutant, which indicates a critical role of the *arf2* product in *M. circinelloides* during anaerobic growth. Although Arf1 and Arf2 share certain common functional aspects, such as those indicated by the reduction of spore production and radial growth in their mutant strains, the molecules also perform distinct functions; we observed that Arf1 is involved specifically during hyphal germination and Arf2 is required for adequate yeast development and, to our knowledge, this is the first report showing regulation of yeast growth by an Arf protein in a dimorphic fungus. Arf1 and Arf2 were grouped with other Arf homologues known to be involved in the secretion pathway, such as ArfA from *A. nidulans* (Lee and shaw 2008) and ARF1 and ARF2 from *S. cerevisiae* (Stearns et al. 1990b), which suggests that Arf1 and Arf2 participate in secretion. We are currently investigating the role of Arf1 and Arf2 in the morphogenesis and secretion pathways of *M. circinelloides*.

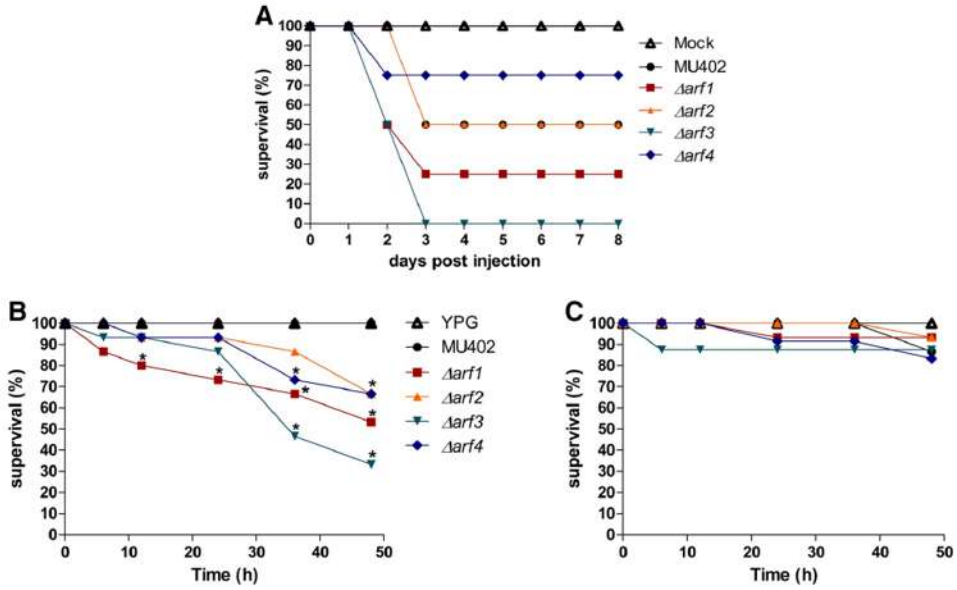

Fig. 8 Virulence of *arf*-mutant strains of *M. circinelloides*. **a** Mice (six per treatment) were inoculated intraperitoneally with 2×10^7 spores from different M. circinelloides strains. **b** Adult C. elegans worms (20) were inoculated with1 mL cell-free media obtained from different strains of M. circinelloides after 12 h of growth in liquid YPG medium. **c** Same as in **b**, but the cell-free media were treated with a protease for 2 h before incubation with the worms. Figures show the average of three independent experiments. Statistically significant differences are indicated by asterisks (ANOVA and Fisher's tests; $p \leq 0.05$)

Arf3 and Arf4 could be involved in polarised growth of *M. circinelloides*, because both single-mutant strains showed dichotomy in 30% of the hyphal tips, and the strains also exhibited diminished spore production (30–40% reduction in both strains) compared to the wild-type strain. Similar defects were previously observed in the *arfB* mutant strain (Lee et al. 2008), although the defect was less drastic in *M. circinelloides*, probably due to the likely functional redundancy between the two genes. Moreover, the heterokaryon genotype observed in the double-mutant strain suggests an essential role of *arf3* and *arf4* in *M. circinelloides*. Arf3 and Arf4 were grouped in Arf class III, similar to *A. nidulans* ArfB and human ARF6, which are involved in the endocytic pathway; this finding suggests that *M. circinelloides* Arf3 and Arf4 are involved in endocytosis.

Our observations imply that these Arf proteins could act as regulators of dimorphism in this Mucoral. It has been described several factors in the *M. circinelloides* morphogenesis, such as carbon source and the O_2/CO_2 ratio (Lübbehüsen et al. 2003). Moreover, oxidative stress regulates fungal morphogenesis and virulence (Huarte-Bonnet et al. 2015). Dysfunctional CnaA, a calcineurin catalytic subunit, led to monomorphic yeast growth (Lee et al. 2013). It would be interesting to investigate a regulatory network with these factors and Arf proteins in *M. circinelloides*.

Vesicle trafficking across the cell wall in fungal cells could be important for delivering harmful substances required for infecting tissues (Casadevall et al. 2009). For example, in *Cryptococcus neoformans*, secretion vesicles are produced during infection of mouse macrophages, and the secreted fungal molecules can modulate key cellular functions such as phagocytosis (Kronstad et al. 2011). In fungi, some of the virulence factors include hydrolases such as proteases and hyaluronidases, which must reach the cell surface or the extracellular space to be effective. The secretion of these molecules could involve active transport by vesicles. Thus, certain Arf proteins and their regulators are involved in virulence, such as *C. albicansAGE3*, which encodes a GAP protein (an allosteric effector that activates Arf GTPase activity) required for hyphal growth (Lettner et al. 2010) and full virulence (Epp et al. 2010). Recently, *C. albicans* showed that *ARF2* and *ARL1* mutations diminished virulence rate, together with defects related to mycelial growth (Labbaoui et al. 2017).

All *arf*-mutant strains of *M. circinelloides* showed distinct levels of virulence against diabetic mice, but the spores from *Δarf1* and *Δarf3* strains exhibited higher virulence compared to the spores from the wild-type strain and the other *arf*-mutant strains. The higher virulence of these two mutants could arise from an export/import imbalance

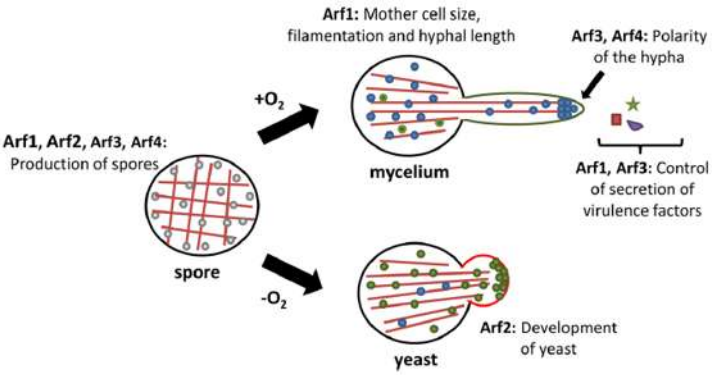

Fig. 9 Proposed model of the role of Arf proteins in morphology and virulence of *M. circinelloides*.Spore production is mainly controlled by Arf1 and Arf2, although the absence of Arf3 and Arf4 also moderately reduces sporulation. During aerobic growth, the absence of Arf1 leads to an enlargement of mother cells, as well as to an increase in the number of hyphae per cell and a decrease in hyphal length. Arf3 and Arf4 are involved in the maintenance of the tip polarity of hyphae, and their absence leads to tip dichotomy in 30% cells. Meanwhile, during anaerobic growth, Arf2 is necessary for the development of yeast cells. Arf1 and Arf3 participate in the secretion of virulence factors, including proteins. The cell wall in hyphae (green) or yeast cells (red) must be synthesised to promote cell growth. Red lines indicate the cytoskeleton and blue and green circles represent specific vesicles involved in hyphal and yeast growth, respectively. Stars, squares, and triangles illustrate secreted molecules (figure modified from Park and Bi 2007)

that might result in the accumulation of certain virulence-inducing molecules in the media. The low viability of nematodes in the presence of cell-free media collected from mycelial cultures of *Δarf1* and *Δarf3* mutants supports the view that these strains secrete a protein (or proteins) responsible for the increase in virulence. The total protein content in the cell-free media of *arf* mutant strains of *M. circinelloides* was similar except for those of *Δarf1, Δarf2, and Δarf4* mutant strains that significantly registered up to 20% more protein compared to the wild-type or other *arf* mutant strains. Probably, some proteins are over-secreted in the *Δarf1* and *Δarf3* strains that contribute to their virulent phenotype. In addition, a recent study in *M. circinelloides* identified that Myo5, a motor protein involved in actin-based vesicle trafficking, is required for polarised growth and virulence phenotype (Tidreu et al. 2017). Myo5 could interact with several types of vesicles, which could explain its essential role in *M. circinelloides* growth and virulence. More experiments in terms of genetic and biochemical interactions are required to dissect these possible scenarios.

The four Arf proteins in *M. circinelloides* participate in different aspects of morphogenesis and virulence, possibly by regulating vesicle trafficking (Fig. 9). To our knowledge, this is the first report describing the regulation of secreted virulence factors by Arf proteins in fungi, and information on the signalling network utilised by these proteins could be used to control the virulence of *M. circinelloides* or other fungi. We are currently attempting to identify the molecule(s) responsible for the increased virulence of the *Δarf1* and *Δarf3* mutant strains of *M. circinelloides*.

Acknowledgements This work was supported by grants from Coordinación de la Investigación Científica, UMSNH, México (2.6, 2.35), Consejo Nacional de Ciencia y Tecnología, México (CONACYT; 181747, 167071, and 256119), and Fundación Séneca-Agencia de Ciencia y Tecnología de la Región de Murcia, Spain (19339/PI/14). JA P-M, G M-H, MI V-M, and NY R-M were supported by postgraduate fellowships from CONACYT and CP-A by Ministerio de Educación, Cultura y Deporte of Spain (FPU-14/01832).

Author contributions JAP-M, GM-H, MIV-M, CP-A, VA-C, NYR-M, RO-A, data acquisition and interpretation; RO-A, IEJ-G, JC-G, MIR-D, VG, reagents, critical analysis, and revision of the article for intellectual content; MIR-D, VG, VM-C, conception and design of the work and data analysis and interpretation; VM-C, drafting of the article.

Compliance with ethical standards

Conflict of interest All authors declared that they have no potential conflict of interest.

Research involving human/animal participants This article does not contain any studies with human participants.

References

Ackema KB, Hench J, Böckler S, Wang SC, Sauder U, Mergentaler H, Westermann B, Bard F, Frank S, Spang A (2014) The small GTPase Arf1 modulates mitochondrial morphology and function. EMBO J 33:2659–2675

Agrawal G, Subramani S (2013) Emerging role of the endoplasmic reticulum in peroxisome biogenesis. Front Physiol 4:286

Arnau J, Strøman P (1993) Gene replacement and ectopic integration in the zygomycete *Mucor circinelloides*. Curr Genet 23:542–546

Avalos J, Limón MC (2015) Biological roles of fungal carotenoids. Curr Genet 61:309–324

Bahn YS, Xue C, Idnurm A, Rutherford JC, Heitman J, Cardenas ME (2007) Sensing the environment: lessons from fungi. Nat Rev Microbiol 5:57–69

Benito EP, Campuzano V, López Matas MA, De Vicente JI, Estava A (1995) Isolation, characterization and transformation, by autonomous replication, of *Mucor circinelloides* OMPdecase-deficient mutants. Mol Gen Genet 248:126–135

Binder U, Maurer E, Lass-Flörl C (2014) Mucormycosis from the pathogens to the disease. Clin Microbiol Infect 20(Suppl 6):60–66

Brenner S (1974) The genetics of *Caenorhabditis elegans*. Genetics 77:71–94

Casadevall A, Nosanchuk JD, Williamson P, Rodrigues ML (2009) Vesicular transport across the fungal cell wall. Trends Microbiol 17:158–162

Colicelli J (2004) Human RAS superfamily proteins and related GTPases. Sci STKE 2004, RE13

Corrochano LM, Kuo A, Marcet-Houben M, Polaino S, Salamov A, Villalobos-Escobedo JM et al (2016) Expansion of Signal Transduction Pathways in Fungi by Extensive Genome Duplication. Curr Biol 26:1577–1584

De laCruz JO, García-Soto J, Uriostegui C, Carranza L, Novoa G, Reyna G, Martínez-Cadena G (2007) Differential expression of Rho1GTPase and Rho3GTPase during isotropic and polarized growth of *Mucor circinelloides*. Can J Microbiol 53:168–176

Dijksterhuis J, Molenaar D (2013) Vesicle trafficking via the Spitzenkörper during hyphal tip growth in *Rhizoctonia solani*. Antonie Van Leeuwenhoek 103:921931

Epp E, Vanier G, Harcus D, Lee AY, Jansen G, Hallett M, Sheppard DC, Thomas DY, Munro CA, Mullick A, Whiteway M (2010) Reverse genetics in *Candida albicans* predicts ARF cycling is essential for drug resistance and virulence. PLoS Pathog 6:e1000753

Gutiérrez A, López-García S, Garre V (2011) High reliability transformation of the basal fungus *Mucor circinelloides* by electroporation. J Microbiol Methods 84:442–446

Hsu JW, Lee FJ (2013) Arf3p GTPase is a key regulator of Bud2p activation for invasive growth in *Saccharomyces cerevisiae*. Mol Biol Cell 24:2328–2339

Huarte-Bonnet C, Juárez MP, Pedrini P (2015) Oxidative stress in entomopathogenic fungi grown on insect-like hydrocarbons. Curr Genet 61:289–297

Jackson CL, Bouvet S (2014) Arfs at a glance. J Cell Sci 127:4103–4109

Kahn RA, Gilman AG (1984) Purification of a protein cofactor required for ADP-ribosylation of the stimulatory regulatory component of adenylate cyclase by cholera toxin. J Biol Chem 259:6228–6234

Kahn RA, Cherfils J, Elias M, Lovering RC, Munro S, Schurmann A (2006) Nomenclature for the human Arf family of GTP-binding proteins: ARF, ARL, and SAR proteins. J Cell Biol 172:645–650

Kronstad JW, Attarian R, Cadieux B, Choi J, D'Souza CA, Griffiths EJ, Geddes JM, Hu G, Jung WH, Kretschmer M, Saikia S, Wang J (2011) Expanding fungal pathogenesis: *Cryptococcus* breaks out of the opportunistic box. Nat Rev Microbiol 9:193–203

Labbaoui H, Bogliolo S, Ghugtyal V, Solis NV, Filler SG, Arkowitz RA, Bassilana M (2017) Role of Arf GTPases in fungal morphogenesis and virulence. PLoS Pathog 13:e1006205

Lambert AA, Perron MP, Lavoie E, Pallotta D (2007) The *Saccharomyces cerevisiae* Arf3 protein is involved in actin cable and cortical patch formation. FEMS Yeast Res 7:782–795

Lee SC, Shaw BD (2008b) Localization and function of ADP ribosylation factor A in *Aspergillus nidulans*. FEMS Microbiol Lett 283:216–222

Lee SC, Schmidtke SN, Dangott LJ, Shaw BD (2008a) *Aspergillus nidulans* ArfB plays a role in endocytosis and polarized growth. Eukaryot Cell 7:1278–1288

Lee SC, Li A, Calo S, Heitman J (2013) Calcineurin plays key roles in the dimorphic transition and virulence of the human pathogenic zygomycete *Mucor circinelloides*. PLoS Pathog 9:e1003625

Lettner T, Zeidler U, Gimona M, Hauser M, Breitenbach M, Bito A (2010) *Candida albicans* AGE3, the ortholog of the S. cerevisiae ARF-GAP-encoding gene GCS1, is required for hyphal growth and drug resistance. PLoS One 5:e11993

Lübbehüsen TL, Nielsen J, McIntyre M (2003) Characterization of the *Mucor circinelloides* life cycle by on line image analysis. J Appl Microbiol 95:1152–1160

Mizuno-Yamasaki E, Rivera-Molina F, Novick P (2012) GTPase networks in membrane traffic. Ann Rev Biochem 81:637–659

Moss J, Vaughan M (1998) Molecules in the ARF orbit. J Biol Chem 273:21431–21434

Nicolás FE, de Haro JP, Torres-Martínez S, Ruiz-Vázquez RM (2007) Mutants defective in a *Mucor circinelloides* dicer-like gene are not compromised in siRNA silencing but display developmental defects. Fungal Genet Biol 44:504–516

Ocampo J, Fernández Nuñez L, Silva F, Pereyra E, Moreno S, Garre V, Rossi S (2009) A subunit of protein kinase a regulates growth and differentiation in the fungus *Mucor circinelloides*. Eukaryot Cell 8:933–944

Ocampo J, McCormack B, Navarro E, Moreno S, Garre V, Rossi S (2012) Protein kinase A regulatory subunit isoforms regulate growth and differentiation in *Mucor circinelloides*: essential role of PKAR4. Eukaryot Cell 11:989–1002

Park HO, Bi E (2007) Central roles of small GTPases in the development of cell polarity in yeast and beyond. Microbiol Mol Biol Rev 71:48–96

Punt PJ, Seiboth B, Weenink XO, van Zeijl C, Lenders M, Konetschny C, Ram AF, Montijn R, Kubicek CP, van den Hondel CAMJJ (2001) Identification and characterization of a family of secretion-related small GTPase-encoding genes from the filamentous fungus *Aspergillus niger*: a putative SEC4 homologue is not essential for growth. Mol Microbiol 41:513–525

Rangel-Porras RA, Meza-Carmen V, Martinez-Cadena G, Torres-Guzmán JC, González-Hernández GA, Arnau J, Gutiérrez-Corona JF (2005) Molecular analysis of an NAD-dependent alcohol dehydrogenase from the zygomycete *Mucor circinelloides*. Mol Genet Genomics 274:354–363

Roden MM, Zaoutis TE, Buchanan WL, Knudsen TA, Sarkisova TA et al (2005) Epidemiology and outcome of zygomycosis: a review of 929 reported cases. Clin Infect Dis 41:634–653

Rodríguez-Andrade E, Hernández-Ramírez KC, Díaz-Peréz SP, Díaz-Magaña A, Chávez Moctezuma MP, Meza Carmen V, Ortíz Alvarado R, Cervantes C, Ramírez-Díaz MI (2016) Genes from pUM505 plasmid contribute to *Pseudomonas aeruginosa* virulence. Antonie Van Leeuwenhoek 109:389–396

Roncero MI (1984) Enrichment method for the isolation of auxotrophic mutants of *Mucor* using the polyene antibiotic *N* glycosylpolyfungin.Carlsberg Res Commun 49:685–690

Salcedo-Hernandez R, Ruiz-Herrera J (1993) Isolation and characterization of a mycelial cytochrome aa3-deficient mutant and the role of mitochondria in dimorphism of *Mucor rouxii*. Exp Mycol 17:142–154

Sambrook J, Russell RW (2001) Molecular cloning: A laboratory manual, 3rd edn. Cold spring harbor laboratory press, Cold Spring Harbor

Sánchez-León E, Bowman B, Seidel C, Fischer R, Novick P, Riquelme M (2015) The Rab GTPase YPT 1 associates with Golgi cisternae and Spitzenkörper microvesicles in *Neurospora crassa*. Mol Microbiol 95:472–490

SecretaríadeAgricultura, G, Desarrollo Rural, Pesca y Alimentación (SAGARPA) (2001) NORMA Oficial Mexicana NOM-062-ZOO 1999. Especificaciones técnicas para la producción, cuidado

y uso de los animales de laboratorio. Diario Oficial de la Federación 2:107–167 (**In Spanish**)

Smaczynska-de Rooij II, Costa R, Ayscough KR (2008) Yeast Arf3p modulates plasma membrane PtdIns(4,5)P2 levels to facilitate endocytosis. Traffic 9:559–573

Stearns T, Kahn RA, Botstein D, Hoyt MA (1990a) ADP ribosylation factor is an essential protein in *Saccharomyces cerevisiae* and is encoded by two genes. Mol Cell Biol 10:6690–6699

Stearns T, Willingham MC, Botstein D, Kahn RA (1990b) ADP-ribosylation factor is functionally and physically associated with the Golgi complex. Proc Natl Acad Sci USA 87:1238–1242

Stiernagle T (2006) Maintenance of *C. elegans*. WormBook. edn. The *C. elegans* Research Community

Thompson JD, Desmond GH, Toby JG (1994) CLUSTAL W: improving the sensitivity of progressive multiple sequence alignment through sequence weighting, position-specific gap penalties and weight matrix choice. Nucleic Acids Res 22:4673–4680

Trieu TA, Navarro-Mendoza MI, Pérez-Arques C, Sanchis M, Capilla J, Navarro-Rodriguez P, Lopez-Fernandez L, Torres-Martínez S, Garre V, Ruiz-Vázquez RM, Nicolás FE (2017) RNAi-Based Functional Genomics Identifies New Virulence Determinants in Mucormycosis. PLoS Pathog 13:e1006150

Valle-Maldonado MI, Jácome-Galarza IE, Díaz-Pérez AL, Martínez-Cadena G, Campos-García J, Ramírez-Díaz MI, Reyes-De la Cruz H, Riveros-Rosas H, Díaz-Pérez C, Meza-Carmen V (2015a) Phylogenetic analysis of fungal heterotrimeric G protein-encoding genes and their expression during dimorphism in *Mucor circinelloides*. Fungal Biol 119:1179–1193

Valle-Maldonado MI, Jácome-Galarza IE, Gutiérrez-Corona F, Ramírez-Díaz MI, Campos-García J, Meza-Carmen V (2015b) Selection of reference genes for quantitative real time RT-PCR during dimorphism in the zygomycete *Mucor circinelloides*. Mol Biol Rep 42:705–711

Van Heeswijck R, Roncero MIG (1984) High frequency transformation of *Mucor* with recombinant plasmid DNA. Carlsberg Res Commun 49:691–702

Wang L, Lin X (2012) Morphogenesis in fungal pathogenicity: shape, size, and surface. PLoS Pathog 8:1003027

Wennerberg K, Rossman KL, Der CJ (2005) The Ras superfamily at a glance. J Cell Sci 1:843–846

Wolff AM, Arnau J (2002) Cloning of Glyceraldehyde-3-phosphate Dehydrogenase-Encoding Genes in *Mucor circinelloides* (*Syn. racemosus*) and Use of the gpd1 Promoter for Recombinant Protein Production. Fungal Genet Biol 35:21–29

Yorimitsu T, Sato K, Takeuchi M (2014) Molecular mechanisms of Sar/Arf GTPases in vesicular trafficking in yeast and plants. Front Plant Sci 5:411

Fungal Genetics and Biology 129 (2019) 40–51

Contents lists available at ScienceDirect

Fungal Genetics and Biology

journal homepage: www.elsevier.com/locate/yfgbi

Role of Arf-like proteins (Arl1 and Arl2) of *Mucor circinelloides* in virulence and antifungal susceptibility

J. Alberto Patiño-Medina[a], Marco I. Valle-Maldonado[a], Guadalupe Maldonado-Herrera[a], Carlos Pérez-Arques[b], Irvin E. Jácome-Galarza[c], César Díaz-Pérez[d], Alma L. Díaz-Pérez[a], Carlos A. Araiza-Cervantes[a], Julio C. Villagomez-Castro[e], Jesús Campos-García[a], Martha I. Ramírez-Díaz[a], Victoriano Garre[b], Víctor Meza-Carmen[a,*]

[a] Instituto de Investigaciones Químico Biológicas, Universidad Michoacana de San Nicolás de Hidalgo, 58038 Morelia, Michoacán, Mexico
[b] Departamento de Genética y Microbiología, Facultad de Biología, Universidad de Murcia, 30100 Murcia, Spain
[c] Laboratorio Estatal de Salud Pública del Estado de Michoacán, 58279 Morelia, Michoacán, Mexico
[d] Facultad de Agrobiología, Campus Salvatierra. Universidad de Guanajuato. 38900 Salvatierra, Guanajuato, Mexico
[e] Departamento de Biología, División de Ciencias Naturales y Exactas, Campus Guanajuato, Universidad de Guanajuato, Noria Alta S/N, Col. Noria Alta, 36000 Guanajuato, Guanajuato, Mexico

ARTICLE INFO

Keywords:
ADP-ribosylation factor
Arl proteins
Antifungal
Mucor circinelloides
Vesicle trafficking
Virulence

ABSTRACT

Mucor circinelloides is an etiologic agent of mucormycosis, a fungal infection produced by Mucorales often associated with mortality due to unavailability of antifungal drugs. Arl proteins belong to the Arf family and are involved in vesicle trafficking and tubulin assembly. This study identified two Arl (Arf-like)-encoding genes, *arl1* and *arl2*, in *M. circinelloides* and explored their function in morphogenesis, virulence, and antifungal susceptibility. Although Arl1 and Arl2 proteins shared 55% amino acid sequence identity, *arl1* and *arl2* genes showed distinct transcriptional expression patterns. *arl1* was expressed at higher levels than *arl2* and induced in mycelia, suggesting a role in morphological transitions. Disruption of the *arl1* and *arl2* genes led to heterokaryon ($\Delta arl1^{(+)(-)}$) and homokaryon ($\Delta arl2$) genotypes, respectively. The incapacity to generate homokaryon mutants for *arl1* suggested that it is essential for growth of *M. circinelloides*. Deletion of each gene reduced the expression of the other, suggesting the existence of a positive cross-regulation between them. Thus, deletion of *arl2* resulted in a ~60% reduction of *arl1* expression, whereas the $\Delta arl1^{(+)(-)}$ showed ~90% reduction of *arl1* expression. Mutation of *arl2* showed no phenotype or a mild phenotype between $\Delta arl1^{(+)(-)}$ and wild-type (WT), suggesting that all observed phenotypes in both mutant strains corresponded to *arl1* low expression. The $\Delta arl1^{(+)(-)}$ produced a small amount of spores that showed increased sensitivity to dodecyl-sulfate and azoles, suggesting a defect in the cell wall that was further supported by decrease in saccharide content. These defects in the cell wall were possibly originated by abnormal vesicle trafficking since FM4-64 staining of both mutants $\Delta arl1^{(+)(-)}$ and $\Delta arl2$ revealed less well-localized endosomes compared to the WT. Moreover, aberrant vesicle trafficking may be responsible for the secretion of specific virulence-related proteins since cell-free medium from $\Delta arl1^{(+)(-)}$ were found to increase killing of *Caenorhabditis elegans* compared to WT.

1. Introduction

Mucor circinelloides is a dimorphic fungus responsible for mucormycosis, an infection rare but can be fatal (Roden et al., 2005). Four ADP-ribosylation factor (Arf)-encoding genes involved in morphogenesis and virulence have been characterized in this *Mucor* specie (Patiño-Medina et al., 2018). Arf family members belonging to the Ras superfamily are the most divergent among small G proteins; they are grouped into Arf proteins, Arf-like proteins (Arl), and Sar proteins (Kahn et al., 2006). Arf proteins were first described as positive allosteric modulators of cholera toxin activity (Kahn and Gilman, 1984; Moss and Vaughan, 1998). Contrary to Arf, Arl proteins do not activate cholera toxin (Kahn et al., 2006).

Arl proteins participate in extracellular vesicles, biogenesis, and

* Corresponding author at: Laboratorio de Diferenciación Celular, Instituto de Investigaciones Químico Biológicas, Universidad Michoacana de San Nicolás de Hidalgo, Ciudad Universitaria 58030, Morelia, Michoacán, Mexico.
E-mail address: victor_meza2004@yahoo.com.mx (V. Meza-Carmen).

https://doi.org/10.1016/j.fgb.2019.04.011
Received 9 January 2018; Received in revised form 17 April 2019; Accepted 19 April 2019
Available online 20 April 2019
1087-1845/

transport of molecules between cell compartments, possibly through the exocytic and endocytic pathways (Mizuno-Yamasaki et al., 2012). Although the molecular function of many Arl factors remains unclear, some play important roles in tubulin assembly, vesicle trafficking, and ciliogenesis (Burd et al., 2004; Kahn et al., 2006; Gillingham and Munro, 2007).

In the best studied fungal model, *Saccharomyces cerevisiae*, three ARL-encoding genes have been reported: ARL1, ARL2, and ARL3 (Burd et al., 2004). ARL1 is involved in vesicle trafficking, as indicated by decreased protein secretion to the plasma membrane in its absence and is required for starvation-induced autophagy under high-temperature stress (Rosenwald et al., 2002; Yang and Rosenwald, 2016). ARL2 (also known as ARF3) is necessary for tubulin assembly, whereas ARL3 is required for vacuolar protein transport and morphogenesis (Huang et al., 1999; Bhamidipati et al., 2000). Lack of ARL1 in *Candida albicans* results in multiple defects, such as shorter hyphae, increased secretion, and a less virulent phenotype (Labbaoui et al., 2017).

Growth conditions are key to *M. circinelloides*, as differing conditions determine the fate of asexual spores, which develop either as mycelia or yeast cells; this process, known as dimorphism, depends mostly on the availability of oxygen and carbon sources (McIntyre et al., 2002; Lübbehüsen et al., 2003a). Morphological changes are also related to fungal pathogenesis and disease development. *M. circinelloides* can become a human opportunistic pathogen associated to its mycelia morphology (Lee et al., 2013; Lewis and Kontoyiannis, 2013). The lethal phenotype in humans is associated in part with the limited availability of antifungal therapies targeted against Mucorales. For example, some clinical strains of *M. circinelloides* have been described as resistant to amphotericin and posaconazole, which are the primary antifungal compounds utilized in mucormycosis therapy (Rogers, 2008).

Our group previously characterized four Arf-encoding genes from *M. circinelloides*. Arf1 is involved in regulation of mother cell size and hyphae defects, Arf2 is essential for adequate yeast development, whereas Arf3 and Arf4 seem to be involved in the control of hyphal tip growth (Patiño-Medina et al., 2018). Moreover, deletion of *arf1* or *arf3* leads to increased virulence of *M. circinelloides* via secretion of virulence factors (Patiño-Medina et al., 2018).

In the present study, we focused on functional characterization of Arl1- and Arl2-encoding genes in *M. circinelloides* and their participation in morphogenesis, virulence, and antifungal susceptibility. Our results showed that mutation of *arl1* is involved in the vesicle trafficking, cell wall maintenance, increased susceptibility to antifungal and secretion of virulence factors of proteinaceus nature.

2. Material and Methods

2.1. Fungal strains and growth media

M. circinelloides R7B (*leuA*$^-$) and MU402 (*leuA*$^-$, *pyrG*$^-$) were utilized in this study (Roncero, 1984; Nicolás et al., 2007). Spore production and culture conditions were as described previously (Patiño-Medina et al., 2018). Briefly, spores were obtained after propagation on YPG or YNB solid media for 5 days at 28 °C in the presence of light. Spores were counted in a hemocytometer chamber.

2.2. Aerobic and self-anaerobic spore germination and growth quantification

Aerobic and anaerobic growth was quantified as described previously (Valle-Maldonado et al., 2015). Germination percentage was calculated for aerobic or anaerobic conditions, as the number of germinal stage or budding yeast in a total of 100 cells. Mycelium from *M. circinelloides* or yeast cells were collected from appropriate cultures, filtered, and dried in pre-weighed filter paper (Whatman No 5). Cells were washed twice with distilled H_2O. Filters were dried for 96 h at 80 °C, then cooled at room temperature and cell dry weight determined.

2.3. Spore production, and radial growth

The process of sporangium development included the following steps. Fifty spores were seeded on slides covered with YPG agar medium supplemented with uracil and placed in the presence of light; growth was recorded after 4 days. Next, 50 spores were inoculated on YPG plates supplemented with uracil. Plates were incubated for 6 days at 28 °C in the presence of light, accompanied by daily measurements of colony diameter. Finally, the spores were harvested and counted at the end of day 5.

2.4. Arl protein identification in M. circinelloides

Homologous genes to *S. cerevisiae* ARL1 were found in the BLAST genome database of *M. circinelloides* 2.0 (https://genome.jgi.doe.gov/Mucci2/Mucci2.home.html). Identification criteria for Arl proteins from *M. circinelloides* included identity percentages and the presence of conserved domains. *M. circinelloides* Arl homologues used in protein alignments and dendrograms included: Arf1 (157293), Arf2 (156501), Arf3 (155350), Arf4 (32250), Arl1 (155647), and Arl2 (112008). Accession numbers for *S. cerevisiae* genes were: ARF1 (CAA98769), ARF2 (CAA65622), ARF3 (CAA99291), ARL1 (CAA85125), ARL2 (5CYA_A), ARL3 (DAA11379), and SAR1 (NP_015106). *Aspergillus nidulans* genes comprised: ArfA (AN1126) and ArfB (AN5020). *Homo sapiens* genes comprised: ARF1 (NP_001019398), ARF3 (NP_001650), ARF4 (NP_001651), ARF5 (NP_001653), ARF6 (CAG46762), ARL1 (P40616), ARL2 (P36404), ARL3 (P36405), ARL4 (NP_001182325), ARL5 (Q9Y689), ARL6 (NP_001265222), and SAR1 (AAF81741). Alignments were carried out using Clustal W software (Thompson et al., 1994).

2.5. Phylogenetic analysis

Phylogenetic analysis was completed using the phylogeny program "a la carte" mode (http://www.phylogeny.fr/alacarte.cgi) (Dereeper et al., 2008). Muscle software was employed for alignment and Maximum Likelihood software for tree construction. An approximate likelihood-ratio test was used to conduct statistical tests for branch support (Fig. S1).

2.6. Oligonucleotide design and quantitative real time reverse transcription polymerase chain reaction (RT-qPCR)

Primers and hydrolysis probes for *arl1 and arl2* genes from *M. circinelloides* with minimal secondary structures were designed using Biosearch Technologies software (www.biosearchtech.com) to ensure specificity of detections during RT-qPCR assays (Table S1). Hydrolysis probes showed more than 85% PCR efficiency (Table S2). The protocol followed was as described previously (Valle-Maldonado et al., 2015).

In order to evaluate relative *arl1* and *arl2* gene expression, an estimation of the efficiency (*E*) of a real time PCR assay for each of the studied genes was required. In this work, estimation was carried out using a calibration dilution curve and slope calculation. A 5-fold dilution series (500–0.05 ng total RNA) was prepared and used as a sample in the RT-qPCR. Briefly, efficiency (*E*) was obtained from standard curves using the formula $E = ((10^{(-1/\text{slope})} - 1) \times 100)$. Relative expression levels were determined with the efficiency correction method, which takes into account amplification efficiencies between target and reference genes (Pffafl, 2001). Using of reference *tfc-1* gene for RT-qPCR analysis during dimorphism in *M. circinelloides* was according as described before (Valle-Maldonado et al., 2015). The *tfc-1* gene encodes a subunit of the transcription factor TFIIIC required for the RNA polymerase III pre-initiation complex assembly. mRNA isolation from *M. circinelloides* R7B strain was performed as described previously for RT-

qPCR analysis (Patiño-Medina et al., 2018).

2.7. Targeted deletion of arl1 and arl2 in M. circinelloides

2.7.1. Targeted deletion of arl1

The full *arl1* open reading frame (ORF), including a region 1 kb upstream of the ATG codon (5́ region) and 1 kb downstream of the stop codon (3′ region), was amplified by PCR using oligonucleotides FW-*Sma*I-*arl1* and RV-*Eco*RI-*arl1* and genomic DNA from *M. circinelloides* MU402 as a template (Table S3). The 3-kb fragment was cloned into the pUC18 vector, generating vector pMAT1575. This was then used as a template to amplify the whole vector, except the *arl1* ORF, using Herculase Enzyme (Agilent) and oligonucleotides FW-*Bgl*II-*arl1* and RV-*Bgl*II-*arl1*. Further enzyme digestion with *Bgl*II was performed in this amplicon, which was then kept at −20 °C. Separately, the 3.4-kb fragment corresponding to the selection marker *pyrG* was obtained from vector pEMP1 (Benito et al., 1995) by *Bam*HI digestion, and was subsequently purified and ligated in the *Bgl*II sites on pMAT1575 (containing the 5′ and 3́UTR regions) to generate vector pMAT1578. The *arl1* 5.7-kb recombinant fragment 5′UTR-*pyrG*-3′UTR from pMAT1578 was obtained after digestion with *Eco*RI and *Sma*I.

2.7.2. Targeted deletion of arl2

A recombinant fragment containing *arl2* gene and *pyrG* selection marker was generated by fusion PCR using three PCR fragments with overlapping sequences between them (Trieu et al., 2017; Patiño-Medina et al., 2018). Oligonucleotides (1) *arl2*-UFwd and (3) *arl2*-URev-*pyrG* amplified a region 1 kb upstream of the start codon of the *arl2* gene, whereas oligonucleotides (2) *arl2*-DRev and (4) *arl2*-DFwd-*pyrG* (Table S3) amplified a region 1 kb downstream of its stop codon. In oligonucleotide (3) *arl2*-URev-*pyrG*, a nucleotide sequence was added at its 3′ end, so it could hybridize to the 5′ end of the *pyrG* gene; whereas in oligonucleotide (4) *arl2*-DFwd-*pyrG*, a nucleotide sequence was added at its 5′ end, so it could hybridize to the 3′ end of the *pyrG* gene. The *pyrG* gene was amplified by PCR using oligonucleotides *pyrG*-FWR and *pyrG*-REV, with pMAT1700 as the template (Trieu et al., 2017). Three individual PCRs were performed to obtain three DNA fragments spanning the 5′ region, the *pyrG* gene (2 kb), and the 3′ region, which were then purified. Fusion PCR was performed using 100 ng/μL of each template; 10 μM of (1) *arl2*-UFwd and (2) *arl2*-DRev oligonucleotides, and 1 μL Herculase II Fusion Enzyme (Agilent). The ratio of the amplicons used in the PCR was 1:2:1.

Protoplasts of *M. circinelloides* obtained from strain MU402 were transformed using the 4.2-kb recombinant DNA fragment (3 μg per transformation event) as detailed previously (Gutiérrez et al., 2011). Transformants were selected on MMC agar plates without uracil. Monosporic cultures were obtained after five cycles of sporulation on either selective or rich medium.

2.8. Molecular identification of arl-mutant strains from M. circinelloides

2.8.1. arl1 gene deletion

Transformed strains were identified by PCR using oligonucleotides FW-INT-*arl1* and RV-INT-*arl1* (Table S3). A homologous integration event was determined by PCR amplification of a 5.7-kb band, whereas a 3-kb band indicated the wild-type genotype.

2.8.2. arl2 gene deletion

Mutants were identified by PCR using oligonucleotides *arl2*-5′CR, which hybridized outside the recombination fragment used to delete *arl2*, and *pyrG*-R2, which hybridized in the selective marker sequence (Table S3). Deletion mutants generated an amplicon of 1.6 kb, whereas lack of amplification identified a wild-type genotype. As a PCR control for a positive amplification, oligonucleotides (2) *arl2*-DRev and (4) *arl2*-DFwd-*pyrG* (Table S3) that hybridize in the flanking 3́ non-coding region of *arl2* were used and an amplicon of 1.1 kb was expected for both wild-type and *arl2* genotypes.

2.8.3. Southern blot to identify the deletion of arl2

Briefly, 1 μg of genomic DNA from strain MU402 and possible mutants in the *arl2* gene were digested with *Eco*RI, separated by DNA electrophoresis, and transferred to nylon membranes (HybondTM-N+, Amersham Biosciences) following the protocol by Sambrook and Russell (2001). Southern blot hybridization was carried out under stringent conditions. DNA probes were labeled with -dCTP [α-32P] Ready-To-Go Labeling Beads (GE Healthcare Life Science). The DNA probe was amplified directly from genomic DNA using primer pairs (1) *arl2*-UFwd and (3) *arl2*-Urev-*pyrG* (Table S3).

2.8.4. RT-qPCR confirmation

This assay was carried out as described in section 2.6 using as template the total RNA from each *arl* mutant and wild-type strains of *M. circinelloides*.

2.9. Complementation of the Δarl2 strain

The Δ*arl2* + *arl2*wt strain (*pyrG*$^+$, *leuA*$^+$, *carRP*$^-$) was obtained by integrative transformation with the *arl2* wild-type allele at the *carRP* gene locus of the Δ*arl2* mutant strain (*pyrG*$^+$, *leuA*$^-$, *carRP*$^+$). The *carRP* gene encodes a lycopene cyclase which catalyzes the transformation of lycopene to beta-carotene, and the general procedure of integrative transformation, was reported previously (Garcia et al., 2017). As a consequence, the complemented strain Δ*arl2* + *arl2*wt had albino colonies instead of the Δ*arl2* yellowish colonies. Transformation fragment included about 1.1 kb upstream of the start of the *carRP* gene ORF and approximately 1.1 kb downstream the stop codon. These two fragments border the *leuA* (4.4 kb) and *arl2* (1.8 kb). Both genes are under the regulation of their native promoter and terminator sequences. The size of this transformation fragment is around 8.2 kb. For selection, single spore colonies from the YNB minimal medium were transferred after 5 days onto new minimal medium agar plates at 28 °C and used for subsequent sporulation cycles until homokaryotic albino colonies were observed. The integration event was also demonstrated by PCR using the oligonucleotides forward *arl2*-F1 (which hybridize in *arl2*) and reverse *carRP* (which hybridize in *carRP*, outside of the recombinant fragment) (Table S3). A 3 kb amplicon size showed the positive integration event.

2.10. Laser scanning confocal microscopy (LSCM)

In order to carry out live-hyphal imaging, the "inverted agar block" method was used (Hickey et al., 2002). MU402, Δ*arl1*$^{(+)(-)}$, Δ*arl2* and Δ*arl2* + *arl2*wt strains were grown on solid YPG for 18 h at 28 °C, then 0.5 cm^3 agar plugs were taken and stained with five mM FM4-64 (Molecular Probes, Eugene, OR) for 20 min. This is a general cytological stain and endocytosis marker for living hyphae (Fisher-Parton et al., 2001). For taking microphotographs, an inverted laser scanning microscope FV1000 FluoView™ (Olympus, Japan) was employed. This microscope is attached to a Multi-line Ar laser that was used for FM4-64 excitation at 543 nm, and fluorescence was detected at 612 nm. An UPlanSapo 20×/0.75 objective and an UPlanFLN 60×, (NA 1.42) oil immersion were employed.

2.11. Analysis of cell wall polymers

Spores were inoculated for 10 h in YPG, the corresponding mycelia was washed with H_2O and disrupted in 50 mM Tris-HCl pH 8.0, using a Precellys homogenizer, 5000×g, during 15 min. Cell walls were centrifuged and washed five times with 1 M NaCl. The pellet was suspended in SDS 2%, 0.3 M ß-mercaptoethanol and 1 mM EDTA, 50 mM Tris, pH 7.5 and heated 10 min at 100 °C. Cell walls were boiled with 2 M trifluoroacetic acid for 3 h. Next, the acid was evaporated and

samples were resuspended in deionized water. Samples were analyzed by High-Performance Anion-Exchange Chromatography coupled to Pulsed Amperometric Detection (HPAEC-PAD, Thermo Fisher Scientific) (Martinez-Álvarez et al., 2017).

2.12. Susceptibility of M. circinelloides to antifungal agents

Susceptibility to sodium dodecyl sulfate (SDS), itraconazole, and fluconazole (Sigma) was assayed by adding these compounds to YPG solid or liquid media aerobically grown at indicated concentrations; radial growth expressed in centimeters, or percentage of germinated cells was registered, respectively. Minimum inhibitory concentrations (MIC) and their corresponding 95% confidence intervals were calculated employing Nonlinear regression (curve fit), log (inhibitor/inductor) vs response (variable slope), R^2 = 0.95–0.99 (GraphPrism 7.0). MIC_{50} for solid and aerobic liquid growths were evaluated at the end of day 5 and 6 h, respectively and data from the alteration in colony diameter or cell germination ratio for antifungal treatments compared to YPG were employed, respectively.

Growth measurements included: (1) radial development on YPG agar plates during 5 days of incubation at 28 °C in the presence of light; (2) germination rate in aerobic liquid YPG medium after 6 h of aerobic growth; and (3) length of hyphae developed in aerobic liquid YPG medium after 6 h of aerobic growth.

2.13. Caenorhabditis elegans killing assays

Caenorhabditis elegans Bristol N2 worms were synchronized by hypochlorite isolation of eggs from gravid adults, followed by hatching of eggs in S-basal medium (Brenner, 1974; Stiernagle, 2006). L1 larvae were transferred onto nematode growth medium plates seeded with the *E. coli* OP50 strain previously grown on the plates as a food source, then incubated at 18 °C for 4–5 days until they reached the young adult phase (Stiernagle, 2006). Worms were incubated with either spores or cell-free medium collected from mycelia grown for 12 h in YPG as previously described (Patiño-Medina et al., 2018). For some experiments, 1 mL of cell-free media acquired from the different *M. circinelloides* strains was incubated with pronase (25 µL, equivalent to 5 U; Sigma, USA) for 2 h at 37 °C) prior to the *C. elegans* killing assays.

2.14. Statistical analysis

Data were evaluated by Student's t–test or one way ANOVA. Means with different letters are significantly different ($p < 0.05$). STATISTICA 7 (StatSoft) was employed.

3. Results

3.1. Identification of arl genes in M. circinelloides

Using Blast-alignment tool and ARL1 from *S. cerevisiae* to query the *M. circinelloides* reference genome (https://genome.jgi.doe.gov/Mucci2/Mucci2.home.html), two ARL1 homologues were found. Both presented the canonical motif for myristoylation on glycine at position + 2 and the five G boxes (G1-G5) (Fig. 1), typical of ADP-ribosylation factors which are essential in the guanine nucleotide-binding site (Wennerberg et al., 2005). The two Arf-like (Arl1 and Arl2) proteins present in the *M. circinelloides* genome showed 55% identity and 81% similarity between them (Table S4), and 49 to 59% identity with Arf from *M. circinelloides* (Patiño-Medina et al., 2018). Arl1 and Arl2 from *M. circinelloides* exhibited 73 and 46.9% identity with ARL1 from *S. cerevisiae* and ARL5 from *H. sapiens*, respectively (Table S5). Arl1 homologues possess a conserved cysteine residue at position 80 in the inter-switch II (Fig. 1); this was present also in *M. circinelloides* Arl1 but not in Arl2 (Burd et al., 2004). This residue is needed for the recognition of Arl1 protein by the GRIP domain from golgins, important proteins involved in Golgi transport and maintenance of its structure (Setty et al., 2003).

Arl1 and Arl2 from *M. circinelloides* were grouped with Arl homologues but were phylogenetically separated from Arf subfamily proteins (Fig. S1). Arl1 from *M. circinelloides* was grouped with ARL1 from both *H. sapiens* and *S. cerevisiae*, whereas Arl2 from *M. circinelloides* was grouped in a different clade with ARL5 from *H. sapiens*. This analysis suggests that Arl1 and Arl2 from this fungus could be the result of a duplication event that took place early in the evolution of eukaryotes. This is supported by the distinct number of introns in the two genes, four in *arl1* and six in *arl2*, without coincidence in their localization (Fig. S2).

3.2. Expression of arl genes during dimorphism in M. circinelloides

We previously described the function of four *arf* (*arf1-4*) genes in *M. circinelloides*, finding that mRNA of *arf2* is mainly accumulated during yeast growth, the mutation of *arf2* led to a significant decreased of yeast development (Patiño-Medina et al., 2018). The possible correlation between *arl* gene expression during the dimorphic process and the corresponding biological function in *M. circinelloides* prompted us to quantify the accumulation of *arl* mRNAs during the dimorphic event. mRNA levels were determined by RT-qPCR using total RNA isolated from spores or vegetative cells (mycelia or yeast) at 3, 6, and 12 h. The highest transcript levels in mycelia and spores corresponded to *arl1*, which showed a 2-fold and 1.5-fold increase compared to the levels in yeasts, respectively. By the other hand, *arl2* mRNA levels were lower than those levels of *arl1* under all tested conditions and the expression pattern was unrelated to the studied morphological stages (Fig. 2). Thus, data indicated that *arl1* transcript levels were positively influenced by the morphological spore and mycelial stages.

3.3. Targeted deletion of arl genes in M. circinelloides

The role of *arl1* and *arl2* genes was studied through the generation of the corresponding deletion mutants by homologous recombination with replacement fragments containing the *pyrG* marker (see Materials and Methods). The *arl1* replacement fragment containing *pyrG* flanking by upstream and downstream sequences of *arl1*, was purified and used to transform protoplasts of wild-type strain MU402 (*leuA*$^-$,*pyrG*$^-$), which is auxotrophic for leucine and uracil (Nicolás et al., 2007) (Fig. 3A). Transformants grown in selective MMC medium were recovered and subsequent successive vegetative cycles in the selective medium were performed to obtain homokaryotic *arl1*$^-$mutants. Following 5 cycles, none of the 10 independent transformants showed 100% *ura*$^+$ spores, indicating a heterokaryon state ($\Delta arl1^{(+)(-)}$).

Molecular confirmation of homologous recombination in the *arl1* locus was conducted by PCR using oligonucleotides that hybridized outside of this locus (Table S3). The presence in the transformed strain of a 3-kb and 5.7-kb PCR fragment corresponding to the wild-type and mutant *arl1* allele, respectively (Fig. 3A), revealed the heterokaryotic genotype of the transformant, generating the strain called $\Delta arl1^{(+)(-)}$. The inability to obtain homokaryons (in transformation-independent experiments) suggests an essential role of the *arl1* gene in *M. circinelloides*.

A similar strategy was followed to delete *arl2*, a recombinant fragment containing the selective marker *pyrG* flanked by 1-kb regions upstream and downstream of the *arl2* start and stop codon, respectively, was generated, and used to transform strain MU402. The selection was performed on MMC medium without uracil; two of six transformant clones screened were mutants. Molecular confirmation of homologous recombination for mutation of *arl2* was performed by PCR using oligonucleotides *arl2*-5′CR and *pyrG*-R2 (Table S3). The presence of a 1.6-kb PCR product, indicated a homokaryon *arl2* deletion mutant (Δ*arl2*) (Fig. 3B). Hybridization of a 4.7-kb band observed in the transformant clone by Southern blot assay confirmed the presence of a unique

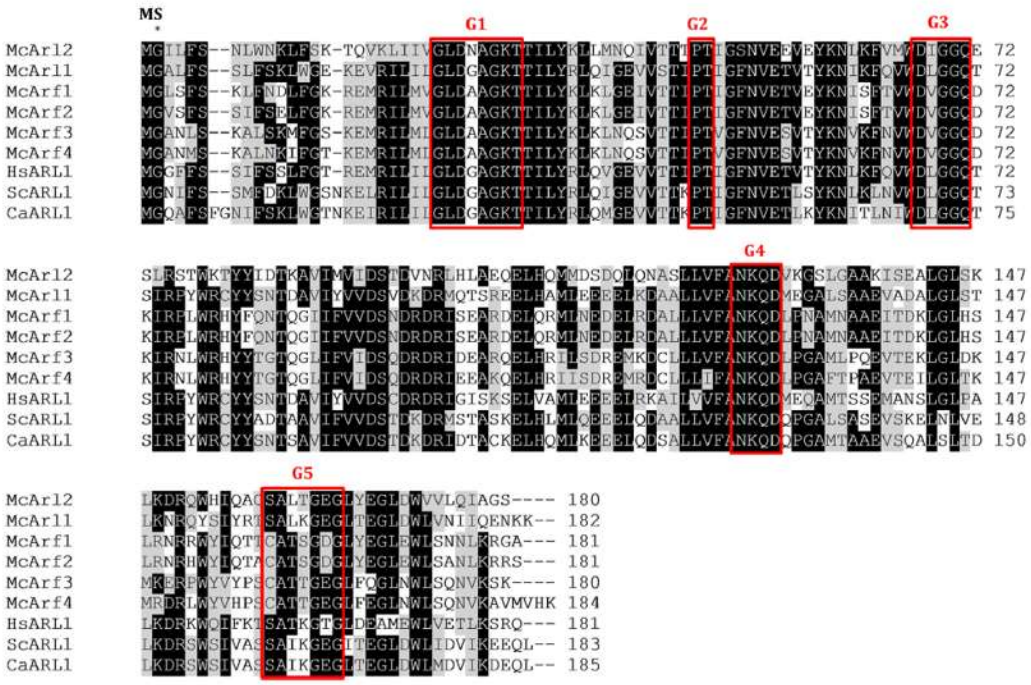

Fig. 1. Alignment of putative Arf-like proteins from *M. circinelloides*. *M. circinelloides* Arl1 and Arl2 protein members (Mc) were aligned with Arl homologues from *S. cerevisiae* (Sc), *C. albicans* (Ca), and *H. sapiens* (Hs). Guanine binding domains composed of G1-G5 motifs are shown in boxes. The consensus sequences for G1 (GxxxxGKS/T), G2 (PT), G3(DxxGQ/H/T), G4(T/NKxD), G5 (C/SAK/L/T), and the myristoylation site (MS) were obtained from Wennerberg et al. (2005). Shaded areas in black correspond to identical amino acids in the protein sequences.

integration event at the desired locus and homokaryon in *arl2* knockout mutant (Fig. 3C). All experiments below were carried out for two independent clones $\Delta arl1^{(+)(-)}$ and *Δarl2* mutant strains, revealing similar results at all times between each mutant strain.

The *Δarl2* + *arl2*wt restored strain was obtained by integrative transformation with the *arl2* wild-type allele at the *carp* locus as has been described (Garcia et al., 2017).

Expression analysis confirmed the null expression for *arl2* in the *Δarl2* and a 93.34% reduction in mRNA levels for *arl1* in the $\Delta arl1^{(+)(-)}$ strains, compared to wild-type (Fig. S3). These results were particularly relevant for $\Delta arl1^{(+)(-)}$, as this could be considered a hypomorphic mutant.

It is interesting to notice that the mutations of *arl1* or *arl2* led to decreased of mRNA levels of *arl2* or *arl1* in 62.4 or 64%, respectively compared to the wild-type strain (Fig. S3). These results showed that mutation of any of these genes led to a decreased in the transcript levels of the other, suggesting a transcriptional a cross-regulation between them.

3.4. Contribution of the arl1 and arl2 genes to mycelium growth, and sporulation in M. circinelloides

The high expression of *arl1* during mycelia stages (Fig. 2) prompted us to investigate the role of this gene in sporulation by analyzing the production of spores in the heterokaryon $\Delta arl1^{(+)(-)}$. Spore size in the heterokaryon was slightly smaller than that of the parent strain (Fig. 4A) and the total amount of spores produced was nearly 70% lower than in the parental strain MU402 (Fig. 4B), indicating the importance of *arl1* for spore production. Meanwhile, *Δarl2* exhibited lower reduction in spore production (~40%) with respect to the wild-type (Fig. 4B) and, again, a slightly smaller spore size (Fig. 4A). Further, the *Δarl2* + *arl2wt* strain showed no differences in spore size or production in comparison to the MU402 strain. A quantitative analysis indicated slightly defects in spore size in both mutant strains (Fig. 4C).

Next, we determined if the spores from *arl* mutant strains germinated properly under aerobic conditions. The hyphae from germinated spores of the mutant strains showed morphologies similar to the wild-type strain (Fig. 5A), reaching in all the strains 100% germination after 6 h of growth under aerobic conditions (Fig. 5B). However, shorter hyphae, and fewer hyphae per mother cell were observed in $\Delta arl1^{(+)(-)}$ with respect to the other strains (Fig. 5C and D). In addition, while radial growth rate was reduced (< 20%) in $\Delta arl1^{(+)(-)}$ (Fig. S4A), no reduction in biomass was observed for any of the *arl* mutants when aerobically grown in YPG liquid medium (Fig. S4B).

Under anaerobic conditions, no differences in morphology could be observed between the strains, although $\Delta arl1^{(+)(-)}$ and *Δarl2* germinated faster compared to *Δarl2* + *arl2wt* or the wild-type strains (Fig. 6). Nevertheless, the faster germination rate did not contribute to increased biomass generation after 24 h of growth (Fig. 6).

3.5. Role of Arl1 and Arl2 in vesicle trafficking and cell wall composition

In an effort to describe the possible roles of the products from *arl1* and *arl2* genes in vesicle trafficking from *M. circinelloides*, we performed FM4-64 staining of aerobic germinated spores. This approach has been used to observe the vesicle distribution of other *Mucorales spp.* such as *Phycomyces blakesleeanus*, where the vesicles showed an apical distribution (Fisher-Parton et al., 2001).

Confocal microscopy revealed that FM4-64 staining of *Δarl2* + *arl2wt* and wild-type strain showed a zone of bright fluorescence in a region that corresponds to the expected location of apical vesicles (Fig. 7A), as reported previously in *Phycomyces*. For both

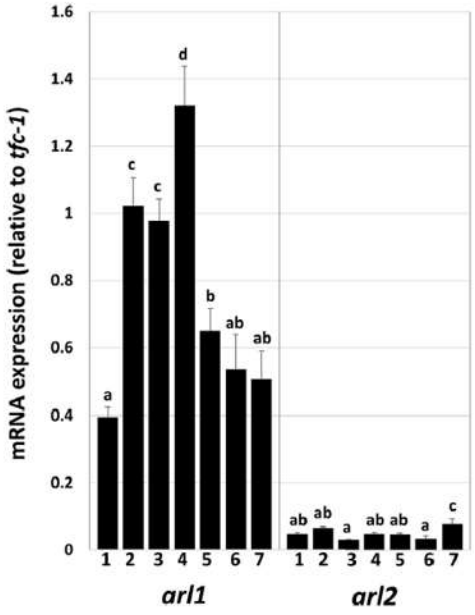

Fig. 2. *arl1* and *arl2* mRNA expression patterns in *M. circinelloides* during spore or vegetative growth. Transcript levels of *arl1* and *arl2* genes were measured during *M. circinelloides* dimorphism by RT-qPCR. Morphological stages are numbered as follows: 1, spores; 2, 3, 4, aerobic growth (at 6, 12, and 24 h, respectively); and 5, 6, 7, self-anaerobic growth (at 6, 12, and 24 h, respectively). Transcript levels are relative to *tfc-1* gene expression. Three independent experiments were carried out, the average is shown, bars correspond to standard error. Statistically significant differences (shown by letters) were determined by Student's t–test ($p < 0.05$).

$\Delta arl1^{(+)(-)}$ and $\Delta arl2$ strains, a total disruption of the wild-type pattern was observed with a loss of the bright FM4-64 staining at the apical region and a more disperse distribution of the staining within the hyphae (Fig. 7A).

In order to described the deposition of polymers, like chitin, in the cell wall. We performed the quantification of glucosamine from cell walls from *arl*-mutants mycelium of *M. circinelloides*. Significantly lower glucosamine content (μg) in the fungal cell walls was found for the $\Delta arl1^{(+)(-)}$ (43% average reduction) and $\Delta arl2$ (23% average reduction) mutant strains in comparison to the already determined $\Delta arl2$ + *arl2wt* or the wild-type strains (Fig. 7B). These results showed impaired intracellular vesicle distribution in both *arl* mutant strains, which could contribute in reduced chitin content in their cell wall.

3.6. Very low expression of arl1 increases M. circinelloides virulence

Many molecules involved in fungal virulence are secreted; then, in order to reach the exterior, they have to be enclosed into vesicles. Therefore, we investigated if $\Delta arl1^{(+)(-)}$ and $\Delta arl2$ were different compared to the wild-type in terms of virulence rates. A virulence assay was performed utilizing the nematode *C. elegans*, in which the worms were seeded in the presence of either spores or cell-free supernatants of cultures from previously grown strains. The spores from strain $\Delta arl1^{(+)(-)}$ were more virulent than those from $\Delta arl2$, $\Delta arl2$ + *arl2wt*, and the wild-type strain, which were almost non-virulent in our experiments (Fig. 8A). Importantly, the cell-free supernatant from the culture medium obtained from the $\Delta arl1^{(+)(-)}$ after 24 h of growth reproduced the lethality of *C. elegans* observed with spores (Fig. 8B), whereas those obtained from $\Delta arl2$, $\Delta arl2$ + *arl2*wt or the wild-type strain were non-virulent.

Previously, we demonstrated that $\Delta arf1$ and $\Delta arf3$ strains from *M. circinelloides* were involved in the secretion of proteins that increased virulence rate (Patiño-Medina et al., 2018). Protease treatment of cell-free medium obtained from $\Delta arl1^{(+)(-)}$ cultures grown for 24 h, caused inactivation of the killing factor secreted in the cell-free medium, indicating the proteinaceous nature of the secreted virulent factor (Fig. 8C). It should be noted that the total amount of protein in the cell-free medium was similar in all strains (Fig. S5). These results suggested that the low *arl1* expression led to virulence increased could be associated with the secretion of one or several specific proteins.

3.7. Susceptibility of M. circinelloides arl1 and arl2 mutants to antifungal compounds

Cell wall and plasma membrane inhibitors are widely used as antifungal drugs, but *M. circinelloide*s exhibits an intrinsic tolerance to them (Salas et al., 2012). Given that an adequate flux of vesicles to the apical region of the hyphae is critical for the biogenesis of new cell structures, such as the cell wall and plasma membrane (Gow et al., 2017). We analyzed the susceptibility of $\Delta arl1^{(+)(-)}$ and $\Delta arl2$ to different antifungal compounds. Radial growth indicated that $\Delta arl1^{(+)(-)}$ was more sensitive to fluconazol or itraconazole with respect to the wild-type strain (Fig. S6). $\Delta arl2$ was generally as tolerant as $\Delta arl2$ + *arl2wt* or the wild-type strain to all compounds. The detergent SDS has been used to observe defects in the fungal cell wall and plasma membrane (Lettner et al., 2010). The higher sensitivity of $\Delta arl1^{(+)(-)}$ to antifungal compounds was observed under aerobic atmosphere in liquid medium, where this strain displayed reduced germination rate (Figs. S7 and S8) and hyphae length (Figs. S7 and S8), as well as defects in hyphal morphology (Figs. S7 and S8). For example, $\Delta arl1^{(+)(-)}$ strain grown in presence of fluconazole, itraconazole or SDS showed 69, 81 or 50% of reduction in the hyphae length, respectively, compared to the wild-type (Figs. S7 and S8). Also, the $\Delta arl2$ mutant showed reduction in hyphae length in lesser extent than $\Delta arl1^{(+)(-)}$. MIC_{50} data revealed a more exacerbated susceptibility of $\Delta arl1^{(+)(-)}$ aerobically grown in liquid media, in presence of itraconazole, a 64.2% less germination rate compared to the wild-type strain was observed, while the $\Delta arl2$ only showed 38.6% less germination (Table 1). In general, similar hyphae length was observed between $\Delta arl2$ + *arl2wt* and the wild type strain (Figs. S7 and S8).

Taken together, these data indicated that the Arl1 protein plays an important function in maintaining intrinsic resistance to the antifungal compounds tested, whereas Arl2 has only a minor role.

4. Discussion

M. circinelloides is an important basal fungus, with multiple and relevant implications in understanding cell differentiation, lipid metabolism, gene regulation silencing, and mucormycosis (Morin-Sardin et al., 2017). Therefore, we have chosen this fungus to study the function of Arf members in early-divergent fungi. All Arf members, Arf, Sar, and Arl, are involved in vesicle biogenesis and vesicle trafficking, one of the most important ways of transporting molecules into eukaryotic cells (Kahn, 2006). In a previous study, we demonstrated Arf member proteins are implicated in the regulation of morphogenesis and virulence in this *Mucor* species (Patiño-Medina et al., 2018). Following up that work, two additional members of the Arf family have been studied: Arl1 and Arl2.

The *arl1* is highly expressed during aerobic growth compared to *arl2* in the wild-type strain, which strongly suggests an important function during these morphological stages. The targeted deletion of *arl1* led to a heterokaryon strain, confirming the essential role of *arl1* in *M. circinelloides*. Arl1 homologues seem to be essential in other organisms such as *Drosophila melanogaster*, where the *ARL1* mutation led to a zygotic lethality (Tamkun et al., 1991).

Low expression of *M. circinelloides arl1* in a heterokaryon mutant led

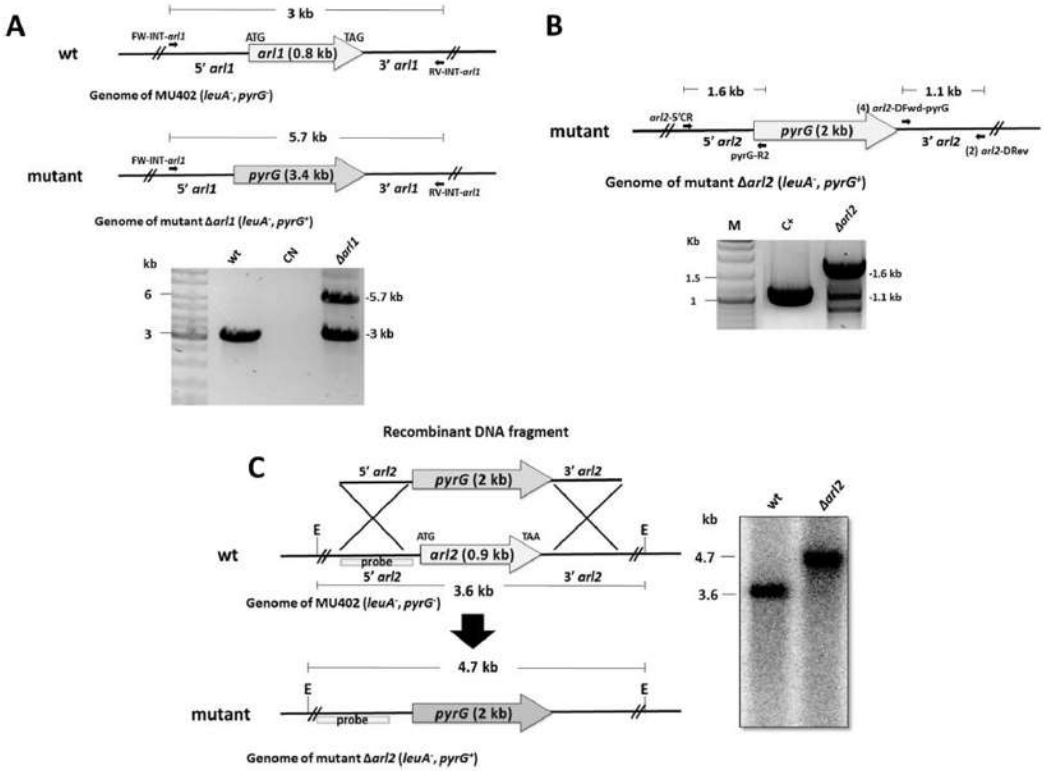

Fig. 3. Deletion of *arl* genes in *M. circinelloides*. The 5′ and 3′ *arl* regions upstream and downstream of the start and stop codons, respectively, were used to flank the *pyrG* selection marker. This diagram shows the recombinantion processes hat was used to transform protoplasts of strain MU402 (*leuA*⁻, *pyrG*⁻). The position of relevant primers and expected fragments after PCR or digestion are also displayed. (A) Molecular confirmation through PCR using primers FW-INT-*arl1* and RV-INT-*arl1* was used to show the recombination event in corresponding *arl1*, and (B) *arl2* mutations. CN and C + stand for the negative control (water) and wild-type strain, respectively. (C) Southern blotting was performed using specific probes for the *arl2* gene showed specific recombination in the corresponding *arl2* locus. Genomic DNA samples from transformed and parental (MU402) strains were digested with *Eco*RI.

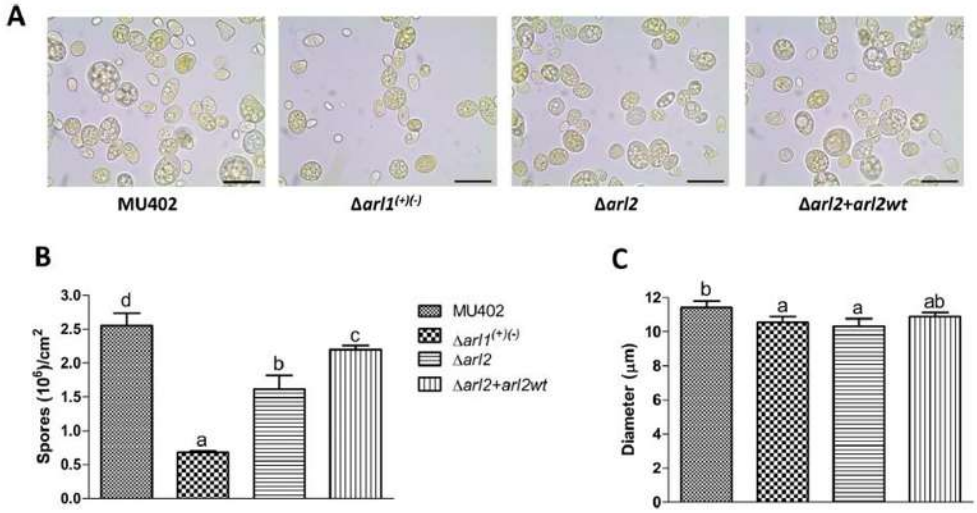

Fig. 4. Spore production in *arl* mutants from *M. circinelloides*. Spore production was evaluated in different strains; spores were grown on YPG solid medium for 5 days in the presence of light, then collected and quantified. (A) Spores observed by light microscope with 100 × magnification, bar = 20 μm. (B) Spore counts. (C) Spore size. Three independent experiments were conducted. Statistically significant differences ($p \leq 0.05$) are indicated by letters, Student's t–test ($p < 0.05$).

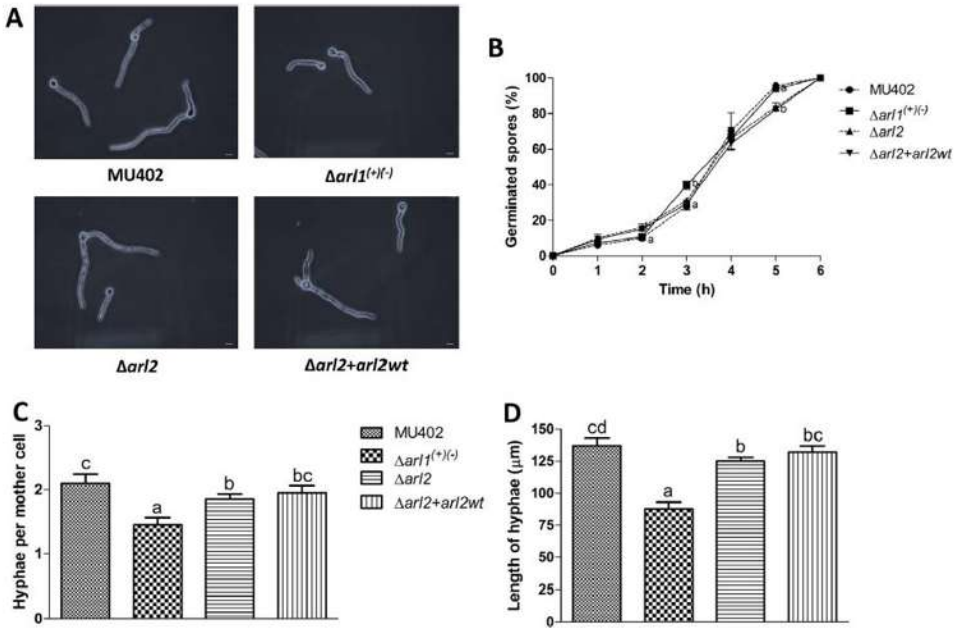

Fig. 5. Effect of *arl1* and *arl2* mutations on *M. circinelloides* germination under aerobic growth. Spores from different strains of *M. circinelloides* were grown in YPG liquid medium for the indicated times. (A) Mycelial morphology observed under a light microscope with 40 × magnification (bar = 20 μm) after 6 h of growth. (B) Percentage of germinated spores at the respective times. (C) Number of hyphae per mother cell after 6 h of growth. (D) Length of each hypha after 6 h of growth. Three independent experiments were conducted. Statistically significant differences (shown by letters) were determined by Student's t–test ($p < 0.05$).

to multiple defects during aerobic growth, of which spore production was the most affected. Deletion of *arl2* also affected spore production, but to a lower extent. In addition, other genes have been described to influence spore production in *M. circinelloides*. One of them is *Mcwc-1b*, which encodes a White Collar-1-like receptor that regulates carotenogenesis and sporulation; another is *pkaR1*, whose dysfunction leads to reduced spore production (Ocampo et al., 2009; Navarro et al., 2013). Other Arf proteins from *M. circinelloides* play important positive

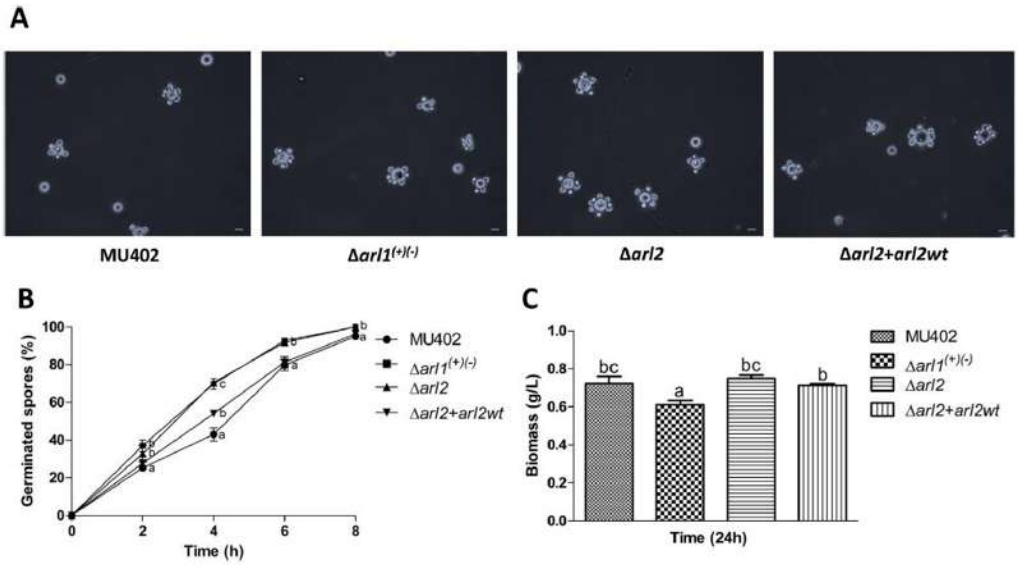

Fig. 6. Effect of *arl1* and *arl2* mutations in *M. circinelloides* on germination under anaerobic growth. Spores from different strains of *M. circinelloides* were grown in YPG liquid medium for the indicated times. (A) Yeast morphology observed under a light microscope with 40 × magnification (bar = 20 μm) after 6 h of growth. (B) Number of germinated spores at the respective times. (C) Biomass generated after 24 h of growth. Statistically significant differences (shown by letters) were determined by Student's t–test ($p < 0.05$).

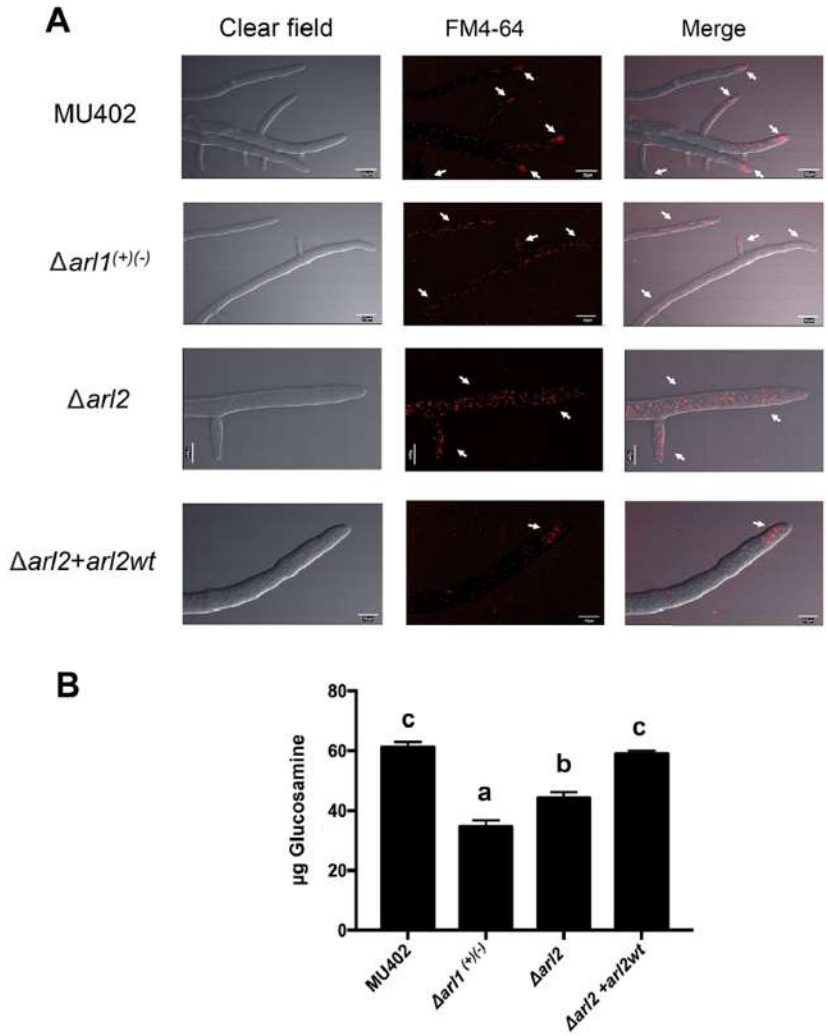

Fig. 7. *arl1* and *arl2* genes regulate vesicle trafficking and chitin content in the cell wall in *M. circinelloides*. (A) FM4-64 staining in *arl* mutants in *M. circinelloides*. MU402, $\Delta arl1^{(+)(-)}$, $\Delta arl2$, $\Delta arl2$ + *arl2wt* strains were stained with FM4-64. Making use of the "inverted agar block method" (Hickey et al., 2002), strains were incubated with five mM FM4-64 to stain mature endosomes or vacuoles. Confocal microscopy showed distinct FM4-64 staining distribution patterns among $\Delta arl1^{(+)(-)}$ and $\Delta arl2$; compared to wild-type and $\Delta arl2$ + *arl2wt* strains. White arrowheads depict staining of endosomes. NA 1.42 with oil. Bars = 10 µm for $\Delta arl2$ and $\Delta arl2$ + *arl2wt*, or 20 µm for MU402 and $\Delta arl1^{(+)(-)}$. (B) Glucosamine content determination in fungal cell walls. Spores from different strains were inoculated (5×10^5 mL^{-1}) into liquid YPG media for 10 h under constant shaking. Cells were prepared as previously described. Then glucosamine content (µg) was determined by High-Performance Anion-Exchange Chromatography coupled to Pulsed Amperometric Detection (HPAEC-PAD). Three independent experiments were conducted. Statistically significant differences ($p \leq 0.05$) are indicated by letters, Student's t–test ($p < 0.05$).

roles in the spore production process, like Arf1, which mutation reduced at nearly 90% the spore production (Patiño-Medina et al., 2018). Understanding how interactions among all of these genes regulate sporulation will require generation of strains with mutations in several genes. Mutant strains $\Delta arl1^{(+)(-)}$ and $\Delta arl2$ increased germination under anaerobic conditions, which was previously observed in the *arf* mutant strains (Patiño-Medina et al., 2018). Yeast morphology in *M. circinelloides* correlates with fermentative metabolism (McIntyre et al., 2002; Lübbehüsen et al., 2003a, 2003b), suggesting a possible increase in the fermentative metabolism of all *arf* and *arl* mutant strains.

M. circinelloides has been reported as a human opportunistic pathogen. Certain fungal virulence factors such as hydrolases (e.g., proteases and hyaluronidases) need to reach the extracellular space (Casadevall et al., 2009). Exocytosis of these molecules could involve active transport through vesicles. Arl1 homologues participate in secretion processes; for example, ARL1 from *S. cerevisiae* localizes with vesicles in the Golgi apparatus and is involved in yeast protein secretion, whereas Arl1 from *C. albicans* is localized in the late-Golgi apparatus (Rosenwald et al., 2002, Labbaoui et al., 2017). ARL1 in mammalian cells is also localized in the Golgi apparatus, where it participates in the exocytic pathway (Lowe et al., 1996; Lu et al., 2001).

Some Arf members and their regulators are involved in virulence. In *C. albicans, Age3* encodes an ARF-GAP protein (allosteric effector responsible for activating the GTPase of ARF proteins) that is required for hyphal growth and its mutation led to a decreased in virulence (Epp et al., 2010; Lettner et al., 2010). In addition, the *arl1* mutant strain in *C. albicans* has been characterized as being less virulent (Labbaoui et al., 2017).

Here, we show that spores from the heterokaryon $\Delta arl1^{(+)(-)}$ are more virulent against a nematode model than those of the parental strain. The proteinaceous killing factor was present in the cell-free medium, possibly suggesting that it was secreted or released to the cell exterior by the $\Delta arl1^{(+)(-)}$ strain. Similar results were observed in $\Delta arf1$ and $\Delta arf3$ strains, where both spores or their cell-free grown medium led to more lethality in mice or nematodes, respectively (Patiño-Medina et al., 2018). Overall, total protein in the cell-free medium was similar in $\Delta arf1$, $\Delta arf3$, $\Delta arl1^{(+)(-)}$ and wild-type strain, suggesting that the absence of these genes triggers over-secretion of proteins contributing to virulence. Interestingly, *M. circinelloides* is able to induce the dead of immune cells in zebra fish infections (López-Muñoz et al., 2018), suggesting that wild-type strains could regulate the secretion of virulence factors during the infection process. Accordingly,

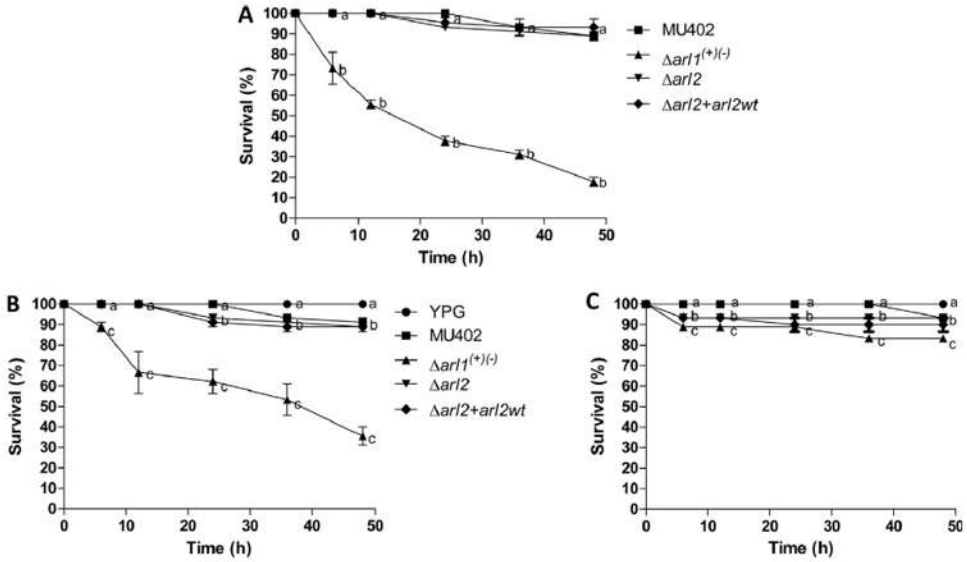

Fig. 8. Effect of *arl1 and arl2* genes from *M. circinelloides* on the viability of *C. elegans*. Twenty adult *C. elegans* worms were inoculated with (A) 10,000 spores; (B) 1 mL of cell-free medium obtained from the different *M. circinelloides* strains grown in YPG for 24 h; (C) mycelium cell-free culture filtrates treated with proteases for 2 h. Three independent experiments were conducted. Statistically significant differences (shown by letters) were determined by Student's t–test ($p < 0.05$).

Table 1
Fluconazole, Itraconazole or SDS were added to solid[A] or liquid media [B], respectively. MIC_{50}: Half radial growth for [A] of half germination rate for [B] doses and their corresponding 95% confidence intervals were calculated employing Nonlinear regression (curve fit), log (inhibitor/inductor) vs response (variable slope), $R^2 = 0.95$ for [A]; 0.99 for [B]. (GraphPrism 7.0). Parenthesis stand for ± . MIC_{50} for solid and liquid growths were evaluated at the end of day 5 and 6 h respectively.

Viability MIC_{50} (μg/mL)				
Substance	Strain			
	MU402	*Δarl1*$^{(+)(-)}$	*Δarl2*	*Δarl2 + arl2wt*
Fluconazole[A]	480.20 (11.34)	390.43 (2.43)	477.53 (9.26)	474.79 (23.27)
Itraconazole[A]	441.25 (2.76)	273.76 (33.14)	399.47 (75.75)	418.60 (49.73)
SDS[A]	72.52 (0.22)	67.77 (0.77)	72.98 (1.03)	73.10 (0.93)
Fluconazole[B]	302.12 (4.99)	261.45 (15.11)	285.44 (11.37)	298.57 (7.08)
Itraconazole[B]	22.64 (2.40)	8.09 (1.79)	13.89 (0.84)	16.41 (3.49)
SDS[B]	29.48 (4.41)	17.67 (2.41)	32.63 (8.86)	32.62 (6.27)

future work will focus on identifying the virulent proteins secreted by *Δarf1*, *Δarf3*, or *Δarl1*$^{(+)(-)}$ mutant strains during mycelial growth of *M. circinelloides*.

Arf proteins are also involved in antifungal susceptibility. In *C. albicans*, dysfunction of a GAP protein, AGE3, has led to increased sensitivity to the plasma membrane or cell wall synthesis inhibitors (Epp et al., 2010). Thus, imbalance in the activated state of some Arf members could be due to the role of Arf proteins in vesicle formation and/or transport of specialized vesicles such as chitosomes, which enclose chitin synthase (Bracker et al., 1976). Moreover, some proteins in the plasma membrane play critical roles in resistance to antifungal drugs, such as the efflux pumps of the ABC transporter and major facilitator superfamilies, iron uptake ferroxidase, and an iron permease (Morschhäuser, 2010; Kim et al., 2012). These proteins could reach their cellular location via vesicular transport. Here, we provide evidence that links *arl1* and *arl2* genes to vesicle trafficking in this fungus. When these two genes were disrupted, endosome staining was more diffuse compared to that in wild-type or *Δarl2 + arl2wt* strains. Similarly, it has been reported previously that disruption of fungal Arf proteins led to aberrant endosome staining at the hyphal apical region, and endosome distribution was more diffuse and less well-localized (Lee et al., 2008). These results suggest that imbalances in vesicle trafficking in *Δarl1*$^{(+)(-)}$ strain might lead to higher sensitivity to SDS and azoles, compared to *Δarf2* strain. Despite this, both *arl*-mutant strains showed differences in intracellular endosome staining patterns when compared to the wild-type strain. These observations suggest that different populations of endosomes could be regulated by Arl1 or Arl2 in *M. circinelloides*.

The cell wall and plasma membrane are the main targets of antifungal drugs but few such drugs with reduced efficacy (amphotericin B and posaconazole) are available to treat mucormycosis (Pagano et al., 2013; Mazu et al., 2016). Moreover, *M. circinelloides* is intrinsically resistant to fluconazole and itraconazole (Almyroudis et al., 2007; Alastruey-Izquierdo et al., 2009). Recently, it has been reported that this intrinsic fluconazole resistance in Mucormycetes is due to a discrete change in the mitochondrial P450 homologue, lanosterol 14α-demethylase (Caramalho et al., 2017). Therefore, it is important to find new molecular targets for antimycotic drugs that could generate better treatments for mucormycosis or other fungal infections. Here, the *Δarl1*$^{(+)(-)}$ mutant strain was more sensitive to compounds that are known to interfere with the plasma membrane and cell wall synthesis, such as SDS, fluconazole, and itraconazole, suggesting that these cellular structures could be abnormal in this heterokaryon strain. Accordingly, cell glucosamine content in the cell wall of the *Δarl1*$^{(+)(-)}$ was significantly lower (43%) than that in the wild-type strain. All these results showed that *arl1* disruption displays aberrant vesicle trafficking, that could lead to depletion of cell wall chitin deposition, which finally might explain the hypersensibility deployed to antifungal compounds in this mutant. The results from this work open the way for future studies relating to Arl1-mediated virulence regulation and antifungal control.

All the defects showed by *arl1* could be consequence of an impaired vesicle transport, like the lower aerobic growth, spore production,

chitin content in the cell wall from hyphae cells, additionally this mutation increased the susceptibility to antifungal compounds, and promote the secretion of proteins that function as virulence factors. Moreover, the defects observed in the Δ*arl2* could be attributed to the decreased in the mRNA of *arl1*, almost all the defects in the phenotypes in Δ*arl2* are similar to those observed in the $\Delta arl1^{(+)(-)}$ but in lesser extend.

5. Conclusions

We found that the *M. circinelloides* genome encodes two Arl proteins, Arl1 and Arl2. Our data suggested that Arl1 plays a major role in this fungus during mycelial growth. A low expression level of *arl1* resulted in defects during aerobic growth, enhanced virulence, sensitivity to the cell wall, and plasma membrane synthesis inhibitors. Both genes regulate in *M. circinelloides* vesicle trafficking and cell wall composition. Future identification of the protein(s) responsible for increased virulence in the *arl1* heterokaryon, and elucidation of the pathway of transport will expand our knowledge of vesicle trafficking in *M. circinelloides* and facilitate the discovery of suitable targets to generate novel antifungals against Mucorales.

6. Submission declaration and verification

This manuscript has not been previously published or submitted to another agency for publication.

Role of the funding source

This work was by funded by grants from Coordinación de la Investigación Científica-UMSNH, IDCA-PRODEP, Consejo Nacional de Ciencia y Tecnología, and Fundación Séneca-Agencia de Ciencia y Tecnología de la Región de Murcia, Spain (19339/PI/14). CP-A was supported by the Ministerio de Educación, Cultura y Deporte of Spain (FPU-14/01832). "Grant funding sources were not involved directly with this study."

Author contributions

JA P-M, MI V-M, GM-H, C P-A, IE J-G, C D-P, AL D-P, CA A-C, JC V-C contributed to data acquisition, analysis, and data interpretation; JC V-C, J C-G, MI R-D, and VG contributed to critical analysis, data interpretation, and critical revision of the article for intellectual content of manuscript; VG and V M-C contributed to conception and design of the work, data analysis, and interpretation; V M-C wrote the majority of the article with minor contributions from the other authors.

Conflict of interest

None.

Acknowledgments

We want to thank Dr. Diego Delgado-Alvarez from Experimental Microbiology, CICESE, Ensenada, Baja California, Mexico for assistance in the confocal microscopy assay.

Funding

This work was supported by grants from Coordinación de la Investigación Científica (UMSNH; 2.6, 2.35), IDCA-PRODEP (9305), Consejo Nacional de Ciencia y Tecnología (CONACYT; 181747, 167071), and Fundación Séneca-Agencia de Ciencia y Tecnología de la Región de Murcia, Spain (19339/PI/14). JAP-M, GM-H, and MIV-M were supported by postgraduate fellowships from CONACYT and CP-A by Ministerio de Educación, Cultura y Deporte of Spain (FPU-14/01832).

Appendix A. Supplementary material

Supplementary data to this article can be found online at https://doi.org/10.1016/j.fgb.2019.04.011.

References

Alastruey-Izquierdo, A., Castelli, M.V., Cuesta, I., Zaragoza, O., Monzón, A., Mellado, E., Rodríguez-Tudela, J.L., 2009. In vitro activity of antifungals against zygomycetes. Clin. Microbiol. Infect. 15, 71–76.
Almyroudis, N.G., Sutton, D.A., Fothergill, A.W., Rinaldi, M.G., Kusne, S., 2007. In vitro susceptibilities of 217 clinical isolates of zygomycetes to conventional and new antifungal agents. Antimicrob. Agents Chemother. 51, 2587–2590.
Benito, E.P., Campuzano, V., López-Matas, M.A., De Vicente, J.I., Eslava, A.P., 1995. Isolation, characterization and transformation, by autonomous replication, of *Mucor circinelloides* OMPdecase-deficient mutants. Mol. Gen. Genet. 248, 126–135.
Bhamidipati, A., Lewis, S.A., Cowan, N.J., 2000. ADP ribosylation factor-like protein 2 (Arl2) regulates the interaction of tubulin-folding cofactor D with nativetubulin. J. Cell. Biol. 149, 1087–1096.
Bracker, C.E., Ruiz-Herrera, J., Bartnicki-Garcia, S., 1976. Structure and transformation of chitin synthetase particles (chitosomes) during microfibril synthesis in vitro. Proc. Natl. Acad. Sci. U. S. A. 73, 4570–4574.
Brenner, S., 1974. The genetics of *Caenorhabditis elegans*. Genetics 77, 71–94.
Burd, C.G., Strochlic, T.I., Setty, S.R., 2004. Arf-like GTPases: not so Arf-like after all. Trends. Cell Biol. 14, 687–694.
Caramalho, R., Tyndall, J.D.A., Monk, B.C., Larentis, T., Lass-Flörl, C., Lackner, M., 2017. Intrinsic short-tailed 1 azole resistance in mucormycetes is due to an evolutionary conserved aminoacid substitution of the lanosterol 14α-demethylase. Sci. Rep. 7, 15898.
Casadevall, A., Nosanchuk, J.D., Williamson, P., Rodrigues, M.L., 2009. Vesicular transport across the fungal cell wall. Trends Microbiol. 17, 158–162.
Dereeper, A., Guignon, V., Blanc, G., Audic, S., Buffet, S., Chevenet, F., Dufayard, J.F., Guindon, S., Lefort, V., Lescot, M., Claverie, J.M., Gascuel, O., 2008. Nucl. Acids Res. 1 (36(Web Server issue)), W465–9.
Epp, E., Vanier, G., Harcus, D., Lee, A.Y., Jansen, G., Hallett, M., Sheppard, D.C., Thomas, D.Y., Munro, C.A., Mullick, A., Whiteway, M., 2010. Reverse genetics in *Candida albicans* predicts ARF cycling is essential for drug resistance and virulence. PLoS Pathog. 6, e1000753.
Fisher-Parton, S., Parton, R.M., Hickey, P.C., Dijksterhuis, J., Atkinson, H.A., Read, N.D., 2001. Confocal microscopy of FM4-64 as a tool for analysing endocytosis and vesicle trafficking in living fungal hyphae. J. Microsc. 198, 246–259.
Garcia, A., Adedoyin, G., Heitman, J., Lee, S.C., 2017. Construction of a recyclable genetic marker and serial gene deletions in the human pathogenic mucorales Mucor circinelloides. G3 (Bethesda) 7, 2047–2054.
Gillingham, A.K., Munro, S., 2007. The small G proteins of the Arf family and their regulators. Annu. Rev. Cell. Dev. Biol. 23, 579–611.
Gow, N.A.R., Latge, J.P., Munro, C.A., 2017. The fungal cell wall: structure, biosynthesis, and function. Microbiol Spectr. 5 (3).
Gutiérrez, A., López-García, S., Garre, V., 2011. High reliability transformation of the basal fungus *Mucor circinelloides* by electroporation. J. Microbiol. Methods 84, 442–446.
Hickey, P.C., Jacobson, D.J., Read, N.D., Glass, N.L., 2002. Live-cell imaging of vegetative hyphal fusion in *Neurospora crassa*. Fungal Genet. Biol. 37, 109–119.
Huang, C.F., Buu, L.M., Yu, W.L., Lee, F.J., 1999. Characterization of a novel ADP-ribosylation factor-like protein (yARL3) in *Saccharomyces cerevisiae*. J. Biol. Chem. 6, 3819–3827.
Kahn, R.A., Gilman, A.G., 1984. Purification of a protein cofactor required for ADP-ribosylation of the stimulatory regulatory component of adenylate cyclase by cholera toxin. J. Biol. Chem. 10, 6228–6234.
Kahn, R.A., Cherfils, J., Elias, M., Lovering, R.C., Munro, S., Schurmann, A., 2006. Nomenclature for the human Arf family of GTP-binding proteins: ARF, ARL, and SAR proteins. J. Cell Biol. 5, 645–650.
Kim, J., Cho, Y.J., Do, E., Choi, J., Hu, G., Cadieux, B., Chun, J., Lee, Y., Kronstad, J.W., Jung, W.H., 2012. A defect in iron uptake enhances the susceptibility of *Cryptococcus neoformans* to azole antifungal drugs. Fungal Genet. Biol. 49, 955–966.
Labbaoui, H., Bogliolo, S., Ghugtyal, V., Solis, N.V., Filler, S.G., Arkowitz, R.A., Bassilana, M., 2017. Role of ArfGTPases in fungal morphogenesis and virulence. PLoS Pathog. 13, e1006205.
Lee, S.C., Li, A., Calo, S., Heitman, J., 2013. Calcineurin plays key roles in the dimorphic transition and virulence of the human pathogenic zygomycete *Mucor circinelloides*. PLoS Pathogen. 9, e1003625.
Lee, S.C., Schmidtke, S.N., Dangott, L.J., Shaw, B.D., 2008. *Aspergillus nidulans* ArfB plays a role in endocytosis and polarized growth. Eukaryot Cell. 7, 1278–1288.
Lettner, T., Zeidler, U., Gimona, M., Hauser, M., Breitenbach, M., Bito, A., 2010. *Candida albicans*AGE3, the ortholog of the *S. cerevisiae* ARF-GAP13 encoding gene GCS1, is required for hyphal growth and drug resistance. PLoS One 5, e11993.
Lewis, R.E., Kontoyiannis, D.P., 2013. Epidemiology and treatment of mucormycosis. Future Microbiol. 8, 1163–1175.
López-Muñoz, A., Nicolás, F.E., García-Moreno, D., Pérez-Oliva, A.B., Navarro-Mendoza, M.I., Hernández-Oñate, M.A., Herrera-Estrella, A., Torres-Martínez, S., Ruiz-Vázquez, R.M., Garre, V., Mulero, V., 2018. An Adult Zebrafish model reveals that

mucormycosis induces apoptosis of infected macrophages. Sci Rep. 8, 12802.
Lowe, S.L., Wong, S.H., Hong, W., 1996. The mammalian ARF-like protein 1 (Arl1) is associated with the Golgi complex. J. Cell Sci. 109, 209–220.
Lu, L., Horstmann, H., Ng, C., Hong, W., 2001. Regulation of Golgi structure and function by ARF-like protein 1 (Arl1). J. Cell Sci. 114, 4543–4555.
Lübbehüsen, T.L., Nielsen, J., McIntyre, M., 2003a. Characterization of the *Mucor circinelloides* life cycle by on-line image analysis. J. App. Microbiol. 95, 1152–1160.
Lübbehüsen, T.L., Nielsen, J., McIntyre, M., 2003b. Morphology and physiology of the dimorphic fungus *Mucor circinelloides* (*syn. M. racemosus*) during anaerobic growth. Mycol Res. 107, 223–230.
Martínez-Álvarez, J.A., Pérez-García, L.A., Mellado-Mojica, E., López, M.G., Martínez-Duncker, I., López-Bezerra, L.M., Mora-Montes, H.M., 2017. *Sporothrix schenckii sensu stricto* and *Sporothrix brasiliensis* Are Differentially Recognized by Human Peripheral Blood Mononuclear Cells. Front. Microbiol. 8, 1–15.
Mazu, T.K., Bricker, B.A., Flores-Rlozas, H., Ablordeppey, S.Y., 2016. The mechanistic targets of antifungal agents: an overview. Mini Rev. Med. Chem. 16, 555–578.
McIntyre, M., Breum, J., Arnau, J., Nielsen, J., 2002. Growth physiology and dimorphism of *Mucor circinelloides*(*syn. racemosus*) during submerged batch cultivation. Appl. Microbiol. Biotechnol. 58, 495–502.
Mizuno-Yamasaki, E., Rivera-Molina, F., Novick, P., 2012. GTPase networks in membrane traffic. Annu. Rev. Biochem. 81, 637–659.
Morin-Sardin, S., Nodet, P., Coton, E., Jany, J.L., 2017. *Mucor*: A Janus faced fungal genus with human health impact and industrial applications. Fungal Biol. Rev. 31, 2–32.
Morschhäuser, J., 2010. Regulation of multidrug resistance in pathogenic fungi. Fungal Genet. Biol. 47, 94–106.
Moss, J., Vaughan, M., 1998. Molecules in the ARF orbit. J. Biol. Chem. 273, 21431–21434.
Navarro, E., Peñaranda, A., Hansberg, W., Torres-Martínez, S., Garre, V., 2013. A white collar 1-like protein mediates opposite regulatory functions in *Mucor circinelloides*. Fungal Genet. Biol. 52, 42–52.
Nicolás, F.E., De Haro, J.P., Torres-Martínez, S., Ruiz-Vázquez, R.M., 2007. Mutants defective in a *Mucor circinelloides* dicer-like gene are not compromised in siRNA silencing but display developmental defects. Fungal Genet. Biol. 44, 504–516.
Ocampo, J., Fernandez-Nuñez, L., Silva, F., Pereyra, E., Moreno, S., Garre, V., Rossi, S., 2009. A subunit of protein kinase A regulates growth and differentiation in the fungus *Mucor circinelloides*. Eukaryot. Cell. 8, 933–944.
Pagano, L., Cornely, O.A., Busca, A., Caira, M., Cesaro, S., Gasbarrino, C., Girmenia, C., Heinz, W.J., Herbrecht, R., Lass-Flörl, C., Nosari, A., Potenza, L., Racil, Z., Rickerts, V., Sheppard, D.C., Simon, A., Ullmann, A.J., Valentini, C.G., Vehreschild, J.J., Candoni, A., Vehreschild, M.J., 2013. Combined antifungal approach for the treatment of invasive mucormycosis in patients with hematologic diseases: a report from the SEIFEM and FUNGISCOPE registries. Haematologica 98, e127–30.
Patiño-Medina, J.A., Maldonado-Herrera, G., Pérez-Arques, C., Alejandre-Castañeda, V., Reyes-Mares, N.Y., Valle-Maldonado, M.I., Campos-García, J., Ortiz-Alvarado, R., Jácome-Galarza, I.E., Ramírez-Díaz, M.I., Garre, V., Meza-Carmen, V., 2018. Control of morphology and virulence by ADP-ribosylation factors (Arf) in *Mucor circinelloides*. Curr. Genet. 4, 853–869.
Pfaffl, M.W., 2001. A new mathematical model for relative quantification in real-time RT-PCR. Nucl. Acids Res. 29, 2000–2007.
Roden, M.M., Zaoutis, T.E., Buchanan, W.L., Knudsen, T.A., Sarkisova, T.A., Schaufele, R.L., Sein, M., Sein, T., Chiou, C.C., Chu, J.H., Kontoyiannis, D.P., Walsh, T.J., 2005. Epidemiology and outcome of zygomycosis: a review of 929 reported cases. Clin. Infect. Dis. 41, 634–653.
Rogers, T.R., 2008. Treatment of zygomycosis: current and new options. J. Antimicrob. Chemother. 1, 35–40.
Roncero, M.I., 1984. Enrichment method 1 for the isolation of auxotrophic mutants of *Mucor* using the polyene antibiotic N-glycosylpolyfungin. Carlsberg Res. Commun. 49, 685–690.
Rosenwald, A.G., Rhodes, M.A., Van Valkenburgh, H., Palanivel, V., Chapman, G., Boman, A., Zhang, C.J., Kahn, R.A., 2002. ARL1 and membrane traffic in *Saccharomyces cerevisiae*. Yeast 12, 1039–1056.
Salas, V., Pastor, F.J., Calvo, E., Alvarez, E., Sutton, D.A., Mayayo, E., Fothergill, A.W., Rinaldi, M.G., Guarro, J., 2012. In vitro and in vivo activities of posaconazole and amphotericin B in a murine invasive infection by *Mucor circinelloides*: poor efficacy of posaconazole. Antimicrob. Agents Chemother. 56 2246-2245.
Sambrook, J., Russell, R.W., 2001. Molecular Cloning: A Laboratory Manual, 3rd 15 ed. Cold spring harbor laboratory press, Cold Spring Harbor, N.Y.
Stiernagle, T., 2006. Maintenance of C. elegans. WormBook.ed. The C. elegans Research Community.
Setty, S.R., Shin, M.E., Yoshino, A., Marks, M.S., Burd, C.G., 2003. Golgi recruitment of GRIP domain proteins by Arf-like GTPase 1 is regulated by Arf-like GTPase 3. Curr. Biol. 13, 401–404.
Tamkun, J.W., Kahn, R.A., Kissinger, M., Brizuela, B.J., Rulka, C., Scott, M.P., Kennison, J.A., 1991. The arf like gene encodes an essential GTP-binding protein in *Drosophila*. Proc. Natl. Acad Sci. U. S. A. 88, 3120–3124.
Thompson, J.D., Higgins, D.G., Gibson, T.J., 1994. CLUSTAL W: improving the sensitivity of progressive multiple sequence alignment through sequence weighting, position-specific gap penalties and weight matrix choice. Nucl. Acids Res. 22, 4673–4680.
Trieu, T.A., Navarro-Mendoza, M.I., Pérez-Arques, C., Sanchis, M., Capilla, J., Navarro-Rodriguez, P., Lopez-Fernandez, L., Torres-Martínez, S., Garre, V., Ruiz-Vázquez, R.M., Nicolás, F.E., 2017. RNAi-based functional genomics identifies new virulence determinants in mucormycosis. PLoS Pathog. 13, e1006150.
Valle-Maldonado, M.I., Jácome-Galarza, I.E., Gutiérrez-Corona, F., Ramírez-Díaz, M.I., Campos-García, J., Meza-Carmen, V., 2015. Selection of reference genes for quantitative real time RT-PCR during dimorphism in the zygomycete *Mucor circinelloides*. Mol. Biol. Rep. 42, 705–711.
Wennerberg, K., Rossman, K.L., Der, C.J., 2005. The Ras superfamily at a glance. J. Cell. Sci. 1, 843–846.
Yang, S., Rosenwald, A.G., 2016. Autophagy in *Saccharomyces cerevisiae* requires the monomeric GTP-binding proteins, Arl1 and Ypt6. Autophagy 12, 1721–1737.

Journal of Microbiology (2019) Vol. 57
DOI 10.1007/s12275-019-8680-z
eISSN 1976-3794
pISSN 1225-8873

Alcohol dehydrogenase 1 participates in the Crabtree effect and connects fermentative and oxidative metabolism in the Zygomycete *Mucor circinelloides*[§]

Rosa Angélica Rangel-Porras[1], Sharel P. Díaz-Pérez[2], Juan Manuel Mendoza-Hernández[1], Pamela Romo-Rodríguez[1], Viridiana Alejandre-Castañeda[2], Marco I Valle-Maldonado[2,3], Juan Carlos Torres-Guzmán[1], Gloria Angélica González-Hernández[1], Jesús Campos-Garcia[2], José Arnau[4], Víctor Meza-Carmen[2], and J. Félix Gutiérrez-Corona[1]*

[1]*Department of Biology, Division of Natural and Exact Sciences, University of Guanajuato, 36050, Guanajuato, Gto., Mexico*
[2]*Institute of Chemical-Biological Research, Universitary City, Michoacán University, 58030, Morelia, Mich., Mexico*
[3]*Michoacán State Public Health Laboratory, 58279 Morelia, Mich., Mexico*
[4]*Department of Fungal Strain Technology, Novozymes A/S Krogshoevej 36, Bagsvaerd, Denmark*

(Received Dec 10, 2018 / Revised Mar 11, 2019 / Accepted Mar 25, 2019)

Mucor circinelloides **is a dimorphic Zygomycete fungus that produces ethanol under aerobic conditions in the presence of glucose, which indicates that it is a Crabtree-positive fungus. To determine the physiological role of the alcohol dehydrogenase (ADH) activity elicited under these conditions, we obtained and characterized an allyl alcohol-resistant mutant that was defective in ADH activity, and examined the effect of *adh* mutation on physiological parameters related to carbon and energy metabolism. Compared to the Adh$^+$ strain R7B, the ADH-defective (Adh$^-$) strain M5 was unable to grow under anaerobic conditions, exhibited a considerable reduction in ethanol production in aerobic cultures when incubated with glucose, had markedly reduced growth capacity in the presence of oxygen when ethanol was the sole carbon source, and exhibited very low levels of NAD$^+$-dependent alcohol dehydrogenase activity in the cytosolic fraction. Further characterization of the M5 strain showed that it contains a 10-bp deletion that interrupts the coding region of the *adh1* gene. Complementation with the wild-type allele *adh1*$^+$ by transformation of M5 remedied all the defects caused by the *adh1* mutation. These findings indicate that in *M. circinelloides*, the product of the *adh1* gene mediates the Crabtree effect, and can act as either a fermentative or an oxidative enzyme, depending on the nutritional conditions, thereby participating in the association between fermentative and oxidative metabolism. It was found that the spores of *M. circinelloides* possess low mRNA levels of the ethanol assimilation genes (*adl2* and *acs2*), which could explain their inability to grow in the alcohol.**

Keywords: *Mucor circinelloides*, ADH1 enzyme, Crabtree effect, fermentative and oxidative metabolism

*For correspondence. E-mail: felixg@ugto.mx; Tel.: +52-473-732 0006 Ext: 8148; Fax: +52-473-732 0006 Ext: 8151
[§]Supplemental material for this article may be found at http://www.springerlink.com/content/120956.

Introduction

Zygomycetes are saprophytes that are ubiquitous in natural environments, and contribute to the transformation of organic matter. In recent years, Zygomycetes have attracted interest in various areas, such as biotechnology and the health sector. These organisms have been studied and used to produce a wide range of metabolic products, including organic acids, enzymes, fatty acids, and biofuels; furthermore, the biomass of Zygomycetes contains proteins, lipids, amino acids, chitin, and chitosan, and is considered useful for the production of animal feed, human food, and chitosan (Ferreira *et al.*, 2013; Karimi and Zamani, 2013). Regarding their interest to the health sector, some Zygomycetes have been described as opportunistic pathogens in humans because they can cause mucormycosis. The reported species include *Absidia trapeziformis*, *Cunninghamella* spp., *Mucor* spp., *Rhizomucor* spp., and *Rhizopus* spp. (Chayakulkeeree *et al.*, 2006; Ibrahim and Spellberg, 2006; Mendoza *et al.*, 2015).

The yeast–hyphae dimorphism of some *Mucor* species has been considered important for industrial applications such as the production of heterologous proteins (Wolff and Arnau, 2002), or metabolites and fuel ethanol in large-scale fermentation plants (Ferreira *et al.*, 2013; Karimi and Zamani, 2013). In aspects related to pathogenicity, for instance, the hyphae of *Mucor* species have been associated with infected tissues in humans (Khan *et al.*, 2009), and in a murine mucormycosis system (Lee *et al.*, 2013).

Depending on the environmental conditions in which dimorphic species of *Mucor* are cultivated, the germination of spores produces vegetative hyphae cells (a mycelium) or spherical budding cells (yeast) (Bartnicki-García, 1963; Sypherd *et al.*, 1978); the production of a mycelium or yeast cells can occur under aerobic or anaerobic conditions, accor-

ding to the carbon source and/or the addition to the medium of morphogenetic compounds. Mycelial cells are capable of adopting an oxidative or fermentative metabolism, depending on the cultivation conditions. In contrast, the production of yeast cells requires the presence of hexoses, and such cells adopt a fermentative metabolism, producing high levels of ethanol after growth under various conditions; yeast cells can grow by anaerobiosis or aerobiosis in the presence of morphogenetic compounds, such as dibutyryl cyclic-AMP, certain amino acids, and phenethyl alcohol (PEA) (Orlowski, 1991). Metabolic studies have shown that when *Mucor circinelloides* is incubated under aerobic conditions in the presence of glucose, it produces a mycelium that exhibits an oxidative metabolism, although it also produces appreciable levels of ethanol; these observations indicate that *M. circinelloides* is a Crabtree-positive microorganism (McIntyre *et al.*, 2002). The ethanol produced by the fungus under these conditions is consumed after the glucose has been exhausted. However, yeast cells produced under anaerobic conditions do not utilize ethanol because they require hexoses as a carbon source (Lübbehüsen *et al.*, 2004).

In *M. circinelloides*, the mRNA of *adh1* gene is expressed in spores (Valle-Maldonado *et al.*, 2015), hyphae, and yeast cells, and produces a cytoplasmic enzyme that appears to be the major alcohol dehydrogenase (ADH) in the fungus; during mycelial growth under aerobic conditions, the level of expression of the *adh1* gene is correlated with the concentration of glucose in the culture medium (Rangel-Porras *et al.*, 2005). Kinetic characterization of purified ADH1 suggests that it mainly works as a fermentative enzyme and converts acetaldehyde to ethanol in an $NADH+H^+$-dependent reaction (Rangel-Porras *et al.*, 2005); furthermore, adh1 mRNA accumulates in higher levels in yeast cells than in hyphae or spores (Valle-Maldonado *et al.*, 2015). In the yeast *Saccharomyces cerevisiae*, the fermentative enzyme ADH1 participates in the production of ethanol, whereas the oxidative enzyme ADH2–in conjunction with the enzymes aldehyde dehydrogenase (ALD1/ALD2) and acetyl-CoA synthetase (ACS2)-participates in the utilization of ethanol as a carbon source (Wills, 1990; de Kok *et al.*, 2012).

To determine the physiological function of the ADH1 enzyme in *M. circinelloides*, we obtained and characterized an allyl alcohol-resistant mutant that was defective in ADH activity; this mutant had an *adh1* gene with an altered open reading frame (ORF), and produced a protein lacking the NAD^+-binding domain. It therefore produced a protein with abolished ADH activity. This mutation was examined for its effect on physiological parameters related to carbon and energy metabolism.

Materials and Methods

Fungal strains and cultivation conditions

We used the leucine-requiring *Mucor circinelloides* strain R7B (ATCC90608; Roncero, 1984) as the wild-type reference strain throughout this study; the M5 strain is a spontaneous allyl alcohol-resistant ($Ally^r$) mutant derived from R7B (see below). For the growth experiments, we used yeast-peptone-glucose (YPG) complete medium (Bartnicki-García and Nickerson, 1962) and Lee's minimal medium (LMM) (Lee *et al.*, 1975), modified as described by Acevedo-Aguilar *et al.* (2006) and containing 0.25% KH_2PO_4, 0.20% $MgSO_4$, 0.50% $(NH_4)_2SO_4$, 0.5% NaCl, and glucose or ethanol at 2% as the carbon source. When necessary, LMM was supplemented with 20 mg/L leucine as a requirement for the auxotrophy of R7B and its derivative M5. The strains were maintained, and spores were obtained after growth in YPG medium as described (Bartnicki-García and Nickerson, 1962). To obtain aerobic mycelia, we grew liquid cultures (600 ml) in 2-L Erlenmeyer flasks containing YPG medium inoculated with spores at a final cell density of 5×10^5/ml, and incubated them in a shaken water bath at 28°C for the indicated period. In some experiments, we inoculated the cultures with swollen spores; these cells were obtained by inoculating YPG medium with intact spores and incubating the cultures under aerobic conditions at 28°C for 4 h. The obtained cells were centrifuged at 3,500 × *g*. The resulting pellets were thoroughly washed by centrifugation in sterile distilled water, and then transferred to a solid or liquid medium, as indicated. For growth in the solid medium under anaerobic conditions, we used LMM with 2% glucose, with or without leucine. After inoculating the medium with spores of the indicated strains, Petri dishes containing the inoculated medium were incubated in an anaerobic jar using the GasPak system (Becton Dickinson). Self-anaerobic growth was facilitated using 125-ml flasks filled completely with culture medium and sealed with rubber stoppers provided with a needle, to allow the exit of excess of CO_2 (Salcedo-Hernández and Ruiz Herrera, 1993). Self-anaerobic cultures containing 125 ml of YPG medium were inoculated with 1×10^6 spores/ml of *M. circinelloides*; this condition causes the spores to grow and produce budding yeast cells, as previously described (Salcedo-Hernández and Ruiz-Herrera, 1993). The germination percentage under aerobic or anaerobic conditions was calculated from the number of germinules or budding yeast cells in at least 100 cells.

For the transition experiments, swollen spores were incubated in YPG medium for 4 h under aerobic conditions or yeast cells in YPG medium for 12 h under self-anaerobic conditions, and then centrifuged the obtained cells at 3,500 × *g*. The harvested pellets were washed five times with 40 ml of sterile distilled water, transferred to LMM containing glucose or ethanol as the sole carbon source, and incubated at 28°C while shaking at 150 rpm.

Isolation and sequencing of genomic clones of the M5 *adh1* gene

The sequencing strategy was based on the polymerase chain reaction (PCR) amplification of fragments of the ORF of the *adh1* gene from the M5 mutant strain using the following oligonucleotides: adh-xhoF (5′ CTC GAG ATG TCT GAA GAA ACT TTC ACT GCC TGG G 3′); adh-notR (5′ GCG GCC GCG TTC ATG ACG ACA GCT CTG TAA CG 3′); adh31F (5′ GAC AAC GCT ACC AAG GAC AAG ACC 3′); and adh32R (5′ TTG TAG TGA GGC TCC ATT TGC TCT 3′). These oligonucleotides were designed based on the sequence from the *adh1* gene of the wild-type strain R7B as described in our previous study (Rangel-Porras *et al.*, 2005). The oligonucleotides adh-xhoF and adh-notR correspond to regions at the 5′ and 3′ ends of the *adh1* gene, respectively,

and contain *Xho*I and *Not*I restriction sites (underlined in the oligonucleotides sequences). Oligonucleotides adh31F and adh32R amplify an internal fragment of the central region of the *adh1* gene. The nucleotide sequence of the genomic and cDNA versions of the wild-type R7B *adh1* gene are available at GenBank under the Accession nos. AY702961 and AY702962, respectively. The nucleotide sequence of the genomic version of the M5 mutant *adh1* gene is available at GenBank under the Accession number MH130382.

The amino acid sequence of the ADH1 protein predicted from the sequenced *adh1* gene of the M5 mutant was aligned with the corresponding ADH1 protein predicted by the *adh1* gene of the wild-type R7B strain (Rangel-Porras *et al.*, 2005) using DNASTAR software.

Total RNA isolation and quantitative reverse transcription polymerase chain reaction (qRT-PCR)

The biological samples of *M. circinelloides* were: 1) spores, grown for 4 h under aerobic conditions to produce swollen spores (SS), 2) spores grown under self anaerobic conditions for 12 h to produce anaerobic swollen spores (ASS) (these cells were produced by the mutant M5, which, unlike the wild-type strain R7B, is unable to grow in the presence of low oxygen tension, which is why it fails to develop and grow as yeast cells), 3) mycelium grown for 12 h (M), and 5) yeast cells grown for 12 h (Y); in all cases, the growth was performed in YPG medium. The cells were collected by filtration (using Whatman No. 6 filter paper), and washed with sterile distilled water. RNA was isolated as described previously (Valle-Maldonado *et al.*, 2015). *M. circinelloides* gene-specific oligonucleotides and hydrolysis probes for *ald2* (aldehyde dehydrogenase) and *acs2* (acetyl-CoA synthetase) genes were designed using Biosearch Technologies software (http://www.biosearchtech.com) to ensure the specificity of all detections during the qRT-PCR assays (Supplementary data Table S1). The qRT-PCR assays, amplifications, and PCR efficiency determinations; the relative expression level calculations and the data analyses; and the use of hydrolysis probes and primers for the *adh1* (alcohol dehydrogenase) and *tfc1* (subunit of the transcription factor TFIIIC from RNA polymerase III) genes, all were carried out according to a previously described method (Valle-Maldonado *et al.*, 2015).

Northern blot analyses

Total RNA was extracted from aerobic mycelium of strains R7B and M5 cultured in YPG medium for 13 h and Northern blot analysis was performed as described by Sambrook *et al.* (1989); the incubation time selected was used because under these conditions the wild-type strain R7B shows the optimum level of ADH activity (Rangel-Porras *et al.*, 2005). The hybridization was performed using ^{32}P-labelled DNA probes, consisting of a 475 bp fragment of the *adh1* gene cDNA or a 774 bp fragment of the *leuA* gene, both obtained from R7B strain.

Construction of plasmid vector pEUKA7/adh1 and fungal transformation

For the complementation experiments, the 1,044-bp DNA fragment corresponding to the ORF of the *adh1* gene was amplified by PCR using the wild-type R7B strain genomic DNA (gDNA) and the oligonucleotides adh-xhoF and adh-notR. The amplified product was directionally cloned into the plasmid pEUKA 7.1 (Wolff and Arnau, 2002) using *Xho*I and *Not*I restriction sites, thereby generating the plasmid pEUKA7/adh1. In this vector, *adh1* gene expression is under the control of the promoter and the transcriptional terminator of the *M. circinelloides gpd1* gene. This construct was introduced into protoplasts of the *adh1*-deficient mutant strain M5. Leu$^+$ prototroph transformants were selected and purified by monosporic isolation, as described previously (Wolff and Arnau, 2002).

Preparation of cell-free extracts

Aerobic mycelia cells were disrupted in an MSK cell homogenizer (Braun) and the crude extract or the cytosolic fraction (164,500 × *g* supernatant) was prepared according to a previously described procedure (Rangel-Porras *et al.*, 2005).

ADH activity assay

NAD$^+$ or NADP$^+$-dependent ADH activity was determined spectrophotometrically in crude extracts or in the cytosolic fraction. All enzyme assays were conducted in a final volume of 2 ml, and the ADH activity was assayed in the oxidative direction, according to the method described by Bergmeyer (1983). The assays were performed in a reaction mixture containing 50 mM Tris-HCl (pH 8.5), 1.9 mM NAD$^+$ or NADP$^+$, cell-free extract (100–200 µg protein), and 0.8 M ethanol. The reaction was started by adding ethanol, and a reduction of NAD$^+$ or NADP$^+$ was monitored by the increase in absorbance at 340 nm. One unit of enzyme activity was defined as the amount required to reduce 1 µmol of NAD$^+$ or NADP$^+$ per min at 25ºC. The specific ADH activity was expressed as units (U) per mg of protein.

The NAD$^+$-dependent ADH activity of the crude extracts was also determined by zymography, which was performed following electrophoresis on non-denaturing 10% polyacrylamide gels (Nikolova and Ward, 1991), as previously described (Torres-Guzmán *et al.*, 1994). The image shown in Fig. 8 comes from an electrophoretic separation in which the crude extracts of the indicated strains were loaded in the same gel, separated between them by an empty lane, to avoid cross-contamination. ADH activity was revealed in the complete gel and then the gel was photographed. The photographic image of the gel was cut to remove the empty lanes of the gel; Fig. 8 shows the image of the lanes in which the samples of extracts of the strains were loaded.

Determination of the ethanol content of the culture

Mycelium biomass (1 g) obtained from cultures grown under aerobic conditions in LMM with 2% glucose for 24 h was transferred to the same medium, and incubated under aerobic conditions. Subsequently, 1-ml samples were obtained from the culture after 12, 24, and 48 h of incubation, fil-

tered through 0.22-μm filters, and used for determination of ethanol content. The ethanol content in the supernatants was determined by gas chromatography with a flame ionization detector (GC-FID, Agilent Technologies 7890B) using an Agilent J&W HP-Innowax 19091N-136 column (60 m × 250 μm × 0.25 μm) with nitrogen as the mobile phase supplied at a flow rate of 1 ml/min. We injected 0.5 μl of each sample using an auto-sampler in split 20:1 mode at 240°C, whereas for the flame ionization detector the temperature was 260°C. The column temperature was held at 50°C for 2 min, increased to 240°C at 5°C/min, and held for 15 min. Quantification was based on a calibration curve using ethanol as a standard and 2-pentanol as the internal standard (both from Sigma-Aldrich) (López-Álvarez *et al.*, 2012).

The values shown in the results are the mean from three independent experiments conducted with duplicate determinations. The error bars represent standard deviations. The one-way analysis of variance (ANOVA) post hoc Bonferroni test was used to analyse the data regarding ethanol production and the ADH activity levels in the cytosolic fraction of the *M. circinelloides* strains. We carried out all the tests using Statistica 11 software, and set a significance level of 0.05 (indicated by letters in the figures) for the analyses.

Results

Isolation and characterization of a mutant deficient in ADH activity

In a previous study, we observed marked expression of the *M. circinelloides adh1* gene in cultures incubated under aerobic conditions in a medium containing glucose (Rangel-Porras *et al.*, 2005). Therefore, these conditions were chosen to select spontaneous mutants that were deficient in ADH activity using allyl alcohol resistance. This procedure has been used to elucidate the physiological role of *adh* gene-encoded enzymes in microorganisms, plants, and animals (Lutstorf and Megnet, 1968; Wills and Phelps, 1975; Freeling and Bennett, 1985; Jacobs *et al.*, 1988; Williamson *et al.*, 1991; Zheng *et al.*, 2009). For this purpose, we incubated spores of strain R7B under aerobic conditions in solid YPG medium containing 2% glucose and supplemented with 100 mM allyl alcohol (a sufficient concentration to inhibit the growth of R7B spores). One resistant colony appeared after 7 days of incubation, and the isolate was purified twice by single-spore colony formation in the same selective medium used to produce the spores, which were able to grow in a medium containing allyl alcohol. The strain was named M5.

The stability of the Ally^r phenotype of the M5 mutant was tested by performing three complete vegetative cycles under non-selective conditions and inoculating the spores onto plates containing solid YPG medium. The top row of Fig. 1 shows that M5 and R7B were able to grow similarly in YPG medium when the cultures were incubated under aerobic conditions. However, under similar incubation conditions in YPG medium containing allyl alcohol, only the spores of the mutant strain M5 and not those of strain R7B were able to germinate and produce a mycelium (Fig. 1 middle row), which illustrates the Ally^r and Ally^s phenotypes of M5 and R7B, respectively. However, in cultures incubated in YPG medium under hypoxic conditions, only the spores of strain R7B and not those of M5 managed to germinate and produce a visible mycelium, which indicated that strain M5 is unable to grow under conditions of low oxygen tension (Fig. 1 bottom row). We obtained similar results for liquid YPG medium inoculated with spores and incubated under self-anaerobic conditions, defined as those stablished due to the displacement of oxygen from the cultures by the CO_2 produced during microbial metabolism. Under self-anaerobic conditions the wild-type strain R7B generated budding yeasts, as previously described (Salcedo-Hernandez and Ruíz Herrera, 1993), whereas the M5 mutant strain was unable to reach the yeast phase and produced only swollen spores (Supplementary data Fig. S1A). At difference of spores, which are metabolically dormant, swollen spores constitute a later stage in the spore germination process, characterized by isodiametric growth and by an active biosynthesis of macromolecules, formation of organelles and development of a new cell wall (Bartnicki-Garcia *et al.*, 1968; Orlowski and Sypherd, 1978); for that reason, from a metabolic point of view, swollen spores are considered fully active, as vegetative cells.

Furthermore, when we transferred yeast cells of the wild-type strain R7B to LMM and incubated them under aerobic conditions with either glucose or ethanol as the carbon source, they exhibited high rates of transition to hyphae formation (approximately 90% for glucose and 75% for ethanol) (Supplementary data Fig. S1B). We carried out a complementation analysis of strain M5 to determine whether the alterations exhibited by the M5 mutant including, allyl-alcohol resistance under aerobic conditions and growth impairment under anaerobic conditions, are due to the mutation in the *adh1* gene. These complementation analysis were performed

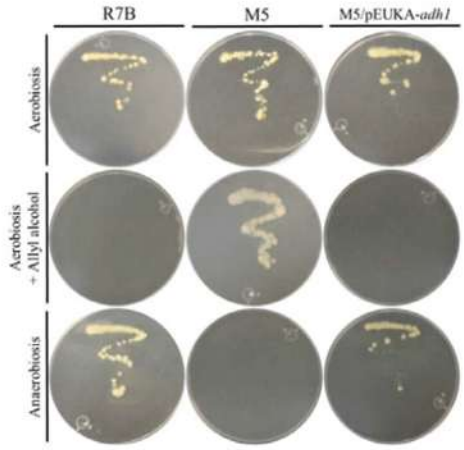

Fig. 1. Plate growth of *Mucor circinelloides* strains under various culture conditions. We inoculated plates of solid Lee's minimal medium (LMM) with or without allyl alcohol with spores of the strains, and incubated under aerobic conditions. We also incubated other inoculated plates without allyl alcohol under anaerobic conditions. In all cases, we photographed the growth of the resulting colonies over 3 days of incubation. For the growth of the wild-type R7B and M5 mutant strains, we supplemented the medium with leucine, whereas we omitted leucine from the medium used to grow complemented strain M5/pEUKA-*adh1*.

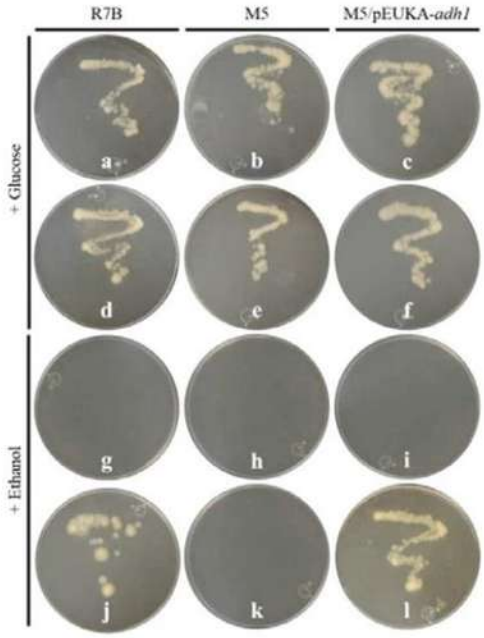

Fig. 2. Plate growth of the *Mucor circinelloides* strains under aerobic conditions in Lee's minimal medium (LMM) with 2% glucose or ethanol as the sole carbon source. We inoculated the cultures with spores (a,b,c and g,h,i) or with swollen spores (d,e,f and j,k,l), and photographed the growth of the colonies after 3 days of incubation. For the growth of the wild-type R7B and M5 mutant strains, we supplemented the medium with leucine, whereas we omitted leucine from the medium used to grow complemented strain M5/pEUKA-*adh1*.

using protoplast transformation with the pEUKA-*adh1* construct, which contains the *adh1*$^{+}$ allele from R7B under the control of the promoter and transcriptional terminator of the *M. circinelloides gpd1* gene. Selection for leucine prototrophy resulted in the M5-derived transformant M5/pEUKA-*adh1*. Figure 1 shows that, as with strain R7B, the presence of the wild-type *adh1* allele in the M5/pEUKA-*adh1* transformant caused allyl alcohol-sensitivity in this strain because it was unable to grow in medium containing allyl alcohol under aerobic conditions (Fig. 1 middle row). Furthermore, similar to the wild-type strain R7B, the transformant M5/pEUKA-*adh1* was able to grow under conditions sustaining anaerobiosis (Fig. 1 bottom row) and self-anaerobiosis (Supplementary data Fig. S1A), in which the mutant strain M5 was unable to grow.

In the next experiment, we compared the abilities of strains R7B and M5 to grow under aerobic conditions in solid LMM media with glucose or ethanol as the carbon source by inoculating the medium with spores or with swollen spores. In the medium containing glucose, the spores (Fig. 2a) and swollen spores (Fig. 2d) of strain R7B were able to grow and produce mycelial colonies; we observed similar results for the spores (Fig. 2b) and swollen spores (Fig. 2e) of the M5 mutant incubated in the same medium. In the LMM solid medium containing ethanol as the carbon source, the spores of the wild-type strain R7B (Fig. 2g) and those of the mutant M5 (Fig. 2h) failed to produce mycelial colonies. Interestingly, in the medium containing ethanol, the R7B swollen spores (Fig. 2j) managed to grow and produce mycelial colonies, but those of M5 did not (Fig. 2k). The inability of the M5 swollen spores to grow in medium containing ethanol is specifically due to *adh1* mutation as demonstrated by the

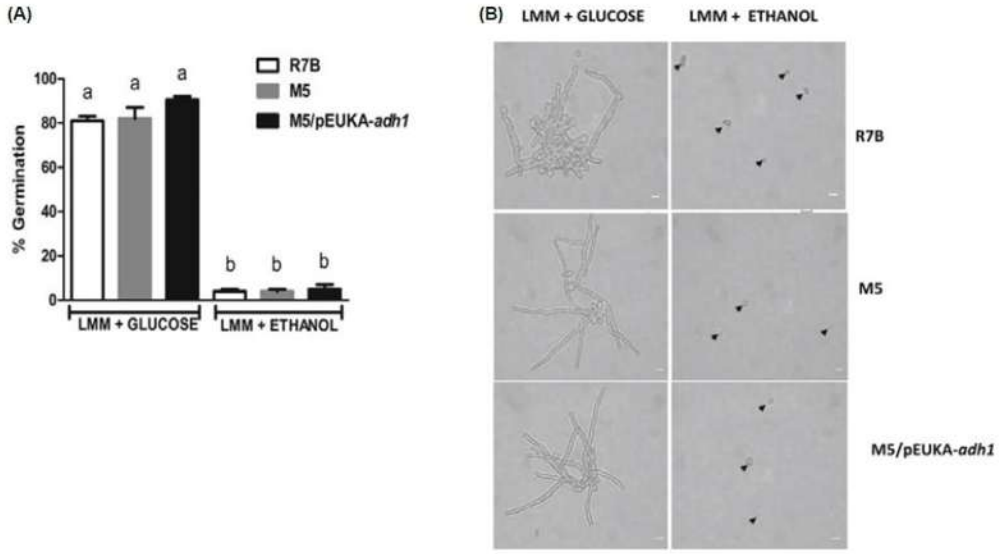

Fig. 3. Spore germination of *Mucor circinelloides* in liquid Lee's minimal medium (LMM) with glucose or ethanol as the sole carbon source. (A) Bars represent the percentage of spores germinated independently of number or size per mother cell. The data are the mean ± SD, and three independent experiments were performed for each condition. The letters denote statistically significant differences (analysis of variance (ANOVA), Fisher, $P < 0.05$). (B) Morphology of spores grown in the presence of glucose or ethanol as the sole carbon source after 12 h of incubation. The arrow heads indicate ungerminated spores; scale bar = 10 μm. For the growth of the wild-type R7B and M5 mutant strains, we supplemented the medium with leucine, whereas we omitted leucine from the medium used to grow complemented strain M5/pEUKA-*adh1*.

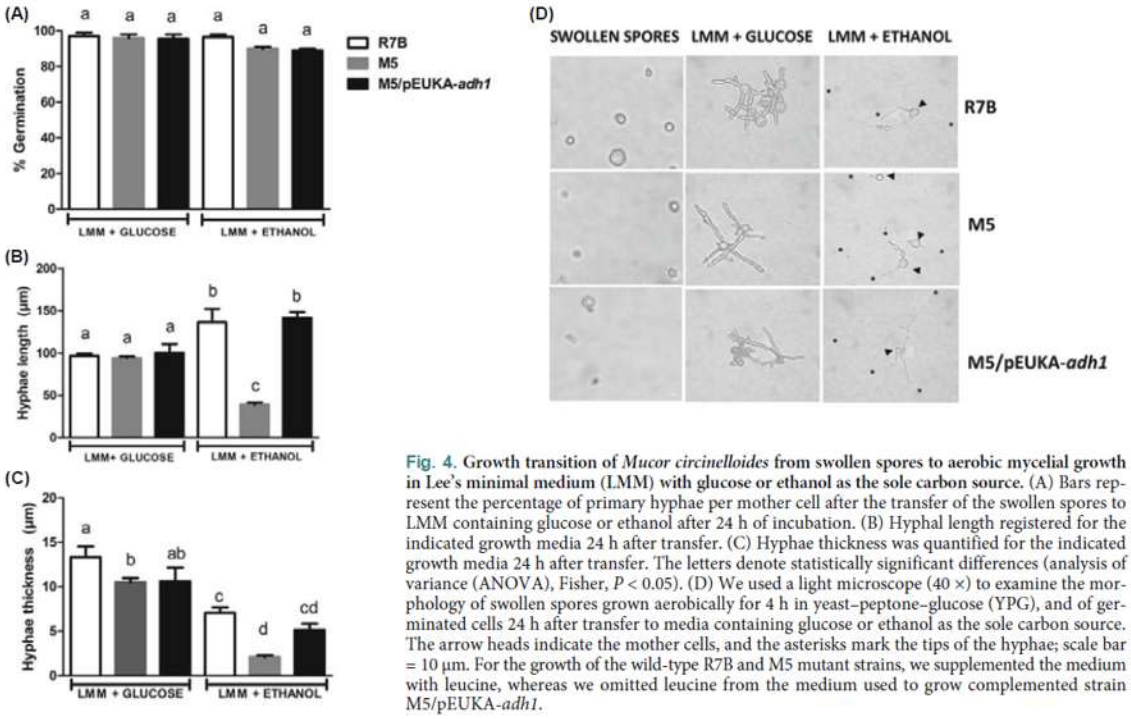

Fig. 4. Growth transition of *Mucor circinelloides* from swollen spores to aerobic mycelial growth in Lee's minimal medium (LMM) with glucose or ethanol as the sole carbon source. (A) Bars represent the percentage of primary hyphae per mother cell after the transfer of the swollen spores to LMM containing glucose or ethanol after 24 h of incubation. (B) Hyphal length registered for the indicated growth media 24 h after transfer. (C) Hyphae thickness was quantified for the indicated growth media 24 h after transfer. The letters denote statistically significant differences (analysis of variance (ANOVA), Fisher, $P < 0.05$). (D) We used a light microscope (40 ×) to examine the morphology of swollen spores grown aerobically for 4 h in yeast–peptone–glucose (YPG), and of germinated cells 24 h after transfer to media containing glucose or ethanol as the sole carbon source. The arrow heads indicate the mother cells, and the asterisks mark the tips of the hyphae; scale bar = 10 µm. For the growth of the wild-type R7B and M5 mutant strains, we supplemented the medium with leucine, whereas we omitted leucine from the medium used to grow complemented strain M5/pEUKA-*adh1*.

fact that the swollen spores of the complemented strain+ M5/pEUKA-*adh1* were able to grow and produced mycelial colonies, as readily as the R7B swollen spores, in medium containing ethanol as the only carbon source (Fig. 2i).

To confirm these observations under different conditions, we decided to grow the strains in liquid LMM containing either glucose or ethanol, using intact spores or swollen spores as inoculum and incubating the cultures under aerobic conditions. Spores from the wild-type R7B, the mutant M5, as well as those from the complemented M5/pEUKA-*adh1* strain were able to germinate at similar levels (> 80%) in medium with glucose as the carbon source, whereas spores of these three strains were unable to germinate when ethanol was the carbon source (Fig. 3A and B). Moreover, when we transferred swollen spores from R7B, M5, and the complemented M5/pEUKA-*adh1* to LMM containing either glucose or ethanol, they exhibited high germination rates of at least 90% (Fig. 4A). However, the hyphae that emerged from the swollen M5 spores incubated in LMM with ethanol were much shorter (Fig. 4B) and narrower (Fig. 4D) than those produced by R7B. These last two phenotypes were remediated by introduction of the *adh1* wild-type allele into the M5 strain as length and thickness of the complemented M5/pEUKA-*adh1* strain were comparable to those shown by the R7B wild-type strain. These results may explain, in part, why swollen M5 spores in solid LMM containing ethanol did not generate visible mycelial colonies to any appreciable extent (Fig. 2k), in contrast to the wild-type strain R7B, which shows robust colonies in this medium (Fig. 2j). In general, the development of hyphae was less extensive in

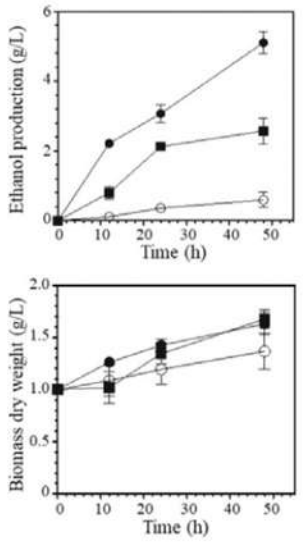

Fig. 5. Ethanol production and growth rate in *Mucor circinelloides* strains incubated in medium containing glucose under aerobic conditions. The cultures were grown in Lee's minimal medium (LMM) containing 2% glucose under aerobic conditions; at the indicated incubation times, we collected aliquots from the cultures to determine the ethanol concentration by gas chromatography with a flame ionization detector (GC-FID) (top) and growth (bottom), as described in the 'Materials and Methods' section. Wild-type R7B (●), mutant M5 (○), and complemented mutant M5/pEUKA-*adh1* (■).

swollen cells grown in ethanol than those grown in glucose, and the difference was particularly evident in the mutant strain M5 (Fig. 4D). These observations indicate that under the conditions tested, the vegetative cells, but not the spores of *M. circinelloides* grow well in ethanol as the carbon source and that this process requires a functional ADH1 enzyme.

Ethanol production of M5 mutant deficient in ADH activity

We sought to evaluate the involvement of ADH1 in the production of ethanol. To this end, the ethanol levels were measured in aerobic cultures of R7B and M5 grown for 48 h on LMM with 2% glucose. The top panel of Fig. 5 shows that in cultures of R7B, ethanol production increased starting at 12 h of incubation, and reached a production level of approximately 5 g/L ethanol at 48 h. However, in the M5 cultures, the level of ethanol produced was very low (< 0.15 g/L) at 12 h and markedly low thereafter (0.5 g/L). This difference in ethanol production between R7B and M5 was statistically significant ($P < 0.05$). The presence of the wild-type *adh1*$^{+}$ gene in the complemented M5/pEUKA-*adh1* strain partially restored ethanol production (Fig. 5 top panel).

Although there was a slight difference in the production of biomass between the strains, being lower in M5, the difference in growth does not explain why the ethanol content

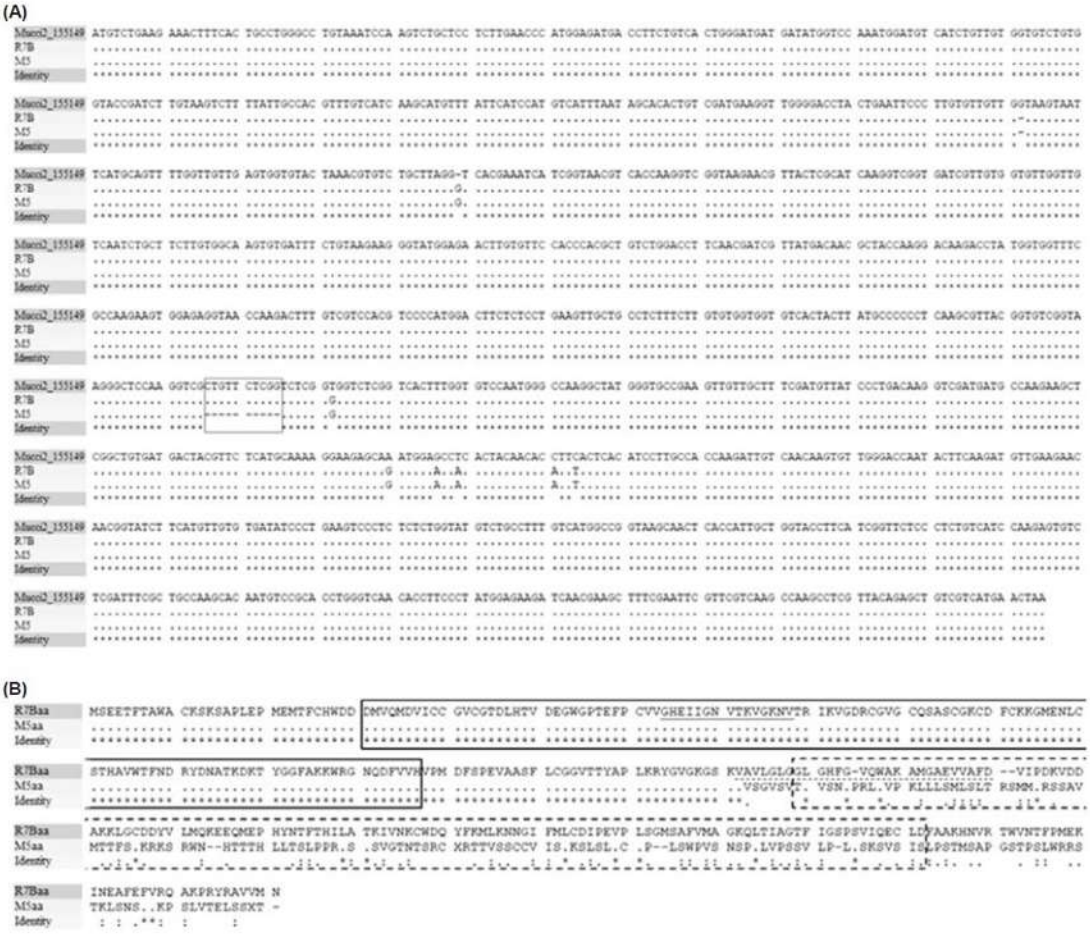

Fig. 6. **Sequence analysis of the *Mucor circinelloides adh1* gene.** (A) DNA sequence alignment of the *adh1* open reading frame (ORF) from the wild-type CBS277.49 strain (JGI genome Mucci_155149), the wild-type R7B strain (GenBank AY702961), and the M5 mutant strain (GenBank MH130382). A 10-bp deletion in the *adh1* gene from the M5 mutant (boxed in the figure) is indicated. A seven-nucleotide difference is also indicated between the ORFs of the *adh1* gene of strains R7B and M5, with respect to the sequence (Mucci2|155149) (gi 309952144|) of the genome of the reference strain *M. circinelloides* CBS277.49 V2. (B) Amino acid sequence alignment between the *adh1*-encoded ADH enzyme from the wild-type R7B and M5 mutant strains. The ADH N-terminal domain (31–147, IPR013154, solid line box), the ADH C-terminal domain (189–312, IPR013149, dashed line box), the ADH zinc-type conserved site (64–78, IPR002328, solid underlined), and the NAD-binding domain conserved site (182–209, IPR029752, dashed underlined) are indicated. The seven-nucleotide difference between the ORFs of the *adh1* gene of strains R7B and M5 with respect to the sequence (Mucci2|155149) (gi 309952144|) of the genome of the reference strain *M. circinelloides* CBS277.49 V2 is also indicated. All alignments were made using the ClustalW algorithm of the DNASTAR software program.

Table 1. NAD- and NADP-dependent alcohol dehydrogenase (ADH) activity in the cytosolic fraction[a] of aerobically grown mycelial cells of *Mucor circinelloides* strains

Strain	ADH-specific activity (U/mg)	
	Assay with NAD as cofactor	Assay with NADP as cofactor
R7B	13.5 ± 1.4	0.015 ± 0.003
M5	0.04 ± 0.003	< 0.001
M5/pEUKA-*adh1*	15.5 ± 1.3	0.020 ± 0.003

[a]The cytosolic fraction for the determination of ADH activity was obtained from mycelia developed in yeast-peptone-glucose medium in cultures incubated for 24 h under aerobic conditions.

produced by the M5 mutant was 10-fold lower than that by R7B strain (Fig. 5, bottom panel). These observations indicate that the mutation present in M5 negatively affected the ethanol production.

Biochemical characterization of the ADH-deficient strain M5

ADH enzymes can use NAD^+ and/or $NADP^+$ as a cofactor (Reid and Fewson, 1994). In a previous study, we observed that in the cytosolic fraction of R7B, the NAD^+-dependent ADH activity was approximately 750 times higher than the $NADP^+$-dependent ADH activity (Rangel-Porras *et al.*, 2005). To determine if the mutation present in M5 affected the activity of an enzyme dependent on NAD^+, $NADP^+$, or both cofactors, we determined the ADH activity in the cytosolic fraction obtained from cell-free extracts of R7B and M5, and performed the assays in the presence of ethanol as a substrate. The results obtained (Table 1) show that in the extracts of strain R7B, the ADH activity was approximately 900 times higher when using NAD^+ as a cofactor (specific activity 13.5 U/mg) compared to $NADP^+$ (specific activity 0.015 U/mg). In the cell-free extracts of M5, the NAD^+-dependent ADH activity was approximately 338 times lower (a specific activity of 0.04 U/mg) than the corresponding activity of R7B, and the $NADP^+$-dependent ADH activity was at least 15 times lower (specific activity < 0.001 U/mg) than the corresponding activity in the cell-free extracts of R7B. The difference in NAD^+- and $NADP^+$-dependent ADH activity between R7B and M5 was statistically significant ($P < 0.05$). Cell-free extracts of the complemented strain M5/pEUKA-*adh1* exhibited levels of NAD^+- and $NADP^+$-dependent ADH activity similar to those detected in the R7B strain (Table 1), indicating the observed effects are indeed specific to *adh1*.

The expression and activity of the *Adh1* introduced into the complemented strain M5/pEUKA-*adh1* was confirmed by electrophoresis. The zymograms revealed that the electrophoretic mobility of the ADH activity band of the transformant M5/pEUKA-*adh1* was similar to that of the wild-type strain R7B (Fig. 8) and not ADH activity was detected in the M5 mutant strain. These results demonstrate that the ADH enzyme present in the cytosolic fraction of *M. circinelloides* is mainly NAD^+-dependent, and that $NADP^+$ use is very inefficient. Furthermore, our data support the model that the activity of the ADH1 enzyme is dramatically affected by the mutation present in the M5 mutant strain.

Analysis of the *adh1* gene in the Ally^r M5 mutant

In a previous study using a reverse genetics approach (Rangel-Porras *et al.*, 2005), we cloned the gene encoding the ADH1 enzyme from the wild-type strain R7B (GenBank AY702961) (Supplementary data Fig. S2A). We used the deduced amino acid sequence of ADH1 in an *in silico* search for paralogous genes of the *M. circinelloides* CBS277.49 V2 genomic database (https://genome.jgi.doe.gov/Mucci2/Mucci2.home.html).

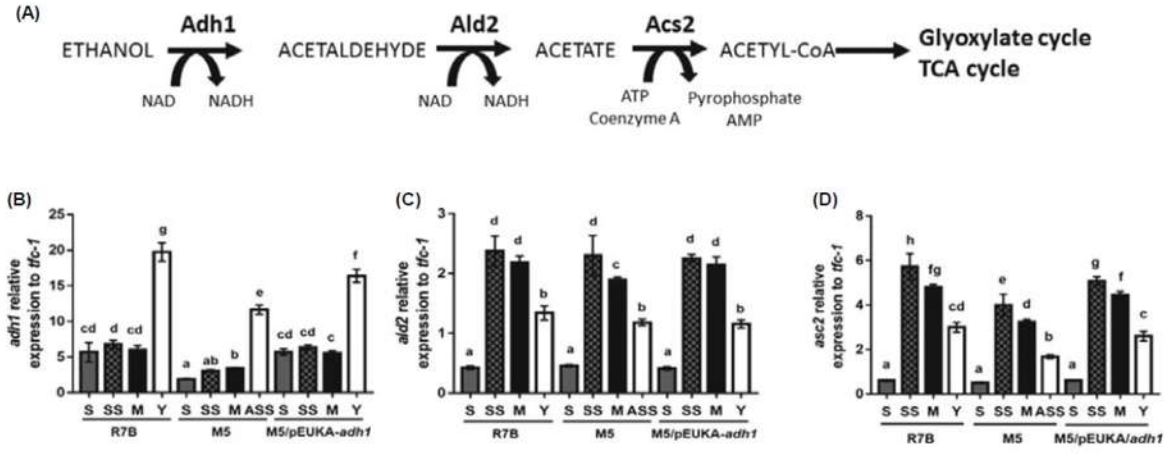

Fig. 7. Quantification of mRNA levels of genes encoding enzymes involved in ethanol consumption in spores and vegetative cells from *Mucor circinelloides*. (A) Initial steps of ethanol metabolism in *M. circinelloides* for its use as a carbon source for growth, involving the participation of alcohol dehydrogenase 1 (Adh1), aldehyde dehydrogenase 2 (Ald2) and acetyl CoA synthetase (Acs2). Ethanol is consumed to produce acetyl-CoA, which finally could be used to supply the glyoxylate or tricarboxylic acid cycles. We measured the mRNA levels by performing quantitative reverse transcription polymerase chain reaction (qRT-PCR) on: (B) *adh1*, alcohol dehydrogenase 1; (C) *ald2*, aldehyde dehydrogenase 2; and (D) *acs2*, acetyl CoA synthetase. We carried out Ct analyses to compare mRNA levels between spores (S), spores aerobically grown for 4 h (SS), mycelium grown under aerobic conditions for 12 h (M) and yeast cells (Y) cultured for 12 h under conditions of self-anaerobiosis; all the cells were grown in yeast-peptone-glucose (YPG) medium. We performed three independent experiments for each condition. The letters denote statistically significant differences (analysis of variance (ANOVA), Fisher, $P < 0.05$).

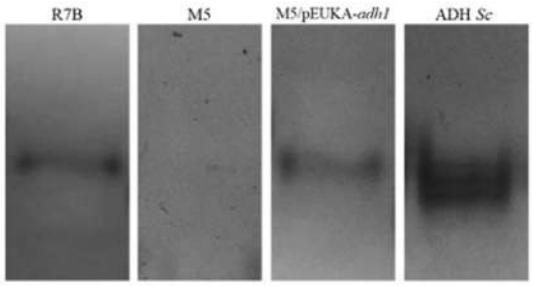

Fig. 8. Zymogram band pattern of ADH activity in cell-free extracts of the *Mucor circinelloides* strains. We electrophoresed and stained crude extracts obtained from aerobic mycelia grown in yeast-peptone-glucose (YPG) medium for 18 h, as described in the Materials and Methods section. The upper part of each lane indicates the strain source of the extract or the enzyme used for the ADH activity assay: wild-type R7B, mutant M5, complemented strain M5/pEUKA-*adh1*, and commercial *Saccharomyces cerevisiae* ADH enzyme (Sigma). Note that, as described in 'Materials and Methods', all samples were analysed on the same gel, leaving an empty lane between each sample to avoid sample contamination across contiguous lanes. The empty lanes were excised-off and the gel strips containing samples were photographed.

We found 100% identity with a sequence (Mucci2|155149) (gi 309952144|) corresponding to the *adh1* gene (Supplementary data Fig. S2B), and 44–59% identity with six additional *adh* paralogous sequences (Mucci2|157439|, Mucci2|34200|, Mucci2|90838|, Mucci2|140177|, Mucci2|120424|, and Mucci2|152844|).

The northern blot analysis of the expression of the *adh1* gene in the aerobic mycelium of R7B and M5 incubated in YPG medium revealed that a 1.15-kb transcript is produced in both strains (Supplementary data Fig. S3). This observation refutes the notion that the mutation in M5 affects a region or regulatory product involved in the transcription of the *adh1* gene. The coding region of the *adh1* gene has been sequenced to determine whether the sequence of *adh1* is altered in the M5 strain. A PCR amplification strategy of overlapping DNA fragments was followed by the use of oligonucleotides adh-xhoF, adh-notR, adh31F, and adh32R, which were designed based on the sequence of the *adh1* gene of strain R7B (Rangel-Porras *et al.*, 2005). As with the wild-type *adh1* allele (Rangel-Porras *et al.*, 2005), sequence analysis of the M5 *adh1* allele revealed a non-continuous ORF resulting from the presence of two small introns at positions 142–202 and 251–306 (Supplementary data Fig. S2C). The alignment of the *adh1* allele in R7B and M5 revealed a deletion of 10 bp at position 666 of the *adh1* gene ORF in the mutant M5 (Fig. 6A). This alteration results in the deletion of three amino acids and a frameshift, which leads to the formation of a smaller predicted protein (243 amino acids with an approximate molecular weight of 28 kDa) than that encoded by the wild-type *adh1* gene (348 amino acids with a calculated molecular mass of 37 kDa) (Rangel-Porras *et al.*, 2005). Importantly, the predicted M5 ADH1 protein lacks the cofactor (NAD^+/$NADP^+$)-binding domain (Fig. 6B). These sequence-deduced alterations in the M5 ADH1 enzyme account for the defective physiological phenotype displayed by the M5 mutant.

The enzymes ADH2, ALD2, and ACS2 are involved in the utilization of ethanol as a carbon source in *S. cerevisiae* (Wills, 1990) (Fig. 7A). Using ALD2 and ASC2 as targets, we identified the corresponding homologues in the *M. circinelloides* genome with the highest identity and similarity scores with the respective yeast genes (Supplementary data Tables S2 and S3). To ascertain whether the genes involved in ethanol consumption are differentially expressed during the morphological development of *M. circinelloides*, we designed specific probes to determine the *adh1*, *ald2*, and *acs2* mRNA levels in spores or vegetative cells. In general, the levels of mRNA of the *adh1* gene in the different morphological stages, including spores, aerobic swollen spores and mycelium of the strains R7B, M5, and M5/pEUKA-*adh1* are approximately similar, being a little lower in the cells of the M5 mutant (Fig. 7B). These results agree with those from a previous study, which found similar *adh1* mRNA levels in both spores and in aerobic mycelium of the R7B strain (Valle-Maldonado *et al.*, 2015). However, the *adh1* mRNA levels were significantly higher in the yeast phase of the R7B and M5/pEUKA-*adh1* strains, and in the anaerobic swollen spores of the M5 mutant strain (Fig. 7B). In these three strains the spores show very low *ald2* (Fig. 7C) and *asc2* (Fig. 7D) mRNA levels, compared with the stages of swollen spore and aerobic mycelium, as well as in comparison with the yeast phase of R7B and M5/pEUKA-*adh1* strains and the anaerobic swollen spores of the M5 mutant. These results suggest that the low expression of the *ald2* and *asc2* genes in spores may result in the spores' inability to use ethanol as a carbon source. Finally, our observations also indicate that the *adh1* mutation does not noticeably affects the expression of the *adh1*, *ald2*, and *asc1* genes in the morphogenetic stages tested in M5 strain.

Discussion

Previous studies have shown that under aerobic conditions and in the presence of glucose, *M. circinelloides* produces significant amounts of ethanol, which suggests that it is a Crabtree-positive microorganism (McIntyre *et al.*, 2002). Moreover, the ethanol produced by the aerobic mycelium of *M. circinelloides* is consumed after glucose depletion in the medium, and the yeast cells produced under anaerobic conditions cannot use ethanol owing to their requirement for hexoses as a carbon source (Lübbehüsen *et al.*, 2004).

Alcohol dehydrogenases play an important role in the metabolism of alcohols, and participate in the last steps of fermentative metabolism or in the first steps of oxidative metabolism (Reid and Fewson, 1994). In a previous study, we observed that glucose positively regulates the production of the ADH1 enzyme at the transcriptional level in *M. circinelloides*. Furthermore, the kinetic characterization of purified ADH1 indicates that it acts as a fermentative enzyme and reduces acetaldehyde to ethanol (Rangel-Porras *et al.*, 2005).

In the present study, we attempted to determine the physiological function of ADH1 in connection with its role in the Crabtree effect and in ethanol metabolism in *M. circinelloides*. We obtained and characterized the allyl alcohol-resistant strain M5 for this purpose. Compared with the reference strain R7B, in addition to allyl alcohol resistance,

M5 exhibited deficiencies in several physiological parameters related to carbon and energy metabolism: 1) an inability to grow in a medium containing glucose in the absence of oxygen; 2) a failure to utilize ethanol as a carbon source for growth under aerobic conditions; and 3) a reduced ability to produce ethanol from glucose under aerobic conditions. In agreement with these characteristics, M5 exhibited dramatically reduced levels of NAD-dependent ADH activity in the cytosolic fraction.

Sequence analysis of the *adh1* allele from M5 showed that it contains a deletion of 10 bp at position 666 of the coding sequence of the *adh1* gene. This sequence alteration causes a deletion of three amino acids and a frameshift that results in a modification of the downstream sequence, which leads to the formation of a smaller predicted protein that lacks the cofactor (NAD^+/$NADP^+$)-binding domain. This alteration affects the enzymatic activity of the ADH1 protein and provides an explanation for the physiological alterations exhibited by M5. The reintroduction of the wild-type allele *adh1* into M5 allowed us to verify that in the resultant transformant (M5/pEUKA-*adh1*), the physiological and biochemical characteristics of R7B were restored in the M5 background. This observation indicates that the product of the *M. circinelloides adh1* gene mediates the Crabtree effect in the fungus, and functions as either a fermentative or an oxidative enzyme, depending on the culture conditions.

The *in silico* analysis performed in this work indicated that the *M. circinelloides adh1* gene (Rangel-Porras *et al.*, 2005) corresponds to sequence (Mucci2|155149) in the *Mucor circinelloides* CBS277.49 V2 genomic database, although the existence of additional sequences encoding paralogous ADH proteins with a significant degree of identity to the Adh1 enzyme (i.e., Mucci2|152844, 59% identity; Mucci2|120424, 48% identity; Mucci2|140177 and Mucci2|90838, 47% identity) was noted. However, it seems that the physiological replacement of the ADH1 enzyme by another paralogous ADH enzyme is eliminated based on the pronounced phenotype of the M5 mutant in relation to its complete inability to grow under anaerobic conditions or to use ethanol as a carbon source. This is corroborated by the absence of other bands of ADH activity in the zymogram activity patterns of the wild-type strain R7B and the M5 mutant. The altered phenotype of M5 indicates that ADH1 is active in R7B from the germination of the spores and in vegetative cells obtained under aerobic or anaerobic conditions in the presence of glucose, or under aerobic conditions in the presence of ethanol.

Our findings suggest that *M. circinelloides* spores are less prone to assimilate ethanol as the sole carbon source than vegetative cells, because the mRNA levels of genes involved in the initial steps of ethanol metabolism for its use as a carbon source, such as *ald2* and *acs2*, are notably lower in spores than in vegetative cells. These findings explain why spores grow poorly in ethanol as the only carbon source, both in solid and liquid media. The observation that the germination of swollen spores in LMM containing ethanol was practically the same in M5, R7B, and in the complemented strain M5/pEUKA-*adh1*, and that there was an obvious difference in the degree of hyphae elongation between the M5 mutant and the other strains that contained the $adh1^+$ allele, could indicate that ADH activity is required after the germination of the spores, possibly in sustaining the growth of the hyphae. A previous study revealed that the spores of the dimorphic zygomycete *M. racemosus* contain pre-transcribed mRNA, which is packed into the spores (Linz and Orlowski, 1982). Thus, the finding in this work of the presence in the spores of *adh1*, *ald2*, and *acs2* mRNAs, may derive from packing these mRNAs into the spores, rather than from transcription in the spores. We find that the lack of ADH activity in the M5 mutant does not affect its development from spore to swollen spore and swollen spore to hypha, although the hyphae formed fails to growth. These results support the interpretation that ADH1 activity is not required for the breakdown of the spore's dormant state nor the passage to the swollen cell stage and the polarization of growth to form hyphae, but rather, ADH1 activity is required to support hyphal growth.

When the filamentous ascomycete *Fusarium oxysporum* is grown in the presence of glucose, ethanol production is low under aerobic conditions and high under anaerobic conditions (Panagiotou *et al.*, 2005; Corrales-Escobosa *et al.*, 2011), which indicates that this fungus is a Crabtree-negative organism. Adh1 participates in the production of ethanol in *F. oxysporum*. Furthermore, ethanol is used as a carbon source by conidia and mycelia, and Adh1 participates in this capacity and is required for full expression of virulence by the fungus (Corrales-Escobosa *et al.*, 2011).

The ascomycete yeast *Saccharomyces cerevisiae* is a Crabtree-positive organism that, in the presence of oxygen and a high concentration of glucose, uses glycolysis and fermentation pathways to obtain energy for growth (Pronk *et al.*, 1996). In *S. cerevisiae* and other Crabtree-positive yeasts, glucose is completely depleted when the ethanol concentration reaches a maximum and begins to be utilized as a carbon source, which constitutes a close connection between fermentative and respiratory metabolism (Hagman *et al.*, 2013). It has been proposed that in *S. cerevisiae*, the duplication of the genome–in particular the duplication of the *ADH* gene (to generate ADH1 and ADH2) and the duplication of hexose transporter coding genes-constitutes the molecular background for the development of the Crabtree effect (Hagman *et al.*, 2013; Pfeiffer and Morley, 2014). In *S. cerevisiae*, ADH1 regenerates NAD and converts acetaldehyde into ethanol, whereas ADH2 is responsible for the oxidation of ethanol as one of the initial steps in the use of this alcohol as a carbon source. Although ADH1p and ADH2p exhibit a high degree of identity at the nucleotide level of the encoding genes and amino acids, the difference in their physiological roles lies in the regulation of their production according to the culture conditions (de Smidt *et al.*, 2008). Because there is no paralog enzyme exhibiting a high degree of identity to the ADH1 protein in the *M. circinelloides* genome, our finding that ADH1 may act as either a fermentative or oxidative enzyme, depending on the nutritional conditions, indicates the different characteristics of the elements involved in determining the activity of ADH with regard to the connection between fermentative and oxidative metabolism, and the operation of the Crabtree effect in the fungus. A perspective of interest is the determination of the role of paralogous ADH1 enzymes in ethanol metabolism, and their possible participation in the connection between the two types of metabolism in *M. circinelloides*.

Acknowledgements

This work was supported by grants 29078N, 41590, and 167071 from SEP-CONACyT, México. RARP, SPDP, VAC, MIVM, and JMMH each received a fellowship from CONACyT, México. We thank María E. Cardenas for critical reading of the manuscript.

Conflicts of Interest

The authors declare no conflicts of interest.

References

Acevedo-Aguilar, F.J., Espino-Saldaña, A.E., León-Rodríguez, I.L., Ávila-Rodríguez, M., Wrobel, K., Wrobel, K., Lappe, P., Ulloa, M., and Gutiérrez-Corona, J.F. 2006. Hexavalent chromium removal *in vitro* and from industrial wastes, using chromate-resistant strains of filamentous fungi indigenous to contaminated wastes. *Can. J. Microbiol.* **52**, 809–815.

Bartnicki-García, S. 1963. Symposium on biochemical bases of morphogenesis in fungi III Mold-yeast dimorphism of *Mucor*. *Bacteriol. Rev.* **27**, 293–304.

Bartnicki-Garcia, S., Nelson, N., and Cota-Robles, E. 1968. Electron microscopy of spore germination and cell wall formation in *Mucor rouxii*. *Arch. Mikrobiol.* **63**, 242–255.

Bartnicki-García, S. and Nickerson, W.J. 1962. Nutrition, growth, and morphogenesis of *Mucor rouxii*. *J. Bacteriol.* **84**, 841–858.

Bergmeyer, H.U. 1983. Reagents for enzymatic analysis, pp. 139. *In* Bergmeyer, H.U. (ed.), Methods of enzymatic analysis. Verlag Chemie, Weinheim, Germany.

Chayakulkeeree, M., Ghannoum, M., and Perfect, J. 2006. Zygomycosis: the re-emerging fungal infection. *Eur. J. Clin. Microbiol. Infect. Dis.* **25**, 215–229.

Corrales-Escobosa, A.R., Rangel-Porras, R.A., Meza-Carmen, V., Gonzalez-Hernandez, G.A., Torres-Guzman, J.C., Wrobel, K., Wrobel, K., Roncero, M.I.G., and Gutierrez-Corona, J.F. 2011. *Fusarium oxysporum* Adh1 has dual fermentative and oxidative functions and is involved in fungal virulence in tomato plants. *Fungal Genet. Biol.* **48**, 886–895.

de Kok, S., Kozak, B.U., Pronk, J.T., and van Maris, A.J.A. 2012. Energy coupling in *Saccharomyces cerevisiae*: selected opportunities for metabolic engineering. *FEMS Yeast Res.* **12**, 387–397.

de Smidt, O., du Preez, J.C., and Albertyn, J. 2008. The alcohol dehydrogenases of *Saccharomyces cerevisiae*: a comprehensive review. *FEMS Yeast Res.* **8**, 967–978.

Ferreira, J.A., Lennartsson, P.R., Edebo, L., and Taherzadeh, M.J. 2013. Zygomycetes-based biorefinery: Present status and future prospects. *Bioresour. Technol.* **135**, 523–532.

Freeling, M. and Bennett, D.C. 1985. Maize *Adh1*. *Annu. Rev. Genet.* **19**, 297–323.

Hagman, A., Säll, T., Compagno, C., and Piskur, J. 2013. Yeast "Make-Accumulate-Consume" life strategy evolved as a multi-step process that predates the whole genome duplication. *PLoS One* **8**, e68734.

Ibrahim, A.S. and Spellberg, B. 2006. Zygomycetes as agents of infectious disease in humans, pp. 429–440. *In* Heitman, J., Filler, S.G., Edwards, Jr.J.E., and Mitchell, A.P. (eds.), Molecular principles of fungal pathogenesis. American Society for Microbiology Press, Washington, D.C., USA.

Jacobs, M., Dolferus, R., and Van den Bossche, D. 1988. Isolation and biochemical analysis of ethyl methanesulfonate induced alcohol dehydrogenase null mutants of *Arabidopsis thaliana* (L.) Heynh. *Biochem. Genet.* **26**, 105–122.

Karimi, K. and Zamani, A. 2013. *Mucor indicus*: biology and industrial application perspectives: a review. *Biotechnol. Adv.* **31**, 466–481.

Khan, Z.U., Ahmad, S., Brazda, A., and Chandy, R. 2009. *Mucor circinelloides* as a cause of invasive maxillofacial zygomycosis: an emerging dimorphic pathogen with reduced susceptibility to posaconazole. *J. Clin. Microbiol.* **47**, 1244–1248.

Lee, K.L., Buckley, H.R., and Campbell, C.C. 1975. An aminoacid liquid synthetic medium for the development of mycelial and yeast forms of *Candida albicans*. *Sabouraudia* **13**, 148–153.

Lee, S.C., Li, A., Calo, S., and Heitman, J. 2013. Calcineurin plays key roles in the dimorphic transition and virulence of the human pathogenic zygomycete *Mucor circinelloides*. *PLoS Pathog.* **9**, e1003625.

Linz, J.E. and Orlowski, M. 1982. Stored mRNA in sporangiospores of the fungus *Mucor recemosus*. *J. Bacteriol.* **150**, 1138–1144.

López-Alvarez, A., Díaz-Pérez, A.L., Sosa-Aguirre, C., Macías-Rodríguez, L., and Campos-García, J. 2012. Ethanol yield and volatile compound content in fermentation of agave must by *Kluyveromyces marxianus* UMPe-1 comparing with *Saccharomyces cerevisiae* baker's yeast used in tequila production. *J. Biosci. Bioeng.* **113**, 614–618.

Lübbehüsen, T.L., Nielsen, J., and McIntyre, M. 2004. Aerobic and anaerobic ethanol production by *Mucor circinelloides* during submerged growth. *Appl. Microbiol. Biotechnol.* **63**, 543–548.

Lutstorf, U. and Megnet, R. 1968. Multiple forms of alcohol dehydrogenase in *Saccharomyces cerevisiae*. I. Physiological control of ADH-2 and properties of ADH-2 and ADH-4. *Arch. Biochem. Biophys.* **126**, 933–944.

McIntyre, M., Breum, J., Arnau, J., and Nielsen, J. 2002. Growth physiology and dimorphism of *Mucor circinelloides* (syn. *racemosus*) during submerged batch cultivation. *Appl. Microbiol. Biotechnol.* **58**, 495–502.

Mendoza, L., Vilela, R., Voelz, K., Ibrahim, A.S., Voigt, K., and Lee, S.C. 2015. Human fungal pathogens of mucorales and entomophthorales. *Cold Spring Harb. Perspect. Med.* **5**, a019562.

Nikolova, P. and Ward, O.P. 1991. Production of L-phenylacetyl carbinol by biotransformation: product and by-product formation and activities of the key enzymes in wild-type and ADH isoenzyme mutants of *Saccharomyces cerevisiae*. *Biotechnol. Bioeng.* **20**, 493–498.

Orlowski, M. 1991. Mucor dimorphism. *Microbiol. Rev.* **55**, 234–258.

Orlowski, M. and Sypherd, P.S. 1978. Regultion of macromolecular synthesis during hyphal germ tube emergence from *Mucor racemosus* sporangiospores. *J. Bacteriol.* **134**, 76–83.

Panagiotou, G., Villas-Boas, S.G., Christakopoulos, P., Nielsen, J., and Olsson, L. 2005. Intracellular metabolite profiling of *Fusarium oxysporum* converting glucose to ethanol. *J. Biotechnol.* **115**, 425–434.

Pfeiffer, T. and Morley, A. 2014. An evolutionary perspective on the Crabtree effect. *Front. Mol. Biosci.* **1**, 17.

Pronk, J.T., Yde Steensma, H., and Van Dijken, J.P. 1996. Pyruvate metabolism in *Saccharomyces cerevisiae*. *Yeast* **12**, 1607–1633.

Rangel-Porras, R.A., Meza-Carmen, V., Martínez-Cadena, G., Torres-Guzmán, J.C., González-Hernández, G.A., Arnau, J., and Gutiérrez-Corona, J.F. 2005. Molecular analysis of an NAD-dependent alcohol dehydrogenase from the zygomycete *Mucor circinelloides*. *Mol. Genet. Genomics* **274**, 354–363.

Reid, M.F. and Fewson, C.A. 1994. Molecular characterization of microbial alcohol dehydrogenases. *Crit. Rev. Microbiol.* **20**, 13–56.

Roncero, M.I.G. 1984. Enrichment method for the isolation of auxotrophic mutants of Mucor using the polyene antibiotic N-glycosyl-polifungin. *Carlsberg Res. Commun.* **49**, 685–690.

Salcedo-Hernández, R. and Ruiz-Herrera, J. 1993. Isolation and

characterization of a mycelial cytochrome aa_3-deficient mutant and the role of mitochondria in dimorphism of *Mucor rouxii*. *Exp. Mycol.* **17**, 142–154.

Sambrook, J., Fritsch, E.F., and Maniatis, T. 1989. Molecular cloning: a laboratory manual (2nd ed.). Cold Spring Harbor Laboratory Press, Cold Spring Harbor, NY, USA.

Sypherd, P., Borgia, P.T., and Paznokas, J.L. 1978. Biochemistry of dimorphism in the fungus *Mucor*. *Adv. Microb. Physiol.* **18**, 67–104.

Torres-Guzmán, J.C., Arreola-García, G.A., Zazueta-Sandoval, R., Carrillo-Rayas, T., Martínez-Cadena, G., and Gutiérrez-Corona, F. 1994. Genetic evidence for independence between fermentative metabolism (ethanol accumulation) and yeast-cell development in the dimorphic fungus *Mucor rouxii*. *Curr. Genet.* **26**, 166–171.

Valle-Maldonado, M.I., Jácome-Galarza, I.E., Gutiérrez-Corona, F., Ramírez-Díaz, M.I., Campos-García, J., and Meza-Carmen, V. 2015. Selection of reference genes for quantitative real time RT-PCR during dimorphism in the zygomycete *Mucor circinelloides*. *Mol. Biol. Rep.* **42**, 705–711.

Williamson, V.M., Long, M., and Theodoris, G. 1991. Isolation of *Caenorhabditis elegans* mutants lacking alcohol dehydrogenase activity. *Biochem. Genet.* **29**, 313–323.

Wills, C. 1990. Regulation of sugar and ethanol metabolism in *Saccharomyces cerevisiae*. *Crit. Rev. Biochem. Mol. Biol.* **25**, 245–280.

Wills, C. and Phelps, J. 1975. A technique for the isolation of yeast alcohol dehydrogenase mutants with altered substrate specificity. *Arch. Biochem. Biophys.* **167**, 627–637.

Wolff, A.M. and Arnau, J. 2002. Cloning of glyceraldehyde-3-phosphate dehydrogenase-encoding genes in *Mucor circinelloides* (Syn. *racemosus*) and use of the *gpd1* promoter for recombinant protein production. *Fungal Genet. Biol.* **35**, 21–29.

Zheng, Z., Luo, S., Li, X., Wu, X., Pan, L., and Jiang, S. 2009. Screening of allyl alcohol resistant mutant of *Rhizopus oryzae* and its fermentation characterization. *Afr. J. Biotechnol.* **8**, 280–284.

Microbial Pathogenesis 137 (2019) 103737

Contents lists available at ScienceDirect

Microbial Pathogenesis

journal homepage: www.elsevier.com/locate/micpath

Sporulation on blood serum increases the virulence of *Mucor circinelloides*

J. Alberto Patiño-Medina[a,1], David Vargas-Tejeda[a,1], Marco I. Valle-Maldonado[a,b], Viridiana Alejandre-Castañeda[a], Irvin E. Jácome-Galarza[b], Javier Villegas-Moreno[a], Rosa E. Nuñez-Anita[c], Martha I. Ramírez-Díaz[a], Rafael Ortiz-Alvarado[d,2], Victor Meza-Carmen[a,*,2]

[a] Instituto de Investigaciones Químico Biológicas, Universidad Michoacana de San Nicolás de Hidalgo, 58030, Morelia, Michoacán, Mexico
[b] Departamento de Biología Molecular, Laboratorio Estatal de Salud Pública del Estado de Michoacán, 58279, Morelia, Michoacán, Mexico
[c] Facultad de Medicina Veterinaria y Zootecnia, Universidad Michoacana de San Nicolás Hidalgo, 58130, Morelia, Michoacán, Mexico
[d] Facultad de Químico Farmacobiología, Universidad Michoacana de San Nicolás de Hidalgo, 58240, Morelia, Michoacán, Mexico

ARTICLE INFO

Keywords:
Mucor circinelloides
Fungal sporulation
Virulence
Blood serum

ABSTRACT

Mucor circinelloides is an opportunistic human pathogen that is used to study mucormycosis, a rare but lethal infection in susceptible immunosuppressed patients. However, the virulence characteristics of this pathogen have not been fully elucidated. In this study, sporangiospores (spores) produced on YPG medium supplemented with native blood serum increased the virulence of *M. circinelloides* compared with spores produced on YPG supplemented with denatured blood serum or on YPG alone. The spores produced from YPG supplemented with native blood serum increased nematode death and led to significant increases in interleukin (*IL*)-*6*, *IL-1β*, macrophage inhibitory protein-2, and tumour necrosis factor α mRNA levels in liver and lung tissues from infected diabetic mice compared with those in tissues from animals infected with spores produced in the presence of YPG supplemented with denatured blood serum or of YPG alone. Moreover, spores produced from cultures supplemented with native blood serum showed increased germination rates and longer hyphae compared with other spores. The spores produced in YPG supplemented with native blood serum also enhanced resistance to stress factors and H_2O_2 and increased thermotolerance compared with spores produced under other conditions. In addition, spores produced in presence of blood serum increased the ability of the pathogen to survive in the presence of macrophages. Taken together, our results showed that these factors were important features for fungal virulence in humans and suggested that thermolabile components in the blood serum may induce *M. circinelloides* virulence.

1. Introduction

Mucormycosis is a fungal opportunistic infection that is lethal in certain populations, particularly those at high risk, such as patients with ketoacid diabetes [1] and transplant recipients [2]. Mucormycosis is named based on the ethylogical agents that belong to the fungal order of Mucorales; the genus *Rhizopus* is the most common genus causing mucormycosis, followed by *Lichtheimia*, *Apophysomyces*, *Rhizomucor*, *Mucor*, and *Cunninghamella* [3]. The global incidence of mucormycosis is increasing, with rates 34% and 28% higher in Europe and the Americas, respectively, during the period from January 2000 through January 2017 [4]. This fungal infection is considered the third most important disease among patients with haematological conditions in Europe [5]. The worldwide incidence is 1.23 per 100,000 persons [6], although the low sensitivity of diagnostic tests could underestimate the true incidence of mucormycosis [3].

Mucor circinelloides has been used to elucidate the basic virulence mechanisms involved in mucormycosis [7–10]. Moreover, *M. circinelloides* is the most well-studied biological model among Mucorales organisms, and many molecular manipulation tools have been developed for this fungus [11–13].

Fungal interactions with the host can enhance some genetic traits in fungi to increase virulence; for example, in *Bauveria bassiana*, consecutive spore propagation cycles through malaria mosquitoes (*Anopheles coluzzii*) leads to selection of variants with increased virulence rates [14]. A similar effect was observed in the ascomycete

* Corresponding author. Laboratorio de Diferenciación Celular, Instituto de Investigaciones Químico Biológicas, Universidad Michoacana de San Nicolás de Hidalgo, Ciudad Universitaria, 58030, Morelia, Michoacán, Mexico.
E-mail address: victor_meza2004@yahoo.com.mx (V. Meza-Carmen).
[1] J. Alberto Patiño-Medina and David Vargas-Tejeda contributed equally to this work.
[2] Rafael Ortiz-Alvarado and Victor Meza-Carmen are the senior authors.

https://doi.org/10.1016/j.micpath.2019.103737
Received 4 May 2019; Received in revised form 6 August 2019; Accepted 8 September 2019
Available online 09 September 2019

Metarhizium anisopliae, in which spores produced by consecutive passages through the tick *Rhipicephalus microplus* increase the virulence against the host [15]. Entomopathogenic fungal strains have shown this type of natural selection, and fungal plant pathogens, such as *Botritis cinereae* [16] and *Fusarium oxysporum f. sp. vasinfectum* [17], have also been shown to induce increased virulence through spores produced by serial passages in their corresponding plant hosts.

Mucor circinelloides can infect animals and humans under certain conditions, e.g., in immunosuppressed patients [6]. However, the virulence characteristics of this pathogen have not been fully elucidated. Therefore, the primary goal of this study was to investigate the influence of *Mucor circinelloides* spores produced on blood serum on virulence. The findings provided important insights into the virulence of this important pathogen.

2. Material and methods

2.1. Strains and culture conditions

Mucor circinelloides strain R7B (*leuA*$^-$) [18] was used throughout this study. Microbiological cultures were grown in YPG medium containing 3 g/L yeast extract, 10 g/L peptone, and 20 g/L glucose in water. For solid medium, 20 g/L agar was added.

Spore production of *Mucor circinelloides* was carried out by inoculation of 100 spores on YPG agar plates supplemented with or without 10% human blood serum or denatured human blood serum incubated at 28 °C for 5 days in the presence of light. Denatured blood serum was obtained after 12 h at 55 °C; this temperature and time were sufficient to inactivate cell growth factors, as has been reported previously [19]. Native or denatured human serum blood was added to the cultures after sterilisation.

The spores were collected from the plates by adding 5 mL distilled sterile water to each plate, followed by gentle scraping with a glass loop; these spores were collected by aspiration and deposited into 50-mL conical tubes. The spores were pelleted by centrifugation at 5000 × *g* for 10 min at 25 °C and then washed with 10 mL distilled sterile water. Finally, the spores were suspended in 10 mL distilled sterile water and counted using a hemocytometer. All spore samples were maintained at 4 °C and used within 15 days.

Aerobic spore germination was observed after inoculation of 5×10^5 spores/mL in 125-mL Erlenmeyer flasks with 10 mL YPG and incubation at 28 °C with constant shaking. Germination rate estimation was carried out considering the number of hyphae per mother cell, independent of the number or length, as has been reported previously [8].

Spore resistance to H_2O_2 was evaluated in 0.5 mL distilled sterile water with 24,000 spores/mL obtained from different conditions. This suspension was treated with 4 mM H_2O_2 for 30 min at 4 °C. Subsequently, 100 spores were taken from spore suspensions previously treated with H_2O_2, spread onto YPG plates, and incubated at 28 °C for 24 h.

For thermoresistance assays, 100 untreated spores were spread on YPG plates and incubated at 37 °C for 24 h. Viability was measured as the number of germlings grown on the plates after 24 h. Viability (%) was calculated as the number of treated spores divided by the number of untreated spores.

2.2. Total Mucor circinelloides RNA and DNA isolation from in vitro cultures, macrophages, and mouse tissues

Total RNA and genomic DNA were isolated from *Mucor circinelloides*, mouse tissues, and macrophages using an RNAeasy mini kit and a QIAamp DNA Mini Kit, respectively (Quiagen, Venlo, the Netherlands).

Mouse tissues were collected at 15 days after infection by *Mucor circinelloides* spore inoculation. Approximately 25 mg tissue from each mouse was transferred into a tube containing MagNA Lyser Green Beads (Roche, Basel, Switzerland) precooled on ice. Denaturing RLT buffer (700 µL) from an RNeasy Mini Kit or buffer ATL (180 µL) from a QIAamp DNA Mini Kit was added immediately before homogenisation to obtained total RNA or genomic DNA, respectively. For cell disruption, tubes were placed in a MagNA Lyser Instrument and processed twice at 4500 × *g* for 40 s with cooling on ice for 1 min between each step. The samples were then centrifuged for 1 min at 20,000 × *g* (Eppendorf 5417), and the supernatants were used for total RNA or genomic DNA isolation by applying the corresponding kit, according to the manufacturer's instructions. To eliminate DNA contamination from RNA samples, samples were treated with DNase I (Promega, Madison, WI, USA) according to the manufacturer's protocol. RNA was eliminated from DNA samples using RNAse A (Roche). RNA or genomic samples were separated on nondenaturing 1% or 2% agarose gels stained with ethidium bromide. The samples were visualised using a Gel Doc XR+ Imager (Bio-Rad, Hercules, CA, USA) and quantified using a SmartSpec Plus spectrophotometer (Bio-Rad).

2.3. Reverse transcription quantitative polymerase chain reaction (RT-qPCR) assays

The primers and hydrolysis probes were modified at their 5′ ends with 6-carboxy fluorescein and at their 3′ ends with Black Hole Quencher. Probes were used as described previously [20]. For amplification and detection of the candidate genes, probes targeting the *pkaR1* gene, which encodes regulatory subunit 1 of protein kinase A [21], and the *tfc-1* gene, which encodes a subunit of the transcription factor TFIIIC required for the RNA polymerase III pre-initiation complex assembly, were used as described previously [20]. The *cnaA* probe from *Mucor circinelloides* was designed based on a previously reported sequence [7], and the *Mucor circinelloides pex3* (ID: 158038) gene, which encodes the peroxin 3 homolog from *Saccharomyces cerevisiae*, was retrieved from the *Mucor circinelloides* genome [22] (Table 1S). Mouse interleukin (*IL*)-6, *IL-1β*, macrophage inhibitory protein-2 (*MIP-2*), and tumour necrosis factor α (*TNF-α*) probes were design based on GenBank accession numbers DQ88722.1, NM_008361.4, NM_009140.2, and BC137720.1, respectively. The mouse β-actin gene was used as a reference gene for RT-qPCR analysis (Table 1S). All probes were purchased from Biosearch Technologies, Inc. (Novato, CA, USA). RT-qPCR assays were performed in a single tube using the 5′ exonuclease probe method. RT-qPCR was performed with a LightCycler 480 II System (Roche Molecular Diagnostics, Pleasanton, CA, USA) using a SuperScript III Platinum One-step RT-qPCR reagent kit (Invitrogen, Carlsbad, CA, USA). Each 25-µL reaction volume contained 5 µL extracted total RNA template (50 ng), 0.5 µL enzyme mix, 12.5 µL of 2× reaction mix, 0.5 µL of 10 µM forward primer, 0.5 µL of 10 µM reverse primer, 0.5 µL of 5 µM probe, and 5.5 µL water.

RT-qPCR was initiated by RT (50 °C, 30 min) and initial denaturation (95 °C, 5 min), followed by 45 amplification cycles at 95 °C for 30 s and 60 °C for 30 s. Similar conditions were employed for qPCR without the reverse transcription step. Fluorescence signals were collected at 60 °C for each cycle. The amplification signal curves were analysed at absorption wavelengths of 530 nm. Appropriate positive and non-template controls were included in each test run.

2.4. Ethics statement

The mouse virulence model protocol was carried out following the recommendations of the Mexican Federal Regulations for the Use and Care of Laboratory Animals (approval no. NOM-062-ZOO-1999; Especificaciones té para la producción, cuidado y uso de los animales de laboratorio/Technical specifications for production, use and care of laboratory animals) [23]. The Internal Biosecurity and Bioethics Committee of Instituto de Investigaciones Químico Biológicas de la Universidad Michoacana de San Nicolás de Hidalgo reviewed and approved

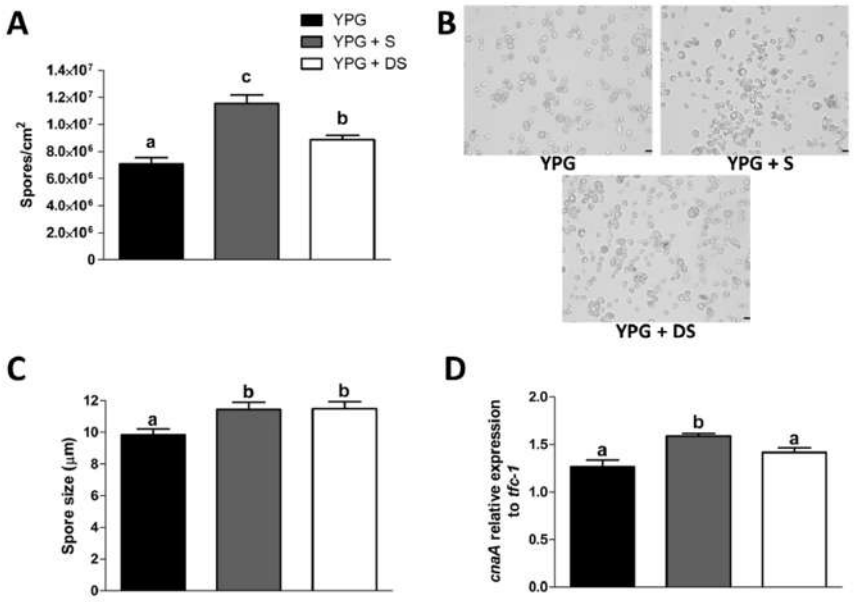

Fig. 1. Effects of blood serum on spore production from *Mucor circinelloides*. **(A)** Spores were produced on YPG plates, YPG supplemented with 10% blood serum (YPG + S), or YPG supplemented with 10% denatured blood serum (YPG + DS) for 5 days at 28 °C. Spores were harvested and counted. **(B)** Spores were observed directly by light microscopy (40 ×). Bar: 10 µm. **(C)** Spore size was determined by measuring 100 spores for each condition. **(D)** The mRNA levels from *cnaA* were quantified by RT-qPCR in spores produced under different conditions, and a ΔCt analysis was performed to compare the transcript levels of *cnaA*. Figures show the average of three independent experiments. Statistically significant differences are indicated by different letters (ANOVA and Fisher's tests; $p \leq 0.05$).

the experimental protocols (trade number 06–13/2016). Blood samples were collected from healthy male volunteers. All enrolled volunteers signed written informed consent form.

2.5. Mouse- and Caenorhabditis elegans-killing assays

Spore virulence of *Mucor circinelloides* was assessed in mice as described previously [24], with minor modifications. Briefly, male BALB/c mice (12–16 weeks old, weighing ~20 g) were treated with streptozotocin (200 mg/kg; Sigma, USA) to induce a diabetic state (≥250 mg/dL glucose). Each group of mice (n = 6 mice each) was inoculated with 2×10^7 spores from *Mucor circinelloides* by intraperitoneal injection.

Virulence assays using the nematode *Caenorhabditis elegans* Bristol N2 [25] were performed as described previously [8]. For each experiment, 10–20 worms in L1 stage were dispensed into each well of a 24-well plate (Costar; Corning, Inc., Corning, NY, USA), followed by incubation with 1000 spores obtained from different conditions with 1 mL YPG medium. The plates were then incubated at 18 °C for 48 h, and live worms were scored at 12, 24, and 48 h. For statistical purposes, two replicates per experiment were used. YPG medium was used as a negative control. A worm was considered dead when it no longer responded to a touch stimulus. Any worm that died because of sticking to the plate wall was excluded from the analysis. Three independent assays were conducted for each worm group.

2.6. Macrophage spore killing assays

Mouse RAW267.4 monocytes/macrophages (TIB-71) were purchased from American Type Culture Collection (Manassas, VA, USA). Cells were maintained in Dulbecco's modified Eagle's medium (DMEM; Sigma) supplemented with 10% foetal bovine serum (Sigma), 100 U/mL penicillin, and 100 µg/mL streptomycin (basal medium) at 37 °C in an atmosphere containing 5% CO_2 for 24 h before treatment.

Macrophages were seeded at 8×10^5 cells/well in DMEM basal medium without antibiotics and incubated at 37 °C in 6-well plates. After incubation overnight, the basal medium in each well was replaced with fresh medium, and the macrophages were then cocultured with 2×10^5 spores from *Mucor circinelloides* either in YPG medium alone or in YPG medium supplemented with native blood serum or denatured blood serum for 1 or 6 h. Immediately after, the supernatants, cells, and spores were removed and placed in independent tubes. Then, cells and spores were centrifuged at 2000 × *g* for 5 min. Pellets were recovered and frozen until nucleic acid extraction.

2.7. Image analysis

An Olympus CKX41 microscope equipped with a 40 × objective lens and a DMC-T25 camera (Panasonic, Kadoma, Japan) was used to capture images of spores or spore germination. Hyphal lengths and spore sizes were determined using QCapture Pro 7 and Leica Application Suite software.

2.8. Statistical analysis

All data, including virulence assays, were evaluated using analysis of variance (ANOVA). Fisher's tests were used for analysis. Differences with *p* values of less than or equal to 0.05 were considered significant.

3. Results

3.1. Effects of blood serum on spore production by Mucor circinelloides

Spore production in a host increases the virulence of various fungi [14–17]. Accordingly, in this study, *Mucor circinelloides* strain R7B was sporulated on plates containing YPG medium supplemented with or without native blood serum at 10%. We used a serum concentration similar to those used for experiments in *Candida albicans* [26]. Our data indicated that spore production was higher (63.1%) in plates containing native blood serum compared with that in plates without native blood serum (Fig. 1A). In order to determine whether the increased spore production involved a thermolabile compound found in the native blood serum, the serum was denatured by heating at 55 °C for 12 h and used under the same conditions as the native blood serum. The results showed that medium supplemented with denatured serum significantly increased the number of spores (25.2%) when compared with spores produced in medium alone (Fig. 1A). However, a significant decrease in the number of spores was observed on medium supplemented with denatured serum (37.9%) when compared with that in medium

supplemented with native blood serum (Fig. 1A).

Spores produced in the presence of native or denatured blood serum (Fig. 1B) were larger (16–17%; 11.45 and 11.5 µm, respectively; Fig. 1C) than spores produced in YPG alone (9.84 µm; Fig. 1B and C). In *Mucor circinelloides*, the mutation of *cnaA*, which encodes the catalytic subunit of the calcium-dependent phosphatase calcineurin, is related to increased sporangiospore size [7]. To determine whether *cnaA* expression was modified by native or denatured blood serum, we quantified *cnaA* mRNA levels. The results showed that the mRNA levels of *cnaA* from spores produced in the presence of native (15.5%) or denatured (11.9%) blood serum were altered compared with those from spores produced in YPG alone (Fig. 1D). Thus, spores from native or denatured blood serum did not decrease *cnaA* mRNA levels, suggesting that another molecular element could affect the spore size produced in the presence of blood serum.

3.2. Aerobic germination of spores from Mucor circinelloides produced in the presence of blood serum

In order to elucidate whether spores produced on YPG supplemented with native or denatured blood serum germinated at similar rates relative to spores produced on YPG medium, aerobic germination was measured. Our data indicated that the spores produced on medium supplemented with native blood serum germinated faster (31.8%) after 2 h than that with spores produced on YPG medium alone (Fig. 2A). Moreover, spores produced from denatured blood serum germinated at a rate similar to that of spores produced in YPG after 2 h of growth (Fig. 2A).

Furthermore, the hyphal length of germinules derived from spores produced on YPG medium supplemented with native blood serum was longer (average: 27.6 µm) compared with either the hyphae generated from spores produced from YPG supplemented with denatured blood serum (12.9 µm) or YPG medium alone (7.2 µm) after 2 h of growth (Fig. 2B and C). Additionally, mRNA of *pkaR1*, which accumulates more in hyphae than spores [20], was quantified by RT-qPCR during germination of spores produced under different conditions. Our results showed that accumulation of *pkaR1* mRNA in hyphae cells after 2 h of growth was higher for spores produced on YPG medium supplemented with native blood serum than for spores produced on YPG medium alone (~50%) or supplemented with denatured blood serum (~36%; Fig. 2D). These results showed that native blood serum induced faster aerobic germination with longer hyphae in *Mucor circinelloides*.

3.3. Effects of Mucor circinelloides spores produced in the presence of blood serum on virulence

Faster spore germination leads to higher rates of virulence in *Mucor circinelloides* [7]. In order to elucidate whether spores produced on YPG supplemented with native or denatured blood serum improved the virulence ability of *Mucor circinelloides*, spores produced from different conditions were used to treat *Caenorhabditis elegans* nematodes. Our results showed that spores produced from YPG medium alone or supplemented with denatured blood serum were not able to affect the viability of the nematodes in the time analysed (Fig. 3A). In contrast, observation of spores produced from native blood serum at the end of the experiment resulted in a significant 30% increase in death in the nematode population compared with spores produced under other conditions (Fig. 3A).

Virulence assays using streptozotocin-induced diabetic mice were carried out by intraperitoneal injection of 2×10^7 spores/mouse from spores obtained under different conditions. Mouse death was not induced by this treatment under our conditions tested. At 15 days after infection with the different spores, the mice were euthanised, and their livers and lungs were removed. *tfc-1* gene levels were then quantified as an indicator of fungal burden using qPCR. *tfc-1* levels were higher in the liver (146%) and lungs (84%) from mice infected with spores produced from YPG medium supplemented with native blood serum compared with that of spores produced on medium alone (Fig. 3B). Notably, *tfc-1* levels were similar between tissues of mice infected with spores produced from medium supplemented with denatured blood serum or medium alone (Fig. 3B).

Moreover, mRNA levels of general inflammation markers, i.e., *IL-6*, *IL-1β*, *MIP-2* and *TNF-α*, were then quantified by RT-qPCR in tissues from mice infected with the spores from *M. circinelloides* produced

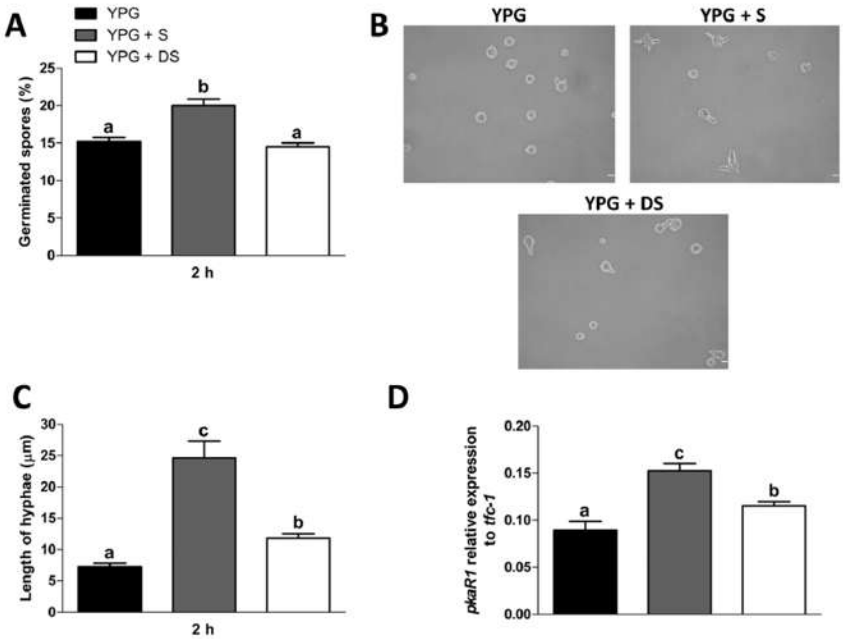

Fig. 2. Aerobic germination of spores from *Mucor circinelloides* produced in blood serum. **(A)** Spores produced from YPG, YPG supplemented with native blood serum (YPG + S), or YPG supplemented with denatured (YPG + DS) blood serum were germinated in YPG liquid medium (5×10^5 spores/mL) for 2 h. Cells were then observed, and germination represented the spores that had germinated independent of the number of hyphae or their length per mother cell. **(B)** Spores produced under different conditions germinated in YPG liquid medium for 2 h were observed directly by light microscopy (40×). Bar: 10 µm. **(C)** Hyphal length (100 hyphae per condition) was determined from spores produced under different conditions germinated after 2 h of growth. **(D)** mRNA levels of *pkaR1* were quantified by RT-qPCR for spores produced under different conditions after 2 h of aerobic growth. ΔCt analysis was performed to compare the transcript levels of *pkaR1*. Figures show the average of three independent experiments. Statistically significant differences are indicated by different letters (ANOVA and Fisher's tests; $p \leq 0.05$).

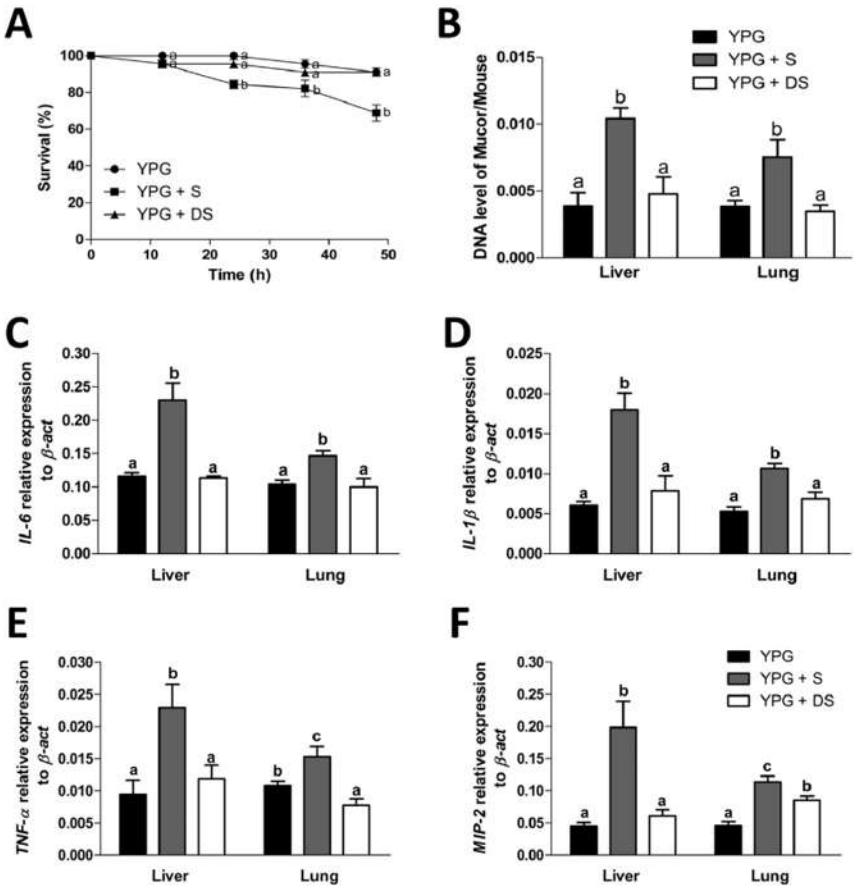

Fig. 3. Virulence of the spores from *Mucor circinelloides* produced in blood serum. (A) Spores produced in YPG, YPG + S, or YPG + DS were germinated in YPG medium in presence of 20 nematodes. Nematode death was evaluated at the indicated times. (B) Fungal burden was quantified by qPCR using *tfc-1* from *M. circinelloides* in mouse tissues analysed 15 days after infection with the respective spores obtained under different conditions. ΔCt analysis was performed to compare the gene expression levels of *tfc-1* between samples. mRNA levels of the inflammation markers (C) *IL-6*, (D) *IL-1β*, (E) *TNF-α*, and (F) *MIP-2* were determined by RT-qPCR from mouse tissues infected with the corresponding spores at 15 days after infection. ΔCt analysis was performed to compare the mRNA levels between samples. Figures show the average of three independent experiments. Statistically significant differences are indicated by different letters (ANOVA and Fisher's tests; $p \leq 0.05$).

under different conditions. The mRNA levels of these inflammatory markers were higher in the liver (91–300%) and lungs (50–200%) of mice infected with spores produced on YPG supplemented with native blood serum compared with that of mice infected with spores produced in YPG supplemented with or without denatured blood serum (Fig. 3C–F). Our results indicated that infection of mice with spores produced on medium supplemented with native blood serum induced an increase in the systemic inflammatory response in the analysed tissues.

3.4. Effects of stressors and macrophage phagocytosis on the viability of spores from Mucor circinelloides produced on blood serum

In order to investigate the physiological implications of higher virulence rates from spores produced in YPG supplemented with native blood serum, the effects of oxidative stress and thermotolerance at 37 °C on spore germination were then evaluated.

The spores produced on YPG supplemented with native blood serum germinated significantly better in at 37 °C, yielding 25.7% and 37.5% more colony forming units (CFUs) than those from YPG supplemented with denatured blood serum or YPG alone, respectively (Fig. 4A). Moreover, spores produced from native blood serum grew significantly better in the presence of 4 mM H_2O_2, yielding 12.2% and 76.6% more CFUs compared with those from YPG supplemented with denatured blood serum or YPG alone, respectively (Fig. 4A). Our results indicated that the addition of native blood serum enhanced the thermotolerance and stress factor resistance of spores from *Mucor circinelloides*.

The peroxisome is one of the most important organelles for detoxifying H_2O_2 [27]. *PEX3* encodes a peroxosimal integral membrane protein involved in peroxisome biogenesis in *S. cerevisiae* [28] and mammals [29]. We identified Pex3 in the *M. circinelloides* genome, and used the protein sequence to compared with two PEX 3 homologs already described, human [30] and yeast [31]. Pex3 from *M. circinelloides* showed 35.7 and 32.2% of similarity, with the human and yeast homologs, respectively (Fig. S1). Accordingly, *pex3* mRNA levels were then quantified by RT-qPCR. *pex3* mRNA was upregulated (33.2% and 76.7%) in the mycelium of spores produced from native blood serum grown for 4 h in YPG compared with that in the mycelium of spores generated from denatured blood serum or YPG alone, respectively (Fig. 4B). This result suggested that native blood serum induced the generation of peroxisomes in *Mucor circinelloides*.

Fungal resistance to H_2O_2 correlates with increased resistance to macrophage phagocytosis [32]. In order to determine whether spores produced from YPG supplemented with blood serum could influence resistance to macrophage phagocytosis in *Mucor circinelloides*, corresponding phagocytosis experiments were conducted with murine RAW264.7 macrophages. After 1 h of incubation with macrophages, fungal spores produced from all conditions were observed in the interior of macrophages (Fig. 5A). Subsequent quantification of spore germination during macrophage interactions based on mRNA levels of the mycelium marker *pkaR1* [20] showed that spores produced from YPG medium with native blood serum increased the mRNA levels of *pkaR1* (by 111.1% and 131%) after 1 h of interaction compared with that in spores produced from either medium supplemented with

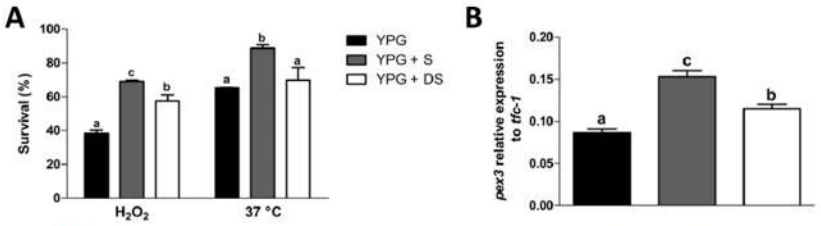

Fig. 4. Effects of stressors on the viability of spores from *Mucor circinelloides* produced in blood serum. (A) Spores produced on YPG, YPG + S, or YPG + DS were incubated with or without 4 mM H_2O_2 at 28 °C. Alternatively, spores produced under different conditions were incubated at 37 or 28 °C. Survival was determined from colonies grown for 24 h by dividing the number of colonies in treated samples by the number of colonies for untreated samples. (B) The mRNA levels of *pex3* were determined by RT-qPCR for spores produced under different conditions. ΔCt analysis was performed to compare mRNA and gene expression levels between samples. Statistically significant differences are indicated by different letters (ANOVA and Fisher's tests; $p \leq 0.05$).

denatured blood serum or medium alone, respectively (Fig. 5B). After 1 h of spore incubation with macrophages, fewer spores (~5269 spores) produced from native blood serum were killed by macrophages compared with the number of spores produced from denatured blood serum (~19,121 spores) or from YPG alone (~24,330; Fig. 5C). Moreover, after 6 h of spore/macrophage interactions, significantly fewer spores produced from native blood serum were killed by macrophages (~106,484 spores) compared with those from denatured blood serum (~158,092 spores) or YPG medium alone (~168,366; Fig. 5C). Thus, these results suggested that in *Mucor circinelloides*, spores produced from native blood serum were resistant to spore killing, potentially through an oxidative resistance mechanism.

4. Discussion

Mucor circinelloides has been shown to have the potential to infect humans and animals under certain conditions, e.g., in immunosuppressed patients [6]. Interestingly, our study showed that *Mucor circinelloides* grown in medium supplemented with blood serum increased sporulation compared with that grown on YPG alone, suggesting that components of native blood serum are responsible of this increase. In order to determine whether the increased spore production involved a thermolabile compound, the serum was denatured by heating, and the level of sporulation was analysed. Our results showed that denaturalisation of blood serum decreased spore production levels, suggesting that molecules present in the blood serum were degraded after incubation under denaturing conditions (55 °C for 12 h). Cell growth factors, such as transforming growth factor β1, nerve growth factor, and calcitonin gene-related peptide, and some plasma proteins may be denatured after incubation at 50–55 °C for 2 h [19,33]. Moreover, some growth factors or proteins present in the blood serum participate in regulating *Mucor circinelloides* physiology, resulting in increased spore production. Additionally, we found that spores produced in the presence of native or denatured blood serum were slightly larger than spores produced in YPG alone; therefore, we next determined whether blood serum modified *cnaA* mRNA levels. Mutations in the gene encoding catalytic subunit calcineurin A (*cnaA*) produced larger, more virulent spores compared with those produced by the wild-type strain with reduced size [7]. However, the results showed that the mRNA level of *cnaA* was not decreased in spores produced in the presence of blood serum, suggested that blood serum and *cnaA* regulated the sizes of spores through a different mechanism.

Next, we evaluated whether native or denatured blood serum could modify the rates of spore germination. Spores that were produced from native blood serum increased the germination rate and correlated with increased *pkaR1* mRNA levels, a transcript that accumulates more in hyphae than spores [20], compared with that in other spores. These results suggested that a thermolabile component in the blood serum favoured faster aerobic germination. Indeed, denatured blood serum induced a germination rate similar to that of spores produced in medium alone. Notably, in other fungal systems, spores produced in different media germinate at different rates; for example, in *Metarhizium robertsii*, spores produced on minimal medium germinate faster than those produced on complex rich medium [34]. In several fungi,

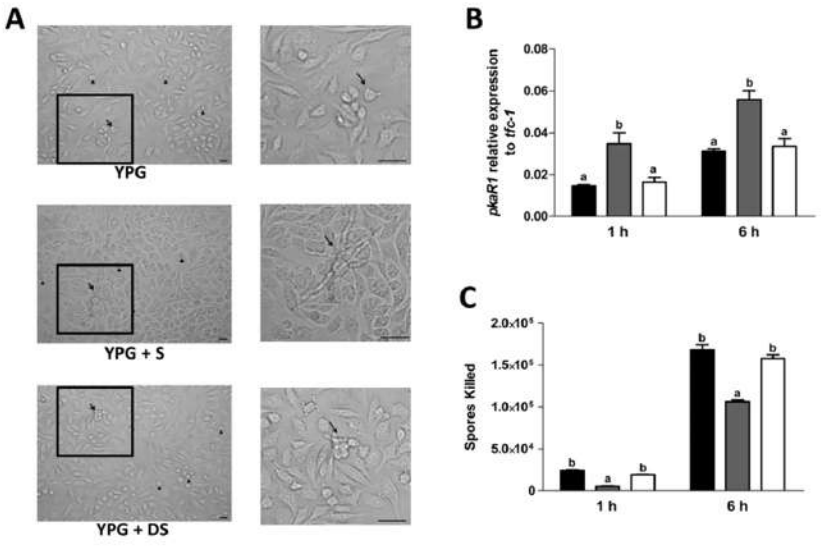

Fig. 5. Macrophage phagocytosis of spores produced on blood serum. Macrophages were seeded at 8×10^5 cells/well in DMEM basal medium were co-cultured with 2×10^5 spores from *Mucor circinelloides* produced either on YPG, YPG + S, or YPG + DS for 1 or 6 h. (A) Germination of spores with macrophage interactions were observed under direct observation by light microscopy (40×). Bar: 20 μm. Arrows indicate germinating hyphae, and arrowheads indicate swelling spores. Rectangular regions show amplification of the images to the right in order to depict spore germination. (B) *pkaR1* mRNA levels were quantified by RT-qPCR at 1 or 6 h after initiation of spore and macrophage interactions. ΔCt analysis was performed to compare mRNA and gene expression levels between samples. (C) Quantification of killed spores by qPCR using *tfc-1* after 1 or 6 h of incubation with mouse macrophages. Figures show the average of three independent experiments. Statistically significant differences are indicated by different letters (ANOVA and Fisher's tests; $p \leq 0.05$).

including *Mucor circinelloides* [7] and *Metarhizium anisopliae* [35], faster germination is correlated with increased virulence. These data indicated that the blood serum may enhance the germination rate of spores of *Mucor circinelloides* and suggested that thermolabile components from human blood elicited the induction of virulent traits in *Mucor circinelloides*. In entomopathogens, such as *B. bassiana* [14] and *Metarhizium anisopliae* [15], and phytopathogens, such as *F. oxisporum* [17], passages through the host or components of the host enhance virulent genetic traits. For example, conidia from *Metarhizium robertsii* produced on minimal medium germinated faster, had increased heat tolerance, and were more virulent to insects than those from complex medium [34]. In *Mucor circinelloides*, an epigenetic mechanism could be involved during the interaction with components from the host, as has been described in several pathogens with their respective hosts, including fungal models such as *Candida albicans* [36].

We found that spores produced on native blood serum, in addition to being thermotolerant, were also more resistant to the presence of H_2O_2, which also correlates with reduced macrophage killing. This perhaps is due to the increased peroxisome proliferation in *Mucor circinelloides*, as we detected more *pex3* mRNA than in spores produced either on denatured blood serum or YPG alone. The *pex3* gene encodes a peroxosimal integral membrane protein involved in peroxisome biogenesis in *S. cerevisiae* [31] and mammals [30]. In many fungal pathogens, such as the phytopathogens *Colletotrichum orbiculare* and *Magnaporthe oryzae*, the entomopathogen *Metarhizium robertsii*, and the human pathogens *Candida albicans*, *Aspergillus fumigatus*, and *Cryptococcus neoformans*, peroxisomes are required for virulence [37].

Moreover, we evaluated the effects of spore production in the presence of blood serum on the virulence of *Mucor circinelloides*. We observed that blood serum increased the virulence of spores of *Mucor circinelliodes* on *C. elegans* and increased fungus proliferation in lung and liver tissues of mice compared with that of mice infected with spores produced in YPG supplemented with or without denatured blood serum. Moreover, mRNA levels of general inflammation markers, such as *IL-6*, *IL-1β*, *MIP-2*, and *TNF-α*, were increased in mouse tissues after infection by spores produced on native blood serum. *IL-6* is a general response chemokine involved in inflammatory processes [38]; *IL-1β* is an important chemokine involved in cellular inflammatory responses and apoptosis [39]; *MIP*-2 mRNA expression is influenced by liver injury [40]; and *TNF-α* is a pro-inflammatory cytokine expressed in response to tissue damage [41]. From our results, we concluded that spores produced on native blood serum were able to increase the invasion of mouse tissues and induce a stronger systemic inflammatory response.

The influence of blood and serum on transcriptional regulation of virulence has been reported for several bacterial pathogens, including the bacteria *Bordetella bronchiseptica* [42] and *Staphylococcus aureus* [43]. In *Candida albicans*, a fungal model in which the effects of blood serum have been thoroughly studied with regard to morphogenesis and virulence, blood stimulates the conversion from yeast to hyphal growth [44], increases biofilm formation [45], and stimulates the transcription of genes involved in the antioxidant response [46].

We still do not know the chemical nature of the molecules present in the blood serum that are involved in increased virulence on *Mucor circinelloides*. Moreover, the functions of components of the blood serum in the pathogenesis of Mucorales are still unclear, although patients with increased serum levels of available iron have been shown to be more susceptible to mucormycosis [47]. Therefore, it is important to describe blood serum molecules that regulate the virulence of *M. circinelloides* and the signalling pathways that are controlled by these blood serum molecules.

5. Conclusion

In this study, we found that sporulation by *Mucor circinelloides* in the presence of native blood serum significantly affected spore production and stimulated the virulence of the fungus. Further studies in our laboratory are underway to determine the chemical nature of the molecules in the blood serum that are involved in the increase in virulence in this Mucoral. In addition, knowledge of these molecules could provide insights into the signalling pathways involved in this process.

Conflicts of interest

The authors declare that they have no conflicts of interest regarding this study.

Author contributions

JA P-M, D V-T, V A-C, MI V-M, IE J-G, RE N-A, and R O-A participated in data acquisition and data interpretation; J V-M, RE N-A, MI R-D and R O-A provided reagents and participated in critical analysis, data interpretation, and revision of the article for intellectual content; R O-A and V M-C participated in the conception and design of the study, data analysis and interpretation, and drafting of the article.

Acknowledgments

We would like to thank to SEP-CONACYT, México (grant no. CB-2011-01-167071) and CIC/UMSNH, Mxico (grant no. 2.36) for partially funding this project. JA P-M, D V-T, V A-C, and MIV-M were postgraduate students with CONACyT scholarship.

Appendix A. Supplementary data

Supplementary data to this article can be found online at https://doi.org/10.1016/j.micpath.2019.103737.

References

[1] B. Spellberg, J. Edwards Jr., A. Ibrahim, Novel perspectives on mucormycosis: pathophysiology, presentation, and management, Clin. Microbiol. Rev. 18 (2005) 556–569.
[2] Y. Song, J. Qiao, G. Giovanni, G. Liu, H. Yang, J. Wu, J. Chen, Mucormycosis in renal transplant recipients: review of 174 reported cases, BMC Infect. Dis. 17 (2017) 283.
[3] H. Prakash, A.J. Chakrabarti, Global Epidemiology of Mucormycosis, Fungi (Basel) vol. 5, (2019), p. E26 pii.
[4] W. Jeong, C. Keighley, R. Wolfe, W.L. Lee, M.A. Slavin, D.C.M. Kong, S.C. Chen, The epidemiology and clinical manifestations of mucormycosis: a systematic review and meta-analysis of case reports, Clin. Microbiol. Infect. 25 (2018) 26–34.
[5] A. Skiada, F. Lanternier, A.H. Groll, L. Pagano, S. Zimmerli, R. Herbrecht, O. Lortholary, G.L. Petrikkos, Diagnosis and treatment of mucormycosis in patients with hematological malignancies: guidelines from the 3rd European Conference on Infections in Leukemia (ECIL 3), Haematologica 98 (2013) 492–504.
[6] M.I.A. Hassan, K. Voigt, Pathogenicity patterns of mucormycosis: epidemiology, interaction with immune cells and virulence factors, Med. Mycol. 1 (57) (2019) S245–S256.
[7] S.C. Lee, A. Li, S. Calo, J. Heitman, Calcineurin plays key roles in the dimorphic transition and virulence of the human pathogenic zygomycete *Mucor circinelloides*, PLoS Pathog. 9 (2013) e1003625.
[8] J.A. Patiño-Medina, G. Maldonado-Herrera, C. Pérez-Arques, V. Alejandre-Castañeda, N.Y. Reyes-Mares, M.I. Valle-Maldonado, J. Campos-García, R. Ortíz-Alvarado, I.E. Jácome-Galarza, M.I. Ramírez-Díaz, V. Garre, V. Meza-Carmen, Control of morphology and virulence by ADP-ribosylation factors (Arf) in *Mucor circinelloides*, Curr. Genet. 64 (2018) 853–869.
[9] M.I. Navarro-Mendoza, C. Pérez-Arques, L. Murcia, P. Martínez-García, C. Lax, M. Sanchis, J. Capilla, F.E. Nicolás, V. Garre, Components of a new gene family of ferroxidases involved in virulence are functionally specialized in fungal dimorphism, Sci. Rep. 8 (2018) 7660.
[10] J.A. Patiño-Medina, M.I. Valle-Maldonado, G. Maldonado-Herrera, C. Pérez-Arques, I.E. Jácome-Galarza, C. Díaz-Pérez, A.L. Díaz-Pérez, C.A. Araiza-Cervantes, J.C. Villagomez-Castro, J. Campos-García, M.I. Ramírez-Díaz, V. Garre, V. Meza-Carmen, Role of Arf-like proteins (Arl1 and Arl2) of *Mucor circinelloides* in virulence and antifungal susceptibility, Fungal Genet. Biol. 129 (2019) 40–51.
[11] G. Nagy, C. Szebenyi, Á. Csernetics, A.G. Vaz, E.J. Tóth, C. Vágvölgyi, T. Papp, Development of a plasmid free CRISPR-Cas9 system for the genetic modification of *Mucor circinelloides*, Sci. Rep. 7 (2017) 16800.
[12] S. Vellanki, M.I. Navarro-Mendoza, A. Garcia, L. Murcia, C. Perez-Arques, V. Garre, F.E. Nicolas, S.C. Lee, *Mucor circinelloides*: growth, maintenance, and genetic manipulation, Curr Protoc Microbiol 49 (2018) e53.

[13] A. Garcia, S. Vellanki, S.C. Lee, Genetic tools for investigating Mucorales fungal pathogenesis, Curr Clin Microbiol Rep 5 (2018) 173–180.
[14] C.A. Valero-Jiménez, J.A.L. van Kan, C.J.M. Koenraadt, B.J. Zwaa, S.E. Schoustra, Experimental evolution to increase the efficacy of the entomopathogenic fungus *Beauveria bassiana* against malaria mosquitoes: effects on mycelial growth and virulence, Evol Appl 10 (2017) 433–443.
[15] M. Adames, M. Fernández-Ruvalcaba, G. Peña-Chora, V.M. Hernández-Velázquez, Effects of passages through a suitable host of the fungus, *Metarhizium anisopliae*, on the virulence of acaricide-susceptible and resistant strains of the tick, *Rhipicephalus microplus*, J. Insect Sci. 11 (1) (2011) 21.
[16] J. Breen, L. Mur, A. Sivakumaran, A. Akinyemi, M. Wilkinson, C.M. Rodriguez-Lopez, *Botrytis Cinerea* Loss and Restoration of Virulence during in Vitro Culture Follows Flux in Global DNA Methylation, (2016) 059477bioRxiv.
[17] B. Wang, C.L. Brubaker, W. Tate, M.J. Woods, J.J. Burdon, Evolution of virulence in *Fusarium oxysporum f. sp.* vasinfectum using serial passage assays through susceptible cotton, Phytopathology 98 (2008) 296–303.
[18] M.I.G. Roncero, L.P. Jepsen, P. Strøman, R. van Heeswijck, Characterization of a *leuA* gene and an ARS element from *Mucor circinelloides*, Gene 84 (1989) 335e343.
[19] J.C. Bradley, J. Simoni, R.H. Bradley, D.L. McCartney, S.M. Brown, Time- and temperature-dependent stability of growth factor peptides in human autologous serum eye drops, Cornea 28 (2009) 200–205.
[20] M.I. Valle-Maldonado, I.E. Jácome-Galarza, F. Gutiérrez-Corona, M.I. Ramírez-Díaz, J. Campos-García, V. Meza-Carmen, Selection of reference genes for quantitative real time RT-PCR during dimorphism in the zygomycete *Mucor circinelloides*, Mol. Biol. Rep. 42 (2015) 705–711.
[21] J. Ocampo, L. Fernandez Nuñez, F. Silva, E. Pereyra, S. Moreno, V. Garre, S. Rossi, A subunit of protein kinase A regulates growth and differentiation in the fungus *Mucor circinelloides*, Eukaryot. Cell 8 (2009) 933–944.
[22] L.M. Corrochano, A. Kuo, M. Marcet-Houben, S. Polaino, A. Salamov, Villalobos-Escobedo, J. Grimwood, M.I. Alvarez, J. Avalos, D. Bauer, E.P.I. Benito, G. Burger, L.P. Camino, D. Canovas, E. Cerda-Olmedo, J.F. Cheng, A. Dominguez, M. Elias, A.P. Eslava, F. Glaser, G. Gutierrez, J. Heitman, B. Henrissat, E.A. Iturriaga, B.F. Lang, J.L. Lavin, S.C. Lee, W. Li, E. Lindquist, S. Lopez-Garcia, E.M. Luque, A.T. Marcos, J. Martin, K. McCluskey, H.R. Medina, A. Miralles-Duran, A. Miyazaki, E. Munoz-Torres, J.A. Oguiza, R.A. Ohm, M. Olmedo, M. Orejas, L. Ortiz-Castellanos, A.G. Pisabarro, J. Rodriguez-Romero, J. Ruiz-Herrera, R. Ruiz-Vazquez, C. Sanz, W. Schackwitz, M. Shahriari, E. Shelest, F. Silva-Franco, D. Soanes, K. Syed, V.G. Tagua, N.J. Talbot, M.R. Thon, H. Tice, R.P. de Vries, A. Wiebenga, J.S. Yadav, E.L. Braun, S.E. Baker, V. Garre, J. Schmutz, B.A. Horwitz, S. Torres-Martinez, A. Idnurm, A. Herrera-Estrella, T. Gabaldon, I.V. Grigoriev, Expansion of signal transduction pathways in fungi by extensive genome duplication, Curr. Biol. 12 (2016) 1577–1584.
[23] Secretaría de de Agricultura, Ganadería, Desarrollo Rural, Pesca y Alimentación (SAGARPA) NORMA Oficial Mexicana NOM-062- ZOO-1999. Especificaciones técnicas para la producción, cuidado y uso de los animales de laboratorio, Diario Oficial de la Federación 2 (2001) 107–167 (In Spanish).
[24] E. Rodríguez-Andrade, K.C. Hernández-Ramírez, S.P. Díaz-Peréz, A. Díaz-Magaña, M.P. Chávez-Moctezuma, V. Meza-Carmen, R. Ortíz-Alvarado, C. Cervantes, M.I. Ramírez-Díaz, Genes from pUM505 plasmid contribute to *Pseudomonas aeruginosa* virulence, Antonie Leeuwenhoek 109 (2016) 389–396.
[25] S. Brenner, The genetics of *Caenorhabditis elegans*, Genetics 77 (1974) 71–94.
[26] C. Sánchez-Martínez, J. Pérez-Martín, Gpa2, a G-protein alpha subunit required for hyphal development in *Candida albicans*, Eukaryot. Cell 1 (2002) 865–874.
[27] J.J. Smith, J.D. Aitchison, Peroxisomes take shape, Nat. Rev. Mol. Cell Biol. 1 (2013) 803–817.
[28] J. Höhfeld, M. Veenhuis, W.H. Kunau, PAS3, a *Saccharomyces cerevisiae* gene encoding a peroxisomal integral membrane protein essential for peroxisome biogenesis, J. Cell Biol. 114 (1991) 1167–1178.
[29] K. Ghaedi, S. Tamura, K. Okumoto, Y. Matsuzono, Y. Fujiki, The peroxin pex3p initiates membrane assembly in peroxisome biogenesis, Mol. Biol. Cell 11 (6) (2000) 2085–2102.
[30] M. Soukupovaa, C. Sprengera, K. Gorgasb, W.-H. Kunaua, G. Dodt, Identification and characterization of the human peroxin PEX3, Eur. J. Cell Biol. 78 (1999) 357–374.
[31] E.H. Hettema, W. Girzalsky, M. van der Berg, R. Erdmann, B. Distel, *Saccharomyces cerevisiae* Pex3p and Pex19p are required for proper localization and stability of peroxisomal membrane proteins, EMBO J. 19 (2) (2000) 223–233.
[32] M. Sasada, R.B. Johnston Jr., Macrophage microbicidal activity. Correlation between phagocytosis-associated oxidative metabolism and the killing of *Candida* by macrophages, J. Exp. Med. 152 (1980) 85–98.
[33] R. Vazquez, D.F. Larson, Plasma protein denaturation with graded heat exposure, Perfusion 28 (2013) 557–559.
[34] D.E. Rangel, G.U. Braga, É.K. Fernandes, C.A. Keyser, J.E. Hallsworth, D.W. Roberts, Stress tolerance and virulence of insect-pathogenic fungi are determined by environmental conditions during conidial formation, Curr. Genet. 61 (2015) 383–404.
[35] C.E. Morales-Hernández, I.E. Padilla Guerrero, G.A. Gonzalez Hernandez, Catalase overexpression reduces the germination time and increases the pathogenicity of the fungus *Metarhizium anisopliae*, Appl. Microbiol. Biotechnol. 87 (2010) 1033.
[36] E. Gómez-Díaz, M. Jordà, M.A. Peinado, A. Rivero, Epigenetics of host-pathogen interactions: the road ahead and the road behind, PLoS Pathog. 8 (2012) e1003007.
[37] X.L. Chen, Z. Wang, C. Liu, Roles of peroxisomes in the rice blast fungus, BioMed Res. Int. 2016 (2016) 9343417.
[38] M. Rincon, Interleukin-6: from an inflammatory marker to a target for inflammatory diseases, Trends Immunol. 11 (2012) 571.
[39] K. Ren, R. Torres, Role of interleukin-1beta during pain and inflammation, Brain Res. Rev. 1 (2009) 57–64.
[40] C.C. Qin, Y.N. Liu, Y. Hu, Y. Yang, Z. Chen, Macrophage inflammatory protein-2 as mediator of inflammation in acute liver injury, World J. Gastroenterol. 17 (2017) 3043–3052.
[41] N.M. Wheelhouse, Y.S. Chan, S.E. Gillies, H. Caldwell, J.A. Ross, D.J. Harrison, S. Prost, TNF-alpha induced DNA damage in primary murine hepatocytes, Int. J. Mol. Med. 6 (2003) 889–894.
[42] M.C. Gestal, I. Rivera, L.K. Howard, K.K. Dewan, I.H. Soumana, M. Dedloff, T.L. Nicholson, B. Linz, E.T. Harvill, Blood or serum exposure induce global transcriptional changes, altered antigenic profile, and increased cytotoxicity by classical bordetellae, Front. Microbiol. 9 (2018) 1969.
[43] Y. Oogai, M. Matsuo, M. Hashimoto, F. Kato, M. Sugai, H. Komatsuzawa, Expression of virulence factors by *Staphylococcus aureus* grown in serum, Appl. Environ. Microbiol. 77 (2011) 8097–8105.
[44] Q. Feng, E. Summers, B. Guo, G. Fink, Ras signaling is required for serum-induced hyphal differentiation in *Candida albicans*, J. Bacteriol. 181 (1999) 6339–6346.
[45] Y.H. Samaranayake, B.P. Cheung, J.Y. Yau, S.K. Yeung, L.P. Samaranayake, Human serum promotes Candida albicans biofilm growth and virulence gene expression on silicone biomaterial, PLoS One 8 (2013) e62902.
[46] C. Fradin, M. Kretschmar, T. Nichterlein, C. Gaillardin, C. D'Enfert, B. Hube, Stage-specific gene expression of *Candida albicans* in human blood, Mol. Microbiol. 47 (2003) 1523–1543.
[47] A.S. Ibrahim, B. Spellberg, T.J. Walsh, D.P. Kontoyiannis, Pathogenesis of mucormycosis, Clin. Infect. Dis. 54 (Suppl 1) (2012) S16–S22.

PLOS ONE

RESEARCH ARTICLE

Heterotrimeric G-alpha subunits Gpa11 and Gpa12 define a transduction pathway that control spore size and virulence in *Mucor circinelloides*

J. Alberto Patiño-Medina[1☯], Nancy Y. Reyes-Mares[1☯], Marco I. Valle-Maldonado[1], Irvin E. Jácome-Galarza[2], Carlos Pérez-Arques[3], Rosa E. Nuñez-Anita[4], Jesús Campos-García[1], Verónica Anaya-Martínez[5], Rafael Ortiz-Alvarado[6], Martha I. Ramírez-Díaz[1], Soo Chan Lee[7], Victoriano Garre[3], Víctor Meza-Carmen[1]*

1 Instituto de Investigaciones Químico Biológicas, Universidad Michoacana de San Nicolás de Hidalgo (UMSNH), Morelia, Michoacán, México, **2** Departamento de Biología Molecular, Laboratorio Estatal de Salud Pública del Estado de Michoacán, Morelia, Michoacán, México, **3** Departamento de Genética y Microbiología, Facultad de Biología, Universidad de Murcia, Murcia, España, **4** Facultad de Medicina Veterinaria y Zootecnia, Universidad Michoacana de San Nicolás Hidalgo, Morelia, Michoacán, Mexico, **5** Facultad de Ciencias de la Salud, Universidad Anáhuac, Naucalpan de Juarez, Estado de México, México, **6** Facultad de Químico Farmacobiología, Universidad Michoacana de San Nicolás de Hidalgo, Morelia, Michoacan, México, **7** Department of Biology, South Texas Center of Emerging Infectious Diseases (STCEID), University of Texas at San Antonio, San Antonio, Texas, United States of America

☯ These authors contributed equally to this work.
* victor_meza2004@yahoo.com.mx

Citation: Patiño-Medina JA, Reyes-Mares NY, Valle-Maldonado MI, Jácome-Galarza IE, Pérez-Arques C, Nuñez-Anita RE, et al. (2019) Heterotrimeric G-alpha subunits Gpa11 and Gpa12 define a transduction pathway that control spore size and virulence in *Mucor circinelloides*. PLoS ONE 14(12): e0226682. https://doi.org/10.1371/journal.pone.0226682

Editor: Sung-Hwan Yun, Soonchunhyang University, REPUBLIC OF KOREA

Received: April 3, 2019

Accepted: December 3, 2019

Published: December 30, 2019

Data Availability Statement: All relevant data are within the manuscript and its Supporting Information files.

Funding: V M-C, MI R-D Coordinación de la Investigación Científica, Universidad Michoacana de San Nicolás de Hidalgo, México (2.6, 2.35). https://www.cic.umich.mx V M-C, MI R-D, J C-G Consejo Nacional de Ciencia y Tecnología, México (CONACYT; 181747, 167071, and 256119).

Abstract

Mucor circinelloides is one of the causal agents of mucormycosis, an emerging and high mortality rate fungal infection produced by asexual spores (sporangiospores) of fungi that belong to the order Mucorales. *M. circinelloides* has served as a model genetic system to understand the virulence mechanism of this infection. Although the G-protein signaling cascade plays crucial roles in virulence in many pathogenic fungi, its roles in Mucorales are yet to be elucidated. Previous study found that sporangiospore size and calcineurin are related to the virulence in *Mucor*, in which larger spores are more virulent in an animal mucormycosis model and loss of a calcineurin A catalytic subunit CnaA results in larger spore production and virulent phenotype. The *M. circinelloides* genome is known to harbor twelve *gpa* (*gpa1* to *gpa12*) encoding G-protein alpha subunits and the transcripts of the *gpa11* and *gpa12* comprise nearly 72% of all twelve *gpa* genes transcript in spores. In this study we demonstrated that loss of function of Gpa11 and Gpa12 led to larger spore size associated with reduced activation of the calcineurin pathway. Interestingly, we found lower levels of the *cnaA* mRNAs in sporangiospores from the Δ*gpa12* and double Δ*gpa11*/Δ*gpa12* mutant strains compared to wild-type and the Δ*cnaA* mutant had significantly lower *gpa11* and *gpa12* mRNA levels compared to wild-type. However, in contrast to the high virulence showed by the large spores of Δ*cnaA*, the spores from Δ*gpa11*/Δ*gpa12* were avirulent and produced lower tissue invasion and cellular damage, suggesting that the *gpa11* and *gpa12* define a signal pathway with two branches. One of the branches controls spore size through regulation of calcineurin pathway, whereas virulences is controlled by an independent

https://www.conacyt.gob.mx V G Fundación Séneca-Agencia de Ciencia y Tecnología de la Región de Murcia, Spain (19339/PI/14). https://www.fseneca.es The funders had no role in study design, data collection and analysis, decision to publish, or preparation of the manuscript.

Competing interests: The authors have declared that no competing interests exist.

pathway. This virulence-related regulatory pathway could control the expression of genes involved in cellular responses important for virulence, since sporangiospores of Δ*gpa11*/Δ*gpa12* were less resistant to oxidative stress and phagocytosis by macrophages than the Δ*cnaA* and wild-type strains. The characterization of this pathway could contribute to decipher the signals and mechanism used by Mucorales to produce mucormycosis.

Introduction

Mucor circinelloides is a basal fungus that belongs to the Phylum Zygomycota [1]. This organism produces three types of spores, zygospores are produced by mating of hyphae of opposite sex: (+) and (-). Arthrospores are generated by hyphae in submerged cultures after the end of the exponential growth or under unfavorable growth conditions. Sporangiospores are produced by asexual reproduction on solid substrate in large number [2, 3]. Several growth conditions determine whether *M. circinelloides* sporangiospores (spores) will produce mycelium or yeast; the most well-studied being the presence of carbon source and atmospheric conditions during spore germination [4–6]. *M. circinelloides* is one of the etiological agents of the mucormycosis, a fungal infection that affects mainly immunocompromised patients [7–8]. This infection has called medical attention as its incidence has risen worldwide recently [9–11], and relatively high mortality rates have been reported [12–13]. In this sense, the fate of vegetative cells in *M. circinelloides* has implications for infectiveness, as the mycelial stage usually shows virulent morphology [14–15], while the yeast morphology is less virulent [15]. Furthermore, the ability to germinate of the Mucorales sporangiospores in the immunocompromised patient is a critical step for stablishing the infection [12, 16].

Larger spores lead to a faster germination rate that, in turn, correlates with a more virulent phenotype in *M. circinelloides* [17]. Spore size in *M. circinelloides* is controlled in part by CnaA, which is the catalytic subunit A of the phosphatase Ca^{+2}-dependent calcineurin [15]. We have previously described that ADP-ribosylation factor-1 (Arf1) dysfunction also increases spore size and virulence and generates defects during the aerobic growth in *M. circinelloides* [18]. Moreover, additional molecular regulators of dimorphism in *M. circinelloides* have been reported. Thus, deletion of the calcineurin regulatory subunit CnbB-encoding gene promotes the yeast rather than mycelial form, even in the presence of oxygen, and this mutant is less virulent compared to its wild-type form [15]. Additionally, deletion of *arf2* leads to difficulty in the generation of the yeast morphology [18]. In fungi, the protein kinase A (PKA) pathway is a key signaling pathway that controls spore production, spore germination, resistance to different stress conditions, and virulence [19]; deletion of *pkaR1*, which encodes a regulatory subunit 1 of PKA, leads to a decrease in spore production and shorter hyphae length after yeast-mycelium transition in *M. circinelloides* [20].

Heterotrimeric G proteins are regulators of the PKA pathway, and their canonical functions are involved in the control of the activity of several effectors; for example, adenylyl cyclase, lipid modifying enzymes like phospholipase C, and ion channels [21–22]. In the ascomycetes *Aspergillus nidulans* and *A. parasiticus*, the Gα subunit FadA stimulates the cAMP levels leading to the activation of the PkaC subunit, which ultimately controls the gene transcription involved in sporulation [23–24].

Our group previously reported that the largest number of members of genes encoding heterotrimeric G proteins in the Fungi kingdom is present in *M. circinelloides* [25]. The twelve Gα-encoding genes (*gpa*1-12) were grouped into three (I-III) of the four groups of the Gα

fungal phylogenetic classification [25–26]. In *M. circinelloides*, Gpa11 and Gpa12, which belong to group I ($G\alpha_s$) and group III ($G\alpha_i$), respectively, showed increased transcript levels during the spore stage (~69% of the total *gpa* transcript levels), suggesting that these genes have an important role in spore production or germination in this Mucoral [25]. However, the molecular role of these subunits in spore function is still unknown.

The aim of this work was to functionally characterize the role of the heterotrimeric Gα subunits Gpa11 and Gpa12 in sporulation and vegetative growth and determine their role in the virulence of *M. circinelloides*.

Results

Deletion of *gpa11* and *gpa12* in *M. circinelloides*

M. circinelloides exhibits twelve Gα subunits (Gpa1-Gpa12). The mRNA of two of these subunits, Gpa11 and Gpa12, have been reported to accumulate mainly in the spore stage and decrease during vegetative growth [25]. To determine whether these genes are relevant to spore physiology, we created *gpa11 and gpa12* deletion mutants. Replacement fragments of *gpa11* and *gpa12* that contained 5′ upstream and 3′ downstream regions from *gpa11* or *gpa12* flanking the selective marker *pyrG* were used to transform protoplasts of the *M. circinelloides* wild-type strain MU402 (*leuA*$^-$, *pyrG*$^-$), which is auxotrophic for leucine and uracil [27], to generate *gpa11* and *gpa12* deletion strains (Fig 1). Transformants grown in selective medium (MMC) were recovered and subsequent vegetative cycles in selective medium were performed to obtain homokaryotic Δ*gpa11* and Δ*gpa12* mutants. After 5 cycles of vegetative growth/

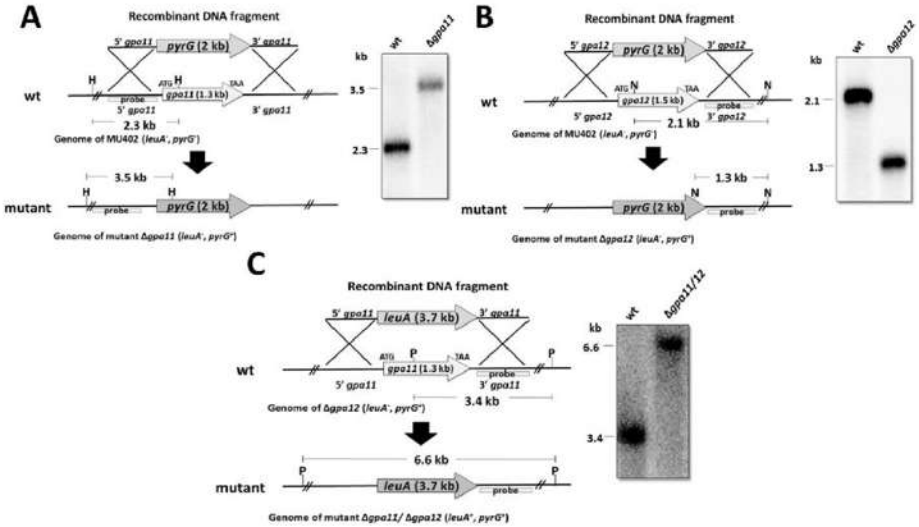

Fig 1. Deletion of *gpa11* and *gpa12* in *M. circinelloides* confirmed by Southern-blot. A) *gpa11*; B) *gpa12*; and C) *gpa11/gpa12* deletion. The 5′ and 3′ regions (1.1 kb for each) upstream and downstream from the start and stop codons, respectively, of *gpa11* or *gpa12* were designed to flank the *pyrG* selection marker for gene deletion (A and B). For the deletion of *gpa11* in Δ*gpa12*, the 5′ and 3′ regions (1.1 kb for each) upstream and downstream from the start and stop codons, respectively, of *gpa11* were designed to flank *leuA* (C). For each diagram, the recombinant fragments that were used to transform protoplasts of the strain MU402 (*pyrG*$^-$, *leuA*$^-$) are shown. Molecular confirmation by Southern blotting was performed using specific probes for each *gpa* gene. DNA samples from transformed and parental (MU402) strains were digested with the indicated restriction enzymes (H, *Hin*cII; N, *Nco*I; P, *Pvu*II).

https://doi.org/10.1371/journal.pone.0226682.g001

sporulation, we obtained two independent transformants for *gpa11* and four for *gpa12* that showed 100% Ura$^+$ spores, confirming the homokaryosis.

The presence of 2.3-kb and 3.5-kb hybridization fragments in wild-type and Δ*gpa11*, respectively; confirmed the presence of a unique integration event in the desired locus, and homokaryosis of the *gpa11* deletant (Fig 1A). Meanwhile, the presence of 2.1-kb and 1.3-kb hybridization fragments in wild-type and *gpa12*, respectively revealed the mutation in *gpa12* (Fig 1B).

A mutant lacking both genes was generated by transformation of the Δ*gpa12* strain with a replacement fragment containing the selective marker *leuA* flanked by 5′ upstream and 3′ downstream regions of *gpa11*. Transformants grown in selective media (without uracil and leucine) were characterized by Southern blot hybridization. A 6.6-kb hybridization band in the selected transformant confirmed the presence of a unique integration event in the desired locus and the homokaryosis of the double Δ*gpa11*/Δ*gpa12* knockout mutant (Fig 1C).

Expression analysis of *gpa11* and *gpa12* in spores generated from single and double knock-out mutants confirmed the null expression of those genes (Fig 2).

For the further analysis, we used two independent strains for each gene mutation revealing similar results for these independent strains in all experiment tested. Furthermore, single Δ*gpa11* and Δ*gpa12* mutant strains were complemented with their respective wild-type gene by

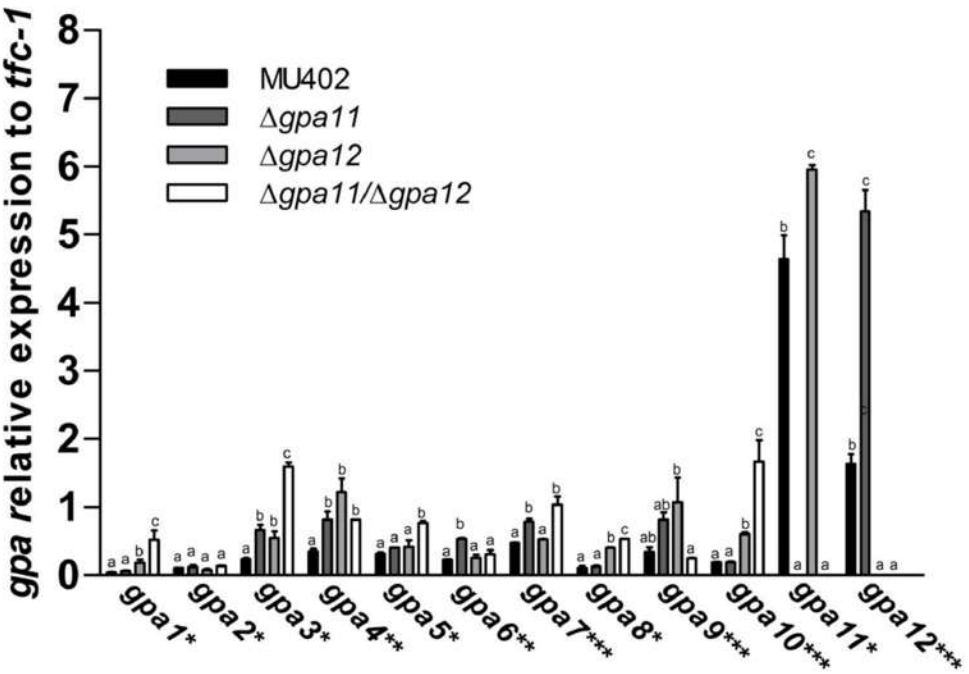

Fig 2. mRNA quantitation of *gpa* genes in sporangiospores in *gpa11* and *gpa12* deletion mutants of *M. circinelloides*. Total RNA was isolated from spores of the wild-type, Δ*gpa11*, Δ*gpa12*, and Δ*gpa11*/Δ*gpa12*. The mRNA from each *gpa* gene was determined by qRT-PCR. Asterisks denote the phylogenetic group of the Gpa proteins in *M. circinelloides* (* I; ** -II, and *** -III) [25]. Four independent experiments were performed under the same conditions. Different letters denote statistically significant differences (ANOVA, Fisher, $p<0.05$).

https://doi.org/10.1371/journal.pone.0226682.g002

expression in the pEUKA4 vector [28] generating the Δ*gpa11*+*gpa11*wt and Δ*gpa12*+*gpa12*wt strains.

Interestingly, the single mutation of each *gpa* gene provoked a significant upregulation of the other. Thus, deletion of *gpa11* led to an ~30% increase in *gpa12* mRNA levels, while deletion of *gpa12* resulted in an ~226% increase of *gpa11* mRNA levels, suggesting a compensatory mechanism (Fig 2, S1 Table). Moreover, single deletion of *gpa11* and *gpa12* led to a significant increase in the mRNA levels of several *gpa* genes. The expression of some *gpa* genes was increased more than two folds in Δ*gpa11* (*gpa3*, *gpa4*, *gpa6*, *gpa9*, and *gpa12*), and in Δ*gpa12* (*gpa1*, *gpa3*, *gpa4*, *gpa8*, *gpa9*, and *gpa10*) (Fig 2, S1 Table). In addition, deletion of both genes led to a further rise in mRNA levels of some *gpa* genes, including *gpa1* (~11.73 folds), *gpa3* (~6.8 folds), and *gpa8* (~4.78 folds), which encode proteins that belong to group I of the Gα phylogenetic fungal classification ($G\alpha_s$). Also, the mRNA levels of a gene, *gpa10*, encoding a protein belonging to group III ($G\alpha_i$) of the phylogenetic fungal classification was highly increased (~8.77 folds) in the double-*gpa* mutant strain (Fig 2, S1 Table).

Gpa11 and Gpa12 are involved in sporangiospore size and germination rate in *M. circinelloides*

In order to investigate the physiological role of *gpa11* and *gpa12*, radial growth and spore production of the different strains were assessed. The radial growth of all the mutant strains was similar to the wild-type strain at the end of the experiment (Fig 3A). After 5 days of incubation, there was around 42–46% decrease in spore production in all single and double mutant strains compared to the wild-type strain (Fig 3B), indicating that both genes participate in spore production. Additionally, the Δ*gpa12* strain produced slightly less spores compared to other mutant strain. The Δ*gpa11*+*gpa11*wt and Δ*gpa12*+*gpa12*wt complemented strains did not show significant difference in spore production compared to the wild-type strain.

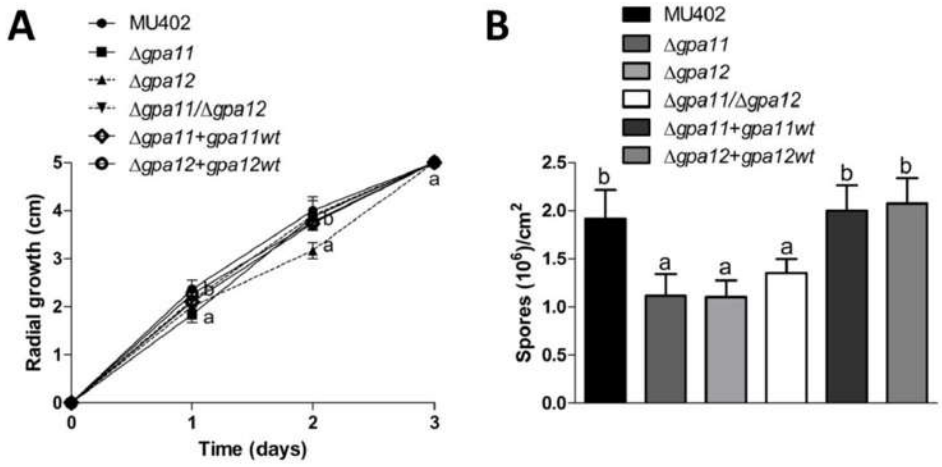

Fig 3. Sporangiospore production in Δ*gpa11* and Δ*gpa12* mutants of *M. circinelloides*. 50 spores were grown in YPG agar plates and A) radial growth was recorded each day during the experiment. B) Spores grown after 5 days were counted. Four independent experiments were performed for each condition. Statistically significant differences are indicated by different letters (ANOVA and Fisher's tests; $p \leq 0.05$).

https://doi.org/10.1371/journal.pone.0226682.g003

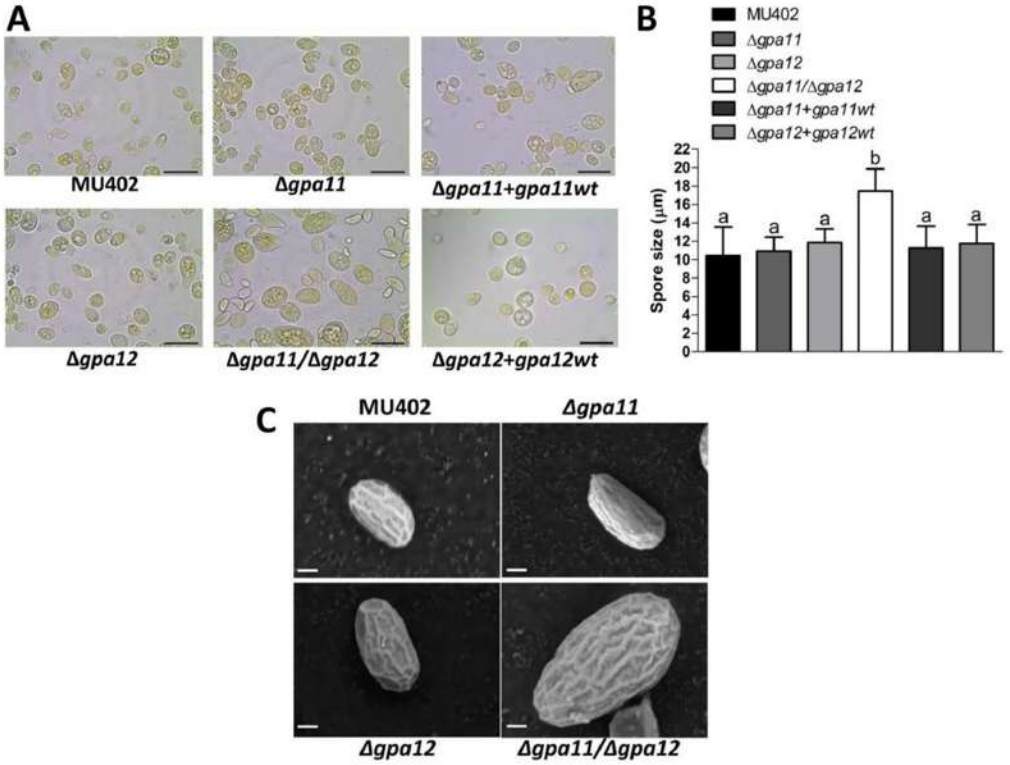

Fig 4. Influence of *gpa11* and *gpa12* on sporangiospore size in *M. circinelloides*. The spores from the different *M. circinelloides* knockout strains produced in YPG were observed under A) light microscope (100 X), scale bar equal to 20 μm. B) The spore size of each strain was quantified using the Leica Application Suite. C) The spores obtained after five days of incubation on solid YPG media were observed under scanning electron microscope. Representative photographs from the corresponding strains of *M. circinelloides* under 10,000 magnifications. Scale bar is equal to 1 μm. Statistically significant differences are indicated by different letters (ANOVA and Fisher's tests; $p \leq 0.05$).

https://doi.org/10.1371/journal.pone.0226682.g004

The spores produced on YPG media were observed by light microscopy. The spores from the Δ*gpa11* mutant strain were morphologically similar (in size) to those produced from the wild-type strain (on average 10.3 and 10.2 μm, respectively) (Fig 4). While the Δ*gpa12* spores were slightly larger than those of the wild-type strain, at 11.4 μm diameter on average. Interestingly, the Δ*gpa11*/Δ*gpa12* mutant strain generated the largest spore size, compared to the rest of the strains, at 16.3 μm diameter on average (Fig 4), but some of them were up to 20 μm of size. Interestingly, the Δ*gpa11*+*gpa11*wt and Δ*gpa12*+*gpa12*wt complemented strains showed similar size as the wild-type strain (Fig 4A and 4B). The spore size was also evaluated by scanning electron microscopy, confirming that the spores from the Δ*gpa11*/Δ*gpa12* mutant were larger than those of the other strains and all had a similar surface shape (Fig 4C). Similar results in terms of spore size were observed with independent *gpa* mutant strains (S1 Fig).

It has been described in *M. circinelloides* that an increase in spore size correlates with a faster aerobic germination rate [17]. To confirm this assumption, we measured the germination rate of the different strains grown in YPG. The double *gpa*-mutant strain had a 50% higher germination rate after 2 h of growth compared to the wild-type strain (Fig 5A).

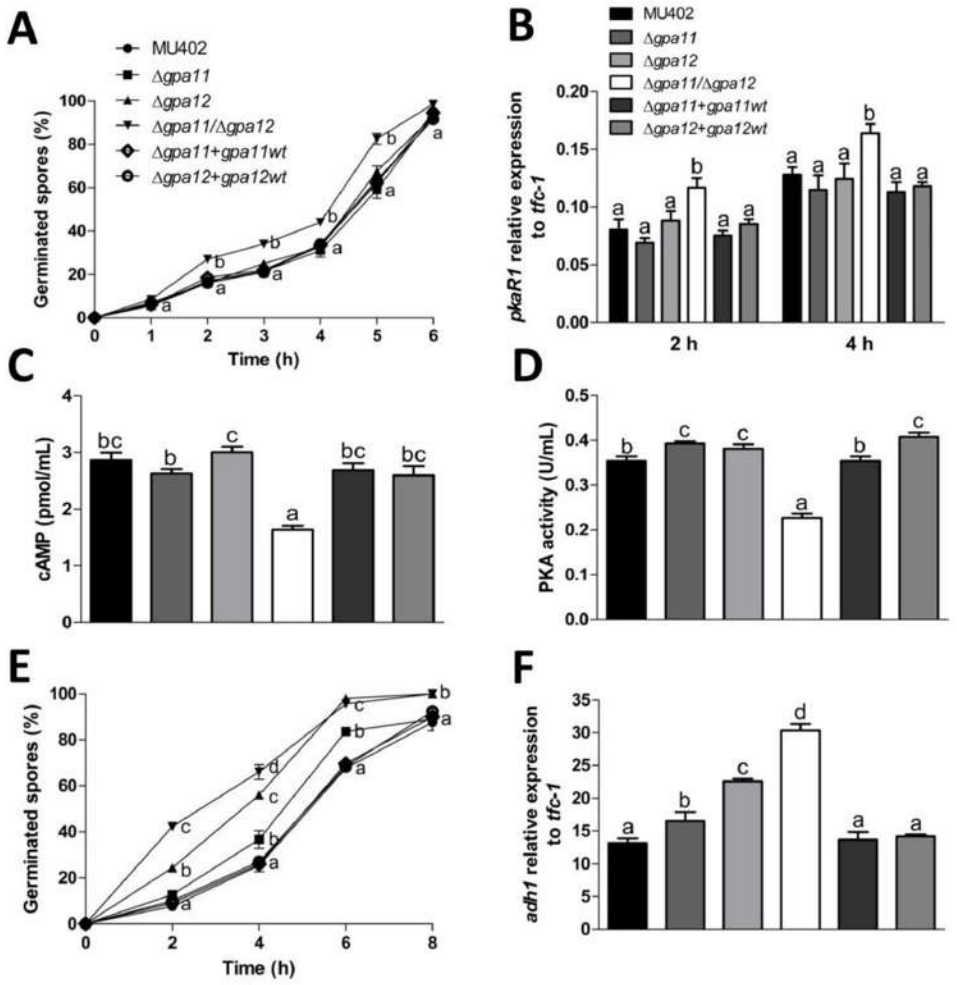

Fig 5. Sporangiospore germination of *M. circinelloides gpa11* and *gpa12* deletion mutants. A) Percentage of germinated spores in aerobic conditions from each strain in YPG. Aerobic germinated cells were considered independent of hyphae length or number of mother cells. B) Relative expression of *pkaR1*, quantified by qRT-PCR using *tfc-1* as reference gene from hyphae obtained from each strain grown at 2 and 4 h. ΔCT analysis was performed to compare the mRNA levels between strains. Spores from the different strains from *M. circinelloides* were inoculated into YPG media and incubated with constant shaking (150 rpm) for 3 h, and C) intracellular cAMP levels, and D) PKA activity were determined. E) Percentage of spores germinated under anaerobic conditions in YPG media. F) Relative expression of *adh1* determined from yeast cells at 4 h of growth, ΔCT analysis was performed to compare mRNA levels between strains. Four independent experiments were performed for each condition. Statistically significant differences are indicated by different letters (ANOVA and Fisher's tests; $p \leq 0.05$).

https://doi.org/10.1371/journal.pone.0226682.g005

However, both single *gpa*-mutant and complemented strains germinated at very similar rates to the wild-type strain (Fig 5A).

Aerobic germination was corroborated using the gene marker *pkaR1*, which is a gene expressed preferentially during hyphae growth compared to the yeast or spore stage [29]. Only

the Δ*gpa11*/Δ*gpa12* mutant strain accumulated significantly more *pkaR1* mRNA observed in the germinating spores after 2 (40%) and 4 h (28%) in YPG with respect to other strains (Fig 5B). The higher mRNA levels of *pkaR1* in the Δ*gpa11*/Δ*gpa12* mutant strain suggest a repression in the PKA pathway. To probe this hypothesis, we conducted the quantification of cAMP levels and PKA activity in the different strains after 3 h of aerobic germination. In correlation with the mRNA levels, the only strain that showed lower cAMP levels and PKA activity was the Δ*gpa11*/Δ*gpa12* mutant strain, meanwhile the rest of the strains showed similar levels as the wild-type strain (Fig 5C and 5D).

Germination rate under anaerobic conditions revealed that Δ*gpa12* and Δ*gpa11*/Δ*gpa12* mutants germinated faster than the Δ*gpa12*, complemented and wild-type strains. The double *gpa*-mutant strain demonstrated a higher rate of germination (5.52 folds) after 2 h compared to the wild-type strain (Fig 5E). The mRNA levels of *adh1*, which is preferentially expressed during anaerobic growth [29–30], were significantly higher in Δ*gpa11* (21%), Δ*gpa12* (71%) and Δ*gpa11*/Δ*gpa12* (130%) strains after 4 h of growth compared to the wild-type strain (Fig 5F).

These results indicated that the products of *gpa11* and *gpa12* genes are involved in the control of the regulation of sporangiospore size as well as the aerobic and anaerobic germination rates in *M. circinelloides*.

Mutation of *gpa12* and the double mutation of *gpa11* and *gpa12* decreased *cnaA* mRNA levels in sporangiospores in *M. circinelloides*

It has been reported that dysfunction of the calcineurin catalytic subunit A (CnaA) leads to an increase in the spore size of *M. circinelloides* [15]. Based on the larger spore phenotype observed in the Δ*gpa11*/Δ*gpa12* mutant strain, we performed mRNA quantitation by qRT-PCR of *cnaA* in spores and during aerobic germination from *gpa*-mutant strains.

The mRNA levels of *cnaA* in the wild-type and Δ*gpa11* mutant spores were similar to each other, while lower mRNA levels were observed in spores from Δ*gpa12* and Δ*gpa11*/Δ*gpa12* mutants by around 56 and 64% respectively, compared to Δ*gpa11*, Δ*gpa11*+*gpa11*wt, Δ*gpa12*+*gpa12*wt and wild-type strains (Fig 6). Although the mRNA levels of *cnaA* in

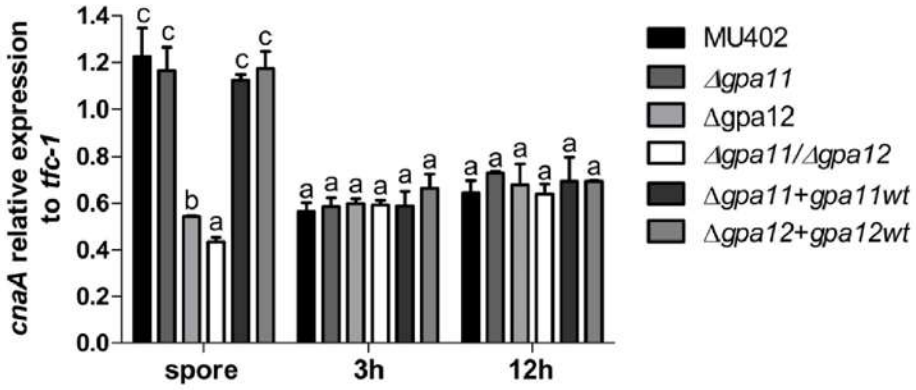

Fig 6. Quantitation of *cnaA* mRNA levels in *M. circinelloides* Δ*gpa11* and Δ*gpa12* mutant strains. Expression of *cnaA* relative to *tfc-1* in total RNA purified from sporangiospores and mycelium grown in aerobic conditions after indicated times in YPG. qRT-PCR was performed to determine the transcript levels of *cnaA* and a ΔCt analysis was performed to compare the mRNA level between the strains. Four independent experiments were performed for each condition. Statistically significant differences are indicated by different letters (ANOVA and Fisher's tests; $p \leq 0.05$).

https://doi.org/10.1371/journal.pone.0226682.g006

mycelium grown for 3 or 12 h in YPG were similar in all strains tested (Fig 6). These results showed that dysfunction of Gpa12 led to down-regulation of *cnaA* mRNA levels in spores of *M. circinelloides*. The lower cnaA expression in Δ*gpa11*/Δ*gpa12* suggested that *gpa11* can partially compensate the absence of *gpa12*.

To investigate if *cnaA* dysfunction affects *gpa11* and *gpa12* mRNA levels during the spore stage, the transcripts of all *gpa* were quantified by qRT-PCR in spores of the Δ*cnaA* mutant form of *M. circinelloides*. The analysis of transcript levels from all *gpa* genes revealed that in the spores from the Δ*cnaA* mutant strain, only *gpa11* and *gpa12* mRNA levels were significantly decreased (61.4 and 57.9%, respectively) compared to the levels from spores of the wild-type (Fig 7). Furthermore, *gpa1*, *gpa2*, *gpa3*, and *gpa8*, whose products belong to group I ($G\alpha_s$), and *gpa4* that belongs to group II showed a significant increase in mRNA levels (1.6–2.3 times) compared to the wild-type (Fig 7, S2 Table). Interestingly, the Δ*gpa11*/Δ*gpa12* mutant strain also showed a significant increase in the mRNA levels of *gpa3*, and *gpa4* (Fig 2). These results suggest a genetic crosstalk between *gpa11*, *gpa12* and *cnaA* gene products.

Activation of the calcineurin pathway is downregulated in Δ*gpa11*/Δ*gpa12* since the dysfunction of Gpa11 and Gpa12 led to the down-regulation of *cnaA* mRNA levels in spores, we investigated if elements downstream of the calcineurin pathway could also be deregulated in *gpa*-mutant strains. In the methylotrophic yeast *Hansenula polymorpha*, the transcription of the gene *ena1*, which encodes a plasma membrane Na^+/K^+-ATPase, is induced by the

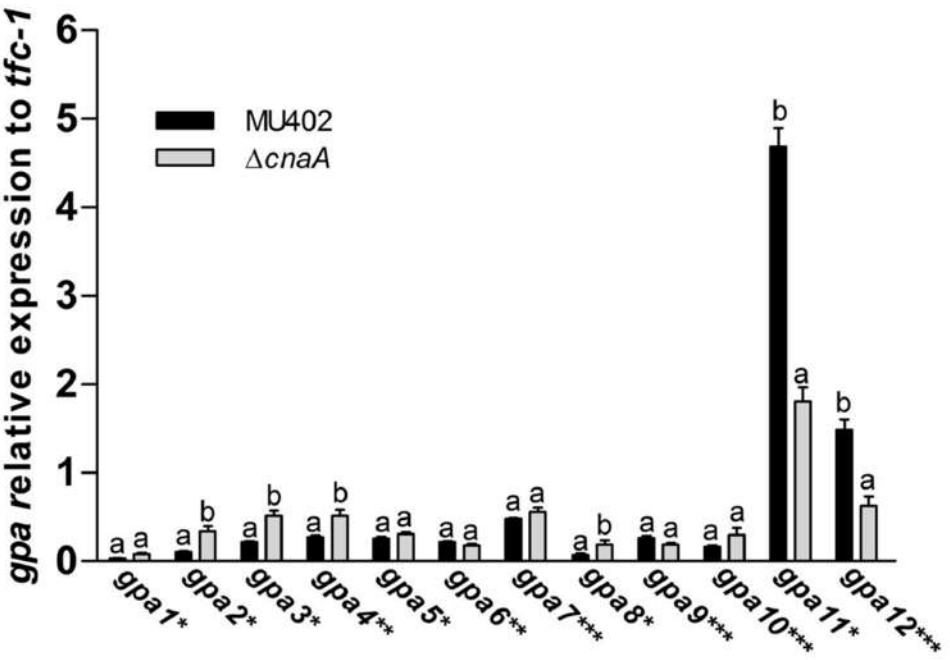

Fig 7. Quantitation of *gpa* mRNA levels in *M. circinelloides* Δ*cnaA*. Changes in levels of mRNA from different *gpa* genes from total RNA purified from sporangiospores of wild-type (closed bars) and Δ*cnaA* (open bars). qRT-PCR was carried out to determine the transcript levels of *gpa* genes, ΔCt analysis was performed to compare the mRNA levels between the strains. Four independent experiments were performed for each condition. Statistically significant differences are indicated by different letters (ANOVA and Fisher's tests; $p \leq 0.05$).

https://doi.org/10.1371/journal.pone.0226682.g007

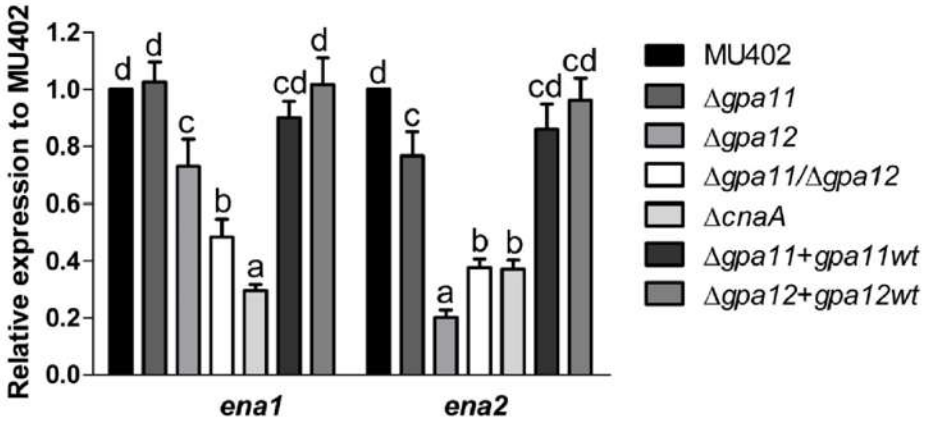

Fig 8. Influence of Gpa11, Gpa12, and CnaA on mRNA levels of *ena* genes in *M. circinelloides*. Levels of A) *ena1* and B) *ena2* measured by qRT-PCR from total mRNA from sporangiospores. ΔΔCt analysis was performed to compare mRNA levels between strains. Four independent experiments were performed for each condition. Different letters denote statistically significant differences (ANOVA, Fisher, $p<0.05$).

https://doi.org/10.1371/journal.pone.0226682.g008

activation of the calcineurin signaling pathway [31]. In order to investigate if a similar scenario could be present in *M. circinelloides*, we quantified the mRNA levels of *ena* homologues in spores from all strains. Firstly, we identified in *M. circinelloides* two Ena homologues, Ena1 and Ena2, with 35.8 and 35.3% identity and 59.2 and 51.6% similarity, respectively, to Ena1 from *H. polymorpha* and 63.1 and 77.3% identity and similarity between them (S2 Fig). The mRNA levels of *ena1* and *ena2* from spores of Δ*cnaA* mutant strain were 70.5 and 62.8% lower, respectively, compared to those levels of the wild-type strain (Fig 8). In Fig 8, marked under expression of *ena1* was seen in the double *gpa11*/*gpa12* mutant, while for *ena2*, loss of *gpa12* alone already leads to low expression. For both *ena1* and *ena2*, loss of *gpa11* alone does not have a large effect though it is significant already for *ena2*. In general, this result indicates that *ena1* and *ena2* mRNA levels are under control of CnaA and Gpa12 in *M. circinelloides*.

To determine if the calcineurin signaling pathway could be altered in the Δ*gpa11*/Δ*gpa12* mutant strain, a calcineurin inhibitor, FK506 was employed. It had been previously reported that FK506 impaired mycelia growth in the Δ*cnaA* strain [15]. We assessed the capability of spores from the single and double mutant strains in *gpa11* and *gpa12* to develop mycelia growth in the presence of FK506. Our results showed that only the double mutant Δ*gpa11*/Δ*gpa12* strain showed a phenotype similar to that of the Δ*cnaA* strain when grown on a poor nitrogen source (YNB) supplemented with FK506, while *gpa*-single mutant strains showed a phenotype similar to the wild-type strain independent of the nitrogen source (S3A Fig). It has been shown that the *cnaA* mutation also leads to increased sensitivity to detergent in a rich YPD media [15]. Our results showed that Δ*gpa11* and Δ*gpa12* or double *gpa*-mutant strains were also more sensitive to the detergent Triton X-100 than the wild type strain in YPG or YNB media (S3B Fig).

The role of *gpa11* and *gpa12* in the virulence of *M. circinelloides*

The increase in spore size and faster germination rate are associated with virulence increase in *M. circinelloides* [17]. Based on the fact that the spores of Δ*gpa11*/Δ*gpa12* mutant strain are much larger, germinate faster, and cause a decrease in mRNA levels of *cnaA* compared to the

wild-type strain, we performed virulence assays. In the mouse killing assay, diabetic mice were used which simulates one of the risk factors for acquiring mucormycosis [18]. Mice were injected intraperitoneally with 2×10^7 spores/mouse from each strain and mouse survival was monitored each day. Reduced survival was observed only in the Δ*gpa11*+*gpa11*wt, Δ*gpa12*+*gpa12*wt, Δ*cnaA* and wild-type strains. 50 and 75% of the mouse population died after 5 days post-inoculation with the spores from wild-type and Δ*cnaA* strains, respectively (Fig 9A).

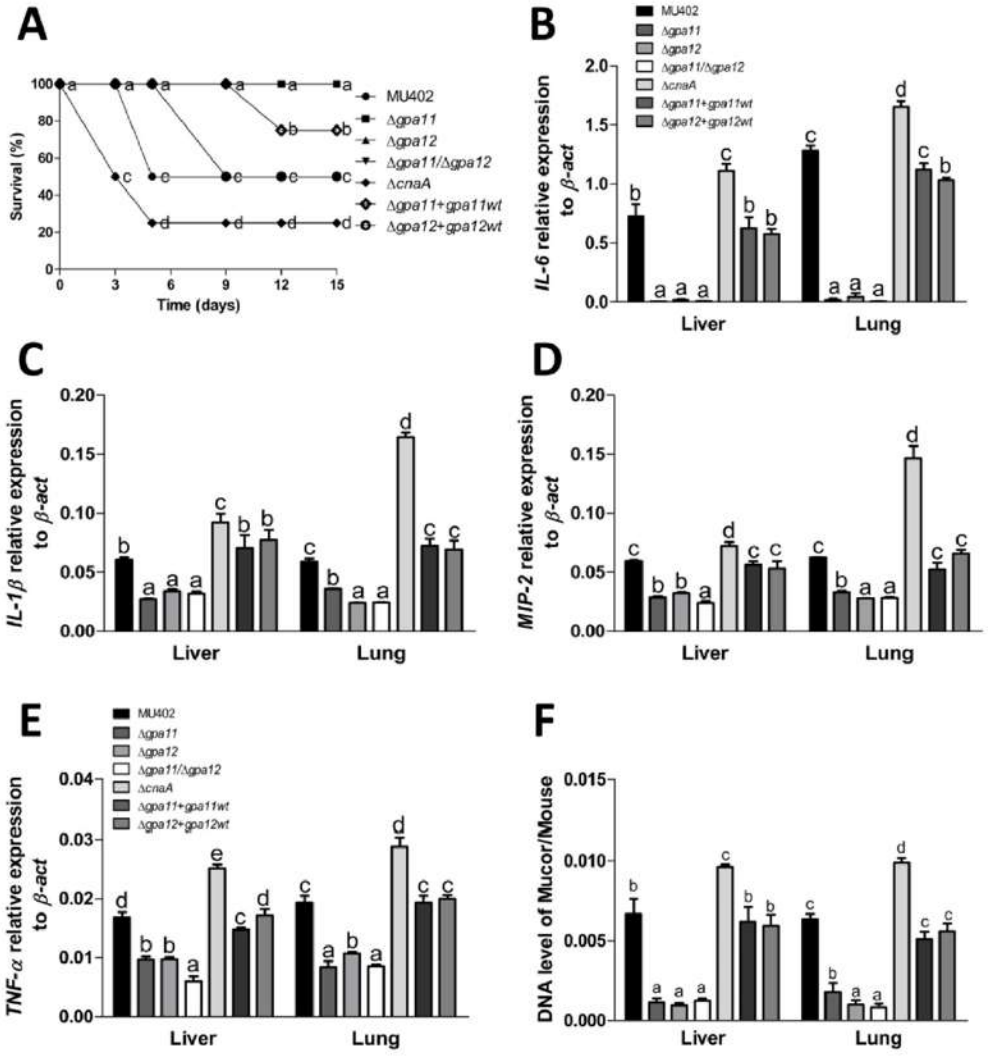

Fig 9. Role of *gpa11* and *gpa12* in the virulence of *M. circinelloides*. A) Survival of diabetic mice infected intraperitoneally with 2×10^7 sporangiospores from different *M. circinelloides* strains recorded each day post-injection. N = 8, two independent experiments. Relative expression of inflammation markers B) *IL-6*, C) *IL-1β*, D) *MIP-2*, E) *TNF-α* used to monitor tissue damage in the liver and lung of mice infected with spores from the different *M. circinelloides* strains (N = 4). F) Fungal burden, determined by qPCR, from the liver and lung of infected mice. Three independent experiments were performed for each condition. Statistically significant differences are indicated by different letters (ANOVA and Fisher's tests; $p \leq 0.05$).

https://doi.org/10.1371/journal.pone.0226682.g009

We quantified by qRT-PCR the mRNA levels of the inflammation markers *IL-6*, *IL-1β*, *MIP-2* and *TNF-α* in the liver and lung of mice infected with the different strains (Fig 9B–9E). The mice infected with the Δ*gpa11*+*gpa11*wt, Δ*gpa12*+*gpa12*wt and wild-type strains, showed significantly increased mRNA levels of *Il-6* (130 times in liver and 124 times in lung), *Il-1β* (96% in liver and 118% in lung), *MIP-2* (115% in liver and 110% in lung) and *TNF-α* (109% in liver and 112% in lung) compared to mRNA levels from animals infected with *gpa*-mutants (Fig 9B–9E). Also, the Δ*cnaA* mutant strain produced significantly higher mRNA levels of all inflammation markers in liver (21–53%) or lung (28–178%) compared to the wild-type strain (Fig 9B–9E). These results indicate that mice infected with the Δ*gpa11*, Δ*gpa12*, or the Δ*gpa11*/Δ*gpa12* mutants induce a weaker inflammatory response compared to those infected with the Δ*cnaA*, Δ*gpa11*+*gpa11*wt and Δ*gpa12*+*gpa12*wt or wild-type strains.

Fungal burden was quantified in tissues (liver and lung) of the mice infected with all the strains by qPCR using the *tfc-1* as gene marker for *M. circinelloides* [29]. The quantity of *tfc-1* from the Δ*gpa11*, Δ*gpa12*, the Δ*gpa11*/Δ*gpa12* mutant strains were lower (up to 82% in liver and 87% in lung) than in those infected with the wild-type strain. Moreover, the Δ*cnaA* strain fungal burden was 26 and 32% more in liver and lung, respectively, compared to the wild-type strain (Fig 9F). These results indicate that mice infected with spores from Δ*gpa11*, Δ*gpa12*, or the Δ*gpa11*/Δ*gpa12* mutant strains induce a weaker inflammatory response and less mouse tissue invasion compared to those infected with the Δ*cnaA*, complemented or wild-type strains.

To explain the mechanism of low virulence of the Δ*gpa11*/Δ*gpa12* spores despite their bigger size, we tested the effect of H_2O_2 on spore survival as previously reported [32, 33]. The Δ*gpa11*, Δ*gpa12*, and the Δ*gpa11*/Δ*gpa12* mutant strains showed a significant decrease in spore survival compared to the wild-type strain in YPG (up to 55%) media supplemented with H_2O_2. The lowest levels of survival were registered for Δ*gpa11*/Δ*gpa12* spores, compared to the wild-type. While Δ*cnaA* strain showed no significant difference in survival rate compared to the wild-type strain (Fig 10A), meanwhile the complemented mutant strains showed similar survival rate as the wild-type strain after the challenged with H_2O_2.

Based on this result, we conducted a confrontation assay with all the *M. circinelloides* strains against the murine macrophage cell line RAW264.7. After 3 h of interaction of macrophages and spores, we observed spore germination in presence of the macrophages (Fig 10B). The germination rate was quantified indirectly by the mRNA levels of *pkaR1* by qRT-PCR, which is used as a molecular marker for hyphae development [28], after 1 or 3 h of macrophage and spore interaction. We observed lower *pkaR1* transcript levels after 1 (≈26%) and 3 h (≈22%) in the single *gpa*-mutant strains compared to the wild-type strain (Fig 10C). The Δ*gpa11*/Δ*gpa12* mutant strain showed the lowest levels of *pkaR1* mRNA after 1 (≈44%) or 3 h (≈45%) compared to the wild-type (Fig 10C), meanwhile the complemented mutant strains showed similar survival rate as the wild-type strain after the challenged with H_2O_2. Based on a standard curve using different amounts of spores from *M. circinelloides*, we quantified by qPCR the *tfc-1* levels from spores that were digested by macrophages after the interaction as described previously [32, 33]. The spores from the Δ*gpa11*+*gpa11*wt, Δ*gpa12*+*gpa12*wt, Δ*cnaA* and wild-type strains showed fewer spores killed after the interaction with the macrophages (Fig 10D) compared to the Δ*gpa11*, Δ*gpa12* and Δ*gpa11*/Δ*gpa12* mutant strains that showed more spores killed in this assay (Fig 10D). These results indicate that the spores from the Δ*gpa11*/Δ*gpa12* mutant strain are the most susceptible to the macrophages compared to the spores from the Δ*cnaA*, Δ*gpa11*+*gpa11*wt, Δ*gpa12*+*gpa12*wt and wild-type strains. This could be explained, in part, by their higher susceptibility to oxidative damage.

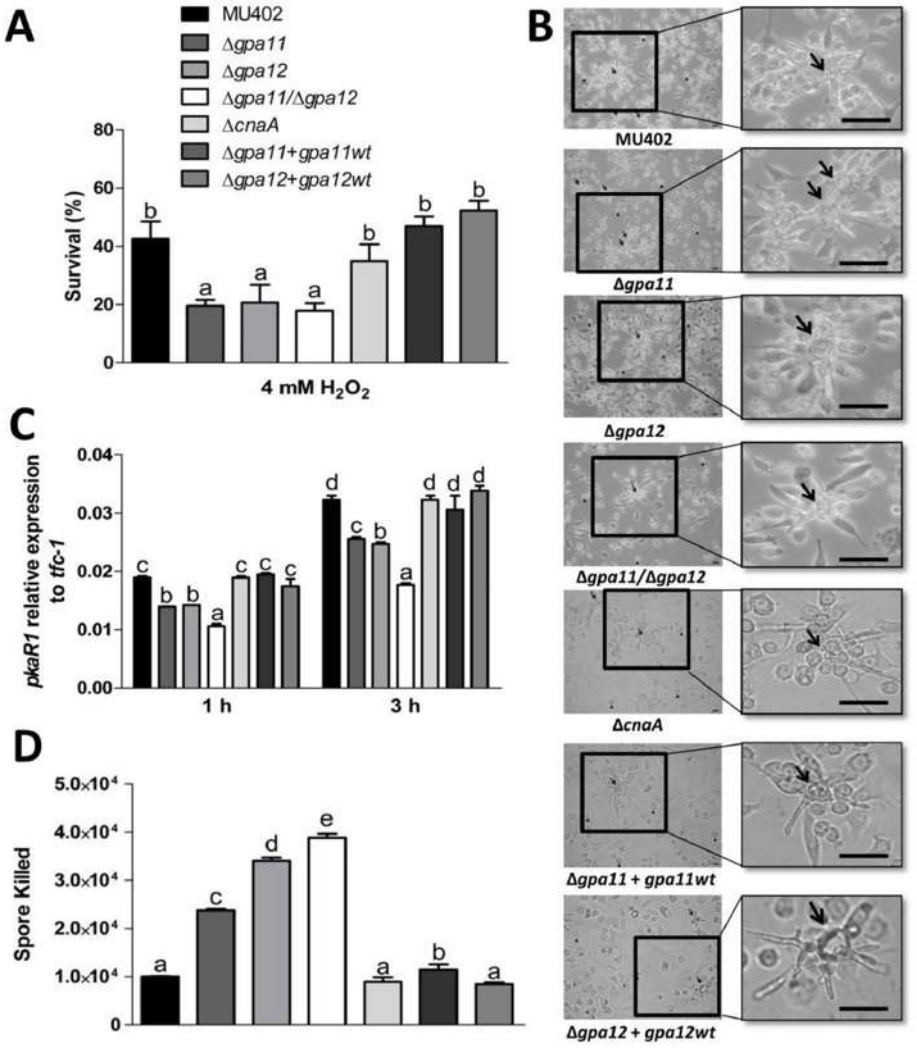

Fig 10. Effect of mutations in *gpa11* and *gpa12* in the viability of sporangiospores from *M. circinelloides* in H_2O_2 and macrophage interaction. A) Spores from different strains were treated or not with 4 mM H_2O_2 and incubated at 28 ˚C on YPG. Survival was obtained from colonies grown for 24 h from the quotient of colonies from treatment versus no treatment. B) Germination of spores during macrophage interaction after 3 h was observed under direct observation by light microscopy (40 X) Scale bar = 20 μm. Arrows indicate germinating hyphae and head of arrows indicate swelling spores. C) The *pkaR1* mRNA levels were quantified by qRT-PCR after 1 and 3 h of spore and macrophage interaction. D) Quantitation of killed spores by qPCR using *tfc-1* after 3 h of incubation with mouse macrophages. A ΔCt analysis was performed to compare the mRNA and gene levels between the samples. Figures show the average of three independent experiments. Statistically significant differences are indicated by different letters (ANOVA and Fisher's tests; $p \leq 0.05$).

https://doi.org/10.1371/journal.pone.0226682.g010

Discussion

M. circinelloides produces several types of spores through its life cycle, and each type of spore has a specific cellular fate [2, 3]. The most well described spore is the sporangiospore, which is

an asexual spore and is produced after the mycelium reaches a certain stage on solid surfaces, producing an aerial structure known as the sporangiophore. Several factors have been described that contribute to sporangiospore production in *M. circinelloides*; for example, light is a positive stimulator of sporulation and carotenogenesis [34]. The detailed molecular mechanism of how sporangiospores are produced in *M. circinelloides* is still not known. Transcript levels from *gpa11* and *gpa12* from *M. circinelloides*, have been shown to mainly accumulate in the sporangiospore, suggesting an important function either in spore formation, production, and/or germination [25].

Our work showed that *gpa11* and *gpa12* has an important function in the spore since Δ*gpa12* and specially Δ*gpa11*/Δ*gpa12* showed increased spore sizes compared to Δ*gpa11* and wild-type strains. Spore size in *M. circinelloides* is known to be controlled by the calcineurin pathway. Thus, mutation of *cnaA*, which encodes the catalytic subunit A of calcineurin, leads to large spore size, faster germination, and increased virulence, among other defects [15]. Interestingly, *cnaA* mRNA levels in spores of Δ*gpa12* and Δ*gpa11*/Δ*gpa12* strains were lower than those of the wild-type strain, suggesting that *gpa12* positively controls the levels of *cnaA* in the spore, a function that can be compensated by *gpa11* in absence of *gpa12* as indicated the more severe effect observed in Δ*gpa11*/Δ*gpa12* compared to Δ*gpa12*. Moreover, the mRNA levels of *ena1* and *ena2*, used as a marker for the activated calcineurin pathway [31], were decreased in Δ*gpa12*, Δ*gpa11*/Δ*gpa12* and Δ*cnaA* strains compared to the wild-type strain. Additionally, the spore size increase could be result of the low *ena1* and *ena2* expression because dysfunction of Ena homologues leads to cell swelling in human renal cells, as dysfunction of Na^+-K^+ ATPases leads to the accumulation of sodium ions in cells, which allows water entry into the cell to compensate the osmotic gradient [35]. Also, *Saccharomyces cerevisiae* mutants in the regulatory subunit of the calcineurin decreased the expression of ENA1 and accumulated Na^+ and Li^+ ions [36]. Therefore, it is tempting to speculate that something similar occurs in the Δ*gpa11*/Δ*gpa12* strain of *M. circinelloides*, it will be interesting to know if the mutation of *ena1* or/and *ena2* could altered the spore size in this Mucoral (Fig 11). Overall, these findings suggest that the calcineurin pathway is under the control of Gpa12, and Gpa11 in a lesser extent, in spores from *M. circinelloides*, and consequently absence of *gpa12* and *gpa11* or *cnaA* results similar phenotypes such as spore enlargement (Fig 4), accelerated germination (Fig 5) and sensibility to the calcineurin inhibitor FK506 (S2 Fig). In addition, the double mutation of *gpa11* and *gpa12* led to lower cAMP levels and PKA activity compared to the the Δ*gpa11* or Δ*gpa12* after 3 hours of aerobic growth (Fig 5). Similar levels of cAMP and PKA activity between Δ*gpa11*/Δ*gpa12* and Δ*cnaA* were observed (data not shown), indicating a crosstalk in the regulation of PKA pathway between Gpa11/Gpa12 and CnaA (Fig 11). Interestingly, although Δ*gpa12* decreased the mRNA from *cnaA*, this mutation did not alter the levels of cAMP and PKA activity, suggesting different pathways in the regulation of activation of PKA by Gpa12 or Gpa11/Gpa12.

Additionally to the regulation of the calcineurin pathway by *gpa12* and *gpa11*, the calcineurin pathway also regulates the expression of *gpa12* and *gpa11* in the spore since their mRNA levels was down regulated in the Δ*cnaA* strain (Fig 7). This observation revealed a regulatory crosstalk between *gpa12* and *gpa11* and the calcineurin pathway. Alteration of this regulatory system by deletion of some key element seems to affect the expression of other *gpa* genes. Thus, Δ*cnaA* strain showed a significant mRNA increase of *gpa2-4*, which codes for products belonging to Group I ($G\alpha_s$) and Group II of the Gα phylogeny. The mRNA levels of *gpa3* and *gpa4* were also increased in the Δ*gpa12* and Δ*gpa11*/Δ*gpa12* mutant strains, suggesting a correlation between *gpa11* with *gpa12* and *cnaA* in terms of regulation of *gpa3* and *gpa4* mRNA levels in spores from *M. circinelloides*, although more experiments are needed to clarify this possible correlation.

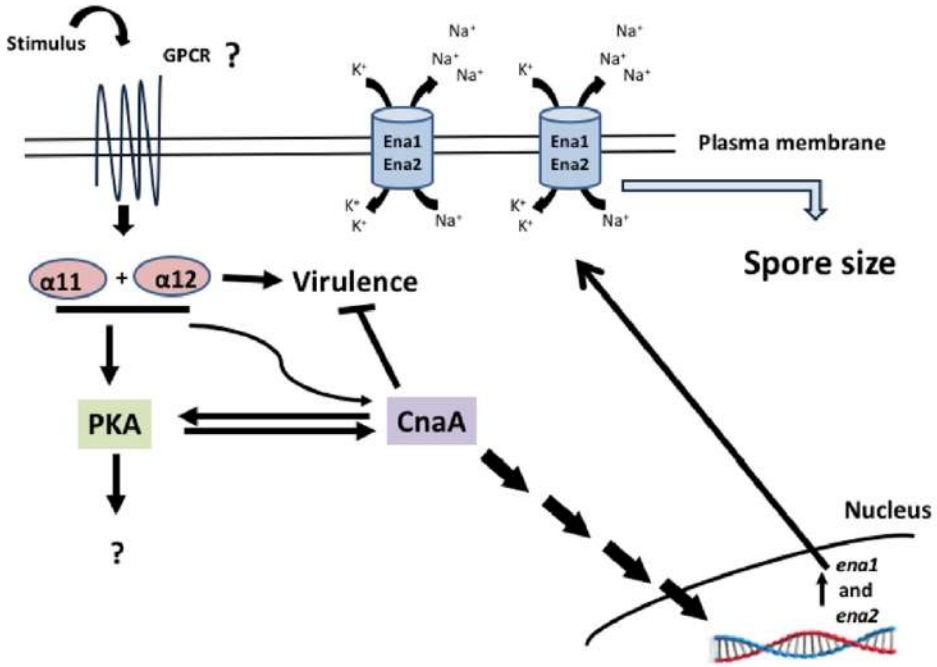

Fig 11. Proposed model of the function of Gpa11 and Gpa12 regulating sporangiospore size and virulence in *M. circinelloides*. Through one or more GPCRs, Gpa11 and Gpa12 in the spores of *M. circinelloides* activate CnaA, which in turn activates the calcineurin pathway. The calcineurin pathway leads to the expression of genes regulated by this pathway, like *ena1* and *ena2*. The dysfunction of Ena1 and Ena2, which are Na^+-K^+ ATPases, could increase cytosolic levels of sodium ions, allowing the influx of water, leading to an increase in spore size in *M. circinelloides* as was observed in the Δ*gpa11*/Δ*gpa12* strain. The CnaA negatively regulates the virulence and stimulates the PKA pathway, meanwhile Gpa11 or Gpa12 positively regulate the virulence and activate the PKA pathway during aerobic germination, but unknown elements are implied in the avirulent phenotype by the mutations in *gpa11* and *gpa12*.

https://doi.org/10.1371/journal.pone.0226682.g011

Deletion of *M. circinelloides* in *cnaA* showed an elevated virulence (Fig 9) that has been attributed in part to the larger spore size that result in increased germination rate, allowing faster destruction of the host [17]. Surprisingly, single and double mutants of *gpa11* and *gpa12* were completely avirulent in a diabetic mouse model, despite the Δ*gpa11*/Δ*gpa12* displayed low *cnaA* mRNA levels and mutant produce large spores that show high germination rate compared to the wild-type strain (Fig 5). Moreover, the inability to infect mice could not be attributed to a poor growth of the *gpa11* and *gpa12* mutants (Fig 3). The defect in virulence of *gpa11* and *gpa12* mutants and the higher virulence of the mutant of *cnaA* were confirmed by the figures of fungal burden and the levels of chemokines (*IL-6*, *IL-1β*, *TNF-α*, and *MIP-2*) known to be induced under filamentous infections [37–39], including *M. circinelloides* [40].

The single and double mutants of *gpa11* and *gpa12* did not show a significant increase in the mRNA levels of these inflammation markers in diabetic mice tissues compared to the levels from the wild-type or Δ*cnaA* strains, despite larger spore size and higher germination rate of Δ*gpa11*/Δ*gpa12* mutant compared to the wild-type strain. Despite these similarities, spores of Δ*gpa11*/Δ*gpa12* and Δ*cnaA* strains behave in a totally different manner in terms of H_2O_2 resistance, since Δ*cnaA* spores are more resistant to H_2O_2 than those from Δ*gpa11*/Δ*gpa12*, and also single mutants of this genes (Fig 10). Moreover, it has been also reported that the spores

from Δ*cnaA* strain are more resistant to phagocytosis [15], but the single and double *gpa*-mutant strains were more efficiently killed by macrophages than spores from the wild-type strain. This result could in part explain that *gpa11* and *gpa12* mutants are unable to infect diabetic mice (Fig 9) The combination of large spores and inability to cause infection shown by mutants of *gpa11* and *gpa12*, especially the double mutant, suggests that both phenotypes are controlled by the same regulatory pathway (Fig 11). This regulatory pathway in some point diverge in two branches, one that controls spore size through the calcineurin pathway and another that regulates the expression of genes important for the virulence. This model could explain the higher virulence of *cnaA* mutants that keep functioning the virulence-specific regulatory branch and simultaneously produce large spores with accelerated germination, it seems that a total lack of CnaA is needed to display a virulent phenotype. Therefore, *gpa11* and *gpa12* define a signal transduction pathway that play pivotal role in fungal infection in *M. circinelloides*. The dissection of this pathway with the identification of receptor to unknown signals, other components of the signal cascade, and targets genes will provide a better knowledge of the understudied process of fungal colonization by Mucorales.

Our work is important to the fungi field revealing new hypothesis to test. Fungal spore size has been found to be an important virulence determinant in fungal pathogens including ascomycetes (*Beauveria bassiana*, *Botrytis cinerea*), basiodiomycetes (*Cryptococcus neoformans*) or mucorales (*Mucor circinelloides*). In the entomopathogenic fungus *B. bassiana*, when the vacuolar ATPase subunit H encoding gene was disrupted, conidia diameter was reduced by 16% when compared to the wild-type strain. Moreover, this mutant displayed significantly attenuated virulence against the *Galleria mellonella* larvae [41]. In both fungal phytopathogens *B. cinera* and *M. fructicola*, environmental conditions regulate spore size. It has been reported that in *B. cinerea*, when grown on culture medium that contains 30% glucose (w/v), spores were about 50% larger than those grown on 2% glucose (w/v). Notably, these larger spores had enhanced aggressiveness against the flowers of *Rosa hybrida* [42]. Comparative analysis of spore sizes from different *C. neoformans* strains revealed that spores from serotype A are around 10% larger in diameter when compared to the serotype D [43]. Noteworthy, serotype A is the major responsible of *C. neoformans* infections (95%) and it has been associated with more severe infections in immunocompromised patients [44]. Interestingly, to the best of our knowledge, the first report for larger fungal spores (>10 μm in diameter) In *M. circinelloides* that does not imply a more virulent phenotype when compared to the wild-type strain.

Our work provides evidence for a genetic and functional linkage between *gpa11* and *gpa12* with the calcineurin pathway in *M. circinelloides*, suggesting that *cnaA* is under control of *gpa11* and *gpa12* and these elements are associated with a larger spore phenotype. However, larger spore phenotype by itself is not a prerequisite for virulence, suggesting that *gpa11* and *gpa12* also regulate a set of genes that are specifically involved in virulence.

Methods

Fungal strains, culture media, and growth conditions

M. circinelloides f. *lusitanicus* MU402 (*leuA*$^-$, *pyrG*$^-$) [27] was used for the *gpa11* and *gpa12* gene deletion studies. Additionally, the MU636 strain (*leuA*$^-$, *pyrG*$^+$) derived from *M. circinelloides* MU402 was also employed in this work [45], although it is not shown, this strain exhibits similar phenotypes as the wild-type strain MU402. A *M. circinelloides* Δ*cnaA* mutant strain [15] derived from MU402 was kindly provided by Dr. Soo Chan Lee (University of Texas at San Antonio, USA). Yeast–peptone–glucose (YPG) medium (pH 4.5); 1 L medium containing 3 g yeast extract (BD Bioxon, USA), 10 g gelatin peptone (BD Bioxon, USA), 20 g glucose (BD Bioxon, USA). Yeast nitrogen base (YNB) (Sigma, USA) or MMC (minimal medium with

casamino acids), which contained 10 g/L casamino acids (BD Difco, USA), 20 g/L glucose, and 0.5 g/L yeast nitrogen base, supplemented with uracil (200 mg/L) (Sigma, USA) as required; 15 g/L agar (BD Bioxon, USA) was added when solid media were prepared. For spore production and culture conditions, germination under self-anaerobic and aerobic atmosphere, as well as the quantitation of growth, spore size, and hyphae length protocols described previously were followed with no modifications [18, 46].

100 spores from the different strains were treated or not with 4 mM H_2O_2 for 1 h at 4 ˚C and spread on YNB or YPG plates and incubated for 24 h at 28 ˚C. YNB or YPG solid media were supplemented or not with 0.005% Triton X-100 and 100 spores from different strains were spread on the plates, incubation was carried out for 1 day at 28 ˚C.

Targeted deletion in *M. circinelloides*

Targeted deletion of *gpa11*. Using genomic DNA from MU402 wild-type strain *of M. circinelloides* 1.1-kb fragments that correspond to the 5′ upstream or 3′ downstream regions from the start or stop translation codon from *gpa11*, respectively, were amplified by PCR. The pair of oligonucleotides Gpa11-P-Fwd and Gpa11-P-Sac-Rev was used to amplify the 5′ region, with a *Sac*I site added to the 3′ end of the Gpa11-P-Sac-Rev primer. The oligonucleotides Gpa11-T-Sac-Fwd and Gpa11-T-Xba-Rev were used to amplify the 3′ region, with a *Sac*I site added to the 5′ end of the Gpa11-T-Sac-Fwd primer and an *Xba*I site to the 3′ end of the Gpa11-T-Xba-Rev primer. A 2-kb fragment that corresponds to the *pyrG* gene was PCR-amplified using the primers PyrG-Sac-Fwd and PyrG-Sac-Rev and *Sac*I sites were added to its 5′ end and 3′ end (S3 Table).

The 5′ and 3′ fragments from *gpa11* and *pyrG* were independently cloned into pJET1.2/blunt resulting in the pGpa11-5′ (for the *gpa11* 5′-region), pGpa11-3′ (for the *gpa11* 3′-region), and pPyrG (for the *pyrG* gene) vectors. The *Sac*I sites in the different fragments allowed the subcloning of *pyrG* into pGpa11-5′, resulting in pGpa115′-pyrG. Finally, 1.1-kb from the 3′ region of *gpa11* was cut using the *Sac*I and *Xba*I enzymes, and subcloned into pGpa115′-pyrG—the resulting plasmid was named pGpa115′-pyrG-3′. This resulting plasmid was used as template to obtain the recombinant fragment (Gpa115′-pyrG-3′ of 4.2 kb) by PCR with the oligonucleotides Gpa11-P-Fwd and Gpa11-T-Xba-Rev. All recombinant plasmids were confirmed by PCR and restriction enzyme patterns.

Targeted deletion of *gpa12*. The *gpa12* recombinant fragment coupled with the *pyrG* selection gene was generated through overlapping-PCR. In this process, three PCR fragments containing overlapping sequences between them were PCR-amplified using the following oligonucleotides (S3 Table): 12pUFow-PstI and 12pURev-pyrG, which amplified 1-kb from the 5′ upstream region of the start translation codon of *gpa12*; and oligonucleotides 12pDRev-NotI and 12pDFow-pyrG, which amplified 1-kb from the 3′ downstream region of the stop translation codon of *gpa12*. In oligonucleotide 12pURev-pyrG, an added nucleotide sequence at the 3' end hybridized to the 5′ end of *pyrG*; and in oligonucleotide 12pDFow-pyrG, an added nucleotide sequence at its 5' end hybridized to the 3' end of *pyrG*. The gene *pyrG* was PCR-amplified using the oligonucleotides PyrG-Sac-Fwd and PyrG-Sac-Rev, with pMAT1700 [47] as a template. Three individual PCR reactions were performed to obtain 3 DNA fragments. The *gpa12* 5′ region, *pyrG* (2 kb), and the *gpa12* 3′ region, which were all purified. Overlapping-PCR was performed using 100 ng/μL of each template; 10 μM each of the oligonucleotides 12pUFow-PstI and 12pDRev-NotI and 1 μL of Herculase II Fusion Enzyme (Agilent Technologies, USA), at a molar ratio of 1:1:1, were used to generate the recombinant fragment of *gpa12*.

Targeted deletion of *gpa11* in Δ*gpa12* strain: To generate the Δ*gpa11*/Δ*gpa12* double-mutant strain, the plasmid pGpa115′-pyrG-3'-previously obtained for the *gpa11* mutation was used. The gene *leuA*, which is required for leucine synthesis [48], was obtained by PCR with the oligonucleotides leuA-Sac-Fwd and leuA-Sac-Rev, and *Sac*I restriction sites were added to both oligonucleotides at their 5′ ends (S3 Table), and then annealed into the plasmid pLeu4 [49]. Both *leuA* (3.7 kb) and the pGpa113′-pyrG-5′ vector were digested with *Sac*I, and both products were ligated using the enzyme T4 DNA ligase (Promega, USA); the resulting plasmid was named pGpa115′-leuA-3′. The plasmid pGpa115′-leuA-3′ was used as a template and using the oligonucleotides Gpa11-P-Fwd and Gpa11-T-Xba-Rev, PCR amplification was carried out to obtain the recombinant fragment (5.9-kb) to delete *gpa11* in the Δ*gpa12* strain. All recombinant plasmids were identified by PCR and restriction fragment patterns.

Protoplasts obtained from *M. circinelloides* MU402 were transformed with the recombinant DNA fragments (3 μg/transformation) according to a previously described protocol [50]. Transformants were obtained under selective conditions on MMC agar plates lacking uracil for single deletion mutants or YNB agar plates lacking uracil and leucine for the double mutants. Monosporic cultures were obtained after 5 cycles of sporulation in either selective medium or rich medium, at which point, 100% of the spores could grow on the selective medium, indicating the transformation of all nuclei.

Molecular identification of *gpa11* and *gpa12* mutant strains from *M. circinelloides*

PCR confirmation of *gpa11* gene deletion. Transformed strains were identified by PCR using the oligonucleotides 11-C-Fwd (forward) and pyrG-R2 (reverse) (S3 Table); 11-C-Fwd hybridized outside the recombination fragment used to delete the *gpa11* gene and pyrG-R2 (S3 Table) that hybridize in the selectable marker sequence to determine a homologous integration event, a positive recombination event was determined by PCR amplification of 1.4-kb band. A lack of amplification band indicated the wild-type genotype (S4 Fig).

PCR confirmation of *gpa12* gene deletion. Using a similar approach, the transformants were identified by PCR with the pair of oligonucleotides 12-C-Fwd, which hybridizes outside the recombination fragment used to delete *gpa12* gene, and pyrG-R2 (S3 Table), which hybridizes in the selectable marker sequence. Those which generated an amplicon of 1.3-kb was the mutant genotype, but non-amplification confirmed a wild-type genotype. (S4 Fig).

PCR confirmation of double mutant Δ*gpa11*/Δ*gpa12*. Using the oligonucleotides 11-C-Fwd (forward) and leuA-C-Rev (reverse) (S3 Table); 11-C-Fwd hybridized outside the recombination fragment used to delete the *gpa11* gene and leuA-C-Rev (S3 Table) hybridized in the selectable marker sequence to determine a homologous integration event. A positive recombination event was determined by PCR amplification of 2.2-kb band, while no amplification confirmed the wild-type genotype (S4 Fig).

As a positive control for DNA integrity that was used for PCR reactions, the pair of oligonucleotides, Gpa11-T-Sac-Fwd / Gpa11-T-Xba-Rev, which hybridized with the 3′-end region of *gpa11* were used for Δ*gpa11* and a 1.1-kb amplicon indicated a positive reaction. For Δ*gpa12* the pair of primers, 12pUFow-PstI / 12pURev-pyrG, which hybridized with the 5' region of *gpa12* were used and 1.1 kb was considered as positive control. The pair of oligonucleotides 11-C-Fwd / Gpa11-P-Sac-Rev was used in a PCR reaction for positive controls for Δ*gpa11*/Δ*gpa12* and a 1.3 kb amplicon indicated a positive PCR reaction; the wild-type strain also amplified an identical PCR size band as well as each mutant strain (S4 Fig).

Southern blot to identify the deletions of *gpa11* and *gpa12*

A total of 1 μg of genomic DNA from MU402 and the mutants of *M. circinelloides* were digested with indicated restriction enzyme. DNA was electrophorized and transferred to nylon membranes (HybondTM-N+, Amersham Biosciences, UK) following the recommended protocol [51]. Southern blot hybridization was performed under stringent conditions. DNA probes were labelled with [α-32P] dCTP using Ready-To-Go Labeling Beads (GE Healthcare Life Science). For Southern blot experiments, a DNA probe (1 kb) was directly amplified from genomic DNA from *M. circinelloides* using the primer pairs that amplified the 5′ region upstream of the start translation codon from *gpa11*, for *gpa12* identification a fragment (1 kb) corresponding to the 3′ region downstream from the stop translation codon was used as a probe and finally the primer pairs that amplified the 3′ region downstream from the stop translation codon (1 kb) from *gpa11* for the double mutation.

Complementation of Δ*gpa11* and Δ*gpa12* strains

The *gpa11* and *gpa12* wild-type ORFs were PCR-amplified using the genomic DNA of *M. circinelloides* MU402 as the template and the oligonucleotides *gpa11*-FWR-*Xho*I/*gpa11*-REV-*Not*I and *gpa12*-FWR-*Sal*I/*gpa11*-REV-*Not*I (S3 Table), which introduced restriction sites for *Xho*I and *Not*I at the 5' and 3' ends, respectively. Wild-type *gpa11* and *gpa12* genes were cloned in pEUKA4 vector [28] under the control of *gpd1* promoter from *M. circinelloides* in the *Xho*I and *Not*I sites; the resulting plasmids were confirmed based on restriction patterns and DNA sequencing. Both recombinant plasmids were used to transform the Δ*gpa11* and Δ*gpa12* strains and selection was performed in YNB media (Difco, Franklin Lakes, NJ, USA) medium.

qRT-PCR confirmation

Total RNA isolated from *gpa11* and *gpa12* single and double mutant strains was used as a template and qRT-PCR was performed to determine all *gpa* transcript levels, as described previously [25].

Specimen preparation for scanning electron microscope (SEM) imaging of spores

SEM was performed according to Oshell 1997 [52], 4 h post-fixation with osmium tetroxide (1% diluted in cacodylate buffer 0.01 M, pH 7.4). The samples were dehydrated in ethanol solutions of 60, 70, 80 and 90%, and three times in 100% ethanol for 15 min each.

For hexamethyldisilazane (HMDS) drying the samples were rinsed in ethanol- HMDS in proportions of 2:1, 1:1, 1:2, 1:3, and HMDS 100% for 15 min each. The samples were transferred to a desiccator for 24 h. Samples were mounted on stubs and examined with a Zeiss GeminiSEM scanning electron microscope.

Ethics statement

The ethics agreement was made for the mouse virulence model protocol following the recommendations of the Mexican Federal Regulations for the Use and Care of Laboratory Animals (NOM-062-ZOO-1999) (Especificaciones técnicas para la producción, cuidado y uso de los animales de laboratorio/Technical specifications for production, use and care of laboratory animals) [53]. The Internal Biosecurity and Bioethics Committee of Instituto de Investigaciones Químico Biológicas de la Universidad Michoacana de San Nicolás de

Hidalgo firstly reviewed the experimental protocols and authorized them (trade number 06-13/2016).

Mouse virulence assays

To assess the virulence of *M. circinelloides* strains, we used methods described previously [18, 54] with some modifications. Briefly, each group consisting of eight male BALB/c mice (12–16 weeks old, weighing ~20 g, obtained from CINVESTAV, Zacatenco. México) were treated with streptozotocin (200 mg/kg) (Sigma, USA) to induce a diabetic state (>300 mg/dL glucose in blood), and then independent mice groups were inoculated with 2×10^7 spores from each strain of *M. circinelloides*. The spores were suspended in saline solution and injected intraperitoneally into mice, and survival of mice was monitored daily. Three independent assays were conducted for each group.

Macrophages spore killing assay

Mouse monocyte/macrophage RAW 267.4 (TIB-71) was purchased from American Type Culture Collection (ATCC). Cells were maintained in DMEM medium supplemented with 10% FBS (Sigma, USA), 100 U/mL penicillin (Sigma, USA), and 100 μg/mL streptomycin (Sigma, USA) (basal medium) at 5% CO_2 and 37 °C for 24 h before treatments.

Macrophages were seeded at 8×10^5 cells/well in DMEM basal medium (GIBCO, Thermo Fisher Scientific, USA) without antibiotics and incubated at 37 °C in 6-well plates. After incubation overnight, the basal medium in each well was replaced with fresh medium, then the macrophages were co-cultured with 2×10^5 spores produced in YPG for 1 or 3 h. Immediately, the supernatants and cells and spores were removed and placed in independent tubes. Then, cells and spores were centrifuged at 1,500 x g for 5 min. Pellet was recovered and frozen until nucleic acid extraction was performed.

Total *M. circinelloides* RNA and DNA isolation from *in vitro* cultures, from macrophages or from mouse tissues

Total RNA and genomic DNA from *M. circinelloides*, mice tissues and macrophages were isolated using RNAeasy mini kit and QIAamp DNA Mini Kit, respectively (Qiagen, Venlo, Netherlands).

M. circinelloides cultures were obtained by filtration in 5 μm membrane filters (Millipore, USA), the mouse tissues were collected following infection with *M. circinelloides* after 15 days of spore inoculation. Approximately 25–50 mg of tissue sample from each mouse was transferred into a tube with MagNA Lyser Green Beads (Roche, Switzerland) pre-cooled on ice. Denaturing RLT buffer (700 μL) from the RNeasy Mini Kit or buffer ATL (180 μL) of QIAamp DNA Mini Kit were added immediately before homogenization to obtain total RNA or genomic DNA, respectively. For cell disruption, tubes were placed in the MagNA Lyser Instrument (Roche, Switzerland) and processed twice at 5,500 x g for 40 s with cooling on ice for 1 min between each step. Then, samples were centrifuged for 1 min at 20,000 *x g* (Eppendorf 5417) and the supernatants were used for total RNA or genomic DNA isolation using the corresponding kit, according to the manufacturer's instructions. To eliminate DNA contamination from RNA samples, samples were treated with DNase I (Promega, USA) according to the manufacturer's protocol. The RNA was eliminated from DNA samples using RNAse A (Roche, Switzerland). RNA or genomic samples were separated on non-denaturing 2% and 1% agarose gel, respectively stained with ethidium bromide (Sigma, USA), visualized using a Gel Doc XR+ Imager (Bio-Rad, Hercules, CA, USA), and quantified using a SmartSpec Plus spectrophotometer (Bio-Rad).

Determination of abundance of DNA from *M. circinelloides* by qPCR

Abundance of *M. circinelloides* from mice tissues or macrophages was compared based in a spore standard curve of *M. circinelloides*. MU402 spore concentrations between 1 x 10^2 and 1 x 10^7 mL^{-1} by 10-fold serial dilutions were employed. Consequently, DNA was extracted as previously reported, to generate a spore standard curve by qPCR by detection of the validated *tfc-1* nuclear gene.

Oligonucleotide design and quantitative reverse transcription polymerase chain reaction (qRT-PCR)

The primers and hydrolysis probe for the calcineurin catalytic subunit (*cnaA*, NCBI gene bank accession number AGJ95088.1); the Na^+-K^+ ATPases *ena1* (ID number 105213), and *ena2* (ID number 113279) DNA sequences were obtained from *M. circinelloides* genome database [55]. Design of the primers and hydrolysis probes for each gene was performed using Biosearch Technologies software (www.biosearchtech.com) to ensure the specificity of all detections during qRT-PCR assays (S4 Table). To evaluate the relative gene expression of *gpa*, *pkar1*, and *adh1* from *M. circinelloides* protocols described previously were followed [25, 29]. Genomic DNA and total RNA isolation were performed as described previously [18].

Quantification of intracellular cAMP levels and protein kinase A activity

Spores from MU402, Δ*gpa11*, Δ*gpa12*, Δ*gpa11*/ Δ*gpa12*, Δ*cnaA*, Δ*gpa11*+*gpa11wt* or Δ*gpa12* +*gpa12wt* strains were inoculated into YPG media and incubated with constant shaking (150 rpm) for 3 h. Biological samples that were obtained under these conditions were used in either cAMP or PKA measurements.

cAMP levels

Cells were separated from media and frozen in liquid nitrogen. Upon nitrogen evaporation, 60 mg of biological samples were weighed, and resuspended in 1 mL of 0.1 M HCl, and 250 μL of glass beads (0.1 mm) (BioSpec Products, Inc., Bartlesville, OK, USA) were added. Samples were homogenized by receiving three pulses at full speed for 30 s, with 1 min incubation on ice intermittently, in a beadbeater (607-BioSpec Products, Inc., Bartlesville, OK, United States). The supernatants were used for cAMP measurements using the Direct cAMP ELISA kit (Enzo Life Science, San Diego, USA). Protocols were followed accordingly to the manufacturer's instructions. The OD was measured at 405 nm on a microplate reader (Bio-Rad Benchmark; Bio-Rad Laboratories, Hercules, CA, USA).

PKA activity

We obtained crude protein extract (0.5 μg) from each sample, and a PKA-specific kinase activity was quantified by using the PKA Colorimetric Activity Kit (Invitrogen, Carlsbad, CA, United States), as described previously [15].

Statistical analysis

All data were evaluated by analysis of variance (ANOVA, level of statistically significant difference at $\alpha<0.05$). Fisher post-hoc test was used.

Supporting information

S1 Fig. The spores from the independent *M. circinelloides* knockout strains produced in YPG were observed under **A)** light microscope (100 X), scale bar is equal to 20 μm. **B)** Under scanning electron microscope. Representative photographs from the corresponding strains of *M. circinelloides* (1000 X), scale bar is equal to 10 μm.
(DOCX)

S2 Fig. Identification of Ena1 and Ena2 from *M. circinelloides*. Ena1 from *Hansenulla polymorpha* was used as bait to find Ena homologues in *M. circinelloides*. **A)** Clustal W alignment analysis. Identical and similar amino acid residues are shown in black and grey boxes, respectively. **B)** Identity analysis of Ena homologues in *M. circinelloides* is shown as identity/similarity in percentage, Mc: *M. circinelloides*; Hp: *H. polymorpha*.
(DOCX)

S3 Fig. Effect of inhibitor of calcineurin FK506 and Triton X-100 on the viability *M. circinelloides gpa11* and *gpa12* mutants. A) Effect of inhibitor of calcineurin FK506 on the growth of *M. circinelloides*. Radial growth of spores grown on YPG or YNB agar plates recorded each day during the experiment. Representative photos show radial growth after 3 days. Three independent experiments were performed for each condition. **B)** 100 spores from each strain were inoculated by spreading on YPG and YNB plates supplemented with 0.005% Triton X-100. Plates were incubated for 1 day. The bars represent the number of colonies formed with treatment versus the colonies formed without treatment. Three independent experiments were performed for each condition. *Statistically significant difference (ANOVA, Fisher, $p<0.05$).
(DOCX)

S4 Fig. Deletion of *gpa genes* in *M. circinelloides* confirmed by PCR. A) *gpa11*; **B)** *gpa12* and **C)** *gpa11/gpa12* mutation strategy. The 5′ and 3′ regions upstream and downstream from the start and stop translation codons, respectively, were used to flank the *pyrG* (single mutants) or *leuA* (double mutant) selective marker. The diagrams show the recombinant fragments used to delete the *gpa* genes in protoplasts of *M. circinelloides* MU402 wild-type strain. The photographs show the molecular confirmation by PCR with specific primers for each gene showing specific PCR-bands that indicate recombination in the corresponding *gpa loci*. **M**: Molecular size markers (kb). C+: PCR control for positive amplification (*wt*: 1.1 kb amplicon to identify the wt *gpa11* or *gpa12* genes); Δ*gpa11*: 1.4 kb amplicon to identify the deletion of *gpa11* gene; Δ*gpa12*: 1.3 kb amplicon to identify the deletion of *gpa12* gene; and Δ*gpa11*/Δ*gpa12*: 2.2 kb amplicon to identify the deletion of *gpa11* gene in the mutant Δ*gpa12*.
(DOCX)

S1 Table. Sporangiospore mRNA levels of *gpa* genes from *gpa11* and *gpa12* mutant strains from *M. circinelloides*.
(DOCX)

S2 Table. Sporangiospore mRNA levels of *gpa* genes from *cnaA* mutant strain from *M. circinelloides*.
(DOCX)

S3 Table. Oligonucleotides used for PCR assays.
(DOCX)

S4 Table. Oligonucleotides for qRT-PCR.
(DOCX)

Author Contributions

Conceptualization: Marco I. Valle-Maldonado, Rafael Ortiz-Alvarado, Victoriano Garre, Víctor Meza-Carmen.

Data curation: J. Alberto Patiño-Medina, Nancy Y. Reyes-Mares, Carlos Pérez-Arques, Rosa E. Nuñez-Anita, Verónica Anaya-Martínez, Martha I. Ramírez-Díaz, Víctor Meza-Carmen.

Formal analysis: Verónica Anaya-Martínez, Rafael Ortiz-Alvarado, Martha I. Ramírez-Díaz, Soo Chan Lee, Víctor Meza-Carmen.

Funding acquisition: Jesús Campos-García, Victoriano Garre, Víctor Meza-Carmen.

Investigation: J. Alberto Patiño-Medina, Nancy Y. Reyes-Mares, Marco I. Valle-Maldonado, Irvin E. Jácome-Galarza, Martha I. Ramírez-Díaz, Victoriano Garre, Víctor Meza-Carmen.

Methodology: Nancy Y. Reyes-Mares, Irvin E. Jácome-Galarza, Carlos Pérez-Arques, Rosa E. Nuñez-Anita, Jesús Campos-García, Verónica Anaya-Martínez, Rafael Ortiz-Alvarado, Martha I. Ramírez-Díaz, Victoriano Garre, Víctor Meza-Carmen.

Project administration: Víctor Meza-Carmen.

Resources: Martha I. Ramírez-Díaz, Victoriano Garre, Víctor Meza-Carmen.

Supervision: Víctor Meza-Carmen.

Validation: Víctor Meza-Carmen.

Writing – original draft: Víctor Meza-Carmen.

Writing – review & editing: Martha I. Ramírez-Díaz, Soo Chan Lee, Victoriano Garre, Víctor Meza-Carmen.

References

1. Wijayawardene NN, Pawłowska J, Letcher PM, Kirk PM, Humber RA, Schüßler A et al. Notes for genera: basal clades of fungi (including Aphelidiomycota, Basidiobolomycota, Blastocladiomycota, Calcarisporiellomycota, Caulochytriomycota, Chytridiomycota, Entomophthoromycota, Glomeromycota, Kickxellomycota, Monoblepharomycota, Mortierellomycota, Mucoromycota, Neocallimastigomycota, Olpidiomycota, Rozellomycota and Zoopagomycota). Fungal Divers. 2018; 92: 43–129. https://doi.org/10.1007/s13225-018-0409-5.
2. Orlowski M. Mucor dimorphism. Microbiol Rev. 1991; 55(2): 234–58. PMID: 1886520
3. Morin-Sardin S, Nodet P, Coton E, Jany JL. A Janus-faced fungal genus with human health impact and industrial applications. Fungal Biol Rev. 2017; 31(1):12–32. https://doi.org/10.1016/j.fbr.2016.11.002.
4. McIntyre M, Breum J, Arnau J, Nielsen J. Growth physiology and dimorphism of *Mucor circinelloides* (syn. *racemosus*) during submerged batch cultivation. Appl Microbiol Biotechnol. 2002; 58:495–502. https://doi.org/10.1007/s00253-001-0916-1 PMID: 11954797
5. Lübbehüsen TL, Nielsen J, McIntyre M. Characterization of the *Mucor circinelloides* life cycle by on-line image analysis. J Appl Microbiol. 2003; 95:1152–60. https://doi.org/10.1046/j.1365-2672.2003.02098.x PMID: 14633045
6. Lübbehüsen T L, Nielsen J, McIntyre M. Morphology and physiology of the dimorphic fungus *Mucor circinelloides* (syn. *M. racemosus*) during anaerobic growth. Mycol Res. 2003; 107:223–30. https://doi.org/10.1017/S0953756203007299 PMID: 12747334
7. Hassan MIA, Voigt K. Pathogenicity patterns of mucormycosis: epidemiology, interaction with immune cells and virulence factors. Med Mycol. 2019; 1; 57(Supplement_2):S245–S256. https://doi.org/10.1093/mmy/myz011 PMID: 30816980
8. Baldin C, Ibrahim AS. Molecular mechanisms of mucormycosis-The bitter and the sweet. PLoS Pathog. 2017; 3; 13(8):e1006408. https://doi.org/10.1371/journal.ppat.1006408 PMID: 28771587
9. Jeong W, Keighley C, Wolfe R, Lee WL, Slavin MA, Kong DCM, et al. The epidemiology and clinical manifestations of mucormycosis: a systematic review and meta-analysis of case reports. Clin Microbiol Infect. 2019; 25(1):26–34. https://doi.org/10.1016/j.cmi.2018.07.011 PMID: 30036666

10. Chander J, Kaur M, Bhalla M, Punia RS, Singla N, Bhola K et al. Changing Epidemiology of Mucoralean Fungi: Chronic Cutaneous Infection Caused by *Mucor irregularis*. Mycopathologia 2015; 180(3–4):181–6. https://doi.org/10.1007/s11046-015-9908-z PMID: 26170185
11. Lewis RE, Kontoyiannis DP. Epidemiology and treatment of mucormycosis. Future Microbiol. 2012; 8(9):1163–1175. https://doi.org/10.2217/fmb.13.78
12. Skiada A, Lass-Floerl C, Klimko N, Ibrahim A, Roilides E, Petrikkos G. Challenges in the diagnosis and treatment of mucormycosis. Med Mycol. 2018;1; 56(suppl_1):93–101. https://doi.org/10.1093/mmy/myx101 PMID: 29538730
13. Jenks JD, Reed SL, Seidel D, Koehler P, Cornely OA et al. Rare mould infections caused by *Mucorales*, *Lomentospora prolificans* and *Fusarium*, in San Diego, CA: the role of antifungal combination therapy. Int J Antimicrob Agents. 2018; 52(5):706–12. https://doi.org/10.1016/j.ijantimicag.2018.08.005 PMID: 30099056
14. Ibrahim AS, Spellberg B, Walsh TJ, Kontoyiannis DP. Pathogenesis of mucormycosis. Clin Infect Dis. 2012; 54 Suppl 1:S16–22. https://doi.org/10.1093/cid/cir865
15. Lee SC, Li A, Calo S, Heitman J. Calcineurin plays key roles in the dimorphic transition and virulence of the human pathogenic zygomycete *Mucor circinelloides*. PLoS Pathog. 2013; 9: e1003625. https://doi.org/10.1371/journal.ppat.1003625 PMID: 24039585
16. Sephton-Clark PCS, Muñoz JF, Ballou ER, Cuomo CA, Voelz K. Pathways of Pathogenicity: Transcriptional Stages of Germination in the Fatal Fungal Pathogen *Rhizopus delemar*. mSphere. 2018; 3(5). https://doi.org/10.1128/mSphere.00403-18
17. Li CH, Cervantes M, Springer DJ, Boekhout T, Ruiz-Vazquez RM, Torres-Martinez SR, et al. Sporangiospore size dimorphism is linked to virulence of *Mucor circinelloides*. PLoS Pathog. 2011; 7(6): e1002086. https://doi.org/10.1371/journal.ppat.1002086 PMID: 21698218
18. Patiño-Medina JA., Maldonado-Herrera G, Pérez-Arques C, Alejandre-Castañeda V, Reyes-Mares NY, Valle-Maldonado MI, et al. Control of morphology and virulence by ADP-ribosylation factors (Arf) in *Mucor circinelloides*. Curr Genet. 2018; 64:853–69. https://doi.org/10.1007/s00294-017-0798-0 PMID: 29264641
19. Fuller KK, Rhodes JC. Protein kinase A and fungal virulence: a sinister side to a conserved nutrient sensing pathway. Virulence. 2012; 3(2):109–21. https://doi.org/10.4161/viru.19396 PMID: 22460637
20. Ocampo J, Fernandez Nuñez L, Silva F, Pereyra E, Moreno S, Garre V, et al. A subunit of protein kinase A regulates growth and differentiation in the fungus *Mucor circinelloides*. Eukaryot Cell. 2009; 8:933–44. https://doi.org/10.1128/EC.00026-09 PMID: 19411621
21. Tesmer JJ. The quest to understand heterotrimeric G protein signaling. Nat Struct Mol Biol. 2010; 17: 650–2. https://doi.org/10.1038/nsmb0610-650 PMID: 20520658
22. Syrovatkina V, Alegre KO, Dey R, Huang XY. Regulation, Signaling, and Physiological Functions of G-Proteins. J Mol Biol. 2016; 428(19):3850–68. https://doi.org/10.1016/j.jmb.2016.08.002 PMID: 27515397
23. Hicks JK, Yu JH, Keller NP, Adams TH. *Aspergillus* sporulation and mycotoxinproduction both require inactivation of the FadA G alpha protein-dependent signaling pathway. EMBO J. 1997 16(16):4916–23. https://doi.org/10.1093/emboj/16.16.4916 PMID: 9305634
24. Roze LV, Beaudry RM, Keller NP, Linz JE. Regulation of aflatoxin synthesis by FadA/cAMP/protein kinase A signaling in *Aspergillus parasiticus*. Mycopathologia. 2004; 158: 219–32. https://doi.org/10.1023/B:MYCO.0000041841.71648.6e PMID: 15518351
25. Valle-Maldonado MI, Jácome-Galarza IE, Díaz-Pérez AL, Martínez-Cadena G, Campos-García J, Ramírez-Díaz MI, et al. Phylogenetic analysis of fungal heterotrimeric G protein-encoding genes and their expression during dimorphism in *Mucor circinelloides*. Fungal Biol. 2015; 119(12):1179–93. https://doi.org/10.1016/j.funbio.2015.08.009 PMID: 26615741
26. Bölker M. Sex and crime: heterotrimeric G proteins in fungal mating and pathogenesis. Fungal Genet Biol. 1998; 25(3):143–56. https://doi.org/10.1006/fgbi.1998.1102 PMID: 9917369
27. Nicolás FE, de Haro JP, Torres-Martínez S, Ruiz-Vázquez RM. Mutants defective in a *Mucor circinelloides* dicer-like gene are not compromised in siRNA silencing but display developmental defects. Fungal Genet Biol. 2007; 44(6):504–16. https://doi.org/10.1016/j.fgb.2006.09.003 PMID: 17074518
28. Wolff A. M., Arnau J. Cloning of Glyceraldehyde-3-phosphate Dehydrogenase-Encoding Genes in *Mucor circinelloides* (Syn. *racemosus*) and Use of the *gpd1* Promoter for Recombinant Protein Production. Fungal Genet Biol. 2002; 35 (1): 21–29. https://doi.org/10.1006/fgbi.2001.1313 PMID: 11860262
29. Valle-Maldonado MI, Jácome-Galarza IE, Gutiérrez-Corona F, Ramírez-Díaz MI, Campos-García J, Meza-Carmen V. Selection of reference genes for quantitative real time RT-PCR during dimorphism in the zygomycete *Mucor circinelloides*. Mol Biol Rep; 2015; 42(3):705–11. https://doi.org/10.1007/s11033-014-3818-x PMID: 25391770

30. Rangel-Porras RA, Meza-Carmen V, Martínez-Cadena G, Torres-Guzmán JC, González-Hernández GA, Arnau J, et al. Molecular analysis of an NAD-dependent alcohol dehydrogenase from the zygomycete *Mucor circinelloides*. Mol Genet Genomics. 2005; 274(4):354–63. https://doi.org/10.1007/s00438-005-0025-4 PMID: 16179992

31. Rodríguez C, Galindo LR, Siverio JM. Nitrogen-dependent calcineurin activation in the yeast *Hansenula polymorpha*. Fungal Genet Biol. 2013; 53:34–41. https://doi.org/10.1016/j.fgb.2013.01.007 PMID: 23403359

32. Patiño-Medina J. A., Vargas-Tejedaa D., Valle-Maldonado M. I., Alejandre-Castañed V, Jácome-Galarz I. E., Villegas-Moreno J., et al. Sporulation on blood serum increases the virulence of *Mucor circinelloides*. Microbial Pathogenesis. 2019; 137: 103737. https://doi.org/10.1016/j.micpath.2019.103737 PMID: 31513895

33. Díaz-Pérez SP, Patiño-Medina JA, Valle-Maldonado MI, López-Torres A, Jacome-Galarza IE, Anaya Martínez V, et al. Alteration of fermentative metabolism enhances Mucor circinelloides virulence. Infect Immun; 2019. (In press) https://doi.org/10.1128/IAI.00434-19 PMID: 31685547

34. Navarro E, Lorca-Pascual JM, Quiles-Rosillo MD, Nicolás FE, Garre V, Torres-Martínez S, et al. A negative regulator of light-inducible carotenogenesis in *Mucor circinelloides*. Mol Genet Genomics. 2001; 266(3):463–70. https://doi.org/10.1007/s004380100558 PMID: 11713676

35. Yordy MR, Bowen JW. Na,K-ATPase expression and cell volume during hypertonic stress in human renal cells. Kidney Int. 1993; 43(4):940–8. https://doi.org/10.1038/ki.1993.132 PMID: 8386782

36. Mendoza I, Rubio F, Rodriguez-Navarro A, Pardo JM. The protein phosphatase calcineurin is essential for NaCl tolerance of *Saccharomyces cerevisiae*. J Biol Chem. 1994; 269(12):8792–6. PMID: 8132612

37. Peng XD, Zhao GQ, Lin J, Jiang N, Xu Q, Zhu CC, et al. Fungus induces the release of IL-8 in human corneal epithelial cells, via Dectin-1-mediated protein kinase C pathways. Int J Ophthalmol. 2015; 8 (3):441–7. https://doi.org/10.3980/j.issn.2222-3959.2015.03.02 PMID: 26085988

38. Chamilos G, Lewis RE, Lamaris G, Walsh TJ, Kontoyiannis DP. Zygomycetes hyphae trigger an early, robust proinflammatory response in human polymorphonuclear neutrophils through toll-like receptor 2 induction but display relative resistance to oxidative damage. Antimicrob Agents Chemother. 2008; 52:722–4. https://doi.org/10.1128/AAC.01136-07 PMID: 18025115

39. Wüthrich M, Deepe GS Jr, Klein B. Adaptive immunity to fungi. Annu Rev Immunol. 2012; 30:115–48. https://doi.org/10.1146/annurev-immunol-020711-074958 PMID: 22224780

40. López-Muñoz A, Nicolás FE, García-Moreno D, Pérez-Oliva AB, Navarro-Mendoza MI, Hernández-Oñate MA et al. An Adult Zebrafish Model Reveals that Mucormycosis Induces Apoptosis of Infected Macrophages. Sci Rep. 2018; 8(1):12802. https://doi.org/10.1038/s41598-018-30754-6 PMID: 30143654

41. Zhu J, Zhu XG, Ying SH, Feng MG. Effect of vacuolar ATPase subunit H (VmaH) on cellular pH, asexual cycle, stress tolerance and virulence in *Beauveria bassiana*. Fungal Genet Biol. 2017; 98:52–60. https://doi.org/10.1016/j.fgb.2016.12.004 PMID: 28011319

42. Phillips DJ, Margosan DA, Mackey BE. Size, nuclear number, and aggressiveness of *Botrytis cinerea* on media of varied glucose concentrations. Phytopathology. 1987; 77: 1606–1608.

43. Velagapudi R, Hsueh YP, Geunes-Boyer S, Wright JR, Heitman J. Spores as infectious propagules of *Cryptococcus neoformans*. Infect Immun 2009; 77(10):4345–55. https://doi.org/10.1128/IAI.00542-09 PMID: 19620339

44. Desnos-Ollivier M, Patel S, Raoux-Barbot D, Heitman J, Dromer F. Cryptococcosis serotypes impact outcome and provide evidence of *Cryptococcus neoformans* speciation. mBio. 2015; 6(3): e00311–15. https://doi.org/10.1128/mBio.00311-15 PMID: 26060271

45. Navarro-Mendoza MI, Pérez-Arques C, Panchal S, Nicolás FE, Mondo SJ, Ganguly P, et al. Early Diverging Fungus Mucor circinelloides Lacks Centromeric Histone CENP-A and Displays a Mosaic of Point and Regional Centromeres. Curr Biol. 2019; 29(22):3791–3802. https://doi.org/10.1016/j.cub.2019.09.024 PMID: 31679929

46. Salcedo-Hernandez R, Ruiz-Herrera J. Isolation and characterization of a mycelial cytochrome aa_3-deficient mutant and the role of mitochondria in dimorphism of *Mucor rouxii*. Exp Mycol. 1993; 17:142–54. https://doi.org/10.1006/emyc.1993.1013

47. Trieu TA, Navarro-Mendoza MI, Pérez-Arques C, Sanchis M, Capilla J, Navarro-Rodriguez P, et al. RNAi-Based Functional Genomics Identifies New Virulence Determinants in Mucormycosis. PLoS Pathog. 2017; 13: e1006150. https://doi.org/10.1371/journal.ppat.1006150 PMID: 28107502

48. van Heeswijck R, Roncero MIG. High frequency transformation of *Mucor* with recombinant plasmid DNA. Carlsberg Research Communications. 1984; 49:691–702. https://doi.org/10.1007/BF02907500.

49. Arnau J, Strøman P. Gene replacement and ectopic integration in the zygomycete *Mucor circinelloides*. Curr Genet. 1993; 23(5–6):542–6. https://doi.org/10.1007/BF00312649 PMID: 8319313

50. Gutiérrez A, López-García S, Garre V. High reliability transformation of the basal fungus *Mucor circinelloides* by electroporation. J Microbiol Methods. 2011; 84:442–6. https://doi.org/10.1016/j.mimet.2011.01.002 PMID: 21256886

51. Sambrook JF, Russell DW. *Molecular cloning*: *A laboratory manual*, 3 ed. Ed. Cold Spring Harbor Press; 2001.

52. Oshel P. HMDS and specimen drying for SEM. Micros today. 1997; 5(4): 16–7 https://doi.org/10.1017/S155192950006140X.

53. Secretaría de Agricultura, Ganadería, Desarrollo Rural, Pesca y Alimentación (SAGARPA) NORMA Oficial Mexicana NOM-062- ZOO-1999. Especificaciones técnicas para la producción, cuidado y uso de los animales de laboratorio. Diario Oficial de la Federación 2. 2001; 107–67 (In Spanish).

54. Rodríguez-Andrade E, Hernández-Ramírez KC, Díaz-Peréz SP, Díaz-Magaña A, Chávez-Moctezuma MP, Meza-Carmen V et al. Genes from pUM505 plasmid contribute to *Pseudomonas aeruginosa* virulence. Antonie Van Leeuwenhoek. 2016; 109: 389–96. https://doi.org/10.1007/s10482-015-0642-9 PMID: 26739475

55. Corrochano LM, Kuo A, Marcet-Houben M, Polaino S, Salamov A, Villalobos-Escobedo JM, et al. Expansion of Signal Transduction Pathways in Fungi by Extensive Genome Duplication. Curr Biol. 2016; 26(12):1577–84. https://doi.org/10.1016/j.cub.2016.04.038 PMID: 27238284

AMERICAN SOCIETY FOR MICROBIOLOGY | Infection and Immunity®

FUNGAL AND PARASITIC INFECTIONS

Alteration of Fermentative Metabolism Enhances *Mucor circinelloides* Virulence

Sharel P. Díaz-Pérez,[a] J. Alberto Patiño-Medina,[a] Marco I. Valle-Maldonado,[a] Adolfo López-Torres,[b] Irvin E. Jácome-Galarza,[c] Verónica Anaya-Martínez,[d] Verónica Gómez-Ruiz,[e] Jesús Campos-García,[a] Rosa E. Nuñez-Anita,[f] Rafael Ortiz-Alvarado,[g] Martha I. Ramírez-Díaz,[a] J. Félix Gutiérrez-Corona,[h] Víctor Meza-Carmen[a]

[a]Instituto de Investigaciones Químico Biológicas, Universidad Michoacana de San Nicolás de Hidalgo (UMSNH), Morelia, Michoacán, México
[b]Universidad Papaloapan, Campus Tuxtepec, Tuxtepec, Oaxaca, México
[c]Departamento de Biología Molecular, Laboratorio Estatal de Salud Pública del Estado de Michoacán, Morelia, Michoacán, México
[d]Facultad de Ciencias de la Salud, Universidad Anáhuac, Huixquilucan, Estado de México, México
[e]Laboratorio de Patología, Hospital Civil "Dr. Miguel Silva," Morelia, Michoacán, México
[f]Facultad de Medicina Veterinaria y Zootecnia, Universidad Michoacana de San Nicolás Hidalgo, Morelia, Michoacán, México
[g]Facultad de Químico Farmacobiología, Universidad Michoacana de San Nicolás Hidalgo, Morelia, Michoacán, México
[h]Departamento de Biología, División de Ciencias Naturales y Exactas, Universidad de Guanajuato, Guanajuato, Guanajuato, México

J. Félix Gutiérrez-Corona and Víctor Meza-Carmen are co-senior authors.

ABSTRACT The fungus *Mucor circinelloides* undergoes yeast-mold dimorphism, a developmental process associated with its capability as a human opportunistic pathogen. Dimorphism is strongly influenced by carbon metabolism, and hence the type of metabolism likely affects fungus virulence. We investigated the role of ethanol metabolism in *M. circinelloides* virulence. A mutant in the *adh1* gene (M5 strain) exhibited higher virulence than the wild-type (R7B) and the complemented (M5/pEUKA-*adh1*$^{+}$) strains, which were nonvirulent when tested in a mouse infection model. Cell-free culture supernatant (SS) from the M5 mutant showed increased toxic effect on nematodes compared to that from R7B and M5/pEUKA-*adh1*$^{+}$ strains. The concentration of acetaldehyde excreted by strain M5 in the SS was higher than that from R7B, which correlated with the acute toxic effect on nematodes. Remarkably, strain M5 showed higher resistance to H_2O_2, resistance to phagocytosis, and invasiveness in mouse tissues and induced an enhanced systemic inflammatory response compared with R7B. The mice infected with strain M5 under disulfiram treatment exhibited only half the life expectancy of those infected with M5 alone, suggesting that acetaldehyde produced by *M. circinelloides* contributes to the toxic effect in mice. These results demonstrate that the failure in fermentative metabolism, in the step of the production of ethanol in *M. circinelloides*, contributes to its virulence, inducing a more severe tissue burden and inflammatory response in mice as a consequence of acetaldehyde overproduction.

KEYWORDS *Mucor circinelloides*, fermentative metabolism, alcohol dehydrogenase, acetaldehyde, ethanol, virulence, alcohol, mucoral, mucormycosis, oxidoreductases, dimorphism

Fungal infections are a major threat to immunosuppressed patients (1) and contribute significantly to nosocomial infections in critical care units (2). Fungal infections can be superficial or invasive, with invasive infections being a major cause of morbidity and mortality in patients with cancer and immunosuppression (3). Mucormycoses are among the fungal infections becoming the most common in the last decade, along with invasive aspergillosis, which is in part a consequence of improved laboratory diagnoses (4). Members of the genera *Rhizopus*, *Rhizomucor*, *Mucor*, and *Absidia* are the

Citation Díaz-Pérez SP, Patiño-Medina JA, Valle-Maldonado MI, López-Torres A, Jácome-Galarza IE, Anaya-Martínez V, Gómez-Ruiz V, Campos-García J, Nuñez-Anita RE, Ortiz-Alvarado R, Ramírez-Díaz MI, Gutiérrez-Corona JF, Meza-Carmen V. 2020. Alteration of fermentative metabolism enhances *Mucor circinelloides* virulence. Infect Immun 88:e00434-19. https://doi.org/10.1128/IAI.00434-19.

Editor Liise-anne Pirofski, Albert Einstein College of Medicine

Address correspondence to Víctor Meza-Carmen, victor_meza2004@yahoo.com.mx.

Received 6 June 2019
Returned for modification 11 July 2019
Accepted 22 October 2019
Accepted manuscript posted online 4 November 2019
Published 22 January 2020

most frequent etiological agents isolated from patients with mucormycosis (5), which yields an overall mortality of up to 90% when left untreated in susceptible populations (6). *Rhizopus* and *Mucor* species cause the majority of mucormycosis, with mortality rates of up to 50%, even in the presence of antifungal therapy (7). Neutropenia, elevated blood serum iron concentration, and malignancies represent risks associated with poor prognosis of mucormycosis (8).

Few virulence factors with well-known biochemical and molecular bases have been described in *Mucorales*. In *Mucor circinelloides*, the size of the spores, which is modulated by calcineurin, is a virulence factor, since mutations in the *cnaA* gene, encoding the calcineurin subunit A, cause the production of spores that are larger and more virulent than spores produced by the wild-type strain (9). Morphological transitions also contribute to virulence during host infection by *M. circinelloides*. Under aerobic conditions the wild-type strain develops abundant hyphae, whereas mutants in the *cnbR* gene, which encodes the *M. circinelloides* calcineurin regulatory subunit B, produced yeast cells and exhibited reduced virulence compared to the wild-type strain (9). Mutation of genes encoding ADP-ribosylation factor 1 (Arf 1) and Arf 3 and Arf-like (Arl) protein 1 led to the secretion of a harmful protein(s) that contributed to increasing the pathogenesis of *M. circinelloides* (10, 11). *Rhizopus oryzae* uses the GRP78 surface protein, which is overproduced during diabetic ketoacidosis, to cause endothelial cell invasion and damage in mice (12). Spores of *M. circinelloides* produced on medium supplemented with native blood serum are more resistant to H_2O_2 and macrophage phagocytosis and increase the virulence capacity compared to *M. circinelloides* spores produced on medium supplemented with denatured blood serum or on medium alone (13).

Other fungal pathogens utilize an extended repertoire of virulence factors, including toxins (aflatoxins produced by some *Aspergillus flavus* strains), hydrolases (lipases, proteases), and glycoproteins for host cell binding (14). In the most common human fungal pathogen, *Candida albicans*, the ability to form biofilms constitutes a major virulence factor (15). Two lines of study suggest a link between ethanol metabolism and biofilm formation. Ethanol inhibits biofilm development; moreover, genetic alteration of the alcohol dehydrogenase (Adh) enzyme increases the capacity of *C. albicans* to form biofilms in which the ethanol level is low but the level of acetaldehyde is high (16). In *Aspergillus fumigatus*, ethanol metabolism has been implicated in the adaptation to hypoxia conditions during mouse infection. The *alcC* gene from *A. fumigatus*, encoding an alcohol dehydrogenase, is highly expressed in the fungus infecting the lungs from immunosuppressed mice. Moreover, *alcC* mutation results in reduced fungal presence in tissues and increases the inflammatory response (17). In relation to *M. circinelloides*, biochemical and genetic evidence indicates that the ADH1 enzyme is responsible for ethanol production from acetaldehyde reduction and that *adh1* gene expression is greater in yeast cells than mycelial cells (18, 19). *M. circinelloides adh1* gene mutation prevents growth under anaerobic conditions and leads to decreased ethanol production and reduced capacity to grow in ethanol, confirming its role in fermentative and oxidative metabolism (20).

Because *Mucor* dimorphism and carbon metabolism are strongly linked (20, 21), we sought to determine the effects of ethanol metabolism on *M. circinelloides* virulence. To this end, we tested the effect of the *adh1*$^-$ mutation on the virulence as well as the inflammatory response in both mouse and nematode infection models.

RESULTS

***adh1* gene mutation increases *M. circinelloides* virulence.** *M. circinelloides* exhibits a dimorphic process, and the hyphal growth has been suggested to increase its virulence (9). Our group observed that the *M. circinelloides adh1* mutant (M5) is unable to grow under anaerobic conditions and shows diminished ethanol production (20). To determine the role of Adh1 in *M. circinelloides* virulence, we tested the effects of *adh1* mutation in a survival assay using normal nonimmunodepressed BALB/c mice and the nematode *Caenorhabditis elegans* as infection models.

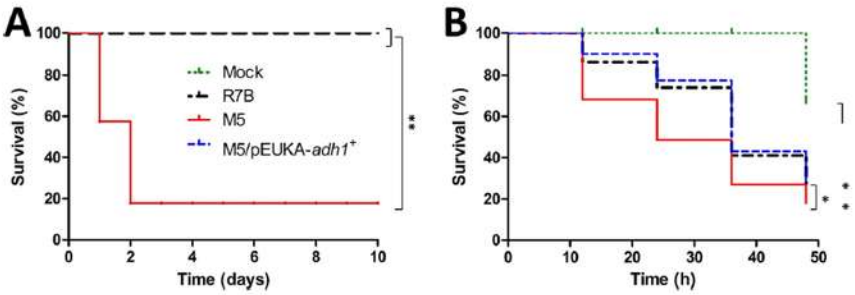

FIG 1 The *adh1*$^-$ mutation increases virulence in *M. circinelloides*. (A) A total of 5×10^6 spores from each of the different strains (M5, *adh1*$^-$ mutant; R7B, *adh1* wild type; M5/pEUKA-*adh1*$^+$, *adh1* mutant complemented) were inoculated using intraperitoneal administration in normal male BALB/c mice. Groups of 8 animals were treated with the different strains. The animals were observed daily until their death. (B) For *C. elegans* infection assays, 24-well flat-bottom plates were incubated with 10,000 spores and 20 nematodes per well in 1 ml of Lee medium; living nematodes were monitored every 12 h. Three independent experiments were registered in each host model of infection. The data were statistically analyzed using the Kaplan-Meier test. *, $P < 0.05$; **, $P < 0.01$; ***, $P < 0.001$. When results were not considered significant, we did not provide an additional indication ($P < 0.1$).

Intraperitoneal injection of spores from wild-type (R7B), *adh1*$^-$ (M5), and complemented M5 mutant (M5/pEUKA-*adh1*$^+$) strains clearly showed that M5 dramatically increased *M. circinelloides* virulence compared to R7B or M5/pEUKA-*adh1*$^+$. Strain M5 administration resulted in 82.14% lethality 2 days postinoculation, whereas all mice inoculated with spores from R7B or M5/pEUKA-*adh1*$^+$ survived throughout all assayed periods (Fig. 1A). In correlation, nematode inoculation with spores from strain M5 led to a significant increase in virulence compared to R7B or the M5/pEUKA-*adh1*$^+$ spores (Fig. 1B). This result indicated that the *adh1* mutation leads to increased fungal virulence.

Mutation of *adh1* affects *M. circinelloides* germination and growth during aerobic development. It has been reported that an increase in germination correlates with a higher virulence rate in *M. circinelloides* (11). Thus, we next addressed whether enhanced strain M5 virulence is due to an increase in the germination and/or growth rate. Strain M5 exhibited a significantly lower germination rate (Fig. 2A) and diminished biomass production (growth) in minimal medium (Fig. 2B) compared to strains R7B and M5/pEUKA-*adh1*$^+$. These results indicated that virulence enhancement in M5 did not correlate with an increase of germination or growth rate in the strain. Assessment of hyphal morphology in mycelia growing under aerobic conditions did not reveal any significant morphological change in the M5 mutant compared to the wild-type R7B

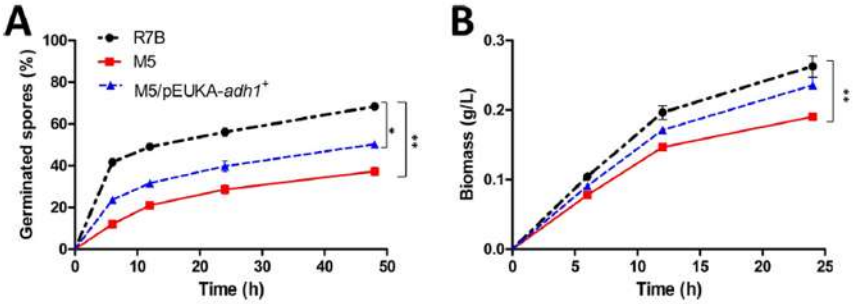

FIG 2 The aerobic development of *M. circinelloides* is affected by mutation of the *adh1* gene. A total of 5×10^5 spores per ml were inoculated into minimal (Lee) liquid medium supplemented with leucine at 28°C with constant shaking. The germination rate (A) and growth (B) were registered at the indicated times for the three strains (M5, *adh1*$^-$ mutant; R7B, *adh1* wild type; M5/pEUKA-*adh1*$^+$, *adh1* mutant complemented). Four independent experiments were performed under the same conditions. Significance testing was performed using the unpaired Student's *t* test. *, $P < 0.05$; **, $P < 0.01$; ***, $P < 0.001$. When results were not considered significant, we did not provide an additional indication ($P < 0.1$).

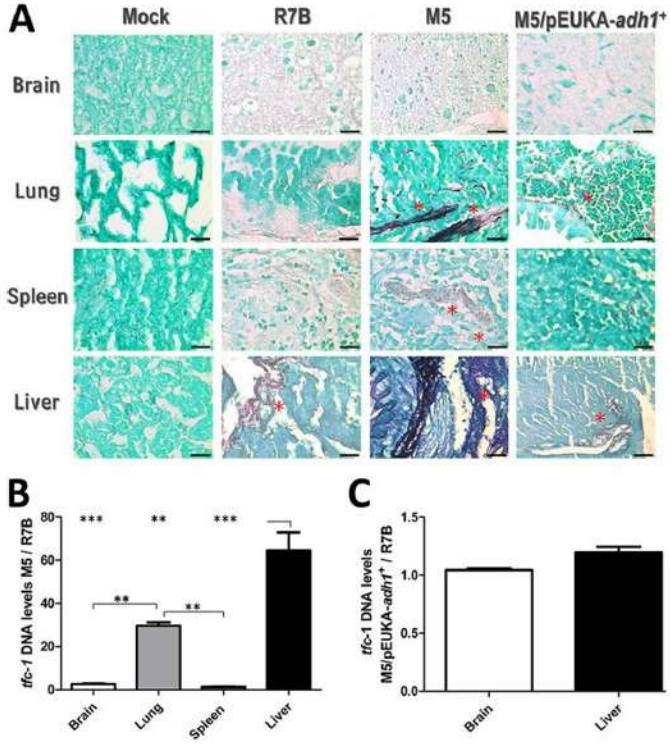

FIG 3 Mutation in the *adh1* gene increases the invasiveness of *M. circinelloides*. A total of 5×10^6 spores from each of the different strains of *M. circinelloides* (M5, *adh1*$^-$ mutant; R7B, *adh1* wild type; M5/pEUKA-*adh1*$^+$, *adh1* mutant complemented with *adh1* wild type [WT]) were inoculated independently per mouse. Following 48 h of incubation, animals were sacrificed and the organs were removed to be observed (A). Asterisks indicate the presence of *M. circinelloides* hyphae in tissues subjected to Grocott staining. Images were taken with ×100 magnification under light microscopy. Bar = 200 μm. (B) Quantification of fungal load in the different mouse tissues by qPCR using *tfc-1* from *M. circinelloides*. The values shown in the ordinate of the graph correspond to the ratio of the *tfc-1* gene signal detected in the tissues by treatment with strain M5 or R7B. (C) We also analyzed the ratio of the *tfc-1* gene from the tissues infected with M5/pEUKA-*adh1* or R7B. Mouse β-actin gene was used to validate the use of the same amount of DNA from the different mouse tissues. Four independent experiments were performed under the same conditions. Significance testing was performed using the unpaired Student's *t* test. *, $P < 0.05$; **, $P < 0.01$; ***, $P < 0.001$. When results were not considered significant, we did not provide an additional indication ($P < 0.1$).

strain (see Fig. S1 in the supplemental material). *M. circinelloides* spore size has been associated with virulence changes, with a larger spore size correlating with higher virulence (22). However, spore size determination by flow cytometry and optical microscopy showed that all three strains produced spores of equivalent size (Fig. S2).

Mutation of *adh1* enhances mouse organ invasion by *M. circinelloides*. Fungal cells' infectivity largely depends on their capability of deep tissue invasion (23), that is, being able to penetrate organs such as the lung, liver, spleen, and brain. The different *M. circinelloides* strains were intraperitoneally inoculated to simulate acute sepsis in the murine model, and all animals were sacrificed and the organs removed prior to natural death. Fungal tissue invasion and burden were determined qualitatively with Grocott staining of the tissue sections and quantitatively with real-time quantitative PCR (qPCR) using the *M. circinelloides tfc-1* gene (19). In general, the histological analysis revealed that in all tissues studied, the presence of the fungus (dark color) was more evident in the mouse tissues infected with strain M5 (Fig. 3A). Following infection with strain M5, the organ with the highest signs of fungal burden was the liver, followed by the lungs, whereas the brain and spleen demonstrated lower fungal presence (Fig. 3A). Using the same amount of mouse genomic DNA isolated from the tissues of mice infected with

the different *M. circinelloides* strains, fungal DNA was quantified using qPCR analysis (Fig. S3), and the results obtained were consistent with the cytology, indicating that after infection with M5, the liver and lungs from mice displayed ~80-fold higher fungal load than that following R7B infection (Fig. 3B). M5 also yielded higher fungal content in the brain and spleen, although this proportion was no more than 5-fold higher than that of R7B. In general, these findings indicated that M5 has a higher capacity to invade and colonize tissues than strains R7B and M5/pEUKA-*adh1*$^+$, which did not markedly differ in their capacity (Fig. 3C).

Trying to explain the increased capability of strain M5 to invade tissues, we evaluated the capability of *M. circinelloides* strains to survive under oxidative stress, determining the ability of the spores to germinate on yeast-peptone-glucose (YPG) medium after the addition of H_2O_2. The spores from strain M5 showed the highest levels of resistance to H_2O_2, with ~64% of spores germinated, strain M5/pEUKA-*adh1*$^+$ showed ~54% of spores germinated, and the spores from the wild-type strain showed ~37% germination compared to the control without H_2O_2 (Fig. 4A). After obtaining this result, we performed a phagocytosis assay with the spores from all the strains using the murine macrophage cell line RAW 264.7. We observed spore germination in the presence of the macrophages after 3 h of interaction, and spores from strain M5 seemed to germinate faster than those from the other strains (Fig. 4B). To quantify the spore germination, mRNA of *pkaR1* was used to indirectly estimate the aerobic spore germination (19). The mRNA levels of *pkaR1* were determined by real-time quantitative reverse transcription-PCR (qRT-PCR) after 1, 3, or 6 h of macrophage and spore interaction. The *pkaR1* transcript levels after 1 h (~264 or ~118%), 3 h (~143 or ~42%), and 6 h (~122 or ~36%) were higher in the M5 strain than the wild-type or M5/pEUKA-*adh1*$^+$ strain (Fig. 4C). We quantified the number of spores that were digested by macrophages after the interaction by qPCR using the *tfc-1* gene levels (see Materials and Methods). Our results showed that the lowest number of spores digested by the macrophages after 6 h of interaction corresponded to strain M5 (94,054 spores digested), followed by strain M5/pEUKA-*adh1*$^+$ (with 151,444 spores digested) and the wild-type strain (160,000 spores digested); this means that the spores digested in the mutant M5 correspond to only 60% and 65% of the spores digested in the wild-type and M5/pEUKA-*adh1*$^+$ strains, respectively (Fig. 4D). Additionally, we quantified the CFU produced from spores that survive the digestion by the macrophage after 6 h of interaction. Spores from the mutant M5 strain produced 36.6 or 42.6% more CFU after the macrophage interaction than the wild type or M5/pEUKA *adh1*$^+$ strain, respectively (Fig. 4E). These results indicate that the spores from the M5 mutant strain are less susceptible to digestion by the macrophages than the spores from the wild-type or M5/pEUKA-*adh1*$^+$ strain. Thus, these observations demonstrated that the genetic alteration of *M. circinelloides* fermentative metabolism by loss of function of the ADH1 enzyme increased the survival of spores after oxidative stress exposure and caused in the spores a greater resistance to the digestion by macrophages, which could explain in part the increased ability to invade and colonize tissues.

The *M. circinelloides adh1* gene mutation enhances the inflammatory response in mouse tissues. As the invasion of mouse tissues by *M. circinelloides* could trigger some response in the animal, it was of interest to determine whether there were changes in the inflammatory response as a result of the presence of the fungus and if such changes were differential between the M5, R7B, and complemented mutant (M5/pEUKA-*adh1*$^+$) strains of *M. circinelloides*. We utilized hematoxylin and eosin staining to analyze the morphological changes occurring in mouse tissues after infection with the various strains. Animals that had not been infected showed normal tissue appearance (Fig. 5A), whereas infection with the R7B or M5/pEUKA-*adh1*$^+$ strain caused mild inflammatory response in almost all tissues compared to tissues from noninfected animals (Fig. 5A). However, the tissues from mice infected with strain M5 showed more pronounced inflammation in brain and lungs. In the latter case, the alveolar structures were disrupted and erythrocytes were observed in the lung tissue, suggesting severe tissue damage. In addition, in mice infected with M5, the liver showed infiltration of

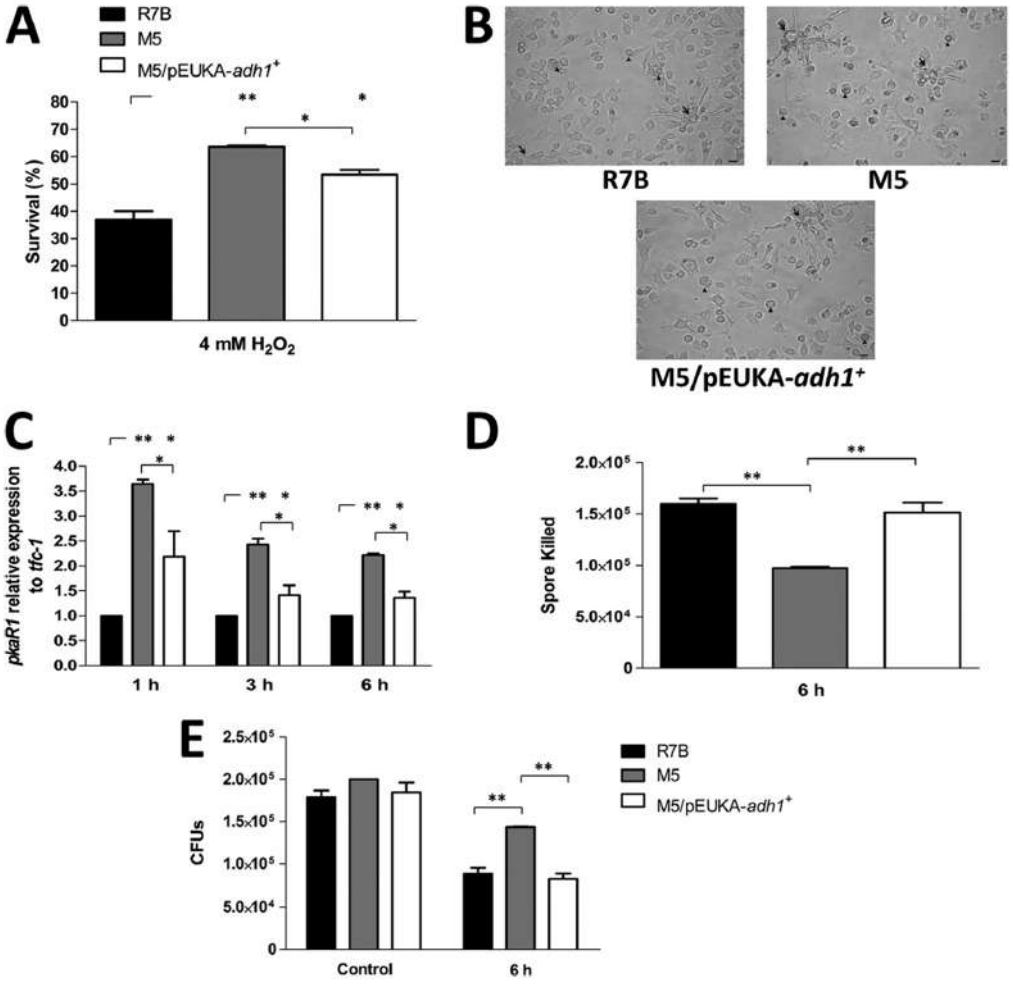

FIG 4 Role of the *adh1* mutation in the survival of *M. circinelloides* spores after H_2O_2 damage or macrophage phagocytosis. (A) Spores produced on YPG from the different strains were incubated with or without 4 mM H_2O_2 and incubated at 28°C. The survival rate was obtained after 24 h from the quotient of colonies from treatment versus no-treatment groups. (B) Germination of spores in the interaction with macrophages was seen under direct observation by light microscopy (×40). Scale bar = 20 μm. Arrows indicate germinating hyphae, and arrowheads indicate swelling spores. (C) The *pkaR1* mRNA levels were quantified using qRT-PCR 1, 3, and 6 h after the spores and macrophages interacted. (D) Quantitation of killed spores by qPCR using *tfc-1* after 6 h of incubation with mouse macrophages. A ΔCT analysis was performed to compare the mRNA and gene levels between the samples. (E) Quantitation of CFU from spores after 6 h of incubation with mouse macrophages. Figures show the average of three independent experiments. Significance testing was performed using the unpaired Student's *t* test. *, $P < 0.05$; **, $P < 0.01$; ***, $P < 0.001$. When results were not considered significant, we did not provide an additional indication ($P < 0.1$).

Kupfer cells and production of binucleated hepatocytes, indicating a more exacerbated inflammatory response than that seen in the tissue from animals infected with strains bearing functional ADH1 activity (Fig. 5A).

qRT-PCR analysis of some inflammatory responses (*Mip2*, *Il-1β*, and *Il-6*) in mice infected with *M. circinelloides* strains confirmed the observations made using histological analysis. The mice that were infected with strain M5 showed significantly higher transcript levels of these inflammation markers than did those infected with strains retaining functional ADH1 activity (Fig. 5B to D). Upregulated transcriptional activity of *Il-1β* and *Il-6* correlated with significantly elevated protein expression of interleukin 1β (IL-1β) and IL-6 in mouse liver and lung tissues that were previously infected with the mutant M5 strain (Fig. 6). These results indicate that the *adh1* mutation in *M. circinel-*

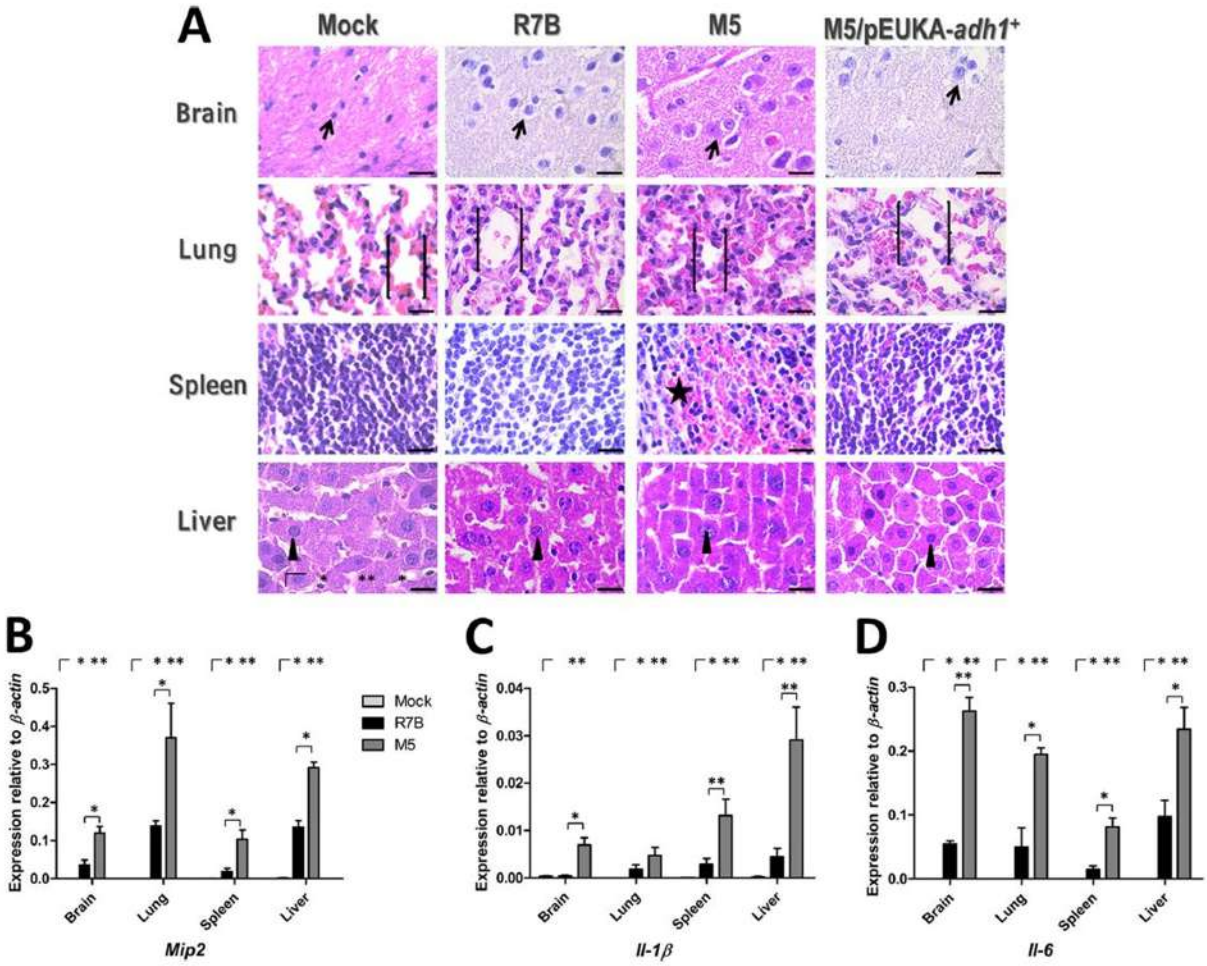

FIG 5 The *adh1*$^-$ mutant strain M5 of *M. circinelloides* triggers an enhanced inflammation response in mice. Spores from the different strains of *M. circinelloides* were inoculated in mice, and 48 h postinfection, the animals were sacrificed and the organs were removed for histological analysis using hematoxylin and eosin (A). The arrows show the glial brain cells. Alveolar structures are enclosed in brackets. The stars show the erythrocytes in the spleen, and the triangles show the hepatocyte morphology in the liver. Images were taken with ×100 magnification under light microscopy. Bar = 200 μm. mRNA quantification was performed in the organs, and levels of (B) *Mip2*, (C), *Il-1β*, and (D) *Il-6* were determined using qRT-PCR. Expression is relative to *Mus musculus* β-actin. Significance testing was performed using the unpaired Student's *t* test. *, $P < 0.05$; ** $P < 0.01$; ***, $P < 0.001$. When results were not considered significant, we did not provide an additional indication ($P < 0.1$).

loides induces a more pronounced systemic inflammatory response that could contribute to the lethal effect in infected mice.

Toxic effect of cell-free supernatant from the *M. circinelloides adh1* mutant. To understand the basis of the enhanced tissue burden and inflammation conferred by the *adh1* mutation, we tested if toxicity is mediated by excreted or secreted products of strain M5. To this end, cell-free culture medium (SS) from the different strains was collected and assayed for its effects on *C. elegans* viability in incubation performed at 20°C. The SS from strain M5 grown for 12 h caused the most pronounced loss of viability in *C. elegans* compared to strains R7B and M5/pEUKA-*adh1*$^+$ (Fig. 7A). M5-derived SS preincubated at 37°C or 37°C with addition of protease (pronase E) prior to nematode incubation similarly abolished the toxic effects on nematode viability (Fig. 7B and C). Moreover, the SS from all three strains incubated for 12 h at 25°C did not trigger any toxic effect on the nematode (Fig. 7D). Taken together, these results indicate that the M5 SS toxic effect is due to a thermolabile molecule of a nonprotein nature.

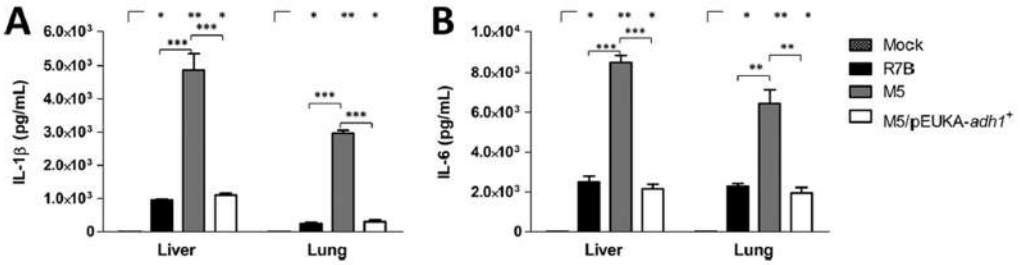

FIG 6 The *adh1*⁻ mutant strain M5 of *M. circinelloides* increased the protein expression of cytokines in mouse tissue. The cytokine expression of (A) IL-1β and (B) IL-6 was determined using ELISA in liver and lung from mice previously infected for 48 h with the different strains. Significance testing was performed using the unpaired Student's *t* test. *, $P < 0.05$; **, $P < 0.01$; ***, $P < 0.001$. When results were not considered significant, we did not provide an additional indication ($P < 0.1$).

Toxic effect of the *M. circinelloides adh1* mutant is associated with excreted acetaldehyde. Because the toxic secreted compounds from strain M5 are temperature labile at 25°C as well as 37°C and because the *adh1* mutation impairs the synthesis of ethanol from acetaldehyde (20), we reasoned that among the possible compounds excreted in the culture medium of this strain, acetaldehyde best matches the characteristic of evaporation (acetaldehyde evaporates at 21°C). Strikingly, the SS acetaldehyde concentrations for strains R7B and M5/pEUKA-*adh1*⁺ were 0.5 and 15 mM, respectively, whereas that of the M5 mutant strain was 47.5 mM (Fig. 8A). The SS from the M5 mutant strain was incubated for 12 h at 25°C or 37°C to promote the possible evaporation of acetaldehyde, and the concentration of acetaldehyde in the SS from strain M5 showed significantly reduced levels after incubation at 25°C (18 mM) and 37°C

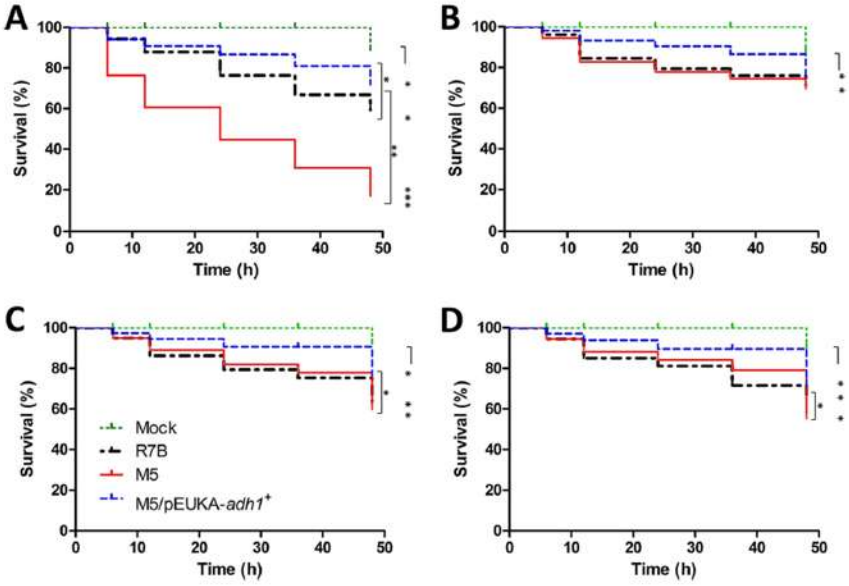

FIG 7 Cell-free medium from cultures of the *adh1*⁻ mutant strain M5 of *M. circinelloides* is toxic to *Caenorhabditis elegans*. (A) Spores from the indicated strains were inoculated in Lee medium and grown under aerobic conditions at 28°C with constant shaking for 12 h, and then the cultures were filtered using 2-μm Millipore filters to obtain the cell-free medium culture (SS), which then was incubated in the presence of *C. elegans*. (B) The SS from all the strains were treated for 2 h at 37°C with pronase E or (C) at 37°C prior to incubation with the nematode. (D) The SS from all the strains were treated for 12 h at 25°C. All the SS were incubated with the nematodes. A total of 20 nematodes were used per well and incubated at 20°C for 2 h. The results presented are the average of four independent experiments. The data were statistically analyzed using the Kaplan-Meier test. *, $P < 0.05$; **, $P < 0.01$; ***, $P < 0.001$. When results were not considered significant, we did not provide an additional indication ($P < 0.1$).

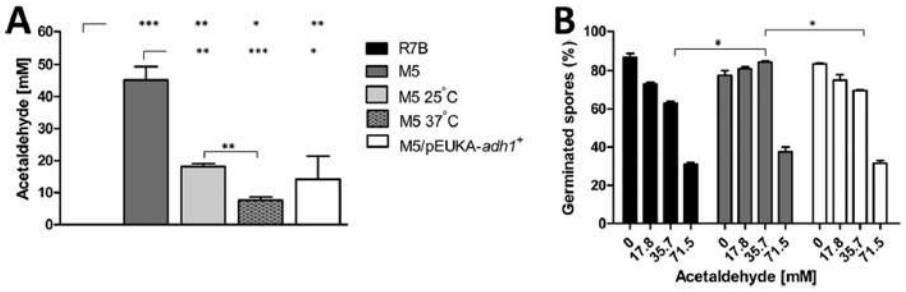

FIG 8 Acetaldehyde accumulation and its toxic effect during spore germination in *M. circinelloides adh1*⁻ and *adh1*⁺ strains. (A) The acetaldehyde from cell-free medium culture (from 12 h of fungal growth) was quantified using a mass spectrometry/flame ionization detector (MS-FID) method from different strains of *M. circinelloides* (M5, *adh1*⁻ mutant; R7B, *adh1* wild type; M5/pEUKA-*adh1*⁺, *adh1* mutant complemented). M5 cell-free medium culture was untreated (M5) or treated for 12 h at 25°C (M5 25°C) or at 37°C (M5 37°C). (B) Spore germination in the presence of exogenous addition of acetaldehyde in the various culture media. Four independent experiments were performed employing the same conditions. Significance testing was performed using the unpaired Student's *t* test. *, $P < 0.05$; **, $P < 0.01$; ***, $P < 0.001$. When results were not considered significant, we did not provide an additional indication ($P < 0.1$).

(7 mM) (Fig. 8A). Further experiments showed that the exogenous addition of acetaldehyde to *C. elegans* at a concentration of 37.5 mM led to a 60% viability loss (Fig. S4), indicating that this acetaldehyde concentration is toxic to *C. elegans* and explaining the high toxicity of M5 SS. Notably, acetaldehyde at 37.5 mM did not affect the spore germination rate of strain M5 at 6 h, although a 30% decrease of R7B spore germination was observed (Fig. 8B). This result indicates that strain M5 is uniquely able to cope with this acetaldehyde concentration, perhaps through its conversion to acetate.

In *Saccharomyces cerevisiae*, the *ald2*-encoded aldehyde dehydrogenase catalyzes the conversion of acetaldehyde to acetate (20). *ald2* mRNA quantitation from *M. circinelloides* strains showed that the *ald2* transcript level of R7B was 13.69-fold lower than that of strain M5 (Fig. 9A); moreover, the accumulation of acetate was 3.6-fold higher in strain M5 than strain R7B (Fig. 9B). These results suggest that the high accumulation of acetaldehyde in the M5 mutant strain activates a detoxification mechanism involving increased expression of the *ald2* gene, resulting in a greater tolerance to acetaldehyde in this strain.

Increased acetaldehyde production in the M5 *adh1* gene mutant strain contributes to its virulence in mice. In mammalian cells, acetaldehyde is metabolized to acetate by aldehyde dehydrogenase (ALD) activity; accordingly, when disulfiram, a competitive inhibitor of ALD activity, is used to control alcohol addiction, the resulting unpleasant symptoms and toxicity are due to acetaldehyde accumulation (24).

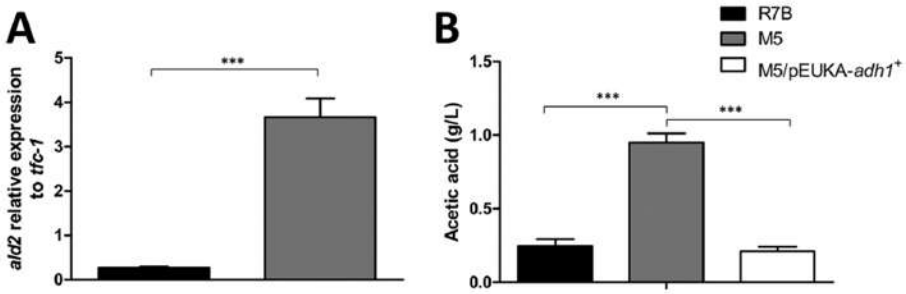

FIG 9 The *adh1*⁻ mutant M5 from *M. circinelloides* detoxifies acetaldehyde through acetaldehyde dehydrogenase (*ald2*) overexpression. (A) Quantitation of the transcript levels of the acetaldehyde dehydrogenase gene (*ald2*) from wild-type (R7B) and *adh1*⁻ mutant (M5) at 12 h of fungal growth. (B) Acetic acid levels were measured in the cell-free culture medium at 12 h of growth. Four independent experiments were performed under the same conditions. Significance testing was performed using the unpaired Student's *t* test. *, $P < 0.05$; **, $P < 0.01$; ***, $P < 0.001$. When results were not considered significant, we did not provide an additional indication ($P < 0.1$).

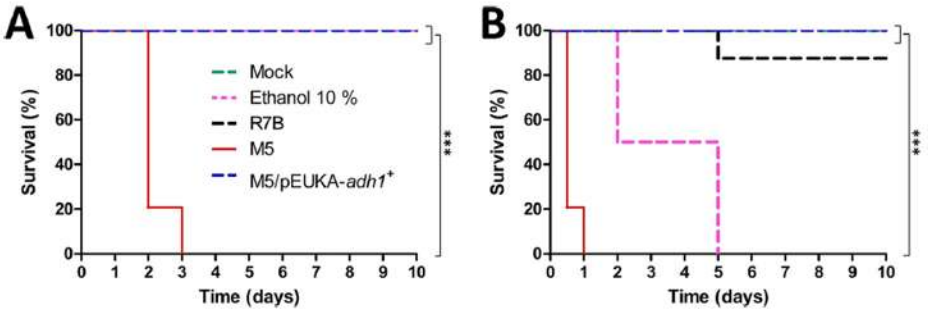

FIG 10 Mouse ALD activity inhibition increases the virulence of the *adh1*$^-$ mutant M5 of *M. circinelloides*. Spores from the different strains of *M. circinelloides* were inoculated independently per mouse. Mice were separated into two groups, which were not treated (A) or treated (B) with disulfiram and inoculated with spores from the *M. circinelloides* strains (M5, *adh1*$^-$ mutant; R7B, *adh1* wild type; M5/pEUKA-*adh1*$^+$, *adh1* mutant complemented). A positive control was used (mice with disulfiram treatment under the presence of ethanol at 10% *ad libitum*). Two independent experiments were performed employing the same conditions using 8 mice under each condition tested. The data were statistically analyzed using the Kaplan-Meier test. *, $P < 0.05$; **, $P < 0.01$; ***, $P < 0.001$. When results were not considered significant, we did not provide an additional indication ($P < 0.1$).

In the present study, disulfiram treatment was used in mice infected with the different strains of *M. circinelloides*, with treatment 48 h prior to spore infection and every 48 h postinfection. The administration of ethanol *ad libitum* did not generate mouse deaths (Fig. 10A), in contrast to the death of all mice at day 5 when ethanol was administered under disulfiram treatment (Fig. 10B). Remarkably, disulfiram treatment increased the virulence of strain M5, as shown by a decreased time until lethality compared to the result for mice that were infected with M5 alone (Fig. 10). In addition, 10% of the mice infected with R7B under disulfiram treatment were killed, in contrast to the 100% survival of mice infected with R7B spores without disulfiram treatment, suggesting that although much lower acetaldehyde is produced by mycelium from the wild-type R7B strain than strain M5 (Fig. 8A), it could be accumulated by the inhibitory effect of disulfiram on the ALD activity in strain R7B. This result suggests that the acetaldehyde accumulation, resulting from the inhibition of mouse ALD activity, enhanced the virulence effect of *M. circinelloides* strain M5.

DISCUSSION

Several zygomycetous species belonging to the order *Mucorales* function as human fungal pathogens to cause the lethal infection mucormycosis; these species include *Mucor* spp., *Rhizopus* spp., *Rhizomucor* spp., *Cunninghamella* spp., and *Apophysomyces trapeziformis* (25–27). In dimorphic species of *Mucor*, spore germination can lead to either filamentous (mycelium) or spherical (yeast) cell production, depending on environmental conditions (28, 29). The hyphal or the yeast phase of development can be obtained both in the presence of oxygen and under anaerobic conditions, depending on the carbon source and/or the presence of morphogenetic compounds. Development of the yeast form requires hexoses and invariably correlates with fermentative metabolism, whereas the hyphal phase can exhibit either oxidative or fermentative metabolism, depending on culture conditions (30). However, the type of metabolism is not a mandatory requirement for any of the *Mucor* dimorphism alternatives. Thus, as a consequence of altered *Mucor rouxii* fermentative metabolism by mutation of the *adh1* gene, the fungus loses its capacity to grow under anaerobic conditions. However, its spores maintain the ability to differentiate toward the yeast phase when incubated under aerobic conditions in the presence of phenethyl alcohol or to the hyphal phase upon incubation under aerobic conditions in medium without phenethyl alcohol (30). In *M. circinelloides*, the *adh1* gene is expressed in both hyphae and yeast cells, producing a cytoplasmic enzyme that appears to account for the major fungal ADH activity (18, 19). In addition, in *M. circinelloides* and *M. rouxii* the *adh1* gene mutation impairs growth under anaerobic conditions and negatively affects ethanol production

in aerobic cultures but does not affect the yeast-hypha dimorphism in aerobic conditions (20, 30). In recent years, specific signaling cascades, including the protein kinase A (31–34) and calcineurin pathways (9), have been implicated in the modulation of yeast-hyphal dimorphic transitions of *M. circinelloides*. Furthermore, it was shown that the pathogenicity of the fungus was negatively impacted upon calcineurin mutation (9).

In the present study, we show that alteration of the fermentative metabolism of *M. circinelloides* by *adh1* mutation exacerbates the pathogenic capacity of the fungus. In particular, the lack of ADH1 activity in the M5 mutant strain led to a higher mortality rate upon infection on mice or nematodes than that seen with the wild-type R7B and the complemented mutant M5/pEUKA-*adh1*$^+$ strains bearing functional ADH1 activity. Our previous kinetic studies showed that the *M. circinelloides* ADH1 enzyme possesses greater affinity for acetaldehyde than ethanol, revealing that *in vivo*, the main role of this enzyme is to convert acetaldehyde to ethanol (18). Our observations indicated that strain M5 produces higher acetaldehyde concentrations in the SS (45 mM) than do strains R7B (0.5 mM) and M5/pEUKA-*adh1*$^+$ (15 mM), lending further support to the fermentative function of the fungal ADH1 enzyme. This result also explains the higher toxic effects on *C. elegans* viability when exposed to SS from M5 than when exposed to SS from strains with functional ADH1 activity. Further observations supporting the model that the high concentration of acetaldehyde in the M5 SS accounts for the marked *C. elegans* loss of viability include (i) the decrease in the *M. circinelloides* strain-mediated SS toxicity effect by its incubation at 25°C and 37°C, which triggers acetaldehyde evaporation, and (ii) exogenous addition of acetaldehyde to *C. elegans* at a concentration similar to that produced by the M5 mutant, which recapitulates the M5 SS toxic effect in nematode viability. Notably, M5 overexpresses the *ald2* gene, which could be an acetaldehyde-induced response, as previously described in *S. cerevisiae* (35), aimed at acetaldehyde detoxification by its conversion to acetate.

Acetaldehyde is a highly toxic and carcinogenic product of alcohol fermentation and metabolism in microorganisms (36). In the dimorphic pathogen *C. albicans*, the ability to form biofilms constitutes a major virulence factor (37). Specifically, alcohol dehydrogenase is downregulated in *C. albicans* biofilms, and *ADH1* disruption significantly enhances the ability of the fungus to form biofilms in which the production of ethanol is low and that of acetaldehyde is high. Thus, it was concluded that ADH1 activity restricts the ability of *C. albicans* to form biofilms *in vitro* and *in vivo* and that the protein restricts biofilm formation through an ethanol-dependent mechanism (16). It was shown that in the presence of D,L-2-hydroxyisocaproic acid, *C. albicans* restricts biofilm formation and negatively affects the production of acetaldehyde from glucose; apparently, the latter process may be due to the upregulation of genes responsible for acetaldehyde catabolism (37, 38).

By using a chemotherapeutic murine model of invasive pulmonary aspergillosis and a metabolomics approach, ethanol was detected in the lungs of mice infected with *Aspergillus fumigatus*; it was demonstrated that during infection, the fungus is exposed to oxygen depleted microenvironments (17). An Δ*alcC* mutant (which has the alcohol dehydrogenase encoding gene *alcC* deleted) of *A. fumigatus* showed no growth defects under hypoxic conditions and yielded wild-type levels of mortality in different murine models. However, lung immunohistopathology and flow cytometry analyses revealed an increase in the inflammatory response in mice infected with the Δ*alcC* mutant strain, which corresponded to a reduction in fungal burden. It was concluded that in *A. fumigatus*, a functional ADH1 contributes to fungal pathogenesis in the lung, to hypoxia adaptation, and to growth (17).

The high degree of virulence of the *M. circinelloides* M5 *adh1* mutant in mice or in *C. elegans* demonstrates that altered fermentative metabolism, producing acetaldehyde accumulation, confers a greater capacity of pathogenesis and does not appear to negatively affect hypoxia adaptation during infection of mice, since the mutant M5 is not affected in its ability to colonize the host. In a previous study, we observed that the growth of the M5 mutant is drastically affected in *in vitro* cultures made under

anaerobic or in self-anaerobic conditions (20). Thus, the normal colonization of mice by the M5 mutant could indicate that nonfermentable carbon sources exist and could be used for growth in the environment of the animal's tissues and/or that hypoxia is not very strict in these tissues. Our findings reveal a mechanistic difference between *A. fumigatus* and *M. circinelloides* regarding the importance of the ADH1 enzyme in connection with pathogenic potential: in the former fungus, a functional ADH1 is required to sustain hypoxia adaptation and host colonization (18), whereas in *M. circinelloides*, the aforementioned enzymatic activity is not required for adaptation to hypoxia or for colonization of mice, and rather, the possession of a nonfunctional ADH1 increases the pathogenic potential of the fungus. Our results coincide in some aspects with those obtained in *C. albicans*, mainly with the observation that a decrease in ADH activity causes an increase in virulence. In *Candida*, this process is associated with an increase in biofilm formation, which constitutes a major virulence factor (37). In our observations, the mouse tissues (mainly liver and lungs) invaded by the M5 mutant showed fungal growth accumulation, but we were unable to determine if these hyphae were organized in biofilms. However, the fact that the S5 from the three *M. circinelloides* strains studied were able to cause mortality in *C. elegans* indicated that hyphae are not the direct cause of damage to the nematode, but rather the acetaldehyde produced and excreted by strain M5 is the cause.

Wild-type *Candida* strains can produce acetaldehyde from ethanol or glucose in *in vitro* cultures (38). Our results show that in cultures grown in medium with glucose, the wild-type *M. circinelloides* strain R7B does not produce significant amounts of acetaldehyde. This may explain R7B's low degree of virulence compared to the M5 mutant strain, which produces acetaldehyde under these conditions, and indicates a metabolic difference between *Candida* and *Mucor*.

When cultured *in vitro* under aerobic conditions in the presence of glucose, the *M. circinelloides* M5 mutant showed a 35% decrease in germination rate and produced 33% less biomass than R7B. As *M. circinelloides* produces high levels of ethanol under aerobic conditions (18, 20), most likely such metabolism contributes to energy production, possibly through the regeneration of NAD^+, catalyzed by the ADH1 enzyme (18, 20). We propose that these detrimental effects could be the result of a lack of NAD^+ regeneration through the ADH1 activity in the M5 mutant strain. Unexpectedly, despite its reduced growth in cultures, the colonization of tissues by M5 was more extensive than that observed with strains R7B and M5/pEUKA-*adh1*$^+$. Probably, this is because strain M5 is more resistant to macrophage digestion in mice, as we observed in macrophage culture analysis.

In chronic lung inflammation in smokers (39) or heavy drinkers (40), acetaldehyde acts as a toxic compound that drives the inflammatory tissue response. The infection of mice with the Δ*alcC* mutant of *A. fumigatus* triggers an inflammatory response in their bronchoalveolar fluids (17). In the present study, we observed a similar effect in infections with the *M. circinelloides* M5 mutant, with an enhanced inflammatory response in all mouse tissues analyzed compared to that following R7B or M5/pEUKA-*adh1*$^+$ infection. We propose that overproduction of acetaldehyde contributes significantly to the M5 mutant's virulence and enhanced tissue burden in mice. Notably, 4.5 mM acetaldehyde inhibits phagocytosis and chemotaxis of monocytes and polymorphonuclear cells (41). This inhibitory effect may partially explain the enhanced tissue colonization by the M5 mutant strain compared to that of strains with functional ADH1 activity.

Our results indicated that the infection of mice with *M. circinelloides* M5 induced a systemic inflammatory response, even in brain tissue, suggesting a process of cell degranulation and blood histamine release. To test this assumption, we assessed the mRNA levels of three inflammatory response markers: (i) *Mip2*, whose mRNA expression is influenced by the presence of histamine (42), (ii) *Il-1β*, which is an important chemokine in the cell inflammatory response and apoptosis (43), and (iii) *Il-6*, the general response chemokine in inflammatory processes (44). These inflammatory response markers were expressed at a higher level of transcript (*Mip2*, *Il-1β*, and *Il-6*) and

protein (IL-1β and IL-6) in mouse tissues infected with the M5 mutant strain than those infected with *M. circinelloides* strains with functional ADH1 activity, indicating that strain M5 triggers a more pronounced inflammatory response.

In support of our model that acetaldehyde produced by *M. circinelloides* strain M5 is in part responsible for M5-associated pathology, treatment with the ALD inhibitor disulfiram, which increases acetaldehyde accumulation, exacerbated M5 virulence.

Acetaldehyde is produced by a conserved metabolic pathway in diverse human pathogens, including bacteria (*Enterobacteria* species), fungi (Ascomycetes: *C. albicans*, Zygomycetes: *Mucor* species), and protozoa (*Entamoeba* species); most of these organisms use fermentative metabolism during their infection process (45). To our knowledge, this is the first report that links ethanol metabolism and virulence in an early-diverging fungus. Furthermore, as *M. circinelloides* is a versatile fungus able to utilize diverse nutrients and oxygen concentrations to colonize its environment, it would be of considerable interest to identify a possible relationship between the prevalence and virulence of Mucorales strains (not only exclusive for *M. circinelloides*) from clinical origins and their characteristics in relation to ethanol metabolism.

MATERIALS AND METHODS

Strains and growth conditions. The *M. circinelloides* R7B (*leuA*$^-$) strain was originally derived from the (−) mating type *M. circinelloides* f. *lusitanicus* CBS 277.49 (46), M5 (*leuA*$^-$, *adh1*$^-$) is a spontaneous *adh1* mutant strain obtained by growth selection in allyl alcohol (20), and M5/pEUKA-*adh1*$^+$ is an M5 strain carrying a self-replicative plasmid (pEUKA-7) harboring the wild-type *adh1* gene from *M. circinelloides* R7B.

Spores were grown on yeast-peptone-glucose (YPG) medium containing 0.3% yeast extract, 1% gelatin peptone, and 2% glucose and supplemented as necessary with 2% bacteriological agar at pH 4.5. Minimum Lee medium was also employed, using 2% glucose, 0.5% sodium chloride, 0.25% potassium dihydrogen phosphate, 0.20% magnesium sulfate, 0.20% ammonium sulfate, 0.005% leucine as necessary, and 2% bacteriological agar supplemented when producing solid medium (adjusted pH 5.3).

Aerobic and self-anaerobic spore germination and growth quantification. Aerobic growth was performed in a 250-ml flask with 25 ml YPG inoculated with 5×10^5 *M. circinelloides* spores per ml. Liquid cultures were maintained at 28°C for 24 h with constant shaking at 150 rpm. Self-anaerobic spore germination was performed using 125-ml flasks with 125 ml YPG medium; 5×10^5 *M. circinelloides* spores per ml were incubated as described previously (47). The germination percentage was calculated for aerobic or anaerobic conditions as germinules or budding yeasts counted in a total of 100 cells. To determine biomass production, mycelia were collected from liquid cultures using filtration, and the dry weight was determined.

To evaluate the oxidative stress, 100 spores from each of the different strains were treated or not treated with 4 mM H_2O_2 for 1 h at 4°C and spread on YPG plates and incubated for 24 h at 28°C.

Total genomic DNA isolation from mouse tissues. DNA from mouse tissues infected or not infected with *M. circinelloides* strains was isolated as follows. Organs (brain, lung, spleen, and liver) were removed from the mouse postinoculation; tissue lysis was performed using 50 mg from each organ. Mouse tissue samples were transferred into a tube with MagNA Lyser green beads (Roche, Madison, WI, USA) and precooled on ice. Denaturing binding buffer (200 μl) and proteinase K (10 mg/ml, 40 μl) from the High Pure PCR template preparation kit (Roche) were added immediately before homogenization. For cell disruption, tubes were placed in the MagNA Lyser instrument (Roche) and processed twice at 4,200 $\times$ *g* for 40 s. Samples were cooled on ice for 1 min between each processing step. Samples were then centrifuged for 1 min at 15,000 $\times$ *g* (Eppendorf 5417), and the supernatants were used for DNA isolation following the manufacturer's protocol. Total genomic DNA was quantified using a Smart Spec Plus spectrophotometer (Bio-Rad, Berkeley, CA, USA).

Total RNA isolation from mouse tissues or *M. circinelloides*. Biological samples from the different *M. circinelloides* strains were collected 24 h after aerobic growth in YPG or Lee medium, filtered through Whatman filter paper (Sigma, St. Louis, MO, USA), and washed with distilled water. Mouse tissues (brain, lung, spleen, or liver) were also collected following *M. circinelloides* strain infection.

Approximately 50 mg of mycelia or mouse tissue samples was then transferred into a tube with MagNA Lyser green beads (Roche) precooled on ice. Denaturing RLT buffer (700 μl) from the RNeasy minikit (Qiagen, Venlo, The Netherlands) was added immediately before homogenization. For cell disruption, tubes were placed in the MagNA Lyser instrument and processed twice at 6,500 rpm for 40 s with cooling on ice for 1 min between each step. Then, samples were centrifuged for 1 min at 20,000 $\times$ *g* (Eppendorf 5417), and the supernatants were used for RNA isolation following the RNeasy minikit protocol (Qiagen). To eliminate DNA contamination, samples were treated with DNase I (Promega, Madison, WI, USA) according to the manufacturer's protocol. RNA samples were separated on nondenaturing 2% agarose gels stained with ethidium bromide, visualized using a Gel Doc XR+ imager (Bio-Rad, Hercules, CA, USA), and quantified using a SmartSpec Plus spectrophotometer (Bio-Rad).

Oligonucleotide design and real-time quantitative reverse transcription-PCR (qRT-PCR). Primers and hydrolysis probes for the *ald2* gene from *M. circinelloides* encoding the homolog to ALD2 from *Saccharomyces cerevisiae* were used as reported previously (20), and the β-actin (*Act*β), interleukin 1β

(*Il-1β*), interleukin 6 (*Il-6*), and murine macrophage inflammatory protein 2 (*Mip2*) genes from mice were used as described before (13).

qRT-PCR was performed using the LightCycler 480 II system (Roche Molecular Diagnostics, Pleasanton, CA, USA) employing the SuperScript III Platinum one-step qRT-PCR reagent kit (Invitrogen, Carlsbad, CA, USA). Each 25-μl reaction volume comprised 5 μl extracted total RNA template (50 ng), 0.5 μl enzyme mix, 12.5 μl reaction mix (2×), 0.5 μl each 10-μM forward and reverse primer, 0.5 μl probe (5 μM), and 5.5 μl nuclease-free water. qRT-PCR was initiated with reverse transcription (50°C, 30 min) and initial denaturation (95°C, 5 min), followed by 45 amplification cycles at 60°C for 30 s, 72°C for 30 s, and 95°C for 15 s; fluorescence signals were collected at each 60°C stage. Appropriate positive, nontemplate, and extraction controls were included in each test run.

Fungal load determination by real-time quantitative PCR from mouse tissues. The qPCR assay was performed using the LightCycler 480 II system with the Platinum quantitative PCR SuperMix-UDG kit (Invitrogen). Reactions were as above for qRT-PCR but with 5 μl extracted total DNA template (500 ng). qPCR was performed as indicated for qRT-PCR (without reverse transcriptase) and included the same controls as those employed for qRT-PCR; fluorescence signals were collected at each 60°C stage at 530 nm.

qRT-PCR and qPCR amplification efficiency, relative expression level calculation, and data analysis. To evaluate relative gene expression, a calculation for estimating the efficiency of a real-time PCR assay for each studied gene is required. Here, estimation was performed using a calibration dilution curve and slope calculation. A 5-fold dilution series (500 to 0.05 ng total RNA) was utilized as qRT-PCR samples. Briefly, E was obtained from standard curves using the formula $E = \{[10^{(-1/slope)} - 1]/100\}$. Relative expression levels were determined using the efficiency correction method, considering amplification efficiencies between target and reference genes (48). *M. circinelloides tfc-1*, which encodes a subunit of the transcription factor TFIIIC required for the RNA polymerase III preinitiation complex assembly, served as the reference gene in qRT PCR analysis during dimorphism in *M. circinelloides* (19).

***Caenorhabditis elegans* killing assays.** *C. elegans* Bristol N2 worms (49) were synchronized by hypochlorite isolation of eggs from gravid adults, followed by hatching in S-basal medium (50). L1 larvae were transferred onto nematode growth medium (50) plates seeded with the *Escherichia coli* OP50 strain previously grown on the plates as a food source and incubated at 20°C for 4 to 5 days until reaching young adult phase. Worms were rinsed from the plates and washed in S basal medium. *M. circinelloides* cultures were grown at 12 or 24 h in YPG medium supplemented with leucine at 28°C and, after centrifugation, the SS was recovered by filtration (Millipore 0.2-μm filters; Billerica, MA, USA) for further experiments. For each experiment, 10 to 20 worms were dispensed into each well of 24-well Costar plates (Corning, Inc., Armonk, NY, USA). Then, worms were incubated with 1 ml SS or 10,000 spores from each strain contained in a total volume of 1 ml Lee medium, and the plates were incubated for 48 h at 20°C and scored for live worms at 6, 12, 24, and 48 h. For statistical purposes, three replicates per experiment were performed. YPG and Lee medium served as negative controls. A worm was considered dead when it no longer responded (moved) to a touch stimulus. Worms that died after sticking to the plate wall were excluded from the analysis.

For all assays, fungal inoculum concentrations were confirmed by dilution plating and counting. We conducted three independent assays for each worm group. The SS (1 ml) obtained from each *M. circinelloides* strain was treated with 25 μl pronase (Sigma), equivalent to 5 units, and incubated for 2 h at 37°C or heated at 90°C for 2 h prior to its use in the *C. elegans* killing assays.

Mouse virulence and disulfiram treatment. The protocol for the mouse virulence model followed the recommendations of the Mexican Federal Regulations for the Use and Care of Animals (NOM-062-ZOO-1999) (SAGARPA 2001) (51).

To assess *M. circinelloides* strain virulence, groups of approximately 10- to 12-week-old male BALB/c mice (CINVESTAV, Zacatenco, México) (20 g average weight) were used. At day 0, mice were inoculated with spores from the different *M. circinelloides* strains in 200 μl total volume of sterile phosphate-buffered saline containing 5×10^5 spores/dose administered intraperitoneally. Mouse survival was monitored each day. At least three independent assays were conducted for each group.

An ALD activity inhibitor (disulfiram; Sigma) was administered to the mice prior to and during the infection assay; each mouse was injected intraperitoneally with 300 mg/kg of body weight 48 h prior to spore inoculation and at day 0 of infection, followed by dosing each 48 h during the infection period. Mouse survival was monitored each 12 h after infection. Ethanol was administered by ingestion in drinking water at a concentration of 10% (vol/vol) supplied *ad libitum* to groups of male mice with or without disulfiram treatment.

Macrophage spore killing assay. Mouse monocyte/macrophage RAW 264.7 (TIB-71) was purchased from the American Type Culture Collection (ATCC). Cells were maintained in Dulbecco modified Eagle (DMEM) medium supplemented with 10% fetal bovine serum (FBS) (Sigma, USA), 100 U/ml penicillin (Sigma, USA), and 100 μg/ml streptomycin (Sigma, USA) (basal medium) at 5% CO_2 and 37°C 24 h before treatments.

Macrophages were seeded at 8×10^5 cells/well in DMEM basal medium (Gibco, Thermo Fisher Scientific, USA) without antibiotics and incubated at 37°C in 6-well plates. After incubation overnight, the basal medium in each well was replaced with fresh medium, and then the macrophages were cocultured with 2×10^5 spores produced in YPG for 1 or 6 h. Afterwards, the culture medium and cells and spores were separated by centrifugation at 1,000 × *g* for 10 min. The cell and spore pellet was recovered and resuspended in 0.1 ml and separated into two tubes with 0.05 ml each. One tube was maintained at −80°C until nucleic acid extraction was performed, and the other was diluted (1:50) and used to plate 200 of the initial spores to evaluate CFU in YPG solid medium. For the CFU assay, the control was the

spores in DMEM basal medium without antibiotics. The CFU were quantified 24 h after incubation in the presence of light at 28°C.

Preparation of tissue homogenate supernatants and ELISA. Spores from the different strains of *M. circinelloides* were inoculated intraperitoneally in BALB/c mice, and 48 h postinfection the animals were sacrificed and the organs were removed. Liver and lung organs were harvested, and the organs were transferred to a 2.0-ml microcentrifuge tube containing 0.8 ml phosphate-buffered saline (PBS) and protease inhibitor (cOmplete ultra tablets, mini, EDTA-free; Roche Diagnostics, Mannheim, Germany). The organs were homogenized by a Potter-Elvehjem glass homogenizer, and the supernatants were collected from the mixture following centrifugation at 10,000 × *g* for 10 min at 4°C and stored at −80°C prior to analysis. The protein expression level of IL-1β and IL-6 in the liver and lungs was determined using enzyme-linked immunosorbent assay (ELISA) following the manufacturer's instructions (Sigma, USA).

Determination of abundance of DNA from spores of *M. circinelloides* using qPCR. The abundance of spores of *M. circinelloides* from macrophage interaction was compared based on a spore standard curve of *M. circinelloides*. Wild-type R7B spore concentrations between 1×10^2 and 1×10^7 ml^{-1} by 10-fold serial dilutions were employed. Consequently, DNA was extracted to generate a spore standard curve by qPCR by detection of the validated *tfc-1* nuclear gene.

Histopathology. BALB/c mice were inoculated as described above and sacrificed at set time points after *M. circinelloides* inoculation. Organs were removed and fixed in 10% phosphate-buffered formalin, embedded in paraffin, sectioned at 5 μm, and stained with hematoxylin and eosin or Gomori methenamine silver using standard histological techniques. Microscopic examinations of the stained tissues were performed on a Leica M80/MSV266 instrument using a Leica DFC295 camera and the Leica Application Suite version 3.8.5 imaging system (Leica Microsystems Inc., Buffalo Grove, IL, USA).

Acetaldehyde and acetic acid quantitation. Acetaldehyde quantitation was performed using gas chromatography with a flame ionization detector on a 7890A series gas chromatograph (Agilent Technologies, Palo Alto, CA, USA) equipped with a WAX column (30 m length by 0.25 mm inside diameter [i.d.] by 0.25 μm film thickness) (Phenomenex, Torrance, CA, USA). Nitrogen was run as a carrier gas at a constant column flow rate of 0.7 ml/min. The temperature program was as follows: 40°C hold for 2 min, 5°C/min up to 60°C, 40°C up to 200°C for 0.5 min. The Split 20 injector was set at 200°C. Flame ionization detector temperatures were set at 250°C with H_2/airflow of 45/450 ml/210°C. Acetaldehyde was quantified using a calibration curve.

Acetic acid quantitation was performed as follows. Sodium hydroxide (NaOH) 0.05 N was prepared with cold water previously boiled for 3 min to eliminate dissolved CO_2; this NaOH solution was standardized with a 0.01 N HCl solution.

For preparation of each *M. circinelloides* supernatant sample, 100 ml previously boiled distilled water was added to a 250-ml Erlenmeyer flask, adjusted to pH 8.2 with 0.05 N NaOH solution and a Sartorius Professional PP-15 pH meter (Bohemia, NY, USA), and 5 ml supernatant was added. The solution was placed in a burette for titration to pH 8.2. The 0.05 N NaOH volume (in ml) necessary to neutralize the acid is directly proportional to the total acidity of acetic acid. The mathematical formula employed was:

$$\mathrm{TA\%} = 100\ (V_{\mathrm{titrate}} \times N_{\mathrm{titrate}} \times \text{citric acid Eqv. Wt.}) \cdot (V_S \times 100)$$

where TA is total acidity, $V_{titrate}$ is the volume of NaOH titrate employed, $N_{titrate}$ is the normality of the NaOH used in the reaction, citric acid Eqv. Wt. is 60.05, and V_s is the volume of sample. Using this approach, the quantity of total acetic acid produced was determined (g/liter).

Statistical analysis. Significance testing was performed using the unpaired Student's *t* test. *, $P < 0.05$; **, $P < 0.01$; ***, $P < 0.001$. When results were not considered significant, we did not provide an additional indication ($P < 0.1$).

SUPPLEMENTAL MATERIAL

Supplemental material is available online only.

SUPPLEMENTAL FILE 1, PDF file, 7.3 MB.

ACKNOWLEDGMENTS

We thank A.Y. Guzman-Hernandez for technical support in the initial mouse infection assays.

This work was supported by grants from Coordinación de la Investigación Científica (UMSNH; 2.6, 2.35) and Consejo Nacional de Ciencia y Tecnología (CONACYT; 181747, 167071). S.P.D.-P., J.A.P.-M., and M.I.V.-M. were supported by postgraduate fellowships from CONACYT.

S.P.D.-P., J.A.P.-M., M.I.V.-M., A.L.-T., I.E.J.-G., V.A.-M., V.G.-R., J.C.-G., R.E.N.-A., and R.O.-A. contributed to data acquisition, analysis, and data interpretation. J.C.-G., M.I.R.-D., J.F.G.-C., and V.M.-C. contributed to critical analysis, data interpretation, and critical revision of the article for intellectual content of the manuscript. J.F.G.-C. and V.M.-C. contributed to the conception and design of the work, data analysis, and interpretation. J.F.G.-C. and V.M.-C. wrote the majority of the article with minor contributions from the other authors.

We declare no conflicts of interest.

REFERENCES

1. Kim JY. 2016. Human fungal pathogens: why should we learn? J Microbiol 54:145–148. https://doi.org/10.1007/s12275-016-0647-8.
2. Matthaiou DK, Christodoulopoulou T, Dimopoulos G. 2015. How to treat fungal infections in ICU patients. BMC Infect Dis 15:205. https://doi.org/10.1186/s12879-015-0934-8.
3. Douglas AP, Chen SC, Slavin MA. 2016. Emerging infections caused by non-*Aspergillus* filamentous fungi. Clin Microbiol Infect 22:670–680. https://doi.org/10.1016/j.cmi.2016.01.011.
4. Pak J, Tucci VT, Vincent AL, Sandin RL, Greene JN. 2008. Mucormycosis in immunochallenged patients. J Emerg Trauma Shock 1:106–113. https://doi.org/10.4103/0974-2700.42203.
5. Petrikkos G, Skiada A, Lortholary O, Roilides E, Walsh TJ, Kontoyiannis DP. 2012. Epidemiology and clinical manifestations of mucormycosis. Clin Infect Dis 54:S23–S34. https://doi.org/10.1093/cid/cir866.
6. Neto FM, Camargo PC, Costa AN, Teixeira RH, Carraro RM, Afonso JE, Jr, Campos SV, Samano MN, Fernandes LM, Abdalla LG, Pêgo-Fernandes PM. 2014. Fungal infection by *Mucorales* order in lung transplantation: 4 case reports. Transplant Proc 46:1849–1851. https://doi.org/10.1016/j.transproceed.2014.05.033.
7. Cornely OA, Arikan-Akdagli S, Dannaoui E, Groll AH, Lagrou K, Chakrabarti A, Lanternier F, Pagano L, Skiada A, Akova M, Arendrup MC, Boekhout T, Chowdhary A, Cuenca-Estrella M, Freiberger T, Guinea J, Guarro J, de Hoog S, Hope W, Johnson E, Kathuria S, Lackner M, Lass-Flörl C, Lortholary O, Meis JF, Meletiadis J, Muñoz P, Richardson M, Roilides E, Tortorano AM, Ullmann AJ, van Diepeningen A, Verweij P, Petrikkos G, European Society of Clinical Microbiology and Infectious Diseases Fungal Infection Study Group, European Confederation of Medical Mycology. 2013. ESCMID and ECMM joint clinical guidelines for the diagnosis and management of mucormycosis. Clin Microbiol Infect 3:5–26. https://doi.org/10.1111/1469-0691.12371.
8. Binder U, Maurer E, Lass-Flörl C. 2014. Mucormycosis: from the pathogens to the disease. Clin Microbiol Infect 6:60–66. https://doi.org/10.1111/1469-0691.12566.
9. Lee SC, Li A, Calo S, Heitman J. 2013. Calcineurin plays key roles in the dimorphic transition and virulence of the human pathogenic zygomycete *Mucor circinelloides*. PLoS Pathog 9:e1003625. https://doi.org/10.1371/journal.ppat.1003625.
10. Patiño-Medina JA, Maldonado-Herrera G, Pérez-Arques C, Alejandre-Castañeda V, Reyes-Mares NY, Valle-Maldonado MI, Campos-García J, Ortiz-Alvarado R, Jácome-Galarza IE, Ramírez-Díaz MI, Garre V, Meza-Carmen V. 2018. Control of morphology and virulence by ADP-ribosylation factors (Arf) in *Mucor circinelloides*. Curr Genet 64:853–869. https://doi.org/10.1007/s00294-017-0798-0.
11. Patiño-Medina JA, Valle-Maldonado MI, Maldonado-Herrera G, Pérez-Arques C, Jácome-Galarza IE, Díaz-Pérez C, Díaz-Pérez AL, Araiza-Cervantes CA, Villagomez-Castro JC, Campos-García J, Ramírez-Díaz MI, Garre V, Meza-Carmen V. 2019. Role of Arf-like proteins (Arl1 and Arl2) of *Mucor circinelloides* in virulence and antifungal susceptibility. Fungal Genet Biol 129:40–51. https://doi.org/10.1016/j.fgb.2019.04.011.
12. Liu M, Spellberg B, Phan QT, Fu Y, Fu Y, Lee AS, Edwards JE, Jr, Filler SG, Ibrahim AS. 2010. The endothelial cell receptor GRP78 is required for mucormycosis pathogenesis in diabetic mice. J Clin Invest 120:1914–1924. https://doi.org/10.1172/JCI42164.
13. Patiño-Medina JA, Vargas-Tejeda D, Valle-Maldonado MI, Alejandre-Castañeda V, Jácome-Galarza IE, Villegas-Moreno J, Nuñez-Anita RE, Ramírez-Díaz MI, Ortiz-Alvarado R, Meza-Carmen V. 2019. Sporulation on blood serum increases the virulence of *Mucor circinelloides*. Microb Pathog 137:103737. https://doi.org/10.1016/j.micpath.2019.103737.
14. Brunke S, Mogavero S, Kasper L, Hube B. 2016. Virulence factors in fungal pathogens of man. Curr Opin Microbiol 32:89–95. https://doi.org/10.1016/j.mib.2016.05.010.
15. Ramage G, Mowat E, Jones B, Williams C, Lopez-Ribot J. 2009. Our current understanding of fungal biofilms. Crit Rev Microbiol 35:340–355. https://doi.org/10.3109/10408410903241436.
16. Mukherjee PK, Mohamed S, Chandra J, Kuhn D, Liu S, Antar OS, Munyon R, Mitchell AP, Andes D, Chance MR, Rouabhia M, Ghannoum MA. 2006. Alcohol dehydrogenase restricts the ability of the pathogen *Candida albicans* to form a biofilm on catheter surfaces through an ethanol-based mechanism. Infect Immun 74:3804–3816. https://doi.org/10.1128/IAI.00161-06.
17. Grahl N, Puttikamonkul S, Macdonald JM, Gamcsik MP, Ngo LY, Hohl TM, Cramer RA. 2011. *In vivo* hypoxia and a fungal alcohol dehydrogenase influence the pathogenesis of invasive pulmonary aspergillosis. PLoS Pathog 7:e1002145. https://doi.org/10.1371/journal.ppat.1002145.
18. Rangel-Porras RA, Meza-Carmen V, Martinez-Cadena G, Torres-Guzmán JC, González-Hernández GA, Arnau J, Gutiérrez-Corona JF. 2005. Molecular analysis of an NAD-dependent alcohol dehydrogenase from the zygomycete *Mucor circinelloides*. Mol Genet Genomics 274:354–363. https://doi.org/10.1007/s00438-005-0025-4.
19. Valle-Maldonado MI, Jácome-Galarza IE, Gutiérrez-Corona F, Ramírez-Díaz MI, Campos-García J, Meza-Carmen V. 2015. Selection of reference genes for quantitative real time RT-PCR during dimorphism in the zygomycete *Mucor circinelloides*. Mol Biol Rep 42:705–711. https://doi.org/10.1007/s11033-014-3818-x.
20. Rangel-Porras RA, Díaz-Pérez SP, Mendoza-Hernández JM, Romo-Rodríguez P, Alejandre-Castañeda V, Valle-Maldonado MI, Torres-Guzmán JC, González-Hernández GA, Campos-Garcia J, Arnaud J, Meza-Carmen V, Gutiérrez-Corona JF. 2019. Alcohol dehydrogenase 1 participates in the Crabtree effect and connects fermentative and oxidative metabolism in the Zygomycete *Mucor circinelloides*. J Microbiol 57:606–617. https://doi.org/10.1007/s12275-019-8680-z.
21. McIntyre M, Breum J, Arnau J, Nielsen J. 2002. Growth physiology and dimorphism of *Mucor circinelloides* (syn. *racemosus*) during submerged batch cultivation. Appl Microbiol Biotechnol 58:495–502. https://doi.org/10.1007/s00253-001-0916-1.
22. Li CH, Cervantes M, Springer DJ, Boekhout T, Ruiz-Vazquez RM, Torres-Martinez SR, Heitman J, Lee SC. 2011. Sporangiospore size dimorphism is linked to virulence of *Mucor circinelloides*. PLoS Pathog 7:e1002086. https://doi.org/10.1371/journal.ppat.1002086.
23. Sheppard DC, Filler SG. 2014. Host cell invasion by medically important fungi. Cold Spring Harb Perspect Med 5:a019687. https://doi.org/10.1101/cshperspect.a019687.
24. Karamanakos PN, Pappas P, Boumba VA, Thomas C, Malamas M, Vougiouklakis T, Marselos M. 2007. Pharmaceutical agents known to produce disulfiram-like reaction: effects on hepatic ethanol metabolism and brain monoamines. Int J Toxicol 26:423–432. https://doi.org/10.1080/10915810701583010.
25. Chayakulkeeree M, Ghannoum M, Perfect J. 2006. Zygomycosis: the reemerging fungal infection. Eur J Clin Microbiol Infect Dis 25:215–229. https://doi.org/10.1007/s10096-006-0107-1.
26. Ibrahim AS, Spellberg B. 2006. Zygomycetes as agents of infectious disease in humans, p 429–440. *In* Heitman J, Filler SG, Edwards JE, Jr, Mitchell AP (ed), Molecular principles of fungal pathogenesis. ASM Press, Washington, DC.
27. Neblett Fanfair R, Benedict K, Bos J, Bennett SD, Lo YC, Adebanjo T, Etienne K, Deak E, Derado G, Shieh WJ, Drew C, Zaki S, Sugerman D, Gade L, Thompson EH, Sutton DA, Engelthaler DM, Schupp JM, Brandt ME, Harris JR, Lockhart SR, Turabelidze G, Park BJ. 2012. Necrotizing cutaneous mucormycosis after a tornado in Joplin, Missouri. N Engl J Med 367:2214–2225. https://doi.org/10.1056/NEJMoa1204781.
28. Bartnicki-Garcia S. 1963. Symposium on biochemical bases of morphogenesis in fungi. III. Mold-yeast dimorphism of *Mucor*. Bacteriol Rev 27:293–304.
29. Sypherd PS, Borgia PT, Paznokas JL. 1978. Biochemistry of dimorphism in the fungus *Mucor*. Adv Microb Physiol 18:67–104. https://doi.org/10.1016/s0065-2911(08)60415-4.
30. Torres-Guzman JC, Arreola-Garcia GA, Zazueta-Sandoval R, Carrillo-Rayas T, Martinez-Cadena G, Gutierrez-Corona F. 1994. Genetic evidence for independence between fermentative metabolism (ethanol accumulation) and yeast-cell development in the dimorphic fungus *Mucor rouxii*. Curr Genet 26:166–171. https://doi.org/10.1007/bf00313806.
31. Wolff AM, Appel KF, Petersen JB, Poulsen U, Arnau J. 2002. Identification and analysis of genes involved in the control of dimorphism in *Mucor circinelloides* (syn. *racemosus*). FEMS Yeast Res 2:203–213. https://doi.org/10.1111/j.1567-1364.2002.tb00085.x.
32. Lübbehüsen T, González Polo V, Rossi S, Nielsen J, Moreno S, McIntyre M, Arnau J. 2004. Protein kinase A is involved in the control of morphology and branching during aerobic growth of *Mucor circinelloides*. Microbiology 150:143–150. https://doi.org/10.1099/mic.0.26708-0.
33. Ocampo J, Fernandez Nunez L, Silva F, Pereyra E, Moreno S, Garre V, Rossi S. 2009. A subunit of protein kinase A regulates growth and

differentiation in the fungus *Mucor circinelloides*. Eukaryot Cell 8:933–944. https://doi.org/10.1128/EC.00026-09.
34. Ocampo J, McCormack B, Navarro E, Moreno S, Garre V, Rossi S. 2012. Protein kinase A regulatory subunit isoforms regulate growth and differentiation in *Mucor circinelloides*: essential role of PKAR4. Eukaryot Cell 11:989–1002. https://doi.org/10.1128/EC.00017-12.
35. Aranda A, del Olmo M. 2003. Response to acetaldehyde stress in the yeast *Saccharomyces cerevisiae* involves a strain-dependent regulation of several ALD genes and is mediated by the general stress response pathway. Yeast 20:747–759. https://doi.org/10.1002/yea.991.
36. Seitz HK, Stickel F. 2010. Acetaldehyde as an underestimated risk factor for cancer development: role of genetics in ethanol metabolism. Genes Nutr 5:121–128. https://doi.org/10.1007/s12263-009-0154-1.
37. Nieminen MT, Novak-Frazer L, Rautemaa V, Rajendran R, Sorsa T, Ramage G, Bowyer P, Rautemaa R. 2014. A novel antifungal is active against *Candida albicans* biofilms and inhibits mutagenic acetaldehyde production in vitro. PLoS One 9:e97864. https://doi.org/10.1371/journal.pone.0097864.
38. Uittamo J, Siikala E, Kaihovaara P, Salaspuro M, Rautemaa R. 2009. Chronic candidosis and oral cancer in APECED-patients: production of carcinogenic acetaldehyde from glucose and ethanol by *Candida albicans*. Int J Cancer 124:754–756. https://doi.org/10.1002/ijc.23976.
39. Sapkota M, Wyatt TA. 2015. Alcohol, aldehydes, adducts and airways. Biomolecules 5:2987–3008. https://doi.org/10.3390/biom5042987.
40. Setshedi M, Wands JR, Monte SM. 2010. Acetaldehyde adducts in alcoholic liver disease. Oxid Med Cell Longev 3:178–185. https://doi.org/10.4161/oxim.3.3.12288.
41. Schopf RE, Trompeter M, Bork K, Morsches B. 1985. Effects of ethanol and acetaldehyde on phagocytic functions. Arch Dermatol Res 277:131–137. https://doi.org/10.1007/bf00414111.
42. Wolpe SD, Cerami A. 1989. Macrophage inflammatory proteins 1 and 2: members of a novel superfamily of cytokines. FASEB J 3:2565–2573. https://doi.org/10.1096/fasebj.3.14.2687068.
43. Henao-Mejia J, Elinav E, Strowig T, Flavell RA. 2012. Inflammasomes: far beyond inflammation. Nat Immunol 13:321–324. https://doi.org/10.1038/ni.2257.
44. Antachopoulos C, Roilides E. 2005. Cytokines and fungal infections. Br J Haematol 129:583–596. https://doi.org/10.1111/j.1365-2141.2005.05498.x.
45. Müller M, Mentel M, van Hellemond JJ, Henze K, Woehle C, Gould SB, Yu R-Y, van der Giezen M, Tielens AGM, Martin WF. 2012. Biochemistry and evolution of anaerobic energy metabolism in eukaryotes. Microbiol Mol Biol Rev 76:444–495. https://doi.org/10.1128/MMBR.05024-11.
46. Roncero MIG, Jepsen LP, Strøman P, van Heeswijck R. 1989. Characterization of a *leuA* gene and an *ARS* element from *Mucor circinelloides*. Gene 84:335–343. https://doi.org/10.1016/0378-1119(89)90508-8.
47. Salcedo-Hernández R, Ruiz-Herrera J. 1993. Isolation and characterization of a mycelial cytochrome aa_3-deficient mutant and the role of mitochondria in dimorphism of *Mucor rouxii*. Exp Mycol 17:142–154. https://doi.org/10.1006/emyc.1993.1013.
48. Pfaffl MW. 2001. A new mathematical model for relative quantification in real-time RT-PCR. Nucleic Acids Res 29:e45. https://doi.org/10.1093/nar/29.9.e45.
49. Brenner S. 1974. The genetics of *Caenorhabditis elegans*. Genetics 77:71–94.
50. Stiernagle T. 2006. Maintenance of *C. elegans*. Worm Book 11:1–11. https://doi.org/10.1895/wormbook.1.101.1.
51. Secretaría de Agricultura, Ganadería, Desarrollo Rural, Pesca y Alimentación (SAGARPA) NORMA Oficial Mexicana NOM-062-ZOO-1999. 2001. Especificaciones técnicas para la producción, cuidado y uso de los animales de laboratorio. Diario Oficial de la Federación 2:107–167. (In Spanish.)

Fungal Biology 124 (2020) 619–628

Contents lists available at ScienceDirect

Fungal Biology

journal homepage: www.elsevier.com/locate/funbio

Arf-like proteins (Arl1 and Arl2) are involved in mitochondrial homeostasis in *Mucor circinelloides*

J. Alberto Patiño-Medina [a], Marco I. Valle-Maldonado [a, b], David Vargas-Tejeda [a], Víctor M. Chávez-Jacobo [a], Alma R. Corrales-Escobosa [c], Joel Ramírez-Emiliano [d], León F. Ruiz-Herrera [a], Martha I. Ramírez-Díaz [a], Victoriano Garre [e], Víctor Meza-Carmen [a, *]

[a] Instituto de Investigaciones Químico Biológicas, Universidad Michoacana de San Nicolás de Hidalgo, 58038, Morelia, Mich, Mexico
[b] Laboratorio Estatal de Salud Pública del Estado de Michoacán, 58279, Morelia, Mich, Mexico
[c] Departamento de Química, Universidad de Guanajuato, 36000, Guanajuato, Gto., Mexico
[d] Departamento de Ciencias Médicas, Universidad de Guanajuato, 37320, León, Gto, Mexico
[e] Departamento de Genética y Microbiología, Universidad de Murcia, 30100 Murcia, Spain

ARTICLE INFO

Article history:
Received 5 November 2019
Received in revised form
17 February 2020
Accepted 25 February 2020
Available online 9 March 2020

Corresponding Editor: Julian Rutherford

Keywords:
Arf member
Fermentation
Glycolysis
Mitochondria
Mucoral
Virulence

ABSTRACT

Mucor circinelloides is an opportunistic dimorphic pathogen, with the dimorphic process controlled in parts by fermentative and oxidative metabolisms, which lead to yeast or mycelial growth, respectively. Dimorphic transition is important for pathogenesis since the mycelium represents the virulent morphology. We previously reported that the deletion of *arl1* or *arl2* stimulate anaerobic germination in *M. circinelloides*, suggesting an augmented fermentative metabolism. In the present study, we demonstrate that the heterokaryon $\Delta arl1^{(+)(-)}$ and homokaryon $\Delta arl2$ strains contain low number of mitochondria, which possibly results in a dysfunctional oxidative metabolism, marked by a low oxygen consumption in glucose and poor growth in glycerol as the unique carbon source. This dysfunction is compensated for by an increase in the glycolysis and fermentation in aerobic conditions, demonstrating growth kinetics similar to that in the wild-type strain. Moreover, as a consequence a high fermentative activity, the $\Delta arl1^{(+)(-)}$ and $\Delta arl2$ strains possibly increased the yeast cell growth during low oxygen concentrations in presence of glucose.

To the best of our knowledge, this is the first study to demonstrate the control of members of Arf family on the mitochondrial population in a *Mucor* species.

1. Introduction

Dimorphism in *Mucor circinelloides* is described as the property by which sporangiospores grow as yeast or mycelial vegetative cells; the carbon source and the presence of oxygen are the principal growth conditions determining the vegetative fate of spores (McIntyre et al., 2002; Lübbehüsen et al., 2003). In *M. circinelloides*, in general the yeast development is associated with a fermentative metabolism; meanwhile the mycelial growth is correlated with an oxidative metabolism (McIntyre et al., 2002; Rangel-Porras et al., 2005, 2019) and is reported to be the invasive and virulent form (Lee et al., 2013; Lewis and Kontoyiannis, 2013). Higher aerobic germination rates of *M. circinelloides* spores resulted in macrophage destruction (Li et al., 2011), suggesting that the initial steps in the formation of a germ tube could determine the success of host invasion.

The oxidative metabolism seems to be critical to mycelial growth in *M. circinelloides* (McIntyre et al., 2002; Lübbehüsen et al., 2003) as well as in other dimorphic species of *Mucor* (Orlowski, 1991). Thus, inhibition of electron chain transport in several dimorphic species of *Mucor* led to the growth of yeast cells in aerobic conditions as well (Orlowski, 1991). Numerous genes appear to contribute to adequate yeast or mycelial growth in *M. circinelloides*; for example, *adh1* that encodes the alcohol

* Corresponding author. Laboratorio de Diferenciación Celular, Instituto de Investigaciones Químico Biológicas, Universidad Michoacana de San Nicolás de Hidalgo, Ciudad Universitaria, 58030, Morelia, Michoacán, Mexico. Fax: +52 443326 5788 ext.120.
E-mail address: victor_meza2004@yahoo.com.mx (V. Meza-Carmen).

https://doi.org/10.1016/j.funbio.2020.02.016
1878-6146/

dehydrogenase 1, which is essential for growth of yeast cells, and its mutation leads to monomorphic mycelia (Rangel-Porras et al., 2019). *pkaR1*, that encodes for one of the regulatory subunits of the protein kinase A, is essential for adequate hyphal growth (Ocampo et al., 2009), and the calcineurin B regulatory subunit gene, *cnbR*, is essential for mycelial growth under aerobic conditions, which is suggestive of its importance in the oxidative metabolism of this *Mucor* species (Lee et al., 2013). Moreover, the deletion of ADP-Ribosylation Factor 2-encoding gene, *arf2*, decreased the growth rate of yeast considerably (Patiño-Medina et al., 2018). Arf family members belong to the Ras superfamily, which includes Arf-like proteins (Arl) and Sar (Secretion-associated and Ras-related) proteins as well (Kahn et al., 2006).

Selected Arf members, including Arl1 (Arf-like protein 1), are known to contribute to mitochondrial function and morphology (Ackema et al., 2014, 2016; Newman et al., 2014). In selected cases, Arf members control the site of contact between the endoplasmic reticulum (ER) and the mitochondria, and are essential in influencing mitochondrial morphology and function (Ackema et al., 2016).

We previously reported two Arl proteins in *M. circinelloides*, Arl1 and Arl2 that share around 55 % of identity between them and share 72.63 % and 52.46 % of identity with ARL1 from *S. cerevisiae*, being Arl1 the orthologous of ARL1. The *arl1* mRNA is high and mainly accumulated during the mycelial growth, meanwhile the mRNA levels of *arl2* are much lower that *arl1*, and showed stable expression during the dimorphism (Patiño-Medina et al., 2019).

The mutation of these *arl* genes renders the heterokaryon $\Delta arl1^{(+)(-)}$ indicating an essential role in this mucoral, and the homokaryon Δ*arl2* strains in *M. circinelloides*. The mutation of *arl1* or *arl2* genes resulted in vesicle mislocalization specially in the apical region, these mutants were also more susceptible to fluconazole and SDS, explained in part by lower quantity of glucosamine in the cell wall. Moreover, the mycelial growth from $\Delta arl1^{(+)(-)}$ increased the virulence by the secretion of molecule(s) susceptible to protease (Patiño-Medina et al., 2019). Additionally, $\Delta arl1^{(+)(-)}$ and Δ*arl2* strains led to a modest, yet significant increase in the germination rate under anaerobic conditions, suggesting an increase in glycolysis rate in the mutant strains (Patiño-Medina et al., 2019).

The main objective of this work was to demonstrate that Arl1 or Arl2 control fermentative and oxidative metabolism, possibly through mitochondrial homeostasis, and if these processes correlates with the virulence phenotype in these mutant strains of *M. circinelloides*.

2. Material and methods

2.1. Strains and media cultures

The strain of *M. circinelloides* MU402 (*leuA*$^-$, *pyrG*$^-$), which is an uracil and leucine auxotroph derived from R7B strain, was employed in this study (Nicolás et al., 2007). The MU636 strain (*leuA*$^-$, *pyrG*$^+$) derived from *M. circinelloides* MU402 was also employed in this work. In MU636 strain the wild-type *pyrG* gene was integrated into the genome, and we used this strain to prevent the possible interference *pyrG* mutation in the phenotype (Navarro-Mendoza et al., 2019). The MU402 and MU636 strains showed similar results in the experiments performed. $\Delta arl1^{(+)(-)}$ and Δ*arl2* strains derived from MU402, and Δ*arl2* strain complemented with the *arl2* wild-type allele were also used (Patiño-Medina et al., 2019). *M. circinelloides* was cultured in yeast–peptone glucose (YPG) medium (pH 4.5); 1 L medium contained 3 g yeast extract, 10 g peptone, and 20 g glucose (111 mM) or Yeast Nitrogen Base (YNB, Difco) supplemented with 111 mM glucose or 111 mM glycerol; 15 g/L agar was added to the preparation of the medium.

Spores were harvested after 5 d of incubation on solid media, counted, and preserved until use for up to 2 weeks at 4 °C.

2.2. Spore germination under normal aerobic conditions or low oxygen levels

Normal aerobic germination was performed in a 125-mL flask with 20 mL of YPG, inoculated with 5×10^5 *M. circinelloides* spores per mL; cultures were maintained at 28 °C under constant shaking conditions at 160 rpm.

Low levels of oxygen were achieved by constant shaking at 50 rpm in an orbital incubator, which facilitated 7.3 ± 0.56 % of oxygen. Meanwhile, shaking at 160 rpm increased dissolved oxygen to approximately 14.4 ± 1.2 %. Oxygen levels were determined using an oximeter. Germination percentage, determined by germinules or budding yeasts per 100 cells, was calculated for all conditions.

2.3. Total RNA and DNA isolation of M. circinelloides

Total RNA and genomic DNA of *M. circinelloides* were isolated using RNAeasy mini kit and QIAamp DNA Mini Kit, respectively (Qiagen, Venlo, Netherlands). *M. circinelloides* cultures were obtained by filtering through 6 μm membrane filters (Millipore, USA). Approximately 50 mg of biomass sample was transferred into a tube with MagNA Lyser Green Beads (Roche, Switzerland) precooled on ice. Denaturing RLT buffer (700 μL) from the RNeasy Mini Kit or buffer ATL (180 μL) of QIAamp DNA Mini Kit were added immediately before homogenization to isolate total RNA or genomic DNA, respectively. To disrupt cells, tubes were placed in the MagNA Lyser Instrument (Roche, Switzerland) and processed twice at 5500×*g* for 40 s and cooled on ice for 1 min in between each step. Samples were centrifuged for 1 min at 20 000×*g* (Eppendorf 5417) and the supernatant obtained was used for total RNA or genomic DNA isolation using the corresponding kit, following the manufacturer's protocol. To eliminate DNA contamination from RNA samples, samples were treated with DNase I (Promega, WI, USA), according to the manufacturer's protocol. RNA was eliminated from DNA samples using RNAse A (Roche, Switzerland). RNA and genomic samples were separated on denaturing and non-denaturing agarose gel, respectively, stained with ethidium bromide (Sigma, MO, USA), and visualized using a Gel Doc XR + Imager (Bio-Rad, CA, USA).

2.4. Oligonucleotide design and quantitative reverse transcription polymerase chain reaction (qRT-PCR)

To ensure specificity of all detections during qRT-PCR assays, the primers and hydrolysis probe for a subunit of the membrane proton channel domain (F_0) (*atp9*, ID number:156648, Fig. S1), the phosphofructokinase 1 subunit (*pfk1*, ID number:1330920, Fig. S2); pyruvate kinase 1 (*pyk1*, ID number:1454448, Fig. S3) (Table S1) were designed using Biosearch Technologies software (www.biosearchtech.com). *adh1* and *tfc-1* oligonucleotides and primers were used as described previously (Valle-Maldonado et al., 2015a). DNA sequences were obtained from *M. circinelloides* genome database (Corrochano et al., 2016). To evaluate the relative gene expression of genes of interest from *M. circinelloides*, protocols described previously were followed (Valle-Maldonado et al., 2015a, b).

2.5. Quantitation of ADH1 activity

A GENESYS™ 10 UV–Vis spectrophotometer (ThermoFisher Scientific. MA, USA) spectrophotometer was used for all Adh1 enzyme assays, which were carried out in a final volume of 1 mL.

NADH-dependent Adh1 activity was assayed in the reductive direction following procedures specified previously (Rangel-Porras et al., 2005). The assays were performed using reaction mixtures containing 50 mM Tris–HCl (pH 8.5), 0.5 mM NADH, cell-free extract (100 μg protein), and 0.5 M acetaldehyde. Addition of acetaldehyde initiated the reaction, and oxidation of NADH was monitored by the decrease in absorbance at 340 nm.

2.6. Determination of mitochondrial DNA abundance in M. circinelloides by qPCR

In order to determine the ratio between mitochondrial and nuclear DNA in each strain of *M. circinelloides*, assays were carried out as follows. Total DNA was extracted from spores, or vegetative growths, as described previously. DNA extractions were quantified by a spectrophotometer (Nanophotometer Pearl, Implen. Munich, Germany). A total of 100 ng of DNA was used as a template for every qPCR reaction. Specific primers and hydrolysis probes were employed to detect the *atp9* and *tfc-1* genes, which are mitochondrial or nuclear genes, respectively. The *M. circinelloides atp9* gene is a mitochondrial gene that encodes a part of the F_0 membrane proton channel domain of the mitochondrial membrane ATP synthase (Fig. S1). Meanwhile, the *tfc-1* gene, which encodes a subunit of the transcription factor TFIIIC required for the RNA polymerase III pre-initiation complex assembly, was used following methods described previously (Valle-Maldonado et al., 2015a, b). The primers and hydrolysis probes were modified at the 5′ends with 6-carboxyfluorescein (FAM) and at their 3′ends with Black Hole Quencher (BHQ1). All probes were purchased from Biosearch Technologies, Inc. (Novato, CA, USA). qPCR experiments were conducted in a single tube using the 5′ exonuclease probe method. qPCR was conducted with a LightCycler 480 II System (Roche Molecular Diagnostics, CA, USA) using a Super-Script III Platinum One-step RT-qPCR reagent kit (Invitrogen, CA, USA). Each 25-μL reaction volume contained 5 μL extracted total DNA template (100 ng), 0.5 μL enzyme mix, 12.5 μL of 2 × reaction mix, 0.5 μL of 10 μM forward primer, 0.5 μL of 10 μM reverse primer, 0.5 μL of 5 μM probe, and 5.5 μL water. qPCR was initiated by initial denaturation (95 °C, 5 min), followed by 45 amplification cycles (95 °C, 30 s and 60 °C, 30 s). Fluorescence signals were detected in each cycle at 60 °C. The amplification signal curves were analysed at absorption wavelengths of 530 nm. Appropriate positive and non-template controls were included in each test run. The mitochondrial/nuclear DNA ratio was calculated using the ΔCt formula:

$$\frac{\text{Mitochondrial DNA}}{\text{Nuclear DNA}} = 2^{(Ct\ tfc-1)-(Ct\ atp9)}$$

2.7. Determination of glucose levels

Strains were cultured in YPG media (20 g/L of glucose) for 6, 12 or 24 h. The supernatant was separated to determine the residual glucose using spectrometric method (Trinder, 1969). The residual glucose reacts with glucose-oxidase to form gluconic acid and free hydrogen peroxide, which further reacts with phenol and ampirone in presence of a peroxidase to form a colorimetric product (quinone). All samples were observed at 505 nm using GENESYS™ 10 UV–Vis spectrophotometer (ThermoFisher Scientific. MA, USA). The concentration of glucose was expressed in g/L.

2.8. Determination of ethanol levels

The culture supernatants were analysed using the flame ionization detection method (GC-FID, Clarus 500, Perkin Elmer, MA, USA) of gas chromatography. The samples were centrifuged, diluted, and injected directly into the deactivated (5 m × 0.25 mm) pre-column, connected to a Phenomenex capillary (ZB-WAX 30 m x 0.25 mm, 0.25 μm) (Pontes et al., 2009).

2.9. Caenorhabditis elegans killing assays

Growth of *C. elegans* Bristol N2 worms was synchronized by hypochlorite isolation of eggs from gravid adults, followed by hatching of eggs in.

S-basal medium (Brenner, 1974; Stiernagle, 2006). L1 larvae were transferred onto nematode growth medium plates seeded with the *Escherichia coli* OP50 strain previously grown on plates as a food source, and incubated at 18 °C for 4–5 d until they reached the young adult phase (Stiernagle, 2006). The worms were incubated with cell-free medium collected from mycelia, or with medium containing YPG in which yeast cells were grown for 12 h, as previously described (Patiño-Medina et al., 2018).

2.10. Respiration measurements

Respiration of cells was determined at 28 °C at 3 h of germination in YPG liquid media using 5×10^7 spores of different strains. After washing in sterile distilled water, cells were suspended in 10 mM potassium phosphate buffer (pH 7.4) containing 20 mM glucose. Oxygen consumption was measured at 28 °C with an Oxytherm oxygraph (Hansatech Instruments Ltd., Norfolk, England). Respiration rates were expressed as nanomoles of oxygen consumed per millilitre per second.

2.11. Fluorescence detection

For fluorescent staining, spores were germinated in YPG liquid media containing 100 nM of MitoTracker Green FM (Invitrogen, MA, USA) for 3 h. The samples were rinsed in water and mounted in 50 % (v/v) glycerol on microscope slides. The samples were observed at a wavelength specific to MitoTracker Green FM, using a confocal microscope (Olympus FV1000, Japan) with a 500–523 nm emission filter (488 nm excitation line). Green fluorescence was quantified by determining the green pixels present in an area comprised of the 20 germinules, using the ImageJ software (http://rsbweb.nih.gov/ij/), and expressed as 5 micrographs per genotype and treatment. We then obtained an arbitrary unit value (AU = green pixels/μm) for each individual, and means were obtained from whole data sets. AU means for wild type were given a value of 1, and the mutant densities were adjusted relative to these and are thus referred to in figures as relative fluorescence.

2.12. Image analysis

An Olympus CKX41 microscope (Tokyo, Japan) equipped with a 40× objective lens and a DMC-T25 camera (Panasonic, Kadoma, Japan) was used to capture images of spores or spore germination.

2.13. Statistical analysis

All the data were evaluated by analysis of variance (ANOVA, statistically significant differences ($\alpha \leq 0.05$) shown in letters) with Fisher's exact test.

3. Results

3.1. Arl1 or Arl2 control the glucose consumption and glycolysis rate in M. circinelloides

Our previous study demonstrated that under anaerobic conditions, Δ*arl1*$^{(+)(-)}$ and Δ*arl2* strains germinate at significantly greater speed than the wild-type (WT) strain (Patiño-Medina et al., 2019). This result suggests that both *arl* mutant strains metabolize glucose more rapidly than the WT strain. In order to test this hypothesis, we measured the glucose concentration in the supernatant of cultures of these strains, grown for 24 h in aerobic conditions, in comparison with the WT and a Δ*arl2* mutant complemented with the wild-type allele of *arl2*, which is phenotypically similar to the WT strain (Patiño-Medina et al., 2019). *arl1*$^{(+)(-)}$ strain showed higher glucose consumption rates compared to the other strains, including the WT strain after 6, 12 or 24 h of aerobic growth (Fig. 1A). These results suggest glycolysis upregulation in both mutant strains. mRNA levels of the genes encoding phosphofructokinase 1 (Pfk1) alpha subunit and the pyruvate kinase 1 (Pyk1), two key enzymes of the glycolytic pathway, were analyzed in spores and mycelium grown in aerobic liquid culture. The *pfk1* and *pyk1* mRNA levels were significantly higher in both *arl* mutant strains compared to the WT, for spores as well as for cultures grown under aerobic conditions (Fig. 1B and C). These results collectively indicate that the deletion of *arl1* or *arl2* led to an increase in glycolysis, along with a greater consumption of glucose, in *M. circinelloides*.

3.2. Dysfunction of Arl1 or Arl2 increased the fermentation in M. circinelloides

Despite the higher glycolytic flux in both *arl* mutants, they accumulate biomass in quantities comparable to that of WT strain (Patiño-Medina et al., 2019). Since *M. circinelloides* is a Crabtree-positive organism (McIntyre et al., 2002), we analysed if fermentation could be increased in the single *arl* mutant strains under aerobic conditions. Both *arl* mutants showed higher levels of *adh1* mRNA, a gene induced during fermentation (Rangel-Porras et al., 2005; Valle-Maldonado et al., 2015a), when compared with the WT strain, with the differences being more pronounced at the beginning of the culture, from spore formation stage to up to 6 h of growth (Fig. 2A). The *adh1* mRNA levels correlated with ADH1 activity under aerobic conditions, measured at 8 h of aerobic growth (Fig. 2B), and with ethanol production after 24 h of growth (Fig. 2C). These results suggest that fermentation is accelerated in the Δ*arl1*$^{(+)(-)}$ and Δ*arl2* strains.

3.3. Deletion of arl1 or arl2 decreased the hyphal growth in M. circinelloides under low oxygen conditions

The Δ*arl1*$^{(+)(-)}$ and Δ*arl2* strains displayed significantly faster cell germination under anaerobic conditions than that displayed by the WT strain (Patiño-Medina et al., 2019). Based on these results, we hypothesize that compared to the WT, the Δ*arl1*$^{(+)(-)}$ and Δ*arl2* strains will generate more yeast cells under lower oxygen conditions. We generally produce mycelia under constant shaking conditions at 160 rpm; this condition enables oxygen dissolution of 14.4 ± 1.2 %, contrary to shaking at 50 rpm, which enables oxygen dissolution of 7.3 ± 0.56 %. We previously demonstrated that germination rates of Δ*arl1*$^{(+)(-)}$ and Δ*arl2* were comparable to that of the WT under 160 rpm (Patiño-Medina et al., 2019). However, under low oxygen conditions, the Δ*arl1*$^{(+)(-)}$ and Δ*arl2* strains showed increase in number of yeast cells compared to the WT or Δ*arl2* restored strains (Fig. 3A). Thus, the WT strain consisted of 85 % hyphae and 15 % yeast cells after 8 h of growth (Fig. 3B), whereas both Δ*arl1*$^{(+)(-)}$ and Δ*arl2* strains consisted of 40 % yeast

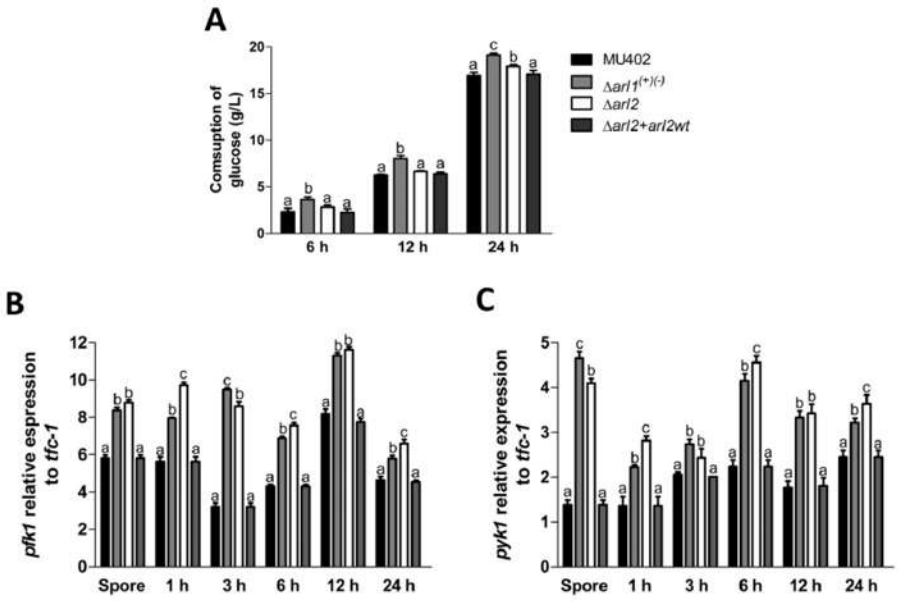

Fig. 1. Deletion of *arl1* or *arl2* in *M. circinelloides* increased the transcription levels of glycolytic genes as well as glucose consumption. In YPG liquid medium, 5×10^5 spores/mL from different strains were grown. (**A**) After 6, 12 and 24 h of incubation, the glucose consumption was determined. (**B**) mRNA levels of phosphofructokinase 1 subunit (*pfk1*) or (**C**) pyruvate kinase 1 (*pyk1*) encoding genes were determined in spores (time 0 h), or after aerobic growth at indicated times. Transcript levels were quantified relative to *tfc-1* expression; ΔCt analysis was performed. The data is represented as the average from three biological replicates of independent cultures, ± correspond to standard error (SE). Significance testing was performed using ANOVA with Fisher's exact test. In each condition (time) assayed the different letters above the bars denote statistically significant, values with identical letter were not considered significantly different ($p < 0.05$).

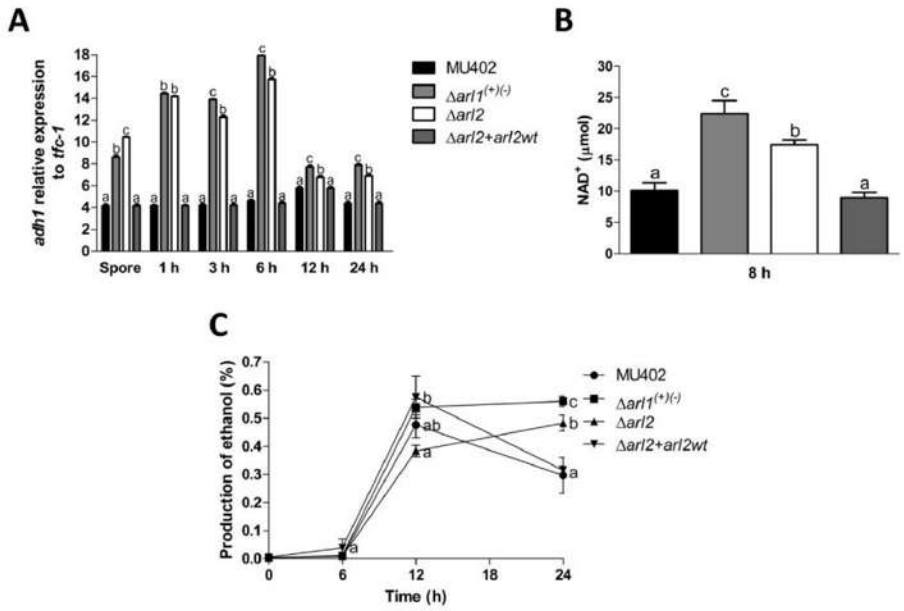

Fig. 2. Mutation of *arl1* or *arl2* in *M. circinelloides* increased fermentation. In YPG liquid medium, 5×10^5 spores/mL from different strains were grown. (**A**) *adh1* mRNA levels were determined in spores, or after aerobic growth at indicated times. Transcript levels were quantified relative to *tfc-1* expression; ΔCt analysis was performed. (**B**) ADH1 activity was determined after 8 h of aerobic growth in YNB liquid medium. (**C**) Ethanol production was quantified at indicated times. The data is represented as the average from three biological replicates of independent cultures, ± correspond to standard error (SE). Significance testing was performed using ANOVA with Fisher's exact test. In each condition (time) assayed the different letters on the bars or lanes indicate statistically significant, values with identical letter were not considered significantly different ($p < 0.05$).

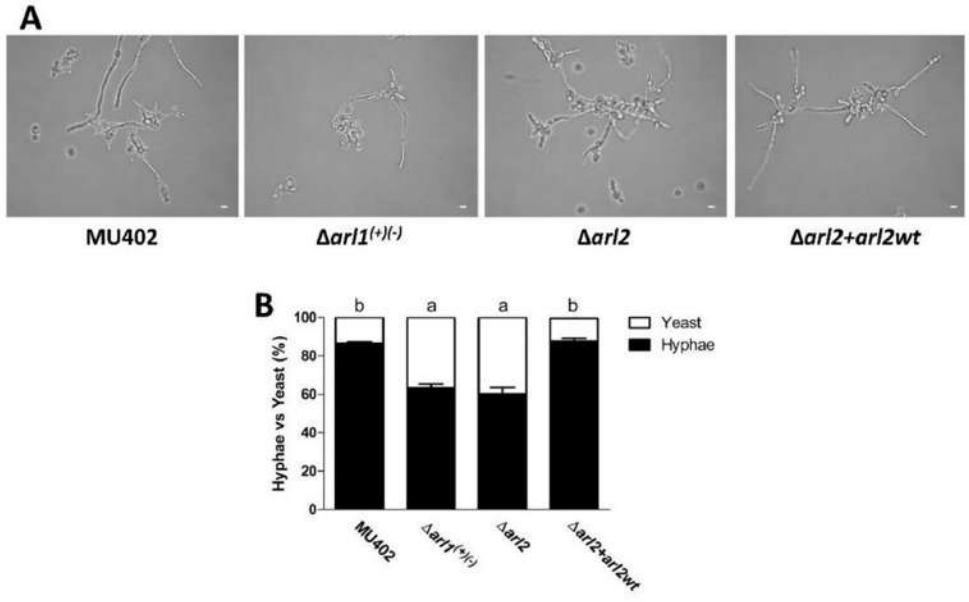

Fig. 3. Mutation of *arl1* or *arl2* decreased the hyphal development under low oxygen concentration in *M. circinelloides*. Spores from the different strains of *M. circinelloides* were inoculated into YPG media and incubated in constant shaking conditions (50 rpm). Cell were analysed at 8 h of growth. (**A**) Microphotographs taken by light microscopy (40 ×) revealed representative cellular morphology, scale bar = 20 μm. (**B**) Quantitation of hyphal or yeast cells for each strain was performed. The data is represented as the average from three biological replicates of independent cultures, ± correspond to standard error (SE). Significance testing was performed using ANOVA with Fisher's exact test. The different letters above the bars denote statistically significant, values with identical letter were not considered significantly different ($p < 0.05$).

cells and 60 % hyphal cells (Fig. 3B). These results indicate that compared to the WT strains, Δ*arl1*$^{(+)(-)}$ and Δ*arl2* strains are more prone to germinate to yeast cells under low oxygen conditions.

3.4. *Arl1 and Arl2 are associated with the ability of* M. circinelloides *to grow on non-fermentable carbon source*

M. circinelloides is able to growth in mediums with different carbon sources. A relatively high glucose concentration (2 % w/v) facilitates the fermentative metabolism even in presence of oxygen, whereas a non-fermentable carbon source favours oxidative metabolism (McIntyre et al., 2012). We compared the growth of the Δ*arl1*$^{(+)(-)}$ and Δ*arl2* strains on YNB supplemented with glucose or glycerol as sole carbon source in order to investigate the role of *arl1* or *arl2* in oxidative metabolism. Both the WT strain and the Δ*arl2* complemented strain cultures formed colonies on the entire plate after 4 d of growth either in glucose or glycerol (Fig. 4A and B), which was different from both *arl* mutant strains that demonstrated growth similar to the control strain on glucose (Fig. 4A), but produced very small radial colonies on the plates with glycerol (Fig. 4B). Similarly, after 8 h of growth in the glucose-containing media, spores from all strains were a 100 % germinated (Fig. 4C). However, the germination rate in presence of glycerol was up to 10 % in Δ*arl1*$^{(+)(-)}$ and Δ*arl2* strains at the end of the experiment (Fig. 4D), compared to the 30 % of germination reached by the WT and the Δ*arl2* complemented strains grown in similar conditions (Fig. 4D). These results indicate that oxidative metabolism is impaired in the Δ*arl1*$^{(+)(-)}$ and Δ*arl2* strains.

3.5. *Mutations of* arl1 *or* arl2 *led to decreased mitochondrial numbers in* M. circinelloides

Defects in oxidative metabolism can be attributed to mitochondrial function, which is modulated by Arf1 homologues (Ackema et al., 2014; Zhang et al., 2018). Therefore, the mitochondrial number was estimated by quantifying the copy number of the mitochondrial gene *atp9* using qPCR, using the nuclear gene *tfc-1* as a reference. During aerobic growth in glucose medium, compared to the control strains, the quantity of mitochondrial DNA was lower in Δ*arl1*$^{(+)(-)}$ and Δ*arl2* strains. The mitochondrial DNA level was significantly low in both *arl* mutant strains at the beginning of the culture process, with around 80 % decrease compared to the WT strain and the Δ*arl2*-complemented strain, and up to 40 % increase at the end of the culture process (Fig. 5A). We also measured the *atp9* mRNA levels during aerobic growth and found a reduction in mRNA levels across the time of assay in both *arl* mutant strains, the decline (around 70–80 %) being more evident in spores or at points of early aerobic germination (Fig. 5B). These results suggest that the impaired growth in non-fermentable carbon source, such as glycerol, is a consequence of the reduced mitochondrial number in Δ*arl1*$^{(+)(-)}$ and Δ*arl2* strains.

In order to visualize the mitochondrial content in the *M. circinelloides* hyphae, we used MitoTracker green FM dye. In general, after 3 h of aerobic growth in liquid media, the fluorescence signal of mitochondrial content in Δ*arl1*$^{(+)(-)}$ and Δ*arl2* strains reduced in comparison to that of the WT and Δ*arl2* complemented strains (Fig. 5C). The quantitation of fluorescence signal in the Δ*arl1*$^{(+)(-)}$ and Δ*arl2* strains showed 50 or 70 % reduction, respectively, compared to the WT strain (Fig. 5D). In addition, the oxygen consumption rate in the Δ*arl1*$^{(+)(-)}$ and Δ*arl2* strains was significantly lower compared to the WT or the Δ*arl2* complemented strains (Fig. 5E). These results clearly indicate a lower mitochondrial number in the Δ*arl1*$^{(+)(-)}$ and Δ*arl2* strains compared to the WT and agree with the *atp9* gene copy numbers and decrease in mRNA levels during aerobic growth.

3.6. *Deletion of* arl1 *induces the secretion of virulent factors in yeast cells of* M. circinelloides

M. circinelloides is an emergent opportunistic human pathogen and its mycelial form corresponds to its virulent morphology (Lee et al., 2013), the yeast cells being practically avirulent (Lee et al.,

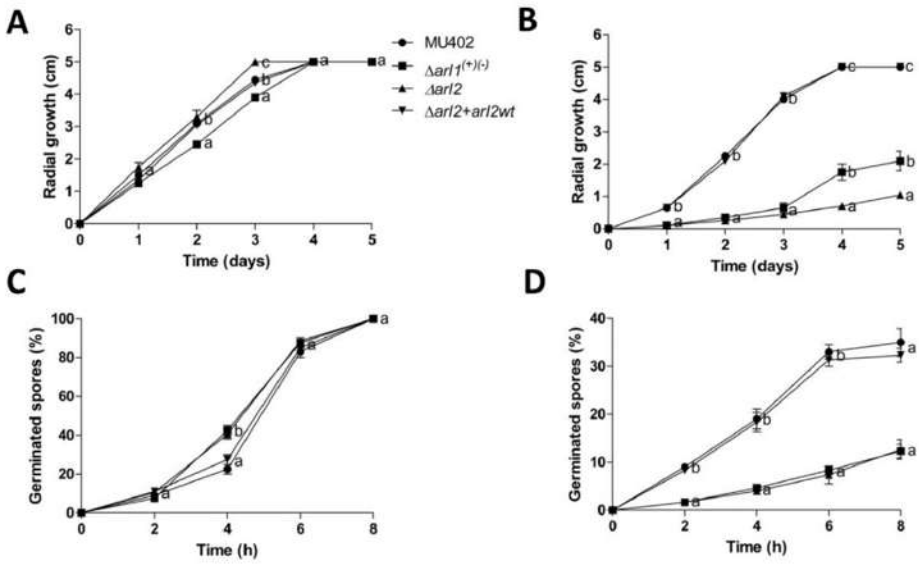

Fig. 4. Mutation of *arl1* or *arl2* impaired growth in non-fermentable carbon source and decreased the mitochondrial number in *M. circinelloides*. Fifty spores from different strains from *M. circinelloides* were inoculated on YNB plates supplemented with (**A**) glucose 2 % (111 mM) or (**B**) glycerol (111 mM), and the diameter was measured at indicated times. In all, 5 × 10^5 spores/mL were inoculated in YNB liquid supplemented with (**C**) glucose or (**D**) glycerol, and the germination rate was determined at indicated times. The data is represented as the average from three biological replicates of independent cultures, ± correspond to standard error (SE). Significance testing was performed using ANOVA with Fisher's exact test. In each condition (time) assayed the different letters on the lanes indicate statistically significant, values with identical letter were not considered significantly different ($p < 0.05$).

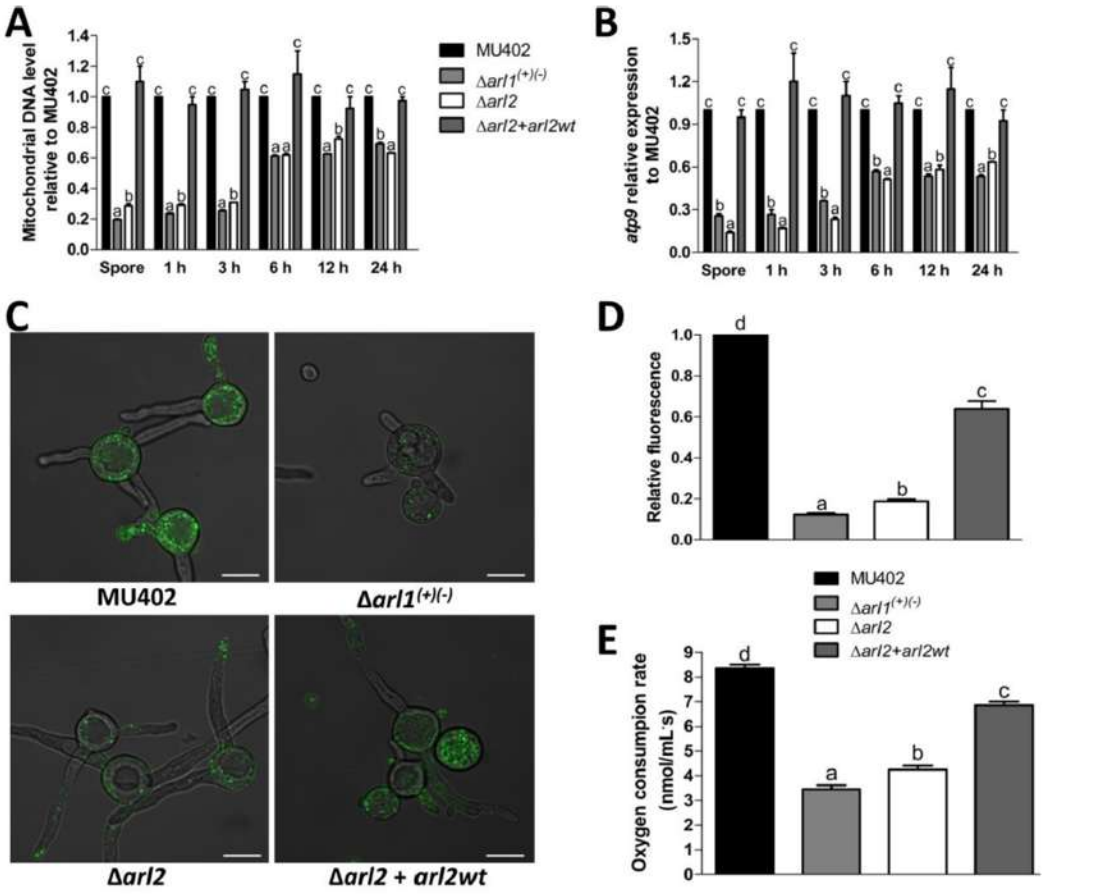

Fig. 5. Arl1 or Arl2 are involved in mitochondrial number determination in *M. circinelloides*. In YPG, 5×10^5 spores from different strains of *M. circinelloides* strains were aerobically grown, and the mitochondrial content was determined in YPG by (**A**) *atp9* gene quantitation using qPCR and based on (**B**) mRNA levels of *atp9* determined using RT-qPCR. Germinules formed at 3 h of growth were visualized (**C**) in presence of MitoTracker Green FM, and then the cells were visualized by confocal microscopy (120 ×), bars = 20 μm. (**D**) Fluorescence signal was quantified and (**E**) oxygen consumption was measured after 3 h of growth. The data is represented as the average from three biological replicates of independent cultures, ± correspond to standard error (SE), ± correspond to standard error (SE). Significance testing was performed using ANOVA with Fisher's exact test. In each condition (time) assayed the different letters above the bars denote statistically significant, values with identical letter were not considered significantly different ($p < 0.05$) (For interpretation of the references to colour in this figure legend, the reader is referred to the Web version of this article).

2013). Previously, we reported that the mycelial growth of Δ*arl1*$^{(+)(-)}$ strain led to the secretion of virulent factors (Patiño-Medina et al., 2019). As the Δ*arl1*$^{(+)(-)}$ and Δ*arl2* strains generate more yeast cells than does the WT strain under low oxygen levels (Fig. 3), we wanted to determine if the yeast and/or the cell-free culture obtained from yeast cell culture of these strains could contribute to the virulence process.

Yeast cells obtained after 24 h of anaerobic growth of the different strains were used in virulence assays against the nematode model. The yeast cells from Δ*arl1*$^{(+)(-)}$ were the only ones to demonstrate the highest rates of virulence against the nematode, compared to the other strains including the WT (Fig. 6A).

Moreover, the cell-free supernatant (SS) obtained from yeast cultures of Δ*arl1*$^{(+)(-)}$ and Δ*arl2* grown for 12 h were used to treat the nematode *C. elegans*. We observed that only the SS from Δ*arl1*$^{(+)(-)}$ yeast demonstrated higher virulence compared to that from the Δ*arl2* or the WT (Fig. 6B). The virulence of SS from Δ*arl1*$^{(+)(-)}$ was also associated with a proteinaceous molecule, since protease pre-treatment disrupted its virulence (Fig. 6A). This result demonstrates that Δ*arl1*$^{(+)(-)}$ secretes virulence factors during yeast cell growth, although the virulence in SS from yeast cultures was much lower than that in SS from mycelial growth (Fig. 6C).

Our results indicate that the yeast and/or secreted molecules of proteinaceous nature derived from yeast cells enhance virulence. To examine whether the yeast cells from Δ*arl1*$^{(+)(-)}$ incubated with the nematode in the virulence assays transform to mycelial cells faster than do the other strains, we measured the yeast–mycelium transition rate. The Δ*arl1*$^{(+)(-)}$ had lesser hyphal cells after the yeast–mycelium transition (Fig. 7A and B). Moreover, the hyphal length was much lower for Δ*arl1*$^{(+)(-)}$ compared to the other strains (Fig. 7A and C). These results indicate that virulence observed in Δ*arl1*$^{(+)(-)}$ yeast cells after interaction with the nematode could not be attributed to a faster transition to hyphal cells; in fact, this strain demonstrated the lowest rates of yeast–mycelium transition.

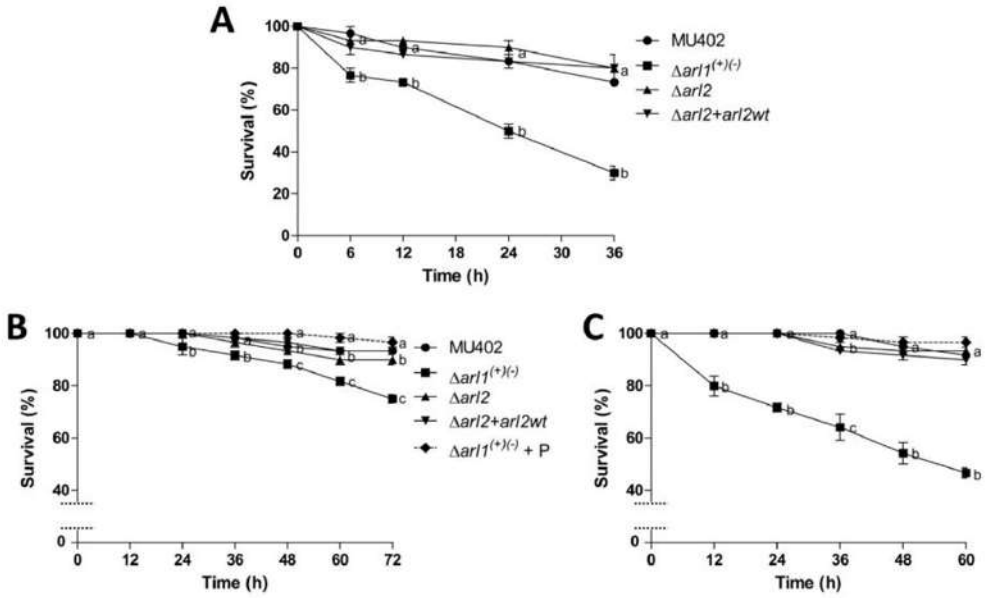

Fig. 6. Virulence of $\Delta arl1^{(+)(-)}$ and $\Delta arl2$ mutant strains of *M. circinelloides*. Adult *Caenorhabditis elegans* worms (15) were inoculated with (**A**) 10 000 yeast cells from each strain; the cells and nematodes were incubated in 1 mL of YPG. Also, 15 nematodes were inoculated with 1 mL cell-free media obtained from different strains of *M. circinelloides* after 12 h of growth in liquid YPG medium under (**B**) anaerobiosis or (**C**) aerobiosis. Sample $\Delta arl1^{(+)(-)}$ +P was treated with proteinase K for 2 h before incubation with the *Caenorhabditis elegans*. Figures represent the average of three independent experiments, ± correspond to standard error (SE). Significance testing was performed using ANOVA with Fisher's exact test. In each time assayed the different letters on the lines indicate statistically significant, values with identical letter were not considered significantly different ($p < 0.05$).

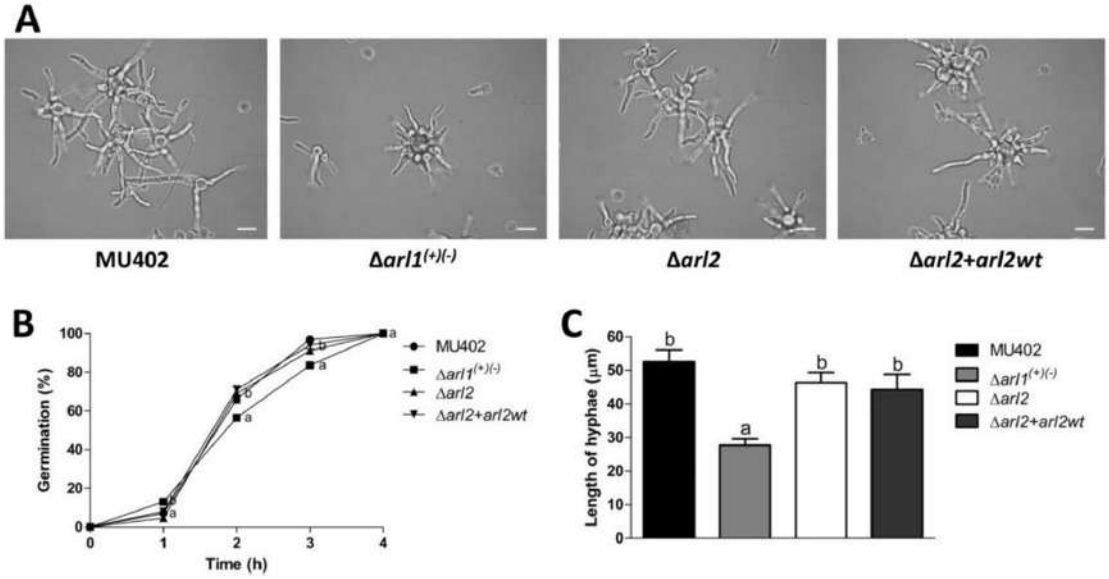

Fig. 7. Role of Arl1 and Arl2 in the yeast-mycelial transition of *M. circinelloides*. Spores from the different strains were first incubated anaerobically in YPG for 24 h, the yeast cells were recovered, inoculated once again in fresh YPG liquid medium, and incubated aerobically for 4 h. (**A**) Cell morphologies of the different strains after yeast–mycelial transition for 4 h were visualized by light microscopy. (**B**) hyphal cells after yeast–mycelial transition were quantified and (**C**) hyphal length was registered for each strain after 4 h of yeast–mycelial transition. The data is represented as the average from three biological replicates of independent cultures, ± correspond to standard error (SE). Significance testing was performed using ANOVA with Fisher's exact test. In each condition (time) assayed the different letters above the bars denote statistically significant, values with identical letter were not considered significantly different ($p < 0.05$).

4. Discussion

Mitochondrial function is decisive in mycelial growth in several dimorphic species of *Mucor* (Orlowski, 1991). Both mitochondrial function and morphology are regulated in multiple organisms by members of Arf superfamily, for example, Arf (Ackema et al., 2014), Arl (Newman et al., 2014), and Sar proteins (Ackema et al., 2016), or accessory Arf-GAP proteins, like yeast GCS1, which encodes a GTPase Activating Protein (Huang et al., 2002). This study provides evidences of the critical role of Arl1 or Arl2 in mitochondrial maintenance in *M. circinelloides*, since deletion of the corresponding genes resulted in a low number of mitochondria, which resulted in a defective oxidative metabolism. A reduced oxygen consumption and a poor growth in glycerol as sole carbon source, as observed in the *arl* mutants, further supports this finding. Conversely, the glucose consumption by glycolytic and fermentative pathways increased in both *arl* mutant strains, eliciting similar growth kinetics as the WT strain. It is common knowledge that inhibition of oxidative phosphorylation is an effective method of increasing glycolytic flux. This mechanism, which compensates for the energy shift, had been described in bacteria (Jensen and Michelsen, 1992; Sekine et al., 2001), yeast (Dechant et al., 2010), and mammalian cells (Burns and Manda, 2017).

The increased fermentation rate did not promote yeast cell growth in $\Delta arl1^{(+)(-)}$ or $\Delta arl2$ strains during normal aerobic growth ($\approx$14 % of dissolved oxygen); however, we observed that they are more likely to generate yeast cells under low dissolved oxygen ($\approx$7 %), contrary to the observation in WT strain. This suggests that under low physiological oxygen availability, the $\Delta arl1^{(+)(-)}$ and $\Delta arl2$ mutant strains could maintain a higher proportion of yeast cells when compared to the WT, possibly through an increased fermentative metabolism, which has been observed to promote yeast cell morphology in this specie of *Mucor* (McIntyre et al., 2002).

The $\Delta arl1^{(+)(-)}$ strain induces aberrant vesicle trafficking that could participate directly or indirectly in the secretion of specific virulent factors during aerobic growth (Patiño-Medina et al., 2019). In this study, we observed that $\Delta arl1^{(+)(-)}$ secretes virulence factors when it grows as yeast cells, although their virulence activity rate was much lower than those secreted during mycelial growth. The rate of growth could be a factor responsible for the difference in virulence of the cell-free supernatant obtained from yeast cells and from mycelia, since growth of yeast cells generates lesser biomass than mycelial growth (Valle-Maldonado et al., 2015a). Further experiments are required to discern whether the factors secreted by $\Delta arl1^{(+)(-)}$ are identical in both morphologies, and to determine the chemical nature of these unknown virulent factors secreted by the $\Delta arl1^{(+)(-)}$ mutant strain.

Our findings also indicate that the virulence of *M. circinelloides* is not necessarily linked to increased oxidative metabolism. $\Delta arl1^{(+)(-)}$ demonstrated that despite having reduced oxidative metabolism, and higher tendency of developing into yeast cells, it still has an enhanced virulent activity compared to the other strains, including the WT. The yeast cells from $\Delta arl1^{(+)(-)}$ have higher virulence than the other strains, and this is not due to the high speed of their yeast–mycelium transition. Our results clearly demonstrated that the yeast cells from $\Delta arl1^{(+)(-)}$ develop a hyphal morphology at a lower speed than the rest of the strains, despite that a higher aerobic germination rate had been linked to the virulent phenotype of *M. circinelloides* (Lee et al., 2013).

A full mitochondrial content and activity seems to be irrelevant for the optimal mycelia development of *M. circinelloides* under the presence of relative high levels of oxygen, as has been described for other *Mucor* species, such as *Mucor genevensis*, in where the oxidative metabolism is not essential for mycelial development (Rogers et al., 1974; Orlowski, 1991). Hence, in $\Delta arl1^{(+)(-)}$ and $\Delta arl2$ strains, the mitochondrial content decreased by nearly 70 % when compared to the WT, but maintained same rate of aerobic germination and hyphal growth. This is in contrast to the observation that in a low-oxygen atmosphere, both *arl* mutant strains develop significantly higher number of yeast cells compared to the WT. It seems Arl1 or Arl2 are needed for an adequate signalling that culminates in mycelium morphology of *M. circinelloides* when the levels of oxygen in the atmosphere decreased. The oxygen availability during the fungal infection could have an important role in the outcome either for the fungus or the host (Grahl et al., 2012). For example, *Aspergillus fumigatus* secretes the nonribosomal peptide gliotoxin that contributes to the inhibition of the angiogenesis, this pathogenic process could prevent tissue repair and led to tissue necrosis (Ben-Ami et al., 2009).

In general, the mitochondrial homeostasis in fungi plays a critical role in at least two aspects of the antifungal susceptibility and virulence processes (Verma et al., 2018; Neubauer et al., 2015). For example, in the dimorphic ascomycete *Candida albicans*, the increase in mitochondrial respiration is necessary for yeast–mycelial transition, since the mycelial morphology is associated with a more virulent phenotype; moreover, mitochondrial activity is also required for initial biofilm formation, which correlates with the increase in virulence (Calderone et al., 2015). Additionally, mitochondrial dysfunction can lead to both resistance and susceptibility to azoles (Shingu-Vazquez and Traven, 2011). The decrease in number of mitochondria correlates with azole susceptibility in $\Delta arl1^{(+)(-)}$ derived from *M. circinelloides*; however, contrary to expectation, the strain maintains higher levels of virulence despite lower-than-expected hyphal length development (Patiño-Medina et al., 2019). We still cannot explain the apparent discrepancy in $\Delta arl1^{(+)(-)}$. However, the secretion of virulence factors are not completely dependent on the mitochondrial metabolism in $\Delta arl1^{(+)(-)}$; we are trying to identify new cellular and molecular elements that explain the increment in virulence of $\Delta arl1^{(+)(-)}$.

5. Conclusions

To the best of our knowledge, this is the first report on the members of the Arf family proteins, Arl1 and Arl2, and their influence on the mitochondrial cell population in a species of *Mucor*. Arl1 and Arl2 control the mitochondrial number in *M. circinelloides*, and their dysfunction leads to an increase in the glycolytic and fermentative pathways under aerobic conditions. Interestingly, the yeast cells or secreted molecules from this stage could be involved in virulence of *M. circinelloides*.

Author contributions

JA P-M, MI V-M, D V-T, VM C-J, AR C-E, J R-E and LF R–H, data acquisition, analysis, and data interpretation, AR C-E and MI R-D, reagents, analysis; AR C-E, JR-E, MI R-D and V G critical analysis, data interpretation, and critical revision of the article for intellectual content; V M–C, conception and design of the work, data analysis and interpretation, and drafting of the article.

Declaration of Competing Interest

The author declare that they have no conflict of interest.

Acknowledgments

We would like to thank to SEP-CONACYT for the grant (CB- 2011-01-167071) for partially funding this project and CIC/UMSNH for the grant 2.36, grants. JA P-M, MIV-M and D V-T were postgraduate student with a CONACyT scholarship.

Appendix A. Supplementary data

Supplementary data to this article can be found online at https://doi.org/10.1016/j.funbio.2020.02.016.

References

Ackema, K.B., Hench, J., Böckler, S., Wang, S.C., Sauder, U., Mergentaler, H., Westermann, B., Bard, F., Frank, S., Spang, A., 2014. The small GTPase Arf1 modulates mitochondrial morphology and function. EMBO J. 33, 2659–2675.

Ackema, K.B., Prescianotto-Baschong, C., Hench, J., Wang, S.C., Chia, Z.H., Mergentaler, H., et al., 2016. Sar1, a novel regulator of ER-mitochondrial contact sites. PloS One 11, e0154280.

Ben-Ami, R., Lewis, R.E., Leventakos, K., Kontoyiannis, D.P., 2009. *Aspergillus fumigatus* inhibits angiogenesis through the production of gliotoxin and other secondary metabolites. Blood 114, 5393–5399.

Brenner, S., 1974. The genetics of *Caenorhabditis elegans*. Genetics 77, 71–94.

Burns, J.S., Manda, G., 2017. Metabolic pathways of the warburg effect in health and disease: perspectives of choice, chain or chance. Int. J. Mol. Sci. 8, e2755.

Calderone, R., Li, D., Traven, A., 2015. System-level impact of mitochondria on fungal virulence: to metabolism and beyond. FEMS Yeast Res. 15, fov027.

Corrochano, L.M., Kuo, A., Marcet-Houben, M., Polaino, S., Salamov, A., Villalobos-Escobedo, J.M., et al., 2016. Expansion of signal transduction pathways in Fungi by extensive genome duplication. Curr. Biol. 26, 1577–1584.

Dechant, R., Binda, M., Lee, S.S., Pelet, S., Winderickx, J., Peter, M., 2010. Cytosolic pH is a second messenger for glucose and regulates the PKA pathway through V-ATPase. EMBO J. 29, 2515–2526.

Grahl, N., Shepardson, K.M., Chung, D., Cramer, R.A., 2012. Hypoxia and fungal pathogenesis: to air or not to air? Eukaryot. Cell 11, 560–570.

Huang, C.F., Chen, C.C., Tung, L., Buu, L.M., Lee, F.J., 2002. The yeast ADP-ribosylation factor GAP, Gcs1p, is involved in maintenance of mitochondrial morphology. J. Cell Sci. 115, 275–282.

Jensen, P.R., Michelsen, O., 1992. Carbon and energy metabolism of atp mutants of *Escherichia coli*. J. Bacteriol. 174, 7635–7641.

Kahn, R.A., Cherfils, J., Elias, M., Lovering, R.C., Munro, S., Schurmann, A., 2006. Nomenclature for the human Arf family of GTP-binding proteins: ARF, ARL, and SAR proteins. J. Cell Biol. 5, 645–650.

Lee, S.C., Li, A., Calo, S., Heitman, J., 2013. Calcineurin plays key roles in the dimorphic transition and virulence of the human pathogenic zygomycete *Mucor circinelloides*. PLoS Pathog. 9, e1003625.

Lewis, R.E., Kontoyiannis, D.P., 2013. Epidemiology and treatment of mucormycosis. Future Microbiol. 8, 1163–1175.

Li, C.H., Cervantes, M., Springer, D.J., Boekhout, T., Ruiz-Vazquez, R.M., Torres-Martinez, et al., 2011. Sporangiospore size dimorphism is linked to virulence of *Mucor circinelloides*. PLoS Pathog. 7, e1002086.

Lübbehüsen, T.L., Nielsen, J., McIntyre, M., 2003. Characterization of the *Mucor circinelloides* life cycle by on-line image analysis. J. Appl. Microbiol. 95, 1152–1160.

McIntyre, M., Breum, J., Arnau, J., Nielsen, J., 2002. Growth physiology and dimorphism of *Mucor circinelloides* (*syn. racemosus*) during submerged batch cultivation. Appl. Microbiol. Biotechnol. 58, 495–502.

Navarro-Mendoza, M.I., Pérez-Arques, C., Panchal, S., Nicolás, F.E., Mondo, S.J., Ganguly, P., Pangilinan, J., Grigoriev, I.V., Heitman, J., Sanyal, K., Garre, V., 2019. Early diverging fungus *Mucor circinelloides* lacks centromeric histone CENP-A and displays a mosaic of point and regional centromeres. Curr. Biol. 29, 3791–3802.

Neubauer, M., Zhu, Z., Penka, M., Helmschrott, C., Wagener, N., Wagener, J., 2015. Mitochondrial dynamics in the pathogenic mold *Aspergillus fumigatus*: therapeutic and evolutionary implications. Mol. Microbiol. 98, 930–945.

Newman, L.E., Zhou, C.J., Mudigonda, S., Mattheyses, A.L., Paradies, E., Marobbio, C.M., Kahn, R.A., 2014. The ARL2 GTPase is required for mitochondrial morphology, motility, and maintenance of ATP levels. PloS One 9, e99270.

Nicolás, F.E., De Haro, J.P., Torres-Martínez, S., Ruiz-Vázquez, R.M., 2007. Mutants defective in a *Mucor circinelloides* dicer-like gene are not compromised in siRNA silencing but display developmental defects. Fungal Genet. Biol. 44, 504–516.

Ocampo, J., Fernández-Nuñez, L., Silva, F., Pereyra, E., Moreno, S., Garre, V., Rossi, S., 2009. A subunit of protein kinase a regulates growth and differentiation in the fungus *Mucor circinelloides*. Eukaryot. Cell 8, 933–944.

Orlowski, M., 1991. Mucor dimorphism. Microbiol. Rev. 55, 234–258.

Patiño-Medina, J.A., Maldonado-Herrera, G., Pérez-Arques, C., Alejandre-Castañeda, V., Reyes-Mares, N.Y., Valle-Maldonado, M.I., et al., 2018. Control of morphology and virulence by ADP-ribosylation factors (Arf) in *Mucor circinelloides*. Curr. Genet. 64, 853–869.

Patiño-Medina, J.A., Valle-Maldonado, M.I., Maldonado-Herrera, G., Pérez-Arques, C., Jácome-Galarza, I.E., Díaz-Pérez, C., et al., 2019. Role of Arf-like proteins (Arl1 and Arl2) of *Mucor circinelloides* in virulence and antifungal susceptibility. Fungal Genet. Biol. 129, 40–51.

Pontes, H., Guedes_de Pinho, P., Casal, S., Carmo, H., Santos, A., Magalhães, T., et al., 2009. GC determination of acetone, acetaldehyde, ethanol, and methanol in biological matrices and cell culture. J. Chromatogr. Sci. 47, 272–278.

Rangel-Porras, R.A., Meza-Carmen, V., Martinez-Cadena, G., Torres-Guzmán, J.C., González-Hernández, G.A., Arnau, J., Gutiérrez-Corona, J.F., 2005. Molecular analysis of an NAD-dependent alcohol dehydrogenase from the zygomycete *Mucor circinelloides*. Mol. Genet. Genom. 274, 354–363.

Rangel-Porras, R.A., Díaz-Pérez, S.P., Mendoza-Hernández, J.M., Romo-Rodríguez, P., Alejandre-Castañeda, V., Valle-Maldonado, M.I., et al., 2019. Alcohol dehydrogenase 1 participates in the Crabtree effect and connects fermentative and oxidative metabolism in the Zygomycete *Mucor circinelloides*. J. Microbiol. 57, 606–617.

Rogers, P.J., Clark-Walker, G.D., Stewart, P.R., 1974. Effects of oxygen and glucose on energy metabolism and dimorphism of *Mucor genevensis* grown in continuous culture: reversibility of yeast-mycelium conversion. J. Bacteriol. 119, 282–293.

Sekine, H., Shimada, T., Hayashi, C., Ishiguro, A., Tomita, F., Yokota, A., 2001. H^{+}-ATPase defect in Corynebacterium glutamicum abolishes glutamic acid production with enhancement of glucose consumption rate. Appl. Microbiol. Biotechnol. 57, 534–540.

Shingu-Vazquez, M., Traven, A., 2011. Mitochondria and fungal pathogenesis: drug tolerance, virulence, and potential for antifungal therapy. Eukaryot. Cell 10, 1376–1383.

Stiernagle, T., 2006. Maintenance of C. elegans. Worm book 11, pp. 1–11.

Trinder, P., 1969. Determination of glucose in blood using glucose oxidase with an alternative oxygen acceptor. Ann. Clin. Biochem. 6, 24–27.

Valle-Maldonado, M.I., Jácome-Galarza, I.E., Gutiérrez-Corona, F., Ramírez-Díaz, M.I., Campos-García, J., Meza-Carmen, V., 2015a. Selection of reference genes for quantitative real time RT-PCR during dimorphism in the zygomycete *Mucor circinelloides*. Mol. Biol. Rep. 42, 705–711.

Valle-Maldonado, M.I., Jácome-Galarza, I.E., Díaz-Pérez, A.L., Martínez-Cadena, G., Campos-García, J., Ramírez-Díaz, M.I., et al., 2015b. Phylogenetic analysis of fungal heterotrimeric G protein-encoding genes and their expression during dimorphism in *Mucor circinelloides*. Fungal Biol. 119, 1179–1193.

Verma, S., Shakya, V.P.S., Idnurm, A., 2018. Exploring and exploiting the connection between mitochondria and the virulence of human pathogenic fungi. Virulence 9, 426–446.

Zhang, B., Yu, Q., Huo, D., Li, J., Liang, C., Li, H., et al., 2018. Arf1 regulates the ER-mitochondria encounter structure (ERMES) in a reactive oxygen species-dependent manner. FEBS J. 285, 2004–2018.

Current Microbiology
https://doi.org/10.1007/s00284-020-02083-3

Virulence Conferred by PumA Toxin from the Plasmid-Encoded PumAB Toxin-Antitoxin System is Regulated by Quorum System

Karen C. Hernández-Ramírez[1] · Brenda Valerio-Arellano[2] · Marco I. Valle-Maldonado[1] · León F. Ruíz-Herrera[1] · Víctor Meza-Carmen[1] · Martha I. Ramírez-Díaz[1]

Received: 8 January 2020 / Accepted: 8 June 2020

Abstract

Toxin-antitoxin (TA) systems are small genetic elements composed of a toxin gene and its cognate antitoxin that are important for plasmid stabilization (plasmid-encoded) and bacterial virulence (chromosome-encoded). These systems are also related to biofilm and persister cell formations. *Pseudomonas aeruginosa* is an antibiotic-resistant human pathogen that produces virulence factors modulated by quorum sensing (QS) and can form biofilms. The type II PumAB TA system of pUM505, isolated from a clinical strain of *P. aeruginosa*, confers plasmid stability. Additionally, the PumA toxin increases *P. aeruginosa* virulence and is neutralized by the PumB antitoxin. In this study, we determined whether virulence conferred by PumA toxin is regulated by QS. The *pum*A gene was transferred to *P. aeruginosa las*I/*rhl*I, a mutant strain in the LasI and RhlI QS systems, to analyze the effect on virulence of the transformants. *pum*A transfer did not increase bacterial virulence in lettuce and *Caenorhabditis elegans*, suggesting that the virulence conferred by PumA requires QS modulation. *pum*A mRNA levels drastically decreased in the *P. aeruginosa las*I/*rhl*I (pUC_pumA) strain, suggesting positive regulation of *pum*A gene expression by QS. Supplementation of the growth medium of *P. aeruginosa las*I/*rhl*I (pUC_pumA) with C4-AHL and 3-oxo-C12-AHL autoinducers increased *pum*A mRNA levels and restored bacterial virulence, suggesting that both autoinducers complemented the mutations and positively regulated the toxic effects of PumA. This strengthened the hypothesis that QS regulates bacterial virulence conferred by the PumA toxin. Thus, this report establishes an important function of QS in the virulence conferred by plasmid-encoded TA systems in bacterial pathogens.

Introduction

Pseudomonas aeruginosa is one of the most significant opportunistic pathogens in humans. It belongs to the ESKAPE group (*Enterococcus faecium*, *Staphylococcus aureus*, *Klebsiella pneumoniae*, *Acinetobacter baumannii*, *P. aeruginosa*, and *Enterobacter* spp.), which is a group of antibiotic-resistant bacteria that are common causes of life-threatening nosocomial infections [1]. Patients with chronic diseases or compromised immune systems due to immunodeficiency or burns are at a greater risk of *P. aeruginosa* infection [2]. The success of *P. aeruginosa* infections is largely due to the production of virulence factors that elicit disease in both plants and animals and the ability to form biofilms [3]. The production of several virulence factors by *P. aeruginosa* is controlled according to cell density via quorum-sensing (QS) systems. QS produces and releases small chemical signals, called autoinducers, which accumulate at a high population density and interact with cognate receptors to induce the transcriptional expression of various target genes, including those encoding virulence factor production [4]. The *P. aeruginosa* QS network is organized in a multilayered hierarchy consisting of at least four interconnected signaling mechanisms, including *las*, *iqs*, *pqs*, and *rhl* [4]. The *las* and *rhl* systems regulate the production of multiple virulence factors as well as elastase, alkaline protease,

Electronic supplementary material The online version of this article (https://doi.org/10.1007/s00284-020-02083-3) contains supplementary material, which is available to authorized users.

✉ Martha I. Ramírez-Díaz
martha.ramirez@umich.mx

[1] Instituto de Investigaciones Químico-Biológicas, Universidad Michoacana de San Nicolás de Hidalgo, Edificio B-3, Ciudad Universitaria, 58030 Morelia, Michoacán, Mexico

[2] Facultad de Químico Farmacobiología, Universidad Michoacana de San Nicolás de Hidalgo, Morelia, Michoacán, Mexico

Published online: 15 June 2020

exotoxin A, rhamnolipids, pyocyanin, lectins, and superoxidase dismutase [5].

Toxin-antitoxin (TA) systems are small genetic modules found in bacterial mobile genetic elements and bacterial chromosomes [6, 7]. TA systems are prevalent in bacteria and archaea; although they are not essential for normal cell growth, they are implicated in multiple cellular functions associated with survival under stress conditions [8]. Plasmid-encoded TA systems are important for plasmid stabilization by a post-segregation killing mechanism that eliminates daughter cells that have lost the TA-encoding plasmid [9]; chromosomally encoded TA systems are related to bacterial pathogen virulence [10, 11]. TA systems are also involved in biofilm formation and persister cell formation (persister cells are a small fraction of bacteria that demonstrate resistance to antibiotics without genetic change), suggesting that these systems may function in the stress response as regulators of the switch from the planktonic to the biofilm lifestyle [12]. A significant correlation between QS and TA systems in clinical *P. aeruginosa* isolates with a high biofilm formation ability has also been indicated [13].

The PumA toxin has been shown to increase *P. aeruginosa* virulence effects neutralized by the PumB antitoxin [14]. Additionally, the supernatant from *P. aeruginosa* expressing PumA can kill *Caenorhabditis elegans*, suggesting that the toxin could be secreted into the media during bacterial growth. Moreover, purified PumA protein decreased *C. elegans* viability, demonstrating that PumA could act as a bacterial virulence factor [14]. The type II PumAB TA system of pUM505 has also been shown to confer plasmid stability to *Escherichia coli* [14].

The aim of this work was to determine whether the virulence conferred by the PumA toxin from a TA system plasmid-encoded is regulated by QS. We report that QS regulates PumA toxicity and increases bacterial virulence. This establishes an important function for QS in the virulence conferred by plasmid-encoded TA systems in bacterial pathogens.

Materials and Methods

Bacterial Strains, Culture Conditions, and Plasmids

Pseudomonas aeruginosa PAO1 (WT) and *P. aeruginosa rhl*I/*las*I double mutant (donated by Dr. Jesús Campos García, Universidad Michoacana de San Nicolas de Hidalgo, México) were used as recipient strains for recombinant plasmids or virulence assays. The pUC_pumA, pUC_pumB, and pUC_pumAB recombinant plasmids contain the *pum*A, *pum*B, or *pum*AB genes, respectively, and were cloned with their own promoters into the pUCP20 *Escherichia/Pseudomonas* shuttle vector [14]. The recombinant plasmids were transferred to *Pseudomonas* strains by electroporation before selecting transformants in LB plates supplemented with carbenicillin (Sigma, St. Louis, MO, USA).

The culture medium used was Luria–Bertani (LB) broth. 1.5% agar was added to form solid media [14]. M9 salts minimal medium (Sigma) supplemented with 20 mM glucose and 0.1 mM $CaCl_2$. Carbenicillin (400 $\mu g \cdot mL^{-1}$) was added to agar plates when necessary. Cultures were routinely grown overnight at 37 °C with shaking, and growth was monitored based on optical density (OD) at 600 nm (OD_{600}) using a spectrophotometer.

Genetic Techniques and Sequence Analysis

Molecular genetics procedures were carried out using standard methods [15].

Bacterial Growth Assays

Liquid cultures of *P. aeruginosa* PAO1 or *P. aeruginosa las*I/*rhl*I double mutants containing the recombinant plasmids were used to evaluate the effects of QS mutation on transformant growth. Overnight cultures were diluted 1:50 in 250 mL of fresh LB or M9 medium, and growth was monitored at intervals by measuring OD_{600}.

RNA Isolation and RT-qpcr Analysis

To measure *pum*A and *pum*B gene expression in *P. aeruginosa* strains, cultures were incubated in the exponential and stationary phases of growth, and cells were harvested by centrifugation. Total RNA was isolated and quantified as previously described [14]. Oligonucleotide primers and hydrolysis probes for RT-qPCR of the *pumA* gene and *16S* rRNA reference genes were described by Hernández-Ramírez et al. [14]. Amplification of *pumA* and *pumB* genes and *16S* rRNA genes was performed using the 5′ exonuclease probe RT-qPCR method. RT-qPCR was performed with total RNA samples (500 ng) and the SuperScript III Platinum One-Step RT-qPCR Reagent kit (Thermo Fisher Scientific, Waltham, MA, USA) with the LightCycler 480 II System (Roche Molecular Diagnostics, Pleasanton, CA, USA). Amplification signal curves were analyzed at the absorption wavelength of 530 nm. Appropriate positive and non-template controls were included in each test run. Relative expression of the *pumA* and *pumB* genes was normalized to the expression values obtained from the *P. aeruginosa 16S* rRNA gene (accession number AE004091; region: 722096–723631). Relative gene expression was estimated using the classical calibration dilution curve and slope calculation. A fivefold dilution series (500–0.05 ng total RNA) was prepared and used as the sample in the RT-qPCR. Efficiency (E) was obtained from standard curves

using the formula $E=(10^{-1/\text{slope}}-1)\times 100$. For chemical complementation, the *P. aeruginosa* bacterial cultures were supplemented with 0.6 µM of N-decanoyl-DL-homoserine lactone (C4-AHL) (Fluka, USA) or N-(3-oxododecanoyl)-L-homoserine lactone (3-oxo-C12-AHL) (Sigma) before growing overnight at 37 °C to the exponential phase. Total RNA extraction and RT-qPCR were performed as described previously. Relative expression levels were determined using the efficiency correction method, which considers amplification efficiencies between target and reference genes [16].

Virulence Assays

Lettuce-Leaf Model of Infection

Pseudomonas aeruginosa infection on lettuce leaves was performed as previously described [17]. Cultures were grown overnight in LB broth at 37 °C. After centrifugation, the pellets were suspended in fresh LB broth and grown for an additional 4 h. The resulting log-phase cultures were diluted with 10 mM $MgSO_4$ to an OD_{600} of 0.2. Lettuce midribs were washed with distilled H_2O and 0.1% (v/v) bleach before inoculating using pipette tip puncture. We inoculated 1×10^6 ($\pm1\times10^4$) colony-forming units (CFU) in 10 µL of the bacterial suspensions onto lettuce leaves, which were placed on Whatman filter paper moistened with 10 mM $MgSO_4$. Symptoms were monitored daily, and the length and width of the lesions were measured. The lesion area was estimated as previously described [18]. The experiments were repeated at least three times. The number of CFUs present within a lettuce lesion was determined using a procedure adapted from Dong et al. [19]. Briefly, after 4 days of incubation, the infected lettuce leaf region was cut from the midrib and macerated in 5 mL of 10 mM $MgSO_4$ with a mortar and pestle. Serial dilutions of the suspension in 10 mM $MgSO_4$ were plated on LB agar to count the number of bacterial CFUs after incubation at 37 °C for 24 h. Bacterial inoculum concentrations were confirmed for all assays using dilution plating.

C. elegans Killing Assays

Caenorhabditis elegans Bristol N2 [20] worms were synchronized using hypochlorite isolation of eggs from gravid adults before hatching the eggs in S-basal medium [21]. L1 larvae were transferred to NGM (Nematode Growth Medium) [21] in plates seeded with the *E. coli* OP50 strain previously grown on the plates as a food source and incubated at 20 °C for 4–5 days until they reached the young adult phase. Worms were rinsed off the plates and washed in S-basal medium. Cultures of *P. aeruginosa* strains were grown overnight in M9 broth at 37 °C, centrifuged, and the pellets were suspended in fresh M9 broth and grown to an OD_{600} of 0.4. To chemically complement *P. aeruginosa rhlI/lasI*, mutant bacterial cultures in M9 were supplemented with 0.6 µM of N-decanoyl-DL-homoserine lactone (C4-AHL) (Fluka, USA), N-(3-oxododecanoyl)-L-homoserine lactone (3-oxo-C12-AHL) (Sigma) or N-decanoyl-DL-homoserine lactone (C10-AHL) (Fluka) before growing overnight at 37 °C and centrifuged. The pellets were suspended in fresh M9 broth and grown to an OD_{600} of 0.4. For each experiment, 20 worms were dispensed into each well of a 24-well Costar plate (Corning, Inc., Corning, NY, USA). The worms were incubated with 1×10^5 ($\pm1\times10^4$) CFU of the bacterial strain contained in a total volume of 1 mL. The plates were incubated for 36 h at 20 °C and scored for live worms at 6, 12, 24, and 36 h. *P. aeruginosa* PAO1 (pUC_pumA) and M9 medium were used as positive and negative controls, respectively. A worm was considered dead when it no longer responded (moved) to a touch stimulus. Worms that died as a result of adhering to the plate wall were excluded from the analysis. For all assays, bacterial concentrations were confirmed by dilution, plating, and counting. Two independent assays with two replicates were conducted for each worm group.

Statistical Analysis

Data analysis were performed using GraphPad Prism 5 software. Analysis of variance (ANOVA) was performed for all the *Pseudomonas* assays. $P<0.05$ was considered statistically significant.

Results

QS Regulates the Virulence of *P. aeruginosa* Conferred by *pumA*

The PumA toxin of the PumAB TA system increases *P. aeruginosa* virulence [14]. To determine whether the virulence ability of PumA depends on QS, the recombinant plasmids with *pumA* and *pumAB* genes were transferred to *P. aeruginosa lasI/rhlI* (double mutant) and virulence assays were conducted. First, virulence conferred by *pumAB* genes was analyzed using the lettuce-leaf model. The *P. aeruginosa* PAO and *P. aeruginosa lasI/rhlI* strains were transformed with the pUCP20 vector and virulence assays were conducted to discount the possibility that the vector backbone/antibiotic selection marker affects the virulence of the strains; the results showed no significant difference in CFU counts between the strains (Fig. 1). CFUs increased by 69% when the lettuce was inoculated with *P. aeruginosa* PAO1 (pUC_pumA) compared to when the lettuce was inoculated with *P. aeruginosa* PAO1 (pUCP20), empty vector only (Fig. 1). This indicated that PumA increased bacterial

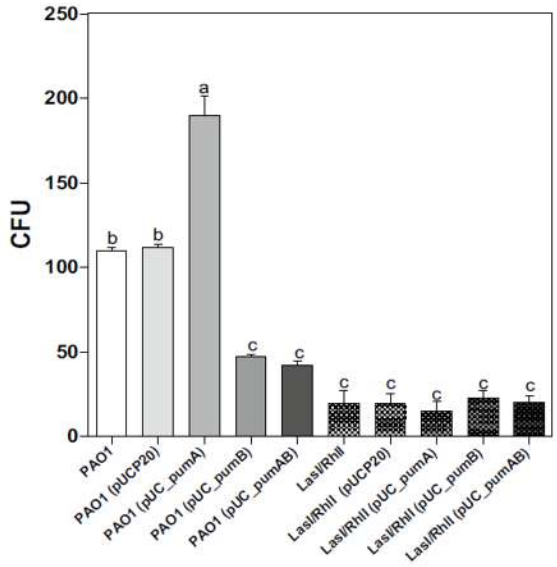

Fig. 1 Virulence conferred by PumA toxin in the *P. aeruginosa lasI/rhlI* double mutant in a lettuce leaf infection model. Colony forming units (CFU) were determined from the lesion areas of lettuce leaves infected with bacterial strains. CFU were quantified as described in the methods section. Data represent the means of six independent experiments with standard deviation (SD). Statistically significant differences are indicated by letters (Tukey's test)

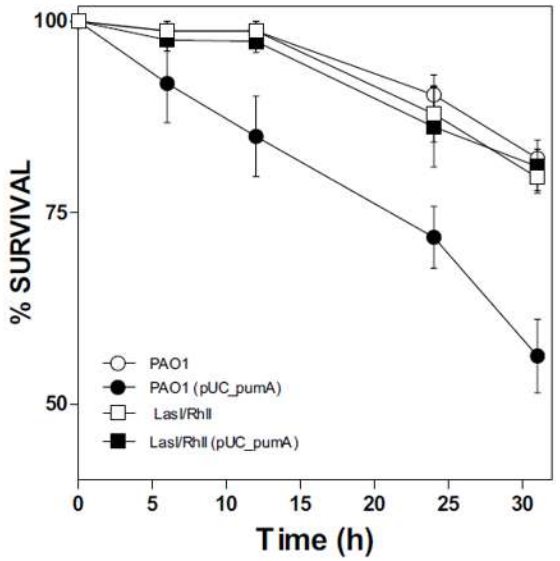

Fig. 2 Effect of *pum*A expression in the *P. aeruginosa lasI/rhlI* double mutant on *Caenorhabditis elegans* survival. Effects of *P. aeruginosa* PAO1 and *P. aeruginosa lasI/rhlI* transformants with *pumA* gene on *C. elegans* viability. Groups of 20 worms were incubated with 1×10^5 ($\pm1\times10^4$) colony-forming units (CFU) of the indicated strains as described in the methods. Mixtures were incubated at 20 °C and scored for live worms at the indicated times. The data shown are the means from the duplicates of four independent assays

virulence in lettuce. Moreover, *P. aeruginosa* PAO1 (pUC_pumAB) decreased the number of CFUs, with values similar to those of the *P. aeruginosa* PAO1 (pUC_pumB) strain. This indicated that, as described [14], PumB neutralizes the toxic PumA effects and does not participate in the bacterial virulence (Fig. 1). The *P. aeruginosa lasI/rhlI* mutant had approximately 82% fewer CFUs in lettuce than *P. aeruginosa* PAO1. This result was expected because several *P. aeruginosa* virulence factors depend on QS function (Fig. 1). However, the *P. aeruginosa lasI/rhlI* (pUC_pumA) strain did not differ in terms of the number of CFUs compared to the *P. aeruginosa lasI/rhlI* (pUCP20), *P. aeruginosa lasI/rhlI* (pUC_pumB), and *P. aeruginosa lasI/rhlI* (pUC_pumAB) strains (Fig. 1). This suggested that the virulence conferred by PumA is LasI/RhlI QS dependent. Additionally, growth kinetics assays were performed to test the possibility that virulence changes were due to growth rate differences in the strains analyzed; these showed no notable variations in growth among the strains (Fig. S1), suggesting that the lack of virulence is due to PumA QS dependence. *P. aeruginosa* containing the *pum*A gene, and also purified PumA toxin alone, has been reported to be toxic to *C. elegans* [14]; therefore, the ability of *pumA* to kill *C. elegans* in the *P. aeruginosa lasI/rhlI* mutant was assessed. We determined that *P. aeruginosa* PAO and *P. aeruginosa lasI/rhlI* strains transformed with the pUCP20 vector were non-virulent to *C. elegans*, as nematodes survival was the same as on M9 medium only (Fig. S2). This indicates again that the vector backbone/antibiotic selection marker does not affect the strain virulence. *P. aeruginosa lasI/rhlI* (pUC_pumA) was non-virulent to *C. elegans* compared with the *P. aeruginosa* PAO1 (pUC_pumA) strain, which decreased *C. elegans* survival by more than 45% (Fig. 2). Additionally, nematodes incubated with *P. aeruginosa lasI/rhlI* (pUC_pumA) showed the same survival values (around 85%) as those incubated only in M9 medium or with the *P. aeruginosa* PAO1 and *P. aeruginosa lasI/rhlI* strains (Fig. 2 and Fig. S2). These results strengthen the hypothesis that PumA function is QS dependent.

QS Positively Regulates *puma* mRna Levels

We determined *pum*A gene expression levels using RT-qPCR assays using RNA from *P. aeruginosa lasI/rhlI* (pUC_pumA) and compared them with the levels obtained for the *P. aeruginosa* PAO1 (pUC_pumA) strain. The *pum*A mRNA was approximately 8 and 4 times less abundant in *P. aeruginosa lasI/rhlI* (pUC_pumA) cultures at exponential and stationary growth phases, respectively, than in

the *P. aeruginosa* PAO1 (pUC_pumA) cultures (Fig. 3a). This suggested *pumA* gene expression was positively regulated by QS. To analyze whether QS regulates *pum*A gene mRNA levels when its gene forms part of the *pum*AB operon, *pum*A mRNA levels from *P. aeruginosa las*I/*rhl*I (pUC_pumAB) were compared with levels from *P. aeruginosa* PAO1 (pUC_pumAB). These results were similar to those for *pum*A cloned without *pum*B: the mRNA levels of *pum*A decreased 11 and 13 times in cultures from exponential and stationary growth phases of *P. aeruginosa las*I/*rhl*I (pUC_pumAB), respectively, compared to the levels in *P. aeruginosa* PAO1 (pUC_pumAB) (Fig. 3). This suggested that the *pum*AB operon was regulated by QS. Although *pum*A mRNA levels decreased in the *P. aeruginosa las*I/*rhl*I mutant strain, *pum*A transcription was detected, suggesting that this gene can be modulated by another QS mechanism or condition of growth. The *pum*B mRNA levels for *P. aeruginosa las*I/*rhl*I (pUC_pumAB) were determined to see whether the *pum*B transcript is also regulated by QS. The results did not show differences in *pum*B mRNA levels in cultures from exponential phase growth of *P. aeruginosa las*I/*rhl*I (pUC_pumAB) compared to the levels of *P. aeruginosa* PAO1 (pUC_pumAB). However, *pum*B transcript levels decreased approximately 3.5 times in cultures from *the P. aeruginosa las*I/*rhl*I (pUC_pumAB) strain compared to those from cultures of *P. aeruginosa* PAO1 (pUC_pumAB) (Fig. 3c). This supports the hypothesis that QS regulates *pum*AB operon expression.

Chemical Complementation of the *P. aeruginosa rhl*I/*las*I (pUC_pumAB) Strain with C4-AHL and 3-oxo-C12-AHL Increased the mRNA Levels of *pum*A and Restored the Virulence Conferred by the Toxin

3-oxo-C12-AHL and C4-AHL are QS autoinducers in *P. aeruginosa*. On binding to their respective receptors, the proteins LasR and RhlR are activated and form complexes that bind to the conserved *las-rhl* boxes in the promoters of target genes and activate their expression [22]. To evaluate whether the expression of *pum*A through QS is regulated by the autoinducer molecules, we added 3-oxo-C12-AHL and C4-AHL to the culture medium of *P. aeruginosa las*I/*rhl*I (pUC_pumA) to complement the *las*I/*rhl*I mutation and determined the mRNA levels of *pum*A. The addition of both autoinducers increased the expression of *pum*A in *P. aeruginosa las*I/*rhl*I (pUC_pumA) in comparison with the absence of autoinducers (Fig. 4) and was more similar to the mRNA expression of the *P. aeruginosa* PAO1 (pUC_pumA) strain; addition of AHLs also increased *pum*A mRNA levels in the *P. aeruginosa* PAO1 (pUC_pumA) (Fig. 4). These results add weight to the hypothesis of positive regulation of *pum*A gene expression by QS.

To demonstrate that the increase in *pum*A expression, via 3-oxo-C12-AHL and C4-AHL complementation of the *las*I/*rhl*I mutation, restored QS-mediated PumA toxin bacterial virulence, we determined the virulence of *P. aeruginosa*

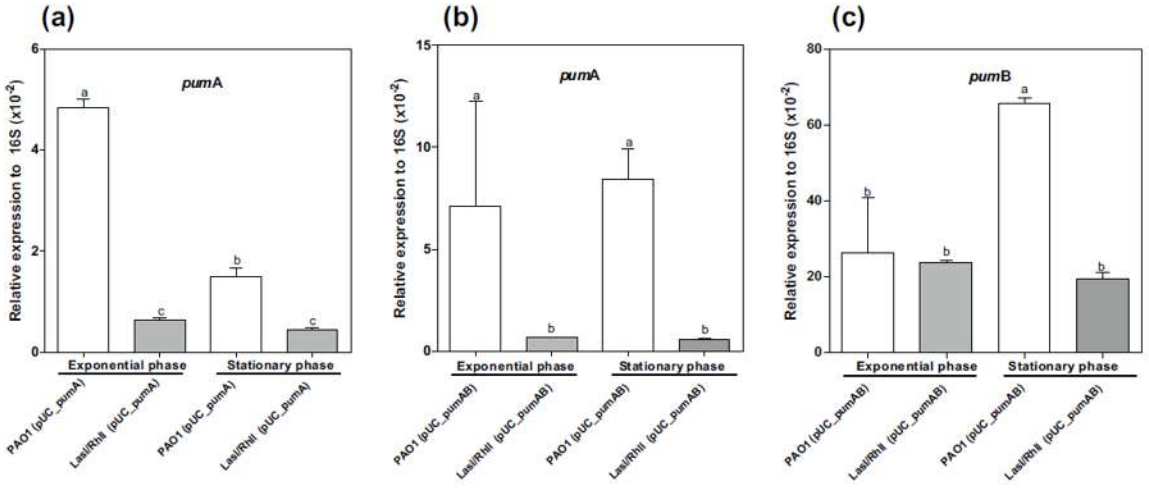

Fig. 3 *pum*A gene expression regulation by the Las and Rhl QS systems. Total RNA (500 ng) from cultures was used to determine the expression levels of the *pum*A or *pum*B genes using RT-qPCR as described in the methods. **a** Expression of *pum*A from *P. aeruginosa* PAO1 (pUC_pumA) (white) and *P. aeruginosa las*I/*rhl*I (pUC_pumA) (gray) cultures grown at the exponential and stationary phases. Expression of *pum*A **b** and *pum*B **c** genes from cultures of *P. aeruginosa* PAO1 (pUC_pumAB) (white), and *P. aeruginosa las*I/*rhl*I (pUC_pumAB) (gray) grown at the exponential and stationary phases. Values represent the means of three independent determinations in duplicate with standard error bars shown. Data were normalized with respect to the transcription of the 16S gene from *P. aeruginosa*. Significant differences ($p<0.0001$) are indicated by the letters

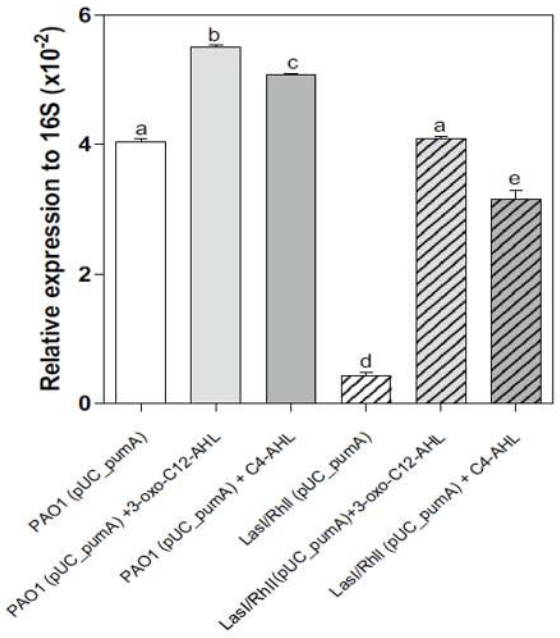

Fig. 4 Chemical complementation with AHLs increased *pum*A mRNA levels in the *P. aeruginosa rhlI*/*las*I mutant. Total RNA (500 ng) from cultures was used to determine the expression levels of *pum*A using RT-qPCR as described in the methods. Expression of *pum*A from *P. aeruginosa* PAO1 (pUC_pumA) and *P. aeruginosa lasI*/*rhl*I (pUC_pumA) cultures grown with or without C4-AHL and 3-oxo-C12-AHL addition. Values represent the means of two independent determinations in duplicate with standard error bars shown. Data were normalized with respect to the transcription of the 16S gene from *P. aeruginosa*. Significant differences ($p < 0.0001$) are indicated by the letters

*las*I/*rhl*I (pUC_pumA) in *C. elegans*. The addition of both AHLs to *P. aeruginosa* PAO1 (pUC_pumA) did not improve the bacterial ability to kill *C. elegans* (Fig. 5a). Interestingly, the addition of 3-oxo-C12-AHL and C4-AHL increased *P. aeruginosa lasI*/*rhl*I (pUC_pumA) virulence (Fig. 5b). However, 3-oxo-C12-AHL clearly restored *P. aeruginosa lasI*/*rhl*I (pUC_pumA) virulence to a greater degree, as its addition limited nematode survival to approximately 48% compared to approximately 71% survival in *C. elegans* obtained under C4-AHL complementation. This suggests that virulence conferred by PumA may respond better to the QS LasI system than the RhlI system. In addition, chemical complementation of the double *rhl*I/*las*I mutant by 3-oxo-C12-AHL and C4-AHL revealed that virulence by *P. aeruginosa* PumA toxin is likely controlled by the LasI and RhlI QS systems.

Interestingly, it has been described that the nosocomial and soil-based *Acinetobacter* species use different signal molecules in bacterial communication. Soil-borne isolates can produce 3-oxo-C8-AHL and C8-AHL, but nosocomial-derived isolates can produce longer-chain signals such as C10-AHL, C12-AHL, C14-AHL, and C16-AHL [23]. In addition, in *P. aeruginosa* clinical isolates, C4-AHL was not detected in the *P. aeruginosa* PAO1 strain, suggesting that the clinical isolates either failed to make short-chain AHLs or the level of the signal molecules was very low [24]. The PumA toxin was identified in pUM505 isolated from a *P. aeruginosa* clinical strain [25], and we therefore determined whether the PumA function could be regulated by other AHL compounds in addition to 3-oxo-C12-AHL and C4-AHL. N-decanoyl-L-homoserine lactone (C10-AHL) was added to the *P. aeruginosa lasI*/*rhl*I (pUC_pumA) cultures and increased the virulence of this strain, with only 53% nematode survival. This was similar to the lethality percentage in *C. elegans* when 3-oxo-C12-AHL was added (Fig. 5c). This suggests that PumA toxin function could also be modulated by different QS long-chain signal molecules.

Discussion

TA systems are found in bacterial mobile genetic elements and bacterial chromosomes. They are linked to many aspects of cell physiology, including plasmid maintenance, stress response, persistence, protection from phage infection, and biofilm formation [12, 26]. The type II PumAB TA system confers plasmid stability, as well as other plasmid-encoded TA systems, and could participate in bacterial virulence via the function of its PumA toxin, such as chromosomally encoded TA systems. The transference of *pum*A to the *P. aeruginosa* PAO1 strain increased bacterial virulence, suggesting that the encoded protein could be a virulence factor [14]. Here, we explored whether QS is involved in the virulence conferred by the PumA toxin from the PumAB plasmid-encoded TA system and evaluated the effects of *pum*A gene in the *P. aeruginosa lasI*/*rhl*I double mutant. We found that PumA did not increase *P. aeruginosa lasI*/*rhl*I virulence in lettuce or against *C. elegans*. This is contrary to what was observed in *P. aeruginosa* PAO1, indicating that the virulence conferred by PumA is QS-dependent. In addition, it was observed that in *P. aeruginosa* PAO1 the transference of *pum*B and *pum*AB genes decreased the bacterial virulence, we do not have an explication of this result; however, this suggests that the PumB antitoxin could, in some way, protect the bacteria from virulence factors and more analyses are required to determine this effect. QS has been shown to control virulence gene expression in gram-negative and gram-positive bacteria, and in some cases, this phenomenon has proven to be relevant for bacterial virulence in vivo [5]. *P. aeruginosa* QS systems play important roles in physiological and metabolic behaviors such as virulence, antibiotic resistance, motility, and biofilm formation [13]. Interestingly, in addition to QS mechanisms that promote biofilm maturation

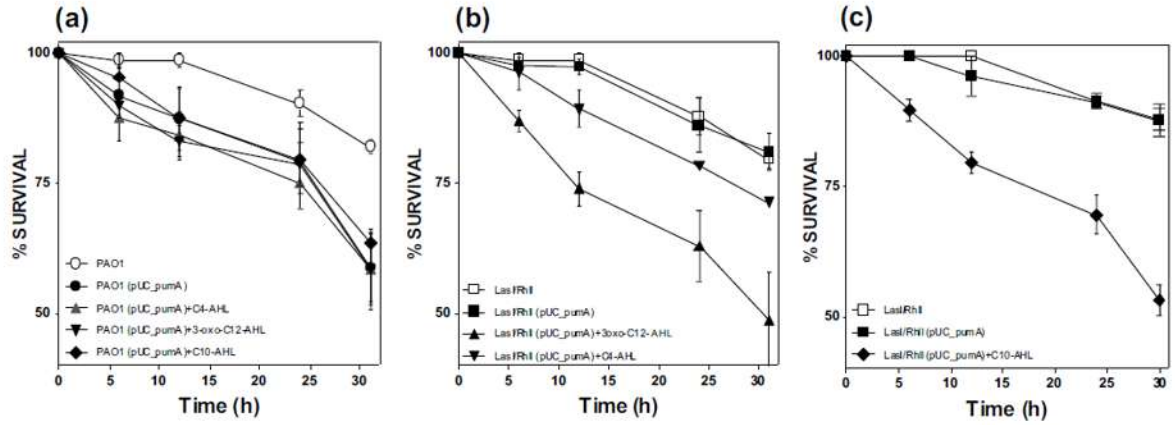

Fig. 5 Restoration of virulence conferred by PumA toxin using chemical complementation with AHLs in the *P. aeruginosa rhlI*/*las*I double mutant. Groups of 20 worms were incubated with 1×10^5 ($\pm1\times10^4$) colony-forming units (CFU) of each strain as described in the Methods section. **a** *C. elegans* viability after incubation with *P. aeruginosa* PAO1 or *P. aeruginosa* PAO1 (pUC_pumA) with or without C4-AHL, 3-oxo-C12-AHL, and C10-AHL addition. **b** *C. elegans* viability after incubation with *P. aeruginosa lasI/rhlI* or *P. aeruginosa lasI/rhlI* (pUC_pumA) with or without C4-AHL and 3-oxo-C12-AHL addition. **c** Effect of C10-AHL addition on *P. aeruginosa lasI/rhlI* virulence conferred by PumA. Mixtures were incubated at 20 °C and scored for live worms at the indicated times. The data shown are the means from the duplicates of four independent assays

[26], multiple TA systems are involved in human pathogenic bacteria biofilm formation [12, 27, 28]. Our data suggest that the PumA toxin acts as a virulence factor that could be regulated by QS. This strengthened the hypothesis of a correlation between QS and TA systems.

In addition, our data showed that *pum*A mRNA levels drastically decreased in the *P. aeruginosa las*I/*rhl*I mutant background, suggesting that *pum*A expression is regulated by QS. In *P. aeruginosa*, QS plays a key role in modulating virulence gene expression, and the Las and Rhl systems regulate the timing and production of multiple virulence factors such as elastase, alkaline protease, exotoxin A, rhamnolipids, pyocyanin, lectins, and superoxidase dismutase [5]. The decrease in the *pum*A transcript in the *P. aeruginosa rhlI*/*las*I mutant background could explain why *pum*A failed to increase the virulence of this strain in both lettuce and *C. elegans*. The *pum*A and *pum*B genes are co-transcribed as a bicistronic mRNA, similar to most genes encoded in TA systems, suggesting that they form an operon [14]. The RT-qPCR results showed that *pum*A mRNA levels also decreased when *pumB* was expressed in the *P. aeruginosa las*I/*rhl*I strain. Moreover, the *pum*B transcript was also decreased in the *P. aeruginosa rhlI*/*las*I mutant. This suggests that the QS system regulates the *pum*AB operon. In addition, it was observed that the *pum*A mRNA levels also decreased the *P. aeruginosa las*I/*rhl*I mutant compared to the *P. aeruginosa* PAO1 background, independent of the bacterial growth phase. This result is not surprising since evidence suggests that although QS occurs at high cell density in many microorganisms, it may play a more central role in the physiology of bacteria, where QS pathways converge with starvation-sensing pathways to regulate cell entry into stationary phase [29].

Several QS systems found in many bacterial pathogens produce and release small chemical signals called autoinducers, which are commonly associated with the regulation of genes encoding virulence factor production and biofilm formation [30–33]. The *las*I gene in *P. aeruginosa* synthesizes 3-oxo-C12-AHL, an acyl homoserine lactone signal (autoinducer), and the *rhl*I gene synthesizes C4-AHL, a second autoinducer [22]. Chemical complementation by addition of 3-oxo-C12-AHL and C4-AHL compounds to *P. aeruginosa las*I/*rhl*I (pUC_pumA) cultures increased the mRNA levels of *pum*A and restored bacterial virulence in *C. elegans*, indicating that both LasI and RhlI systems regulate PumA function. Although both autoinducers restored virulence, 3-oxo-C12-AHL addition restored *P. aeruginosa las*I/*rhl*I (pUC_pumA) virulence to a greater degree than C4-AHL addition, and also induced higher *pum*A mRNA levels than C4-AHL. A study in *P. aeruginosa las*I and *rhl*I mutants revealed that some genes respond well to 3-oxo-C12-AH (e.g., *las*A), while other genes responded well with C4-AHL (e.g., *rhl*AB), and some equally well to both signals [34, 35]. Our data suggested that virulence conferred by PumA responds better to the QS LasI system than the RhlI system.

In summary, this work describes for the first time the role of QS in the regulation of virulence conferred by toxins from plasmid-encoded TA systems in bacterial pathogens.

Acknowledgements This work was supported by grants from Coordinación de la Investigación Científica (UMSNH; 2.6 and 2.35). KCH-R and MIV-M were supported by postgraduate fellowships from CONACYT.

Author contributions KC H-R, B V-A and MI V-M, data acquisition, analysis, and data interpretation, LF R-H and V M-C, reagents, analysis; V M-C data interpretation, and critical revision of the article for intellectual content; MI R-D, conception and design of the work, data analysis and interpretation, and drafting of the article.

Compliance with Ethical Standards

Conflicts of interest The authors declare that they have no conflict of interest.

References

1. Pendleton JN, Gorman SP, Gilmore BF (2013) Clinical relevance of the ESKAPE pathogens. Expert Rev Anti Infect Ther 11:297–308
2. Quick J, Cumley N, Wearn CM, Niebel N, Constantinidou C, Thomas CM, Palle M, Moiemen NS, Bamford A, Oppenheim B, Loman NJ (2014) Seeking the source of *Pseudomonas aeruginosa* infections in a recently opened hospital: an observational study using whole-genome sequencing. BMJ Open 4(11):e006278
3. Rahme LG, Ausubel FM, Cao H, Drenkard E, Goumnerov BC, Lau GW, Mahajan-Miklos S, Plotnikova J, Tan MW, Tsongalis J, Walendziewicz CL, Tompkins RG (2000) Plants and animals share functionally common bacterial virulence factors. Proc Natl Acad Sci USA 97:8815–8821
4. Lee J, Zhang L (2015) The hierarchy quorum sensing network in *Pseudomonas aeruginosa*. Protein Cell 6(1):26–41
5. Antunes LCM, Ferreira RBR, Buckner MMC, Finlay BB (2010) Quorum sensing in bacterial virulence. Microbiology 156:2271–2282
6. Leplae R, Geeraerts D, Hallez R, Guglielmini J, Drèze P, Van Melderen L (2011) Diversity of bacterial type II toxin-antitoxin systems: a comprehensive search and functional analysis of novel families. Nucleic Acids Res 39:5513–5525
7. Page R, Peti W (2016) Toxin-antitoxin systems in bacterial growth arrest and persistence. Nat Chem Biol 12:208–214
8. Fernández-García L, Blasco L, Lopez M, Bou G, García-Contreras R, Wood T, Tomas M (2016) Toxin-antitoxin systems in clinical pathogens. Toxins 8(7):227
9. Yamaguchi Y, Park JH, Inouye M (2011) Toxin-antitoxin systems in bacteria and archaea. Annu Rev Genet 45:61–79
10. Unterholzner SJ, Poppenberger B, Rozhon W (2013) Toxin-antitoxin systems: biology, identification, and application. Mob Genet Elem 1(3):e26219
11. De la Cruz MA, Zhao W, Farenc C, Giménez G, Raoult D, Cambillau C, Gorvel JP, Méresse S (2013) A toxin-antitoxin module of Salmonella promotes virulence in mice. PLOS Pathog 9(12):e1003827
12. Wang X, Wood TK (2011) Toxin-antitoxin systems influence biofilm and persister cell formation and the general stress response. Appl Environ Microbiol 77(16):5577–5583
13. Hemati S, Azizi-Jalilian F, Pakzad I, Taherikalani M, Maleki A, Karimi S, Monjezei A, Mahdavi Z, Reza Fadavi M, Sayehmiri K, Sadeghifard N (2014) The correlation between the presence of quorum sensing, toxin-antitoxin system genes and MIC values with ability of biofilm formation in clinical isolates of *Pseudomonas aeruginosa*. Iran J Microbiol 6(3):133–139
14. Hernández-Ramírez KC, Chávez-Jacobo VM, Valle-Maldonado MI, Patiño-Medina JA, Díaz-Pérez SP, Jácome-Galarza IE, Ortiz-Alvarado R, Meza-Carmen V, Ramírez-Díaz MI (2017) Plasmid pUM505 encodes a Toxin-Antitoxin system conferring plasmid stability and increased *Pseudomonas aeruginosa* virulence. Microb Pathog 112:259–268
15. Green MR, Sambrook J (2012) Molecular cloning: a laboratory manual, 4th edn. Cold Spring Harbor Laboratory, Cold Spring Harbor, NY
16. Pfaffl MW (2001) A new mathematical model for relative quantification in real-time RT-PCR. Nucleic Acids Res 29:2000–2007
17. Rodríguez-Andrade E, Hernández-Ramírez KC, Díaz-Peréz SP, Díaz-Magaña A, Chávez-Moctezuma MP, Meza-Carmen V, Ortíz-Alvarado R, Cervantes C, Ramírez-Díaz MI (2016) Genes from pUM505 plasmid contribute to *Pseudomonas aeruginosa* virulence. Antonie Van Leeuwenhoek 109:389–396
18. Battle SE, Meyer F, Rello J, Kung VL, Hauser AR (2008) Hybrid pathogenicity island PAGI-5 contributes to the highly virulent phenotype of a *Pseudomonas aeruginosa* isolate in mammals. J Bacteriol 190:7130–7140
19. Dong X, Mindrinos M, Davis KR, Ausubel FM (1991) Induction of Arabidopsis defense genes by virulent and avirulent *Pseudomonas syringae* strains and by a cloned virulence gene. Plant Cell 3:61–72
20. Brenner S (1974) The genetics of *Caenorhabditis elegans*. Genetics 77:71–94
21. Stiernagle T (2006) Maintenance of *C. elegans*. Worm Book, pp. 1–11.
22. Pearson JP, Gray KM, Passador L, Tucker KD, Eberhard A, Iglewski BH, Greenberg EP (1994) Structure of the autoinducer required for expression of *Pseudomonas aeruginosa* virulence genes. Proc Natl Acad Sci USA 91:197–201
23. Erdönmez D, Rad AY, Aksöz N (2017) Quorum sensing molecules production by nosocomial and soil isolates *Acinetobacter baumannii*. Arch Microbiol 199(10):1325–1334
24. Boşgelmez-Tinaz G, Ulusoy S, Aridoğan B, Eroğlu F, Kaya S (2005) N-butanoyl-L-homoserine lactone (BHL) deficient *Pseudomonas aeruginosa* isolates from an intensive care unit. Microbiol Res 160(4):399–403
25. Ramírez-Díaz MI, Díaz-Magaña A, Meza-Carmen V, Johnstone L, Cervantes C, Rensing C (2011) Nucleotide sequence of *Pseudomonas aeruginosa* conjugative plasmid pUM505 containing virulence and heavy-metal resistance genes. Plasmid 66(1):7–18
26. Otsuka Y (2016) Prokaryotic toxin-antitoxin systems: novel regulations of the toxins. Curr Genet 62(2):379–382
27. Wen Y, Behiels E, Devreese B (2014) Toxin-Antitoxin systems: Their role in persistence, biofilm formation, and pathogenicity. Pathog Dis 70:240–249
28. Kedzierska B, Hayes F (2016) Emerging roles of toxin antitoxin modules in bacterial pathogenesis. Molecules 21:790
29. Lazazzera BA (2000) Quorum sensing and starvation: signals for entry into stationary phase. Curr Opin Microbiol 3(2):177–182
30. Whitehead NA, Barnard AM, Slater H, Simpson NJ, Salmond GP (2001) Quorum-sensing in gram-negative bacteria. FEMS Microbiol Rev 25:365–404
31. Ng WL, Bassler BL (2009) Bacterial quorum-sensing network architectures. Annu Rev Genet 43:197–222
32. Deng Y, Wu J, Tao F, Zhang LH (2011) Listening to a new language: DSF-based quorum sensing in gram-negative bacteria. Chem Rev 111:160–173
33. Pereira CS, Thompson JA, Xavier KB (2013) AI-2-mediated signaling in bacteria. FEMS Microbiol Rev 37:156–181

34. Schuster M, Lostroh CP, Ogi T, Greenberg EP (2003) Identification, timing, and signal specificity of *Pseudomonas aeruginosa* quorum- controlled genes: a transcriptome analysis. J Bacteriol 185:2066–2079
35. Schuster M, Greenberg EP (2006) A network of networks: quorumsensing gene regulation in *Pseudomonas aeruginosa*. Int J Med Microbiol 296:73–81

Hongos: los inquilinos de nuestro cuerpo

Escrito por Marco Iván Valle Maldonado y Víctor Meza-Carmen

13. REFERENCIAS

Abo Elsoud, M.M., El Kady, E.M. 2019. Current trends in fungal biosynthesis of chitin and chitosan. *Bull Natl Res Cent* 43: 59.

Almyroudis, N.G., Sutton, D.A., Linden, P., Rinaldi, M.G., Fung, J., Kusne, S. 2006. Zygomycosis in solid organ transplant recipients in a tertiary transplant center and review of the literature. *Am J Transplant* 6:2365–2374.

Artemeyev, N.O., Rarick, H.M., Mills, J.S., Skiba, N.P., Hamm. 1992. Sites of Interaction between Rod G-protein α-Subunit and cGMP-phosphodiesterase γ-Subunit. *J Biol Chem* 267(35): 25067-25072.

Aslani, J., Eizadi, M., Kardavani, B., Khoddami-Vishteh, H.R., Nemati, E., Hoseini, S.M.J., Einollahi, B. 2007. Mucormycosis after kidney transplantations: report of seven cases. *Scand J Infect Dis* 39(8): 703-706.

Balzi, E., Wang, M., Leterme, S., Van Dyck L., Goffeau, A. 1994. PDR5, a novel yeast multidrug resistance conferring transporter controlled by the transcription regulator PDR1. *J. Biol Chem* 269: 2206-2214.

Baron S. 1996. Medical Microbiology. University of Texas Medical Branch. United States of America. pp 1273.

Bartnicki-Garcia, S. 1968. Control of Dimorphism in *Mucor* by Hexoses: Inhibition of Hyphal Morphogenesis. *J Bacteriol*. 96: 1586-1594.

Bass, D. , Czech, L. , Williams, B. A. P. , Edric Berney, C. , Dunthorn, M. , Mah E G, F. , Torruella, G. E., Stentiford, G. D. & Williams, T. A. 2018. Clarifying the relationships between Microsporidia and Cryptomycota. *J Eukaryot Microbiol* 65(6), 773-782.

Bastidas, R.J., Shertz, C.A., Lee, S.C., Heitman, J. 2012. Rapamycin exerts antifungal activity in vitro and in vivo against *Mucor circinelloides* via FKBP12-dependent inhibition of Tor. *Eukaryot cell* 11:270-281.

Battaglia, E., Benoit, I., Van Den Brink, J., Wiebenga, A., Coutinho, P.M., Henrissat, B., De Vries, R.P. 2011. Carbohydrate-active enzymes from the zygomycete fungus *Rhizopus oryzae:* a highly specialized approach to carbohydrate degradation depicted at genome level. *BMC Genomics* 12: 38.

Bennet, J.W., Wunch, K.G., Faison B.D. 2002. Use of Fungi Biodegradation. Manual of Environmental Microbiology. Second Edition. ASM Press Washington. United States of America. pp 960-971.

Blattner ,F.R., Plunkett, G., Bloch, C.A., Perna, N.T., Burland, V., Riley, M., Collado-Vides, J., Glasner, J.D., Rode, C.K., Mayhew, G.F., Gregor, J., Davis, N.W., Kirkpatrick, H.A., Goeden, M.A., Rose, D.J., Mau, B., Shao, Y. 1997. The complete genome sequence of *Escherichia coli* K-12. *Science* 277(5331): 1453-1462.

Blumer, J.B., Cismowski, M.J., Sato, M., Lanier, S.M. 2005. AGS proteins: receptor-independent activators of G-protein signaling. *Trends Pharmacol Sci* 26(9): 470-476.

Blumer, J.B., Lanier, S.M. 2014. Activators of G Protein Signaling Exhibit Broad Functionality and Define a Distinct Core Signaling Triad. *Mol Pharmacol* 85(3): 388–396.

Bölker M., 1998. Sex and Crime: Heterotrimeric G Proteins in Fungal Mating and Pathogenesis. *Fungal Genet Biol* 25: 143-156.

Bredenkamp, A., Velankar, H., Van Zyl, W.H., Gorgens, J.F. 2010. Effect of dimorphic regulation on heterologous glucose oxidase production by *Mucor circinelloides. Yeast* 27: 849-860.

Brivanlou, A.H., Darnell Jr, J.E. 2002. Signal Transduction and the Control of Gene Expression. Science 29(5556): 813-818.

Buss, J. E., Mumby, S. M., Casey, P. J., Gilman, A. G. & Sefton, B. M. 1987. Myristoylated *α* subunits of guanine nucleotide-binding regulatory proteins. Proc Natl Acad Sci U S A 8:, 7493–7497.

Cabrera, I.E., Pacentine, I.V., Lim, A., Guerrero, N., Krystofova, S., Li, L., Michkov, A.V., Servin, J.A., Ahrendt, S.R., Carrillo, A.J., Davidson, L.M., Barsoum, A.H., Cao, J., Castillo, R., Chen, W.C., Dinkchian, A., Kim, S., Kitada, S.M., Lai, T.H., Mach, A., Malekyan, C., Moua, T.R., Torres, C.R., Yamamoto, A., Borkovich, K.A. 2015. Global Analysis of Predicted G Protein-Coupled Receptor Genes in the Filamentous Fungus, *Neurospora crassa*. *G3 (Bethesda)* 5(12):2729-2743.

Cerdá-Olmedo, E. 2001. *Phycomyces* and the biology of light and color. *FEMS Microbiol Rev* 25(5): 503-512.

Cismowski, M.J., Takesono, A., Ma, C., Lizano, J.S., Xie, X., Fuernkranz, H., Lanier, S.M., Duzic, E. 1999. Genetic screens in yeast to identify mammalian nonreceptor modulators of G-protein signaling. *Nat Biotechnol* 17(9): 878-873.

Corrochano, L.M., Kuo, A., Marcet-Houben, M., Polaino, S., Salamov, A., Villalobos-Escobedo, J.M., Grimwood, J., Álvarez, M.I., Avalos, J., Diane Bauer,

D., Benito, E.P., Benoit, I., Burger, G., Camino, L.P., Cánovas, D., Cerdá-Olmedo, E., Cheng, J.F., Domínguez, A., Marek Eliáš, M., Eslava, A.P., Glaser, F., Gutiérrez, G., Heitman, J., Henrissat, B., Iturriaga, E.A., Lang, F., Lavín, J.L., Lee, S.C., Li, W., Lindquist, E., López-García, S., Luque, E.M., Marcos, A.T., Martin, J., McCluskey, K., Medina, H.R., Miralles-Durán, A., Miyazaki, A., Muñoz-Torres, E., Oguiza, J.A., Ohm, R.A., Olmedo, M., Orejas, M., Ortiz-Castellanos, L., Pisabarro, A.P., Rodríguez-Romero, J., Ruiz-Herrera, J., Ruiz-Vázquez, R., Sanz, C., Schackwitz, W., Shahriari, M., Sheles, E., Silva-Franco, F., Soanes, D., Syed, K., Tagua, V.G., Talbot, N.J., Thon, M.R., Tice, H., De Vries, R.P., Wiebenga, A., Yadav , J.S., Braun, E.L., Baker, S.E., Garre, V., Schmutz, J., Horwitz, B.A., Torres-Martínez, S., Idnurm, A., Herrera-Estrella, A. Gabaldón, T., Grigoriev, I.V. 2016. Expansion of Signal Transduction Pathways in Fungi by Extensive Genome Duplication. *Curr Biol* 26(12):1577-1584. doi: 10.1016/j.cub.2016.04.038.

Davis, W.J., Amses, K.R., Benny, G.L., Carter-House, D., Chang, Y., Grigoriev, I., Smith, M.E., Spatafora, J.W., dJason E.StajichJames, T.Y. 2019. Genome-scale phylogenetics reveals a monophyletic Zoopagales (Zoopagomycota, Fungi). *Mol Phylogenetics Evol* 133: 152-163.

De Souza, T.D., Alves-Leal, C., Massarolo, K.C., Badiale-Fulong, E. 2019. Profile of Phenolic Compounds Released from Rice Bran by Rhizopus oryzae and Trichoderma reesei : Their Relation with Hydrolases Activity. *J Food Sci* 84(6): 1382-1389.

Díaz-Pérez, S.P., Patiño-Medina, J.A., Valle-Maldonado, M.I., López-Torres, A., Jácome-Galarza, I.E., Anaya-Martínez, V., Gómez-Ruiz, V., Campos-García, J., Nuñez-Anita, R.E., Ortiz-Alvarado, R., Ramírez-Díaz, M.I., Gutiérrez-Corona, J.F., Meza-Carmen, V. 2020. Alteration of Fermentative Metabolism Enhances *Mucor circinelloides* Virulence. *Infect Immun* 88(2):e00434-19.

Dignard, D., André, D., Whiteway, M. 2008. Heterotrimeric G-protein subunit function in *Candida albicans:* both the alpha and beta subunits of the pheromone response G protein are required for mating. *Eukaryot Cell*, 7(9), 1591–1599

Dohlman, H.G., Ma, S.D., Courchesne, W.E., Thorner, J. 1996. Sst2, a negative regulator of pheromone signaling in the yeast Saccharomyces cerevisiae: expression, localization, and genetic interaction and physical association with Gpa1 (the G-protein alpha subunit). *Mol Cell Biol* 16(9): 5194-5209.

Etienne-Manneville, S., Hall, A. 2002. Rho GTPases in cell biology. *Nature* 420(6916): 629-635.

García-Solache, M., Casadevall, A. 2011. Global Warming Will Bring New Fungal Diseases for Mammals. *MBio*, 1, e00061-10.

Galagan, J.E., Henn, M.R., Ma, L.J., Cuomo, C.A., Birren, B. 2005. Genomics of the fungal kingdom: insights into eukaryotic biology. *Genome Res* 15(12): 1620-1631.

Gao, C., Wang, L., Milgrom, E. Winston-Shen, W.C. 2004. On the Mechanism of Constitutive Pdr1 Activator-mediated *PDR5* Transcription in *Saccharomyces cerevisiae. J Bioll Chem* 279(41): 42677-42686.

Gutiérrez, A., López-García, Garre, V. 2011. High reliability transformation of the basal fungus *Mucor circinelloides* by electroporation. *J Microbiol Methods* 84(3): 442-446.

Hammond, S.P., Baden, L.R., Marty, F.M. 2011. Mortality in hematologic malignancy and hematopoietic stem cell transplant patients with mucormycosis, 2001 to 2009*. Antimicrob Agents Chemother* 55(11): 5018-5021.

Hartanti, A.T., Rahayu, G., Hidayat, I. 2015. *Rhizopus* Species from Fresh Tempeh Collected from Several Regions in Indonesia. *HAYATI J Biosci* 22(3): 136-142

Hawksworth, D.L. 2001. The magnitude of fungal diversity: the 1.5 million species estimate revisited. *Mycol Res* 105(12): 1422-1432.

Hibbett, D.S., Binder, M., Bischoff, J.F. Blackwell. M., Cannon, P.F., Eriksson, O.E., Huhndorff, S., James, T., Kirk, P., Lücking, R., Lumbsch, T., Lutzoni, F., Matheny, B., McLaughlin, D.J., Powell, M.J., Redhead, S., Schochk, C.L., Spatafora, J.W., Stalpers, J.A., Vilgalys, R., Aime, M.C., Aptroot, A., Bauer, R., Begerow, D., Benny, G.L., Castlebury, L.A., Crous, P.W., Dai, Y.C., Gams, W., Geiser, D.M., Griffith, G.W., Gueidan, C., Hawksworth, D.L. Hestmark, G., Hosaka, K., Humber, R.A., Hyde, K.D., Ironside, J.E., Kõljalg, U., Kurtzman, C.P., Larsson, K.H., Lichtward, R., Longcore, J., Miądlikowska, J., Miller, A., Moncalvo, J.M., Mozley-Standridge, S., Oberwinkler, F., Parmasto, E., Reeb, V., D. Rogers, J.D., Roux, C., Ryvarden, L., Sampaio, J.P., Schüßleram, A., Sugiyama, J., Thorn, G., Tibell, L., Untereiner, W.A., Walker, C., Wang, Z., Weir, A., Weiss, M., White, M.M., Winka, K., Yao, Y.L., Zhang, N. 2007. A higher-level phylogenetic classification of the Fungi. *Mycol Res* 111(5): 509-547.

Huang, P., Chandra, V., Rastinejad, F. 2010. Structural Overview of the Nuclear Receptor Superfamily: Insights into Physiology and Therapeutics. *Annu Rev Physiol* 72: 247–272.

Huang, C., Tesmer, J.J.G. 2011. Recognition in the Face of Diversity: Interactions of Heterotrimeric G proteins and G Protein-coupled Receptor (GPCR) Kinases with Activated GPCRs. *J Biol Chem* 286: 7715–7721.

Kahn, R.A. 2014. Is the model of signal amplification by GPCRs/GEFs activating multiple GTPases relevant to a broad spectrum of heterotrimeric and RAS superfamily GTPases? *Cell Logist* 4(2): e943602.

Karmakar, M., Ghosh, B., Ray, R.R. 2012. Effect of Extracellular Factors on Growth and Dimorphism of Rhizopus oryzae with Multiple Enzyme Synthesizing Ability. *Indian J Microbiol* 52(2): 215-221.

Köhler, J.R., Casadevall, A., Perfect, J. 2015. The Spectrum of Fungi That Infects Humans. *Cold Spring Harb Perspect Med* 5(1): a019273.

Koretzky, G.A, Picus, Thomas, M.L., Weiss, A., 1990. Tyrosine phosphatase CD45 is essential for coupling T-cell antigen receptor to the phosphatidyl inositol pathway. *Nature* 346(6279): 66-68.

Krauss, G. 2003. Biochemistry of Signal Transduction and Regulation. Third Edition. Wiley-WCH. Germany. pp 541.

Lee, S.C., Li, A., Calo, S., Heitman, J. 2013. Calcineurin plays key roles in the dimorphic transition and virulence of the human pathogenic zygomycete *Mucor circinelloides*. *PLoS Pathog* 9(9): e1003625.

Levitzki, A., Bar-Sinai, A. 1991. The regulation of adenylyl cyclase by receptor-operated G proteins. *Pharmacol Therapeut* 50(3): 271-283.

Li, L., He, L., Lai, Y., Shao, Y., & Chen, F. 2014. Cloning and functional analysis of the Gβ gene Mgb1 and the Gγ gene Mgg1 in Monascus ruber. *J Microbiol* 52(1), 35-43.

Li, L., Wright, S.J., Krystofova, S., Park, G., Borkovich, K.A. 2007. Heterotrimeric G protein signaling in filamentous fungi. *Annu Rev Microbiol* 61: 423–452.

Lübbehüsen, T.L., Nielsen, J., McIntyre, M. 2003. Characterization of the *Mucor circinelloides* life cycle by on-line image analysis. *J Appl Microbiol* 95: 1152–1160.

Ma, L.J., Ibrahim, A.S., Skory, C., Grabherr, M. G., Burger, G., Butler, M., Elias, M., Idnurm, A., Lang, B.F., Sone, T., Abe, A., Calvo, S.E., Corrochano, L.M., Engels, R., Fu, J., Hansberg, W., Kim, J.M., Kodira, C.D., Koehrsen, M.J., Liu, B., Miranda-Saavedra, D., O´Leary, S., Ortiz-Castellanos, L., Poulter, R., Rodriguez-Romero, J., Ruiz-Herrera, J., Shen, Y.Q., Zeng, Q., Galagan, J., Birren, B.W., Cuomo, C.A.,

Wickes, B.L. 2009. Genomic Analysis of the Basal Lineage Fungus *Rhizopus oryzae* Revealis a Whole-Genome Duplication. *PLoS Genet* 5(7): e1000549.

Martins MP, Silva LG, Rossi A, Sanches PR, Souza LDR, Martinez-Rossi NM. 2019. Global Analysis of Cell Wall Genes Revealed Putative Virulence Factors in the Dermatophyte *Trichophyton rubrum*. Front Microbiol 10: 2168.

McCudden C.R., Hains M.D., Kimple R.J., Siderovski D.P., Willard F.S. 2005. G-protein signaling: back to the future. *Cell Mol Life Sci* 62: 551-577.

McIntyre, M., Breum, J., Arnau, J., Nielsen, J. 2002. Growth physiology and dimorphism of *Mucor circinelloides. Appl Microbiol Biot* 58: 495-502.

Meussen, B.J., De Graaff, L.H., Sanders, J.P.M., Sanders, Weusthuis, R.A. 2012. Metabolic engineering of Rhizopus oryzae for the production of platform chemicals. *Appl Microbiol Biotechnol* 94(4): 875–886. doi: 10.1007/s00253-012-4033-0

Mohanta T.K., Bae H. 2015. The diversity of fungal genome. *Biol Proced Online* 17: 8.

Mulligan, T., Farber, S.A. 2011. Central and C-terminus domains of heterotrimeric G protein gamma subunits differentially influence the signaling necessary for primordial germ cell migration. *Cell Signal* 23(10): 1617-1624.

Murcia-Flores, L., Lorca-Pascual, J.M., Garre, V., Torres-Martínez, S, Ruiz-Vázquez, R.M. 2007. Non-AUG Translation Initiation of a Fungal RING Finger Repressor Involved in Photocarotenogenesis. *J Biol Chem* 282: 15394–15403.

Naar, A.M., Thakur, J.K. 2009. Nuclear receptor-like transcription factors in fungi. *Genes Dev* 23: 419-432.

Navarro-Olmos, R., Kawasaki, L., Domínguez-Ramírez, L., Ongay-Larios, L., Pérez-Molina, & R., Coria, R. 2010. The β subunit of the heterotrimeric G protein triggers the Kluyveromyces lactis pheromone response pathway in the absence of the γ Subunit. *Mol Biol Cell*, 21(3), 489–498.

Neer, E.J. 1994. G proteins: Critical control points for transmembrane signals. *Protein Sci* 3: 3-14.

Nielsen, E., Cheung, A.Y., Ueda, T. 2008. The regulatory *RAB* and *ARF* GTPases for vesicular trafficking, *Plant Physiol* 147(4): 1516-1526.

Nishijima, K.A., Wall, M.M. 2011. First Report of Association of *Mucor circinelloides* on Noni (*Morinda citrifolia*) in Hawaii. *Plant Dis* 95(3): 360.

Nishimura, M., Park, G., Xu, J.R. 2003. The G-beta subunit MGB1 is involved in regulating multiple steps of infection-related morphogenesis in *Magnaporthe grisea*. *Mol Microbiol*, *50*(1), 231–243.

Nout, M.J., Rombouts, F.M. 1990. Recent developments in tempe research. *J Appl Microbiol* 69: 609-633.

Ocampo, J., Fernández-Núñez, L., Silva, F., Pereyra, E., Moreno, S., Garre, V., Rossi, S. 2009. A Subunit of Protein Kinase A Regulates Growth and Differentiation in the Fungus *Mucor circinelloides. Eukaryot Cell* 8: 933-944.

Ocampo, J., McCormack, B., Navarro, E., Moreno, S., Garre, V., Rossi S. 2012. Protein kinase A regulatory subunit isoforms regulate growth and differentiation in *Mucor circinelloides*: essential role of PKAR4. *Eukaryot Cell* 11(8): 989-1002.
Orlowski M, 1991. *Mucor* dimorphism. *Microbiol Rev* 55: 234-258.

Patiño-Medina, J.A., Maldonado-Herrera, G., Pérez-Arques, C., Alejandre-Castañeda, V., Reyes-Mares, N.Y., Valle-Maldonado, M.I., Campos-García, J., Ortiz-Alvarado, R., Jácome-Galarza, I.E., Ramírez-Díaz, M.I., Garre, V., Meza-Carmen, V. 2018. Control of morphology and virulence by ADP-ribosylation factors (Arf) in *Mucor circinelloides*. *Curr Genet* 64(4): 853-869.

Patiño-Medina, J.A., Reyes-Mares, N.Y., Valle-Maldonado, M.I., Jácome-Galarza, I.E., Pérez-Arques, C., Nuñez-Anita, R.E., Campos-García, J., Anaya-Martínez, V., Ortiz-Alvarado, R., Ramírez-Díaz, M.I., Lee, S.C. S, Garre, V., Meza-Carmen, V. 2019a. Heterotrimeric G-alpha subunits Gpa11 and Gpa12 define a transduction pathway that control spore size and virulence in *Mucor circinelloides*. *PLoS One* 14(12):e0226682.

Patiño-Medina JA, Valle-Maldonado MI, Maldonado-Herrera G, Pérez-Arques C, Jácome-Galarza IE, Díaz-Pérez C, Díaz-Pérez AL, Araiza-Cervantes CA, Villagomez-Castro JC, Campos-García J, Ramírez-Díaz MI, Garre V, Meza-Carmen V. 2019b. Role of Arf-like proteins (Arl1 and Arl2) of *Mucor circinelloides* in virulence and antifungal susceptibility. *Fungal Genet Biol* 129:40-51.

Patiño-Medina, J.A., Valle-Maldonado, M.I., Vargas-Tejeda, D., Chávez-Jacobo, V.M., Corrales-Escobosa, A.R., Ramírez-Emiliano, J. Ruiz-Herrera, L.F., Ramírez-Díaz, M.I., Garre, V., Meza-Carmen, V. 2020. Arf-like proteins (Arl1 and Arl2) are involved in mitochondrial homeostasis in *Mucor circinelloides. Fungal Biol* 124(7):619-628.

Patiño-Medina, J.A., Vargas-Tejeda, D., Valle-Maldonado, M.I., Alejandre-Castañeda, V., Jácome-Galarza, I.E., Villegas-Moreno, J., Nuñez-Anita, R.E., Ramírez-Díaz, M.I., Ortiz-Alvarado, R., Meza-Carmen, V. 2019c. Sporulation on

blood serum increases the virulence of *Mucor circinelloides*. *Microb Pathog* 137:103737.

Petrikkos, G., Skiada, A., Lortholary, O., Roilides, E., Walsh, T. J., Kontoyiannis, D.P. 2012. Epidemiology and Clinical Manifestations of Mucormycosis. *Clin Infect Dis* 54 Suppl 1:S23-S54.

Prakash, H., Chakrabarti, A., 2019. Global Epidemiology of Mucormycosis. J Fungi (Basel) 5(1): 26.

Rammaert, B., Lanternier, F., Zahar, J.R., Dannaoui, E., Bougnoux, M.E., Lecuit, M., Lortholary, O. 2012. Healthcare-associated mucormycosis. *Clin Infect Dis* 54 Suppl 1:S44-54.

Rangel-Porras, R. A., Díaz-Pérez, S.P., Mendoza-Hernández, J.M., Romo-Rodríguez, P., Alejandre-Castañeda, V., Valle-Maldonado, M.I., Torres-Guzmán, J.C., González-Hernández, G.A., Campos-Garcia, Arnau, J., Meza-Carmen, V., Gutiérrez-Corona, J.F. 2019. Alcohol dehydrogenase 1 participates in the Crabtree effect and connects fermentative and oxidative metabolism in the Zygomycete *Mucor circinelloides. J Microbiol* 57(7): 606-617.

Redman, R.S., Dunigan, D.D., Rodriguez, R.J. 2001. Fungal simbiosis from mutualism to parasitism: who controls the outcome, host or invader? *New Phytol* 151: 705-716.

Repasky, G.A., Chenette, E.J., Der, C.J. 2004. Renewing the conspiracy theory debate: does *Raf* function alone to mediate *Ras* oncogenesis? *Trends Cell Biol* 14(11): 639-647.

Rodrigues M.L. 2018. The Multifunctional Fungal Ergosterol. *MBio* 9(5): e01755-18.

Sagaram, U.S., Shim, W.B. 2007. *Fusarium verticillioides* GBB1, a gene encoding heterotrimeric G protein beta subunit, is associated with fumonisin B biosynthesis and hyphal development but not with fungal virulence. *Mol Plant Pathol* 8(4): 375-384.

Scheib, U., Stehfest, K., Gee, C.E., Körschen, H.G., Fudim, R., Oertner, T.G., Hegemann, P. 2015. The rhodopsin-guanylyl cyclase of the aquatic fungus *Blastocladiella emersonii* enables fast optical control of cGMP signaling. *Sci Signal* 8(389):rs8.

Schwindinger, W.F., Robishaw, J.D. 2001. Heterotrimeric G-protein βγ-dimers in growth and differentiation. *Oncogene* 20(13): 1653-1660.

Sharma P.D. 2005. *Fungi and Allied Organisms.* Alpha Science International. Oxford, United Kingdom. pp. 300.

Sever, R., Glass, C.K. 2013. Signaling by Nuclear Receptors. *Cold Spring Harb Perspect Biol* 5(3): a016709.

Siekhaus, D.E., Drubin, D.G. 2005. Spontaneous receptor-independent heterotrimeric G-protein signaling in an RGS mutant. *Nat Cell Biol* 5: 231-235.

Singh L.P., Gill S.S., Tuteja N. 2011. Unraveling the role of fungal symbionts in plant abiotic stress tolerance. *Plant Signal Behav* 6(2): 175-191.

Smrcka, A.V., Brown, J.H., Holz, G.G. 2012. Role of phospholipase Cε in physiological phosphoinositide signaling networks. *Cell Signal* 24(6): 1333-1343.

Snyder, A., Churey, J.C., Worobo, R.W. 2016. Characterization and control of *Mucor circinelloides* spoilage in yogurt. *Int J Food Microbiol 228:14-21.*

Sorol, M.R., Pastori, R.L., Muro, A., Moreno, S., Rossi, S. 2000. Structural and functional analysis of the cAMP binding domain from the regulatory subunit of Mucor rouxii protein kinase A. Archives of Bbiochemistry and Bbiophysics 382(2): 173-181.

Spatafora, J.W., Chang, Y., Benny, G.L., Lazarus, K., Smith, M.E., Berbee, M.L., Bonito, G., Corradi, N., Grigoriev, I., Gryganskyi, A. 8, James, T.Y., O'Donnell, K., Roberson, R.W., Taylor, T.N., Uehling, J., Vilgalys, R., White, M.M., Stajich. J.E. 2016. A Phylum-Level Phylogenetic Classification of Zygomycete Fungi Based on Genome-Scale Data. *Mycologia* 108(5):1028-1046

Spellberg, B., Ibrahim, A.S., Chin-Hong, P. V., Kontoyiannis, D.P., Morris, M.I., Perfect, J.R. Fredricks, D., Brass, E.P. 2012. The Deferasirox–AmBisome Therapy for Mucormycosis (DEFEAT Mucor) study: a randomized, double-blinded, placebo-controlled trial*. J Antimicrob Chemother* 67(3): 715–722.

Spellberg, B., Ibrahim, A.S. 2010. Recent Advances in the Treatment of Mucormycosis. *Curr Infect Dis Rep* 12(6): 423–429.

Snyder, A.B., Churey, J.J., Worobo, R.W. 2016. Characterization and control of *Mucor circinelloides* spoilage in yogurt. *Int J Food Microbiol* 228:14-21. doi: 10.1016/j.ijfoodmicro.2016.04.008.

Sprang, S.R. 1997. G PROTEIN MECHANISMS: Insights from Structural Analysis. Annu Rev Biochem 66: 639-678

Takahashi, T., Tsuchida, Y., Irie M. 1978. Purification and some properties of three forms of glucoamylase from *Rhizopus* species. *J Biochem* 84(5): 1183-1194.

Takai Y., Sasaki, T., Matozaki, T. 2001. Small GTP-Binding Proteins. Physiol Rev 81(1): 154-188.

Tanabe, Y., Watanabe, M.M., Sugiyama, J. 2005. Evolutionary relationships among basal fungi (Chytridiomycota and Zygomycota): Insights from molecular phylogenetics. *J Gen Appl Microbiol* 51(5): 267-276.

Tesmer, J.J.G. 2010. The Quest to Understand Heterotrimeric G Protein Signaling. *Nat Struct Mol Biol* 17(6): 650-658.

Thongchul, N., Navankasattusas, S., Yang, S.T. 2010. Production of lactic acid and ethanol by *Rhizopus oryzae* integrated with cassava pulp hydrolysis. *Bioproc Biosyst Eng* 33(3): 407-416.

Todd, R.T., Forche, A., Selmecki, A. 2017. Ploidy Variation in Fungi: Polyploidy, Aneuploidy, and Genome Evolution. *Microbiol Spectr* 5(4):10.1128/microbiolspec.FUNK-0051-2016.

Tzima, A.K., Paplomatas, E.J., Tsitsigiannis, D.I., Kang, S. 2012. The G-Protein β subunit controls virulence and multiple growth- and developmet related traits in *Verticillium dahliae*. *Fungal Genet Biol*, 49(4), 271-283.

Valle-Maldonado, M.I., Jácome-Galarza, I.E., Gutiérrez-Corona, F., Ramírez-Díaz, M.I., Campos-García, J., Meza-Carmen, V. 2015a. Selection of reference genes for quantitative real time RT-PCR during dimorphism in the zygomycete *Mucor circinelloides. Mol Biol Rep* 42(3):705-711. doi: 10.1007/s11033-014-3818-x.

Valle-Maldonado, M.I., Jácome-Galarza, I.E., Díaz-Pérez, A.L., Martínez-Cadena, G., Campos-García, J., Ramírez-Díaz, M.I., Reyes-De la Cruz, H., Riveros-Rosas, H., Díaz-Pérez, C,, Meza-Carmen, V. 2015b. Phylogenetic analysis of fungal heterotrimeric G protein-encoding genes and their expression during dimorphism in *Mucor circinelloides*. Fungal Biol 119(12): 1179-1193.

Van Dop, C., Yamada, G., Steinberg, F., Sekura, R. D., Manclark, C. R., Stryer, L. & Bourne, H. R. 1984. *J Biol Chem* 259: 23-26

Vellanki, S., Billmyre R.B., Lorenzen, A., Campbell, M., Turner, B., Huh, E.Y., Heitman, J., Lee, S.C. 2020. A Novel Resistance Pathway for Calcineurin Inhibitors in the Human-Pathogenic Mucorales *Mucor circinelloides.* mBio 11(1): e02949-19. doi: 10.1128/mBio.02949-19.

Vellanki, S., Navarro-Mendoza, M.I., Garcia, A., Murcia, L., Perez-Arques, C., Garre, V., Nicolas, F.E., Lee, S.C. 2018. *Mucor circinelloides*: Growth, Maintenance, and Genetic Manipulation. *Curr Protoc Microbiol* 49(1): e53. doi: 10.1002/cpmc.53.

Versele, M., Lemaire, K., Thevelein, J.M. 2001. Sex and sugar in yeast: two distinct GPCR systems. *EMBO Rep* 2(7): 574-579.

Wacker, D., Stevens, R.C., Roth, B.L. 2017. How Ligands Illuminate GPCR Molecular Pharmacology. *Cel*l 170(3): 414-427.

Walbot V., Petrov D.A. 2001. Gene galaxies in the maize genome. P Natl Acad Sci USA 98(15): 8163-8164.

Wall, M.A., Coleman, D.E., Lee, E., Iñiguez-Lluhi, J.A., Posner, B.A., Gilman, A.G., Sprang, S.R. 1995. The structure of the G protein heterotrimer Gi alpha 1 beta 1 gamma 2. *Cell* 83(6): 1047-1058.

Wang, P., Perfect, J.R., Heitman, J. 2000. The G-protein beta subunit GPB1 is required for mating and haploid fruiting in *Cryptococcus neoformans*. *Mol Cell Biol,* 2(1), 352-362.

Weis, K. 2003. Regulating access to the genome: nucleocytoplasmic transport throughout the cell cycle. *Cell* 112(4): 441-451.

West, R.E., Moss, J, Vaughan, M., Liu, T., Liu, T.Y. 1985. Pertussis toxin-catalyzed ADP-ribosylation of transducin. Cysteine 347 is the ADP-ribose acceptor site. *J Biol Chem* 260(27):14428-14430.

White M.M., James T.Y., O´Donnell K. 2006. Phylogeny of the Zygomycota based on nuclear ribosomal sequence data. *Mycologia* 98(6): 872-884.

Whiteway M., Clark K.L., Leberer C.E., Dignard D., Thomas D.Y. 1994. Genetic Identification of Residues Involved in Association of α and β G-Protein Subunits. *Mol Cell Biol* 14(5): 3223-3229.

Whiteway M., Hougan L., Dignard D., Thomas D.Y., Bell L., Saari G.C., Grant F.J., MacKay V.L. 1989. The STE4 and STE18 genes of yeast encode potential beta and gamma subunits of the mating factor receptor G protein. *Cell* 56(3): 467-477.

Wikandari, R., Millati, R., Lennartsson, P.R., Harmayani, E., Taherzadeh M.J. 2012. Isolation and Characterization of Zygomycetes Fungi from Tempe for Ethanol Production and Biomass Applications. *Appl Biochem Biotechnol* 167(6):1501-1512.

Wolff, A.M., Appel, K.F., Petersen, J.B., Poulsen, U., Arnau, J. 2002. Identification and analysis of genes involved in the control of dimorphism in *Mucor circinelloides (syn. racemosus).* 2002. *FEMS Yeast Res* 2(2): 203-213.

Wright, S.K., Inchausti, R., Eaton, C.J., Krystofova, S., Borkovich, K.A. 2011. *RIC8* is a guanine-nucleotide exchange factor for Galpha subunits that regulates growth and development in *Neurospora crassa*. *Genetics* 189(1): 165-176.

Zaballos, P., Ara, M., Pozo, A., Andrés, R., Gil, J., Ramóny Cajal, S., Carapeto, F.J. 2003. Fulminant rhinocerebral mucormycosis. Actas Dermosifiliogr 94(9): 624-626.

Zerial, M., McBride, H. 2001. Rab proteins as membrane organizers. *Nat Rev Mol* 2(2): 107-117.

Zhang W. 2011. Roles of heterotrimeric G proteins in guard cell ion channel regulation. *Plant Signal Behav* 6(7): 986-990.

Zhang, W., Jeon, B.W., Assmann, S.M. 2011. Heterotrimeric G-protein regulation of ROS signalling and calcium currents in *Arabidopsis* guard cells. *J Exp Bot* 62(7): 2371-2379.

Zhang, Y., Navarro, E., Cánovas-Márquez, J.T., Almagro, L., Chen, H., Chen, Y.Q., Zhang, H., Torres-Martínez, S., Chen, W., Garre, V. 2016. A new regulatory mechanism controlling carotenogenesis in the fungus *Mucor circinelloides* as a target to generate β-carotene over-producing strains by genetic engineering. *Microb Cell Fact* 15:99.

Žifčáková L., Větrovský T., Howe A., Baldrian P. 2016. Microbial activity in forest soil reflects the changes in ecosystem properties between summer and winter. *Environ Microbiol* 18(1): 288-301.

Zininga, J.T., Puri, A.K., Govender, A., Singh, S., Permaul, K. 2019. Concomitant production of chitosan and lipids from a newly isolated *Mucor circinelloides* ZSKP for biodiesel production. *Bioresour Technol* 272: 545-551. doi: 10.1016/j.biortech.2018.10.035.